

THE JOURNAL OF PHYSICAL CHEMISTRY

Volume 74, Number 5 March 5, 1970

Kinetics of Ion-Exchange. Diffusion of Trace Component	H. D. Sharma, R. E. Jervis, and L. W. McMillen	969
Reactions of CF_3 Radicals with Methylfluorosilanes	T. N. Bell and U. F. Zucker	979
Reaction of Hot and Thermal Hydrogen Atoms with Hydrogen Bromide and Bromine	Richard A. Fass	984
Electron Spin Resonance Study of the Kinetics of the Reaction of $O(^3P)$ Atoms with H_2S	Gerald A. Hollinden, Michael J. Kurylo, and Richard B. Timmons	988
Kinetics of the Dehydrofluorination of Vinyl Fluoride in a Single-Pulse Shock Tube	J. M. Simmie, W. J. Quiring, and E. Tschuikow-Roux	992
The Gas-Phase Thermal Decomposition of Chlorocycloalkanes	J. M. Sullivan and W. C. Herndon	995
The Kinetics and Mechanism of the Thermal Decomposition of Nitroglycerin	Chas. E. Waring and Gunar Krastins	999
The Kinetics of the Thermal Decomposition of 1,1,1-Trifluoroacetone	Chas. E. Waring and Alexander J. Fekete	1007
Kinetic Investigation of the Radiation-Induced Isotopic Exchange between Iodobenzene and Iodine in Benzene	R. Riess and H. Elias	1014
The 2537-Å Photochemistry of Azido-Ammine Complexes of Cobalt(III) in Aqueous Solution: Products, Stoichiometry, and Quantum Yields	John F. Endicott, Morton Z. Hoffman, and Laszlo S. Beres	1021
Charge-Transfer Effects on the Absorption and Fluorescence Spectra of Anthroic Acids	T. C. Werner and David M. Hercules	1030
Nuclear Magnetic Resonance Studies on the Intermolecular Association in Some Binary Mixtures. I. Chloroform and Proton-Acceptor Solvents	Wei-chuwan Lin and Shyr-jin Tsay	1037
Dipole Moments of Alkyl Mesityl Ketones and Some Aliphatic and Phenyl Analogs	A. G. Pinkus and H. C. Custard, Jr.	1042
Ethylene-Maleic Anhydride Copolymers and Derivatives. Potentiometric Titrations and Interactions with Polypeptides	E. Bianchi, A. Ciferri, R. Parodi, R. Rampone, and A. Tealdi	1050
On the Viscosity of Concentrated Aqueous Electrolyte Solutions.	Barry R. Breslau and Irving F. Miller	1056
Micellar and Electrolyte Effects upon the H_0'' and H_0''' Acidity Functions	C. A. Euntun and L. Robinson	1062
The Surface Tension of Polyatomic Liquids and the Principle of Corresponding States	D. Patterson and A. K. Rastogi	1067
Electrical Conductivity of Suspensions of Conducting Colloidal Particles	Henry C. Thomas and Adrien Cremers	1072
An Effusion Study of the Reaction of Zirconium Carbide with Calcium Oxide	Juey Hong Rai and N. W. Gregory	1076
Mechanism of Polarographic Reduction of Germanium(IV) in Acidic Catechol Medium	R. G. Canham, D. A. Aikens, Nicholas Winograd, and Glenn Mazepa	1082
Adsorption of Blood Proteins on Metals Using Capacitance Techniques	G. Stoner and S. Srinivasan	1088
Electrical Conductivity of the Nickel Oxide- α -Ferrous Oxide System	Jae Shi Choi and Ki Hyun Yoon	1095
Electron Paramagnetic Resonance Studies of Silver Atom Formation and Enhancement by Fluoride Ions in γ -Irradiated Frozen Silver Nitrate Solutions	Barney L. Bales and Larry Kevan	1098
A Molecular Structure Study of Cyclopentene	Michael I. Davis and T. W. Muecke	1104

INTRODUCING

“CHEMICAL EXECUTIVES AUDIO NEWS”

—an exciting new concept in chemical industry reporting.

To help busy CPI executives overcome their “reading time problem,” the American Chemical Society invites top industry management to enter charter subscriptions to “CHEMICAL EXECUTIVES AUDIONEWS.”

—an exclusive fifteen minute weekly roundup—on audio tape—of major chemical industry developments.

As a charter “CEA” recipient, you’ll benefit *four* ways:

- By entering your charter one year subscription now, you’ll be sent a FREE Panasonic tape recorder/playback unit (*retail value \$50*).
- You will be able to keep and reuse all fifty-two tape cassettes received during the year (*retail value \$78*).
- By hearing industry news *anywhere, at any time*—in your car or on the train or plane—you’ll save costly hours now spent thumbing through page upon page of material.
- You’ll be privy to *first word* of CPI trends, news from the lab, Government plans, executives on the move. Through the ACS’ global information network, reports are *authoritative . . . exclusive*.

Send for the descriptive brochure containing full facts on “CHEMICAL EXECUTIVES AUDIONEWS,” by returning the coupon opposite.



Chemical Executives Audionews
American Chemical Society

1155 16th Street, N.W., Room 601-D
Washington, D.C. 20036

Please send me information on the new “CHEMICAL EXECUTIVES AUDIONEWS” service of the ACS.

NAME _____

TITLE _____

COMPANY _____

ADDRESS _____

CITY _____ STATE _____ ZIP _____

A Refinement Procedure for Determining the Crystallite Orientation Distribution Function . . .	W. R. Krigbaum	1108
First Quantum Corrections to the Second Virial Coefficient of a Stockmayer Gas . . .	M. McCarty, Jr., and S. V. K. Babu	1113
Phosphorus 2p Electron Binding Energies. Correlation with Extended Hückel Charges . . .	M. Pelavin, D. N. Hendrickson, J. M. Hollander, and W. L. Jolly	1116
Chemical Reaction during Electromigration of Ions	J Deman and W. Rigole	1122
Predicted Properties of the Super Heavy Elements. I. Elements 113 and 114, Eka-Thallium and Eka-Lead	O. L. Keller, Jr., J. L. Burnett, T. A. Carlson, and C. W. Nestor, Jr.	1127
Radiation-Induced <i>cis-trans</i> Isomerization of Solutions of 2-Pentene in Cyclohexane	J. W. F. van Ingen and W. A. Cramer	1134

NOTES

Fitting Data with the β Distribution	Gordon H. Fricke, Donald Rosenthal, and George Welford	1139
The Product Energy Distribution on Photolysis of 3-Methyl-1-Pyrazoline	F. H. Dorer	1142
Glass Structure and Electrochemical Selectivity	Michael L. Hair	1145
The Anomalous Frequency Effect in Conductometric Measurements at High Dilution	Estella K. Mysels, Piet C. Scholten, and Karol J. Mysels	1147

COMMUNICATIONS TO THE EDITOR

Density of Liquid Uranium	William G. Rohr and Layton J. Wittenberg	1151
Secondary Valence Force Catalysis. XI. Enhanced Reactivity and Affinity of Cyanide Ion toward N-Substituted 3-Carbamoylpyridinium Ions Elicited by Ionic Surfactants	J. Baumrucker, M. Calzadilla, M. Centeno, G. Lehrmann, P. Lindquist, D. Dunham, M. Price, B. Sears, and E. H. Cordes	1152
Solvent Polarity in Electrochemical and Other Salt Solution Studies.	M. Mohammad and E. M. Kosower	1153

AUTHOR INDEX

- Aikens, D. A., 1082
 Babu, S. V. K., 1113
 Bales, B. L., 1098
 Baumrucker, J., 1152
 Bell, T. N., 979
 Beres, L. S., 1021
 Bianchi, E., 1050
 Breslau, B. R., 1056
 Bunton, C. A., 1062
 Burnett, J. L., 1127
 Calzadilla, M., 1152
 Canham R, G., 1082
 Carlson, T. A., 1127
 Centeno, M., 1152
 Choi, J. S., 1095
 Ciferri, A., 1050
 Cordes, E. H., 1152
 Cramer, W. A., 1134
 Cremers, A., 1072
 Custard, H. C., Jr., 1042
 Davis, M. I., 1104
 Deman, J., 1122
 Dorer, F. H., 1142
 Dunham, D., 1152
 Elias, H., 1014
 Endicott, J. F., 1021
 Fass, R. A., 984
 Fekete, A. J., 1007
 Fricke, G. H., 1139
 Gregory, N. W., 1076
 Hair, M. L., 1145
 Hendrickson, D. N., 1116
 Hercules, D. M., 1030
 Herndon, W. C., 995
 Hoffman, M. Z., 1021
 Hollander, J. M., 1116
 Hollinden, G. A., 988
 Jervis, R. E., 969
 Jolly, W. L., 1116
 Keller, O. L., Jr., 1127
 Kevan, L., 1098
 Kosower, E. M., 1153
 Krastins, G., 999
 Krigbaum, W. R., 1108
 Kurylo, M. J., 988
 Lehrmann, G., 1152
 Lin, W., 1037
 Lindquist, P., 1152
 Mazepa, G., 1082
 McCarty, M., Jr., 1113
 McMillen, L. W., 969
 Miller, I. F., 1056
 Mohammad, M., 1153
 Muecke, T. W., 1104
 Mysels, E. K., 1147
 Mysels, K. J., 1147
 Nestor, C. W., Jr., 1127
 Parodi, R., 1050
 Patterson, D., 1067
 Pelavin, M., 1116
 Pinkus, A. G., 1042
 Price, M., 1152
 Quiring, W. J., 992
 Rai, J. H., 1076
 Rampone, R., 1050
 Rastogi, A. K., 1067
 Riess, R., 1014
 Rigole, W., 1122
 Robinson, L., 1062
 Rohr, W. G., 1151
 Rosenthal, D., 1139
 Scholten, P. C., 1147
 Sears, B., 1152
 Sharma, H. D., 969
 Simmie, J. M., 992
 Srinivasan, S., 1088
 Stoner, G., 1088
 Sullivan, J. M., 995
 Tealdi, A., 1050
 Thomas, H. C., 1072
 Timmons, R. B., 988
 Tsay, S., 1037
 Tschuikow-Roux, E., 992
 van Ingen, J. W. F., 1134
 Waring, C. E., 999, 1007
 Welford, G., 1139
 Werner, T. C., 1030
 Winograd, N., 1082
 Wittenberg, L. J., 1151
 Yoon, K. H., 1095
 Zucker, U. F., 979

THE JOURNAL OF PHYSICAL CHEMISTRY

Registered in U. S. Patent Office © Copyright, 1970, by the American Chemical Society

VOLUME 74, NUMBER 5 MARCH 5, 1970

Kinetics of Ion Exchange. Diffusion of Trace Component

by H. D. Sharma,¹

Department of Chemistry, University of Waterloo, Waterloo, Ontario, Canada

R. E. Jervis, and L. W. McMillen

Department of Chemical Engineering and Applied Chemistry, University of Toronto, Toronto, Ontario, Canada

(Received December 3, 1968)

The diffusion of Cs^+ , Co^{2+} , La^{3+} , Tb^{3+} , and Lu^{3+} ions in ion-exchange beads has been studied in the presence of a large excess of another counterion. The rate laws for the uptake of ions present in trace concentration have been verified, and the agreement between the theory and the experimental results is very good, if contributions due to both film and particle diffusional processes are taken into account. The criteria for distinguishing between "film" and "particle" diffusion-controlled mechanisms have been examined. The \bar{D} values for Cs^+ , Co^{2+} , and La^{3+} in 1 M HCl, 0.5 M CaCl_2 , and 0.17 M LaCl_3 and for Tb^{3+} and Lu^{3+} in HCl solutions indicate that large hydrated ions, having the same charge, have higher mobility inside the resin matrix contrary to the earlier concepts. The \bar{D} values in methanol-water solutions show that the solvent in the resin matrix plays an important role in the transport of ions in the matrix, and thus it is difficult to compare experimentally determined interdiffusion coefficients \bar{D}_{AB} with the ones predicted by Helfferich-Plesset equation because the solvent content of the resin matrix changes as the ionic composition of the matrix changes from one form to the other.

Introduction

It has long been established that the rate of ion exchange is controlled by diffusion, either through a hydrostatic film, called "film control" diffusion or through the pores of the resin matrix, called "particle diffusion control."² In the former case, the rate of exchange of the ion is governed by the thickness of the liquid adhering to the resin and the diffusivity of ions through the film, whereas in the latter case, the rate of exchange depends on the charge and size of the ion, the electrical potential between the diffusing species, and the environment through which the ions are diffusing in the resin matrix. There exist a large number of investigations on the determination of self-diffusion coefficients of ions which indicate the effect of charge and size of ions on the diffusivity in the resin matrix; *i.e.*, the particle diffusion coefficient, \bar{D} , decreases in the order of $\text{Cs}^+ > \text{Rb}^+ > \text{K}^+ > \text{Na}^+ > \text{Zn}^{2+} > \text{La}^{3+} > \text{Hf}^{4+}$ for a moderately cross-linked resin.² However, the order of interdiffusion coefficient is reversed for Cs^+ , Rb^+ , K^+

when the uptake or release of these ions is in trace concentration in the presence of a large excess of another counterion in both ion exchanger and external solution. In such systems the changes in the ion-exchange matrix, ionic composition of the external solution, and the degree of swelling are negligible. In interdiffusion of a trace counterion, hereinafter designated as A^{z+} , and another counterion present in large excess, hereinafter designated B^{z+} , diffusion of the A^{z+} controls the rate of exchange in accordance with Helfferich-Plesset equation.³ The rate laws for isotopic exchange apply, and under batch and flow conditions the following equations have been developed^{2, 4-6}

(1) To whom all correspondence should be addressed.

(2) (a) G. E. Boyd, A. W. Adamson, and L. S. Myers, *J. Amer. Chem. Soc.*, **69**, 2836 (1947); (b) F. Helfferich, "Ion Exchange," McGraw-Hill Book Co., Inc., New York, N. Y., 1962.

(3) F. Helfferich and M. S. Plesset, *J. Chem. Phys.*, **28**, 418 (1958).

(4) G. E. Boyd and B. A. Soldano, *J. Amer. Chem. Soc.*, **75**, 6091 (1953).

$$U(t) = 1 - \frac{6}{\pi^2} \sum_{n=1}^{\infty} \frac{1}{n^2} \exp\left(-\frac{\bar{D}t\pi^2 n^2}{r_0^2}\right) \quad (1)$$

where $U(t)$ is the fractional attainment of equilibrium at time t , \bar{D} is the diffusion coefficient, and r_0 is the radius of resin beads. For the batch condition (finite volume) and also for a particle diffusion-controlled reaction Paterson's equation applies

$$U(t) = 1 - \frac{2}{3w} \sum_{n=1}^{\infty} \frac{\exp(-S_n^2 \tau)}{1 + S_n^2/9w(w-1)} \quad (2)$$

where $w = \bar{C}_A \bar{V}_A / C_A V_A$ and \bar{C}_A and C_A are the concentration of A^{z+} in the resin beads of volume \bar{V} and in solution of volume V , respectively. $k = \bar{C}_A / C_A$, $\tau = \bar{D}t/r_0^2$, and S_n are the roots of equation $S_n \cot S_n = 1 + S_n^2/3w$.

Similarly for film diffusion control for the infinite volume condition

$$U(t) = 1 - \exp\left(-\frac{3DC_A t}{r_0 \delta \bar{C}_A}\right) \quad (3)$$

where δ is the thickness of the film and D is the film diffusion coefficient and for finite volume

$$U(t) = 1 - \exp\left[\frac{3D(\bar{V}_A \bar{C}_A + V_A C_A)}{r_0 \delta \bar{C}_A V_A}\right] \quad (4)$$

In the intermediate range when both film and particle diffusion control and infinite volume conditions are met

$$U(t) = \frac{6\theta^2}{r_0^2} \sum_{n=1}^{\infty} \frac{A_n \sin^2(m_n r_0)}{m_n^4} \exp(-\bar{D}m_n^2 t) \quad (5)$$

where $\theta = C_A D / \bar{C}_A \bar{D} \delta$, $A_n = m_n^2 r_0^2 + (\theta r_0 - 1)^2 / m_n^2 r_0^2 + (\theta r_0 - 1)\theta r_0$, and m_n are the roots of the equation $m_n r_0 = (1 - \theta r_0) \tan m_n r_0$.

Equation 1 has limited applicability since the effect of the film cannot entirely be removed. Our experiments on the uptake of a trace component gave variable \bar{D} in high concentration of B^{z+} . Equation 5 can be applied if the parameter θ is known, which requires the value of \bar{D} and δ . Our experiments indicate the feasibility of determination of D/δ from a rate of uptake curve in the batch method. \bar{D} for A^{z+} can then be evaluated from the data from the flow experiments. For $w < 0.1$ eq 5 gave constant \bar{D} in the batch method since, under these conditions, the boundary conditions approximated to infinite volume solution.

Helferich has analyzed theoretically the effect on diffusion coefficients if the ion-exchange process is accompanied by ionic reaction such as neutralization or complex formation.⁷ A radioactive tracer can conveniently be used for the determination of D or \bar{D} in such processes. However, in surveying the literature, there appeared to be few studies wherein the rate laws have been verified thoroughly for the uptake of A^{z+} in B^{z+} . Boyd, *et al.*, obtained variable \bar{D} in such systems.⁴

It was therefore considered essential to verify the applicability of the equations for the evaluation of D and \bar{D} for various A^{z+} in the presence of a large excess of B^{z+} in both methods. The effect of matrix environment and solvent content on \bar{D} for different A^{z+} has been examined and reported in this paper. A mechanism involving transport of ions in the matrix is also suggested.

Experimental Section

A large quantity (20 lb) from a production batch of Dowex 50-X 8 resin was subjected to the wet elutriation method to obtain resin beads of a constant particle diameter in the manner described by Reichenberg.⁸ About 100 g of beads of constant diameter was obtained, and microscopic examination showed that they were spherical in shape and that diameter variations were less than 3%. The resin beads were stored in water and at no time were they allowed to dry after conditioning them. The water content in the resin beads was estimated by the Karl Fischer method⁹ as given in Table I along with the diameters of the beads.

Table I: Water Content and Size of Resin Beads

Resin environment	Water content, wt % of wet resin	Radius, cm
H ₂ O	52.6 ± 1.0	0.048 ± 0.0015
1 M HCl	50.0 ± 0.7	...
2 M HCl	48.1 ± 0.8	0.046 ± 0.0015
3 M HCl	46.6 ± 0.6	...
6 M HCl	41.2 ± 0.8	0.0443 ^a ± 0.0015
9 M HCl	36.7 ± 0.6	0.0440 ^a ± 0.0015
1 M CaCl ₂	41.9 ± 0.7	0.0460 ± 0.0015
0.17 M LaCl ₃	34.6 ± 0.8	0.0457 ± 0.0015
0.17 M TbCl ₃	37.3 ± 0.6	...
1.94 M HCl- 25% methanol	36.7 ± 0.6	0.045 ^a ± 0.002
1.94 M HCl- 50% methanol	31.2 ± 0.6	0.044 ^a ± 0.002
1.94 M HCl- 80% methanol	17.3 ± 0.5	0.0427 ^a ± 0.002

^a Measured by shrinkage in volume of resin beads.

(a) *Radioisotopes.* Lanthanum, terbium, and lutetium oxides were obtained in 99.9%+ purity in the oxide form. Small portions of these were irradiated with thermal neutrons to produce appropriate radio-tracers La¹⁴⁰ ($t_{1/2} = 40$ hr), Tb¹⁶⁰ ($t_{1/2} = 73$ days), and

(5) A. W. Adamson and J. J. Grossman, *J. Chem. Phys.*, **17**, 1002 (1949).

(6) J. J. Grossman and A. W. Adamson, *J. Phys. Chem.*, **56**, 97 (1952).

(7) F. Helferich, *ibid.*, **69**, 1178 (1965).

(8) D. Reichenberg, *J. Amer. Chem. Soc.*, **75**, 589 (1953).

(9) A. Dickel and J. W. Hartmann, *Z. Phys. Chem. (Frankfurt am Main)*, **23**, 1, 1960; H. D. Sharma and N. Subramanian, *Anal. Chem.*, **41**, 2063 (1969).

Lu^{177} ($t_{1/2} = 6.75$ days). The radiochemical purity of these isotopes was checked by γ -ray spectroscopy using a Ge(Li) detector and a 400-channel pulse height analyzer. No impurities greater than 1% of the expected predominant γ -ray peak were found. The radioactive oxides were dissolved in hydrochloric acid. Radioisotopes Co^{60} ($t_{1/2} = 5.26$ yr) and Cs^{137} ($t_{1/2} = 30$ yr) were procured from the Atomic Energy of Canada Ltd.

(b) *Miscellaneous Chemicals.* Chemicals used in the present experiments were all of reagent grade. The methanol was supplied by Union Carbide and contained no significant impurity and less than 0.5% water.

Kinetic Experiments

(a) *Finite Volume (Batch) System.* The apparatus for the batch experiments was similar to one used by Schwartz, *et al.*¹⁰ The reaction vessel was a 1-l. flask fitted by means of a ground-glass seal to a five-necked lid. The flask was submerged in a thermostatically controlled water bath kept at a temperature of $25 \pm 0.2^\circ$. A peristaltic pump was used for circulating liquid through a sintered-glass tube, which confined the resin to the flask, through a glass coil surrounding a NaI(Tl) scintillation crystal and back into the vessel. The volume in the sampling section of the apparatus was approximately 60 ml, and the flow rate was maintained at 550 ml/min. The residence time of solution in the sampling section was 6.5 sec. Solution in the vessel was stirred by means of an anchor stirrer driven by a variable speed motor. All connections to the flask were of ground-glass fittings, and the otherwise sealed unit was vented through a water condenser to prevent any loss of solution.

The glass coil which surrounded the 2-in. NaI scintillation crystal was shielded from the flask by lead bricks. The pulses from the detector were amplified and displayed on a rate meter as well as continuously recorded on a two-speed, strip-chart recorder. The time constant of the meter was kept at 0.8 sec. A lag of 8 sec was observed for the solution to get from the vessel to the sampling section and to record its radiation.

For all experiments in the batch system, approximately 3 ml of sized resin was used. The resin beads were equilibrated with solution containing B^{2+} and a radioactive tracer as A^{2+} ion. The resin was transferred to a lucite tube having a fine platinum gauze at one end so as to enable removal by means of suction of any liquid adhering to the resin beads. Through a neck in the reaction vessel, containing 650 ml of solution, the beads were transferred rapidly into the solution by applying air pressure to the lucite tube. The activity of the solution was recorded continuously until a sufficient rate data had been compiled (usually $U(t) > 0.8$) at which time the recorder was shut off but the reaction continued until equilibrium was reached. The equilibrium values were checked carefully, often by leaving

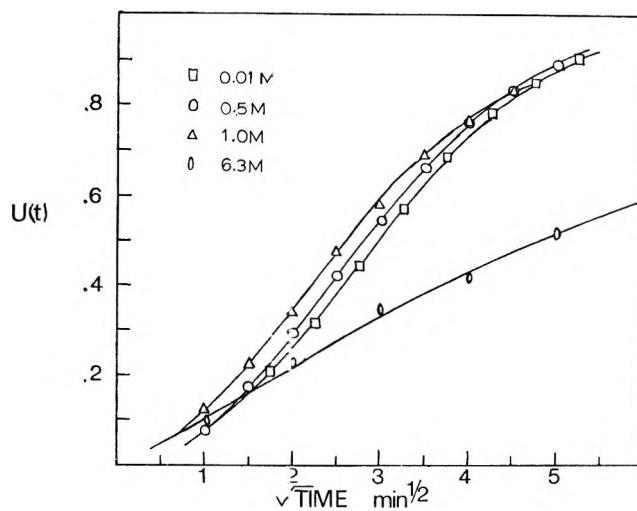


Figure 1. The rate of exchange of trace Tb^{3+} in various hydrochloric acid concentrations, batch system.

the reaction overnight, to ensure that no more exchange was taking place.

In experiments in which the distribution coefficient was sufficiently high, the radioactive tracer was initially added to the macrocomponent solution instead of incorporating it into the resin matrix.

(b) *Infinite Volume (Flow) System.* The apparatus for the flow system was similar to the one used by Boyd, *et al.*^{2a} The peristaltic pump was used to pass a constant flow of the solution over a shallow bed of resin beads. A small portion of resin was preequilibrated with radioisotope in solution (B^{2+}) and transferred into a lucite resin holder. The beads were then rinsed rapidly under suction with a small amount of the solution to remove any activity in the adhering liquid. The resin holder was attached to an acid-resistant butyl tubing and fastened securely to the NaI(Tl) scintillation crystal. The detector and recorder were the same as described for the batch system.

Except for some specific experiments at high flow rates, a flow rate of 500 ± 20 ml/min was used throughout which resulted in a linear flow velocity, v , of ~ 100 cm/sec. This linear flow velocity was calculated as being four times the volumetric rate of flow, divided by the bed area (0.316 cm^2). The factor of 4 used here was the same as that used by Tetenbaum and Gregor¹¹ and was based on the assumption that the bed voids are about 25% of the bed volume.

Verification of Rate Laws

(a) *Analysis of Data for Batch and Flow Systems.* The initial experiments in this work were performed using the batch system. The exchange of Tb^{3+} and H^+ in 1 M HCl solution was studied, and the rate curve

(10) A. Schwartz, J. A. Marinsky, and K. S. Speigler, *J. Phys. Chem.*, **68**, 918 (1964).

(11) M. Tetenbaum and H. P. Gregor, *ibid.*, **58**, 1156 (1954).

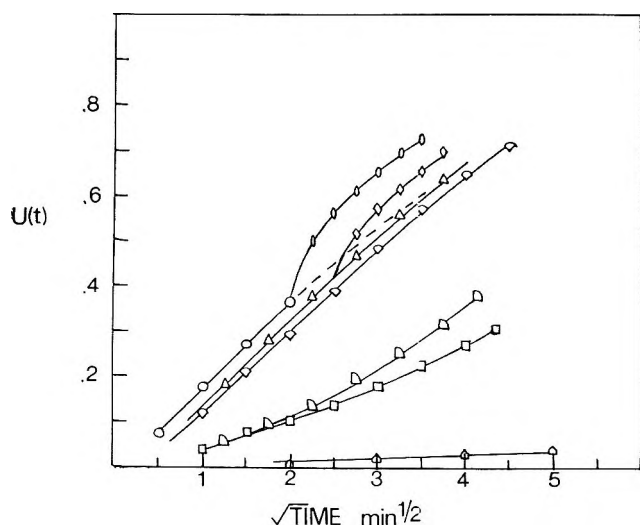


Figure 2. The rate of exchange of Tb^{3+} in HCl at various conditions. Normal flow rate ($v = 103$). \square , 0.25 M ; \square , 0.5 M ; \diamond , 1.0 M ; \circ , 1.94 M ; high flow rate ($v = 190$) \square , 0.5 M ; \triangle , 1.0 M ; Interruption tests \diamond , 1.0 M ; \circ , 1.94 M .

was determined (Figure 1). Applying eq 1 with the infinite volume condition, it was found that the calculated particle diffusion coefficient, \bar{D} , for Tb^{3+} was not constant but increased as the fractional attainment of equilibrium, $U(t)$, increased. To examine this system further, the rate of exchange of Tb^{3+} ion was studied over a wide range of hydrochloric acid concentration (0.01 to 6.3 M). The rate curves of representative experiments are shown in Figure 1. At HCl concentrations of 0.01, 0.1, and 0.5 M , the curves are nearly identical, having the same shape and varying in the half-time of exchange by only 15%. The analysis of data according to eq 4 would predict that changing from 0.01 to 0.5 M should change the slope by approximately 13%. This is in good agreement with the present results if \bar{C} and C are taken as concentrations of A^{2+} . Furthermore, by assuming a constant value of the film diffusion coefficient, D , of 1.17×10^{-5} cm^2/sec , one calculates the film thickness for the batch experiment as 25×10^{-4} cm , which is a reasonable value for the rapid stirring conditions of these experiments. The concentration of B^{2+} has little effect on D/δ . At 1.0 M , the curve takes on a more concave nature and the half-time of exchange decreases. At 6.3 M , the half-time of exchange is significantly larger indicating a decrease in the rate of exchange. Preliminary interruption tests revealed that particle diffusion controlled the rate of exchange for experiments using HCl 1.0 M and higher (Figure 2).

\bar{D} values for the uptake of Tb^{3+} in 1 M HCl were calculated for the flow and the batch systems following eq 1 and 2. It can be seen from Table II that the calculated \bar{D} 's are not constant. Similar treatment of experimental data for Tb^{3+} in 3 M HCl gave \bar{D} 's which varied slightly, and those for Tb^{3+} in 6.3 M HCl gave

Table II: Calculated Particle Diffusion Coefficients, \bar{D} , for Exchange of Tb^{3+} for H^+ in 1.0 M HCl

Fractional attainment of equilibrium, $U(t)$	$\bar{D} \times 10^8$, cm^2/sec	
	(A) Batch system ^a	(B) Flow system ^b
0.11	1.3	4.5
0.18	2.1	6.4
0.30	3.5	8.7
0.49	6.8	11.8
0.68	9.6	14.5

^a (A) Finite volume, batch system, \bar{D} 's calculated are various fractional attainments of equilibrium using the Patterson equation (2) at $w = 0.9$. ^b (B) Infinite volume, flow system, \bar{D} 's calculated at various fractional attainments of equilibrium using the infinite, particle diffusion equation (1).

nearly constant \bar{D} . It appeared that both film and particle diffusion controlled the rate of uptake of Tb^{3+} .

(b) *Application of the Film-Particle Equation.* The rate data for Tb^{3+} in 1 to 3 M HCl were analyzed by applying eq 5 and by setting the film diffusion coefficient D equal to 1.17×10^{-5} cm^2/sec , a value obtained for La^{3+} in a dilute $LaCl_3$ solution,¹² $\delta = 2.5 \times 10^{-3}$ cm for the batch system and experimentally determined value of k . In any event D/δ can be determined in the film diffusion control region. Film thickness for the flow system was obtained and estimated to be 1.0×10^{-3} cm which compared with the reported values by Tetenbaum and Gregor.¹¹ Rate curves were deter-

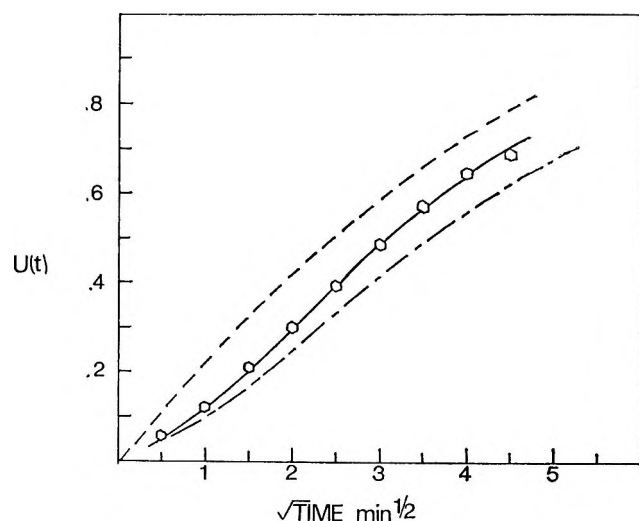


Figure 3. Film-particle diffusion equation to fit experimental data for Tb^{3+} in 1.0 M HCl; flow system, $k = 210$, $\delta = 10 \times 10^{-4}$ cm . \circ , experimental data; —, film-particle equation for $\bar{D} = 20 \times 10^{-8}$ cm^2/sec ; - - -, film-particle equation for $\bar{D} = 15 \times 10^{-8}$ cm^2/sec ; - · - ·, particle diffusion equation for $\bar{D} = 20 \times 10^{-8}$ cm^2/sec .

(12) H. S. Harned and B. B. Owen, "The Physical Chemistry of Electrolytic Solutions," 3rd ed, Reinhold Publishing Corp., New York, N. Y., 1963.

Table III: Parameters Used to Calculate Particle Diffusion Coefficients

A ³⁺ (trace ion)	B ³⁺ (macro-component ion)	Exptl method	Equation applied for calculation	k	$\delta \times 10^4$, cm	$w = K\bar{V}/V$	Calcd $\bar{D} \times 10^6$, cm ² /sec
Tb ³⁺	H ⁺ (0.5 M)	Batch		~2500	25	9.75	(Film)
	(1.0 M)	Batch		210	25	0.9	(Film-particle)
	(6.3 M)	Batch	1		25		5.8 ± 0.3
Cs ⁺	H ⁺ (1.0 M)	Batch	5	9	25	0.04	625 ± 31.0
	Ca ²⁺ (0.5 M)	Batch	5	4	25	0.02	120 ± 6.0
	La ³⁺ (0.17 M)	Batch	5	3	25	0.01	27 ± 1.3
Co ²⁺	H ⁺ (1.0 M)	Batch	5	12	25	0.05	94 ± 4.7
	Ca ²⁺ (0.5 M)	Batch	5	5	25	0.02	13.0 ± 0.6
	La ³⁺ (0.17 M)	Batch	5	2	25	0.01	3.5 ± 0.1
La ³⁺	H ⁺ (1.0 M)	Flow	5	320	10		10.4 ± 0.5
	La ³⁺ (0.17 M)	Batch	5	5	25	0.01	1.6 ± 0.1
Tb ³⁺	Ca ²⁺ (0.5 M)	Batch	5	12	25	0.05	8.7 ± 0.4
Tb ³⁺	H ⁺ (1.0 M)	Flow	5	210	10		20.8 ± 1.1
	(1.94 M)	Flow	5	28	10		16.3 ± 0.8
	(3.0 M)	Flow	5	8	10		14.4 ± 0.7
	(6.0 M)	Flow	1		10		7.5 ± 0.3
	(9.0 M)	Flow	1				1.9 ± 0.1
La ³⁺	H ⁺ (1.94 M)	Flow	5	71	10		3.2 ± 0.1
Tb ³⁺	in 25% methanol)	Flow	5	51	10		7.7 ± 0.3
Lu ³⁺	methanol)	Flow	5	40	10		19.5 ± 0.9
La ³⁺	H ⁺ (1.94 M)	Flow	5	150	10		1.3 ± 0.1
Tb ³⁺	in 50% methanol)	Flow	5	108	10		3.4 ± 0.1
Lu ³⁺	methanol)	Flow	5	75	10		11.3 ± 0.5
La ³⁺	H ⁺ (1.94 M)	Flow	1		10		0.04 ± 0.02
Tb ³⁺	in 85% methanol)	Flow	1		10		0.09 ± 0.02
Lu ³⁺	methanol)	Flow	1		10		0.4 ± 0.2

mined for various assumed values of \bar{D} and compared with the experimental data. Because of the extensive calculations required to determine a curve of $U(t)$ vs. t for even one assumed \bar{D} , a computer program was outlined to calculate $U(t)$ as a function of $\bar{D}t$ for different values of θ ranging from 50 to 100,000 and for a particular value of r_0 . The experimental values for $U(t)$ were then fitted to the calculated ones for \bar{D} .

For Tb³⁺ in 1 M HCl experiment, $k = 210$ and $\delta = 10 \times 10^{-4}$ cm; a value of $\bar{D} = 20 \times 10^{-8}$ cm²/sec was found to fit the experimental data as shown in Figure 3. The $U(t)$ vs. t curve calculated from eq 1 with $\bar{D} = 20 \times 10^{-8}$ cm²/sec and the curve using eq 5, $k = 210$, $\delta = 10 \times 10^{-4}$ cm, and $\bar{D} = 15 \times 10^{-8}$ cm²/sec are included for comparison. It is evident that the film-particle equation provided the most accurate method of determining the particle diffusion coefficients. The particle diffusion coefficients were calculated from the experimental data by applying appropriate equations (Table III).

(c) *Examination of Methods Used to Distinguish Particle and Film Diffusion Control.* The tests suggested to establish particle diffusion as the rate-controlling step are (i) examination of the rate curve on the basis of $U(t)$ vs. $t^{1/2}$; (ii) changing stirring or flow rate; (iii) increasing the external concentration; (iv) varying the particle radius, and (v) performing "interruption tests."²⁶ The applicability of the tests was examined for conditions wherein both film and particle diffusion

affected the rate. The analysis of experimental data revealed the following.

(i) The initial linearity of $U(t)$ vs. $t^{1/2}$ in many systems extends beyond that expected for pure particle diffusion. This is a consequence of the combined control of the particle and film diffusion which is known to exist under these conditions, and thus it is not a reliable test.

(ii) Changing the flow rate is a good test for film effects as long as the experiments are sufficiently accurate to distinguish the small effects produced, as can be seen in Figure 2. Increasing the stirring speed in batch experiments may not always decrease the film thickness to any extent, and therefore the test may be insensitive in establishing that the film control is present. Varying the linear velocity from 103 to 190 cm/sec for 0.5 M HCl increased the rate of uptake of Tb³⁺ while a similar change in flow at 1.0 M HCl resulted in only a slight increase in the rate.

(iii) Increasing the external concentration is not a particularly good test to apply because of the variety of conditions which change. For example, in self-diffusion it has been reported that the diffusion rate increases as external concentration increases, while in this work the diffusion rate decreases as the external concentration increases.

(iv) Examining the rate of exchange at different particle radii is a very sensitive method to distinguish the difference between film and particle diffusion

control. Unfortunately, it is so sensitive that few authors have been able to relate the various experiments accurately enough to distinguish small effects of film control. This is probably due to the fact that completely uniform particles with accurately determined radii are very difficult to obtain. The half-time of exchange varied as $1/r_0^{1.8}$ for Tb^{3+} in 6.3 M HCl.

(v) The "interruption test" as first introduced by Kressman and Kitchener¹³ has been used extensively to establish particle diffusion control. This is an excellent test to establish the effect of particle diffusion control in any particular experiment. However, it cannot reveal any contribution due to film control as shown in the present work (Figure 2).

The rate-controlling mechanism is dependent on the value of θr_0 according to eq 5.^{6,11} The computed values of $U(t)$ for a particular value of r_0 and for θ ranging from 50 to 100,000 indicate that for $\theta r_0 < 1$, film diffusion controls the rate of exchange whereas particle diffusion controls the rate for $\theta r_0 > 5000$.

(d) *Forward and Reverse Exchange Rates.* The condition of trace exchange carries with it the implication that the forward and reverse exchange rates should be the same. This is predicted by the Helfferich-Plasset equation where \bar{D}_{AB} reduces to \bar{D}_A for low concentration of A^{2+} present in the resin. To test this, the forward ($Tb^{3+}-H^+$) exchange was compared to the reverse ($Tb^{3+}-H^+$) exchange for 1.0 M HCl in the external solution. The results revealed that the exchange rate was indeed the same for both experiments. This shows that the particle diffusion coefficients are those of the trace ion only and are not dependent on the macrocomponent ion mobility or the separation factor $\bar{C}_A \bar{C}_B / C_A \bar{C}_B$.

(e) *Trace Exchange at Equilibrium.* Inactive Tb^{3+} was placed in a 1.0 M HCl solution in the batch apparatus and allowed to come to equilibrium with the resin phase such that approximately 1% of the resin was converted into Tb^{3+} form. The rate data were obtained by adding radioactive Tb^{3+} ion in a quantity which increased the equilibrium concentration of inactive Tb^{3+} in the external solution very little. The rate of exchange in this experiment was found to be nearly identical with previous trace, nonequilibrium experiment.

Results and Discussion

(I) *Ionic Charge. Its Direct and Indirect Effect on the Rate of Exchange.* The charge of an ion greatly affects its rate of diffusion through an ion-exchange resin.^{2b} In general, the rate of exchange decreases rapidly as the charge of the exchanging species increases. In our previous work and that of other workers^{4,14-17} it has also been noted that the rate of exchange of A^{2+} is affected by B^{2+} , *i.e.*, the ionic form of the resin phase. To examine this effect further, the exchange rates of a monovalent, a divalent, and a

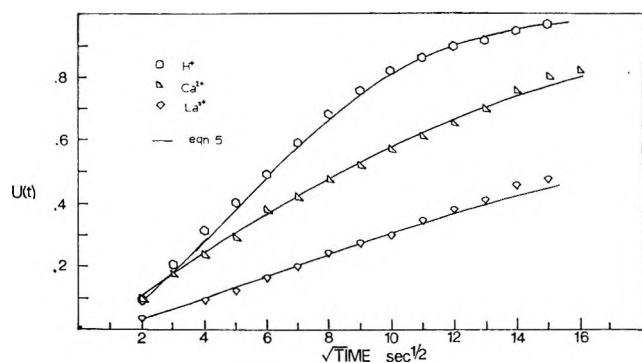


Figure 4. Rate of exchange of Cs^+ in H^+ (1 M HCl), Ca^{2+} (0.5 M $CaCl_2$), and La^{3+} (0.17 M $LaCl_3$), batch system.

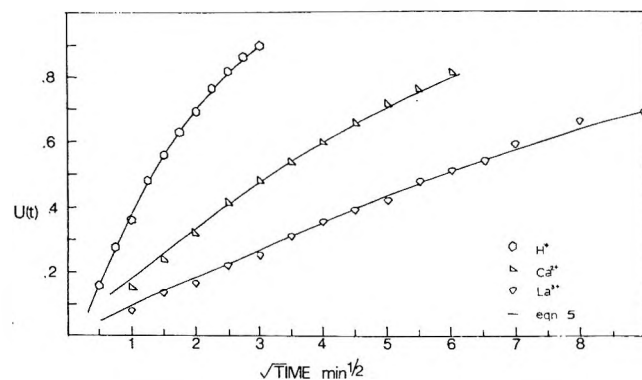


Figure 5. Rate of exchange of Co^{2+} in H^+ (1 M HCl), Ca^{2+} (0.5 M $CaCl_2$), and La^{3+} (0.17 M $LaCl_3$), batch system.

trivalent A^{2+} ion were studied with three different B^{2+} ions. The rate curves are presented in Figures 4, 5, and 6. The particle diffusion coefficients, \bar{D} , calculated for the various trace ions are presented in Table IV. At a constant macrocomponent ion composition, for example, 1 M HCl, the resin environment is established by the solution of B^{2+} . The effect of ionic charge can thus be separated from the other variables, such as solvent content, pore size, swelling effects, etc. The rate of exchange decreases rapidly as the ionic charge increases; *i.e.*, $\bar{D}_{Cs^+} > \bar{D}_{Co^{2+}} > \bar{D}_{La^{3+}}$ (Table IV). This is the expected behavior for these ions which is also reflected in the respective self-diffusion coefficients.⁴ Furthermore, it can be seen that the \bar{D} values for a particular A^{2+} , for example Cs^+ , decrease as the charge of B^{2+} increases, namely $\bar{D}_{Cs^+-H^+} = 625 \times 10^{-8}$; $\bar{D}_{Cs^+-Ca^{2+}} = 120 \times 10^{-8}$; $\bar{D}_{Cs^+-La^{3+}}$

(13) T. R. E. Kressman and J. A. Kitchener, *Discussions Faraday Soc.*, **7**, 90 (1949).

(14) G. E. Boyd, A. W. Adamson, and L. S. Myers, *J. Amer. Chem. Soc.*, **72**, 4807 (1950); G. E. Boyd and B. A. Soldano, *ibid.*, **75**, 6105 (1953).

(15) A. E. Lagos and J. A. Kitchener, *Trans. Faraday Soc.*, **56**, 1245 (1960).

(16) B. A. Soldano and G. E. Boyd, *J. Amer. Chem. Soc.*, **75**, 6099 (1953).

(17) L. W. McMillen, B.A.Sc. Thesis, University of Toronto (1965).

= 27.4×10^{-8} cm²/sec. As has been noted by Soldano and Boyd,¹⁸ the rate of exchange of the trace component decreases if a macrocomponent of a lower mobility is used. Although this statement is consistent with the data, it may be misleading to relate the change in \bar{D}_{AB} to the mobility of the macrocomponent ion. The changes in \bar{D}_{AB} are not nearly as large as one would expect if the ratio of self-diffusion coefficients are considered. For example, the ratio of self-diffusion coefficients $\bar{D}_{Cs^+}/\bar{D}_{La^{3+}}$ is approximately 200 while the ratio $\bar{D}_{Cs^+-H^+}/\bar{D}_{Cs^+-La^{3+}}$ is 18. Similarly, the value $\bar{D}_{La^{3+-H^+}}$ is only seven times as great as for the self-diffusion coefficient of La^{3+} .

Table IV: Calculated Particle Diffusion Coefficients, $\bar{D} \times 10^8$, cm² sec⁻¹

Macrocomponent	Microcomponent		
	Cs ⁺	Co ²⁺	La ³⁺
H ⁺ (1.0 M)	625	94	10.4
Ca ²⁺ (1.0 M)	120	13	4.3 ^a
La ³⁺ (0.5 M)	27	3.5	1.6

^a This experiment was done using the exchange of Tb³⁺ with Ca²⁺ and $\bar{D}_{Tb^{3+}}$ was found to be 8. Since $\bar{D}_{Tb^{3+}}/\bar{D}_{La^{3+}}$ was found to be about 2, a value of 4 was estimated for $\bar{D}_{La^{3+}}$ in Ca²⁺.

Recently, the application of the Helfferich-Plesset equation to ion exchange has received considerable support. The equation predicts that the particle interdiffusion coefficient is not constant but depends on the relative concentration of the two counterions (A and B) as shown below

$$\bar{D}_{AB} = \frac{\bar{D}_A \bar{D}_B (Z_A^2 \bar{C}_A + Z_B^2 \bar{C}_B)}{Z_A^2 \bar{C}_A \bar{D}_A + Z_B^2 \bar{C}_B \bar{D}_B}$$

For $\bar{C}_A \ll \bar{C}_B$, the interdiffusion coefficient, \bar{D}_{AB} , assumes the value of \bar{D}_A . Thus, the rate of diffusion for a trace element should remain constant and equal to the individual diffusion coefficient regardless of the mobility of the macrocomponent ion. This appears to be in disagreement with the results given here and also by others.¹⁸ Such a behavior can be explained, perhaps, by considering the resin environment. In the present set of experiments, the resin phase is different for each of the macrocomponent ions, *i.e.*, H⁺, Ca²⁺, and La³⁺. An important variable of the resin environment is the water content of the resin phase. It is a complex function of the charge of the counterion in the matrix and the swelling pressure and cross linkage of the resin. Since the rate of exchange is known to decrease markedly as the water content of the resin phase decreases,^{2,15} the decrease of \bar{D}_{Cs^+} going from a H⁺ to a La³⁺ environment may be due partially or wholly to this effect (Figure 7). The present results

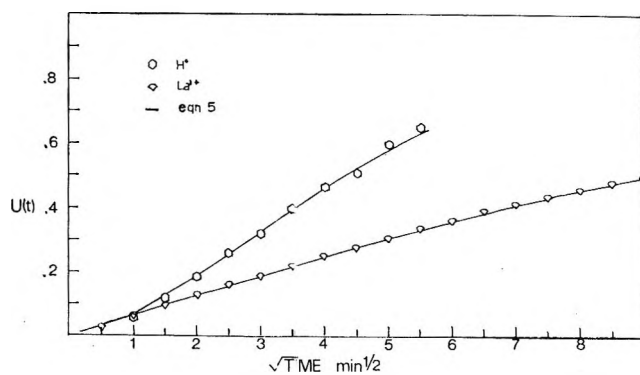


Figure 6. Rate of exchange of trace La^{3+} in H⁺ (1 M HCl) in flow system and for La^{3+} (0.17 M $LaCl_3$) in batch system.

cannot be used to refute or verify the effects predicted by the Helfferich-Plesset equation. However, in the limiting case of trace exchange, the applicability of the simplified equation is clearly indicated. The failure of the equation to explain the present results appears to lie in the definition of individual diffusion coefficients under a particular set of conditions. The equation assumes that the individual diffusion coefficients are constant which is true only if the resin phase under consideration is always in the same condition (*i.e.*, ionic form, water content, etc., are constant).

(II) *Effect of Hydrated Ionic Size on Rate of Exchange.* The values of \bar{D}_{AB} for Cs⁺ and La³⁺ indicate that the charge of the exchanging ion and the solvent environment of the resin phase play an important role in controlling the rate of exchange of the ions. In order to examine the effect of the size and solvation of ions on the rate of exchange, three ions of the lanthanides, namely La³⁺, Tb³⁺, and Lu³⁺ were chosen as A²⁺ ions. These ions have almost identical chemical properties and exhibit a convenient gradation of ionic radii.

The $U(t)$ vs. t curves for the three rare earth ions are given in Figure 8, and the calculated \bar{D} values are listed in Table V. It can be seen that the rate of diffusion is fastest for Lu³⁺, slowest for La³⁺, and intermediate for Tb³⁺. Table V also lists the data on the size and ionic mobility in solution. Lanthanum ion has the largest ionic (crystal) radius while lutetium has the smallest. Conductivity data indicates that the Stokes radius will be the smallest for La³⁺ and largest for Lu³⁺, which is consistent with the generalization that ions with the largest charge density will have the largest hydration sheath. The hydrated size of the ions should be in order of Lu³⁺ > Tb³⁺ > La³⁺. The ions in the resin phase exist as hydrated species similar to those in aqueous solution as indicated by the molal chemical shifts observed in nmr spectra of alkali metal ions.^{19,20}

(18) B. A. Soldano and G. E. Boyd, *J. Amer. Chem. Soc.*, **75**, 6107 (1953).

(19) J. P. de Villiers and J. R. Parrish, *J. Polym. Sci., Part A*, **2**, 1331 (1964).

(20) H. D. Sharma and N. Subramanian, *Can. J. Chem.*, in press.

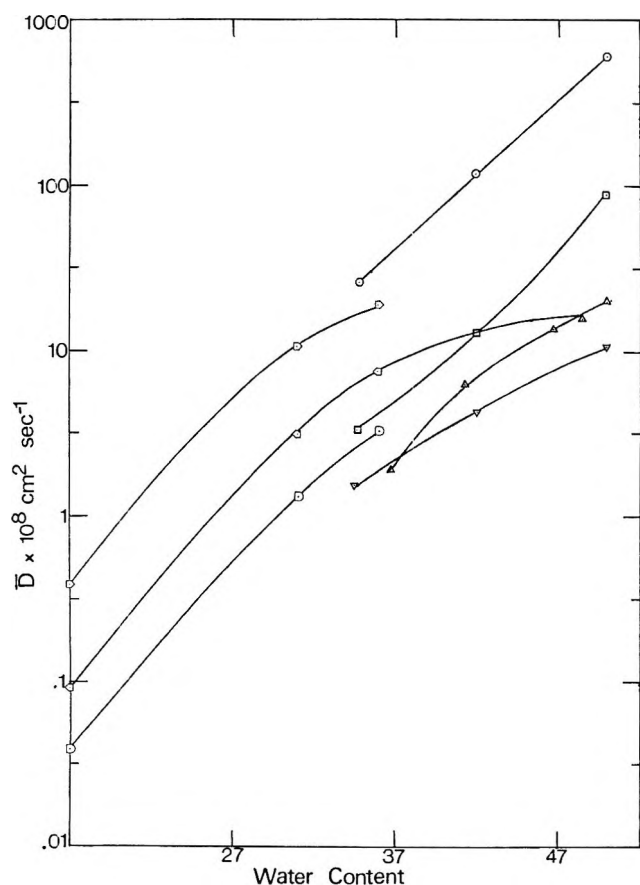


Figure 7. $\log \bar{D}$ vs. wt % of water in swollen resin matrix. \circ , Cs^+ ; \square , Co^{2+} ; and ∇ , La^{3+} in H^+ , Ca^{2+} , and La^{3+} . \triangle , Tb^{3+} in various HCl concentrations. \ominus , Lu^{2+} ; \square , Tb^{3+} ; and \oplus , La^{3+} in 1.94 M HCl methanol-water solutions.

The water content of the resin is sufficient that the lanthanide ions will still retain their water of hydration in the resin phase. The values given in Table V indicate that the largest hydrated species (namely Lu^{3+}) has the highest rate of diffusion inside the resin phase. This appears to be in disagreement with the results of previous workers^{13,15} who examined the self-diffusion of the alkali ions. An analysis of the present results in terms of previous work and a possible explanation is presented under section IV.

Table V: Calculated Particle Diffusion Coefficients, \bar{D} , and Other Pertinent Data for La^{3+} , Tb^{3+} , and Lu^{3+} Ions

$\bar{D} \times 10^8 \text{ cm}^2/\text{sec}$ in 1.94 M HCl	La 8.7	Tb 16.3	Lu 35.0
Ionic (crystal) radius, \AA^a	1.061	0.923	0.848
Limiting equivalent conductivity, λ_0^a	70	67	65
Distribution coefficients, k , in 1.94 M HCl	38	28	20

^a Data from R. A. Robinson and R. H. Stokes, "Electrolyte Solutions," Butterworth and Co. Ltd., London, 1955.

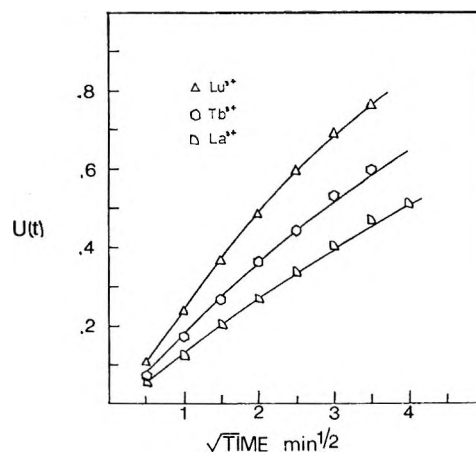


Figure 8. Rate of exchange of La^{3+} , Tb^{3+} , and Lu^{3+} in 1.94 M hydrochloric acid, flow system.

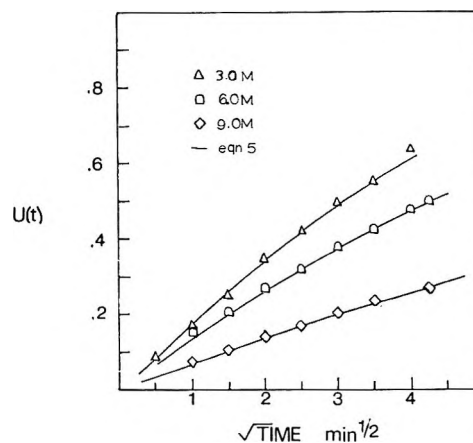


Figure 9. The influence of hydrochloric acid concentration on the rate of exchange of trace Tb^{3+} , flow system.

(III) *Effect of Resin Water Content on Rate of Exchange.* (a) *The Interdiffusion of Tb^{3+} in H^+ -Form Resin.* The \bar{D} values for Cs^+ , Co^{2+} , and La^{3+} decrease as the water content of the resin matrix decreases (Figure 7). It is known that the total water content of the resin phase decreases as the external concentration of electrolyte increases and therefore the rate of exchange of the ions should also decrease. Earlier experimenters,^{11,21,22} however, found that the rate of exchange for self-diffusion increased as the external concentration increased. The rate of uptake of Tb^{3+} was studied in various external concentrations of solution. The rate curves for hydrochloric acid concentration up to 1.94 M are shown in Figures 2 and 3; while those from 3.0 to 9 M are shown in Figure 9. The particle diffusion coefficients, $\bar{D}_{\text{Tb}^{3+}}$, are given in Table III. Since the trace ion (Tb^{3+}) and the macrocomponent ion (H^+) have remained the same throughout the experiments, the decrease of \bar{D} at higher acid

(21) D. Richman and H. C. Thomas, *J. Phys. Chem.*, **60**, 237 (1956).

(22) R. Schlogl, *Z. Elektrochem.*, **57**, 195 (1953).

concentrations is probably due to water content in the resin matrix (Figure 7). Lagos and Kitchener¹⁵ observed that \bar{D}_{Cs^+} decreased with decreasing free water content of the resin in a manner which bears a resemblance to the decrease of $\bar{D}_{Tb^{3+}}$ with acid concentration as reported in this work.

The water content is not the only condition which changes as the acid concentration goes up. The decrease in \bar{D} with increasing concentrations of HCl can also be attributed to changes in the hydration of Tb^{3+} ion, increase in nonexchange electrolyte in the matrix and complexing of Tb^{3+} with Cl^- ions. The effect of each factor cannot easily be separated. However, it can be seen from Figure 7 that up to 6 M HCl, the decrease in \bar{D} is similar to that observed for La^{3+} in resin matrix in H^+ , Ca^{2+} , and La^{3+} form. The sharp decrease in \bar{D} at 9 M HCl can probably be attributed to changes in the hydration shell of Tb^{3+} ion. This effect is further examined by determining \bar{D} in systems where water is partly replaced by another solvent.

(b) *Rate of Exchange of Lanthanide Ions in Methanol-Water Solutions.* The external hydrochloric acid concentration was kept constant at 1.94 M, and the rate of uptake of La^{3+} , Tb^{3+} , and Lu^{3+} was determined at methanol volume percentages of 25, 50, and 85. The calculated \bar{D} 's are listed in Table III. For each ion, the rate of exchange decreased markedly as the methanol concentration increased. The rate of exchange became so slow at 85% methanol that only a small amount of the exchange could be followed using a reasonable amount of solution. Therefore, the absolute values of \bar{D} 's at 85% are in some doubt but have been included to give an easy comparison with previous experiments. The \bar{D} values decrease as the water content of the resin matrix decreases, thus indicating that water in the matrix plays an important role in the transport of ions.

Increasing the methanol concentration in the external solution has, perhaps additional effects apart from decreasing water content of the resin and perhaps decreasing the hydration of ions which affect the rate of exchange. The effects are (a) shrinkage of the resin, (b) decrease the dielectric constant of the solution, (c) increase the electrolyte concentration in the resin, and (d) decrease the degree of dissociation of the fixed sulfonate salt in the resin. Many of these factors are again interrelated; for example, the lower hydration of the ion and the lower dielectric constant are possibly responsible for the shrinking of the resin. The overall effect of adding methanol to the solution would be to cause a more severe atmosphere under which an ion must travel. However, it can be seen that the particle diffusion coefficients, \bar{D} , in the mixed solvents are always in the order of $\bar{D}_{Lu} > \bar{D}_{Tb} > \bar{D}_{La}$ which is consistent with that found in the purely aqueous system. It seems reasonable that the hydration of the ions, although lower in the methanol-water mixtures,

will still be such that Lu^{3+} , with the highest charge density, will remain the largest ion. If such is the case, then the results again indicate that hydration of an ion aids its transport in the resin phase, at least for the particular conditions of these experiments. The exchange rate in pure methanol is expected to be very slow, and thus solvation of ion by methanol does not aid appreciably transport of ion in the mixed solvent system.

By examining the particle diffusion coefficients for all the experiments, a rather interesting phenomenon is noted. From Table III the value of \bar{D} for 0% methanol divided by \bar{D} for 50% methanol for each ion yield the following ratios: for La, $\bar{D}(0\%)/\bar{D}(50\%) = 6.7$; for Tb, $\bar{D}(0\%)/\bar{D}(50\%) = 5.2$; for Lu, $\bar{D}(0\%)/\bar{D}(50\%) = 3.6$. These ratios indicate that the changing resin environment has a greater inhibiting effect on the rate of diffusion for La^{3+} than it does for Lu^{3+} . The reason for this is not clear at this time. It may indicate that a large solvation sheath becomes relatively more important as the conditions in the resin become more severe.

(IV) *Effect of Nonexchange Electrolyte.* The concentration of the diffusible or nonexchange electrolyte increases as the hydrochloric acid concentration goes up as reported by Bauman and Eichhorn.²³ Since the Donnan exclusion is more prominent at low concentrations, the internal HCl solution concentration does not reach 1 M until the outside HCl solution is about 4.3 M. At external HCl solution concentrations of 6 and 9 M the internal concentrations are approximately 2 and 5 M, respectively. Tetenbaum and Gregor¹¹ have related the increase of self-diffusion coefficients with increasing external electrolyte concentration to this build up of nonexchange electrolyte. This effect does not appear to be present in this investigation possibly due to the fact that only trace exchange is studied.

(V) *Effect of Complexing of Ion-Pair Formation.* The complexing of the Tb^{3+} ion should increase in more concentrated HCl solutions although these complexes should be quite labile and have little effect on the rate of exchange. To examine this, an experiment was performed using the lesser complexing medium of 3.0 M perchloric acid. This experiment gave the same rate of diffusion as one performed with hydrochloric acid of the same concentration, indicating that very little effect of complexing on the rate of exchange in the system at least at this concentration.

(VI) *Examination of Results in Terms of a Simple Mechanism.* The experimental results have revealed the following points, namely (a) ion-exchange rate decreases as the charge of the exchanging species increases, (b) ion-exchange rate decreases as the free water content of the resin decreases, and (c) ion-

(23) W. C. Bauman and J. Eichhorn, *J. Amer. Chem. Soc.*, **69**, 2830 (1947).

exchange rate decreases as the size of the hydrated species decreases.

The last statement (c) contradicts the view held by others, based on the self-diffusion of the alkali ions, that the self-diffusion rates of the alkali ions are in the order $\text{Cs}^+ > \text{Rb}^+ > \text{K}^+ > \text{Na}^+$, Cs^+ having the smallest hydrated radius whereas Na^+ has the largest in the series. In order to explain the apparent discrepancy with the results of the present study, the difference between "trace exchange" and self-diffusion has been examined.

In self-diffusion experiments, each ion diffuses in the resin matrix in a completely different atmosphere, since each resin matrix is in a different ionic form and therefore has varying water content and swelling of resin. This factor must be considered before the self-diffusion data can be compared on the basis of the ionic size of the exchanging species. For example, it is known² that a Cs^+ -form resin has a smaller total water content but a larger free water content than does a resin in the Na^+ form. To illustrate it in terms of the resin environment, a hypothetical pore of the resin is shown in the sketch below.



In the matrix, free water content is a more important factor to consider than is total water content for the transport of ion. Free water content can be said to be a gauge of the amount of "free space" inside the resin or in other words, a gauge of the "effective" pore diameter. As shown in the sketch, a Cs^+ -form resin has a larger "effective" pore diameter than does a Na^+ -form resin even though the Cs^+ -form resin has a lower total water content. This means that a Cs^+ ion has a less restrictive atmosphere in which to diffuse and so can diffuse at a faster rate. Thus, it is not possible to compare the diffusion of Cs^+ in a Cs^+ resin and Na^+ in a Na^+ resin on the basis of the size of hydrated ion alone. If it is assumed that a larger hydrated ion will diffuse more rapidly than a smaller one under identical conditions, then it would be predicted that Na^+ should diffuse at a faster rate than Cs^+ if a constant resin environment was maintained. Data reported by Boyd, *et al.*,^{2a} reveal that this is indeed the case. Using trace exchange techniques and a resin in K^+ form, the rate of diffusion of the trace ion was in order of $\text{Na}^+ > \text{Rb}^+ > \text{Cs}^+$, similar to our results on the diffusion rate of lanthanide ions.

The mechanism of diffusion of a hydrated ion inside the pores of the resin matrix is a complex one and can

only be speculated. The diffusion of an ion can perhaps be visualized as a two-step process, namely (a) diffusion in the pore-liquid and (b) diffusion near the surface of the pores in the resin matrix. In the first step, an ion can be channeled inside the pore in a similar manner as in a crystal^{24,25} before experiencing retardation by the fixed charges. A smaller hydrated species having lower charge will travel further inside the matrix than a larger hydrated ion or having higher charge. In the second step, according to Mackay and Meares,²⁶ a smaller hydrated ion would travel closer to the matrix structure than a larger hydrated ion and thereby be more restricted by the high local viscosity due to the electrostriction of solvent in the neighborhood of the fixed charges. An ion of higher charge will be retarded to a greater extent by the resin matrix and thus will have lower diffusivity. The role of the solvent in the pores of the resin matrix is somewhat of a similar nature. An ion traveling in a high dielectric medium will encounter lesser viscous drag than in a lower dielectric medium. The experimental results in methanol-water system support this view, but it is still premature to derive this conclusion. Perhaps, another factor which may yet be very important in the transport of ions in the matrix is the exchange rate of solvent between a solvated ion and free solvent.

In summary, it has been shown that there can be large variations in the calculated \bar{D} values for ions diffusing into the resin matrix if the rate data are not properly analyzed. Constant \bar{D} values are obtained if the effect of diffusion through the film on the resin beads is taken into account. The particle diffusion coefficient, \bar{D} , for various ions in resin matrix are shown to be dependent on the solvent content in the matrix. The value of \bar{D}_{AB} for a microcomponent ion is not equal to \bar{D}_A , self-diffusion coefficient, as predicted by Helfferich-Plasset equation. The solvent content in the resin matrix does not remain constant in different macrocomponent ion. The experimental verification of rate laws derived for ion exchange accompanied by reactions might present the same difficulty.

Acknowledgment. The authors gratefully acknowledge the financial support for this work by the National Research Council of Canada. We are also grateful to Mr. N. Subramanian for providing the results of water-content determinations of resins.

(24) G. R. Percy, F. Brown, J. A. Davies, and M. McCargo, *Phys. Rev. Lett.*, **10**, 399 (1963).

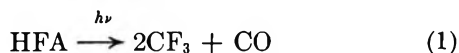
(25) M. T. Robinson and O. S. Oen, *Appl. Phys. Lett.*, **2**, 30 (1963).

(26) D. Mackay and P. Meares, *Trans. Faraday Soc.*, **55**, 1221 (1959).

fractionation at -135° . Repeated tests showed quantitative removal of C_2F_6 , CF_3H , and CF_2CH_2 from the bulk of the reaction mixture using this procedure.

Results

The photolysis of HFA was used as a trifluoromethyl radical source. Equation 1 adequately describes the process occurring⁹



Emission Measurements. The possibility always exists that products ascribed to radical processes may come from some reaction involving excited HFA molecules and the substrate. The effect of the silanes on the emission spectrum of excited HFA was therefore examined and compared with similar measurements for CO_2 and O_2 . With HFA, 10–50 Torr, and $MeSiF_3$ or Me_2SiF_2 , 0–200 Torr, slight enhancement of emission was obtained. This was similar to the effect of CO_2 , 0–200 Torr. Quenching was observed with O_2 , 0–20 Torr. Measurements were made at 25, 80, and 200° . These results suggest that chemical quenching by the silanes is insignificant.

Products of Reaction. Examination of the volatile products of reaction showed the presence of CO , C_2F_6 , CF_3H , and CF_2CH_2 , when HFA was photolyzed in the presence of $(CH_3)_4Si$, $(CH_3)_3SiF$, $(CH_3)_2SiF_2$, and CH_3SiF_3 . In addition SiF_4 was detected with CH_3SiF_3 as substrate. Addition of oxygen reduced the amounts of C_2F_6 , CF_3H , and CF_2CH_2 ; however, some 16 Torr was required to suppress these products to zero.

This is in accord with those products arising from radical reactions, with oxygen acting as a radical scavenger. Further evidence that the CF_3H , C_2F_6 , and CF_2CH_2 arise from CF_3 radical reactions was obtained using hexafluoroazomethane (HFAM) as a radical source, reaction 2



Both the thermolysis and photolysis of HFAM gave the products described above, where HFA was used as the radical source. In no case was methane or products normally expected from methyl radicals observed.

Hydrogen Abstraction. The most probable source of CF_3H is the abstraction reaction 3



C_2F_6 formation can be ascribed to reaction 4



Making the assumption that CF_3H formation from $CF_3 + CH_2Si \rightleftharpoons$ is negligible, we obtain from (3) and (4)

$$\frac{R_{CF_3H}}{R_{C_2F_6}^{1/2}} = \frac{k_3[\text{silane}]}{k_4^{1/2}} \quad (5)$$

That the experimental results fit this equation is seen

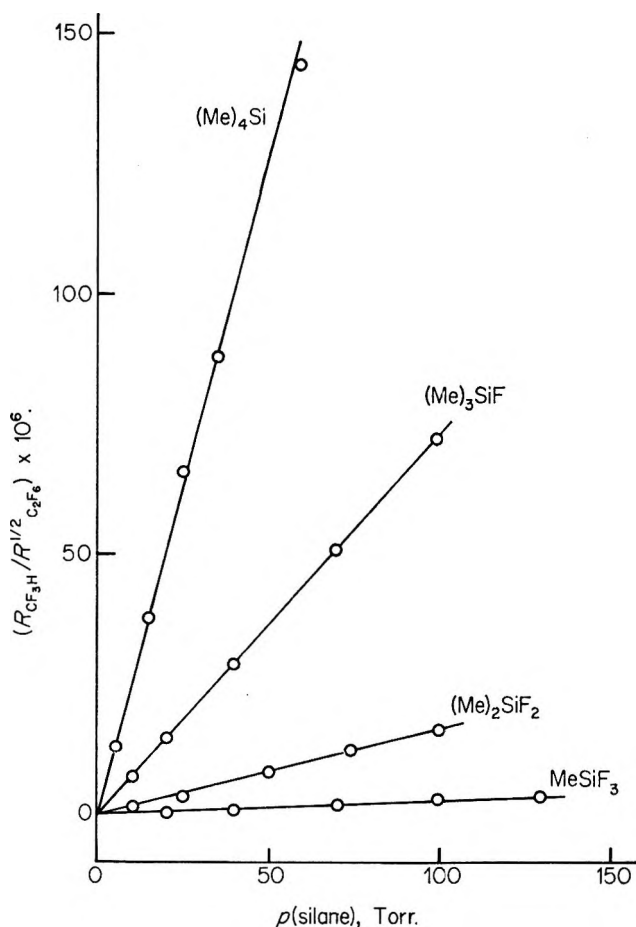


Figure 1. Variation of $R_{CF_3H}/R_{C_2F_6}^{1/2}$ with pressure of silane; temp, 200° .

in Figure 1 where $R_{CF_3H}/R_{C_2F_6}^{1/2}$ is plotted against silane, for a fixed HFA pressure of 20 Torr at a temperature of 200° .

The results of a series of experiments designed to measure $k_3/k_4^{1/2}$ through application of eq 5 for each of the four silanes are shown in Table I, and the corresponding Arrhenius plots in Figure 2. Decomposition of silane was kept to $<2\%$. Variations in HFA pressure caused no change in value of $k_3/k_4^{1/2}$. Using Ayscough's¹⁰ value for k_4 of 2.3×10^{13} cc mol⁻¹ sec⁻¹, the Arrhenius parameters for reaction 3, as determined by the method of least squares, are given in Table II.

CF_2CH_2 Formation. This product was formed with all the silanes from $(CH_3)_4Si$ to CH_3SiF_3 ; the results of a study to determine its origin have been reported elsewhere.¹¹

In summary there are two sources of CF_2CH_2 . (1) During the photolysis the major source is the hot molecule formed in the recombination reaction 6. This

(9) P. B. Ayscough and E. W. R. Steacie, *Proc. Roy. Soc.*, **A476**, 234 (1956).

(10) P. B. Ayscough, *J. Chem. Phys.*, **24**, 944 (1956).

(11) T. N. Bell and U. F. Zucker, *Can. J. Chem.*, **47**, 1701 (1969).

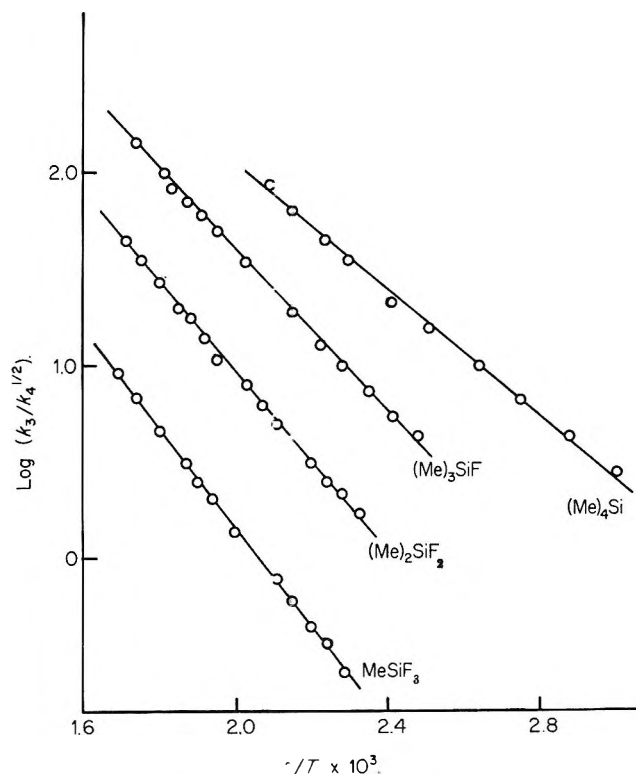
Table I: Rate Data: H Abstraction by CF₃ from Methylfluorosilanes

Temp, °C	P silane, Torr	Substrate (Me) _n Si		
		R _{CF₃} × 10 ¹⁰ mol ml ⁻¹ sec ⁻¹	R _{CF₃H} × 10 ¹⁰ mol ml ⁻¹ sec ⁻¹	k ₃ /k ₄ ^{1/2} ml ^{1/2} m ^{-1/2} sec ^{-1/2}
59.1	57.0	0.045	0.115	2.814
74.1	27.3	0.213	0.183	4.293
90.5	26.0	0.552	0.435	6.626
105.6	25.0	0.831	0.769	9.953
125.3	23.8	1.157	1.360	15.69
141.8	22.8	1.271	1.848	21.19
161.6	21.8	1.113	2.737	35.11
173.3	10.6	0.712	1.359	44.88
192.0	10.2	0.552	1.660	64.73
205.3	9.9	0.309	1.610	86.53
Substrate Me ₃ SiF				
130.1	58.9	1.222	0.932	4.243
140.1	22.9	1.718	0.559	5.495
141.8	57.0	1.179	1.137	5.416
152.4	22.2	1.616	0.706	7.375
165.4	21.6	1.485	0.880	9.874
177.3	21.0	1.300	1.052	12.96
192.0	20.3	1.073	1.319	18.48
219.5	19.2	0.841	2.068	34.70
239.7	18.4	0.626	2.474	49.99
250.4	18.0	0.369	2.225	59.85
261.6	17.7	0.436	2.796	70.40
273.3	4.3	0.734	1.063	84.46
279.3	8.6	0.575	2.251	102.3
301.6	4.1	0.791	1.780	144.4
Substrate Me ₂ SiF ₂				
156.0	54.7	2.436	0.484	1.671
165.4	53.4	2.470	0.623	2.186
173.3	52.6	1.980	0.663	2.522
181.4	51.7	2.265	0.848	3.214
200.8	49.6	1.892	1.169	5.051
209.9	48.6	1.365	1.188	6.172
219.5	47.5	1.455	1.534	7.887
239.7	45.7	1.128	1.767	10.74
247.7	45.1	0.860	1.957	13.80
258.8	44.0	0.825	2.413	17.79
267.4	43.5	0.636	2.330	19.79
282.4	42.3	0.529	2.824	27.08
298.3	41.1	0.383	3.081	35.71
311.6	40.2	0.304	3.326	44.26
311.6	8.1	1.175	1.328	44.60
Substrate MeSiF ₃				
163.5	216.8	1.192	0.207	0.258
173.3	212.1	2.070	0.368	0.355
181.4	208.1	2.234	0.470	0.446
192.0	101.6	2.249	0.305	0.590
200.8	99.7	0.236	0.412	0.793
221.9	95.4	0.210	0.631	1.344
242.3	91.9	1.778	0.854	2.054
253.2	89.8	1.436	0.913	2.501
261.6	88.4	1.434	1.152	3.206
282.4	85.3	1.161	1.437	4.609
301.6	82.3	8.092	1.708	6.798
318.6	80.0	6.276	1.970	9.166

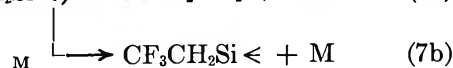
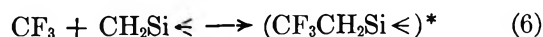
Table II: Arrhenius Parameters for H Abstraction by CF₃^a

Substrate	lg A ₃	E ₃
(CH ₃) ₄ Si	11.91 ± 0.09	7.29 ± 0.14
(CH ₃) ₃ SiF	12.45 ± 0.05	9.48 ± 0.09
(CH ₃) ₂ SiF ₂	12.27 ± 0.06	10.53 ± 0.12
(CH ₃)SiF ₃	11.38 ± 0.04	11.71 ± 0.09

^a Calculation of k₃ for (CH₃)₄Si at 180° yields a value 2.6 × 10⁸ cc mol⁻¹ sec⁻¹. Szwarc⁶ determines this as 3.5 × 10⁸ cc mol⁻¹ sec⁻¹ and Kerr¹⁹ as 2.7 × 10⁸.


 Figure 2. Arrhenius plot, log (k₃/k₄^{1/2}) vs. 1/T.

may decompose (reaction 7a) or be collisionally stabilized (reaction 7b).



(2) The second source is the thermolysis (reaction 8) of the stabilized molecule formed in reaction 7b



Our determination of $k_3 \approx 10^{-5}$ sec⁻¹ for the particular case of MeSiF₃ yields E₃ ≈ 37 kcal assuming A₃ ≈ 10¹². This is in agreement with the thermal decomposition of β-fluorosilanes.^{12,13} From (7a) and (7b)

$$R_{\text{stab}}/R_{\text{Decomp}} = k_{7b}[\text{M}]/k_{7a}$$

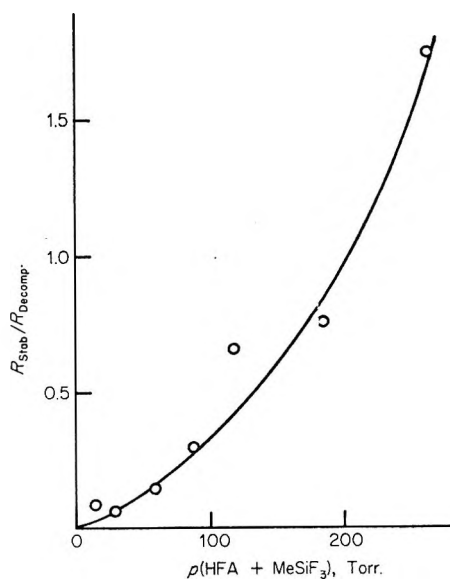


Figure 3. Variation of $R_{\text{Stab}}/R_{\text{Decomp}}$ with pressure for $(\text{CF}_3\text{CH}_2\text{SiF}_3)^*$.

In Figure 3 is seen a plot of $R_{\text{Stab}}/R_{\text{Decomp}}$ plotted against total pressure, HFA + silane, for the particular case of MeSiF_3 at 200° . The significant curvature can be ascribed to two causes.^{14,15} (1) Multicollisional deactivation of the hot molecule. If the strength of the $\text{CF}_3\text{-CH}_2\text{Si}$ bond ≈ 85 kcal, the molecule will have an excess of energy above the activation energy of ~ 45 kcal. (2) The deactivating body M is of two types, HFA and silane, in variable proportions, each having a different third body effect.

Discussion

Previous studies by Kerr, Slater, and Young^{16,17} on the interaction of free radicals with silanes indicate that in H abstraction reactions abnormally high A factors are operative. Doubts on this conclusion have been expressed by these same authors as a result of their more recent work,^{18,19} which is in keeping with our results where normal A factors have been shown to be operative in the $\text{CF}_3\text{-silane}$ system. The small differences observed between the reactions under study may be real, but do not significantly affect the values of k_3 . When normalized per methyl group, the three fluorosilanes have almost identical A factors.

Szwarc⁶ has measured the rate constants for hydrogen abstraction by CF_3 from a series of chlorosilanes and found a trend of decreasing reactivity with increasing chlorine substitution. This trend was not identified with either of the two Arrhenius parameters, but was shown to parallel the chemical shift of the protons, and indicates the importance of polar effects.

Our results tabulated in Table II agree with the findings of Szwarc in showing a marked decrease in reactivity of the silanes with increasing fluorine substitution. In our case the decreased reactivity is clearly the result of a change in activation energy.

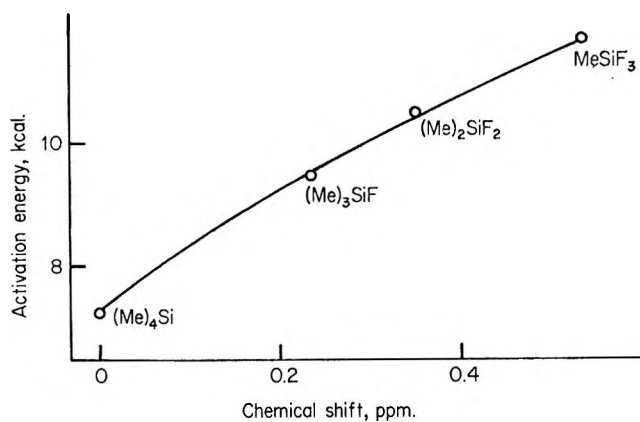


Figure 4. Correlation of activation energy for H abstraction with chemical shift.

The chemical shift of the protons incorporates anisotropy as well as electron density effects. Qualitatively, however, a change in chemical shift in a series of similar compounds can be considered to parallel changes in the electron density around the proton.

The following chemical shift measurements were made (Varian A56/60), in parts per million for the series of silanes under investigation: $\text{Si}(\text{Me})_4$, 0; Me_3SiF , 0.233; Me_2SiF_2 , 0.346; MeSiF_3 , 0.530.

The most negative H atom is associated with $\text{Si}(\text{Me})_4$, and a gradual change to less negative character occurs with increasing fluorine substitution. This observation is compatible with electronegativity considerations (C, 2.5; Si, 1.8; F, 4.0), where the electron drift towards the methyl group in $\text{Si}(\text{Me})_4$ will be lessened on substitution of the strongly electron-withdrawing F atom. Further evidence²⁰ of the correctness of the above conclusions is obtained from the quenching cross sections of $(\text{Me})_4\text{Si}$, $(\text{Me})_3\text{SiF}$, and $(\text{Me})_2\text{SiF}_2$ with respect to $\text{Hg } 6(^3\text{P}_1)$. These decrease markedly along the series, which, if triplet Hg is an electrophile, indicates a decrease in the electron density around the hydrogen atom.

A plot of the activation energy for the H abstraction, reaction 3, against the chemical shift is shown in Figure 4. A striking relationship is observed, which

(12) R. N. Haszeldine, P. J. Robinson, and R. F. Simmons, *J. Chem. Soc.*, 1890 (1964).

(13) G. Fishwick, R. N. Haszeldine, C. Parkinson, P. J. Robinson, and R. F. Simmons, *Chem. Commun.*, 383 (1965).

(14) G. O. Pritchard and R. L. Thomason, *J. Phys. Chem.*, **71**, 1674 (1967).

(15) J. T. Bryant and G. O. Pritchard, *ibid.*, **71**, 3439 (1967).

(16) J. A. Kerr, D. H. Slater, and J. C. Young, *J. Chem. Soc.*, **A**, 104 (1966).

(17) J. A. Kerr, D. H. Slater, and J. C. Young, *J. Chem. Soc.*, **A**, 134 (1967).

(18) J. A. Kerr, A. Stephens, and J. C. Young, *Int. J. Chem. Kinet.*, **1**, 371 (1969).

(19) J. A. Kerr, A. Stephens, and J. C. Young, *ibid.*, **1**, 339 (1969).

(20) M. A. Nay, G. N. C. Woodall, O. P. Strausz, and H. E. Gunning, *J. Amer. Chem. Soc.*, **87**, 179 (1965).

indicates that the greater the electron density on the H atom, the lower is the activation energy for H abstraction. This is in keeping with a strongly polar effect operating, where the attacking radical is the electrophilic CF₃ group.

The measured activation energies for H abstraction by CH₃ from the methylchlorosilanes¹⁷ are between 11.45 and 11.6 kcal while that for tetramethylsilane has been variously reported^{19,21,22} as 11.0, 10.3, and 10.6 kcal. From these values it can be argued that the C-H bond strength is little affected by chlorine substitution, leading to an approximately constant heat of reaction for the abstraction process. If the C-H bond for the methylfluorosilanes is considered in similar light, the expected changes in activation energy along the series due to differences in the heat of reaction would be small.

Thus, the following Polanyi-type relationship is in order

$$E \propto (\text{constant} - \Delta H) - \delta$$

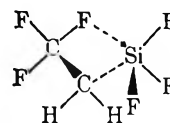
where δ represents a polar effect, and ΔH the heat of reaction, the magnitude of δ increasing with increasing electron density on the hydrogen atom.

It is interesting to note that Chaudhry and Gowenlock²¹ have correlated the energy of activation for H abstraction by methyl radicals from (Me)₄Si, (Me)₄Ge, (Me)₄Sn, and (Me)₄Pb, with the ¹³C-H coupling constant.

Reviewing all the available results, it is very clear that the reactivity of the C-H group towards free

radical attack is markedly dependent on the overall nature of the molecule, and further that polar effects can have a very marked influence on this reactivity.

Elimination reactions from hot radical-combination products, involving CF₃ radicals, are well established in organic systems.^{14,15,23,24} Introduction of a silicon atom leads to a new type of rearrangement-elimination reaction, presumably through the interaction of the empty d orbitals of the silicon atom. We propose



to investigate this reaction in detail and examine the possible generality of this process with systems involving B, Ge, and Sn atoms.

Acknowledgment. We thank the National Research Council for financial support, Mr. F. Wick for construction of apparatus, and Mrs. M. Boonstra for technical help. Mr. R. McDaniel kindly supplied the computer program for the calculation of the rate constants from the raw experimental data.

(21) A. U. Chaudhry and B. G. Gowenlock, *J. Organometal. Chem.* **16**, 221 (1969).

(22) T. N. Bell and A. E. Platt, unpublished work.

(23) R. D. Giles and E. Whittle, *Trans. Faraday Soc.*, **61**, 1425 (1965).

(24) D. C. Philips and A. F. Trotman-Dickenson, *J. Chem. Soc., A*, 1143 (1968).

Reaction of Hot and Thermal Hydrogen Atoms with Hydrogen Bromide and Bromine¹

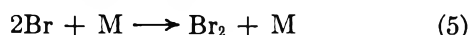
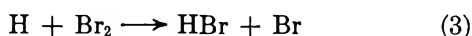
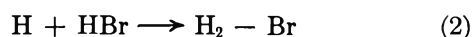
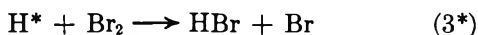
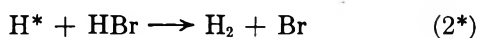
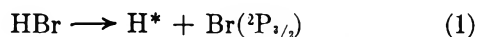
by Richard A. Fass²

Department of Chemistry University of Wisconsin, Madison, Wisconsin (Received September 4, 1969)

The ratios of the rates of the reactions $\text{H} + \text{HBr} \xrightarrow{(2)} \text{H}_2 + \text{Br}$ and $\text{H} + \text{Br}_2 \xrightarrow{(3)} \text{HBr} + \text{Br}$ have been determined for both thermal and unmoderated H atoms in the gas phase at temperatures from 300 to 523°K, using H atoms produced by the photolysis of HBr in the presence of Br₂ at 1850 and 2480 Å. In the absence of inert gas moderators, the ratio k_3^*/k_2^* for the reactions of hot H atoms = 5.3 ± 0.4 at each wavelength, independent of the temperature. The independence of wavelength and temperature suggests that most of the hydrogen atoms react with HBr or Br₂ before being thermalized. He is much more efficient than CO₂ for thermalizing the 2.9-eV H atoms from 1850-Å photolysis. The data for thermal H atoms in the range 300 to 523°K, coupled with earlier data between 900 and 1400°K, give $k_3/k_2 = 6.8 \exp(800/RT)$. The ratio of preexponential factors for the thermal reactions is approximately the same as the ratio of the reaction probabilities for hot hydrogen atoms in the same system.

Introduction

Photodissociation of HBr by 1850 Å and 2480-Å radiation produces H atoms with 2.9 and 1.2 eV of translational energy, respectively.^{3,4} These may react while retaining energy in excess of average thermal energies (H*), or after moderation (H), by the following steps



In pure HBr, all the H atoms must form H₂ by reaction 2* and/or 2, leading to a quantum yield of 2.0 for HBr consumption. As the Br₂ concentration grows [reactions 2* and 2 followed by 5] the quantum yield falls due to reactions 3* and 3. Because (1) HBr is useful as an actinometer for ultraviolet radiation;⁴ (2) there are discrepancies in the literature concerning the reactions of thermal H atoms in the HBr-Br₂ system; and (3) the system is of intrinsic interest for the study of hot reactions, we have investigated the relative probabilities per collision of reactions 2* and 3* and the relative rate constants of reactions 2 and 3.

The ratio k_3^*/k_2^* from the 2537-Å photolysis of HBr has been reported as 0.66,⁵ but parallel results on the HI-I₂ system using the same apparatus have been shown to be in error.^{5,6} Previous measurements of k_3/k_2 in studies of the thermal reaction of Br₂ with H₂

from 228 to 302°,⁷ the photochemical Br₂-H₂ reaction from 160 to 218°,⁸ and the Br₂-H₂ reaction in flames and shock tubes from 327 to 1427°⁹ give values between 8.2 and 10.1, temperature independent within the detection limits of the experiments. Bodenstein and Jung^{7b} reported $k_3/k_2 = 8.6$ from a photochemical experiment at 25°, but Sullivan¹⁰ has shown that at this temperature the photochemical Br₂-H₂ reaction is dominated by a mechanism different than the chain assumed. There is, therefore, no reliable measurement of k_3/k_2 below 160°, and a small temperature coefficient might not have been detected at the higher temperatures. By analogy with the HCl-Cl₂ system¹¹ and the HI-I₂ system,¹² it might be expected that the activation energy for reaction 2 would be about 1 kcal mol⁻¹ higher than that for reaction 3.

(1) This work has been supported in part by the U. S. Atomic Energy Commission under Contract AT(11-1)-1715.

(2) Department of Chemistry, Pomona College, Claremont, Calif. 91711.

(3) R. M. Martin and J. E. Willard, *J. Chem. Phys.*, **40**, 3007 (1964).

(4) (a) R. A. Fass and J. E. Willard, *ibid.*, in press; (b) R. M. Martin, Ph.D. Thesis, University of Wisconsin, Madison, Wis. 1964.

(5) H. A. Schwarz, R. R. Williams, Jr., and W. H. Hamill, *J. Amer. Chem. Soc.*, **74**, 6007 (1952).

(6) J. L. Holmes and P. Rodgers, *Trans. Faraday Soc.*, **64**, 2348 (1968).

(7) (a) M. Bodenstein and S. C. Lind, *Z. Phys. Chem.*, **57**, 168 (1906); (b) M. Bodenstein and G. Jung, *ibid.*, **121**, 127 (1926).

(8) M. Bodenstein and H. Lutkemeyer, *ibid.*, **114**, 208 (1924).

(9) (a) A. Levy, *J. Phys. Chem.*, **62**, 570 (1958); (b) S. D. Cooley and R. C. Anderson, *Ind. Eng. Chem.*, **44**, 1402 (1952); (c) D. Britton and R. M. Cole, *J. Phys. Chem.*, **65**, 1302 (1961).

(10) J. H. Sullivan, *J. Chem. Phys.*, **49**, 1155 (1968).

(11) F. S. Klein and M. Wolfsberg, *ibid.*, **34**, 1494 (1961).

(12) R. D. Penzhorn and B. de B. Darwent, *J. Phys. Chem.*, **72**, 1639 (1968).

Experimental Section

Matheson HBr (99.8% minimum purity) was degassed and distilled under vacuum at -78° . Air Reduction Co. research grade CO₂ and H₂ and Matheson ultrahigh-purity grade He were used without further purification. The quantum yield of decomposition of pure HBr did not vary from the expected value of 2 even when an excess of CO₂, H₂, or He was added, thus verifying the adequacy of the purity of these additives.

Cylindrical quartz cells with 2.5-cm diameter Suprasil end windows and 10-cm path lengths were used for all photolyses. They were fitted with graded seals and greaseless stopcocks which did not react with HBr or Br₂. A ground-glass joint attached to the stopcock allowed attachment of the cell to the mercury-free vacuum line which was used for cell filling. The stopcocks on the vacuum line were lubricated with Kel-F 90 grease. HBr was metered into the cells by means of a click gauge,^{4b} which permitted measurements reproducible to 0.5 Torr. After removal of the cell from the line the HBr pressure was measured on a Cary 14 spectrophotometer, using a molar extinction coefficient of 155 l. mol⁻¹ cm⁻¹ at 2100 Å.¹³ CO₂, He, and H₂ pressures were measured on a mercury manometer isolated from the mercury-free manifold by a U-tube trap cooled to -78° .

An Osram HBO-200W "super-pressure" mercury arc coupled with a Bausch and Lomb uv-visible grating monochromator was used for photolyses at 2480 Å, with a 250-Å bandpass. This arrangement permitted about 10¹⁶ photons sec⁻¹ to be delivered to a cell. Two Hanovia SC 2537 low-pressure mercury lamps with Suprasil windows, one directed at each end of the reaction cell, were used for 1850-Å photolyses, providing about 2×10^{15} photons sec⁻¹. For rapid photolyses designed to build up the Br₂/HBr ratio to a desired level for quantum yield measurements, a low-pressure spiral mercury lamp which provided an 1850-Å intensity of about 10¹⁷ photons sec⁻¹ in the 10-cm cylindrical cells was used. This lamp was constructed by L. C. Glasgow of our laboratory.

Actinometry was done by measuring the rate of Br₂ production from the photolysis of 15 Torr HBr at Br₂/HBr ratios less than 0.01, where reactions 3* and 3 are negligible. The Br₂ concentration was determined on the Cary spectrophotometer using $\epsilon = 170$ l. mol⁻¹ cm⁻¹ at 4160 Å.¹⁴ The decrease in HBr concentration measured at 2100 Å was always greater than the increase of Br₂ by a factor of 2.00 ± 0.02 , as predicted by the mechanism. All experiments were done at HBr pressures in the range from 15 to 7 Torr (optical densities at 1850 Å from ca. 4 to 2) so that even at the highest per cent decompositions studied there was essentially complete absorption of the 1850-Å incident radiation. In the 1850-Å photolyses, approximately 15% of the absorbed light in a 15 Torr HBr sample was

at the 2537-Å mercury line. At this pressure of HBr the 2537-Å optical density is ca. 0.02, so at this wavelength the absorbed light intensity is directly proportional to HBr pressure. Utilizing these facts the total absorbed light intensity was calculated as a function of HBr pressure for the quantum yield measurements. Similar calculations were made for the quantum yield measurements at 2480 Å.

In experiments where the ratio of the rates of reaction 2* to reaction 3* was to be studied using Br₂/HBr ratios produced by prior photolysis of HBr, the H₂ formed in the photolysis was first pumped out to avoid any moderating effect. Likewise, in experiments above room temperature the H₂ concentration was never allowed to reach more than 2% of the HBr concentration. This precluded interference by the inhibiting chain reaction of Br atoms with H₂, represented by the reverse of reaction 2 followed by reaction 3. Calculations using rate constants given by Sullivan¹⁰ indicate that this chain reaction should not contribute significantly at low H₂ pressures, and this was verified in several experiments which showed k_3/k_2 ratios to be independent of H₂ concentration up to at least 3% of the HBr concentration.

Results

Determination of k_3/k_2 and k_3^/k_2^* .* The rate of formation of Br₂ by reactions 1-5 derived from steady-state considerations and applicable to both hot and thermal reactions is given by

$$\frac{d[\text{Br}_2]}{dt} = \frac{I_a}{1 + \frac{k_3'[\text{Br}_2]}{k_2'[\text{HBr}]}} \quad (\text{I})$$

I_a is the rate of light absorption (einsteins l.⁻¹ sec⁻¹), $[\text{Br}_2]$ is in units of mol l.⁻¹, and the "constants" k_3' and k_2' may be either k_3^* and k_2^* applicable to the distribution of H atoms present during unmoderated HBr photolyses, or k_3 and k_2 applicable to thermal H atoms. If photolysis is done under conditions such that I_a is constant and $[\text{Br}_2]/[\text{HBr}]$ is nearly constant (an average value over the time of photolysis can be used if the ratio does not vary substantially), then (I) can be rearranged, giving

$$\frac{1}{\phi_{\text{Br}_2}} = \frac{k_3'[\text{Br}_2]}{k_2'[\text{HBr}]} + 1 \quad (\text{II})$$

where ϕ_{Br_2} is $(d[\text{Br}_2]/dt)/I_a$. In Figure 1, plots of $1/\phi_{\text{Br}_2}$ vs. $[\text{Br}_2]/[\text{HBr}]$ for the photolysis of HBr with and without the 600 Torr of He moderator required to thermalize the H atoms (see below) give straight lines with slopes of $k_3/k_2 = 22.7$ and $k_3^*/k_2^* = 5.3$, respectively.

(13) B. J. Huebert and R. M. Martin, *J. Phys. Chem.*, **72**, 3046 (1968).

(14) A. A. Passchier, J. D. Christian, and N. W. Gregory, *ibid.*, **71**, 937 (1967).

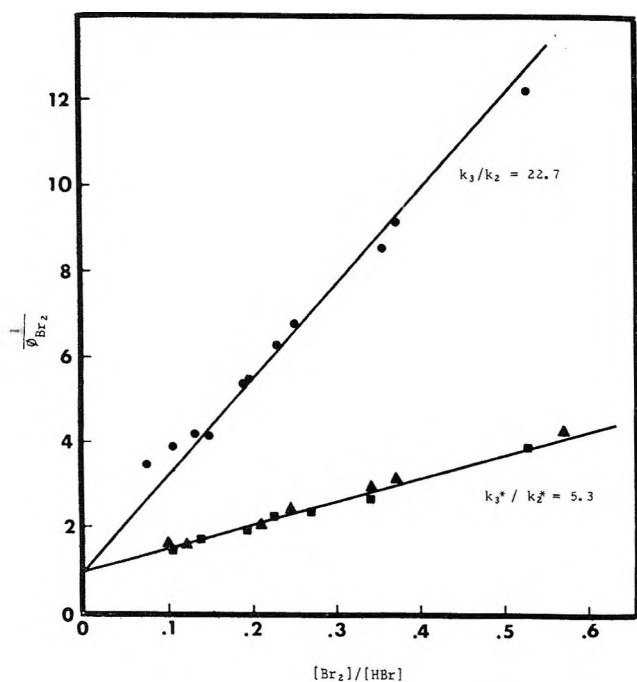


Figure 1. Reciprocal Br_2 quantum yield vs. $[\text{Br}_2]/[\text{HBr}]$ for moderated and unmoderated systems at 27° . Initial HBr pressure, 15 Torr. $[\text{Br}_2]/[\text{HBr}]$ varied by successive photolyses of the same mixture. ●, 600 Torr He at 1850 \AA ; ■, unmoderated at 1850 \AA ; ▲, unmoderated at 2480 \AA .

For experiments in which pure HBr ($[\text{Br}_2]/[\text{HBr}] = 0$) is photolyzed until a significant amount of Br_2 is accumulated, (I) can be integrated to give

$$\frac{k_3'}{k_2'} = \frac{I_a t - [\text{Br}_2]_t}{\frac{[\text{HBr}]_i}{4} \ln \frac{[\text{HBr}]_i - [\text{Br}_2]_t}{[\text{HBr}]_t} - \frac{[\text{Br}_2]_t}{2}} \quad (\text{III})$$

where $[\text{HBr}]_i$ and $[\text{HBr}]_t$ are the initial and final HBr concentrations respectively, $[\text{Br}_2]_t$ is the final Br_2 concentration, and t is the photolysis time. The conditions of eq III were used in one experiment, with an excess of inert moderator. The value of $k_3/k_2 = 25$ at 27° obtained is in good agreement with $k_3/k_2 = 23$ at 27° obtained in separate experiments using eq II, and serves as a check on the validity of the assumed mechanism.

Effect of Moderators on Reaction Probabilities. In order to determine the pressure of inert gas required to eliminate reactions of hot hydrogen atoms the ratios of specific reaction rates k_3'/k_2' were determined as a function of pressure of He and of CO_2 for $1850\text{-}\text{\AA}$ photolysis. These data, including one point for H_2 as moderator, are given in Figure 2.

The point for H_2 moderator indicates that H_2 is more efficient than He or CO_2 as would be expected. If it is assumed that the one point for H_2 and the point at 1400 Torr He represent mixtures in which virtually all of the H atoms are thermalized before reaction with HBr or Br_2 , then it can be estimated that in the mixtures

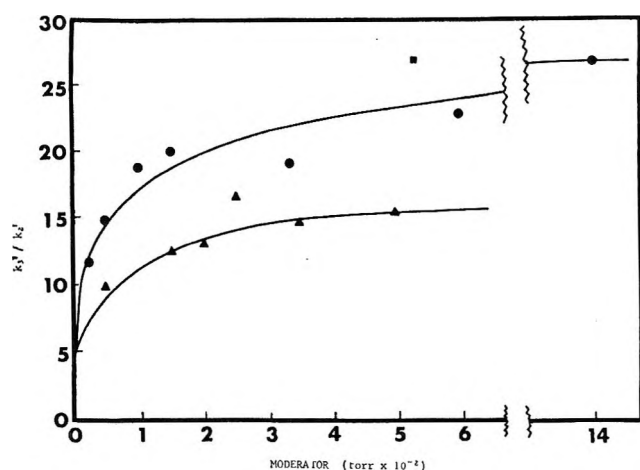


Figure 2. Effect of inert moderators on k_3'/k_2' . Photolyses at 1850 \AA , 27° . HBr pressures, 7–15 Torr: ●, He; ▲, CO_2 ; ■, H_2 .

containing 600 Torr He, ca. 85% of the H atoms are thermalized while the remaining 15% react as hot atoms with $k_3'/k_2' = k_3^*/k_2^* = 5.3$.

In mixtures containing 600 Torr CO_2 ($\text{CO}_2/\text{HBr} \approx 40:1$) only ca. 60% of the H atoms are thermalized, as shown in Figure 2. Similar CO_2 moderator curves have been obtained in the $2400\text{-}2800\text{-}\text{\AA}$ photolysis of HI– I_2 mixtures¹² and in $\text{H}_2\text{S-C}_2\text{H}_4$ mixtures photolyzed at 2138 and 2490 \AA ¹⁵ (both systems producing 1–2 eV H atoms). Reasoning from the apparent plateau in these curves, these authors^{12,15} concluded that all of the H^* atoms are thermalized before reaction at a CO_2/HI or $\text{CO}_2/\text{H}_2\text{S}$ ratio of 40:1. Our data for 2.9 eV H atoms indicate that this ratio does not completely thermalize all H atoms in the $\text{CO}_2\text{-HBr-Br}_2$ system even though the CO_2 curve (Figure 2) appears to be nearly horizontal. The very slow approach to complete thermalization indicated by these moderation curves is probably a result of the lower energy loss per collision at energies near the threshold for reactions 2* and 3*. Considering the scatter of the data of Figure 2 and ref 12 and 15, this suggests that the appearance of a plateau is not sufficient evidence for complete thermalization.

Temperature Coefficient of k_3/k_2 . Data obtained in this work over the temperature range from 27 to 250° are shown in Figure 3 on an Arrhenius plot which includes data from other sources taken at much higher temperatures. The straight line corresponds to an activation energy difference $E_2 - E_3 = 0.8 \pm 0.3 \text{ kcal mol}^{-1}$, where the indicated error limits include the limits placed by the lines of extreme maximum and minimum slopes which could reasonably be drawn through the points and the error introduced by the probability that ca. 15% of the H atoms were not

(15) G. R. Woolley and R. J. Cvetanovic, *J. Chem. Phys.*, **50**, 4697 (1969).

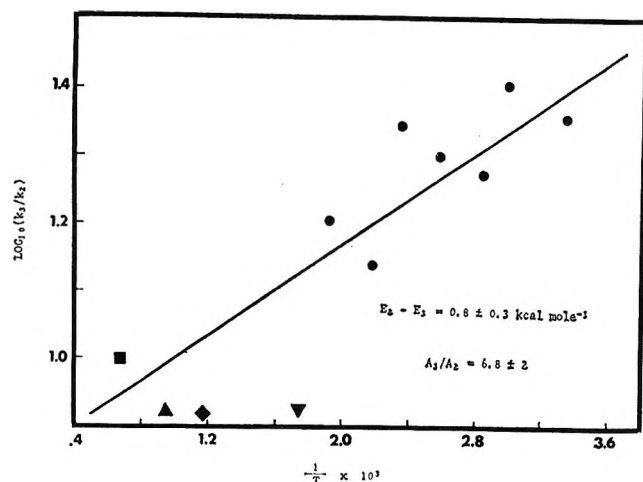


Figure 3. Temperature dependence of k_3/k_2 . ●, this work; ▲, ref 9a; ◆, ref 9b; ■, ref 9c; ▼, ref 7b.

moderated by the 600 Torr of He, as discussed above. The ratio of preexponential factors A_3/A_2 derived from the data of Figure 3 is 6.8 ± 2 .

Discussion

Fraction of H Atoms Which Reacts before Moderation. The data of Figure 2 show that the ratio of reaction of H atoms with Br₂ to their reaction with HBr in the absence of inert gas moderator is the same (5.3) regardless of whether activation is with 1850- or 2480-Å radiation. Since the analogous ratio for reaction of thermalized atoms is much different ($k_3/k_2 = 23$), it may be concluded that in the unmoderated system most of the H atoms produced at each wavelength react before thermalization. This implies that the reaction $\text{HBr} + \text{H}^* \rightarrow \text{H} + \text{BrH}^*$ as a process for producing thermal H atoms is improbable relative to reaction 2*.

k_3^/k_2^* Compared to A_3/A_2 .* The ratio of preexponential factors A_3/A_2 of 6.8 ± 2 obtained from Figure 3 is, within experimental error, the same as the ratio of the corresponding reaction probabilities for hot H atoms, $k_3^*/k_2^* = 5.3 \pm 0.4$. A similar relationship (see Table I) has been found for the reaction of hydro-

Table I: Rate Parameters for Reactions of Hydrogen Atoms

X	$E_2 - E_3$ kcal mole ⁻¹	A_3/A_2	k_3^*/k_2^* ^d
Cl ^a	1.5	6.9	
Br ^b	0.8	6.8	5.3
I ^c	0.6	5.0	4.2

^a Reference 11. ^b This work. ^c Reference 12. ^d This is the ratio of reaction probabilities for hot H atoms. See text.

gen atoms with HI and I₂¹². This is consistent with the collision theory interpretation of the Arrhenius preexponential factor as being directly proportional to the probability that a collision at an energy above the reaction threshold will result in chemical reaction.

Comparison with Literature Values. The data of Figure 3 clearly indicate that reactions 2 and 3 have an activation energy difference. This difference is small enough to have been missed in the high-temperature work using shock tube and flame techniques.⁹ Consequently the value of $E_2 - E_3$ has frequently been quoted as zero. The available data on the analogous reactions in the HCl-Cl₂ and HI-I₂ systems are included in Table I. The parameters for the HBr-Br₂ system found in this work fit into a consistent trend in this series.

The activation energy of reaction 2 has been independently reported to have values of 0.9 to 3.7 kcal mol⁻¹.¹⁶ If these values bracket the correct value, E_3 must lie in the range of 0 to 3.2 kcal mol⁻¹.

Acknowledgment. The author wishes to thank Professor John E. Willard for his helpful suggestions and encouragement during the course of this work.

(16) A. F. Trotman-Dickenson and G. S. Milne, "Tables of Bimolecular Gas Reactions," National Bureau of Standards, NSRDS-NBS9 (1967).

Electron Spin Resonance Study of the Kinetics of the

Reaction of O(³P) Atoms with H₂S^{1a}

by Gerald A. Hollinden,^{1b} Michael J. Kurylo,^{1c} and Richard B. Timmons

Department of Chemistry, The Catholic University of America, Washington, D. C. 20017 (Received September 22, 1969)

Esr atom detection has been employed to measure the O atom concentration as a function of reaction time in the study of the reaction of O + H₂S. The specific rate constant obtained for the reaction O + H₂S → OH + HS was $(1.74 \pm 0.40)10^{11} \exp[-(1500 \pm 100/RT)]$ in units of cm³ mol⁻¹ sec⁻¹. This result is based on an assumed stoichiometry of 3.5 atoms of oxygen consumed per molecule of H₂S. This stoichiometry is inferred from other work plus experimental observations in the current study. The Arrhenius *A* factor obtained in this work is compared with the result calculated on the basis of entropy changes using the method developed by Benson. Excellent agreement is obtained between theory and experiment if one assumes that a loose activated complex is formed in this reaction.

Introduction

The kinetics and mechanism of the oxidation of sulfur-containing compounds are of interest from the aspect of basic rate theory considerations as well as from the standpoint of their practical importance in combustion processes and air pollution. A number of recent studies have been devoted to the detection and identification of radical intermediates in the thermal^{2a} and photochemical^{2b} oxidation of H₂S and from these efforts mechanistic details have emerged. On the other hand, it appears that only one investigation has been devoted to a determination of the kinetics of the O + H₂S reaction. In this work Liuti, Dondes, and Harteck³ employed a flow system and mass spectrometric detection to obtain a rate constant for the reaction O + H₂S at room temperature.

In this paper we report on our study of this reaction over the temperature range of 205 to 300°K. Esr atom detection was employed to measure the O atom concentration as a function of reaction time. The apparatus and procedure we employed were similar to that developed by Westenberg and deHaas.⁴ Although the O + H₂S reaction is very rapid, it was measurable, with good precision, using the esr approach. From the Arrhenius parameters obtained in this work, it is obvious that the speed of this reaction results from a low activation energy.

Experimental Section

The flow apparatus has been described elsewhere.^{5,6} The only significant change from our earlier work was the replacement of the high temperature furnace with an aluminum lined styrofoam box in which the flow tube was suspended. For runs below room temperature, the flow tube was immersed in a liquid (usually methanol) cooled to the appropriate temperature by the addition of Dry Ice.

Oxygen atoms were produced by electrodeless discharge of O₂ in helium carrier gas. It has been shown⁷ that the magnitude of the O-atom esr signal (peak height) is a linear function of the atom concentration, and this fact was used in our work. The usual procedure⁸ of taking "on" and "off" readings of the O atom signal, that is, readings with H₂S flowing through the injector followed by readings with H₂S flowing through the by-pass tubing, were carried out to compensate for the wall loss of O atoms. The esr signal observed for O atoms is the pressure and modulation broadened line of the six transitions between the ³P₁ and ³P₂ states. Thus the specific rate constant observed in this work refers to the reaction of an O(³P) atom. The concentration of O₂ to inert carrier gas entering the discharge was varied from 0.3 to 1.4% (Table I).

Results and Discussion

The rate constant for an atom-molecule reaction using a fixed detector, in this case the esr cavity, and variable injector position for the stable reactant is calculated from the equation⁹

$$\ln ([A]_{B=0}/[A]) = k[B]t \quad (I)$$

(1) (a) This work was supported by the National Science Foundation under Research Grant GP-8699; (b) NSF trainee fellow; (c) NASA trainee fellow.

(2) (a) D. G. H. Marsden, *Can. J. Chem.*, **41**, 2607 (1963). References to earlier work are given in this paper; (b) R. G. W. Norrish and A. D. Zeelenberg, *Proc. Roy. Soc.*, **A240**, 293 (1957).

(3) G. Liuti, S. Dondes, and P. Harteck, *J. Amer. Chem. Soc.*, **88**, 3212 (1966).

(4) A. A. Westenberg and N. deHaas, *J. Chem. Phys.*, **47**, 1393 (1967).

(5) A. A. Westenberg and N. deHaas, *ibid.*, **46**, 490 (1967).

(6) M. J. Kurylo and R. B. Timmons, *ibid.*, **50**, 5076 (1969).

(7) A. Carrington, D. H. Levy, and T. A. Miller, *Proc. Roy. Soc.*, **A293**, 108 (1966).

(8) A. A. Westenberg, *Science*, **164**, 381 (1969).

(9) A. A. Westenberg and N. deHaas, *J. Chem. Phys.*, **46**, 490 (1967).

Table I: Experimental Results Used to Calculate k for the Reaction O + H₂S

$T, ^\circ\text{K}$	P, Torr	$V, \text{cm/sec}$	[H ₂ S], mol/cc	$\frac{[\text{O}_2]}{[\text{He}]}$	$\frac{[\text{H}_2\text{S}]}{[\text{O}_2]}$	$k, \text{cc/mol sec}$
300	1.38	1450	1.91×10^{-10}	1.4	0.18	6.50×10^{10}
	1.40	1540	1.69×10^{-10}	0.5	0.40	6.22×10^{10}
	1.79	1470	1.89×10^{-10}	1.1	0.18	3.82×10^{10}
	1.82	1450	3.05×10^{-10}	1.1	0.30	7.74×10^{10}
	2.25	1430	2.31×10^{-10}	0.3	0.59	5.35×10^{10}
						$k_{\text{av}} = 5.92 \pm 1.07 \times 10^{10}$
273	1.78	1380	1.95×10^{-10}	0.4	0.48	3.24×10^{10}
	1.78	1380	2.33×10^{-10}	0.2	0.92	5.25×10^{10}
	1.99	1350	1.92×10^{-10}	0.9	0.18	2.09×10^{10}
	2.00	1340	2.58×10^{-10}	0.9	0.24	3.13×10^{10}
	2.15	1350	2.38×10^{-10}	0.8	0.47	2.88×10^{10}
						$k_{\text{av}} = 3.34 \pm 0.76 \times 10^{10}$
234	1.68	1170	3.27×10^{-10}	1.2	0.24	1.66×10^{10}
	2.00	1150	4.45×10^{-10}	1.0	0.32	2.72×10^{10}
	2.12	1150	4.43×10^{-10}	0.9	0.32	3.56×10^{10}
						$k_{\text{av}} = 2.31 \pm 0.32 \times 10^{10}$
205	1.18	1080	3.54×10^{-10}	0.3	1.16	1.58×10^{10}
	1.18	1080	4.02×10^{-10}	0.3	1.32	1.81×10^{10}
	1.32	1050	3.31×10^{-10}	0.3	1.05	1.44×10^{10}
	1.32	1050	4.38×10^{-10}	0.3	1.40	2.32×10^{10}
	1.42	1040	4.18×10^{-10}	0.3	1.32	1.40×10^{10}
						$k_{\text{av}} = 1.71 \pm 0.28 \times 10^{10}$

^a From metered flow rates.

The left-hand side represents the ratio of the esr atom signal intensity without B (stable reactant) and with B added through the injector. The time, t , is simply the distance of the injector from some arbitrary zero position divided by the flow velocity. Since all quantities in this equation are known or easily measured, the rate constant k can be obtained.

The derivation has been discussed in detail by Westenberg and deHaas.⁹ With respect to the present investigation, it suffices to say that the only assumption which is questionable is the one which requires that the stable reactant be present in large excess over the atom species, that is, $[\text{B}] \gg [\text{A}]$. In our other studies using esr atom detection this condition was easily achieved. However in the current work, the extreme speed of the O + H₂S reaction placed severe restrictions on the pressure of H₂S which could be employed without completely removing all the O atoms. As shown in Table I, the metered flows of H₂S and O₂ were varied over the range of 0.18 to 1.4. This, on first glance, would not fulfill the requirement that $[\text{H}_2\text{S}] \gg [\text{O}]$. However it is to be noted that not all of the O₂ which enters the discharge dissociates to produce O atoms. Furthermore some of the O atoms will recombine before reaching the reaction zone. In addition, we have observations in this work, as well as from studies on comparable systems, which indicate that the stoichiometry of O atoms removed per H₂S molecule is larger than one and is probably closer to 3 or 4. Both of these factors combine to limit the H₂S depletion

during a kinetic run. In a given run, the O-atom concentration never decreased by more than a factor of two from the innermost to the outermost injector position.

Although we were somewhat disappointed with the relatively small change in the ratio of H₂S to O₂ accessible in this investigation, we do feel there are additional experimental observations which support the assumption that little change in the H₂S concentration occurs during the course of a kinetic run. For example, as shown in Table I, a change in H₂S/O₂ by a factor of 3 had no discernible effect on the measured rate constant at 300°K. In addition, all runs employed in calculating the desired rate constant gave atom-decay plots which were linear with reaction time (see, for example, curves B and C in Figure 1). If significant depletion of the H₂S occurred in these runs, one would anticipate obtaining atom-decay plots which would exhibit downward curvature at the longer reaction time.

It is of interest to note that an apparent complication arose in using higher pressures of H₂S. In this case, the atom-decay plots would show upward curvature, as shown in curve A of Figure 1. Runs involving such curvature were not employed in the kinetic calculations as it is impossible to determine the slope of the atom-decay plot under such conditions. Whenever this curvature was obtained a pronounced chemiluminescence could be observed in the flow tube.

We were also able to observe distinct esr absorption by H atoms and SO radicals in our kinetic runs. How-

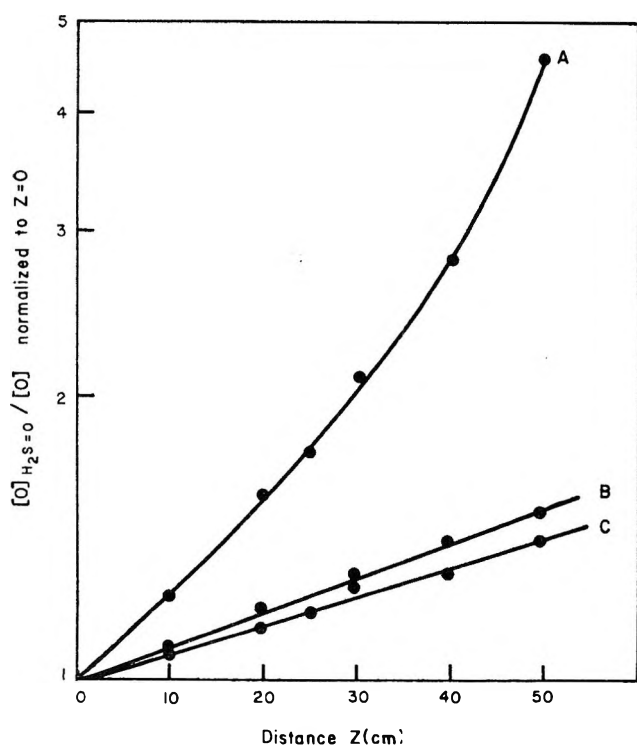
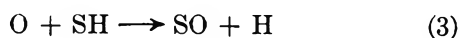
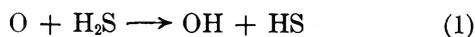


Figure 1. Typical O atom decay plots obtained at 300°K. Curve A: $p = 1.55$ Torr; $v = 1600$ cm sec⁻¹; $[H_2S] = 2.87 \times 10^{-10}$ mol cm⁻³. Curve B: $p = 2.25$ Torr; $v = 1430$ cm sec⁻¹; $[H_2S] = 2.31 \times 10^{-10}$ mol cm⁻³. Curve C: $p = 1.40$ Torr; $v = 1540$ cm sec⁻¹; $[E_2S] = 1.69 \times 10^{-10}$ mol cm⁻³.

ever it was not possible to make exact correlations between the increasing SO and H signals and the decreasing O atom esr signal. This arises from the fact that it is virtually impossible to use a product atom esr absorption for kinetic calculations as one cannot compensate for wall loss of the product species.

In view of the above experimental observations plus results from numerous other flow discharge studies, we feel the following mechanism is applicable in this work.



Under conditions of higher H₂S pressure, the following reaction will also become significant



It is to be noted that reactions 3 and 4 constitute a chain mechanism for removal of O atoms. This presumably accounts for the upward curvature of the atom-decay plots at higher H₂S pressures. The occurrence of this reaction chain will also produce a marked increase in [SO]. This serves to explain the appearance of the chemiluminescence, under these conditions, as it is apparent that this luminescence was produced from the reaction



followed by fluorescence by SO₂*. Thrush and co-workers¹⁰ have studied the chemical reactions in sulfur dioxide afterglow, and they conclude that reaction 5 is the dominant process of SO removal in a flow system containing O atoms.

It has been demonstrated that reaction 2 is very fast and of importance in flow work of the current type.¹¹ The specific rate constant for reaction 2 has been reported^{12,13} to be $\sim 10^{13}$ cm³ mol⁻¹ sec⁻¹, and it is believed to have essentially zero activation energy. At 300°K, k_2 is approximately a 1000 times greater than k_1 , and this difference becomes even greater at the lower temperatures. Although no rate constant is available for reaction 3, it is a highly exothermic reaction and, by analogy with reaction 2, would be expected to be rapid. Thus, on the basis of the proposed mechanism, we obtain a minimum stoichiometry of three oxygen atoms removed per H₂S. However it seems reasonable to expect that reaction 5 would also occur to a certain extent even under our restricted conditions of linear atom-decay plots. This would then set an upper limit of 4 for the reaction stoichiometry if every SO radical were removed by this route. However, since we detect esr absorption by SO, it is apparent that not all of the SO radicals are removed under our reaction conditions. Therefore, we have decided that the best procedure is to assume an average stoichiometry of 3.5. For this reason the rate constants given in Table I are to be divided by this factor.

An Arrhenius plot of the results obtained in this work are shown in Figure 2. From the least-squares treatment of our data and employing the assumed stoichiometry of 3.5, we obtain a value for k_1 of $(1.74 \pm 0.40)10^{11} \exp[-(1500 \pm 100/RT)]$ in units of cm³ mol⁻¹ sec⁻¹. We have also shown the room temperature result of Liuti, Dondes, and Hartek³ in Figure 2. The rate constant they obtained was approximately a factor of 2 higher than we obtain. However in view of the different experimental approaches used and the rather complex reaction sequence involved, the agreement between the two studies can be considered good and the results actually overlap within the large experimental errors quoted.

It is of considerable interest to compare the experimental Arrhenius A factor with the predicted value based on entropy changes employing the procedure developed by Benson.¹⁴ In this method one calculates

(10) (a) M. A. A. Clyne, C. J. Halstead, and B. A. Thrush, *Proc. Roy. Soc.*, **A295**, 355 (1966); (b) C. J. Halstead and B. A. Thrush, *ibid.*, **A295**, 363 (1966).

(11) See, for example, A. A. Westenberg and N. deHaas, *J. Chem. Phys.*, **47**, 4241 (1967).

(12) F. P. Del Greco and F. Kaufman, *Discussions Faraday Soc.*, **33**, 128 (1962).

(13) M. A. A. Clyne and B. A. Thrush, *Proc. Roy. Soc.*, **A275**, 544 (1963).

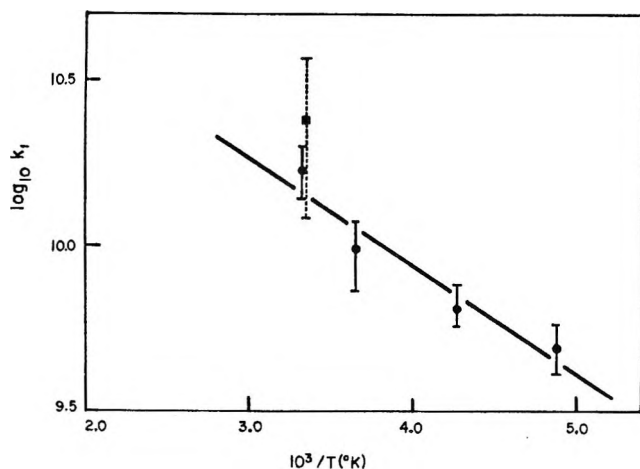


Figure 2. Arrhenius plot of the rate constant for the reaction $O + H_2S \rightarrow OH + HS$. The rate constant obtained in this work is based on an assumed stoichiometry of 3.5 oxygen atoms per H_2S . ●, this work; ■, ref 3.

a lower limit for ΔS , entropy of activation, and thus a lower limit for the calculated preexponential factor. In the current work, we compute the entropy of the [OHS₃] activated complex by comparison with that of H_2S assuming the translational and rotational entropy of this complex are not seriously increased over that of H_2S . That is, one assumes that the main entropy differences between these two species arise from symmetry and spin considerations. Hence, we write

$$S^\circ(\text{OHS}_3)^\ddagger \geq S^\circ(\text{H}_2\text{S}) + R \ln 3 + R \ln 2$$

and

$$\begin{aligned} \Delta S_p^\ddagger (\text{of activation}) &= S^\circ(\text{OHS}_3)^\ddagger - \\ & S^\circ(\text{O}) - S^\circ(\text{H}_2\text{S}) \\ &\geq -S^\circ(\text{O}) + R \ln 6 \end{aligned}$$

Using $S^\circ(\text{O})$ of 38.5 gibbs mol⁻¹,¹² we obtain $\Delta S_p^\ddagger \geq -34.9$ gibbs mol⁻¹. To transform to units of molarity, we use the expression

$$\Delta S_o^\ddagger = \Delta S_p^\ddagger - R \Delta n - (\Delta n)R \ln (RT)$$

and we obtain $\Delta S_o^\ddagger = -26.6$ gibbs mol⁻¹. From the relation $A = (ekT/h) \exp(\Delta S_o^\ddagger/R)$ we calculate a value for A of 2.56×10^{10} cm³ mol⁻¹ sec⁻¹.

At first glance, the calculated value appears much too low compared to the experimental result of 1.74×10^{11} cm³ mol⁻¹ sec⁻¹. However in this particular reaction this is precisely the result we would expect, as the above calculation is based on a "tight" activated complex. The $O + H_2S$ reaction is highly exothermic, and the H-S bond will be only slightly stretched in the activated complex. In view of this, one anticipates the formation of a rather "loose" activated complex, and thus one possessing low bending vibrations. For example, the presence of two degenerate bending modes of 250 cm⁻¹ at 298°K would add 3.5 gibbs mol⁻¹ to the calculated entropy, and we obtain a calculated A factor of 1.63×10^{11} cm³ mol⁻¹ sec⁻¹ in excellent agreement with the experimental result.

It will be of interest, in the future, to apply this method to other reactions as it can potentially supply considerable insight into the nature of the activated complex formed in these bimolecular reactions. The assumption of two weak bending modes in the activated complex in the $O + H_2S$ reaction may seem somewhat arbitrary. However in view of the energetics of this reaction this assumption is quite reasonable. Moreover in order to provide a fair test of the Benson method, the same assumption of low bending vibrations in the activated complex would have to be employed in calculating A factors for other highly exothermic reactions involving H atom transfer from H_2S . Hopefully future work in this area will provide A factors of sufficient precision and accuracy so that meaningful comparisons can be made. This could result in a clearer idea of the geometry and properties of the activated complex formed in such reactions.

(14) For a comprehensive discussion see, S. W. Benson, "Thermochemical Kinetics," John Wiley & Sons, New York, N. Y., 1968.

Kinetics of the Dehydrofluorination of Vinyl Fluoride in a Single-Pulse Shock Tube¹

by J. M. Simmie,² W. J. Quiring,³ and E. Tschuikow-Roux

Department of Chemistry, University of Calgary, Calgary, Alberta, Canada (Received August 27, 1969)

The gas phase decomposition of vinyl fluoride has been studied in a single-pulse shock tube between about 1170 and 1350°K at total reflected shock pressures from 2800 to 3600 Torr. It is shown that vinyl fluoride decomposes by molecular elimination of hydrogen fluoride, $\text{CH}_2=\text{CFH} \xrightarrow{k} \text{C}_2\text{H}_2 + \text{HF}$. The first-order rate constant is given by $k = 10^{14.0 \pm 0.7} \exp[-(70,800 \pm 3600)/RT] \text{ sec}^{-1}$.

Introduction

The thermal gas phase hydrogen halide elimination reactions of alkyl chlorides, bromides, and iodides have been extensively studied.⁴ Comparable data on the decomposition of the alkyl fluorides have only recently been published.^{5,6} In contrast, the kinetic aspects of the dehydrohalogenation reactions of alkenyl halides are but little known. We report here the first direct kinetic study on the decomposition of an alkenyl fluoride, vinyl fluoride. The reaction was carried out under assured homogeneous reaction conditions behind reflected shock waves in a single-pulse shock tube over the temperature range 1174 to 1353°K.

Experimental Section

The single-pulse shock tube, which was of the modified ball-valve type design, and its mode of operation have been described previously.⁷ Helium was used as the driver gas. The channel was filled with pure argon except for the ball valve. The latter was charged with a dilute mixture of vinyl fluoride in argon to a pressure equal to the argon pressure in the rest of the shock tube.

Reflected shock temperatures were calculated from measured incident and reflected shock velocities.⁷ These were determined by recording the transit times of the incident and reflected shocks across two high frequency pressure transducers (Kistler, Model 603A/623F, located 10 and 20 cm, respectively, from the end-plate) using two universal counters of 0.1- μ sec resolution (Hewlett Packard, Model 5325A). The amplified signals were also fed to an oscilloscope (Tektronix, Model 535 A with CA plug-in) operated in a single-sweep mode, and the wave history of interest was photographically recorded to provide a measure of the reaction time and cooling rate.

Vinyl fluoride of 99.95% stated purity was obtained commercially (Matheson Co.) and checked by mass spectrometric and gas chromatographic analysis. No detectable impurities were found, and it was used without further purification. The dilute reaction mix-

ture (0.98% CH_2CHF in Ar) was prepared in a large stainless steel tank and allowed to mix prior to its use.

After a run, the shocked reactant and its decomposition products were isolated in the end section of the shock tube by closing the ball valve, and a sample of the fully mixed gases was withdrawn for analysis. The ratio of the product, acetylene, to reactant was determined by gas chromatography (Varian Aerograph, Model 1740) using a flame ionization detector in conjunction with a 12-ft silica gel column at 75° and helium as carrier gas. Quantitative identification was achieved by means of standard mixtures of acetylene and vinyl fluoride in argon prepared for calibration purposes. At the highest temperatures employed the extent of reaction did not exceed 30%.

Results and Discussion

The thermal decomposition of vinyl fluoride in the temperature range 1174 to 1353°K yields acetylene as the major reaction product, comprising over 90% of the total products, exclusive of hydrogen fluoride. The latter was not analyzed quantitatively because of its reactivity with the walls of the shock tube (after the high-temperature pulse) and the transfer vessel. Small quantities of ethane, ethylene, and 1,1-difluoroethylene were also detected but could not be investigated in detail. Their presence suggests the occurrence of complicated side—or parallel—reactions. Thermochemical considerations would tend to exclude mechanisms based on either C=C, C-F, or C-H bond scission as the primary process. Thus, the carbon-fluorine bond dissociation

- (1) Work supported by the National Research Council of Canada.
- (2) National Research Council Postdoctorate Fellow, 1968–1970.
- (3) Graduate Fellow.
- (4) A. Maccoll and P. J. Thomas, *Progr. React. Kinet.*, **4**, 119 (1967).
- (5) D. Sianesi, G. Nelli, and R. Fontanelli, *Chim. l'Ind. (Milan)*, **50**, 619 (1968).
- (6) M. Day and A. F. Trotman-Dickenson, *J. Chem. Soc., A*, 233 (1969).
- (7) J. M. Simmie, W. J. Quiring, and E. Tschuikow-Roux, *J. Phys. Chem.*, **73**, 3830 (1969).

Table I: Experimental Results

Mach number		P_1 , Torr	T_1 , °K	P_2 , Torr	T_2 , °K	t_d , μ sec	R_t	k , sec $^{-1}$
W_{11}	W_{21}							
2.192	1.272	864	693	2840	1174	641	0.00900	14.0
2.204	1.260	874	702	2848	1184	509	0.00670	13.1
2.212	1.268	880	703	2889	1191	608	0.00639	10.5
2.225	1.273	891	709	2941	1203	706	0.0109	15.4
2.229	1.280	895	711	2973	1211	568	0.00764	13.4
2.237	1.283	904	716	3012	1222	687	0.0172	24.8
2.239	1.276	903	721	2993	1226	668	0.0102	15.2
2.250	1.282	912	722	3041	1232	625	0.0135	21.5
2.258	1.283	919	723	3069	1235	663	0.0199	29.8
2.262	1.286	922	732	3089	1252	688	0.0430	61.3
2.268	1.291	933	731	3139	1253	666	0.0430	63.1
2.287	1.294	946	735	3198	1264	721	0.0308	42.1
2.308	1.298	981	746	3330	1285	731	0.0548	73.0
2.316	1.299	968	748	3290	1289	827	0.0965	111
2.328	1.304	979	753	3343	1302	751	0.120	151
2.334	1.313	990	762	3407	1322	867	0.205	213
2.355	1.309	1003	772	3444	1338	878	0.277	278
2.356	1.298	1003	766	3416	1321	708	0.177	230
2.360	1.307	1007	773	3456	1339	857	0.422	411
2.365	1.324	1018	771	3538	1345	854	0.261	271
2.367	1.309	1012	775	3408	1345	883	0.277	277
2.374	1.324	1019	775	3546	1353	870	0.363	356

tion energy in vinyl fluoride can be evaluated from the known enthalpies of formation of the vinyl radical⁸ (64 ± 2 kcal mol $^{-1}$), the fluorine atom⁹ (18.9 ± 0.2 kcal mol $^{-1}$), and vinyl fluoride¹⁰ (-28 kcal mol $^{-1}$), as 111 ± 3 kcal mol $^{-1}$. The C=C bond dissociation energy is probably intermediate in value between that found in ethylene^{11,12} of 160 kcal mol $^{-1}$, and that in 1,1-difluoroethylene¹¹ of 125 kcal mol $^{-1}$; if it is further assumed that the dissociation energy of the C-H bonds in vinyl fluoride are about 104 kcal mol $^{-1}$ as in ethylene,⁸ then clearly the observed activation energy of 71 kcal mol $^{-1}$ suggests that homolysis is of minor significance. Homolytic initiation followed by radical chain reaction could, of course, proceed with a substantially lower activation energy. Nevertheless, the preponderance of acetylene among the reaction products indicates that the principal reaction is likely to be a unimolecular process involving the elimination of hydrogen fluoride.



Accordingly, the rate constants were evaluated from an assumed first-order rate law

$$k = (1/t_d) \ln(1 + R_t)$$

where R_t is the product/reactant ratio, $R_t = [\text{C}_2\text{H}_2]/[\text{C}_2\text{H}_3\text{F}]$, and t_d is the calculated reaction dwell time.¹³ The latter could be made to correspond closely to the actual measured "transducer dwell time" through a suitable choice of shock tube geometry.^{7,13}

The experimental results are summarized in Table I, where W_{11} and W_{21} are incident and reflected shock Mach numbers, and subscripts 2 and 5 refer to regions of

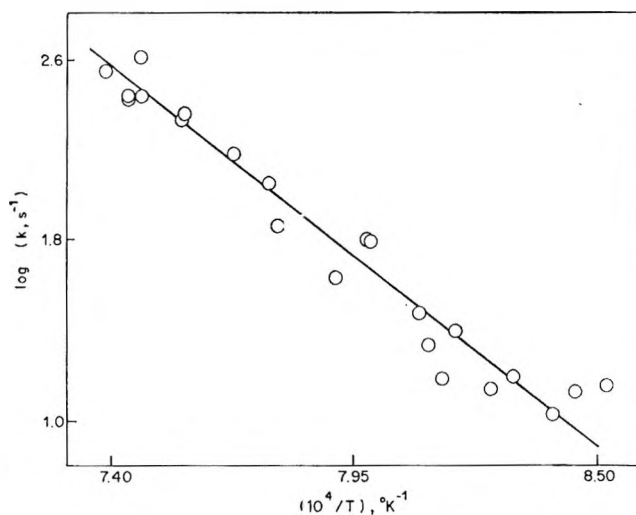


Figure 1. Temperature dependence of the rate constant.

environment behind the incident and reflected shock, respectively. The temperature dependence of the observed rate constants is shown in Figure 1 and is given by the Arrhenius expression

$$k = 10^{14.0 \pm 0.7} \exp[-(70,800 \pm 3,600)/RT] \text{ sec}^{-1}$$

(8) J. A. Kerr, *Chem. Rev.*, **66**, 435 (1966).

(9) "JANAF Interim Thermochemical Tables," Dow Chemical Co., Midland, Mich., 1965.

(10) P. G. Maslov and Yu. P. Maslov, *Tekhnol. Topliv. i Masel.*, **3**, 50 (1958).

(11) J. S. Shapiro and F. P. Lossing, *J. Phys. Chem.*, **72**, 1552 (1968).

(12) Table XXXII of ref 8 gives 167 kcal mol $^{-1}$ in error; the correct value can however be calculated from data supplied in the text.

(13) E. Tschuikow-Koux, *Phys. Fluids*, **8**, 821 (1965).

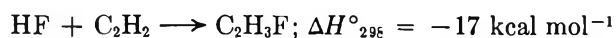
which was obtained from the regression equation for $(1/T)$ on $\log k$. This choice instead of the usual least-squares fit was preferred because the uncertainty in the reflected shock temperature, T_6 , was judged to be greater than the uncertainty in product analysis. The error limits shown are standard deviations.

Over the relatively narrow pressure range from 2840 to 3550 Torr and the temperature range cited above, no discernible trend of the first-order rate constants with the total reflected shock pressure, P_5 , was found. This indicates that the rate constants reported here are probably close to their high pressure limiting values, subject of course, to the usual restriction that the mechanism postulated here is correct.

The effect of finite cooling rates by the expansion fan, which may give rise to some additional decomposition during the quenching process, has been shown⁷ to be quite small for reactions with activation energies of the order of 70 kcal mol⁻¹ and cooling rates in excess of 10⁵ °K sec⁻¹. This was confirmed in the present study from cooling rates obtained from the slope of oscilloscope traces ($-dT/dt \simeq 3 \times 10^5$ °K sec⁻¹) using the expression derived earlier.¹³ The correction was within experimental error and could therefore be neglected.

The elimination of HF from vinyl fluoride is endothermic by only 17 kcal mol⁻¹ (see below). Because of this, and the high dilution factor (<1% C₂H₃F in Ar), as well as by virtue of the very nature^{7,13} of the modified single-pulse shock tube the effect of endothermicity on the reflected shock temperature was within the experimental uncertainty and was also neglected.

The value obtained for the activation energy reduced to 298°K, $E_f = 70$ kcal mol⁻¹, may be used to calculate the activation energy, E_r , for the reverse four-center addition reaction



using the known heats of formation of vinyl fluoride

(-28 kcal mol⁻¹),¹⁰ acetylene (54.2 kcal mol⁻¹),⁹ and hydrogen fluoride (-64.8 kcal mol⁻¹).⁹ Thus, $E_r \simeq E_f + \Delta H \simeq 53$ kcal mol⁻¹. This value is in good agreement with that estimated by Benson and Haugen¹⁴ of 52 ± 2 kcal mol⁻¹, who treat the transition state as an intimate semiion pair and equate the electrostatic interaction energy to the energy of activation.

The preexponential factor was calculated by the method of O'Neal and Benson¹⁵ which was developed for four- and six-center unimolecular reactions. The frequency assignments for the molecule and the complex of ref 16 were used for a "loose" four-center cyclic transition state. The carbon-fluorine stretching mode was chosen as the reaction coordinate with the assumption of α,β elimination.¹⁶ At 1250°K the difference in intrinsic vibrational entropies, ΔS^\ddagger , between the complex and the ground state is -1.12 cal mol⁻¹ deg⁻¹ which gives, on the assumption of unit reaction path degeneracy (*i.e.*, an essentially planar complex), $\log A$ (sec⁻¹) = 13.6. The agreement with our experimental value of $\log A$ (sec⁻¹) = 14.0 ± 0.7 is considered satisfactory in view of the rather arbitrary nature of the model employed and also because there is some uncertainty as to whether the elimination of hydrogen fluoride proceeds *via* α,α or α,β (or both) mechanisms. Pritchard, *et al.*,^{17,18} have shown that some α,α elimination occurs in the decomposition of "hot" 1,1,1-trideuterio-2,2-difluoroethane and suggest that at least two geminal fluorine atoms are required for α,α elimination.

(14) S. W. Benson and G. R. Haugen, *J. Phys. Chem.*, **70**, 3336 (1966).

(15) H. E. O'Neal and S. W. Benson, *ibid.*, **71**, 2903 (1967).

(16) E. Tschuikow-Roux and S. Kodama, *J. Chem. Phys.*, **50**, 5297 (1969).

(17) J. T. Bryant, B. Kirtman, and G. O. Pritchard, *J. Phys. Chem.*, **71**, 1960 (1967).

(18) M. J. Perona, J. T. Bryant, and G. O. Pritchard, *J. Amer. Chem. Soc.*, **90**, 4782 (1968).

The Gas-Phase Thermal Decomposition of Chlorocycloalkanes¹

by J. M. Sullivan²

Rocketdyne, A Division of North American Rockwell Corporation, Canoga Park, California 91304

and W. C. Herndon

Chemistry Department, Texas Technological College, Lubbock, Texas 79406 (Received July 23, 1969)

The thermal decompositions of cyclopentyl chloride, cyclohexyl chloride, cycloheptyl chloride, and cyclooctyl chloride were investigated over the temperature range 350–470° using a gas-phase stirred flow reactor. The rates for cyclopentyl and cycloheptyl chloride were measured relative to cyclohexyl chloride. The Arrhenius expressions for the first-order decomposition of the C₅, C₆, C₇, and C₈ chlorides were $k_5 = 10^{13.44} \exp(-48,570/RT)$ sec⁻¹, $k_6 = 10^{13.90} \exp(-50,250/RT)$ sec⁻¹, $k_7 = 10^{13.88} \exp(-47,340/RT)$ sec⁻¹, $k_8 = 10^{13.16} \exp(-44,950/RT)$ sec⁻¹. The Arrhenius *A* factors are discussed in terms of the loose cyclic transition state postulated by O'Neal and Benson.³

Introduction

Recently, O'Neal and Benson³ have demonstrated a method for estimating the Arrhenius *A* factors for four- and six-center unimolecular reactions *via* application of the transition state expression

$$A = \frac{ekT}{h} \exp(\Delta S^\ddagger/R)$$

The entropy of activation, ΔS^\ddagger , is obtained from estimates based upon their model which portrays the transition state as possessing a loose cyclic structure with semiion-pair charge separation at the reaction centers. Rules are given for assigning bending, stretching, and torsion frequencies for such structures and in general the major contributions to ΔS^\ddagger are found to come from symmetry changes and losses in hindered internal rotations.

An interesting situation arises in the case of the four-center elimination of HX from cyclic haloalkanes. In this case there is no loss in internal rotation and the major contributions to ΔS^\ddagger come from symmetry changes and unique features of the transition complexes such as partial loss of pseudorotation for the cyclopentyl ring and the possibility of the *trans* isomer in the case of the cyclooctyl compound.

We have investigated the gas-phase pyrolysis of cyclopentyl, cyclohexyl, cycloheptyl, and cyclooctyl chloride which decompose to give HCl and the corresponding cyclic olefin. The Arrhenius *A* factors for these unimolecular reactions are discussed in terms of the above model.

Experimental Section

The rate parameters were obtained using a gas-phase stirred flow reactor⁴⁻⁷ which was described previously.⁸ Prepurified nitrogen at 1 atm pressure was passed from a cylinder through a fine needle valve, used to adjust the flow rate, then through a magnesium perchlorate drying

tube, and into a vaporizer containing the compound (or compounds) to be investigated. The vaporizer was thermostated at 0° to ensure a low, constant partial pressure of reactant (or reactants) in the vapor phase. The gases leaving the reactor were analyzed by means of an Areograph Model A-600 "Hi-Fi" gas chromatograph equipped with a flame ionization detector and a 3-ft by 1/8-in. column packed with 20% Dow Corning #550 Silicone fluid on Embacel (60–100 mesh). The 52-ml Pyrex reactor was submerged in a molten-lead bath, the temperature of which was found not to vary by more than ±0.3° over a 3-hr period at 400°. The flow rates of the gases leaving the reactor were measured with a soap bubble flowmeter and were corrected to reactor temperature by means of the ideal gas law.⁹

Cyclopentyl chloride and cyclohexyl chloride of the highest purity available were purchased. Gas chromatographic analysis indicated traces of the lower boiling cyclic olefins which were removed by bubbling prepurified nitrogen through the chlorides for several hours.

Cycloheptyl chloride and cyclooctyl chloride were prepared from reaction of the corresponding cyclic alcohols with thionyl chloride using chloroform as the

(1) Taken from thesis by J. M. S. in partial fulfillment of requirements for M.S., Department of Chemistry, University of Mississippi, 1963.

(2) Division of Chemical Development, Tennessee Valley Authority, Muscle Shoals, Ala. 35660.

(3) H. E. O'Neal and S. W. Benson, *J. Phys. Chem.*, **71**, 2903 (1967).

(4) W. C. Herndon, *J. Chem. Educ.*, **41**, 425 (1964).

(5) A. A. Frost and R. G. Pearson, "Kinetics and Mechanism," John Wiley & Sons, Inc., New York, N. Y., 1956, p 185.

(6) J. M. Sullivan and T. J. Houser, *Chem. Ind.*, 1057 (1965).

(7) M. F. R. Mulcahy and D. J. Williams, *Aust. J. Chem.*, **14**, 534 (1961).

(8) W. C. Herndon, M. B. Henley, and J. M. Sullivan, *J. Phys. Chem.*, **67**, 2842 (1963).

(9) In this investigation the partial pressure of reactant was low in comparison with the carrier gas and no correction of flow rate for reaction was required. It is of interest to note that for a stirred flow reactor no such correction is necessary even at high partial pressures of reactant if the flow rate of the *exit* gas is measured.

solvent. The chloride products were purified by vacuum distillations and the following boiling points and refractive indices were determined: cycloheptyl chloride, $b_{750 \text{ mm}} = 172^\circ$, $n_{25}^D = 1.4728$; cyclooctyl chloride, $b_{19 \text{ mm}} = 87-88^\circ$, $n_{25}^D = 1.4825$.

The cyclic olefins were purchased in the highest purity available and were used without further purification. These olefins were chromatographically identical with those obtained from the pyrolysis of the corresponding cyclic chlorides. The gas chromatographic column used in this investigation did not distinguish between the *cis* and *trans* forms of cyclooctene.

Initial experiments in clean reaction vessels resulted in fast nonconsistent rates characteristic of this system of compounds.¹² However, in seasoned reaction vessels much slower and more consistent results were obtained.

The rates of decomposition of cyclohexyl and cyclooctyl chloride were measured directly, while the rates for cyclopentyl and cycloheptyl chloride were measured relative to cyclohexyl chloride by passing the reactant pair through the reactor simultaneously. Consider the simultaneous unimolecular decomposition of two reactants in a stirred flow reactor



The first-order rate constant for reaction 1 is given by the stirred flow expression

$$k_1 = \frac{(B)}{\tau(A)} \quad (3)$$

where τ is the residence time in the reactor and (A) and (B) are the steady-state concentrations of the reactant and one of the products, respectively, leaving the reactor.

The rate of reaction 1 relative to reaction 2 is given by

$$k_1/k_2 = \frac{(B)(D)}{(A)(E)} \quad (4)$$

In the above expression the residence time has canceled and the relative rates are determined simply from the ratio of products and reactants.

The first-order character of the thermal decompositions investigated is demonstrated in Figures 1, 2, and 3. Figure 1 shows a plot of (olefin)/(chloride) vs. τ for cyclohexyl and cyclooctyl chloride at 452 and 370°, respectively. These plots give straight lines in agreement with eq 3. In Figures 2 and 3 plots of the concentration ratios (cyclohexene)/(cyclohexyl chloride) vs. (cyclopentene)/(cyclopentyl chloride) and (cyclohexene)/(cyclohexyl chloride) vs. (cycloheptene)/(cycloheptyl chloride) at 408 and 422°, respectively, are given. The slopes of these lines are equal to k_6/k_5 and k_6/k_7 , respectively, where k_6 is the first-order rate constant for the decomposition of cyclohexyl chloride

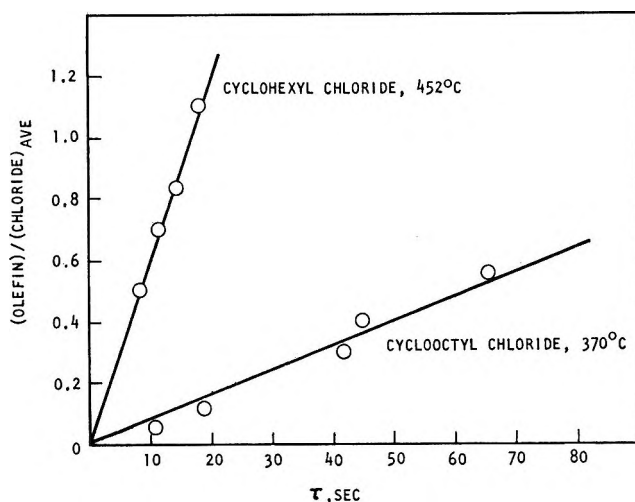


Figure 1. Concentration (olefin)/(chloride)_{ave} vs. τ for cyclohexyl and cyclooctyl chloride at 452 and 370°.

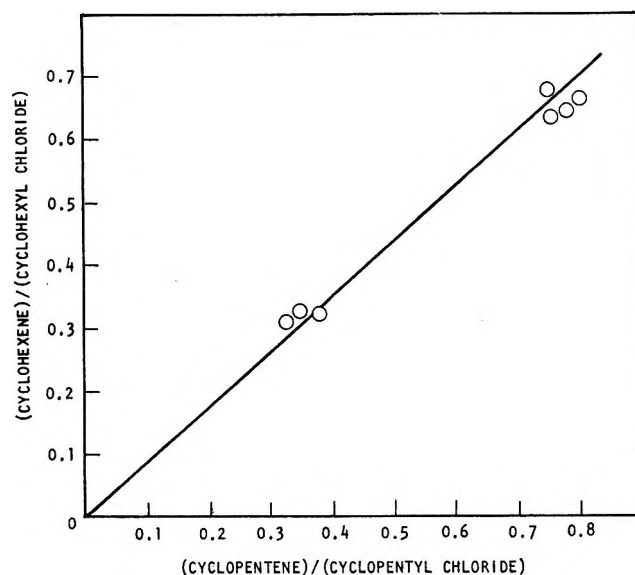


Figure 2. Concentration (cyclohexene)/(cyclohexyl chloride) vs. (cyclopentene)/(cyclopentyl chloride) at 408°.

and k_5 and k_7 are the respective rate constants for cyclopentyl and cycloheptyl chloride.

Table I gives the first-order rate constants, k_6 and k_8 , for the pyrolysis of cyclohexyl and cyclooctyl chloride, while the relative rates, k_6/k_5 and k_6/k_7 , for cyclohexyl chloride/cyclopentyl chloride and cyclohexyl chloride/cycloheptyl chloride are given in Table II. Figures 4 and 5 show plots of $\log k_6/k_5$ and $\log k_6/k_7$ vs. $1/T$ for cyclopentyl and cycloheptyl chloride, respectively.

The plots of the relative rates, k_6/k_5 and k_6/k_7 , result in relative Arrhenius parameters, *i.e.*, ΔE and $\Delta \log A$.

(10) "Beilstein Handbuch der Organischen Chemie," Band V, 450-498, p 29.

(11) S. A. Miller and W. O. Jones (to British Oxygen Co., Ltd.), Brit. 738, 992, Oct 26, 1955; *Chem. Abstr.*, 50, 10768f (1956).

(12) A. Maccoll, *Chem. Rev.*, 69, 33 (1969).

Table I: Rate Coefficients of Cyclohexyl Chloride and Cyclooctyl Chloride at Different Temperatures

Temp, °C	No. of runs	Average k_6 or $k_8 \times 10^2, \text{sec}^{-1}$	Std dev $\times 10^2, \text{sec}^{-1}$
Cyclohexyl Chloride			
350.0	17	0.018	0.006
385.0	15	0.18	0.01
413.8	11	0.81	0.03
438.8	13	3.2	0.4
452.2	18	5.9	0.2
475.8	18	15.5	0.9
Cyclooctyl Chloride			
370.3	22	0.75	0.13
371.5	28	0.86	0.10
380.0	5	1.93	0.08
405.5	5	4.6	0.2
423.6	5	11.7	0.5

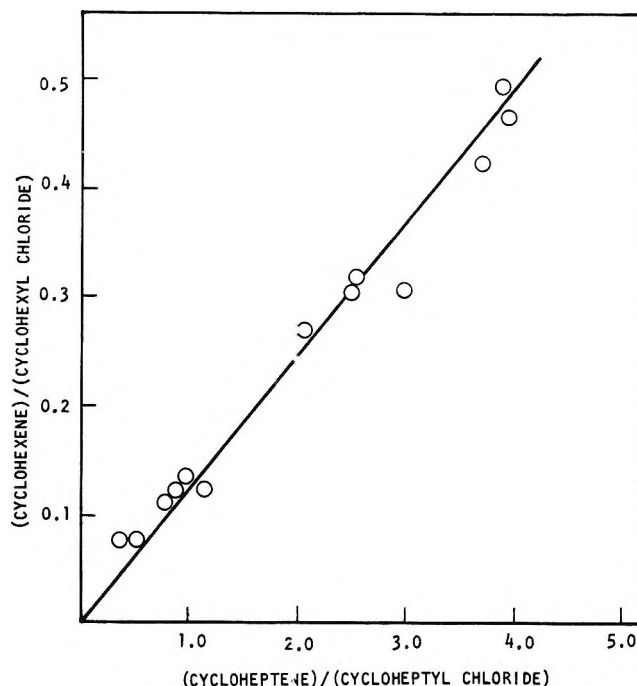
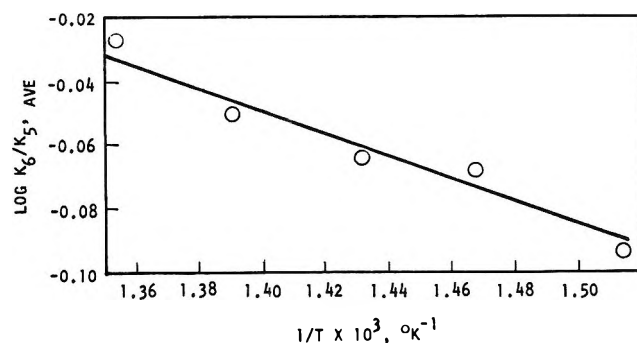
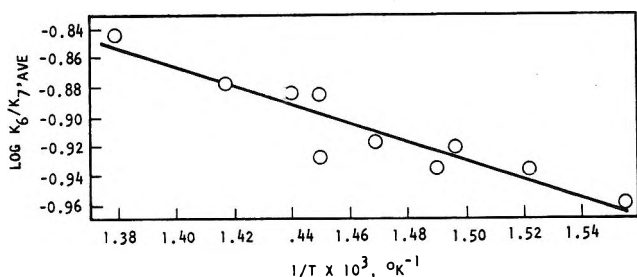
Table II: Relative Rate Coefficients for Cyclohexyl Chloride/Cyclopentyl Chloride and Cyclohexyl Chloride/Cycloheptyl Chloride at Different Temperatures

Temp, °C	No. of runs	Average k_6/k_5 or k_6/k_7	Std dev
Cyclohexyl Chloride/Cyclopentyl Chloride			
387.0	5	0.808	0.034
408.0	8	0.856	0.039
425.0	6	0.863	0.030
445.8	4	0.890	0.013
466.0	7	0.939	0.014
Cyclohexyl Chloride/Cycloheptyl Chloride			
370.4	7	0.109	0.007
384.0	5	0.115	0.004
395.4	4	0.119	0.001
398.3	8	0.116	0.004
407.6	8	0.121	0.020
416.6	6	0.130	0.008
416.7	3	0.121	0.005
421.6	14	0.130	0.017
431.9	6	0.132	0.019
452.0	6	0.143	0.015

Table III: Relative Arrhenius Parameters for Cyclohexyl Chloride/Cyclopentyl Chloride and Cyclohexyl Chloride/Cycloheptyl Chloride

Compound	$\Delta \log A$	$\Delta E, \text{cal/mol}$
Cyclohexyl chloride/cyclopentyl chloride	0.47 ± 0.06	$1,680 \pm 200$
Cyclohexyl chloride/cycloheptyl chloride	0.02 ± 0.10	$2,910 \pm 300$

These results are given in Table III. Table IV gives the Arrhenius parameters and entropy of activation, as determined by the least-squares procedure, for all of the chlorocycloalkanes studied during this investigation. The parameters for cyclopentyl chloride and cyclo-


Figure 3. Concentration (cyclohexene)/(cyclohexyl chloride) vs. (cycloheptene)/(cycloheptyl chloride) at 422°.

Figure 4. $\log k_6/k_{5, \text{AVE}}$ vs. $1/T$ for cyclohexyl chloride/cyclopentyl chloride.

Figure 5. $\log k_6/k_{7, \text{AVE}}$ vs. $1/T$ for cyclohexyl chloride/cycloheptyl chloride.

heptyl chloride were obtained by subtracting the relative Arrhenius constants ΔE and $\Delta \log A$ from E and $\log A$ for cyclohexyl chloride.

Swinbourne has studied the pyrolysis of both cyclopentyl and cyclohexyl chloride in a static system.^{13,14}

Table IV: Arrhenius Parameters and Entropies of Activation for the Pyrolysis of Chlorocycloalkanes

Compounds	Log <i>A</i>	<i>E</i> , cal	ΔS , gibbs/mol
Cyclopentyl chloride	13.44 ± 0.34	48,570 ± 1100	-0.73 ± 1.5
Cyclohexyl chloride	13.90 ± 0.28	50,250 ± 900	+1.42 ± 1.3
Cycloheptyl chloride	13.88 ± 0.38	47,340 ± 1200	+1.32 ± 1.7
Cyclooctyl chloride	13.16 ± 0.28	44,950 ± 900	-1.92 ± 1.3

He found $k_5 = 10^{13.47} \exp(-48,290/RT)$ sec⁻¹ for cyclopentyl chloride and $k_6 = 10^{13.77} \exp(-49,980/RT)$ sec⁻¹ for cyclohexyl chloride. Within experimental error, his results are the same as those found in this work (Table IV).

Discussion

If the procedure of O'Neal and Benson³ is applied to the cycloalkyl chlorides studied during this investigation it is seen that only about +0.2 gibbs/mol of activation entropy is contributed due to the changes in molecular vibrations in passing to the transition state. All other entropy contributions must come from changes in symmetry or from specific features of the individual activated complexes.

For cyclopentyl chloride an entropy contribution of $R \ln 2 = 1.37$ gibbs/mol would be predicted because of two equivalent nonsuperimposable structures for the transition complex. The experimentally obtained $\Delta S^\ddagger = -0.73$ gibbs/mol reflects partial freezing of the pseudorotation¹⁵ of the five-membered ring due to incipient double bond formation.¹⁶

In the case of cyclohexyl chloride an entropy contribution of $R \ln 2 = 1.37$ gibbs/mol would result from transition states with chlorine in the axial position, while an entropy contribution of $R \ln 4 = 2.75$ gibbs/mol is predicted for reaction of an equatorial chlorine atom. Presumably the two positions are nearly equivalent;

hence the observed $\Delta S^\ddagger = 1.42$ gibbs/mol appears slightly low, but certainly within experimental error of the predicted value, $R \ln 3 = 2.18$ gibbs/mol.

The larger C₇ and C₈ rings show considerable ring strain and the chlorine atom occupies the roomier equatorial positions. Hence for cycloheptyl chloride $\Delta S^\ddagger = R \ln 2$ in excellent agreement with the observed value, 1.32 gibbs/mol.

Cyclooctyl chloride is the smallest of the ring compounds whose pyrolysis offers the possibility of an olefin with *trans* configuration about the double bond. The loose cyclic transition state postulated above would favor the formation of the more unstable *trans*-cyclooctene¹⁷ with an attendant loss in entropy. Hence, the entropy contribution of $R \ln 2$ is more than overshadowed by partial formation of the *trans* isomer in the activated complex.

In summary, the loose cyclic transition state accounts very nicely for the results observed during this investigation and is favored over the polar transition state postulated by Maccoll.^{12,18,19} This is particularly true in light of the recent study by Field²⁰ which showed that the activation energies for the formation of benzyl ion and *t*-amyl ion from protonated benzyl acetate and protonated *t*-amyl acetate are identical, despite the fact that the solvolysis of *t*-C₄H₉Cl proceeds much more readily than does the solvolysis of C₆H₅CH₂Cl.

Acknowledgments. Gratitude is extended to the University of Mississippi and the National Science Foundation (G.P. No. 247) for their financial support.

(13) E. S. Swinbourne, *J. Chem. Soc.*, 4668 (1960).

(14) E. S. Swinbourne, *Aust. J. Chem.*, 11, 314 (1958).

(15) J. E. Kilpatrick, K. S. Pitzer, and R. Spitzer, *J. Amer. Chem. Soc.*, 69, 2483 (1947).

(16) O'Neal and Benson attribute the low *A* factor for cyclopentyl bromide to the complete freezing of the pseudorotation mode.³ We do not find this to be the case with cyclopentyl chloride.

(17) A. C. Cope, R. A. Pike, and C. F. Spencer, *J. Amer. Chem. Soc.*, 75, 3212 (1953).

(18) A. Maccoll and P. J. Thomas, *Nature*, 176, 392 (1955).

(19) A. Maccoll in "Theoretical Organic Chemistry," Butterworth and Co., Ltd., London, 1958.

(20) F. H. Field, *J. Amer. Chem. Soc.*, 91, 2827 (1969).

The Kinetics and Mechanism of the Thermal Decomposition of Nitroglycerin

by Chas. E. Waring and Gunar Krastins

Department of Chemistry, University of Connecticut, Storrs, Connecticut 06268 (Received August 9, 1969)

The thermal decomposition of nitroglycerin has been investigated in the vapor and liquid phases over a temperature range of 115–160°. Above 140° the decomposition in the vapor phase is first order but in the liquid phase the order is only approximately first. At all temperatures the rates were found to vary markedly with the ratio of the mass of nitroglycerin to the volume of the reactor. Below 140° the decomposition was autocatalytic. A mechanism is proposed for the vapor-phase reaction that is in agreement with the experimental data.

Introduction

The kinetics of the thermal decomposition of nitroglycerin have been the subject of considerable study. For the most part, the rate constants and order of reaction have been determined by manometric methods. Because of the complexity of the decomposition, this has resulted in irregularities in values of the kinetic constants. Roginskii,¹ for example, reports the reaction to be first order between 150 and 190°. At lower temperatures, the decomposition was found to be autocatalytic. Over three different temperature ranges extraordinarily high values for the frequency factor in the Arrhenius equation were obtained. This was explained as being due to the existence of chains. However, Roginskii's extensive study of the effects of known chain inhibitors on the rate of decomposition of nitroglycerin failed to substantiate their presence.

The autocatalytic decomposition of nitroglycerin has been studied also by Lukin² and more recently by Andreev and Glazkova³ and Gorbunov and Svetlov.⁴ These investigators found that certain oxides of nitrogen, water, and various acids increased the rate of decomposition.

Robertson,⁵ in a brief study on the thermal decomposition of nitroglycerin in the liquid phase, confirmed Roginskii's¹ results and concurred with the latter's explanation of the high-frequency factors and temperature dependency of the activation energy. Phillips,⁶ employing a manometric technique, obtained somewhat lower values for the frequency factor and activation energy for the liquid-phase decomposition than did Roginskii¹ and Robertson.⁵ Svetlov⁷ also investigated the thermal decomposition of nitroglycerin in the liquid phase between 80 and 140° using manometric methods. He noted that, at constant temperatures, different rates were obtained depending on the ratio of the mass of nitroglycerin to the volume of the reaction chamber.

From a review of the literature it is apparent that the thermal decomposition of nitroglycerin is a complex process and one that is sensitive to the conditions of the experiment. It is also evident that manometric studies alone are not in themselves adequate for deter-

mining the mechanism of this reaction. It was decided, therefore, to investigate the thermal decomposition of nitroglycerin using infrared techniques.

Experimental Section

A. Materials. The nitroglycerin used throughout this work was prepared and purified by the method described by Naoum.⁸ All gases employed in the studies on the effect of additives were obtained from commercial sources and were dried by standard methods. Nitric oxide was purified by cooling it to Dry Ice temperature to remove nitrogen dioxide and water.

B. Apparatus for Rate Studies. The apparatus used for studying the rate of decomposition of nitroglycerin vapor consisted of a 220-ml Pyrex flask equipped with side arms for introducing the sample, evacuating the flask, and introducing gaseous additions.

C. Apparatus for Product Analysis. The relatively large number of possible intermediates from the decomposition of nitroglycerin made it desirable to analyze for products throughout the entire course of the decomposition. This was done by the use of a Perkin-Elmer Model 21 double-beam infrared spectrophotometer. The reactor employed in this series of experiments was a 315-ml round-bottom Pyrex flask, equipped with side arms as previously described. A breakable capillary glass seal was used to transfer the decomposition products into the infrared absorption cell.

The infrared absorption cell used in the analytical work was equipped with calcium fluoride windows. Calcium fluoride was found to be inert toward all

- (1) S. Z. Roginskii, *Phys. Z. Sowjetunion*, **1**, 640 (1932).
- (2) A. Lukin, *Zh. Fiz. Khim.*, **3**, 406 (1932).
- (3) K. K. Andreev and A. P. Glazkova, *Dokl. Akad. Nauk SSSR*, **105**, 286 (1955).
- (4) V. V. Gorbunov and B. S. Svetlov, *Teor. Vzrychatykh Veshchestv*, **197** (1963).
- (5) A. J. B. Robertson, *Chem Ind. (London)*, **67**, 221 (1948).
- (6) L. Phillips, *Nature*, **160**, 753 (1947).
- (7) B. S. Svetlov, *Kinet. Katal.*, **1**, 38 (1961).
- (8) P. Naoum, "Nitroglycerine and Nitroglycerin Explosives," The Williams and Wilkins Co., Baltimore, Md., 1928, pp 27–29.

reaction products from the decomposition of nitroglycerin. The limited range of infrared transmittance of CaF_2 was of no concern since all the products determined exhibited absorption between 2 and 9 μ , the useful range of calcium fluoride. This was confirmed by the use of an NaCl cell in some runs.

D. Apparatus for High-Temperature Infrared Study. Because it was suspected that unstable intermediates might be formed in the decomposition of nitroglycerin, a high-temperature infrared absorption system was designed that would permit continuous recording of spectra during the course of the reaction. The system consisted of a small electrically heated oven with sodium chloride windows and a Pyrex absorption cell with calcium fluoride windows.

E. Procedure for Rate Studies. The rates of decomposition of nitroglycerin in both the vapor and liquid phases were determined by measuring the rate of disappearance of the nitrate groups. A sample of nitroglycerin was introduced into the reactor through the side arm and weighed. For safety reasons the maximum amount of NG used was about 0.2 g. The reactor was then evacuated through the side arm, which was subsequently sealed and immersed in a constant-temperature oil bath. Small, experimentally determined corrections were made for the time required to reach the temperature of the bath. The liquid-vapor equilibrium was reached very rapidly, as evidenced by the absence of liquid residue a short time after immersion, if a sufficiently small sample was used.

At the desired time, the reactor was removed from the bath and quenched in cold water. The residual nitroglycerin in the vapor phase was observed to condense on the walls of the reactor. The seals were broken and the reactor flushed with air to remove the gaseous decomposition products. Because of the low vapor pressure of nitroglycerin at room temperature, none of it was removed by this procedure.

The liquid residue was dissolved into a weighed amount of chloroform and introduced into a 0.050 mm thick infrared absorption cell. The concentration of the decomposed nitrate was determined from the intensity of the absorption peaks at 1280 and 1670 cm^{-1} . A calibration curve was prepared of known concentrations of solutions of pure nitroglycerin in chloroform.

This method of analysis does not, of course, enable one to distinguish between the two different nitrate groups, either quantitatively or qualitatively. Only a single, sharp absorption peak was observed at 1670 cm^{-1} , indicating the same absorption frequency for both groups. It was assumed that both nitrate groups exhibit the same absorptivity. This assumption is based on the experimental evidence that solutions of nitroglycerin, ethylene glycol dinitrate, and propyl nitrate⁹ exhibit the same absorptivity if the concentrations are expressed in the number of nitrate groups per unit volume.

It was considered that the spectrographic method had two distinct advantages over the manometric methods employed by previous investigators. First, the absolute rate of disappearance of the nitrate groups could be determined directly, and second, an accurate study of the decomposition of small amounts of nitroglycerin was possible. This made possible the rate studies in the vapor phase.

F. Procedure for Product Analysis. The analyses of the gaseous decomposition products were made by placing 0.063-g samples of nitroglycerin in the 315-ml reactor which was then evacuated, sealed, and immersed in the constant-temperature bath. At the desired time the reactor was removed and quenched in cold water. The gaseous decomposition products were transferred to an infrared absorption cell, and the pressure was measured. The total pressure of the system was then brought to 1 atm with helium, and the infrared spectrum of the products was recorded. The cell was pressurized with helium because the presence of an inert gas intensified the absorption bands of small molecules, thus aiding in the determination of minute quantities of components, and because at low pressures the presence of other products exhibits sufficient pressure effects to cause appreciable error in the quantitative determination of any component.

Carbon monoxide and nitric oxide were determined from the R branches of the 2143 and the 1876- cm^{-1} vibrational bands, respectively. A calibration curve was prepared for both species. The less intense P branch was used for the determination of CO whenever more than just a trace of nitrous oxide was present, because part of the N_2O absorption band coincides with the R branch of CO.

Carbon dioxide was determined from the height of the absorption band at 2350 cm^{-1} .

Nitrogen dioxide was determined from the height of the P branch of the 1620- cm^{-1} vibrational band. The amount of nitrogen tetroxide present was calculated by means of the Verhoek and Daniels¹⁰ expression.

Formic acid was found to be present in very small quantities and was estimated by comparing the absorption peak at 1105 cm^{-1} with prepared standards.

Traces of formaldehyde were observed among the decomposition products but no quantitative determination was attempted because most of the formaldehyde was found to have polymerized to paraformaldehyde on the walls of the reactor.

The sum of the pressures of the individual components was found always to be slightly lower than the measured total pressure. However, the deviation was less than 4%, indicating that only minute amounts of products were unaccounted for.

(9) J. B. Levy and F. J. Adrian, *J. Amer. Chem. Soc.*, **77**, 2015 (1955).

(10) F. H. Verhoek and F. Daniels, *ibid.*, **53**, 1250 (1931).

G. Procedure for High-Temperature Infrared Study.

In this investigation 5–10 mg of nitroglycerin was introduced into the high-temperature absorption cell, and the system was brought to temperature. A continuous scanning of the spectrum was made between 2 and 9 μ .

In this series of experiments the decomposition of nitroglycerin was studied at 132, 140, 145, and 150°. The possibility of autocatalytic effects was essentially eliminated by employing very low mass to volume ratios.

H. Manometric Study. Manometric investigations of the thermal decomposition of nitroglycerin were limited to the low-temperature, autocatalytic reaction. For this, a reaction flask of 216 ml capacity was thermostated and connected to a high-vacuum system. Pressures were measured by a quartz Bourdon gauge.

Results

1. Effect of Mass:Volume Ratio on Rate. The rate of decomposition of nitroglycerin is strongly dependent upon the mass of nitroglycerin and the volume of the reaction vessel in which it is decomposed. Thus, it was found useful to express sample concentrations in terms of the ratio of the mass of nitroglycerin to the volume of the reactor, or the mass:volume (M/V) ratio. Figure 1 shows the effect of the M/V ratio on the rate of decomposition of nitroglycerin at 160°. It is noted that under vacuum the rate falls sharply until a M/V ratio of $20 \times 10^{-4} \text{ g cm}^{-3}$ is reached. Above this value, the rate is independent of the ratio.

It can also be seen that NO_2 strongly inhibits the rate of decomposition at low M/V ratios but is ineffective at higher ratios. It is noted, too, that the inhibited rates at low and high M/V ratios are approximately the same. The inhibiting effect of oxygen is probably due to the oxidation of nitric oxide, which is one of the major decomposition products of nitroglycerin, thus increasing the concentration of nitrogen dioxide.

Figure 2 presents the significant inhibiting effects of relatively small amounts of NO_2 on the rate of decomposition in the vapor phase at 160°. At this NG concentration ($4 \times 10^{-4} \text{ g cm}^{-3}$) a large fraction of the decomposition takes place in the vapor phase.

The possibility that surface effects, causing heterogeneity, might be responsible for the M/V ratio effect led to a study on the influence of surfaces. Such effects were found to be negligible. A threefold change in the surface:volume ratio resulted in no measurable change in rate over a M/V range from 0.5 to $40 \times 10^{-4} \text{ g cm}^{-3}$. In addition, concentrated KOH was refluxed in the reaction vessel for 24 hr in an attempt to alter the surface. No change in the rate was observed.

2. Order of Reaction. **A. Vapor Phase.** Before investigating the order of the vapor-phase decomposition it was necessary to determine the approximate

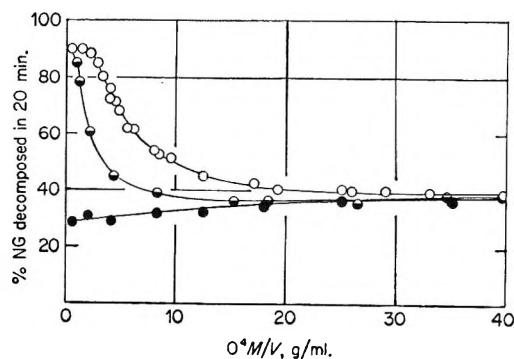


Figure 1. Effect of mass: volume ratio on the rate at 160°: O, vacuum; ◐, 1 atm of O_2 ; ●, 1 atm of NO_2 .

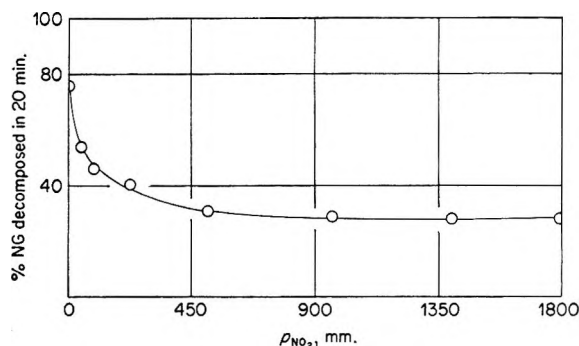


Figure 2. Effect of NO_2 on the rate of decomposition at 160° ($M/V = 4 \times 10^{-4} \text{ g cm}^{-3}$)

vapor pressure of nitroglycerin. This was accomplished by plotting the pressure increase of the decomposition products against time and extrapolating to zero time. The vapor pressure of nitroglycerin was observed to be approximately 17 mm at 160° and 8 mm at 150°. These values are in fair agreement with those obtained by extrapolating the low-temperature data reported by Marshall and Peace.¹¹

By means of the ideal gas law, which was considered a reasonable approximation at these temperatures and pressures, the saturated vapor pressure of nitroglycerin in a 220-ml reactor at 160° corresponds to a M/V ratio of $1.4 \times 10^{-4} \text{ g cm}^{-3}$. The corresponding values for the saturated vapor at 155 and 150° are 1.0×10^{-4} and $0.7 \times 10^{-4} \text{ g cm}^{-3}$, respectively. Therefore, in the determination of the order of the vapor phase decomposition, it was necessary to keep the M/V ratios well below these saturation values in order to assure immediate vaporization and to minimize the effects of decomposition products, such as nitrogen dioxide.

The decompositions were all carried out to the same extent (about 35 and 55%) at all temperatures. The fact that the rate constants were essentially identical over a range of M/V ratios of 0.4–1.2 supports negligible inhibition of the decomposition by the decomposition products in this range.

(11) A. Marshall and G. Peace, *J. Chem. Soc.*, 109, 298 (1916).

The order of the vapor-phase decomposition of nitroglycerin was determined by spectroscopically measuring its rate of disappearance with time. The data presented in Table I are seen to yield first-order rate constants with good consistency when calculated by the usual equation

$$k = \frac{2.3}{t} \log \frac{a}{a-x} \quad (1)$$

Table I: Determination of the Order of the Vapor-Phase Decomposition of Nitroglycerin at Several Temperatures

$10^4 M/V$, g cm^{-3}	Time, sec	% decompn	$10^4 k$, sec^{-1}
160.0°			
1.11	300	52.0	24.4
0.80		52.9	25.0
0.52		53.2	25.3
0.41		53.9	25.8
1.21	180	34.6	23.6
0.92		35.9	24.7
0.67		36.0	24.8
0.39		35.4	24.3
		Av	24.7
155.0°			
0.96	540	54.8	14.7
0.86		55.7	15.1
0.56		56.6	15.4
0.30		54.9	14.7
0.59	300	37.5	15.6
0.56		38.6	16.1
0.47		38.8	16.2
0.33		37.8	15.6
		Av	15.4
150.0°			
0.63	900	55.3	9.0
0.60		55.0	8.9
0.53		54.6	8.8
0.37		56.0	9.1
0.59	450	36.8	10.1
0.53		35.1	9.5
0.53		34.6	9.4
0.37		33.9	9.2
		Av	9.25

B. Liquid Phase. It has been previously reported² that above 140° the liquid-phase decomposition of nitroglycerin followed the first-order rate law. This assumption was made on the basis that the rate of pressure increase from decompositions in dilute solutions was approximately the same as that of pure nitroglycerin.

In the present study, the order of the liquid-phase decomposition was determined from rate measurements at an M/V ratio of $35 \times 10^{-4} \text{ g cm}^{-3}$. At this sample loading the fraction of nitroglycerin decomposing in the vapor phase is small. It can be readily shown from the vapor pressure of nitroglycerin and from the vapor- and

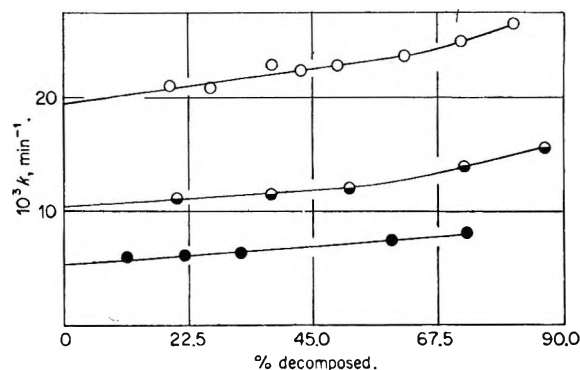


Figure 3. Variation of the first-order rate constant with per cent NG decomposed: O, 160°; ◐, 155°; ●, 150° ($M/V = 35 \times 10^{-4} \text{ g cm}^{-3}$).

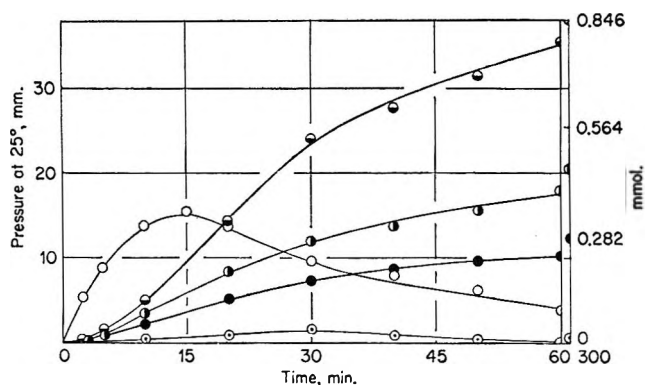


Figure 4. Variation of products of decomposition with time at 160° for a 0.282-mmol sample of NG: O, NO_2 ; ◐, NO ; ●, CO ; ●, CO_2 ; ◐, HCOOH ($M/V = 2 \times 10^{-4} \text{ g cm}^{-3}$).

liquid-phase rate constants (Table I and Figure 3, respectively) that at 160° the initial fraction of decomposition taking place in the vapor phase is 24%. Based on the data presented in Figures 2 and 4, however, the vapor phase rate is very rapidly inhibited to a liquid-phase value, and only 5–10% of the decomposition will take place in the vapor phase. Because at 150° the vapor pressure is only half of the 160° value, the fraction decomposing in the vapor phase will be correspondingly smaller.

In the liquid phase, the first-order rate law was found to be obeyed only approximately. Figure 3 shows that there is a gradual increase in the first-order rate constants as the reaction proceeds. This is considered to be due to small autocatalytic effects. The increase is not caused by a proportionally larger fraction of the decomposition taking place in the vapor phase, because at as low as 10% decomposition of the sample, the vapor-phase rate is nearly fully inhibited, based on Figures 2 and 4, and at 20% decomposition the rates in both phases are equal.

3. Energy of Activation. A. Vapor Phase. From the rate constants in Table I at the various temperatures the Arrhenius equation is found to be

$$k = 3.2 \times 10^{15} e^{-36,000/RT} \text{ sec}^{-1} \quad (2)$$

B. Liquid Phase. It was noted in Figure 3 that the first-order rate constants exhibited a gradual increase as the reaction proceeded. The rate constants were extrapolated to zero time. The resulting values were taken as the true rate constants. At the M/V ratio of $35 \times 10^{-4} \text{ g cm}^{-3}$ the Arrhenius equation is

$$k = 1.6 \times 10^{20} e^{-46,900/RT} \text{ sec}^{-1} \quad (3)$$

The marked difference between the rate expressions for the vapor and liquid phases is immediately apparent.

4. Product Analysis. The results of the analyses of the decomposition products at 150 and 170° are shown in Table II. Figure 4 is a graphical presentation of the

Table II: Analysis of Decomposition Products of Nitroglycerin at 150 and 170° ($M/V = 2 \times 10^{-4} \text{ g cm}^{-3}$)

Time, min	Pressure at 25°, mm					% NG decompm
	CO	CO ₂	NO	NO ₂	HCOOH	
	150°					
10	Trace	Trace	Trace	4.7	...	22
15	1.0	0.6	2.0	6.3
20	1.5	1.0	2.4	7.7	...	40
25	2.0	1.4	3.5	9.0
30	3.0	2.0	4.5	9.4	Trace	58
40	4.3	2.7	8.2	10.0	Trace	68
45	6.7	3.8	9.5	10.7	0.4	...
50	6.2	4.4	10.4	11.7	0.5	79
55	7.0	4.7	16.0	10.8	1.5	...
60	8.0	5.5	16.0	9.9	1.7	83
70	10.0	6.4	17.8	10.8	1.5	...
80	11.2	6.4	25.5	8.3	1.8	90
120	15.0	9.8	29.3	7.5	0.7	...
180	15.1	9.9	33.5	4.0	0.5	...
200	16.5	10.5	34.5	3.8	0.6	...
1100	20.7	13.1	37.1	0.5	Trace	...
	170°					
1	1.0	0.6	1.5	7.2	...	28
2	2.0	1.5	2.5	10.0	...	49
3	13.7
5	5.0	3.2	9.5	17.5	0.4	78
7	8.5	5.5	13.5	18.3	0.4	...
8	16.7
10	10.2	6.8	21.5	13.2	1.3	92
15	13.1	8.4	30.0	6.5	1.7	97
20	15.0	9.2	30.5	6.3	0.7	...
30	17.0	10.4	33.5	4.9	Trace	...
45	19.1	11.0	36.0	3.4
60	19.3	11.5	38.4	2.2

data obtained at 160°. These curves are also typical of the other two temperatures.

Upon examining Table II it is noted that the final products of decomposition are CO, CO₂, and NO. The evolution of these products takes place at an approximately constant ratio of 3:2:6 throughout the reaction. It is also clear from Figure 4 that NO₂ is an

intermediate. The total amount of oxides of nitrogen found accounts for all the nitrogen present in the nitroglycerin sample. The sum of the CO and CO₂, however, account for only about 85% of the original carbon present. This carbon discrepancy is explained by the presence of formaldehyde which condensed to solid paraformaldehyde when the reaction vessel was cooled to room temperature. The white solid was volatilized and identified as formaldehyde in the high-temperature infrared cell. No attempt was made to determine the formaldehyde quantitatively.

The only evidence for the presence of water was the two weak absorption bands at 3600 and 3700 cm⁻¹, also observed in the high-temperature infrared studies. Since the sum of the partial pressures of the products was always essentially identical with the measured total pressure, it was assumed that the inability to detect water was due to its interaction with the decomposition products. The inability to observe absorption peaks of water is consistent with the results of a limited study of the decomposition of ethylene glycol dinitrate and the oxidation of formaldehyde with nitrogen dioxide, both of which almost certainly yield water.

5. High-Temperature Infrared Investigation. The high-temperature infrared analysis of the decomposition products and intermediates was only semiquantitative. Its chief value was to provide information as to the sequence of product evolution. The nonquantitative limitation was due to the lack of information on the absorption intensities of the corresponding compounds at elevated temperatures in the presence of other gases. Attempts to prepare calibration curves presented difficulties because the intensities of absorption were found to be temperature and pressure dependent.

An examination of the spectra recorded during the course of the decomposition of nitroglycerin at 150° reveals that only nitrogen dioxide is evolved during the initial stage of the reaction. This is almost immediately followed by the appearance of formaldehyde. Shortly thereafter the absorption peaks of CO, CO₂, and NO appear simultaneously. Traces of N₂O are formed in the latter stages of the reaction. The two small peaks at 3600 and 3700 cm⁻¹ were attributed to water. These were the only compounds identified during the decomposition of nitroglycerin at 150°. The only unidentified peak in the spectrum was a very small band at about 1780 cm⁻¹.

6. Autocatalytic Decomposition. The investigation of the autocatalytic decomposition of nitroglycerin was limited to manometric studies of the effect of various decomposition products on the rate at 115 and 120°. At these temperatures the vapor pressure of nitroglycerin is negligible and the decomposition takes place in the liquid phase. Figure 5 presents a comparison of the rate of decomposition in a vacuum with rates in the

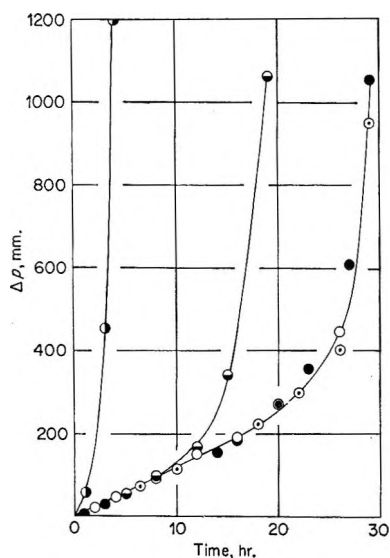


Figure 5. Effect of 300 mm of various additives on the rate of decomposition of NG at 120°: O, vacuum; ⊙, He; ●, NO; ⊕, O₂; ⊗, H₂O.

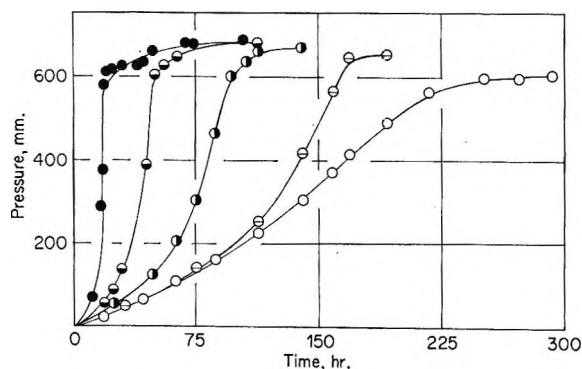


Figure 6. Effect of NO₂ on the rate of decomposition of NG at 115° ($M/V = 8 \times 10^{-4} \text{ g cm}^{-3}$): O, vacuum; ⊙, 55 mm; ⊕, 150 mm; ⊕, 350 mm; ●, 800 mm.

presence of various additives at a M/V ratio of $46 \times 10^{-4} \text{ g cm}^{-3}$.

The curves indicate that helium and nitric oxide have no effect upon the rate, whereas oxygen and water vapor produce a considerable acceleration. The rate of decomposition of nitroglycerin was also found to be unaffected by the presence of nitrogen and carbon dioxide.

The effect of NO₂ on the rate of decomposition was determined at a M/V ratio of $8 \times 10^{-4} \text{ g cm}^{-3}$. The results are shown in Figure 6. Again, it is seen that NO₂ exerts a marked accelerating effect and that there is a pronounced incubation period. This behavior is in sharp contrast with the inhibiting effect that NO₂ produces at temperatures above 140°.

There is some evidence to suggest that other decomposition products, besides nitrogen dioxide and water, may also be responsible for the autocatalytic effects. A spectroscopic examination of the liquid

residue of partially decomposed nitroglycerin revealed the simultaneous appearance of absorption bands at 1750 and 3600 cm^{-1} . The band at 3600 cm^{-1} was very sharp during the initial stage of the reaction but broadened and shifted toward lower frequency as the decomposition proceeded. The sharp, high-frequency absorption was assigned to the free O-H vibration and the broadening effect was attributed to hydrogen bonding between the carboxyl groups. This had the effect of reducing the O-H strength and consequently lowering the vibrational frequency. Flushing the liquid residue with a stream of air for 24 hr failed to reduce the original intensities of these bands, indicating that the acid responsible for these absorptions was non-volatile.

Discussion

The results of this investigation show that the thermal decomposition of nitroglycerin is both complicated and unusual in several ways. First, the reason for the marked difference between the rate expressions for the liquid and vapor-phase decompositions is not immediately apparent. Examination of eq 2 and 3 shows that the apparent activation energy for the liquid-phase decomposition is some 11,000 cal/mol higher than that of the vapor. While such a large difference between the gas- and liquid-phase reaction energies is not unprecedented, it is, nevertheless, unusual. More unexpected is the magnitude of the frequency or entropy factor. The natural inclination is to attempt an explanation in terms of compensating errors. This view, however, would be difficult to reconcile with the fact that comparable high-frequency factor values have been obtained for the decomposition of organic nitrates by other investigators, as seen in Table III. To assume that the same compensating errors of the same magnitude occurred in all of these studies would be somewhat arbitrary.

The other question that arises is why the rate of decomposition is so sensitive to changes in the M/V ratio. The data presented suggest that this and the former anomaly may not be unrelated. The results

Table III: Comparison of Arrhenius Constants for the Thermal Decomposition of Several Organic Nitrates

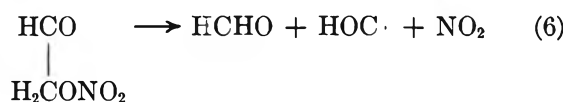
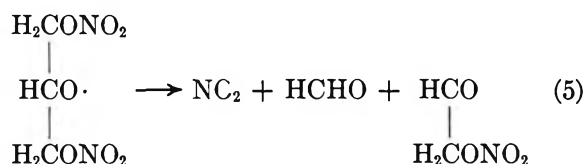
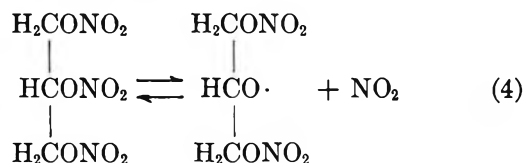
Nitrate	Temp, °C	Log A	E_a kcal/ mol	Phase
Ethylene glycol ⁶	85-105	15.9	39.0	Gas
Nitroglycerin ⁶	75-105	17.1	40.3	Liquid
Nitroglycerin ¹	90-125	18.0	42.6	Liquid
Nitroglycerin	125-150	19.2	45.0	Liquid
Nitroglycerin	150-190	23.3	50.0	Liquid
Pentaerythritol tetranitrate ⁶	161-233	19.8	47.0	Liquid
Pentaerythritol tetranitrate ⁵	171-238	16.1	39.5	5% soln

clearly show that the rate of decomposition of nitroglycerin in the liquid phase is appreciably slower than that in the vapor. In Figure 1, it can be seen that the rate of decomposition under vacuum at 160° is fairly constant over a M/V ratio from 0 to 1.5×10^{-4} g cm⁻³. In this range the decomposition occurs solely in the gas phase. From 1.5×10^{-4} to 20×10^{-4} g cm⁻³ a sharp decrease in rate is noted. Over this range, nitroglycerin is decomposing in both the vapor and the liquid phases, and, as Figures 1 and 2 clearly show, the decomposition in the vapor phase is becoming more and more inhibited by the nitrogen dioxide produced. At M/V ratios above 20×10^{-4} g cm⁻³ the reaction is occurring primarily in the liquid phase. The liquid-phase decomposition is fully self-inhibited and no further change in rate occurs. That this is, indeed, the case is evidenced by the fact that the addition of 1 atm of nitrogen dioxide produces no further reduction in rate in the liquid-phase decomposition range. It would appear, therefore, that the effect of the M/V ratio on the rate is simply due to varying degrees of inhibition of the decomposition by NO₂. In the vapor phase, $0-1.5 \times 10^{-4}$ g cm⁻³, the concentrations of nitroglycerin are very low, and hence the amount of nitrogen dioxide formed is correspondingly too small to produce any measurable inhibition. The rates thus are independent of sample loading and under these conditions the kinetics of the reaction are normal. As the M/V ratio increases, the per cent of nitroglycerin decomposing in the liquid phase steadily increases. Since the nitrogen dioxide produced within the liquid undergoes many collisions before escaping into the vapor phase, its opportunity for an effective, inhibiting collision is greatly enhanced. Consequently, as the ratio of liquid to vapor is increased, the rate decreases until a limiting value is reached.

The situation described above is somewhat analogous to many gas-phase reactions in which the rate of decomposition can be reduced to a limiting value by the addition of small quantities of nitric oxide or propylene. In such cases, it is found that the activation energy of the fully inhibited reaction is generally about 10 kcal/mol higher than that of the uninhibited process. The frequency factor for the fully inhibited reactions, however, is usually no greater than two powers of ten over the uninhibited. The apparent increase in the energy of activation in the liquid-phase decomposition cannot be adequately explained by an increase of the fraction of vapor-phase decomposition (with faster rates) as the temperature increases, because at the high M/V ratio the decomposition products rapidly build up to a concentration which fully inhibits the vapor-phase reaction. It is suggested, however, that a lower temperature dependency of the inhibiting effects of nitrogen dioxide in the liquid-phase decomposition may be a considerable factor contributing to the large apparent energy of activation, which in turn necessitates a high apparent frequency factor to account for the experi-

mental rate. This may be due to either a lower activation energy of the reverse process of the first decomposition step, or to an increase of the rate of escape of the nitrogen dioxide from the liquid phase with temperature.

From the data available it is not possible to write a complete mechanism for this complicated decomposition. The results of this investigation, however, do permit the postulation of a mechanism which can account for the major products from the vapor-phase decomposition of nitroglycerin



The rupture of the O-N bond in step 4 to form a radical and NO₂ is generally agreed to be the initial step in all organic nitrate decompositions. This step is reversible, as indicated by the inhibitive effect of added NO₂. The fact the decomposition of the nitrate groups follows first-order kinetics throughout the reaction suggests that step 4 is also the rate-determining step and that all further steps involving the removal of nitrate groups take place at a faster rate. This is further supported by the fact that no frequency shift of the nitrate absorption band has been observed during the course of the vapor-phase decomposition.

The possibility exists that the initial step might occur through the loss of a nitrate group at the 1 or 3 position. This is unlikely in view of the fact that the stability of a nitrate group has been found to be markedly decreased by the presence of another nitrate group in the vicinal position. Thus, the middle nitrate group in nitroglycerin, having two vicinal groups, would be expected to be less stable. Further, partial nitration of glycerol gives 1,3- and 1,2-glycerol dinitrates in a ratio of 93:7,¹² suggesting a greater stability of the 1,3 compound.

(12) W. Will, *Ber. Deut. Chem. Ges.* **41**, 1107 (1908).

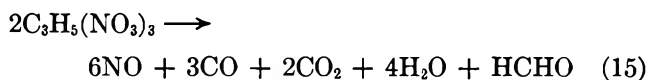
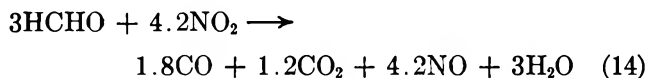
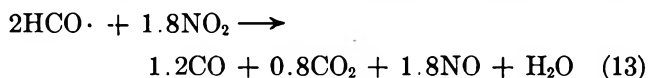
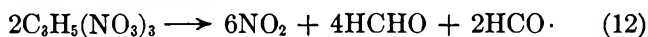
In step 5, the simultaneous rupture of the C-C and O-N in the radical is shown since it is impossible to tell which breaks first. In either case, one would be expected to follow the other immediately. This step is confirmed by the fact that only formaldehyde is observed immediately after the appearance of nitrogen dioxide.

According to the general mechanism for the decomposition of organic nitrates proposed by Adams and Bawn¹³ and Phillips,⁶ step 5 would be the removal of a hydrogen atom from another molecule, forming 1,3- and 1,2-glycerol dinitrates. Such a mechanism is ruled out in the present case since these compounds are relatively stable at 150°, as evidenced by the fact that they can be successfully distilled at this temperature.

Step 6 represents a further degradation of the molecule. This is probably the most uncertain step, and is suggested because it explains the nature and relative ratios of the reaction products.

Steps 7-11 represent the mechanism for the oxidation of formaldehyde by nitrogen dioxide. This mechanism is essentially that of Thomas,¹⁴ who proposes this as the only plausible one that accounts for all the experimental facts observed in the oxidation of formaldehyde, acetaldehyde, and glyoxal with nitrogen dioxide. The ratio of the rates of steps 10 and 9 is assumed to be 3:2 in order to account for the observed CO:CO₂ ratio.

On the basis of the proposed mechanism the overall reaction for the decomposition of nitroglycerin vapor may be written as



The decomposition of nitroglycerin in the liquid phase at temperatures below 140° has been shown by this and other investigators to be autocatalytic. A reasonable

explanation of this effect is a nitric acid catalyzed hydrolysis of the ester. It is suggested that nitric acid is formed according to



As the temperature increases, this equilibrium would be shifted farther and farther to the left. Thus, at temperatures above 140°, the reaction proceeds entirely to the left and the decomposition of nitroglycerin is no longer catalyzed by nitric acid but is inhibited by nitrogen dioxide.

The following facts support this assumption. Dry nitrogen dioxide exhibited a considerably smaller accelerating effect than the wet gas. This argues that since no moisture is present initially, the autocatalytic reaction could not proceed until some water was formed by way of steps 4-11. Similarly, when water was employed as a catalyst, no accelerating effects were noted until some nitrogen dioxide had been formed. Consequently, an incubation period occurred in both instances. No incubation period was observed, however, when nitrogen dioxide was introduced after the reaction had been allowed to proceed for 48 hr. By this time, sufficient water had been formed to catalyze the reaction fully.

The catalytic effects of oxygen at low temperatures in contrast to inhibiting effects above 140° are explained by the oxidation of NO to NO₂. An examination of Figure 5 reveals that initially the rates of decomposition in oxygen and helium are identical. This is also in agreement with the above assumption since the amount of NO formed during the initial stage of the reaction is negligible.

A nitric acid autocatalyzed mechanism for the decomposition explains, in part, why nitroglycerin-containing materials sometimes detonate in storage.

Acknowledgments. The authors are grateful to the Research Department of the Naval Propellant Plant, Indian Head, Md., for the use of their facilities during part of this study.

(13) C. K. Adams and C. E. H. Bawn, *Trans. Faraday Soc.*, **45**, 494 (1949).

(14) J. H. Thomas, *ibid.*, **49**, 630 (1953).

The Kinetics of the Thermal Decomposition of 1,1,1-Trifluoroacetone

by Chas. E. Waring and Alexander J. Fekete¹

Department of Chemistry, University of Connecticut, Storrs, Connecticut 06268 (Received August 13, 1969)

The thermal decomposition of 1,1,1-trifluoroacetone (TFA) has been investigated in a static system between 545 and 600° over initial pressures from 10.6 to 134.8 mm. The order of the reaction was found to be 1.3 both by initial rate measurements and by the rate of disappearance of TFA itself. The order for the rate of formation of such products as CF₃H, CF₃CH₃, and CF₂CH₂, however, was found to be unity. The Arrhenius parameter for the TFA decomposition is given by $k_0 = 3.6 \times 10^{15} e^{-55,200/RT} M^{-0.3} \text{ sec}^{-1}$ while that for CF₃H is $1.5 \times 10^{12} e^{-59,400/RT} \text{ sec}^{-1}$, that for CF₃CH₃ is $1.4 \times 10^{11} e^{-58,600/RT} \text{ sec}^{-1}$, and that for CF₂CH₂ is $1.8 \times 10^{15} e^{-72,000/RT} \text{ sec}^{-1}$. The decomposition of TFA was also investigated in the presence of various foreign gases, one of which inhibited the reaction while the others produced marked catalysis. From a knowledge of the products from the uninhibited and inhibited decompositions a mechanism is proposed to account for the predominant reactions. The activation energies of several of these reactions are evaluated by use of the Arrhenius equations given above.

Introduction

The photolysis of 1,1,1-trifluoroacetone (TFA) was first investigated by Sieger and Calvert,² who found the major reaction products to be CO, CH₄, CF₃H, C₂H₆, CF₃CH₃, and C₂F₆. No CH₃F, CF₄, HF, or F₂ was observed. More recently, Dawidowicz and Patrick³ reinvestigated the TFA photolysis and while they were not in agreement with the mechanism proposed by Sieger and Calvert, they reported the same products of reaction in essentially the same amounts as the earlier investigators.

Although Clark and Pritchard⁴ determined the Arrhenius parameters of TFA by thermally decomposing a mixture of 1% of this compound in toluene at 840°, they made no attempt to study the kinetics and mechanism of the pyrolysis. The purpose of this research, therefore, was to study the kinetics and mechanism of the thermal decomposition of TFA and to compare the reactions of the CF₃ radical with those of the CH₃ radical under similar conditions. It was also thought worthwhile to examine the effect of well-known methyl radical inhibitors on the trifluoromethyl radical.

Experimental Section

A. Apparatus. The thermal decomposition of TFA was studied in a static system employing a spherical quartz reaction flask of 176-ml capacity. This was heated in an electric furnace whose temperature was controlled to within $\pm 0.1^\circ$ in the area of the reaction zone. To prevent condensation, the lines from the furnace, including stopcocks, were wrapped with electrical heating tape and maintained at a constant temperature of 75°.

The reaction system was evacuated by the usual techniques and no run was made unless the pressure in the system was 10^{-5} mm or less, as measured by a McLeod gage. Pressures were measured by an Atco-tran transducer unit, also maintained at 75°, in con-

junction with a modified Leeds-Northrup Speedomax recorder. Before each run the vacuum line was flamed out to eliminate the possibility of oxygen contamination.

A Toepler pump attached directly into the line was employed to remove the gaseous reaction products. Analyses were made on a vapor fractometer and a mass spectrometer.

B. Materials. The 1,1,1-trifluoroacetone used in this study was obtained from Merck Sharp and Dohme. Its purity, as established by a Perkin-Elmer Model 154D vapor fractometer, was 99%. Tetrafluoromethane, 1,1-difluoroethane, 1,1,1-trifluoroethane, trifluoromethane, and hexafluoroethane, obtained commercially, were found to have a purity of 99%—except tetrafluoromethane which was 95%. Since these compounds were used for identification purposes, they were employed without further purification.

1,1,1-Trifluoropropane and 1,1,1-trifluoropropene were synthesized by the method of Hasek, Smith, and Engelhardt⁵ by allowing the corresponding carboxylic acids to react with sulfur tetrafluoride in a 75-ml stainless steel container for 8–48 hr. The products were removed and treated with KOH solution to remove the excess SF₄. Final purification and isolation was accomplished with the vapor fractometer.

Results

1. Nature of the Decomposition. TFA was found to decompose at a conveniently measurable rate between 545 and 600° and at initial pressures from 10.6 to

(1) Presented in partial fulfillment of the requirements for the Ph.D. degree at the University of Connecticut, June 1967.

(2) R. A. Sieger and J. G. Calvert *J. Amer. Chem. Soc.*, **76**, 5197 (1954).

(3) E. A. Dawidowicz and C. R. Patrick, *J. Chem. Soc.*, 4250 (1964).

(4) D. Clark and H. O. Pritchard, *ibid.*, 2136 (1956).

(5) W. R. Hasek, W. C. Smith and V. A. Engelhardt, *J. Amer. Chem. Soc.*, **82**, 543 (1960).

Table I: Change in Pressure with Time for Various Initial Pressures of TFA at 546.2°

<i>t</i> , sec	<i>p</i> _i , mm							
	23.0	47.7	54.5	69.3	99.5	115.2	134.8	141.3
30	23.3	48.4	55.6	70.3	101.5	117.3	137.5	146.1
60	23.7	49.4	56.6	72.0	103.9	120.4	141.3	150.2
120	24.0	51.1	59.0	74.8	108.7	125.5	147.5	156.1
180	24.7	52.5	61.1	76.8	111.8	129.7	151.9	160.5
240	25.0	53.9	62.4	78.5	114.9	133.8	156.4	164.6
300	26.1	55.2	63.5	80.3	117.6	136.9	159.5	168.1
540	27.4	58.7	68.3	86.1	126.2	147.8	170.8	179.1
780	29.8	61.7	71.7	90.2	133.4	156.8	179.4	188.7
1020	30.9	64.3	75.1	94.3	139.3	164.6	187.3	196.9
1260	33.3	67.5	78.2	98.1	144.1	171.2	194.5	205.1
1500	34.0	70.0	81.3	101.2	149.2	177.2	201.7	212.7
1740	35.0	72.4	83.7	103.9	153.3	...	207.5	219.5
1980	36.7	74.3	85.4	107.0	157.4	...	214.0	...
2220	37.7	109.1	161.2

134.8 mm. After the reaction bulb was conditioned by the TFA products of reaction for 2 days, the rates of decomposition were readily reproducible and the reaction was homogeneous. The ratio of the final to the initial pressures, p_t/p_i , was found to be constant at 2.17 over the pressure range from 23 to 128 mm.

2. *Order of Reaction.* Table I presents typical data for the change in pressure with time for various initial pressures of TFA at 546.2°. These data, and all similar data, were programmed on an IBM 1620 computer to solve for k_i , the initial rate constant, and n , the order of reaction, in the equation

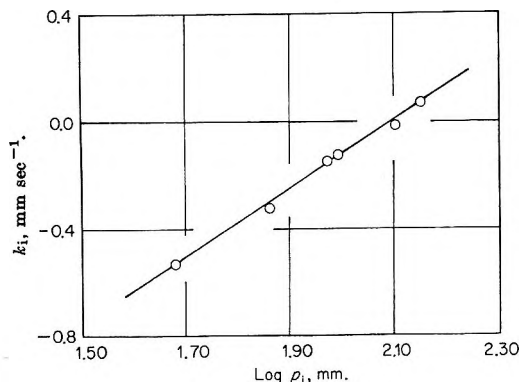
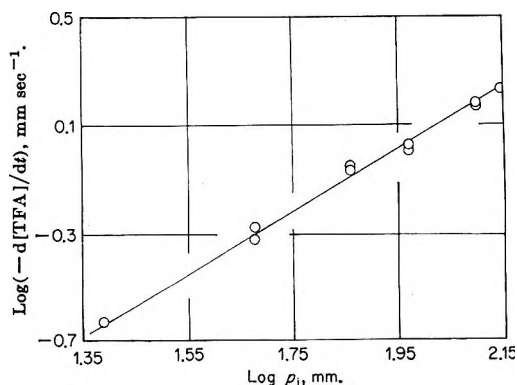
$$\log (dp/dt)_0 = \log k_i + n \log p_i \quad (1)$$

A value of $n = 1.3$ was obtained at each of four different temperatures from 546.2 to 599.1°, indicating that the order of the decomposition lay between 1.0 and 1.5. Visual evidence for the consistency of the data can be seen in Figure 1.

The order of the reaction was also determined by measuring the amount of TFA that decomposed in 1 min. This study was conducted over an initial pressure range from 25 to 150 mm at four different temperatures. Figure 2 is a typical plot of the logarithm of the rate of disappearance of TFA as a function of the logarithm of the initial pressure. The rate constants and order of reaction at the various temperatures were evaluated and are given in Table II.

Table II: The Order and Rate Constants Based upon the Amount of TFA Disappearing in 60 Sec

Temp, °C	Order	$10^4 k_0$, mm ^{-0.3} sec ⁻¹
546.7	1.4	5.83
555.7	1.4	9.25
576.6	1.3	23.3
599.1	1.1	65.3
	Av	1.3

**Figure 1.** Variation of the logarithms of the initial rate constants with the logarithms of the initial pressures of TFA at 599.1°.**Figure 2.** Log of initial rate of disappearance of TFA vs. the log of the initial pressure at 599.1°.

3. *Formation of CF_3H , CF_3CH_3 , and $CF_2=CH_2$.* The initial rates of formation of these three products of the decomposition of TFA were also determined by measuring the number of millimeters of each formed in 60 sec reaction time over an initial pressure range between 17 and 150 mm. The orders of reaction and initial rate constants at various temperatures are presented in Table III.

Table III: Rate Constants and Orders for the Formation of CF_3H , CF_3CH_3 , and CF_2CH_2 at Various Temperatures

Temp, °C	$10^4 k_i, \text{sec}^{-1}$			Order			
	CF_3H	CF_3CH_3	CF_2CH_2	CF_3H	CF_3CH_3	CF_2CH_2	
546.7	2.17	1.10	0.86	1.2	1.1	1.1	
555.7	3.45	1.67	1.37	1.2	1.1	1.0	
576.6	9.12	3.76	3.76	1.1	1.2	0.9	
599.1	19.5	...	12.9	1.0	...	0.8	
				Av	1.1	1.1	0.9

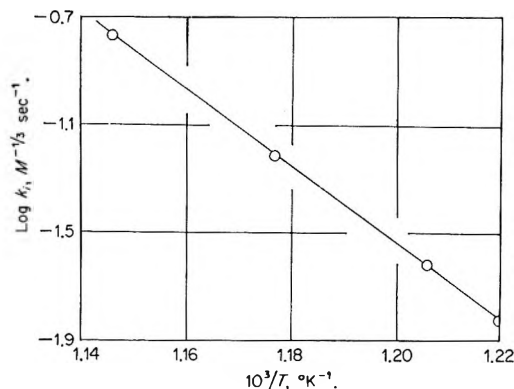


Figure 3. Log of initial rate constants vs. the reciprocals of the absolute temperatures for the disappearance of TFA.

4. *Energies of Activation.* The activation energy for the thermal decomposition of TFA was determined by two methods—one using the rate constants for the disappearance of TFA, k_0 , and the other using the initial rate constants, k_i . As seen in Figure 3, a plot of the logarithms of k_0 as a function of the reciprocals of the absolute temperatures gave excellent linearity. The activation energy and frequency factor associated with k_0 and k_i were calculated by the method of least squares, and the rates of decomposition expressed in terms of the Arrhenius parameters are

$$k_0 = 3.63 \times 10^{15} e^{-65,200/RT} M^{-0.3} \text{sec}^{-1} \quad (2)$$

and

$$k_i = 2.22 \times 10^{15} e^{-66,300/RT} M^{-0.3} \text{sec}^{-1} \quad (3)$$

The close agreement of eq 2 and 3 indicates that the determination of initial rates of pressure increase is, in effect, a measurement of the rate of disappearance of TFA.

The activation energies of CF_3H , CF_3CH_3 , and CF_2CH_2 were determined from the data in Table III by the method of least squares. The rates of formation were found to be

$$k_{\text{CF}_3\text{H}} = 1.50 \times 10^{12} e^{-59,400/RT} \text{sec}^{-1} \quad (4)$$

$$k_{\text{CF}_3\text{CH}_3} = 1.40 \times 10^{11} e^{-56,600/RT} \text{sec}^{-1} \quad (5)$$

$$k_{\text{CF}_2\text{CH}_2} = 1.86 \times 10^{15} e^{-72,000/RT} \text{sec}^{-1} \quad (6)$$

5. *Effect of Foreign Gases.* The thermal decomposition of TFA was examined in the presence of several

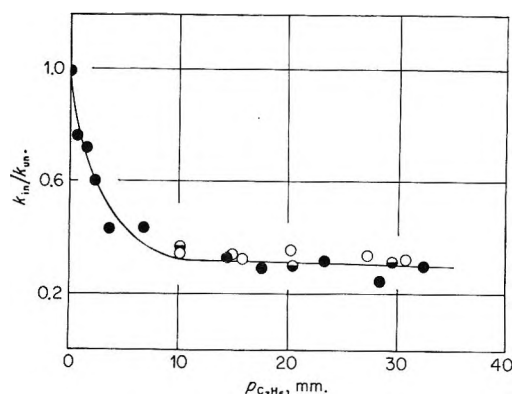


Figure 4. Retardation of decomposition rate by propylene for 50 (O), 100 (●), and 150 mm. (⊖) of TFA at 545.2°.

foreign gases, most significant of which were propylene, perfluoropropylene, and nitric oxide.

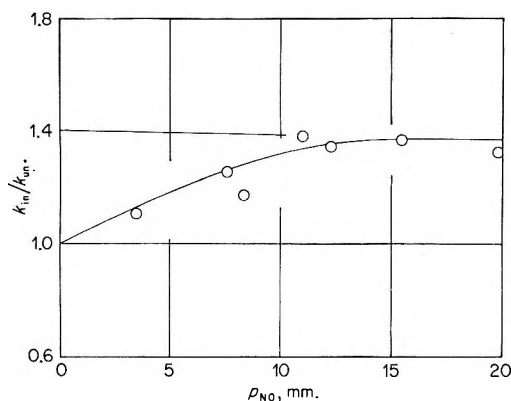
A. *Propylene.* The inhibiting effect of propylene on the decomposition of TFA was studied at three different initial pressures at temperatures of 545.2, 569.6, and 591.3°. The initial rate constants and the order of the inhibited decomposition were determined by the method previously described. A value of $n = 1.3$, identical with that of the uninhibited reaction, was obtained. In Figure 4, the ratio of the inhibited to the uninhibited initial rate constants, k_{in}/k_{un} , is plotted as a function of the partial pressure of propylene. It is seen that the inhibiting effect attains a limiting value at about 10–12 mm of propylene pressure, and, at the limit, the reaction is approximately 70% inhibited. Of interest also is the fact that the amount of inhibition for a given pressure of propylene is independent of the initial pressure of TFA. Similar inhibition curves were also obtained at the other two temperatures investigated. The variation of the initial rate constant with temperature for the propylene-inhibited decomposition of TFA is

$$k_i = 8.02 \times 10^{13} e^{-63,900/RT} M^{-0.3} \text{sec}^{-1} \quad (7)$$

B. *Perfluoropropylene (PFP).* The presence of 1–30 mm of PFP produced a marked catalytic effect on the decomposition TFA at 547°. At this temperature, the PFP was found to increase the rate of decomposition of 50, 100, and 150 mm. initial pressures of TFA over 100%. Although the rates were only approximately

Table IV: Partial Pressures of Gaseous Products from the Uninhibited Decomposition of 106 mm of TFA at 547°

Time, min	<i>p</i> , mm												
	CO	CF ₃ H	CF ₃ CH ₃	CF ₂ CH ₂	CH ₄	CF ₃ CH=CH ₂	CF ₃ C ₂ H ₅	Ketene	C ₂ H ₄	C ₂ H ₆	CO ₂	H ₂	TFA
1	3.0	4.8	2.6	0.3	0.4	3.2	0.4	Neg	Neg	Trace	97.6
3	8.8	8.0	6.1	0.8	0.9	6.3	1.0	0.1	0.2	Trace	81.9
5	13.2	8.9	7.0	0.9	1.2	0.9	0.4	7.4	1.3	0.1	0.4	Trace	84.3
10	23.0	11.4	9.1	1.7	1.8	2.3	1.2	4.3	1.6	0.2	1.3	Trace	81.0
20	37.5	20.8	19.2	6.0	2.6	3.9	2.2	5.9	1.8	0.2	1.8	Trace	60.0
40	53.5	26.5	23.6	8.1	3.8	5.6	2.9	8.5	1.9	0.1	2.6	Trace	44.4
125	84.3	29.8	28.6	17.8	5.9	6.4	2.3	...	1.7	0.2	3.6	Trace	16.9

**Figure 5.** The acceleration in the rate of decomposition of 100 mm of TFA by nitric oxide at 546.7°.

reproducible, it was clear that the catalytic effect was pressure dependent on the initial pressure of TFA.

C. Nitric Oxide. The effect of nitric oxide on the TFA decomposition was studied only at one initial pressure, 100 mm, at 547°. Figure 5 shows that NO, like PFP, strongly catalyzes the reaction. This is consistent with the observation that NO catalyzes the decomposition of all ketones containing a methyl carbonyl group.

6. Products of Reaction. A. Uninhibited Decomposition. Analyses of products from the uninhibited decomposition of TFA were made over various time intervals at 547° by means of a Perkin-Elmer Model 154D vapor-phase chromatograph. The data in Table IV indicate that the predominant reaction products are CO, CF₃H, CF₃CH₃, CF₂CH₂, and ketene. The precision of the analyses was good, especially from 5 min of reaction time on. It is obvious from the data that the sum of the partial pressures of CO, CO₂, ketene, and ketone remaining should equal 106 mm, the initial pressure of TFA. This is seen to be the case at each reaction time within ± 4 mm.

It was suspected that HF might be one of the products of this decomposition. If so, its presence could interfere with the analysis for ketene. A number of samples were, therefore, withdrawn at various time intervals, shaken with distilled water, and qualitatively tested for fluoride ion with zirconium-alizarin indicator.

All tests were negative. Since the possibility existed that any HF formed might react with the reaction flask to form SiF₄ and water, the mass spectra were taken of the products from a 10-min and a 4-hr decomposition. There was no evidence for SiF₄ in the 10-min run but a small peak due to SiF₄ was observed in the 4-hr run. It was concluded, therefore, that the amount of unreacted HF present was too small to interfere with the ketene analyses. In determining the ketene concentrations, appropriate corrections were made for the acidity due to the CO₂ present.

B. Propylene-Inhibited Decomposition. It was seen in Figure 4 that propylene produces a pronounced inhibitory effect on the decomposition of TFA. In order to examine the effect of this inhibition on the reaction products, 100 mm of TFA was decomposed in the presence of 15 mm of propylene at 547°. Analyses were made at five different time intervals from 1 to 10 min. The data corresponding to 12.5% TFA decomposition for the inhibited (8.8 min) and the uninhibited (2.3 min) reactions are compared in Table V. These data indicate that the main effects of propylene are markedly to reduce the amounts of CF₃H and CF₃CH₃ formed and significantly to increase the concentrations of CF₃CH=CH₂ and CH₄. An increase in the methane concentration is not unusual under these conditions and is usually attributed to CH₃ radicals abstracting hydrogen from propylene. That this is true in the present case is uncertain. The data in Table V indicate that only 0.5 mm of C₃H₆ has reacted. In fact, the maximum amount of propylene found to disappear in any analysis was only 0.6 mm. The apparent failure of propylene to be consumed is even more difficult to understand in view of the decreases in concentration of CF₃H and CF₃CH₃. One would normally expect a corresponding increase in CF₃ addition compounds.

C. Effect of Other Foreign Gases on Product Formation. Since 15 mm partial pressure of NO and of PFP were found to catalyze 100 mm of TFA to the extent of about 120% at 547°, analyses of the reaction products of these two systems were made at 10-min reaction times.

The presence of CF₃CH=CH₂ and CF₃C₂H₅ in the uninhibited decomposition products (Table IV) suggested that their formation might be due to the inter-

Table V: Partial Pressures of Reaction Products from the Uninhibited and Propylene-Inhibited Decomposition of TFA after 12.5% Decomposition at 547° ($p_i(\text{un}) = 106 \text{ mm}$; $p_i(\text{in.}) = 100 \text{ mm}$; $p_{\text{C}_2\text{H}_4} = 15 \text{ mm}$)

	$p, \text{ mm}$												
	CO	CF ₃ H	CF ₃ CH ₃	CF ₂ CH ₂	CH ₄	CF ₃ CH=CH ₂	H ₂	Ketene	C ₂ H ₄	C ₂ H ₆	CO ₂	TFA	C ₃ H ₆
Uninhibited	7.0	6.9	5.0	0.7	0.7	5.5	0.8	0.1	0.1	94.0	...
Inhibited	4.9	1.7	0.9	1.8	4.2	2.7	...	5.6	1.6	0.1	0.4	81.0	14.5

Table VI: Partial Pressures (mm) of Reaction Products after 10-min Reaction Time from the Decomposition of 100 ± 5 mm of TFA in the Presence of 15 ± 2 mm of Foreign Gases and 50:50 Mixtures of TFA-Acetone and TFA-HFA at 547°

Products	System					
	TFA ^a	TFA-NO	TFA-PFP	TFA-C ₂ H ₄	TFA-acetone	TFA-HFA
CO	23.0	31.3	27.1	21.0	15.4	20.4
CF ₃ H	11.4	16.0	17.4	9.2	6.3	25.2
CF ₃ CH ₃	9.1	10.8	11.5	7.9	4.0	9.2
CF ₂ CH ₂	1.7	2.5	4.5	3.8	1.6	3.2
CH ₄	1.8	3.3	1.7	7.5	16.2	0.4
CF ₃ CH=CH ₂	2.3	1.4	2.4	5.6	0.6	2.0
CF ₃ C ₂ H ₅	1.2	1.0	0.8	4.4	0.6	0.2
Ketene	4.3	6.4	10.8	6.1	11.3	42.2
C ₂ H ₄	1.6	0.8	1.1	6.8	3.6	0.3
C ₂ H ₆	0.2	0.0	0.1	0.8	0.4	0.0
CO ₂	1.3	3.4	0.6	0.8	1.0	8.7
TFA	81.0	51.9	61.5	83.4	30.8	21.0
NO	...	7.1
PFP	4.9
Acetone	42.1	...
HFA	12.7
C ₃ H ₆	0.5	2.5
C ₂ F ₆	0.2

^a From Table IV.

action of CF₃, or a radical containing CF₃, with ethylene. If this were the case, then the addition of ethylene to the system should result in a corresponding increase in the fluorinated propane and propylene products. To test this hypothesis, 100 mm of TFA was pyrolyzed for 10 min in the presence of 15 mm of C₂H₄ at 547° and the products were analyzed.

Finally, it was thought to be of interest to examine the effect of the addition of CH₃ and CF₃ radicals on the decomposition products of TFA. Consequently, 100 mm of a 50:50 mixture of TFA-acetone and 100 mm of a similar mixture of TFA-hexafluoroacetone (HFA) were allowed to react for 10 min at 547° and the resulting products were analyzed.

The results of the above analyses are reported in Table VI.

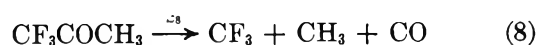
It is seen in Table VI that, with the exception of propylene, the TFA-NO and TFA-PFP reactions yield the same products in approximately the same concentrations. The results of the TFA-acetone and TFA-HFA reactions are those expected. In the TFA-acetone reaction, the CF₃H and CF₃CH₃ concentrations are about half that observed in the decom-

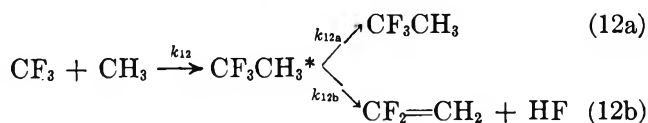
position of TFA alone while the CH₄ concentration has increased eightfold. It should be noted, however, that the concentration of CF₂=CH₂ is essentially the same as in the TFA reaction. On the other hand, in the TFA-HFA reaction, the amounts of CF₃H and CF₂=CH₂ formed are about double those from TFA alone while the CH₄ concentration is fivefold less. It is difficult to understand, however, why the CF₃CH₃ concentration is the same as in the TFA reaction.

It was suspected that radical-scrambling reactions, similar to those reported in analogous photochemical studies, might also occur in the TFA decomposition to produce acetone and hexafluoroacetone. With the columns employed, acetone and hexafluoroacetone could be readily separated and identified. Neither of these compounds, however, was ever detected in the reaction products.

Discussion

The reactions which produce the predominant products found in Table IV may be written as





Although significant concentrations of 1,1,1-trifluoropropylene are found in the latter stages of the decomposition, its formation is undoubtedly due to complicated secondary processes. In Table VI, it is seen that the decomposition of TFA in the presence of ethylene results in a marked increase in the $\text{CF}_3\text{CH}=\text{CH}_2$ concentration as compared to that in TFA alone. Since ketene, a primary product, decomposes into ethylene and carbon monoxide at these temperatures, $\text{CF}_3\text{CH}=\text{CH}_2$ is probably formed according to



where R is one of the free radicals present.

With the exception of C_2F_6 , the products found in this investigation are the same as those reported by Sieger and Calvert² in their photochemical studies. On the basis of having found biacetyl as a product, Dawidowicz and Patrick³ postulated that TFA dissociates initially to give CF_3 and CH_3CO radicals. Rice and Walters,⁶ however, have shown that biacetyl thermally decomposes between 424 and 470°. In the temperature range of the present experiments and owing to the fact that no biacetyl was observed in the products, reaction 8 would be preferred over that proposed by Dawidowicz and Patrick. Reactions 9 and 11 are identical with the mechanisms postulated for the formation of CF_3H and CH_4 in various photolysis investigations. The mechanisms for the formation of 1,1,1-trifluoroethane, however, require further explanation.

Reactions 12a and 12b were first substantiated in the photochemical studies of Alcock and Whittle⁷ and, later, more thoroughly investigated by Giles and Whittle.⁸ The latter show that, as the temperature increases in the range 23–244°, the elimination reaction, (12b), is favored at the expense of the stabilization reaction, (12a). They point out that when a methyl and a trifluoromethyl radical combine in reaction 12 to form the activated complex CF_3CH_3^* , 88 kcal/mol must be removed in order to stabilize the molecule and prevent its dissociation into radicals. While it is unlikely that a single collision with a third body would remove the entire 88 kcal/mol, it may, nevertheless, be deactivated to an extent so as to prevent dissociation but still have sufficient energy to react *via* (12b). From bond energy considerations it can be shown that the activation energy for the formation of CF_2CH_2 cannot be less than

45 kcal/mol. Since the activation energy of (12a) is zero, or nearly so, it is clear as to why a temperature increase would favor reaction 12b over 12a. Based on this argument and the data of Giles and Whittle, it is highly unlikely that reaction 12a would make any significant contribution to the total CF_3CH_3 concentration at the temperatures of the present experiments.

A further argument against reaction 12a being predominant is the high concentration of CF_3CH_3 observed during the initial stages of the decomposition. The probability that such concentrations as shown in Table IV are the result of a radical-radical reaction would be negligible. On the other hand, it is also noted in Table IV that the concentrations of CF_2CH_2 are small initially but become appreciable in the latter stage of the reaction where the concentration of TFA is considerably reduced. It is concluded, therefore, that reaction 10 is the primary source of 1,1,1-trifluoroethane.

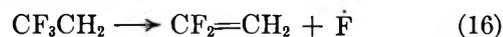
There is, of course, the possibility that CF_3CH_3 could be formed by



However, in the photolysis of azomethane in the presence of hexafluoroacetone between 163 and 265°, Pritchard and Steacie⁹ found only trace amounts of CF_3CH_3 . It is, therefore, unlikely that any appreciable amount of this compound was produced by reaction 15 in the present study.

A question which naturally arises is why do not radical-abstracting-radical reactions similar to (10) occur to produce C_2H_6 and C_2F_6 ? Since no ethane or hexafluoroethane was ever found in the reaction products, one is forced to conclude that, for reasons not yet clear, these particular abstractions do not occur under the existing experimental conditions.

The question may also be raised as to whether $\text{CF}_2=\text{CH}_2$ might not be formed as the result of hydrogen abstraction from CF_3CH_3 followed by



To test this, 81 mm of CF_3CH_3 was allowed to react for 25 min at 547°. Analysis showed that only 2 mm of $\text{CF}_2=\text{CH}_2$ was formed along with trace quantities of C_2H_6 and C_2F_6 . Since this amounted to only a 2.5% decomposition of CF_3CH_3 over a 25-min period, it is safe to conclude that this molecule is essentially stable at this temperature and, therefore, not the primary source of $\text{CF}_2=\text{CH}_2$.

Although it was impossible to identify HF directly, further support for reaction 12b is the previously men-

(6) F. O. Rice and W. D. Walters, *J. Chem. Phys.*, **7**, 1015 (1939).

(7) W. G. Alcock and E. Whittle, *Trans. Faraday Soc.*, **61**, 244 (1965).

(8) R. D. Giles and E. Whittle, *ibid.*, **61**, 1425 (1965).

(9) G. O. Pritchard and E. W. R. Steacie, *Can. J. Chem.*, **35**, 1216 (1957).

tioned presence of SiF_4 in the reaction products. Presumably, this was formed by the reaction of HF on the walls of the quartz reaction vessel. In addition, at the conclusion of this study the walls of the reaction chamber were found to be strongly etched, again indicating the presence of HF.

If one refers to Table IV, it is seen that the ratio $[\text{CF}_3\text{H}]/[\text{CF}_3\text{CH}_3] = 1.8$. Assuming steady-state conditions for the mechanism of eq 8-12b and employing eq 4 and 5, it can be shown that

$$\frac{d[\text{CF}_3\text{H}]/dt}{d[\text{CF}_3\text{CH}_3]/dt} = \frac{k_9}{k_{10}} = \frac{1.5 \times 10^{12} e^{-59,400/RT}}{1.4 \times 10^{11} e^{-56,800/RT}} = 10e^{-2800/RT} \quad (17)$$

or, $E_{10} - E_9 = 2.8$ kcal/mol, the increase in activation energy required for a CF_3 radical to remove a methyl radical from TFA over that required for hydrogen abstraction. Further, at 547° , the ratio k_9/k_{10} was found to be 1.8 by eq 17. This close agreement between the calculated and experimental values for the $[\text{CF}_3\text{H}]/[\text{CF}_3\text{CH}_3]$ ratio provides additional support to the argument that reaction 10 is the predominant source of CF_3CH_3 .

It is of interest to note that the value of 2.8 kcal/mol for $E_{10} - E_9$ is identical with that found by McGee and Waring¹⁰ for the difference in activation energy between the removal of an ethyl radical from methyl ethyl ketone by a CF_3 radical and the corresponding hydrogen-abstraction process. They reported an activation energy of 7.9 kcal/mol for the radical-removal reaction. For the present case, Sieger and Calvert² gave $E_9 = 6.6$ kcal/mol. Employing their value, the activation energy for the removal of a methyl radical from a ketone by a trifluoromethyl radical, E_{10} , becomes 9.4 kcal/mol. It follows, then, that the difference in activation energy for the removal of a methyl over an ethyl radical in ketones by a CF_3 radical becomes $E_{\text{CH}_3} - E_{\text{C}_2\text{H}_5} = 1.5$ kcal/mol.

It can also be demonstrated under steady-state conditions that

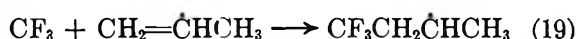
$$d[\text{CF}_2\text{CH}_2]/dt = k_{12b}[\text{CF}_3][\text{CH}_3] = k_8[\text{TFA}] \quad (18)$$

This indicates that the Arrhenius constants for the

rate of decomposition of TFA and the rate of formation of CF_2CH_2 should be quite similar. The agreement between eq 3 and 6 is seen to be reasonably good.

If one compares the products from the uninhibited and propylene-inhibited decompositions of TFA (Table V), the most significant differences are seen to be the marked decrease in CF_3H and CF_3CH_3 and the increase in CH_4 and $\text{CF}_3\text{CH}=\text{CH}_2$. This suggests that propylene is effective in removing CF_3 but not CH_3 radicals. At lower temperatures ($\sim 350^\circ$) there is evidence¹⁰ that CF_3 radicals add to the propylene to form primary and secondary free butyl radicals. These then abstract a hydrogen to form saturated butanes. Since no such butanes were detected in this investigation, it must be concluded that some other mechanism is operative.

A mechanism which could perhaps explain the observed increase in $\text{CF}_3\text{CH}=\text{CH}_2$ concentration may be written as



Such a mechanism is, admittedly, purely speculative. It does, however, account for the formation of 1,1,1-trifluoropropylene and provide an additional source of methyl radicals for the production of methane. On the other hand, this mechanism does not successfully account for the unusually low consumption of propylene.

The mechanisms for the nitric oxide and PFP catalyzed decomposition of TFA appear to be even more subtle than that of the propylene-inhibited process. Although the rates of the catalyzed decompositions are over 100% faster than that of TFA alone, the same products are observed in essentially the same amounts as in the uncatalyzed decomposition.

Acknowledgment. The authors wish to thank Dr. S. R. Smith of this department for his advice and help with the mass spectrographic analyses.

(10) T. H. McGee and C. E. Waring, *J. Phys. Chem.*, **73**, 2838 (1969).

Kinetic Investigation of the Radiation-Induced Isotopic

Exchange between Iodobenzene and Iodine in Benzene

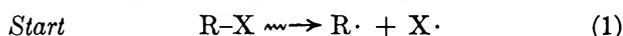
by R. Riess and H. Elias

Lehrstuhl für Kernchemie, Technische Hochschule, Darmstadt, Germany (Received August 7, 1969)

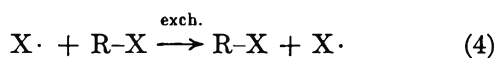
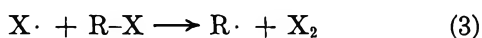
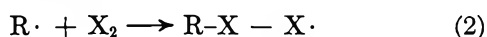
The isotopic exchange between iodobenzene and radioactive elementary iodine induced by ionizing radiation (^{60}Co) has been investigated in benzene as a solvent. The kinetic measurements have been made at 30° in the absence and the presence of oxygen and at different dose rates. The following rate law has been derived both for aerated and oxygen-free solutions: $R = (\alpha[\text{I}_2]^{1/2})/(1 + \beta[\text{I}_2]/[\text{PhI}])$. No dose rate effect has been observed. The mechanism is discussed.

Introduction

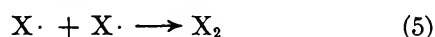
Molecular halogens (especially iodine) are frequently used as radical scavengers by radiation chemists. It has been observed by several authors¹⁻⁶ investigating the radiation chemistry of organic halides that in the presence of a radioactive halogen as radical scavenger, radioactive halide is formed. In the case of aliphatic halides, R-X, the following list of mechanistic steps, as given by various authors,¹⁻⁶ explains this radiation-induced isotopic exchange



Secondary reactions



Termination reactions

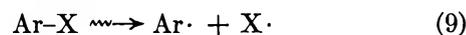


If radioactive halogen, $^*\text{X}_2$, is present, reactions 2, 4, and 7 can contribute to the observed formation of labeled halide, R- $^*\text{X}$. The rate of exchange is reduced considerably in the presence of oxygen,¹⁻⁴ which is understandable on the basis of this radical mechanism and oxygen being a most powerful scavenger for organic radicals. If light is used instead of ionizing radiation,^{7,8} the photochemical dissociation of X_2 has to be considered a start reaction in addition to (1)

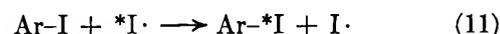


Only scarce information is found in the literature on the radiation-induced isotopic exchange between aromatic halides, Ar-X, and the corresponding radioactive halogen. Investigating the radiation chemistry of iodo-,

bromo-, and chlorobenzene in the presence of radioactive halogen as scavenger, Choi and Willard⁹ observed the same effect as found for aliphatic halides: during the irradiation radioactive halobenzene was formed. On the basis of the mechanistic interpretation given by Choi and Willard⁹ for the radiation chemistry of the halobenzenes it would appear that the observed isotopic exchange is mainly due to the following reactions, which correspond to reactions 1 and 2 for aliphatic halides



However, the observation of the G values for exchange in the system iodobenzene- $^*\text{I}_2$ not being reduced by atmospheric oxygen¹⁰ does not back this radical mechanism. The rate of the photochemically induced isotopic exchange between *o*-iodoanisole and radioactive iodine is proportional to the square root of the iodine concentration.¹¹ This result led Anbar and Rein to postulate the exchange step



Reaction 11 is suggested also by other authors¹²⁻¹⁴ to be

(1) R. C. Petry and R. H. Schuler, *J. Amer. Chem. Soc.*, **75**, 3796 (1953).

(2) R. H. Schuler and R. C. Schuler, *ibid.*, **78**, 3954 (1956).

(3) E. O. Hornig and J. E. Willard, *ibid.*, **79**, 2429 (1957).

(4) R. S. Hanrahan and J. E. Willard, *ibid.*, **79**, 2435 (1957).

(5) R. H. Luebbe and J. E. Willard, *ibid.*, **81**, 761 (1959).

(6) A. H. Young and J. E. Willard, *J. Phys. Chem.*, **66**, 271 (1962).

(7) M. Gazith and R. M. Noyes, *J. Amer. Chem. Soc.*, **77**, 6091 (1955).

(8) I. J. Gardner and R. M. Noyes, *ibid.*, **83**, 2409 (1961).

(9) S. U. Choi and J. E. Willard, *J. Phys. Chem.*, **66**, 1041 (1962).

(10) H. Elias, *Radiochim. Acta*, **6**, 107 (1966).

(11) M. Anbar and R. Rein, *Chem. Ind.*, 1524 (1963).

(12) R. K. Sharma and N. Kharash, *Angew. Chem.*, **80**, (2), 69 (1968).

(13) B. Milligan, R. L. Bradow, J. E. Rose, H. E. Hubbert, and A. Roe, *J. Amer. Chem. Soc.*, **84**, 158 (1962).

the main pathway for the photochemically induced isotopic exchange between aromatic halides and labeled halogen. The photolytic rupture of the carbon-halogen bond (according to reaction 9) followed by its re-formation (according to reaction 10) is assumed to contribute to the isotopic exchange only to a minor extent at low concentrations of halogen.¹⁵⁻¹⁷

There are no kinetic measurements available concerning the radiation-induced isotopic exchange between aromatic halides and labeled halogen. We decided, therefore, to investigate the kinetics of the exchange between iodobenzene and labeled iodine in benzene as solvent, using the γ radiation of a ^{60}Co source. This investigation has practical aspects, because radiation-induced isotopic exchange reactions can be applied to labeling of aromatic halides.^{10,18,19}

Experimental Section

Reagents. Iodobenzene (Schuchhardt, Munich) was distilled over Hg in an atmosphere of dry N_2 at 60° and a pressure of 12 mm. The distillation was repeated until the product was colorless and free of impurities detectable by gas chromatography (7-m Carbowax 20 M column (5 wt % on Chromosorb G) at 200°). Shortly before each run the distilled iodobenzene was finally purified by fractional sublimation *in vacuo* with a cooling finger (see Figure 1). Benzene (Aral AG, Essen) was purified by shaking with concentrated H_2SO_4 , washing with water and NaHCO_3 solution, partial recrystallization with rejection of a 20% fraction of the unfrozen liquid, drying over CaCl_2 , and fractionation over P_2O_5 . Iodine (Merck, Darmstadt) was not further purified.

Sample Preparation. Samples with appropriate concentrations of iodine were obtained by dissolving weighed amounts of I_2 in iodobenzene-benzene mixtures. These solutions were activated by shaking with 0.1-0.01 cc (about 30 μCi) of a carrier-free, aqueous solution of Na^{131}I (Farbwerke Höchst, Frankfurt). After shaking, these solutions were dried with anhydrous Na_2SO_4 . Samples with $[\text{I}_2] < 1 \times 10^{-3} M$ were obtained by diluting solutions of higher iodine concentration. The oxygen-free samples were obtained by degassing with the freeze-thaw-pumping technique.

Irradiation. A 12,000-Ci ^{60}Co source (Gammacell 220, Atomic Energy of Canada, Ltd.) was used for the irradiations (ferrous sulfate dosimetry). The glass tubes containing the samples were mounted reproducibly in the irradiation chamber which had a temperature of 30° . Dose calculations were corrected for the difference in electron density between the dosimeter solution and the samples.

Analysis. The analytical procedure applied by Choi and Willard⁹ in their exchange studies (shaking of the irradiated sample with an aqueous solution of sulfite for iodine reduction and separation; counting of the organic phase) appeared to be unsatisfactory. This

was shown by analyzing the irradiated samples of a given exchange run in three different ways: (1) reduction and separation of the iodine according to the procedure of Choi and Willard⁹ (as described above) and counting of the organic phase (benzene, iodobenzene, and organic radiolysis products) without further purification; (2) analysis of the organic phase by preparative gas chromatography, trapping of the iodobenzene peak, and counting of the purified iodobenzene; (3) partial sublimation of the organic phase (as described below). The comparison revealed that methods (2) and (3) gave identical results (within the limits of error of $\pm 5\%$), whereas method (1) gave values for the fraction exchange which were 1.5-3 times (depending on the dose) higher. This effect was obviously due to the iodine containing radiolysis products diiodobenzene and 4-iodobiphenyl⁹ not being separated from the iodobenzene by method (1). The sublimation procedure (3) is as effective as the gas chromatographic separation (2) because the radiolysis products mentioned above are solids at room temperature which do not sublime upon partial sublimation of the organic phase. Method (3) is experimentally simpler than method (2); therefore, the analysis of the irradiated samples was carried out in the following way.

The irradiated samples were shaken with a few drops of a 0.1 M $\text{Na}_2\text{S}_2\text{O}_3$ solution to reduce the iodine. The organic layer was separated, dried with anhydrous Na_2SO_4 , and transferred to the apparatus for sublimation where it was cooled with liquid nitrogen (see Figure 1). After the apparatus had been evacuated to a pressure of 5-15 mm, the cooling finger was filled with liquid nitrogen. The sublimation started when the liquid nitrogen cooling the sample was removed; it was stopped (by aerating the apparatus) after approximately 50% of the liquid sample had been transferred to the cold finger. The crystals of iodobenzene and benzene deposited on the cold finger were finally thawed and weighed. The ^{131}I activity of the sublimate was measured in a well-type scintillation counter. The concentration of iodobenzene in the sublimated iodobenzene-benzene mixture was determined with a uv spectrophotometer (Model UV 137, Perkin-Elmer) at a wavelength of 277 m μ .

Calculation of the Rate of Exchange, R. The equation given by McKay²⁰ for the description of isotopic exchange reactions can be modified for the radiation-in-

(14) B. Müller and C. Walling *J. Amer. Chem. Soc.*, **79**, 4187 (1957).

(15) R. M. Noyes, *ibid.*, **77**, 2342 (1955).

(16) R. M. Noyes, *J. Phys. Chem.*, **65**, 763 (1961).

(17) J. F. Garst and R. S. Cole, *Tetrahedron Lett.*, **19**, 679 (1963).

(18) H. Elias, R. Riess, and K. Müller, *Naturwissenschaften*, **54**, 114 (1967).

(19) H. Elias, Proceedings of the 2nd International Conference on Methods of Preparing and Storing Labeled Molecules, Brussels, 1966, EURATOM 3776 d.f.e., 881, 1968.

(20) See A. C. Wahl and N. A. Bonner, "Radioactivity Applied to Chemistry," John Wiley & Sons, Inc., New York N. Y., 951, p 7.

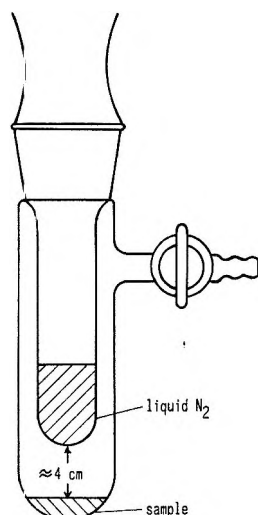


Figure 1. Cooling finger for sublimation.

duced isotopic exchange between iodobenzene and iodine by introducing the radiation dose instead of time

$$\log(1 - F) = -R \frac{(2[I_2] + [\text{PhI}])0.4343D}{2[I_2][\text{PhI}]} \quad (12)$$

where R is the rate of exchange [$\text{mol l}^{-1} \times (\text{eV/g})^{-1}$]; D is the radiation dose (eV/g); F is the fraction exchange, and $[I_2]$ and $[\text{PhI}]$ are concentrations (mol/l). F is given by the ratio of the specific activity of iodobenzene, $a(\text{PhI})$, and its specific activity at exchange equilibrium, $a(\text{PhI})_\infty$, which can be calculated

$$a(\text{PhI})_\infty = a(I_2)_0 \frac{2[I_2]}{2[I_2] + [\text{PhI}]} \quad (13)$$

where $a(I_2)_0$ is the specific activity of iodine before exchange.

According to eq 12, R can be determined from the slope of the curves obtained by plotting $\log(1 - F)$ as a function of the dose D . For most of the runs, these plots gave straight lines up to doses of approximately 1 Mrad and, correspondingly, up to F values of 30–60%. In some cases (especially at low iodine concentrations like $5 \times 10^{-4} \text{ mol/l}$. and in the absence of oxygen) the initially straight lines deviated from linearity with increasing dose (due to the radiolytic formation of iodine on the one hand and of iodine containing compounds on the other hand). In these cases only the linear, *i.e.*, the initial part of the exchange curves (corresponding to relatively small doses and relatively small F values up to approximately 20%) was used for the determination of the slope and of R , the rate of exchange, respectively.

Results and Discussion

The rate law for the radiation-induced isotopic exchange between iodobenzene and iodine in benzene was derived on the basis of the rate of exchange, R , being measured at different concentrations of the exchange partners. The experiments were carried out

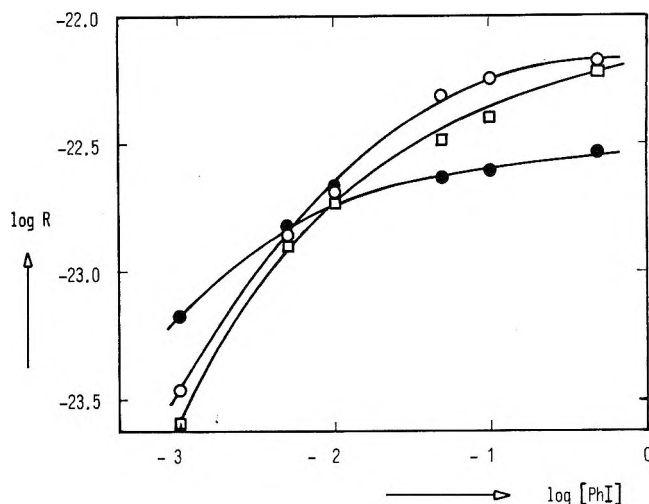


Figure 2. Rate of exchange R as function of the concentration of iodobenzene. $-\circ-\circ-$, $[I_2] = 1 \times 10^{-2} \text{ mol/l}$. (oxygen-free solutions); $-\square-\square-$, $[I_2] = 1 \times 10^{-2} \text{ mol/l}$. (aerated solutions); $-\bullet-\bullet-$, $[I_2] = 2 \times 10^{-3} \text{ mol/l}$. (aerated solutions).

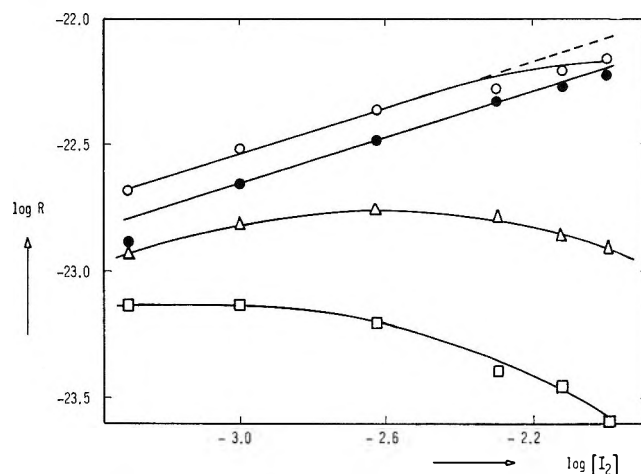


Figure 3. Rate of exchange R as function of the concentration of iodine. $-\circ-\circ-$, $[\text{PhI}] = 5 \times 10^{-1} \text{ mol/l}$. (oxygen-free solutions); $-\bullet-\bullet-$, $[\text{PhI}] = 5 \times 10^{-1} \text{ mol/l}$. (aerated solutions); $-\triangle-\triangle-$, $[\text{PhI}] = 5 \times 10^{-3} \text{ mol/l}$. (aerated solutions); $-\square-\square-$, $[\text{PhI}] = 1 \times 10^{-3} \text{ mol/l}$. (aerated solutions).

with oxygen-free solutions as well as with aerated solutions. The results and reaction conditions are compiled in Table I.

Derivation of the Rate Law. To analyze the concentration dependence of R , $\log R$ was plotted as a function of $\log [\text{PhI}]$ (at constant concentration of I_2) and as a function of $\log [I_2]$ (at constant concentration of PhI). Figures 2 (runs V–VII) and 3 (runs I–IV) show these plots for aerated and oxygen-free solutions. The fact that curves are obtained instead of straight lines proves that the rate law is not a simple exponential one of the form

$$R \sim [\text{PhI}]^m [I_2]^n \quad (14)$$

However, Figure 3 indicates that at relatively high concentrations of iodobenzene ($[\text{PhI}] = 5 \times 10^{-1} \text{ mol/l}$)

Table I: Rate of Exchange $R^{a,b}$ for the Radiation-Induced Isotopic Exchange in the System Iodobenzene- $^{131}\text{I}_2$ -benzene as a Function of Concentration

Run	[PhI], mol/l.	[I ₂], mol/l.					
		5×10^{-4}	1×10^{-3}	2.5×10^{-3}	5×10^{-3}	7.5×10^{-3}	1×10^{-2}
I	5×10^{-1}	1.3	2.2(2.3 ^d)	3.2	4.6	5.3	5.9
II ^c	5×10^{-1}	2.04	3.0	4.2	5.13	6.07	6.67
III	5×10^{-3}	1.18	1.54	1.71	1.65	1.40	—
IV	1×10^{-3}	0.74	0.74	0.63	0.39	0.35	—

Run	[I ₂], mol/l.	[PhI], mol/l.					
		1×10^{-3}	5×10^{-3}	1×10^{-2}	5×10^{-2}	1×10^{-1}	5×10^{-1}
V	2×10^{-3}	0.65	1.52	2.03	2.3	2.55	3.07
VI	1×10^{-2}	0.25	1.24	1.92	3.34	4.13	—
VII ^c	1×10^{-2}	0.34	1.43	2.38	5.10	6.04	—

^a R in $\text{mol l.}^{-1} (\text{eV/g})^{-1} \times 10^{23}$. ^b Unless otherwise stated, the data refer to irradiations at 30° in presence of atmospheric oxygen and at a dose rate between 3.12×10^{19} and 3.36×10^{19} (eV/g) hr^{-1} . ^c Oxygen-free solutions. ^d At a dose rate of 1.20×10^{19} , 0.776×10^{19} , and 0.252×10^{19} (eV/g) hr^{-1} . ^e Ratio R (without air)/ R (with air).

1.) the dependence of $\log R$ on $\log [I_2]$ is practically linear with a slope of approximately 0.5, which means that the relationship $R \sim [I_2]^{1/2}$ holds under these conditions. By plotting the R values compiled in Table I as a function of various concentration parameters it was finally found that the data can be represented by the relationship

$$R = \frac{\alpha [I_2]^{1/2}}{1 + \beta [I_2]/[\text{PhI}]} \quad (15)$$

For the determination of α and β one could plot $[I_2]^{1/2}/R$ against $[I_2]/[\text{PhI}]$. This procedure would put all the points on a single plot. It was found, however, that in such a plot most of the points are concentrated in a rather narrow range of $[I_2]/[\text{PhI}]$, so that the slope of the curve is determined by only a few points at higher values of $[I_2]/[\text{PhI}]$. Therefore, α and β were determined separately for each of the seven runs by using eq 16, a rearranged form of eq 15

$$\frac{1}{R} = \frac{1}{\alpha [I_2]^{1/2}} + \frac{\beta}{\alpha} \frac{[I_2]^{1/2}}{[\text{PhI}]} \quad (16)$$

By plotting $1/R$ against $1/[\text{PhI}]$, α results from the intercept on the ordinate axis at $1/[\text{PhI}] = 0$, whereas β can be evaluated from the slope of the straight line. The results as obtained by the least-squares method are

$$\begin{aligned} \alpha_V &= 5.90 \times 10^{-22} (\text{mol/l.})^{1/2} \times (\text{eV/g})^{-1}; & \beta_V &= 2.18 \\ \alpha_{VI} &= 6.29 \times 10^{-22} (\text{mol/l.})^{1/2} \times (\text{eV/g})^{-1}; & \beta_{VI} &= 2.30 \\ \alpha_{VII} &= 7.14 \times 10^{-22} (\text{mol/l.})^{1/2} \times (\text{eV/g})^{-1}; & \beta_{VII} &= 1.99 \end{aligned}$$

Run V and run VI refer to exchange experiments in the presence of atmospheric oxygen; the agreement between α_V and α_{VI} and also between β_V and β_{VI} is good. The runs which were made at various concentrations of I_2 with $[\text{PhI}] = \text{constant}$ (runs I, II, III, and IV) can be used now for an independent determination of α from the slope of the straight line obtained by plotting $R(1 + \beta [I_2]/[\text{PhI}])$ against $[I_2]^{1/2}$. This plot is based on eq 17

$$R(1 + \beta [I_2]/[\text{PhI}]) = \alpha [I_2]^{1/2} \quad (17)$$

With a mean of $\beta = 2.24$ (from β_V and β_{VI} ; aerated solutions) and $\beta = 1.99$ ($= \beta_{VII}$; oxygen-free solutions) one obtains

$$\begin{aligned} \alpha_{I,III,IV} &= 6.29 \times 10^{-22} (\text{mol/l.})^{1/2} \times (\text{eV/g})^{-1} \\ \alpha_{II} &= 7.23 \times 10^{-22} (\text{mol/l.})^{1/2} \times (\text{eV/g})^{-1} \end{aligned}$$

By averaging the various α values one ends up with the following set of constants.

Aerated solutions

$$\begin{aligned} \alpha &= 6.16 \times 10^{-22} (\text{mol/l.})^{1/2} \times (\text{eV/g})^{-1} \\ \beta &= 2.24 \end{aligned}$$

Oxygen-free solutions

$$\begin{aligned} \alpha &= 7.18 \times 10^{-22} (\text{mol/l.})^{1/2} \times (\text{eV/g})^{-1} \\ \beta &= 1.99 \end{aligned} \quad (18)$$

These numbers have an error of about 5%; they differ slightly from the preliminary results published previously.²¹ To prove the validity of eq 15 and the numbers derived for α and β , Figures 4 and 5 show a summarizing plot of R as a function of the right side of eq

(21) R. Riess and H. Elias, *Radiation Chem. Acta*, **10**, 110 (1968).

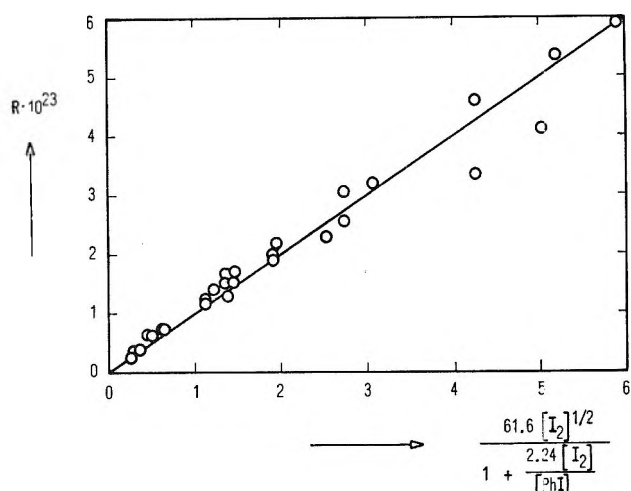


Figure 4. Rate of exchange R as a function of the expression $(\alpha[I_2]^{1/2}/1 + \beta[I_2]/[PhI])$; measurements in the presence of atmospheric oxygen.

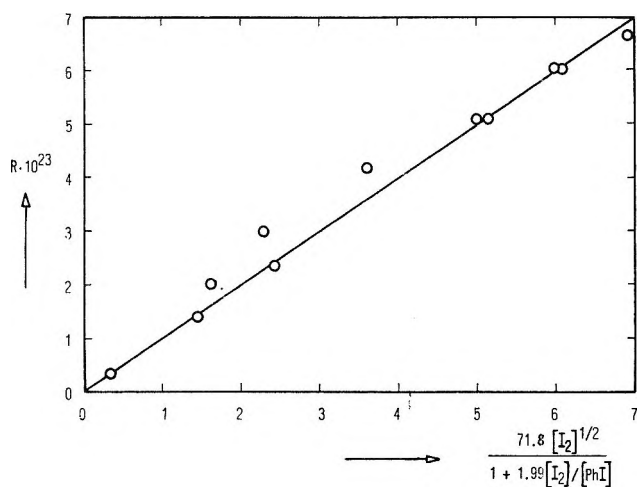


Figure 5. Rate of exchange R as a function of the expression $(\alpha[I_2]^{1/2}/1 + \beta[I_2]/[PhI])$; measurements in the absence of oxygen.

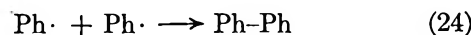
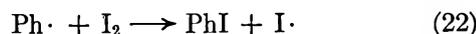
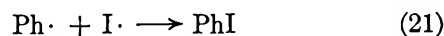
15 for all concentrations investigated. As one can see, the data are well represented by eq 15. There are only very few points which deviate from the straight line (slope = 1.0) by more than 10%.

One finds, therefore, that as well in the presence as in the absence of oxygen the results follow the same type of rate law. The only difference is α being about 17% greater and β being about 11% smaller for oxygen-free solutions. Equation 15 and the numbers given for α and β in (18) imply that for the ratio $[PhI]/[I_2] \geq 200$ the contribution of the denominator term $\beta[I_2]/[PhI]$ becomes negligibly small ($\leq 1\%$). Under these conditions, *i.e.*, in the presence of a large excess of PhI as compared to I_2 , eq 15 is reduced to eq 19, in which R is just proportional to the square root of the iodine concentration

$$R = \alpha[I_2]^{1/2} \quad (19)$$

This simple rate law is in agreement with the results of runs I and II ($[PhI]/[I_2] \geq 50$; see Figure 3) which give practically straight lines with a slope of 0.5 in the $\log R$ vs. $\log [I_2]$ plot.

Discussion of the Mechanism. If the mechanism of the radiation-induced isotopic exchange between iodobenzene and labeled iodine is of the radical type, one would suggest the following sequence of reaction steps.



According to the scavenger experiments done by Fessenden and Schuler,²² oxygen and iodine are competitive scavengers for organic radicals. Therefore, in the presence of air, according to reaction 25



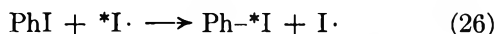
oxygen would compete for phenyl radicals together with iodine according to reaction 22, which—in the presence of radioactive iodine—represents the exchange step. As a consequence, oxygen should reduce the rate of exchange. As can be seen from Table I (runs I/II and VI/VII), there is a small rate-reducing effect of atmospheric oxygen being dissolved in the samples. If one assumes that iodine and oxygen are equally effective scavengers for phenyl radicals and that $[O_2]_{\text{dissolv}} \approx 3 \times 10^{-4}$ mol/l. (estimated), then, at $[I_2] = 5 \times 10^{-4}$ and 1×10^{-3} mol/l. one would expect rate ratios $R(\text{without } O_2)/R(\text{with } O_2)$ of 1.6 and 1.3, respectively. The actually observed values, 1.57 and 1.36, respectively, are in good agreement (see Table I; runs I/II). On the basis of the results obtained by Fessenden and Schuler,²² the rate-reducing effect of oxygen should decrease and finally become negligible with increasing iodine concentration. The results of run I/II (Table I) indicate this trend. However, at $[I_2] = 2.5 \times 10^{-3}$, 5×10^{-3} , 7.5×10^{-3} , and 1×10^{-2} mol/l. one observes the rate ratios 1.31, 1.12, 1.15, and 1.13 instead of 1.12, 1.06, 1.04, and 1.03, as to be expected. So, at higher iodine concentration the oxygen effect is stronger than it should be. Even more inconsistent with the picture of radical scavenging by oxygen are the results of run VI/VIII (Table I). At $[I_2] = 1 \times 10^{-2}$ mol/l. and $[O_2]_{\text{dissolv.}} \approx 3 \times 10^{-4}$ mol/l., one would expect a rate ratio of 1.03 and observes clearly higher values with a mean of 1.35. It follows, therefore, that the results as discussed on the basis of an entirely radical mechanism according to reactions 20–25 are not unambiguous. On the one

(22) R. W. Fessenden and R. H. Schuler, *J. Amer. Chem. Soc.*, **79**, 273 (1957).

hand, the results do not follow strictly the consequences of the suggested radical mechanism with respect to the role of oxygen as scavenger; on the other hand, it cannot be ruled out definitely that there is some contribution of such radical processes.

According to the observed rate law (see eq 15) the rate of exchange is proportional to the square root of the iodine concentration. It has been shown by Hamill, *et al.*,^{23,24} and by Noyes¹⁵ that the competition of a strong radical scavenger like I₂ with geminate recombination reactions like (21) can lead to a square-root dependence for the scavenger. Therefore, the denominator of the observed rate law could be in agreement with the radical mechanism described by reactions 20–25. It is hard to see, however, how this radical mechanism should lead to the observed denominator term $(1 - \beta[I_2]/[PhI])$ (see eq 15). This term obviously describes the competition of iodine molecules and iodobenzene molecules for some relevant species which the radical mechanism does not account for.

For the photochemical exchange between *o*-iodoanisole and labeled iodine Anbar and Rein¹¹ suggested as a rate determining step



If the concentration of iodine atoms is given by a dissociation equilibrium according to



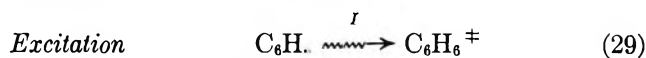
the resulting rate law has the form

$$R \sim [PhI] [I_2]^{1/2} \quad (28)$$

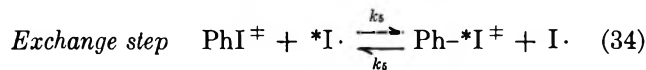
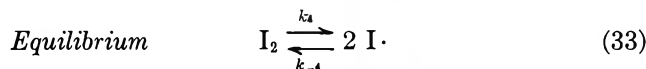
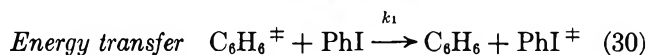
However, there are several arguments against this mechanism being responsible for the radiation-induced isotopic exchange between iodobenzene and iodine. One of these arguments is the observation²⁵ that the rate constant for exchange reaction 26 is very low. Another argument can be derived from photochemical studies.²⁶ If a solution of iodobenzene and labeled iodine in benzene is exposed to a certain number of light quanta from the visible part of a high-pressure mercury lamp spectrum, the degree of isotopic exchange taking place is very small. However, if the same solution is irradiated under identical conditions with the same number of quanta from the uv part of the mercury lamp spectrum, the degree of exchange is about 8 times higher as compared to the irradiation with visible light. This experiment demonstrates that iodobenzene in the ground state plus iodine atoms (as produced by visible light) causes only a slow exchange, whereas excited iodobenzene (as produced by uv light) plus iodine atoms exchanges much faster. Very similar results have been published by Macrae and Shaw.²⁷

If excited iodobenzene molecules cause the radiation-induced isotopic exchange according to eq 26, one has to consider the question of how they are produced. It appears reasonable to assume that excited iodobenzene

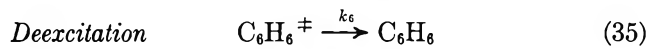
is formed by energy transfer from excited benzene²⁸ because the solvent benzene is the major constituent in the solutions irradiated (the percentage by weight of iodobenzene in the solutions irradiated was 11% for the maximum concentration of $[PhI] = 5 \times 10^{-1}$ mol/l. and less for all other solutions). Taking into account that there can be energy transfer from excited benzene not only to iodobenzene but also to iodine and oxygen, one could suggest the following set of reactions as a mechanism for the observed radiation-induced isotopic exchange



(*I* = dose rate; \ddagger = excited state)



(**I* = radioactive iodine)



The concentration of radioactive iodine is extremely small as compared to inactive iodine. Therefore, the equilibrium concentration of inactive and radioactive iodine atoms, respectively is

$$[I \cdot] = \left(\frac{k_4}{k_{-4}} \times [I_2] \right)^{1/2} = K^{1/2} \times [I_2]^{1/2} \quad (37)$$

$$[*I \cdot] = K^{1/2} \times [I-*I]/[I_2]^{1/2} \quad (38)$$

Stationary-state treatment of the concentration of $C_6H_6^\ddagger$ molecules gives (*I* = dose rate in (eV/g) sec⁻¹; *d* = density of the solution in g/cc; *G* = number of the $C_6H_6^\ddagger$ molecules per 100 eV; *N_L* = Loschmidt number)

$$\frac{d[C_6H_6^\ddagger]}{dt} = 0 = \frac{10GI d}{N_L} - [C_6H_6^\ddagger](k_1[PhI] + k_2[I_2] + k_3[O_2] + k_6) \quad (39)$$

(23) J. C. Roy, R. R. Williams, Jr., and W. H. Hamill, *J. Amer. Chem. Soc.*, **76**, 3274 (1954).

(24) H. A. Gillis, R. R. Williams, Jr., and W. H. Hamill, *ibid.*, **83**, 17 (1961).

(25) R. M. Noyes, private communication.

(26) R. Riess and H. Elias, unpublished data.

(27) J. F. C. Macrae and P. F. D. Shaw, *J. Inorg. Nucl. Chem.*, **24**, 1327 (1962).

(28) W. G. Burns, R. B. Cundall, P. A. Griffiths, and W. R. Marsh, *Trans. Faraday Soc.*, **64**, 129 (1968).

With the abbreviation $a = 10GId/N_L$ one obtains

$$[C_6H_6^\ddagger] = a/(k_1[PhI] + k_2[I_2] + k_3[O_2] + k_6) \quad (40)$$

The stationary-state concentrations of PhI^\ddagger and Ph^*I^\ddagger , respectively, can be determined from eq 41

$$\frac{d[PhI^\ddagger]}{dt} = 0 = k_1[C_6H_6^\ddagger][PhI] - k_7[PhI^\ddagger] \quad (41)$$

$$[PhI^\ddagger] = \frac{k_1}{k_7} [C_6H_6^\ddagger][PhI] \quad (42)$$

$$[Ph^*I^\ddagger] = [PhI^\ddagger][Ph^*I]/[PhI] \quad (43)$$

The rate of formation of radioactive PhI molecules, Ph^*I , is given by the rate of formation of excited radioactive PhI molecules, Ph^*I^\ddagger , according to reaction 34

$$\frac{d[Ph^*I]}{dt} = \frac{d[Ph^*I^\ddagger]}{dt} = k_5([PhI^\ddagger][^*I] - [Ph^*I^\ddagger][I]) \quad (44)$$

Introducing eq 37, 38, 42, and 43 in eq 44 one obtains (s = specific activity = concentration of radioactive species/concentration of inactive species)

$$\frac{d[Ph^*I]}{dt} = \frac{k_1 k_5 K^{1/2}}{k_7} [I_2]^{1/2} [C_6H_6^\ddagger][PhI] (s_{I_1} - s_{PhI}) \quad (45)$$

Therefore, the rate of exchange, R , is ²⁰

$$R = \frac{k_1 k_5 K^{1/2}}{k_7} [I_2]^{1/2} [C_6H_6^\ddagger][PhI] \quad (46)$$

The introduction of eq 40 and rearrangement gives

$$R = \frac{k_5 K^{1/2} GId \cdot 10}{k_7 N_L} \frac{[I_2]^{1/2}}{1 + \frac{k_2[I_2] + k_3[O_2] + k_6}{k_1[PhI]}} \left(\frac{\text{mol}}{\text{l. sec}} \right) \quad (47)$$

R is determined in units of $\text{mol l.}^{-1} (\text{eV/g})^{-1}$ from the slope of the curves obtained by plotting $\log(1 - F)$ as a function of the dose $D (=It)$ (see Experimental Section). Using the abbreviation

$$\alpha = \frac{k_5 K^{1/2} Gd \cdot 10}{k_7 N_L} \quad (48)$$

eq 47 can be rewritten, therefore

$$R = \frac{\alpha [I_2]^{1/2}}{1 + \beta [I_2]/[PhI]} \left(\frac{\text{mol}}{\text{l. eV/g}} \right) \quad (49)$$

In the presence of oxygen, β represents the expression

$$\beta = \frac{k_2}{k_1} + \frac{k_3 [O_2]}{k_1 [I_2]} + \frac{k_6}{k_1} \frac{1}{[I_2]} \quad (50)$$

whereas in the absence of oxygen one obtains

$$\beta = \frac{k_2}{k_1} + \frac{k_6}{k_1} \frac{1}{[I_2]} \quad (51)$$

It turns out, therefore, that β is actually not a constant but a parameter depending on the concentration of oxygen and iodine. In agreement with eq 50 as compared to eq 51 the observed value for β is higher for aerated solutions than for oxygen-free solutions. The small difference of only 11% indicates, however, that the contribution of the term $k_3/k_1 \cdot [O_2]/[I_2]$ (and as well of the term $k_6/k_1 \cdot 1/[I_2]$) to β is small, so that $\beta \approx k_2/k_1 = \text{constant}$. The rate law 49 as derived from the mechanism described by reactions 29–36 would fit the experimental data. It is obvious, however, that the rate-determining step 34 consisting in the collision of excited iodobenzene molecules with iodine atoms is open to discussion. With the assumptions that $k_5 \approx 10^{10}$ l./mol sec and that the mean lifetime of excited iodobenzene molecules is approximately 10^{-6} sec, one can calculate from the observed rate that in a solution with an iodine concentration of 2.5×10^{-3} mol/l., the equilibrium concentration of iodine atoms should be 0.69×10^{-4} mol/l. This would mean that during the irradiation approximately 1% of the iodine molecules should be dissociated into iodine atoms. For a 2.5×10^{-3} M solution of iodine, one can estimate a thermal equilibrium concentration for iodine atoms of approximately 10^{-13} mol/l.^{29,30} One has to conclude that processes other than thermal dissociation lead to the formation of iodine atoms.

It is possible, of course, to assume that the forward reaction of equilibrium 33 is not thermal but radiation induced in the sense that excited iodine molecules, I_2^\ddagger , dissociate



Since $k_4' \gg k_4$, the steady-state concentration of iodine atoms would be increased as compared to the thermal case. This assumption would imply, however, that the rate of exchange, R , is proportional to the square root of the dose rate I , *i.e.*, a dose rate effect should be observed.

To check this, the rate of exchange, R , in units of $(\text{mol/l.})(\text{eV/g})^{-1}$ was determined at four different dose rates I ($I = 3.31 \times 10^{19}$, 1.20×10^{19} , 0.77×10^{19} , 0.252×10^{19} (eV/g) hr⁻¹) under constant conditions of concentration ($[PhI] = 5 \times 10^{-1}$ and $[I_2] = 1 \times 10^{-3}$ mol/l.). As can be seen from Table I, $R = 2.2 \times 10^{-23}$ for the highest dose rate and $R = 2.3 \times 10^{-23}$ for the other dose rates. This means that a variation of the dose rates by a factor of 13 does not reveal a dose rate effect. It follows from these results, therefore, that the suggested mechanism with reaction 34 as rate-determining step does leave an open question with respect to the mechanistic interpretation of how the relatively

(29) J. E. Mayer and M. G. Mayer, "Statistical Mechanics," John Wiley & Sons, New York, N. Y., 1950, p 216.

(30) J. Zimmermann and R. M. Noyes, *J. Chem. Phys.*, **18**, 658 (1950).

high concentration of iodine atoms participating in this reaction is formed. Another point is that the reaction scheme 29-36 cannot explain the fact that $\alpha(\text{oxygen-free solution}) > \alpha(\text{aerated solution})$ (one can see from eq 50 that the concentration of oxygen enters only the expression for β). As indicated above, this could

possibly arise from a small contribution of the radical mechanism (see reactions 20-25) to the exchange.

Acknowledgments. The authors wish to thank Professor R. M. Noyes and Professor R. W. Dodson for helpful discussions and the Deutsche Forschungsgemeinschaft for financial support.

The 2537-Å Photochemistry of Azido-Ammine Complexes of Cobalt(III) in Aqueous Solution: Products, Stoichiometry, and Quantum Yields¹

by John F. Endicott, Morton Z. Hoffman, and Laszlo S. Beres²

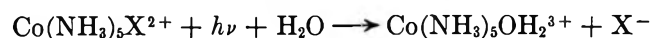
Department of Chemistry, Boston University, Boston, Massachusetts 02215 (Received January 17, 1969)

The principal products of the 2527-Å irradiation of $\text{Co}(\text{NH}_3)_5\text{N}_3^{2+}$ are Co^{2+} , N_2 , and probably $\text{Co}(\text{NH}_3)_4\text{OH}_2\text{N}_3^{2+}$. The yields of Co^{2+} and N_2 have been determined directly under a variety of conditions and exhibit a peculiar dependence on the intensity of absorbed radiation. This dependence of product yields on I_a as well as the spectral features of irradiated solutions imply the formation and subsequent photolysis of a different azido-amine complex of cobalt(III). The source of product N_2 has been shown to be coordinated azide and experiments with $\text{Co}({}^{16}\text{NH}_3)_5\text{N}_3^{2+}$ show that $\text{Co}(\text{NH}_3)_5\text{OH}_2^{3+}$ cannot be an important product of photolysis. $\text{Co}(\text{NH}_3)_4\text{OH}_2\text{N}_3^{2+}$ exhibits kinetic behavior very similar to that of $\text{Co}(\text{NH}_3)_5\text{N}_3^{2+}$. The photochemistry of $\text{Co}(\text{tetraen})\text{N}_3^{2+}$, *cis*- $\text{Co}(\text{NH}_3)_4(\text{N}_3)_2^+$, and *trans*- $\text{Co}(\text{NH}_3)_4(\text{N}_3)_2^+$ appears to be much more straightforward and may not involve photolabilization of an ammine ligand.

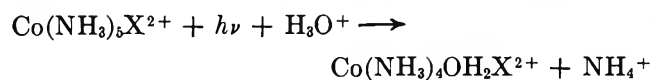
Introduction

Although there have been several investigations of the photochemistry of cobalt(III) complexes, there is still some dispute about the specific role of the excited states which are generated on absorption of radiation.³ Some of the ambiguity concerning the photochemical mechanism arises from a lack of accurate detailed information regarding the over-all products and the over-all reaction stoichiometry of the photoprocess. The identification of all the final products of reaction and the determination of product yields are complicated by the fact that three experimentally distinguishable reaction paths are possible in the photochemistry of simple cobalt(III) complexes.⁴

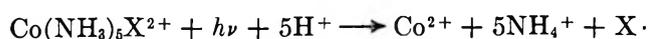
(I) Photolabilization of weakest ligand bond⁵



(II) Photolabilization of the strongest ligand bond^{6,7}



(III) Photoreduction⁵



The photolabilization processes I and II are often difficult to establish experimentally since (1) the chemical and physical properties of any $\text{Co}(\text{NH}_3)_4\text{OH}_2\text{X}^{2+}$ formed are often so similar to the properties of the original $\text{Co}(\text{NH}_3)_5\text{X}^{2+}$ complex as to make *in situ* spectral analyses ambiguous and separations difficult; and (2) X^- is frequently formed from subsequent

(1) This research was supported by the National Science Foundation under Grant GP 7048. The mass spectrometer used was purchased from funds provided by the National Science Foundation under Equipment Grant GP 5561.

(2) Participant, National Science Foundation Undergraduate Research Participation Program Summer 1966 and the 1966-1967 academic year.

(3) (a) For recent reviews see E. L. Wehry, *Quart. Rev. (London)*, **21**, 213 (1967); (b) V. Balzani, L. Moggi, F. Scandola, and V. Carassiti, *Inorg. Chem. Acta Rev.*, **1**, 7 (1967); (c) A. W. Adamson, *Coord. Chem. Rev.*, **3**, 169 (1968); (d) V. Balzani, L. Moggi, and V. Carassiti, *Ber. Bunsenges. Phys. Chem.*, **72**, 238 (1968); (e) L. Moggi, V. Balzani, and V. Carassiti, *ibid.*, 293 (1968); (f) D. Valentine, Jr., *Advan. Photochem.*, **6**, 123 (1968).

(4) For simplicity we confine the present discussion to pentaammine complexes containing simple unidentate ligands X (e.g., Cl^- , N_3^- , NH_3 , OH_2 , etc.).

(5) A. W. Adamson, *Discussions Faraday Soc.*, **29**, 163 (1960).

(6) L. Moggi, N. Sabbatini, and V. Balzani, *Gazz. Chim. Ital.*, **97**, 980 (1967).

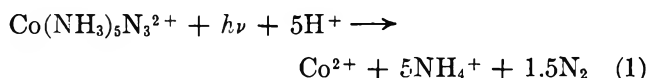
(7) J. F. Endicott and M. Z. Hoffman, *J. Amer. Chem. Soc.*, **90**, 4740 (1968).

reaction of $X \cdot$ ^{5,8} (from III) as well as from thermal aquation. The stoichiometry of photoreduction reactions may be complicated by radical reactions, some of which may involve the cobalt(III) substrate.^{9,10} Finally, the determination of the stoichiometry of photoreduction may be difficult if the products of ligand oxidation are gases^{5,8} (e.g., N_2) and are many oxidation-reduction equivalents removed from the radical initially generated from the ligand (e.g., NH_3).¹¹

Information obtained from reaction stoichiometries is essential to any mechanistic discussion. However, the critical test of mechanism is provided by a kinetic analysis of the photochemical reaction. Two kinds of kinetic information have proved to be particularly useful: the form of the rate law for product formation (i.e., the dependence of product yield on the intensity of absorbed radiation) and the direct or indirect detection of transient reaction intermediates. It is significant that some photolyses of cobalt(III) complexes do not have first-order light intensity dependencies^{3b,8,12} and that some transient species have been detected in flash photolysis studies of $Co(NH_3)_5X^{2+}$ complexes.¹³⁻¹⁵

At present there is much evidence that the radical pair model proposed by Adamson,⁵ for the photochemistry of cobalt(III) is itself not sufficient to account for all of the relevant photochemistry.^{3b,8,16} On the other hand, the present paucity of reliable information about reaction stoichiometries, product yields, or photokinetic behavior do not permit a definitive general examination of any of the proposed models of the photochemistry of cobalt(III).

In this paper we report the results of our investigations of the 2537-Å photochemistry of $Co(NH_3)_5N_3^{2+}$. The first reported studies of the photochemistry of this compound indicated a classically simple photooxidation-reduction behavior^{5,17}



These early studies provide only limited information about yields of nitrogen, do not make very critical evaluation of the extent of the photolabilization paths, and provide no kinetic information. They also report^{5,11,18-20} the generation of some reactive radical (presumably $N_3 \cdot$) during photolysis. Our original interest in reexamining the photochemistry of $Co(NH_3)_5N_3^{2+}$ was to investigate the possibility of scavenging the $[(H_3N)_5Co \cdot N_3]$ radical pairs chemically in much the same way as chemical scavengers have been used to characterize the solvated electron products in the irradiation of I^- .^{21,22} These scavenging studies will be reported separately²³ since at the present time they do not bear directly on the photochemistry of $Co(NH_3)_5N_3^{2+}$.

The 2537-Å photochemistry of $Co(NH_3)_5N_3^{2+}$, produced by absorption in a predominantly $N_3^- \rightarrow Co(III)$

charge-transfer band,^{24,25} has proved to be very complex.⁷ In the present paper we report stoichiometric and photokinetic studies which have led to the identification and estimates of yields of the principal reaction products. Some comparative studies of other azido-amine complexes of cobalt(III) are also reported.

Experimental Section

Preparation of Reagents. $[Co(NH_3)_5N_3]Cl_2$ was prepared by direct air oxidation of $CoCl_2 \cdot 6H_2O$ in ammoniacal solution containing an excess of sodium azide.^{17a} *cis*- and *trans*- $[Co(NH_3)_4(N_3)_2]ClO_4$ were prepared from $[Co(NH_3)_4(OH_2)](ClO_4)_3$ in excess NaN_3 .²⁶ These complexes were recrystallized in the dark by the mixing of saturated aqueous solutions of the respective preparative mixtures with about 2 M $NaClO_4$.

The equilibrium mixture of *cis*- and *trans*- $Co(NH_3)_4OH_2N_3^{2+}$ was generated in solution by the acidification of solutions of either *cis*- or *trans*- $Co(NH_3)_4(N_3)_2^{2+}$.²⁷ We were not successful in attempts to separate or crystallize the $Co(NH_3)_4OH_2N_3^{2+}$ complexes.

The procedures described by House and Garner were used to prepare $[Co(\text{tetraen})N_3](ClO_4)_2$ from β - $[Co(\text{tetraen})Br](ClO_4)_2$.²⁸ Although the β - $[Co(\text{tetraen})$ -

(8) J. F. Endicott and M. Z. Hoffman, *J. Amer. Chem. Soc.*, **87**, 3348 (1965).

(9) T. B. Copestake and N. Uri, *Proc. Roy. Soc. (London)*, **A228**, 252 (1955).

(10) A. Haim and H. Taube, *J. Amer. Chem. Soc.*, **85**, 499 (1963).

(11) R. G. Hughes, J. F. Endicott, and M. Z. Hoffman, *Chem. Commun.*, 195 (1969).

(12) The experimental evidence with regard to $Co(NH_3)_5I^{2+}$ appears to be incorrectly represented in a recent review.^{3f}

(13) S. A. Penkett and A. W. Adamson, *J. Amer. Chem. Soc.*, **87**, 2514 (1965).

(14) G. Caspari, J. F. Endicott, and M. Z. Hoffman, submitted for publication.

(15) The species which have actually been observed are apparently X_2^- radical anions.¹⁴

(16) A. W. Adamson, W. L. Waltz, E. Zinato, D. W. Watts, P. D. Fleischauer, and R. D. Lindholm, *Chem. Rev.*, **68**, 541 (1968).

(17) (a) M. Linhard and H. Flygare, *Z. Anorg. Allg. Chem.*, **262**, 328 (1950); (b) M. Linhard and M. Weigel, *ibid.*, **267**, 121 (1951).

(18) Attempts at the direct detection of these radical species have so far failed,¹³ no doubt owing to the relatively low molar absorptivity of N_3^- .^{19,20} and the very high molar absorptivity of the cobalt(III) substrate. The lack of an easily observable transient when $Co(NH_3)_5N_3^{2+}$ is flashed has been verified in this laboratory (G. Caspari, unpublished observations) and is not accurately represented in a recent review article.^{3f}

(19) F. Barat, B. Hickel, and J. Sutton, *Chem. Commun.*, 125 (1969).

(20) A. Treinin and E. Hayon, *J. Chem. Phys.*, **50**, 538 (1969).

(21) G. Stein, "The Solvated Electron," *Advances in Chemistry Series*, No. 50, American Chemical Society, Washington, D. C., 1965, p 230.

(22) J. F. Endicott and M. Z. Hoffman, *J. Phys. Chem.*, **70**, 3389 (1966).

(23) J. F. Endicott, M. Z. Hoffman, L. S. Beres, and R. W. McQuigg, manuscript in preparation.

(24) M. Linhard, H. Siebert, and M. Weigel, *Z. Anorg. Allg. Chem.*, **278**, 287 (1955).

(25) I. Burak and A. Treinin, *J. Chem. Phys.*, **39**, 189 (1963).

(26) M. Linhard, M. Weigel, and H. Flygare, *Z. Anorg. Allg. Chem.*, **263**, 233 (1950).

(27) A. Haim, *J. Amer. Chem. Soc.*, **86**, 2352 (1964).

Br](ClO₄)₂ complex seemed to be reasonably pure, we obtained from different crystallization fractions two slightly different (in solubility and visible-ultraviolet spectra) samples of [Co(tetraen)N₃](ClO₄)₂. The more slowly crystallizing fraction represented about 80% of the product, and we worked mostly with this material (λ_{max} 308 nm, ϵ_{max} $9.6 \times 10^3 \text{ M}^{-1} \text{ cm}^{-1}$).

A sample of 95 atom % ¹⁵N NH₄Cl was obtained from Bio-Rad Laboratories. Aliquots of this material were diluted (by weight) with normal NH₄Cl to prepare labeled [Co(*NH₃)₅N₃]Cl₂ and labeled solutions of *NH₄Cl.

All complexes were recrystallized at least one and generally two or three times before use. Absorption spectra of complexes agreed to within a few per cent with literature values. The purity of complexes was also assessed by comparing the yield of Co²⁺ after complete photolysis to the theoretical amount of cobalt in the weighed aliquot of complex.²⁹ Theoretical and experimental cobalt yields always agreed to within 2%.

With the exceptions noted, reagent grade chemicals were used without further purification. All solutions were made using triply distilled and/or deionized water.

Analytical Procedures. Co²⁺ was analyzed by the thiocyanate extraction method^{22,30} or the hydrochloric acid method.⁸ For purposes of obtaining a calibration curve for cobalt analysis, a stock solution of Co²⁺ was standardized by titrating the acid eluted when an aliquot of stock solution was passed through an acidic cation-exchange resin.

Ammonia was determined by the indophenol method.³¹ This method is very sensitive to the pH of the solution and was calibrated with reference to standard solutions of NH₄Cl, which contained NH₄⁺ in the concentration range produced from photolysis, were 0.1 M in HClO₄, and were subjected to precisely the same experimental procedure as aliquots of the photolyzed solutions. Stock solutions of Co(NH₃)₅N₃²⁺ did not contain detectable amounts of NH₄⁺, and the complex did not interfere with the analysis.

Gaseous products of reaction were detected and determined quantitatively from photolyses performed *in vacuo*. The system to be photolyzed was purged of air and dissolved gases on a vacuum line. The solution was stirred magnetically before, during, and after photolysis. Any product gases resulting from the photolysis were quantitatively transferred through a cold trap to remove water vapor and collected for mass spectrometry (Nuclide Model RMS-60-6) or quantitative gas chromatography (F & M Model 810) using Linde 5A molecular sieve with thermal conductivity detection. Calibration curves for the chromatograph were obtained by injecting known quantities of various gases and recording the integrated area under the peaks. Replicate samples agreed within less than 5%.

The presence of the following possible oxidized species was investigated by a number of qualitative tests: N₃⁻,³² H₂O₂,³³ NH₂OH,^{34a} and N₂H₄.³⁵ The test for NH₂OH was also performed using the method^{34b} in which 1 ml of a 0.2 M THAM buffer solution, 1 ml of a 2 N Na₂CO₃ solution, and 1 ml of 1% 8-hydroxyquinoline are mixed with the sample. The green color which appears when NH₂OH is present can be monitored at 700 nm. Since Co²⁺ interferes with this test, Co(SCN)₂ was extracted into methyl isobutyl ketone before the NH₂OH was determined (we found that the presence of NCS⁻ does not interfere with this test). In addition, the iodate method³⁶ was used to test for N₂H₄ and NH₂OH. The limits of detectability of the latter two methods were determined using dilute solutions of reagent N₂H₄ or NH₂OH.

In a few cases the reaction products were separated using cation ion-exchange resins (Dowex 50W-X12, 100-200 mesh) either in the magnesium or the lanthanum forms. We also attempted an *in situ* polarographic analysis of partially photolyzed Co(NH₃)₅N₃²⁺ using a Chemtrix Model SSP-2 polarograph. This attempt did not provide any useful information since the broad irreversible reduction waves of Co(NH₃)₅N₃²⁺, Co(NH₃)₄OH₂N₃²⁺, and HN₃ all occurred at about the same potential.

Spectrophotometric analyses of photolyzed solutions, reagents, and various separated products were accomplished using a Cary 14, Unicam SP800, or Beckman DU spectrophotometer.

Photolysis Apparatus. In these studies three different photolysis units were used. One of them, with very high incident light intensity ($I_0 \approx 6.6 \times 10^{-3}$ einstein l⁻¹ min⁻¹) has been described previously.⁸ The other two units consisted of an Ultra-violet Products low-pressure mercury immersion lamp separated from the photolysis solution by at least one quartz jacket and an air space (see Figure 1). One of these systems was designed with two coaxial quartz tubes (separated by about 1 cm) to permit the use of filter solutions, resulting in about a tenfold decrease in the effective path length. The use of the chemical filter

(28) (a) D. A. House and C. S. Garner, *Inorg. Chem.*, **5**, 2097 (1966); (b) D. A. House and C. S. Garner, *J. Amer. Chem. Soc.*, **89**, 727 (1967).

(29) R. G. Hughes, J. F. Endicott, M. Z. Hoffman, and D. A. House, *J. Chem. Educ.*, **48**, 440 (1969).

(30) D. Katakis and A. O. Allen, *J. Phys. Chem.*, **68**, 1359 (1964).

(31) W. Bolleter, C. Bushman and P. Tidwell, *Anal. Chem.*, **33**, 592 (1961).

(32) F. Feigl, "Spot Tests in Inorganic Analysis," Elsevier Publishing Co., Amsterdam, 1958, p 286.

(33) C. J. Hochanadel, *J. Phys. Chem.*, **56**, 587 (1952).

(34) (a) G. Endres, *Ann.*, **518**, 109 (1945); (b) H. Omura, Y. Osajima, S. Hatano, F. Yoshihara, K. Watanabe, and K. Yamafuji, *Daigaku Gakugei Zasshi*, **20**, 179 (1963).

(35) G. W. Watts and J. P. Chrisp, *Anal. Chem.*, **24**, 2066 (1952).

(36) I. M. Kolthoff and R. Becher, "Volumetric Analysis," Vol. III, Interscience, New York, N. Y. 1957.

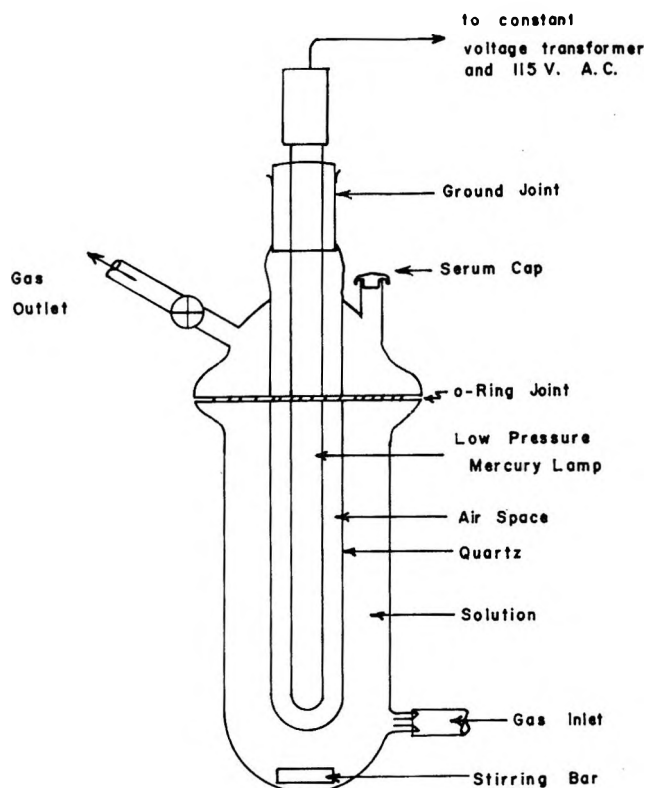


Figure 1. Photolysis unit; $I_0 = 5.5 \times 10^{-4}$ einstein $l^{-1} \text{ min}^{-1}$.

($\text{CoSO}_4\text{-NiSO}_4$ and KI)³⁷ permits isolation of a relatively pure 2537-Å line and virtually eliminates any possibility of significant irradiation with lower energy radiation. The maximum intensity of radiation in the apparatus with the filter solutions was found to be about 8×10^{-5} einstein $l^{-1} \text{ min}^{-1}$ and in the system containing no filter solution about 5.5×10^{-4} einstein $l^{-1} \text{ min}^{-1}$.

Actinometry. Each photochemical apparatus was calibrated with a standard chemical actinometer, either uranyl oxalate³⁸ or potassium ferrioxalate.³⁹ For each apparatus a calibration curve of the variation of I_a with the absorbance of the solution was prepared as described in detail previously.⁸ Quantum yields were calculated by dividing the rate of product formation by the I_a value of the solution of known absorbance. Because the photolysis of $\text{Co}(\text{NH}_3)_5\text{N}_3^{2+}$ exhibited kinetic irregularities, we periodically checked each apparatus and the particular experimental procedures by measuring the yield of Co^{2+} from photolyzed solutions of $\text{Co}(\text{NH}_3)_5\text{Cl}^{2+}$. We have determined⁴⁰ that for $\text{Co}(\text{NH}_3)_5\text{Cl}^{2+}$ in 0.1 M HClO_4 at 25°, $\phi_{\text{Co}^{2+}} = 0.17$, independent of I_a (for $2.0 \times 10^{-5} \leq I_a \leq 6.6 \times 10^{-3}$ einstein $l^{-1} \text{ min}^{-1}$). The 2537-Å photochemistry of $\text{Co}(\text{NH}_3)_5\text{Cl}^{2+}$ has always been found to be kinetically straightforward as is illustrated by two specific examples in Figure 2. The behavior of $\text{Co}(\text{NH}_3)_5\text{N}_3^{2+}$ is shown for comparison.

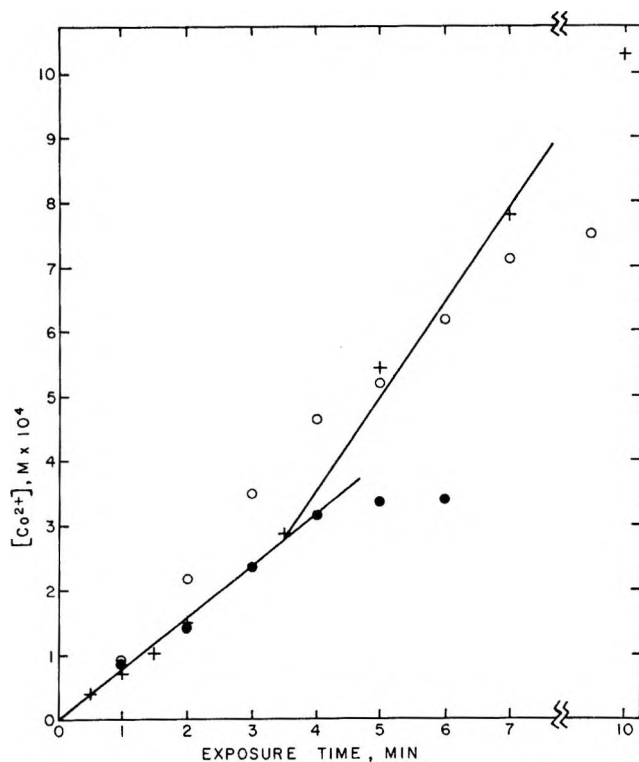


Figure 2. Comparison of photokinetic behavior of $\text{Co}(\text{NH}_3)_5\text{N}_3^{2+}$ and $\text{Co}(\text{NH}_3)_5\text{Cl}^{2+}$: $[\text{Co}(\text{NH}_3)_5\text{N}_3^{2+}] \approx 1.8 \times 10^{-3} \text{ M}$, +; $[\text{Co}(\text{NH}_3)_5\text{Cl}^{2+}] \approx 4.5 \times 10^{-4} \text{ M}$, ●. Their initial absorbancies at 254 nm are nearly the same (~ 1.3) and the initial values of $\phi_{\text{Co}^{2+}}$ are nearly the same (0.17). Simple kinetic behavior is exhibited for $\text{Co}(\text{NH}_3)_5\text{Cl}^{2+}$ at all concentrations in the range 10^{-4} to 10^{-2} M ; kinetic data for $[\text{Co}(\text{NH}_3)_5\text{Cl}^{2+}] = 10^{-3} \text{ M}$ are included for comparison, ○.

Procedure. Solutions were thermostated at 25° in the photolysis cell before (and generally during) irradiation. Aliquots of the photolysis mixture were removed after timed periods of irradiation by means of a syringe equipped with a Teflon needle. Solutions were stirred magnetically during photolysis and (except when otherwise specifically indicated) scrubbed⁸ nitrogen was passed through solutions continually during photolysis. For each kinetic determination of $\phi_{\text{Co}^{2+}}$, the yield of Co^{2+} was plotted as a function of time (Figure 2), and the initial rate was compared to the I_a value of an actinometer solution of the same absorbance.⁸ There are some experimental difficulties which can arise with this technique when the immersion-type lamps are used. First of all, the lamp output varies with temperature and erroneous results can be obtained if a cold lamp is used for short irradiation periods. In our work this problem has been avoided by warming

(37) J. G. Calvert and J. N. Pitts, Jr., "Photochemistry," John Wiley & Sons, Inc., New York, N. Y., 1967, p 729.

(38) W. A. Noyes, Jr., and P. A. Leighton, "The Photochemistry of Gases," Reinhold Publishing Corp., New York, N. Y., 1941.

(39) C. A. Parker and G. C. Hatchard, *Proc. Roy. Soc. (London)*, A235, 518 (1956).

(40) J. F. Endicott and M. Z. Hoffman, unpublished observations.

up the lamp for 15–30 min before the beginning of each kinetic run. The second problem arises because there is some O_2 in the air space between the quartz jacket and the photolysis lamp (Figure 1). During the first 2 min that the lamp is on there is an apparent buildup to a photostationary state of O_3 which acts as a filter to reduce the effective value of I_0 . This effect is eliminated by allowing the jacketed lamp to run for several minutes before the start of an actual experiment. Provided that the above precautions are observed, we have found that for kinetically well-behaved systems (e.g., standard actinometers, $Co(NH_3)_5Cl^{2+}$, etc.), product yields are not detectably dependent on exposure time (at constant I_a) for periods as short as 10 sec or as long as 1 hr.

Results

Photolysis Products. In agreement with the previous reports on the photochemistry of $Co(NH_3)_5N_3^{2+}$, we find that Co^{2+} and N_2 are the major final products of reaction. We have also found that the ultraviolet absorbance of irradiated solutions cannot be accounted for on the basis of mixtures of $Co(NH_3)_5N_3^{2+}$, Co^{2+} , and NH_4^+ in $HClO_4$. There is no noticeable shift in the near-ultraviolet absorbance maximum of $Co(NH_3)_5N_3^{2+}$ (λ_{max} 301 nm); rather this change in ultraviolet absorbance is most noticeably manifested as a shift to longer wavelengths of the ultraviolet absorbance minimum ($\lambda \sim 250$ nm) as exposure time is increased.⁴¹ In this section we report our attempts to isolate and characterize this new absorbing species in the photolyzed solutions. Indirect information about this species will be presented in our discussion of the kinetics of the photochemical decompositions.

We have been unable by any means to detect free N_3^- , NH_2OH , N_2H_4 , or H_2O_2 in the photolyzed solutions (see Table I).⁴² In several attempts at cation-exchange separation of the components of photolyzed solutions we found that the species, mentioned above, which absorbs significantly in the ultraviolet, is not present in solution after passage through the ion-exchange column. Careful elution (using 0.1–1 M $Mg(ClO_4)_2$) of material from the resin showed no evidence for more than about 1% $Co(NH_3)_5OH_2^{3+}$. The ion-exchange studies of $Co(NH_3)_5N_3^{2+}$ were complicated by the observation that the absorption spectra of eluent fractions varied significantly with the length of time the $Co(NH_3)_5N_3^{2+}$ remained on the resin.

The yields of nitrogen gas (based on vpc analysis) are reported (see Tables I and II) as molar ratios, compared to the $[Co^{2+}]$ resulting from the irradiation. We have found that the yield of nitrogen tends to be low unless care is taken to keep the reaction vessel scrupulously clean. For example, after determination of N_2 yields in the $Co(NH_3)_5N_3^{2+}-I^-$ solutions (Table II), there was apparently some water-insoluble residual material in the photolysis cell which could repress the N_2 yield (to

Table I: Relative Yields of Photolysis Products from $Co(NH_3)_5N_3^{2+}$

Possible product	Yield ^a
Co^{2+}	1.00
N_2	1.25 ± 0.15^b
$Co(NH_3)_5OH_2^{3+}$	$<0.05^c$
$Co(NH_3)_4OH_2N_3^{2+}$	$\sim 3^d$
NO_2	$<0.001^e$
NO	$<0.001^e$
N_2O	$\leq 0.03^e$
N_2H_4	<0.01
NH_2OH	<0.01
N_3^-	<0.01
H_2O_2	<0.003

^a All yields relative to $\phi_{Co^{2+}}$. The upper limits represent the largest amount of each substance which could have gone undetected using our analytical techniques. ^b See Table II; error limit reflects the range of the observations. ^c Based on mass spectrometric analysis (Table III). ^d See Discussion section. ^e Based on mass spectrometric analysis.

Table II: Relative N_2/Co^{2+} Yields from the Photolysis of Azido-Ammine Complexes of Cobalt(III)^a

Complex	$[Co(III)]_{initial}$ $10^{-3} M$	Exposure time, min	$[I^-]_{initial}$ $10^{-3} M$	$[N_2]/[Co^{2+}]^b$
$Co(NH_3)_5N_3^{2+}$	6.2	0.50	...	1.27
	3.1	0.50	...	1.37
	5.7	0.50	...	1.12
	4.6	1.00	...	1.32
	3.3	0.50	...	1.22
	2.1	0.50	...	1.08
$Co(tetraen)N_3^{2+}$	4.3	0.50	11.2 ^c	0.0058
	4.2	0.50	4.9 ^c	0.16
	4.3	0.50	0.98 ^c	0.88
$Co(tetraen)N_3^{2+}$	1.5	3.00	...	0.94
	2.2	1.00	...	0.9
	2.3	1.00	...	1.13
$cis-Co(NH_3)_4(N_3)_2^+$	1.2 ^e	0.50	...	1.11
$trans-Co(NH_3)_4(N_3)_2^+$	2.6	0.50	...	1.24

^a Solutions 0.1 M in $HClO_4$; $I_0 \approx 6.6 \times 10^{-3}$ einstein $l^{-1} \text{min}^{-1}$. ^b Concentrations expressed in terms of moles per liter of product formed. ^c $[Co^{2+}] = (3.4-4.5) \times 10^{-4} M$.

as low as 1% of the Co^{2+} yield) from the photolysis of a pure $Co(NH_3)_5N_3^{2+}$ solution. After each run with I^- it was necessary to clean the photolysis cell several times with a mixture of concentrated HNO_3 and ethanol (followed by ethanol and water rinses) before the

(41) It should be noted that the absorptivity changes more rapidly at 254 nm than at 301 nm. The statement in ref 7 that the rates stand in the reverse order is in error.

(42) The absence of these species in the materials recovered from the liquid nitrogen traps used in the photolyses of evacuated solutions has also been established.

Co^{2+} ratio from pure $\text{Co}(\text{NH}_3)_5\text{N}_3^{2+}$ solutions reached the relatively constant value of 1.25.

A few experiments were also performed in which a sample of $\text{Co}(\text{NH}_3)_4\text{N}_3^{2+}$ was irradiated *in vacuo* for 0.50 min, the gases were pumped off (repeating the cycle described in the Experimental Section), and an aliquot of deaerated 0.1 M KIO_3 was added (by means of syringe) to the photolyzed solution. In one of these experiments we detected a very small amount of nitrogen. Based on this small nitrogen yield, we estimate that the ratio $[\text{N}_2\text{H}_4] + 2[\text{NH}_2\text{OH}]/[\text{Co}^{2+}] \leq 0.0026$ in the photolyzed solutions.

In addition to the specific analyses mentioned above, it should be noted that photolyzed solutions of $\text{Co}(\text{NH}_3)_5\text{N}_3^{2+}$ do not contain any substance which can reduce acidic KIO_3 (0.1 M) and only a trace (about 1% with respect to $[\text{Co}^{2+}]$) of a substance which can oxidize acidic I^- (0.1 M).

Mass Spectral Analyses of Gaseous Products. The product gases from the photolysis of $\text{Co}(\text{NH}_3)_5\text{N}_3^{2+}$ were examined mass spectrometrically (m/e 12–52). After short photolysis periods a slight enhancement in m/e 30 (compared to tank nitrogen) was observed which may imply a trace amount of NO or N_2O . Experiments with $^{15}\text{NH}_3$ enriched $\text{Co}(*\text{NH}_3)_5\text{N}_3^{2+}$ (Table III) showed a somewhat greater enhancement of m/e 30 and some enhancement of m/e 29. When irradiation was performed for extended periods or for short periods in the presence of free NH_4^+ , both m/e 44 and 30 were enhanced. Thus it would appear that NO and N_2O are probably not immediate photolysis products. Our investigations of the reactions of the immediate photolysis products with NH_4^+ will be reported in detail later.²³

Table III: Mass Spectrometric Determination of Nitrogen Isotope Ratios in N_2 Resulting from the Photolysis of $\text{Co}(\text{NH}_3)_5\text{N}_3^{2+}$

[Co(III)] _{initial} ^a 10 ⁻³ M	Exposure time, min	—Nitrogen isotope ratios—		Relative to tank N_2 ^b
		m/e 30/28 × 10 ³	m/e 29/28 × 10 ³	
4.15	0.62	0.808	7.63	0.985
3.22 ^c	0.50	1.07	7.83	1.003
4.12 ^{c,d}	20.0	1.22	8.30	...
2.60 ^e	60.0	7.50	139	...

^a $[\text{Co}(\text{NH}_3)_5\text{N}_3^{2+}]$ except as indicated. $[\text{H}^+] = 0.1$ M except as indicated. ^b $[m/e(29/28)_{\text{sample}}]/[m/e(29/28)_{\text{tank N}_2}]$. ^c ~6.5 atom % $^{15}\text{NH}_3$ in $\text{Co}(*\text{NH}_3)_5\text{N}_3^{2+}$. ^d $[\text{H}^+] = 0.001$ M. ^e $\text{Co}(*\text{NH}_3)_5\text{OH}_2^{3+}$ formed from the base hydrolysis of $\text{Co}(*\text{NH}_3)_5\text{N}_3^{2+}$. ^f $[\text{Co}(*\text{NH}_3)_5\text{OH}_2](\text{ClO}_4)_3$ was recrystallized before photolysis.

Kinetics of the Photochemical Reaction. Table IV summarizes our determinations of the quantum yields of the formation of Co^{2+} and, in some cases, the apparent quantum yields of the disappearance of the

original cobalt(III) substrate for several azido-ammine complexes. It appears that the disappearance of the original cobalt(III) substrate (as determined using ϵ_{max} for $\text{Co}(\text{NH}_3)_5\text{N}_3^{2+}$) generally parallels fairly closely the formation of Co^{2+} .

The most startling feature of the photochemistry of $\text{Co}(\text{NH}_3)_5\text{N}_3^{2+}$ has been the kinetic behavior in strongly absorbing solutions. Ordinarily one expects the rate of formation of Co^{2+} to follow the simple rate law^{8,43}

$$\frac{d[\text{Co}^{2+}]}{dt} = \phi I_a = \phi I_0(1 - e^{-\alpha})$$

where I_0 is the maximum light intensity incident on the solution and $\alpha = (\epsilon_{254})([\text{Co(III) substrate}])(\text{path length of photolysis cell})$. The expected kinetic behavior is exhibited by $\text{Co}(\text{NH}_3)_5\text{Cl}^{2+}$, as shown in Figure 2, under identical conditions, using identical techniques as those used for $\text{Co}(\text{NH}_3)_5\text{N}_3^{2+}$. In the case of $\text{Co}(\text{NH}_3)_5\text{N}_3^{2+}$, for the higher light intensities ($I_a \geq 3 \times 10^{-4}$ einstein $\text{l}^{-1} \text{min}^{-1}$), we have generally found that $d[\text{Co}^{2+}]/dt$ increases as $\text{Co}(\text{NH}_3)_5\text{N}_3^{2+}$ is consumed. This kinetic irregularity, noted in a preliminary communication,⁷ is illustrated by another example in Figure 2 and has always been observed for the irradiation of $\text{Co}(\text{NH}_3)_5\text{N}_3^{2+}$ at sufficiently high values of I_a and sufficiently large extents of reaction. We have indicated the observation of such kinetic irregularities in the studies summarized in Table IV by the entry of a minimum value of $\phi_{\text{Co}^{2+}}$ observed at large extents (25–75%) of photolysis ($\phi_{\text{Co}^{2+}, \text{final}}$).

Detailed spectrophotometric analyses of irradiated solutions have shown that the absorption of 2537-Å radiation does not generally decrease in proportion to $[\text{Co}(\text{NH}_3)_5\text{N}_3^{2+}]$ (see Table V). However, I_a at 2537 Å generally does decrease during photolysis; the minimum value of ϕ_{final} in Table IV has been calculated using the initial value of I_a . In one sense the observations cited in Table IV can be interpreted as an increase in ϕ_{app} with I_a . Comparisons of the studies summarized in Table IV shows that $\phi_{\text{Co}^{2+}}$ varies with I_a but is apparently independent of $[\text{Co}(\text{NH}_3)_5\text{N}_3^{2+}]$ at constant I_a (e.g., compare entries 1–4, 12, and 13).

In a few determinations we have followed the change in $\Phi = (\Delta[\text{Co}^{2+}])/(\Delta t)I_{a(\text{av})}$ during a single photolysis experiment, and we find that Φ increases during photolysis if $\text{Co}(\text{NH}_3)_5\text{N}_3^{2+}$ (or $\text{Co}(\text{NH}_3)_4\text{OH}_2\text{N}_3^{2+}$) absorbs a high percentage of the incident radiation during the early stages of photolysis (e.g., see Table V). The percentage of radiation absorbed is a function of both the geometry of the photolysis apparatus and $[\text{Co}(\text{NH}_3)_5\text{N}_3^{2+}]$. In Figure 3 we have compared Φ or

(43) Because of the geometry of our photochemical apparatus, the rates are expected to follow Beer's law only approximately, and the ratio of $\alpha/(\text{absorbance of the Co(III) substrate})$ is an undetermined geometrical factor. It is for this reason that we use actinometry curves over the relevant absorbance range for each photochemical apparatus. See also discussion in ref. 8.

Table IV: Quantum Yields for the 2537-Å Photolysis of $\text{Co}(\text{NH}_3)_5\text{N}_3^{2+}$, $\text{Co}(\text{tetraen})\text{N}_3^{2+}$, *cis*- $\text{Co}(\text{NH}_3)_4(\text{NH}_2)_2^{2+}$, *trans*- $\text{Co}(\text{NH}_3)_4(\text{N}_3)_2^{2+}$, and $\text{Co}(\text{NH}_2)_4\text{OH}_2\text{N}_3^{2+}$

[Co(III)] _{initial} , 10 ⁻³ M	[H ⁺], M	<i>I</i> _a (initial), (10 ⁻⁴ einstein l. ⁻¹ min ⁻¹)	$\phi_{\text{Co}^{2+}}$ Initial	Final ^a	$\phi_{-\text{Co(III)}-\text{N}_3^m}$
Co(NH₃)₅N₃²⁺					
5.60	0.10	44 ^b	0.29		
8.60	0.20	50 ^b	0.28		
19.5	0.10	56 ^b	0.3		
24.7	0.10	58 ^b	0.28		
4.50	0.010	5.5 ^c	0.20	>0.5	0.2 → 0.5 ^d
2.96	0.010	4.4 ^c	0.20		
3.23	0.10	5.0 ^c	0.22	>0.46	0.2 → 0.5 ^d
0.99	0.10	3.3 ^c	0.16	>0.35	
4.70 ^e	0.010	5.5 ^c	0.20	>0.5	
0.26	0.10	0.87 ^c	0.38 ^c	0.38 ^f	
0.154	0.10	0.44 ^c	0.27 ^g	≥0.7	≥1.7 ^g
0.079	0.10	0.23 ^c	0.82 ^f		
2.50	0.32	0.22 ^h	0.64 ^f		0.6
2.50	0.06	0.22 ^h	0.64 ^f		
2.50	0.006	0.22 ^h	0.64 ^f		
2.50	0.003	0.22 ^h	0.68 ^f		
2.50	0.0016	0.22 ^h	0.73 ^f		
2.50	0.0004	0.22 ^h	0.73 ^f		
2.50	0.03	0.22 ^h	0.64 ^{f,i}		
2.50 ^j	0.003	~0.20 ^h	0.7		
2.51 ^j	0.08	~0.20 ^h	0.7		
2.47 ^j	0.16	~0.20 ^h	0.65		
Co(tetraen)N₃²⁺					
2.90	1.0	5.5 ^c	0.30		0.30
2.92	0.047	5.5 ^c	0.29		
3.28	0.0093	5.5 ^c	~0.2 ^k		0.24
3.98	0.0074	5.5 ^c	0.12 ^{l,k}		0.20
<i>cis</i>-Co(NH₃)₄(NH₂)₂²⁺					
2.60	0.020	52 ^b	0.24 ^f		0.20
2.48	0.020	5.5 ^c	0.28 ^f		0.34 ^f
<i>trans</i>-Co(NH₃)₄(N₃)₂²⁺					
2.36	0.040	60 ^b	0.13 ^f		
0.70	0.020	4.8 ^c	0.27		0.36 ^f
Co(NH₂)₄OH₂N₃²⁺					
1.60	0.10	4.3 ^c	0.20	>0.5	0.2 → 0.5 ^d
1.52	0.19	4.2 ^c	0.16	>0.24	

^a A minimum value for the final Co²⁺ yield in cases where kinetic irregularities were observed; see text. ^b *I*₀ ≈ 6.6 × 10⁻³ einstein l.⁻¹ min⁻¹. ^c *I*₀ ≈ 5.5 × 10⁻⁴ einstein l.⁻¹ min⁻¹. ^d $\phi_{-\text{Co(III)}-\text{N}_3}$ increased during photolysis in a manner paralleling the change in $\phi_{\text{Co}^{2+}}$. ^e Solution prepared with a previously photolyzed solution of $\text{Co}(\text{NH}_3)_5\text{N}_3^{2+}$ from which all metal ions had been removed. ^f No break was observed in the kinetics curve. ^g The initial stages of reaction were not well defined. ^h *I*₀ ≈ 8 × 10⁻⁶ einstein l.⁻¹ min⁻¹. ⁱ O₂ bubbled through solution during irradiation. ^j [N₃⁻] = 0.020 M; about 25% of the absorbance at 254 nm was due to N₃⁻. ^k Co²⁺ yields are based on ~10% of reaction. ^l The extraction method for [Co²⁺] did not work well in this experiment. ^m Values of ϕ based on absorbance changes at 275, 308, and 325 nm. The spread of values was about ±10%. ⁿ This quantum yield for the disappearance of "Co(III)" is based on spectral data for the original azido complexes. Since the molar absorptivities of all azido-ammine complexes of Co(III) are not identical at any particular wavelength, and since the kind of azido-cobalt(III) complex appears to change during irradiation in the cases of $\text{Co}(\text{NH}_3)_5\text{N}_3^{2+}$ and $\text{Co}(\text{NH}_2)_4\text{OH}_2\text{N}_3$, these are only "apparent" quantum yields.

Table V: Photokinetic Behavior of $\text{Co}(\text{NH}_3)_5\text{N}_3^{2+}$ and $\text{Co}(\text{NH}_3)_4\text{OH}_2\text{N}_3^{2+}$ at 2537 Å^a

Exposure time, min	$\Delta[\text{Co}^{2+}]$, 10 ⁻⁴ M	Abs ₂₅₄	<i>I</i> _a , 10 ⁻⁴ einstein l. ⁻¹ min ⁻¹	ϕ^b
Co(NH₃)₅N₃²⁺, [Co(III)]_{initial} = 1.80 × 10⁻³ M				
0.0	...	1.27	4.5	0.18
0.5	0.39	1.26	4.5	0.15
1.0	0.71	1.22	4.5	0.14
1.5	1.03	1.17	4.4	0.20
2.0	1.48	1.15	4.4	0.21
3.5	2.86	1.03	4.2	0.49
5.0	5.43	0.63	2.9	0.48
7.0	7.84	0.44	2.1	0.86
10.0	10.26	0.14	0.7	
Co(NH₃)₄OH₂N₃²⁺, [Co(III)]_{initial} = 1.89 × 10⁻³ M				
0.0	...	1.30	4.5	0.18
0.5	0.38	1.08	4.3	0.28
1.5	1.59	1.03	4.2	0.42
2.0	2.40	0.80	3.6	0.54
3.0	4.30	0.78	3.5	0.58
3.5	5.29	0.72	3.3	0.47
5.0	6.07	0.60	2.8	

^a At 25° with [H⁺] = 0.1 M. ^b $\phi = (\Delta[\text{Co}^{2+}]) / (\Delta t) I_{a(\text{av})}$.

ϕ_{initial} for the irradiation of $\text{Co}(\text{NH}_3)_5\text{N}_3^{2+}$ in the three photolysis units used in this study with the per cent of radiation transmitted through the photolysis cell during each stage of the photolysis.

We have also included in Table IV some of our observations of the lack of variation of $\phi_{\text{Co}^{2+}}$ in the presence of potential scavengers. In general we have found $\phi_{\text{Co}^{2+}}$ to be insensitive to the presence of nonabsorbing chemical reagents in the solution being photolyzed.^{7,23} In addition, in one experiment we irradiated an acidic solution of $\text{Co}(\text{NH}_3)_5\text{N}_3^{2+}$ until all the cobalt(III) complex was destroyed (~20 min for *I*₀ = 5.5 × 10⁻⁴ einstein l.⁻¹ min⁻¹). High charge type cationic species were removed from this solution by ion exchange (acidic resin), and the remaining solution was used in the preparation of a solution of $\text{Co}(\text{NH}_3)_5\text{N}_3^{2+}$ for photolysis (60 vol % of this new solution came from the previously irradiated sample). This latter solution exhibited precisely the same photokinetic behavior reported above for solutions which did not initially contain photolysis products.

We determined the ammonia yield from the irradiation of 5.2 × 10⁻³ M $\text{Co}(\text{NH}_3)_5\text{N}_3^{2+}$ in 0.1 M HClO₄ (*I*_a ≈ 5 × 10⁻⁴ einstein l.⁻¹ sec⁻¹). After irradiation for 5 min, $\Delta[\text{Co}^{2+}] = 1.07 \times 10^{-3}$ M and $[\text{NH}_3^+] = (8 \pm 1) \times 10^{-3}$ M; after 10 min, $\Delta[\text{Co}^{2+}] = 2.21 \times 10^{-3}$ M and $[\text{NH}_4^+] = (16 \pm 2) \times 10^{-3}$ M.

Discussion

Stoichiometry of the Photochemical Reaction. The coordinated ¹⁵NH₃ tracer studies reported in Table III can be used to put an upper limit on the amount of

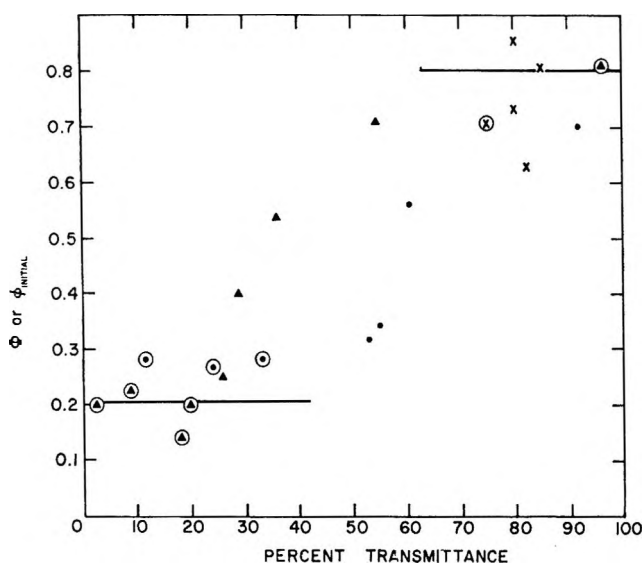


Figure 3. Quantum yields of Co^{2+} formation from the photolysis of $\text{Co}(\text{NH}_3)_5\text{N}_3^{2+}$ as a function of the percent transmittance of the solution. Circled points indicate ϕ_{initial} . Uncircled points indicate $\phi = (\Delta[\text{Co}^{2+}]) / (\Delta t) I_{0(\text{av})}$ within a single kinetic run. Incident light intensities, $I_0 = 6.6 \times 10^{-3}$ einstein $\text{l}^{-1} \text{min}^{-1}$, \bullet and \circ ; 5.5×10^{-4} einstein $\text{l}^{-1} \text{min}^{-1}$, \blacktriangle , and \odot ; $\sim 8 \times 10^{-5}$ einstein $\text{l}^{-1} \text{min}^{-1}$, \times and \otimes . The limiting values at 0 and 100% transmittance are given by the horizontal lines.

photoaquation which occurs in the 2537-Å irradiation of $\text{Co}(\text{NH}_3)_5\text{N}_3^{2+}$. If one assumes that the enrichment of the $^{14}\text{N}^{15}\text{N}$ in the nitrogen from the complete photolysis of $\text{Co}(\text{NH}_3)_5\text{N}_3^{2+}$ has come from the photolysis of $\text{Co}(\text{NH}_3)_5\text{OH}_2^{3+}$ and that this latter complex has come from photoaquation of $\text{Co}(\text{NH}_3)_5\text{N}_3^{2+}$, then the maximum amount of nitrogen gas which could have come from photolysis of $\text{Co}(\text{NH}_3)_5\text{OH}_2^{3+}$ is 0.36% of the total nitrogen. Since the 2537-Å irradiation of $\text{Co}(\text{NH}_3)_5\text{OH}_2^{3+}$ gives 0.0833 mol of N_2 per mole of Co^{2+} ,⁴⁴ the maximum amount of $\text{Co}(\text{NH}_3)_5\text{OH}_2^{3+}$ produced from the 2537-Å irradiation of $\text{Co}(\text{NH}_3)_5\text{N}_3^{2+}$ is 0.054 mol for every mole of Co^{2+} . In fact it now appears that the $\text{N}_3\cdot$ radical reacts with free NH_4^+ to give some scrambling of isotopes (when the NH_4^+ is labeled and N_3^- is not),²³ and it is undoubtedly this reaction which accounts for the enrichment of $^{14}\text{N}^{15}\text{N}$. The quantum yield for photoaquation of $\text{Co}(\text{NH}_3)_5\text{N}_3^{2+}$ must be very nearly zero.

The data shown in Tables II and IV support the suggestions⁶ that the azide radical results from the irradiation of $\text{Co}(\text{NH}_3)_5\text{N}_3^{2+}$ and can be scavenged by I^- .⁴⁶ It is to be noted, however, that we obtain some nitrogen even in the presence of an excess of I^- . This is to be expected since the radical-radical combination reaction (2) would be competitive with scavenging reactions such as (3)



The observation that I^- can nearly completely quench the N_2 yield is certainly strong evidence for the production of $\text{N}_3\cdot$ in the photoreduction of $\text{Co}(\text{NH}_3)_5\text{N}_3^{2+}$.

Despite the apparent stoichiometric defect in the nitrogen yield (Table II), we are inclined at this time to regard reaction 1 as representing the correct stoichiometry for the photoreduction of $\text{Co}(\text{NH}_3)_5\text{N}_3^{2+}$. Our reasons for this are (1) the yield reported in Table I is $83.5 \pm 10\%$ of the expected nitrogen yield which is probably close to the maximum error in the two analytical methods; (2) the radical precursors to N_2 appear to be very reactive and nitrogen yields are very often spuriously low; and (3) small quantities of other gaseous products can be detected and appear to arise from the reaction of the $\text{N}_3\cdot$ radical with NH_4^{+23} thus partially accounting for the apparent stoichiometric defect.

Our results indicate that the yield of ammonia is considerably in excess of that required by (1). The observed 8:1 ratio of $[\text{NH}_4^+]/[\text{Co}^{2+}]$ is consistent with our previous conclusion that photokinetic and other evidence implied photolabilization of an ammine ligand.⁷ This analytical result suggests that three such photolabilization events occur for each photoreduction event with a quantum yield of 0.5 (± 0.1) for the production of $\text{Co}(\text{NH}_3)_4\text{OH}_2\text{N}_3^{2+}$ from the 2537-Å irradiation of $\text{Co}(\text{NH}_3)_5\text{N}_3^{2+}$.

Kinetics of the Photoreduction of $\text{Co}(\text{NH}_3)_5\text{N}_3^{2+}$.

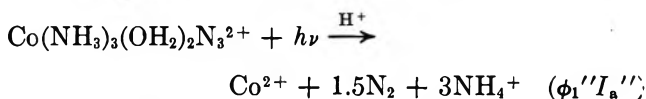
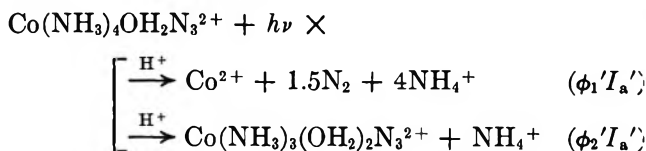
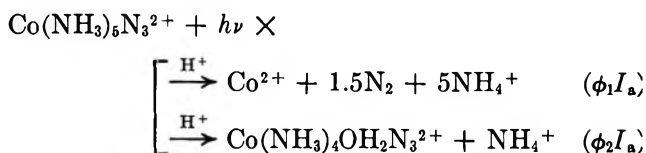
Although the kinetics curves exhibit some features of autocatalysis,⁷ we can rule out the formation of any catalyst from the irradiation of $\text{Co}(\text{NH}_3)_5\text{N}_3^{2+}$ on the following grounds. (1) There is no significant dark reaction; (2) the species associated with the changes in ultraviolet absorbance and with the higher $\phi_{\text{Co}^{2+}}$ is removed by a cation-exchange resin; (3) irradiated solutions of $\text{Co}(\text{NH}_3)_5\text{N}_3^{2+}$, after ion-exchange removal of cobalt(III) complexes, do not catalyze the photoreduction of $\text{Co}(\text{NH}_3)_5\text{N}_3^{2+}$; and (4) the photooxidation-reduction reaction is insensitive to a great variety of potential scavengers or catalysts.^{7,23} The most reasonable explanation of the peculiar photooxidation-reduction behavior of $\text{Co}(\text{NH}_3)_5\text{N}_3^{2+}$ and of $\text{Co}(\text{NH}_3)_4\text{OH}_2\text{N}_3^{2+}$ is the generation of cobalt(III)-azide complexes which are very similar to these complexes both in absorption spectra and in photochemistry.

It was suggested in a preliminary report of this work that the generation of $\text{Co}(\text{NH}_3)_4\text{OH}_2\text{N}_3^{2+}$ account for some of the kinetic irregularities observed in photolysis of $\text{Co}(\text{NH}_3)_5\text{N}_3^{2+}$.⁷ Further investigation shows that

(44) J. F. Endicott and M. Z. Hoffman, unpublished observations. It is to be noted that this is just one-half of the stoichiometric amount of N_2 required if the disproportionation of the oxidized ligand, NH_2^+ , yields only N_2 . A recent study has shown that NH_4^+ is another of the disproportionation products;^{3b} the remaining products are still being identified.

(45) Because of the absorptivity of I^- at 254 nm, we have not been able to carry out these photolyses in solutions as concentrated as reported previously.⁹ In dilute solutions the I^- - N_3 reaction is not exactly stoichiometric (Table II and ref 23). Note that I^- does not affect $\phi_{\text{Co}^{2+}}$.

upon photolysis, $\text{Co}(\text{NH}_3)_4\text{OH}_2\text{N}_3^{2+}$ exhibits kinetic behavior and a photolysis rate very similar⁴⁶ to that of $\text{Co}(\text{NH}_3)_5\text{N}_3^{2+}$. It appears that the simplest mechanism which accounts for our observation is



Then the rate of formation of Co^{2+} is

$$\frac{d[\text{Co}^{2+}]}{dt} = \phi_1 I_a + \phi_1' I_a' + \phi_1'' I_a'' \quad (4)$$

where the various values of I_a are given approximately⁴³ by Beer's law and the absorbancies of the various complexes

$$I_a = I_0(1 - e^{-x})$$

$$I_a' = I_0(1 - e^{-y})$$

$$I_a'' = I_0(1 - e^{-z})$$

and x , y , and z are the absorbancies of $\text{Co}(\text{NH}_3)_5\text{N}_3^{2+}$, $\text{Co}(\text{NH}_3)_4\text{OH}_2\text{N}_3^{2+}$, and $\text{Co}(\text{NH}_3)_3(\text{OH}_2)_2\text{N}_3^{2+}$ at some time t , respectively.

It is useful to consider two different limiting cases. The first important case is that in which $\text{Co}(\text{NH}_3)_5\text{N}_3^{2+}$ initially has a high absorbance. In this limit $d[\text{Co}^{2+}]/dt \rightarrow \phi_1 I_0(1 - e^{-x})$ as $t \rightarrow 0$. This is the lower limit in Figure 3 where $\phi_1 \simeq 0.2$.

The second important limiting case is when $(x + y + z) \rightarrow 0$. To treat this case it is necessary to observe that the experimental values of the quantum yield, Φ_{exp} , are based on the "initial" slopes of plots of $[\text{Co}^{2+}]$ vs. time.⁴⁷ Under such low absorbance conditions the partly aquated species will be photolyzed nearly as rapidly as they are produced, and a photostationary state in $[\text{Co}(\text{NH}_3)_4\text{OH}_2\text{N}_3^{2+}]$ and $[\text{Co}(\text{NH}_3)_3(\text{OH}_2)_2\text{N}_3^{2+}]$ would be quickly achieved. Assuming such photostationary states, $y \simeq \phi_2 x / (\phi_1' + \phi_2')$ and $z \simeq \phi_2' \phi_2 x / (\phi_1' + \phi_2') \phi_1''$. In the limit of low absorbancies, eq 4 becomes

$$\frac{d[\text{Co}^{2+}]}{dt} \simeq \phi_1 I_0 x + \phi_1' I_0 y + \phi_1'' I_0 z \simeq \left\{ \phi_1 + \frac{\phi_1' \phi_2}{\phi_1' + \phi_2'} + \frac{\phi_2' \phi_2}{\phi_1' + \phi_2'} \right\} \alpha I_0 e^{-\lambda t}$$

where αI_0 is the value of I_a at $t = 0$, $\lambda = \epsilon I_0(\phi_1 + \phi_2)$

and ϵ is the molar absorptancy of $\text{Co}(\text{NH}_3)_5\text{N}_3^{2+}$ at 254 nm. At short exposure times, Φ_{exp} may be identified with the time-independent part of this expression

$$\Phi_{\text{exp}} \simeq \phi_1 + \frac{\phi_1' \phi_2}{\phi_1' + \phi_2'} + \frac{\phi_2' \phi_2}{\phi_1' + \phi_2'}$$

Since the photochemistries of $\text{Co}(\text{NH}_3)_5\text{N}_3^{2+}$ and $\text{Co}(\text{NH}_3)_4\text{OH}_2\text{N}_3^{2+}$ are very similar at 2537 Å, we may estimate that $\phi_1 \simeq \phi_1' \simeq 0.2$ and $\phi_2 \simeq \phi_2'$. For $\Phi_{\text{exp}} \simeq 0.8$, these estimates give a value of $\phi_2 \simeq 0.6$, nearly identical with the value estimated from the ammonia yield.⁴⁸

From the work reported here it appears that the photolabilization of an amine ligand is of decreasing importance in the complexes $\text{Co}(\text{NH}_3)_5\text{N}_3^{2+} \geq \text{Co}(\text{NH}_3)_4\text{OH}_2\text{N}_3^{2+} > \text{Co}(\text{tetraen})\text{N}_3^{2+}$. This behavior may not occur at all for $\text{Co}(\text{tetraen})\text{N}_3^{2+}$, and we have not been able to detect such behavior in the $\text{Co}(\text{NH}_3)_4(\text{N}_3)_2^+$ complexes. The instability (*e.g.*, to acid hydrolysis) of the later complexes and the lack of any information about $\text{Co}(\text{NH}_3)_3(\text{OH}_2)_2(\text{N}_3)_2^+$ do not allow detailed conclusions about their photochemistry. On the other hand, careful spectral and kinetic (see Table IV) analyses have shown that $\text{Co}(\text{NH}_3)_4\text{OH}_2\text{N}_3^{2+}$ cannot be an important product of irradiation of either *cis*- or *trans*- $\text{Co}(\text{NH}_3)_4(\text{N}_3)_2^+$.

It appears that the radical pair model proposed⁶ to describe the photochemistry of cobalt(III) complexes cannot account for the formation of $\text{Co}(\text{NH}_3)_4\text{OH}_2\text{N}_3^{2+}$ and the lack of formation of $\text{Co}(\text{NH}_3)_5\text{OH}_2^{2+}$ from the irradiation of $\text{Co}(\text{NH}_3)_5\text{N}_3^{2+}$. At present it seems most likely that the products resulting from the photolysis of cobalt(III) complexes depend on the structure, chemistry, lifetimes, and probabilities of formation of various excited states which are populated when these complexes are irradiated.

Acknowledgment. The authors wish to thank Mr. Ramesh C. Patel for a sample of $[\text{Co}(\text{tetraen})\text{Br}](\text{ClO}_4)_2$ and Miss Zulema Rachmanis for assistance with the ammonia analysis.

(46) Even the molar absorptivities of these complexes are similar: $\epsilon_{254} 0.66 \times 10^3 M^{-1} \text{cm}^{-1}$ for $\text{Co}(\text{NH}_3)_4\text{OH}_2\text{N}_3^{2+}$. A higher value was mistakenly reported previously.

(47) Note that the kinetics curves (*i.e.*, $[\text{Co}^{2+}]$ vs. time) are nearly linear at these low absorptivities (at least up to ~30% of reaction).

(48) A referee has suggested that a "simpler" mechanism would involve the direct production of $\text{Co}(\text{NH}_3)_3(\text{OH}_2)_2\text{N}_3^{2+}$ from the photolysis of $\text{Co}(\text{NH}_3)_5\text{N}_3^{2+}$ without the intermediate formation of $\text{Co}(\text{NH}_3)_4\text{OH}_2\text{N}_3^{2+}$. The production of several $\text{Co}(\text{NH}_3)_n(\text{OH}_2)_{2-n}\text{N}_3^{2+}$ species is certainly possible. However, production of each such species must be associated with a quantum yield, and the sum of these yields must be compatible with the observed stoichiometry in Co^{2+} and NH_3 . Thus, with ϕ_1 and ϕ_2 as defined above and for ϕ_3 ($n = 3$) and ϕ_4 ($n = 2$), then $5\phi_1 + \phi_2 + 2\phi_3 + 3\phi_4 = 1.5$, or $\phi_2 + 2\phi_3 + 3\phi_4 \simeq 0.5$. If ϕ_2 were taken as negligible, then $\phi_3 \leq 0.3$. A photostationary state treatment for such a mechanism, analogous to the treatment described above, would require $\phi_3 \simeq 0.6$ to agree with the low absorbance determinations. Although the uncertainties in these numbers is large (since they are obtained as differences of experimental yields), the formation of some $\text{Co}(\text{NH}_3)_4\text{OH}_2\text{N}_3^{2+}$ seems to be required. It should also be observed that the sum of the concentrations of all $\text{Co}(\text{NH}_3)_n(\text{OH}_2)_{2-n}\text{N}_3^{2+}$ species must necessarily be less than about 20% of the total cobalt(III) in solution at any time.

Charge-Transfer Effects on the Absorption and Fluorescence

Spectra of Anthroic Acids

by T. C. Werner^{1a} and David M. Hercules^{1b}

Department of Chemistry and Laboratory for Nuclear Science, Massachusetts Institute of Technology, Cambridge, Massachusetts 02139 (Received August 21, 1963)

The absorption and fluorescence spectra of 1- and 2-anthroic acids (1-COOH, 2-COOH) and their anions (1-COO⁻, 2-COO⁻) have been investigated. For 1-COOH and 1-COO⁻, smearing of the ¹A → ¹L_a transition by charge-transfer interaction is shown to be greater for carboxyl than for carboxylate substitution. This is attributed to the greater possible resonance interaction between the aromatic ring with the -COOH group than with the -COO⁻ group. When the carboxyl group is substituted at the 2 position of anthracene, the ¹A → ¹L_b transition is enhanced. The fluorescence of 2-COOH originates from the ¹L_b state in polar solvents and from the ¹L_a state in nonpolar solvents. Fluorescence lifetime data support these assignments. Comment is made on the increased basicity in the lowest excited singlet-state aromatic carboxylic acids and their anions. Greater ΔpK_A is expected for the acid than for the anion due to the greater ability of the COOH group to undergo resonance interaction with the ring. Previously published data on the pK_A^{*} of 9-anthroic acid (9-COOH) are found to be too high. An excited-state rotation which occurs for 9-COOH but not for 9-COO⁻ probably invalidates the Forster pK_A equation when fluorescence frequencies are used.

Introduction

Recently, excited-state rotation of the carboxyl group has been shown to occur for 9-anthroic acid (9-COOH) and its esters at room temperature, resulting in a coplanar configuration in the excited state.² In this configuration charge-transfer interaction between the carboxyl group and the ring results in a structureless, highly Stokes-shifted fluorescence. The rotation is not observed for the ionized form of the acid (9-COO⁻).

We have extended these investigations to include the fluorescence and absorption spectra of 1- and 2-anthroic acids (1-COOH, 2-COOH) and their salts. Steric inhibition to coplanarity of the carboxyl group and the ring in the ground state is less important for 1- and 2-COOH than for 9-COOH. As a result, excited-state rotation is not necessary to achieve a coplanar configuration and carboxyl group effects are evident in absorption as well as fluorescence spectra.

Experimental Section

Benzene, acetonitrile, benzonitrile, heptane, cyclohexane, and methylcyclohexane were Matheson Coleman and Bell Spectroquality solvents. U. S. Industrial Chemicals pure grade absolute ethanol and Baker Analyzed methanol were used.

1-Anthroic acid, prepared by the method of Carlson from benzanthrone,³ melted at 244–246° (lit.³ mp 245°). Sodium 1-anthroate was prepared from the acid and was crystallized from ethanol. Both 2- and 9-anthroic acids were obtained from Aldrich Chemical Co. and were recrystallized several times from ethanol. Quinine sulfate was recrystallized several times from ethanol.

Absorption spectra were obtained using a Cary Model 14 spectrophotometer.

Fluorescence spectra were recorded on a G. K. Turner Associates Model 210 "Spectro" absolute spectrofluorometer. This instrument records corrected spectra in quanta per unit wavelength interval. Fluorescence quantum yield measurements were carried out on the Turner Model 210 "Spectro" according to the procedure of Turner.⁴ Quinine sulfate in 0.1 N H₂SO₄ was used as the fluorescent standard (φ_f = 0.57). Both fluorescence standard and sample solutions had absorbances less than 0.02 (1-cm cells) at the exciting wavelength. All sample solutions were deoxygenated by bubbling with prepurified nitrogen.

Fluorescent lifetimes were measured using a TRW Model 31A nanosecond spectral source⁵ and associated system components. The output was recorded on a Tektronix 556 dual-beam oscilloscope employing Type 1A1 dual-trace and Type B plug-in units. A Corning 110-816 filter (color specification 2A) was used to pass emission above 420 nm. All solutions were deoxygenated by nitrogen bubbling before measurement.

Results

The absorption spectra of 1-COOH in acidic ethanol, benzene, and benzonitrile are shown in Figure 1. These spectra are displaced toward lower energy and are con-

(1) (a) National Institutes of Health Predoctoral Fellow, 1967–1968. (b) Address all correspondence to this author at the Department of Chemistry, University of Georgia, Athens, Ga. 30601.

(2) T. C. Werner and D. M. Hercules, *J. Phys. Chem.*, **73**, 2005 (1969).

(3) C. A. Coulson, *J. Chem. Soc.*, 1932 (1930).

(4) G. K. Turner, *Science*, 183 (1964).

(5) "Measurement of Short Decay Times with the TRW Nanosecond Spectral System," Application Note 6, TRW Instruments, El Segundo, Calif.

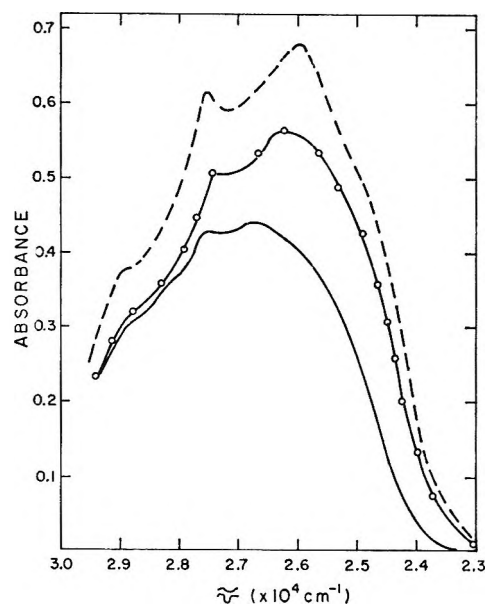


Figure 1. Absorption spectra of 1-anthroic acid in acidic ethanol, benzonitrile, and benzene: —, benzene ($1.2 \times 10^{-4} M$, 1,000-cm cell); - - -, acidic ethanol ($9.5 \times 10^{-5} M$, 1,000-cm cell); $\circ-\circ-\circ$, benzonitrile ($1.1 \times 10^{-4} M$, 1,000-cm cell).

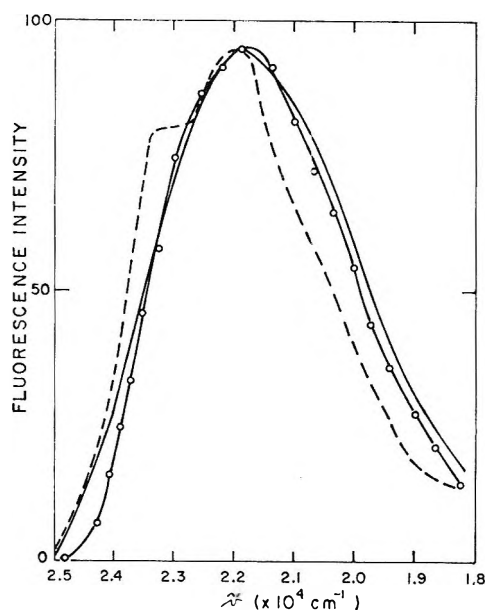


Figure 2. Fluorescence of 1-anthroic acid in acidic ethanol, benzene, and benzonitrile: —, acidic ethanol (*ca.* $10^{-5} M$); - - -, benzene (*ca.* $10^{-5} M$); $\circ-\circ-\circ$, benzonitrile (*ca.* $10^{-5} M$).

siderably more diffuse than the spectra of anthracene or 9-COOH in these solvents. The absorption maxima of 1-COOH are blue shifted by 800 and 200 cm^{-1} in acidic ethanol and benzonitrile, respectively, *vs.* benzene.

Fluorescence spectra of 1-COOH in acidic ethanol, benzene, and benzonitrile shown in Figure 2 are quite diffuse just as for 9-COOH fluorescence in these sol-

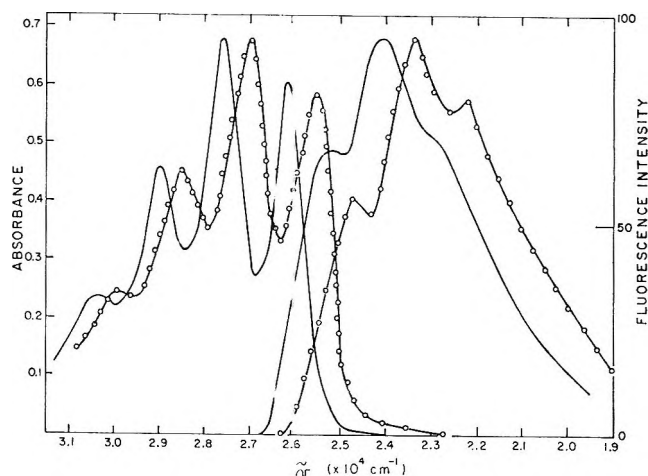


Figure 3. Absorption and fluorescence spectra of sodium 1-anthroate in benzonitrile and in ethanol: —, ethanol (*ca.* $10^{-4} M$, 1,000-cm cell); $\circ-\circ-\circ$, benzonitrile (*ca.* $10^{-4} M$, 1,000-cm cell).

vents. The Stokes shift (absorption to fluorescence maximum) increases from benzene (4000 cm^{-1}) to benzonitrile (4500 cm^{-1}) to acidic ethanol (5000 cm^{-1}). The Stokes shifts are greater than those observed for anthracene but smaller than for 9-COOH.

In Figure 3, the absorption and fluorescence spectra of 1-COONa in ethanol and benzonitrile are shown. The absorption spectrum is red shifted relative to anthracene absorption but, like that of 9-COONa, retains the characteristic anthracene vibronic pattern. A 600- cm^{-1} blue shift of the 0,0 band is observed in ethanol relative to benzonitrile. The fluorescence of 1-COONa is more diffuse than 9-COONa fluorescence (Figures 3 and 1 of ref 2). The fluorescence Stokes shifts for 1-COONa in ethanol and benzonitrile are nearly the same (*ca.* 3500 cm^{-1}).

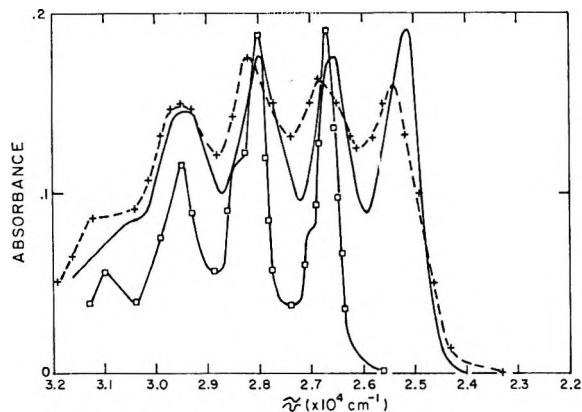
Table I lists the frequency of maximum absorption and fluorescence and the fluorescence Stokes shifts for 1-COOH and 1-COONa in the solvents mentioned above.

The absorption spectra of 2-COOH in cyclohexane and acetonitrile are shown in Figure 4. In heptane, methylcyclohexane, and benzene the absorption spectra are similar to those in cyclohexane while in acidic ethanol or acidic methanol the absorption resembles the acetonitrile spectrum. Relative to cyclohexane, the 0,0 transition is found to shift to higher frequencies with increasing solvent polarity. An absorption spectrum of anthracene in ethanol is included in Figure 4 as a comparison.

In Figure 5 the fluorescence spectra of 2-COOH in cyclohexane, acetonitrile, and acidic methanol are shown. A structured emission is observed in cyclohexane while a diffuse band at *ca.* 23,000 cm^{-1} is obtained in acetonitrile and in acidic methanol. The fluorescence spectra of 2-COOH in heptane and methylcyclohexane are identical with the cyclohexane spectra

Table I: Absorption and Fluorescence Maxima and Stokes Shifts for 1-Anthroic Acid and Sodium 1-Anthroate^a

Compound	Solvent	Abs max $\times 10^{-4}, \text{cm}^{-1}$	Fluor max $\times 10^{-4}, \text{cm}^{-1}$	$\Delta\bar{\nu}, \text{cm}^{-1}$
1-Anthroic acid	Acidic ethanol	2.68 (3.65)	2.18	5.0
	Benzonitrile	2.62	2.17	4.5
	Benzene	2.60	2.20	4.0
Sodium 1-anthroate	Ethanol	2.75 (3.81)	2.40	3.5
	Benzonitrile	2.70	2.34	3.6
2-Anthroic acid	Ethanol	2.55 (3.55)	2.29	
		2.68 (3.55)		
		2.81 (3.58)		
		2.96 (3.52)		
		3.08 (3.30)		
Sodium 2-anthroate	Ethanol	2.61 (3.63)	2.56	
		2.76 (3.69)	2.41	
		2.92 (3.58)	2.29	
		3.03 (3.36)	2.17	

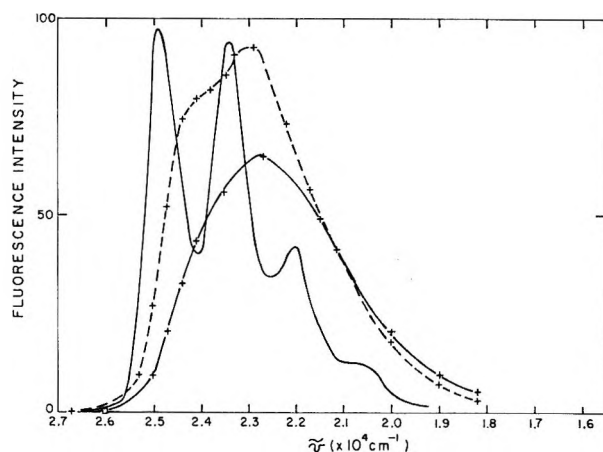
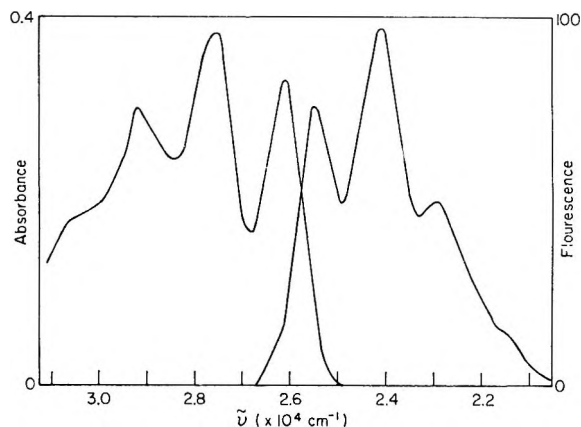
^a Deviation $\pm 100 \text{ cm}^{-1}$.**Figure 4.** Absorption of 2-anthroic acid in cyclohexane and acetonitrile compared with the absorption of anthracene in hexane: $-\square-\square-\square-$, anthracene in hexane ($ca. 2.0 \times 10^{-5} M$, 1,000-cm cell); $+---+$, 2-COOH in acetonitrile ($ca. 5.0 \times 10^{-5} M$, 1,000-cm cell); $---$, 2-COOH in cyclohexane ($ca. 5.0 \times 10^{-5} M$, 10.00-cm cell).

while in acidic ethanol the results are similar to acidic methanol.

The absorption and fluorescence spectra of 2-COO⁻ in basic ethanol are shown in Figure 6. The mirror image relationship is evident. Both absorption and fluorescence spectra resemble anthracene spectra although the 2-COO⁻ absorption is more diffuse than comparable spectra of 1- and 9-COO⁻.

Table I also contains the extinction coefficients and absorption and fluorescence maxima for 2-COOH in basic and weakly acidic ethanol.

Table II contains the fluorescence lifetimes (τ_f), fluorescence quantum yields (ϕ_f), and the calculated

**Figure 5.** Fluorescence of 2-anthroic acid in cyclohexane, acetonitrile, and acidic methanol: $---$, cyclohexane; $+---+$, acetonitrile; $+---+$, methanol + $10^{-3} N HCl$; $c = 1.0 \times 10^{-5} M$.**Figure 6.** Absorption and fluorescence of 2-anthroic acid in basic ethanol; $c = 8.0 \times 10^{-5} M$ for absorption spectrum, 1,000-cm cell.**Table II:** Values of τ_f , τ_f^0 , and τ_f^0 for 2-Anthroic Acid in Cyclohexane and in Acetonitrile

Solvent	ϕ_f	τ_f , nsec	$(\tau_f^0)_{\text{abs}}$, nsec	$(\tau_f^0)_{\text{rad}}$, nsec
Acetonitrile	0.31 ± 0.03	19.5 ± 2	22	63
Cyclohexane	0.49 ± 0.02	13.6 ± 1	(25) ^a	28

^a Estimate based on relative intensities of 2-COOH absorption in acetonitrile and cyclohexane. The very low solubility of 2-COOH in the latter solvent precludes an accurate measurement of concentration needed to measure $(\tau_f^0)_{\text{abs}}$.

intrinsic excited-state lifetimes (τ_f^0) for 2-COOH in acetonitrile and cyclohexane. The τ_f^0 's were calculated by two different methods.

First, $(\tau_f^0)_{\text{rad}}$ was found from the relationship between the measured ϕ_f and τ_f .⁶

(6) E. H. Gilmore, G. E. Gibson, and D. S. McClure, *J. Chem. Phys.*, **23**, 399 (1955).

$$(\tau_f^0)_{\text{rad}} = \frac{\tau_f}{\phi_f}$$

Second, $(\tau_f^0)_{\text{abs}}$ was obtained by integrating the absorption spectrum of 2-COOH plotted as ϵ vs. $\bar{\nu}$ cm^{-1} . The equation below was used for the calculation⁷

$$\frac{1}{(\tau_f^0)_{\text{abs}}} = 2.88 \times 10^{-9} \frac{g_m \bar{\nu}^2}{g_u} (F) \int_{\bar{\nu}_1}^{\bar{\nu}_2} \epsilon(\bar{\nu}) d\bar{\nu}$$

where g is the multiplicity of the states involved in the transition, $\bar{\nu}$ is the average frequency of the transition, and

$$\int_{\bar{\nu}_1}^{\bar{\nu}_2} \epsilon(\nu) d\nu$$

is the integral of the absorption spectrum plotted in $\epsilon(\bar{\nu})$ vs. $\bar{\nu}$ in cm^{-1} .

F is the correction term for the solvent refractive index. The relationship of Rabinowicz was used to calculate this correction term⁸

$$F = \frac{9N}{(N^2 + 2)^2}$$

where N is the solvent refractive index.

The difference in the ground- and excited-state pK_a of 9-COOH was calculated using the Forster equation⁹

$$\Delta pK_a = \frac{hc\Delta\nu}{2.303kT}$$

where $\Delta\nu$ is the difference in the 0,0 transition for the ionized and un-ionized acid.

Previously, the anthracene-like fluorescence of 9-COO⁻ was reported to change in aprotic solvents such as benzonitrile to a structureless, lower energy emission similar to that of 9-COOH.² This observation resulted from a trace of acid-base equilibrium to the molecular form (9-COOH). In acid-free benzonitrile, as in all other solvents, the fluorescence of 9-COO⁻ possesses the anthracene-like structure shown in Figure 1 of reference 2.

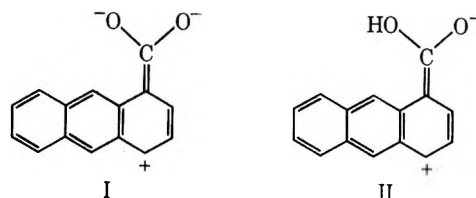
Discussion

1-Anthroic Acid. Absorption Spectra of 1-Anthroic Acid. Molecular models demonstrate that there is less steric hindrance to coplanarity of the carboxyl group and aromatic nucleus for 1-COOH than for 9-COOH. From X-ray analysis of 1-naphthoic acid, where the carboxyl group geometry should be similar to that of 1-COOH, the angle between the ring and carboxyl group is 11°. At this angle significant resonance interaction between aromatic ring and carboxyl group will occur. Some charge-transfer (CT) character is thereby introduced into the ¹A → ¹L_a (or ¹L_a) transition resulting in a red shift and loss of structure relative to the parent hydrocarbon.¹¹ Comparison of the absorption spectra of 1-COOH in Figure 1 with the absorption spectra of 9-COOH² demonstrates this effect.

In benzoic acid the absorption band at 230 nm is assigned to a CT transition, involving a one-electron promotion from the highest bonding π orbital of the ring to the antibonding π orbital of the carboxyl group.¹² The transition is perturbed by the higher energy (ca. 200 nm) ¹L_a state.¹² For 1-naphthoic acid¹³ the ¹L_a state will lie below the CT state and the lowest energy excitation will be a ring $\pi \rightarrow \pi^*$ transition having some CT character.¹⁴ The extent of the mixing depends inversely on the energy separation between the states involved.

The ¹L_a transition is essentially a one-electron transition from the highest bonding (ϕ_{+1}) to the lowest antibonding orbital (ϕ_{-1}) of hydrocarbon.¹⁵ On going from 1-naphthoic acid to 1-anthroic acid the ϕ_{+1} orbital is raised and the ϕ_{-1} orbital is lowered while the carboxyl group antibonding orbital (ϕ'_{-}) does not change significantly. Therefore, both the ¹L_a and CT transitions shift to lower energy, but the shift is greater for the ¹L_a transition. The energy difference between CT and ¹L_a states is therefore greater for 1-anthroic acid. In addition, the electron density at the 1-position of naphthalene is greater than at the 1-position of anthracene.¹⁵ Thus, greater resonance interaction between aromatic ring and carboxyl group is expected for 1-naphthoic acid than for 1-anthroic acid. As a result of these two effects, greater CT character is expected in the ¹L_a state of 1-naphthoic acid. Evidence for this is seen in the red shifts of ¹L_a bands in the acids relative to their parent hydrocarbons. For 1-naphthoic acid the shift is 2400 cm^{-1} , while for 1-anthroic acid the shift is only 1100 cm^{-1} .

Absorption of 1-Anthroate Anion. Resonance forms, such as I, are less important for the ground state of 1-COO⁻ than forms like (II) for 1-COOH. The carboxylate anion, already possessing a negative charge, will not readily accept the second negative charge necessary for resonance interaction.¹⁶ Thus, the inductive



(7) J. G. Calvert, J. M. Pitts, Jr., "Photochemistry," John Wiley and Sons, New York, N. Y., 1967, p 174.

(8) A. Rabinowicz, *Rep. Progr. Phys.*, **12**, 233 (1948-1949).

(9) A. Weller, *Progr. Reaction Kinetics*, **1**, 187 (1961).

(10) J. Trotter, *Acta Cryst.*, **15**, 732 (1962).

(11) J. N. Murrell, "The Theory of the Electronic Spectra of Organic Molecules," John Wiley and Sons, New York, N. Y., 1963, Chapter 9.

(12) H. Suzuki, "Electronic Absorption Spectra and the Geometry of Organic Molecules," Academic Press, New York, N. Y., 1967, p 472.

(13) A. E. Lutskii and L. A. Antropova, *Zh. Fiz. Khim.*, **39**, 1131 (1965).

(14) Reference 11, Chapter 10.

(15) Reference 11, Chapter 12.

effect of the carboxylate anion is smaller than that of the carboxyl group. Introduction of CT character into the 1L_a state therefore is less important for 1-COO⁻ than 1-COOH. As a result the absorption spectrum of COO⁻ retains the characteristic vibronic pattern of the anthracene 1L_a transition. A slight red shift of the 1-COO⁻ absorption relative to anthracene is the only evidence for a carboxylate ion effect on the 1L_a transition.

Owing to the smaller interaction between the carboxylate ion and ring than between the carboxyl group and ring it is likely that 1-COO⁻ ground-state geometry involves a less planar configuration than for 1-COOH.

Solvent Effects. Figure 1 shows a blue shift of the absorption maximum of 1-COOH with increasing solvent polarity. Similar behavior has been reported previously for the 1L_a band of 1-naphthoic acid.¹³ Generally, $\pi \rightarrow \pi^*$ transitions shift red with increasing solvent polarity. The reason for the anomalous behavior of 1-COOH is apparent when the relative effects of polar and nonpolar solvents on the Franck-Condon (FC) and equilibrium excited states are considered. Figure 7 shows a potential energy diagram for the ground and excited states of 1-COOH in benzene and ethanol, as a function of the solute-solvent interaction parameter, r . Essentially, r is the average distance between a solute and a solvent molecule.

Both the ground and excited states of 1-COOH are stabilized in ethanol relative to benzene. The molecular dipole, already in the direction of the carboxyl group in the ground state, will be increased on excitation due to the direction of the 1L_a transition dipole. Interaction between the solvent 1-COOH will therefore increase on excitation, and the equilibrium excited-state solute-solvent distance, r_e^E , will become smaller than the equilibrium ground-state distance, r_e^G . As solvent polarity increases, Δr_e , the distance between r_e^E and r_e^G , should also increase. The resulting displacement of the ground and excited-state potential curves leads to a higher energy FC state, represented by the arrows marked A in Figure 7.

It is worth noting that a blue shift of the CT band of benzoic acid with decreasing concentration in nonpolar solvents¹⁷ is attributed to a dimer-monomer equilibrium. In polar solvents, the dimerization is inhibited resulting in a blue shift of the absorption relative to that in nonpolar solvents. This behavior is similar to that discussed above for 1-COOH. However, since the absorption spectrum of 1-COOH in benzene from 10^{-4} to 10^{-6} M does not change, acid dimer formation for 1-COOH can be ruled out as the cause of the polar solvent blue shift.

In ethanol the 0,0 band of 1-COO⁻ absorption is blue shifted 600 cm^{-1} relative to the 0,0 band in benzonitrile. This is again attributed to the difference in solvation of the ground and FC excited state as discussed earlier for 1-COOH. The 0,0 band of 9-COO⁻

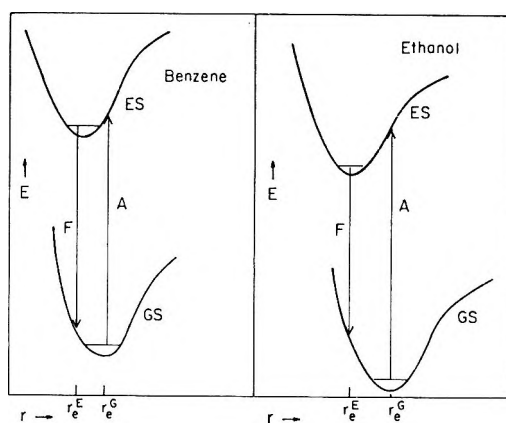


Figure 7. Potential energy curves for ground and excited states of 1-anthric acid in ethanol and benzene as a function of solute-solvent internuclear distance, r : r_e^G solute-solvent internuclear distance in ground state; r_e^E , solute-solvent internuclear distance in excited state; A, absorption; F, fluorescence; GS, ground state; ES, excited state; E, energy.

in ethanol and benzonitrile differs by only 100 cm^{-1} . As would be expected, solvent effects are better transmitted when carboxylate group and ring can approach coplanarity.

Nature of the Emission Process. Since the transition dipole of the 1L_a transition lies perpendicular to the long axis of anthracene, a greater interaction is expected between the carboxyl group and the 1L_a state than with the ground state, introducing greater CT character into the excited state. As a result, the emission of 1-COOH in Figure 2 is more diffuse than its absorption. The diffuseness is increased in polar solvents from the normal polar-solvent excited-state interactions.¹⁸

A consequence of the difference in CT nature of the two states is the observation of a greater Stokes shift for 1-COOH ($4000\text{--}5000\text{ cm}^{-1}$) than for the parent hydrocarbon anthracene (3200 cm^{-1}). The Stokes shift for 1-COOH is smaller than for 9-COOH (6500 cm^{-1}). Several factors account for this. First, the difference in excited-state and ground-state geometries is not as great for 1-COOH as 9-COOH.² Second, theory predicts the electron density in the excited state to be greater at the 9 position than at the 1 position,¹¹ therefore permitting greater resonance interaction in the former. Third, the change in the magnitude of the molecular dipole on excitation is greater for 9-COOH. For 1-COOH the ground-state dipole is larger than for 9-COOH because of the resonance effect of the carboxyl group. Therefore, upon excitation and formation of the planar excited-state, a larger increase in the molecular dipole is expected for 9-COOH.

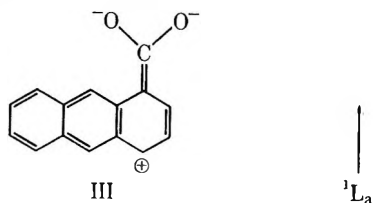
(16) E. S. Gould, "Mechanism and Structure in Organic Chemistry," Reinhold and Winston, New York, N. Y., 1959, Chapter 7.

(17) H. Husoya, J. Tanada, and S. Nagakura, *J. Mol. Spectrosc.*, **8**, 257 (1962).

(18) B. L. Van Duuren, *J. Org. Chem.*, **26**, 2954 (1961).

The Stokes shift of 1-COOH fluorescence increases in going to more polar solvents—*i.e.*, ethanol > benzonitrile > benzene. Referring to Figure 7, such a trend is predicted by the greater Δr_e and corresponding greater displacement of the potential wells in the more polar solvent. The difference in the length of the arrows A (absorption) and F (fluorescence), represents the Stokes shift.

The resonance forms for 1-COO⁻, improbable in the ground state, become more favorable in the excited state due to the electron density change induced by the ¹L_a transition dipole (III). Evidence for this differ-



ence in ground- and excited-state behavior is shown in Figure 3. In the excited state, the carboxylate anion interaction with the aromatic nucleus is sufficient to make the fluorescence spectrum more diffuse than the absorption spectrum. The extent of the interaction is not sufficient to produce the large Stokes shifts observed for 1-COOH. Since the Stokes shift for 1-COO⁻ in both ethanol and benzonitrile is *ca.* 3500 cm⁻¹, one may conclude that the change in the molecular dipole induced by excitation is smaller for 1-COO⁻ than for 1-COOH.

2-Anthroic Acid. Absorption of 2-Anthroic Acid. Molecular models indicate that steric hindrance to carboxyl group and ring coplanarity is negligible. Infrared studies show less steric interaction between the carboxyl group and ring H's for 2-COOH.¹⁹ Substitution of the carboxyl group at the 2 position of anthracene would therefore be expected to have a greater smearing effect than 9 substitution. A comparison of the absorption spectra of 9-COOH² and 2-COOH with anthracene shows this to be true.

The electron density of the highest filled anthracene MO is twice as great at the 1 position as at the 2 position.¹¹ Disregarding the small difference in steric interaction for 1 and 2 substitution, smaller resonance interaction with the carboxyl group would be expected for 2 substitution, introducing a smaller amount of CT character into the ¹L_a transition. As a result, the absorption spectra of 2-COOH in Figure 4 are less diffuse than for 1-COOH.

Closer inspection of the 2-COOH absorption spectra reveals two interesting features. First, the vibronic structure of 2-COOH absorption is different from the vibronic pattern of anthracene. Second, a comparison of the absorption and fluorescence spectra of 2-COOH in Figures 4 and 5 reveals a lack of mirror symmetry. The situation is most apparent in cyclohexane where both absorption and fluorescence show considerable

structure. The most likely explanation for these observations is that the 25,000–31,000-cm⁻¹ absorption band of 2-COOH is composed of two overlapping transitions, although emission occurs only from one excited state.

Besides the well-established ¹A₁ → ¹L_a anthracene transition in the 31,000–26,000-cm⁻¹ region, a second transition designated ¹A₁ → ¹L_b (or ¹L_b) is predicted to occur at nearly the same energy. Because it is less allowed and consequently less intense, the ¹L_b transition of anthracene is obscured by the more intense ¹L_a transition.²⁰ The polarization of the ¹L_b transition is perpendicular to the ¹L_a transition dipole lying along the longitudinal axis of the ring.²⁰

Studies on substituted naphthalene spectra have shown that the position of substitution determines the relative effects of the substituent on the ¹L_a and ¹L_b transitions.¹³ Extension of the molecule in a given direction by substitution primarily affects the transition polarized in that direction. The magnitude of the effect is greatest when there is resonance interaction between the polar forms of a particular state and the substituent. Platt has defined a spectroscopic moment which is a transition moment induced in the ring by the presence of any substituent which destroys the symmetry,²¹ listing a rather large spectroscopic moment for carboxyl group.²¹

The discrepancies between the absorption spectra of anthracene and 2-COOH can therefore be explained on the basis of an enhanced ¹L_b transition for the latter. Suzuki and Baba have used a similar argument to rationalize the spectral behavior of 2-anthranol.^{22–24} Supporting evidence for overlapping transitions in 2-COOH in acetonitrile, calculated from the measured fluorescence lifetime and quantum yield (τ_f^0)_{rad} is three times as long as the one calculated from the absorption spectrum (τ_f^0)_{abs}. Such a large discrepancy in τ_f^0 's is exactly that expected when an absorption band is a composite of two transitions. Hidden transitions in biphenyls and substituted biphenyls have been discovered in this manner.²⁵

The spectra in Figure 4 reveal a variation in the vibronic pattern of the 2-COOH absorption band in polar and nonpolar solvents. This spectral dependence can be attributed to the difference in solvation energy of the Franck-Condon ¹L_a and ¹L_b states. These states are not affected equally by changes in solvent polarity. The blue shift of the 0,0 vibronic

(19) M. Figeys-Fanconnier, H. Figeys, G. Genskens, and J. Nasielski, *Spectrochim. Acta*, **18**, 689 (1932).

(20) J. R. Platt, *J. Chem. Phys.*, **17**, 484 (1949).

(21) J. R. Platt, *ibid.*, **19**, 253 (1951).

(22) H. Baba and S. Suzuki, *Bull. Chem. Soc. Jap.*, **35**, 683 (1962).

(23) H. Baba and S. Suzuki, *J. Chem. Phys.*, **35**, 1501 (1961).

(24) H. Baba and S. Suzuki, *Bull. Chem. Soc. Jap.*, **34**, 82 (1961).

(25) I. B. Berlman and O. J. Steingraber, *J. Chem. Phys.*, **43**, 2140 (1965).

band with increasing solvent polarity is similar to the solvent dependence of 1-COOH absorption. Just as for 1-COOH, this blue shift is attributed to the increasing difference in the ground and excited-state solute-solvent distance with increasing solvent polarity.

Fluorescence of 2-Anthroic Acid. In cyclohexane the fluorescence of 2-COOH, shown in Figure 5, displays anthracene-like structure. This is also the case for other nonpolar solvents. The intrinsic excited-state lifetime $(\tau_f^0)_{rad}$ in Table II, calculated from τ_f and ϕ_f , is considerably shorter in cyclohexane than in acetonitrile. Because of the short lifetime and spectral resemblance to anthracene fluorescence, emission in nonpolar solvents is thought to originate from the 1L_a state of 2-COOH. This assignment is supported by the similar values of τ_f^0 calculated from the absorption spectrum and from fluorescence measurements.

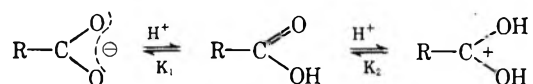
In polar solvents, such as acetonitrile, the calculated and measured values of τ_f^0 do not agree, as seen in Table II. The longer lifetime in acetonitrile indicates the emission results from a transition, less allowed than the 1L_a transition. In addition, the spectrum in polar solvents lacks structure and is red shifted. On this basis, the fluorescence in acetonitrile is assigned to the less-allowed 1L_b transition. In polar solvents, solvent stabilization of the longitudinally polarized 1L_b state of 2-COOH will be greater than stabilization of the transversely polarized 1L_a state due to the position of carboxyl group substitution. This will result in lowering the energy of the 1L_b state, relative to the 1L_a state, to the point where crossover has occurred and the 1L_b state lies lowest in energy. The transition dipole of the 1L_b state will increase the electron density at the 2 position relative to the ground state. This leads to a strong excited-state interaction between the carboxyl group and ring resulting in the almost structureless fluorescence seen in polar solvents. The smaller ϕ_f for 2-COOH in acetonitrile than in cyclohexane is also consistent with the longer intrinsic lifetime of the 1L_b state.

Absorption and Fluorescence for the 2-Anthroate Anion. Inspection of the 2-COO⁻ absorption and fluorescence in Figure 6 reveals a good mirror image relationship. Although the absorption is somewhat smeared, it clearly resembles the anthracene spectrum. Thus, significant contribution from the 1L_b transition can be ruled out. This is consistent with the smaller ground-state resonance interaction with the ring for the carboxylate anion than for the carboxyl group. As a result, a less intense 1L_b band is predicted for 2-COO⁻ than 2-COOH.

Hydrogen bonding between solvent and an aromatic ring substituent is known to produce spectral broadening.²⁶ It is this type of interaction which causes the diffuseness of the 2-COO⁻ absorption. The even more diffuse absorption of 2-COO⁻ in water is further evidence for this phenomenon. From a comparison of

Figures 3 and 6 the broadening effect of the carboxylate anion on the anthracene 1L_a transition is greatest for 2 substitution. This is in agreement with the greater degree of ring and substituent coplanarity for substitution at this position. As might be expected, significant hydrogen-bond interaction with the solvent is best transmitted to the ring *via* a coplanar configuration. The mirror-image relationship of the 2-COO⁻ absorption and fluorescence spectra means that the fluorescence, like the absorption, involves the 1L_a excited state.

Excited-State pK_a 's of Carboxylic Acids. Several workers have shown that the pK_a 's of aromatic carboxylic acids increase in their lowest excited singlet state relative to their ground state.²⁷⁻³⁰ Considering



the increase in pK_a is greater for pK_2 ($\Delta pK_2 \approx 7$) than for pK_1 ($\Delta pK_1 \approx 4$). Charge-transfer-type structures involving electron transfer from the ring to the carboxyl group have been invoked to explain the increased basicity. Porter and Vander Donckt suggested that the C=O bond is most directly affected by the charge migration while the -OH group is only indirectly affected.²⁹ From spectral data on the anthroic acids, another important factor affecting changes in pK_a is the abilities of the -COOH and -COO⁻ groups to undergo resonance with the ring. Both absorption and fluorescence spectra indicate greater charge-transfer interactions for the un-ionized acid. Consequently, on excitation, the ring can contribute more charge to the -COOH group than to the COO⁻ group and a greater increase in basicity results.

Porter and Vander Donckt have calculated the ΔpK_1 's of the three anthroic acids using the Forster cycle.³⁰ For 9-anthroic acid, they report $\Delta pK_1 = 3.5$ ($pK_1 = 3.0$, $pK_1^* = 6.5$). Our data yield $\Delta pK_1 = 3.2$ when the $\Delta \bar{\nu}$ term in the Forster equation is obtained from average values of absorption and fluorescence.

Absorption and fluorescence of 9-COO⁻ are primarily the structured 1L_a transition of anthracene only slightly perturbed. The carboxylate group is not coplanar with the ring and interaction between it and the ring is minimal.² For 9-COOH, absorption still arises from the structured 1L_a anthracene transition but fluorescence results from a CT state caused by rotation of the carboxyl group to a coplanar configuration in the excited state. Therefore, to calculate the change in

(26) H. Baba and S. Suzuki, *J. Chem. Phys.*, **35**, 118 (1961).

(27) A. Weller and W. Urban, *Angew. Chem.*, **66**, 336 (1954).

(28) E. L. Wehry and L. B. Rogers, *J. Amer. Chem. Soc.*, **88**, 351 (1966).

(29) E. Vander Donckt and G. Porter, *Trans. Faraday Soc.*, **64**, 3215 (1968).

(30) E. Vander Donckt and G. Porter, *ibid.*, **64**, 3218 (1968).

basicity of 9-COO^\ominus by using averaged absorption and fluorescence bands probably is not valid. However, excited-state rotation of the carboxyl group does not occur for the carboxylate anion, even in aprotic solvents.² Consequently, the absorption and fluorescence of 9-COO^- are primarily the structured anthracene 1L_a transition with only minor CT perturbation. This implies little transfer of electron density toward the $-\text{COO}^-$ group and a small change in basicity. If ΔpK_1 is calculated by the Forster cycle using the lowest energy vibronic components of the 9-COOH and 9-COO^- absorption spectra, a value of $\Delta pK_1 = 0.5$ is obtained. Such a value seems more consistent with the spectral behavior of 9-COO^- which indicates only a minimal

interaction between the carboxylate group and the ring. Since the excited-state rotation occurs for the un-ionized acid, the Forster assumption of equal entropy for the ground and excited-state ionization is probably not met when fluorescence frequencies are included in calculations. Thus caution must be exercised when calculating excited-state pK_a 's of molecular undergoing excited-state geometry changes.

Acknowledgments. This work was supported in part through funds provided by the Atomic Energy Commission under Contract No. AT(30-1)-905. T. C. W. thanks the National Institutes of Health and the Proctor and Gamble Co. for fellowship support.

Nuclear Magnetic Resonance Studies on the Intermolecular Association

in Some Binary Mixtures. I. Chloroform and Proton-Acceptor Solvents¹

by Wei-chuwan Lin and Shyr-jin Tsay

Department of Chemistry, National Taiwan University, Taipei, Taiwan, Republic of China
(Received February 13, 1969)

A graphic method based on nmr measurements has been developed which enables one to determine the association constant and the chemical shift of the 1:1 molecular complex in binary mixtures. Results obtained for chloroform in various proton-acceptor solvents are presented and discussed in detail.

Introduction

Nuclear magnetic resonance studies have revealed that the chemical shift of the chloroform proton in the medium of a proton acceptor is largely dependent on the chloroform concentration and also on the nature of solvent.² This dependence is attributable to intermolecular association between chloroform and solvent molecules through hydrogen bonding.² Chloroform also associates with benzene to form a complex³ whose bonding is similar to other hydrogen bonds, *i.e.*, essentially electrostatic in character.^{3b} Two types of hydrogen-bonded complex with 1:1^{3a,4} and 2:1^{3a,5} ratios, respectively, have been known between chloroform and a proton-acceptor solvent.

Many different methods of nmr approach, such as curve fitting,^{2,5} limiting slope,⁶ and temperature variation,⁷ as well as a graphic method,^{8,9} have been used to determine the association constant for 1:1 hydrogen-bonded complexes.

The present paper is concerned with the proton magnetic resonance of chloroform in a variety of proton-

acceptor solvents. A graphic method will be developed to determine the association constant and the chemical shift due to its 1:1 hydrogen-bonded complexes.

Theory

In a solution of a 1:1 solute-solvent complex, an equilibrium is considered to exist between the unasso-

(1) Based in part on material submitted for the Master's thesis of S. T.

(2) C. M. Huggins, G. C. Pimental, and J. N. Shoolery, *J. Chem. Phys.*, **23**, 1244 (1955).

(3) (a) G. W. Chantry, H. A. Gebbie, and H. N. Mirza, *Spectrochim. Acta*, **23A**, 2749 (1967); (b) R. J. Abraham, *Mol. Phys.*, **4**, 369 (1961).

(4) L. J. Andrews, *Chem. Rev.*, **54**, 713 (1954).

(5) A. L. McChellan, S. W. Nicksic, and J. C. Guffy, *J. Mol. Spectrosc.*, **11**, 340 (1963).

(6) P. J. Berkeley, Jr., and M. W. Hanna, *J. Phys. Chem.*, **67**, 846 (1963).

(7) R. E. Klinck and J. B. Stothers, *Can. J. Chem.*, **44**, 37 (1966).

(8) R. Marthur, E. D. Becker, P. B. Bradley, and N. C. Li, *J. Phys. Chem.*, **67**, 2190 (1963).

(9) S. Nishimura, C. H. Ke, and N. C. Li, *ibid.*, **72**, 1297 (1968).

ciated and associated forms of the proton donor (D) and the acceptor (A): $A + D \rightleftharpoons AD$. The equilibrium constant in terms of mole fraction (X) can be expressed as

$$K = \frac{X_{AD}}{X_A X_D} = \frac{N_{AD}}{(N_A^0 - N_{AD})(N_D^0 - N_{AD})} \times (N_A^0 + N_D^0 - N_{AD}) \quad (1)$$

where N_D^0 and N_A^0 are the number of moles of proton donor and acceptor initially given, and N_{AD} is the number of moles of 1:1 complex after equilibrium is established.

The observed shift of the chloroform proton (δ_{obsd}) is therefore the weighted average of the shift due to the unassociated solute (δ_D) and that due to the complex (δ_{AD}), *i.e.*

$$\delta_{\text{obsd}} = \frac{N_D^0 - N_{AD}}{N_D^0} \delta_D + \frac{N_{AD}}{N_D^0} \delta_{AD} \quad (2)$$

or

$$\frac{N_{AD}}{N_D^0} = \frac{\delta_{\text{obsd}} - \delta_D}{\delta_{AD} - \delta_D} = \frac{\Delta_{\text{obsd}}}{\Delta_{AD}} \quad (2')$$

where Δ_{obsd} and Δ_{AD} stand, respectively, for $(\delta_{\text{obsd}} - \delta_D)$ and $(\delta_{AD} - \delta_D)$, *i.e.*

$$\Delta_{\text{obsd}} = \delta_{\text{obsd}} - \delta_D \quad (3)$$

$$\Delta_{AD} = \delta_{AD} - \delta_D \quad (4)$$

Substitution of eq 2' into eq 1 gives

$$K = \frac{\Delta_{\text{obsd}}/\Delta_{AD}}{1 - \Delta_{\text{obsd}}/\Delta_{AD}} \left[1 + \frac{X_D^0}{X_A^0 - (\Delta_{\text{obsd}}/\Delta_{AD})X_D^0} \right] \quad (5)$$

where X^0 's denote the initial mole fractions. Equation 5 after expansion becomes

$$\Delta_{\text{obsd}}^2 \frac{1}{K} + \Delta_{\text{obsd}}^2 - \left(\frac{\Delta_{\text{obsd}}}{X_D^0} \right) \frac{\Delta_{AD}}{K} - \frac{\Delta_{\text{obsd}}}{X_D^0} \Delta_{AD} + \left(\frac{1}{X_D^0} - 1 \right) \Delta_{AD}^2 = 0 \quad (6)$$

Rearrangement of eq 6 gives

$$\frac{\Delta_{\text{obsd}}}{1 - X_D^0} = \frac{1}{\Delta_{AD}} \frac{X_D^0 \Delta_{\text{obsd}}^2}{1 - X_D^0} + \frac{\Delta_{AD}}{1 + (1/K)} \quad (7)$$

The plot of $\Delta_{\text{obsd}}/(1 - X_D^0)$ against $X_D^0 \Delta_{\text{obsd}}^2/(1 - X_D^0)$ gives a straight line whose slope and intercept determines the values of Δ_{AD} and K .

In the present study we are mainly interested in the 1:1 solute-solvent complex. However, if the formation of any other non-1:1 complex or self-association of solute proceeds competitively in the system, the plot of $\Delta_{\text{obsd}}/(1 - X_D^0)$ vs. $X_D^0 \Delta_{\text{obsd}}^2/(1 - X_D^0)$ will exhibit a distinct curvature at higher solute concentration, where these processes are expected to become more pro-

nounced. Even in this case, a linear plot obtained at the lower concentration range may be approximated to the behavior due to the 1:1 complex. Accuracy and reliability of association constants thus determined largely depend on the extension of the linear part of the plot.

The product of slope \times intercept for the straight line mentioned above can be given by eq 7 as

$$P = \text{slope} \times \text{intercept} = 1 / \left(1 + \frac{1}{K} \right)$$

One has $P \rightarrow 0$ as $K \rightarrow 0$ and $P \rightarrow 1$ as $K \rightarrow \infty$, indicating that the behavior of the straight line is sensitive to small change in K , as long as K is small, but rather insensitive when K is large.

Now suppose the case in which K for solute dimerization or other non-1:1 complex formation is small⁹ over a certain range of solute concentration. Then a small value of K for 1:1 solute-solvent complex formation will exhibit a plot with pronounced curvature at higher concentration range. If the value of K for 1:1 complex formation is large enough, so that K for dimerization or other non-1:1 complex formation becomes negligibly small, the resulting plot will exhibit good linearity. Thus the straight line obtained over a certain range of solute concentration can determine the association constant for the 1:1 solute-solvent complex and rule out unequivocally a weak dimerization or other competitive non-1:1 complex formation.

Experimental Section

The chemicals used in the present work were obtained from standard commercial sources and were purified mostly according to conventional procedures,¹⁰ but some were purified according to the literature.⁵

The sample solutions were made up by weight under

Table I: The Nmr Data for the Intermolecular Association of Chloroform with a Variety of Proton-Acceptor Solvents at 26°

Proton acceptor	Range of chloroform mole fraction studied	$(\Delta_{\text{obsd}})_{X_D \rightarrow 0}$, ppm	Δ_{AD} , ppm	K , (mf) ⁻¹
Benzene	0.0468–0.3242	0.853	3.33	0.36
Toluene	0.0216–0.3093	0.915	2.31	0.67
Mesitylene	0.0398–0.3624	1.037	2.26	0.86
Acetonitrile	0.0290–0.3364	–0.500	–0.65	3.4
Dimethyl sulfoxide	0.0202–0.4764	–1.250	–1.64	3.2

(10) J. A. Riddick and E. E. Toops, "Organic Solvents," Interscience Publishers, Inc., New York, N. Y., 1955.

Table II: Literature Values of Association Constants for Chloroform-Proton-Acceptor Complex

Proton acceptor	Δ_{AD} , ppm	K , (mf) ⁻¹	Method	Ref
Acetonitrile	-0.63	3.2	Binary mixture	<i>a</i>
	-0.973 ± 0.019	1.14 ± 0.04	Ternary mixture containing CCl ₄ as solvent	<i>b</i>
	-0.752 ± 0.024	0.91 ± 0.05	Ternary mixture containing CCl ₄ as solvent	<i>b</i>
Dimethyl sulfoxide	-1.5	3.8	Binary mixture	<i>c</i>

^a Reference 6. ^b B. B. Howard, C. F. Jumper, and M. T. Emerson, *J. Mol. Spectrosc.*, **10**, 117 (1963). ^c Calculated from ref 5.

open air, degassed at Dry Ice-methanol temperature, and sealed in 5-mm od tubes *in vacuo*.

The 60-MHz nmr experiments were carried out with a Varian HR-60 high-resolution nmr spectrometer system at 26 ± 1°.

The signal position of the chloroform proton was measured with reference to the cyclohexane signal by the side-band technique with use of a Hewlett-Packard HP-200CD wide-range oscillator in conjunction with an HP-521C electronic counter with crystal time base. It was thus possible to hold the average deviation within ± 0.1 Hz.

Results and Discussion

The chloroform proton shift at infinite dilution in the solution of cyclohexane was determined as 5.65 ppm (339.0 Hz) from the plots of chloroform proton shift as a function of chloroform concentration in solution. This value is in good agreement with Jumper's result¹¹ and was taken as δ_D , the chemical shift of pure chloroform monomer.

Several plots of $\Delta_{obsd}/(1 - X_D^0)$ against $X_D^0 \Delta^2_{obsd}/(1 - X_D^0)$ for the binary mixtures under study are shown in Figure 1. The results of the determinations are listed in Table I. In Table II, some nmr data on association constants in the literature are listed for comparison.

Chloroform forms dimers by self-association through weak hydrogen bonding.¹¹ However, as can be seen from Figure 1, these plots generally exhibit good straight lines with the exception of the chloroform-dimethyl sulfoxide system, which on extension to the right-hand side of Figure 1 gives a distinct curvature above 16 mol % chloroform concentration. This indicates that the dimerization effect of chloroform is negligibly small as compared to the effect of chloroform-solvent association, within the range of chloroform concentration studied (below 35 mol %).

Breakdown of linearity in a higher concentration range above 16 mol % for the case of a chloroform-dimethyl sulfoxide system mentioned above seems to be due to the simultaneous formation of the 2:1 complex in addition to the 1:1 complex.⁵ Even in this case, the linear plot obtained below 16 mol % can be used to determine K and Δ_{AD} for the 1:1 complex. The values of K and Δ_{AD} thus determined for the 1:1 com-

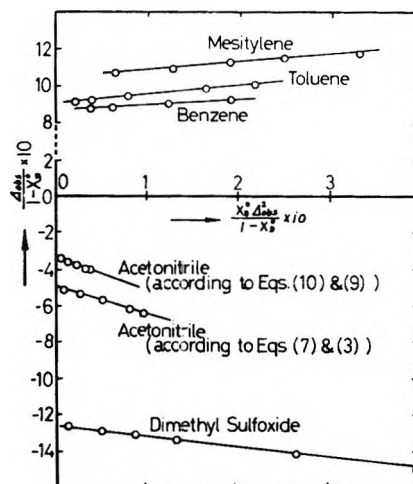


Figure 1. Plots of $\Delta_{obsd}/(1 - X_D^0)$ against $X_D^0 \Delta^2_{obsd}/(1 - X_D^0)$ for chloroform in a variety of proton-acceptor solvents.

plex of chloroform-dimethyl sulfoxide are in good agreement with those obtained by McChellan, *et al.*,⁵ as may be seen on comparing Table I with Table II.

For the $\text{CHCl}_3\text{-CH}_3\text{CN}$ complex, Howard, *et al.*,¹² gave two sets of association constants both from measurements in CCl_4 solution as listed in Table II. The discrepancy between their results on the one hand and those obtained by Berkeley, *et al.*,⁶ and ours on the other hand may be attributable specifically to the fact that Howard, *et al.*, made their measurements in CCl_4 solution. A chloroform-base mixture in the solvent carbon tetrachloride presumably undergoes an appreciable amount of CHCl_3 -solvent association¹¹ which may proceed in competition with the predominant association of CHCl_3 -base type even at very dilute chloroform concentration. A similar discrepancy was noticed by Howard, *et al.*,¹² for association constants of the $\text{Et}_2\text{O-CHCl}_3$ complex; *i.e.*, association constants were determined to be $\bar{K} = 3.76 \pm 0.10$ and $\Delta_{AD} \pm -0.905 \pm 0.008$ ppm from measurements in cyclohexane solution, while these turned out to be $K = 1.46 \pm$

(11) C. F. Jumper, M. T. Emerson, and B. B. Howard, *J. Chem. Phys.*, **35**, 1911 (1961).

(12) B. B. Howard, C. F. Jumper, and M. T. Emerson, *J. Mol. Spectrosc.*, **10**, 117 (1963).

0.04 and $\Delta_{AD} = -1.266 \pm 0.018$ ppm from measurements in CCl_4 solution.

It is obvious from eq 7 that at extreme dilution (*i.e.*, $X_D^0 \rightarrow 0$), the first term of eq 7 becomes zero and one obtains

$$(\Delta_{\text{obsd}})_{X_D^0 \rightarrow 0} = \frac{\Delta_{AD}}{1 + (1/K)} \quad (8)$$

This latter formula is the same as that obtained by Huggins, *et al.*² It is noteworthy that Δ_{AD} should not be approximated by $(\Delta_{\text{obsd}})_{X_D^0 \rightarrow 0}$, unless K is very large. This may find full support in Table I by comparing the data in the third and fourth columns in conjunction with K values given in the fifth column.

The dielectric constant of the solvent may have two effects on the hydrogen bond of solute-solvent complexes, *viz.* (1) reduction of the electrostatic force acting on the charge centers of the hydrogen bond and (2) increased bonding due to increased polar character of the proton-acceptor group toward hydrogen atom. These two effects are counterbalanced in the equilibrium and its extent is best described by K . Thus the dependence of the strength of the hydrogen bond on K is straightforward.

However, the relationship between hydrogen-bond strength and hydrogen-bond shift is rather complicated. Since a more electronegative group favors stronger hydrogen bonding, the stronger the bonding, the larger the low-field shift would be (shift a). At the same time, the proton shift related to the hydrogen bond is also dependent on the specific geometry of the hydrogen bond in the particular complex structure, which causes a low-field shift of the chloroform proton in the medium of a common base like acetone² but yields a high-field shift due to ring currents in the case of aromatic solvents like benzene^{3b} (shift b).

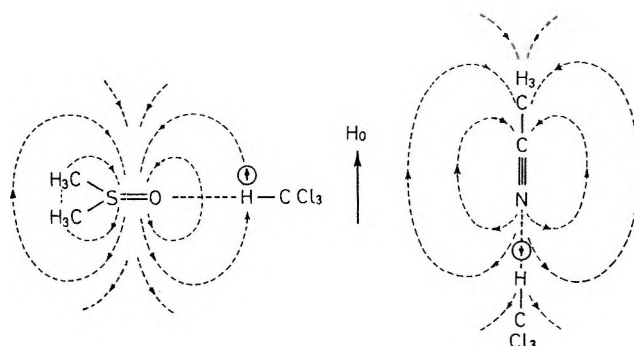
Thus the net shift due to hydrogen bonding is the algebraic sum of shift a and shift b and is not always a direct function of hydrogen-bond strength. This is why no simple regularity is observed for Δ_{AD} or $(\Delta_{\text{obsd}})_{X_D^0 \rightarrow 0}$, when one compares the complexes with different structures in Table I.

Positive values of $(\Delta_{\text{obsd}})_{X_D^0 \rightarrow 0}$ and Δ_{AD} , *i.e.*, the high-field shift of the chloroform proton in the aromatic solvents, as may be seen in Table I, are of course due to the anisotropic effect of the aromatic ring, indicating that a hydrogen-bonded complex is formed between chloroform and the aromatic molecule so as to locate the chloroform proton perpendicular to the benzene ring^{13,14} in such a manner that the dipole axis of chloroform is along the sixfold axis of symmetry of the benzene ring with the proton nearest the benzene.^{3b,14} In this position the proton experiences a high-field shift due to the aromatic ring current.^{3b} As has been pointed out by Abraham,^{3b} the complex bonding between chloroform and the benzene ring, similar to other hydrogen bonds, is essentially electrostatic in character but, due

to the weak ionic character of the C-H bond, is considerably less stable than the more common hydrogen bond. This is consistent with lower values of K obtained by us for chloroform in the medium of benzene, toluene, and mesitylene.

Creswell and Allred¹⁵ studied the chloroform-benzene association in the chloroform-benzene-cyclohexane system with cyclohexane used as an inert solvent to dissolve the equimolar mixture of chloroform and benzene. The K value was then determined as a parameter to be adjusted to make the observed shift *vs.* mole fraction of the 1:1 complex a linear function. They obtained $K = 1.06 \pm 0.30$ (mf)⁻¹ at 25°. However, using this method it seems rather difficult to rule out other competitive non-1:1 complex formation, for instance, the formation of the 2:1 $\text{CHCl}_3\text{-C}_6\text{H}_6$ complex.

In acetonitrile and dimethyl sulfoxide, chloroform exhibits negative values of $(\Delta_{\text{obsd}})_{X_D^0 \rightarrow 0}$ and Δ_{AD} (*i.e.*, low-field shifts). The low-field shift of chloroform in dimethyl sulfoxide solvent is greater than in acetonitrile solvent. This is inconsistent with the prediction simply from the values of K , which according to Table I are nearly equal, indicating that the chloroform proton shifts should be quite close to each other. This inconsistency may well be resolved by assuming the structure of these 1:1 complexes, respectively, as



As far as the effect of magnetic anisotropy is concerned, the double bond of the sulfoxide group must resemble that of the carbonyl group, which results in negative shielding of the proton along the double-bond axis,¹³ in agreement with the low-field shift. The triple bond of the nitrile group must resemble a $\text{-C}\equiv\text{C-}$ bond, which gives positive shielding of the proton along the triple-bond axis,¹³ in accordance with the high-field shift. The diametrical opposition between the magnetic anisotropy effects of =S=O and $\text{-C}\equiv\text{N}$ is expected to give rise to an additional contribution to the relative magnitude of the observed chloroform proton shifts in the two association complexes, *i.e.*, $\text{CHCl}_3\text{-}$

(13) L. M. Jackman, "Application of Nuclear Magnetic Resonance Spectroscopy in Organic Chemistry," Pergamon Press, New York, N. Y., 1959.

(14) W. T. Huntress, Jr., *J. Phys. Chem.*, **73**, 103 (1969).

(15) C. J. Creswell and A. L. Allred, *ibid.*, **66**, 1469 (1962).

DMSO and $\text{CHCl}_3\text{-CH}_3\text{CN}$, and thus makes the relative chloroform shift between $\text{CHCl}_3\text{-DMSO}$ and $\text{CHCl}_3\text{-CH}_3\text{CN}$ much larger than that predicted merely from the relative hydrogen-bonding strength or from the relative magnitude of association constants.

Strictly speaking, K and Δ_{AD} determined by eq 7 might still include the influence both from solvent shift and from self-association of chloroform because of Δ_{obsd} being defined as

$$\Delta_{\text{obsd}} = \delta_{\text{obsd}} - \delta_{\text{D}} \quad (3)$$

If the solvent effect is taken into consideration, Δ_{obsd} at any concentration may be given by the empirical formula^{6,16}

$$\Delta_{\text{obsd}} = \delta_{\text{obsd}} - \Delta^* + y\Delta x \quad (9)$$

In eq 9, Δ^* is the gas-phase difference in shift between pure donor and reference. $y\Delta x$ is the correction for the anomalous shift exhibited by a gaseous solute when infinitely diluted with the acceptor solvent, where y is the characteristic number^{6,16} of the acceptor solvent and Δx is the difference in the x value between donor solute and reference solute, x being the characteristic number^{6,16} of the compound containing the proton.

Substitution of eq 9 into eq 7 gives

$$\frac{[\delta_{\text{obsd}} - \Delta^* + y\Delta x]}{1 - X_{\text{D}}^0} = \frac{1}{\Delta_{\text{AD}}} \frac{X_{\text{D}}^0 [\delta_{\text{obsd}} - \Delta^* + y\Delta x]^2}{1 - X_{\text{D}}^0} + \frac{\Delta_{\text{AD}}}{1 + (1/K)} \quad (10)$$

This equation again enables one to determine K and Δ_{AD} by plotting $[\delta_{\text{obsd}} - \Delta^* + y\Delta x]/(1 - X_{\text{D}}^0)$ against $X_{\text{D}}^0 [\delta_{\text{obsd}} - \Delta^* + y\Delta x]^2 / (1 - X_{\text{D}}^0)$ provided that $y\Delta x$ is known for the specific system.

The values of K and Δ_{AD} thus determined by this refined method, unlike the previous values obtained from eq 7 and 3, eliminate automatically the unfavorable contribution from solvent shift due to donor and reference solutes and also eliminate the effect arising from self-association of chloroform.

Among the series of binary mixtures under study, it is only the chloroform-acetonitrile system whose characteristic number $y\Delta x$ is known.⁶ Application of eq 10 gave $\Delta_{\text{AD}} = -0.63$ ppm and $K = 3.1$ for the chloroform-acetonitrile system, whose plot is also shown in Figure 1 for comparison. Only a small discrepancy is noticed between these two methods of determination. A further improvement in the values of K and Δ_{AD} with application of the refined method would be expected for the rest of the binary mixtures, especially for ones with smaller K values, if their characteristic number $y\Delta x$ were known.

(16) A. A. Bothner-By, *J. Mol. Spectrosc.*, **5**, 52 (1960).

Dipole Moments of Alkyl Mesityl Ketones and

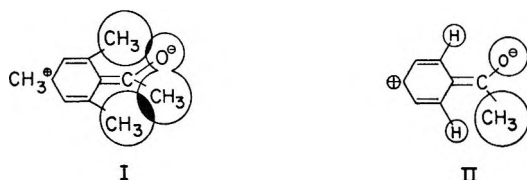
Some Aliphatic and Phenyl Analogs¹

by A. G. Pinkus and H. C. Custard, Jr.

Department of Chemistry, Baylor University, Waco, Texas 76703 (Received July 1, 1969)

Dipole moments (D) on the ketones listed below were obtained in benzene at 30° (alkyl group listed for each series): methyl alkyl: methyl, 2.84; ethyl, 2.86; isopropyl, 2.83; *t*-butyl, 2.70; alkyl phenyl: methyl, 3.05; ethyl, 2.90, isopropyl, 2.93; *t*-butyl, 2.58; alkyl mesityl: methyl, 2.81; ethyl, 2.76; isopropyl, 2.64; *t*-butyl, 2.50. In the methyl alkyl series an increase in C-CO-C angle due to steric interference between methyl and *t*-butyl groups is suggested as a possible explanation of the lower moment of methyl *t*-butyl ketone. In the alkyl phenyl series steric interaction between the *t*-butyl group and *ortho* hydrogens inhibits the coplanar conformation necessary for maximum π - π overlap in *t*-butyl phenyl ketone resulting in the lowest moment; similar interactions in certain conformations for ethyl phenyl and isopropyl phenyl ketones result in moments lower than for methyl phenyl ketone. In the alkyl mesityl ketones the decrease in moments from methyl to *t*-butyl is attributed to varying degrees of π - π conjugation between aromatic ring and carbonyl depending on angle of twist from coplanarity between the plane of the ring and the C-CO-C plane; the smaller the angle, the more conjugation and the larger the moment. *t*-Butyl mesityl ketone is suggested as a more suitable standard for a deconjugated system for use with the Braude-Sondheimer equation for calculation of angles of twist from dipole moment data of aromatic ketones.

In dipole moment studies on some carbonyl compounds, Kadesch and Weller² found that the dipole moment of methyl mesityl ketone^{3,4} (I) (2.71 D) was below that of methyl phenyl ketone⁵ (2.88 D) and about the same as those of aliphatic ketones (2.72 D).² The dipole moment of mesitylaldehyde (2.96 D), however, was found to be about the same as its unhindered analog, benzaldehyde (2.92 D). They explained the reduction of the moment of methyl mesityl ketone to below that of methyl phenyl ketone in terms of steric inhibition of resonance. Thus, introduction of *ortho* methyls in acetomesitylene resulted in interference of *ortho* methyls with carbonyl methyl when a coplanar position was approached and the carbonyl group was thus forced into a noncoplanar orientation (I) with respect to the ring. This prevented formation of the resonance hybrid which would have resulted in a greater charge separation and consequently a higher dipole moment as in the case of methyl phenyl ketone (II). The fact that the mo-



ment was reduced to about the same value as for aliphatic ketones was interpreted by Kadesch and Weller as showing that the maximum reduction in moment had been attained. Mesitylaldehyde and benzaldehyde, however, had nearly the same moments because the hydrogen and oxygen atoms of the aldehyde group were not large enough to cause interference with *ortho* meth-

yls. As a consequence of the postulate of Kadesch and Weller, all alkyl mesityl ketones would be expected to have the same dipole moment based on their interpretation that the maximum reduction in moment was obtained with the methyl derivative.

In connection with a program of studies on alkyl mesityl ketones⁶ further information was desired on the nature of restricted rotation about the carbonyl group and a determination of dipole moments of a series of alkyl mesityl ketones (III) was undertaken. In order to assess more accurately the differences in dipole moments between mesityl ketones and their unhindered analogs, dipole moments of two of the latter series were also obtained under the same conditions: alkyl methyl ketones⁷ (IV) in which conjugation interaction is absent

(1) Presented at the XIXth International Congress of Pure and Applied Chemistry, London, England; see Abstracts, p A3-52.

(2) R. G. Kadesch and S. W. Weller, *J. Amer. Chem. Soc.*, **63**, 1310 (1941).

(3) In order to call attention to the relationships among the classes of compounds studied in the present paper, nomenclature is used in which compounds are named as ketone derivatives in place of the system in which they are named as substituted derivatives of mesitylene, benzene, and methane. Commonly used names of the latter system will be noted as they occur.

(4) Acetomesitylene.

(5) Acetophenone.

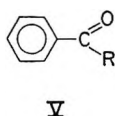
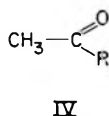
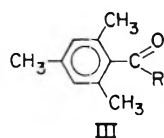
(6) A. G. Pinkus, J. I. Riggs, Jr., and S. M. Broughton, *J. Amer. Chem. Soc.*, **90**, 5043 (1968).

(7) Although dipole moments for compounds in series IV and V have been reported (see Table III), they are not completely comparable with each other because of differences in temperatures, methods of calculation, and solvents; the data reported in the present paper determined under the same conditions are more meaningful especially with regard to comparisons and differences among the compounds measured. The mesityl ketones (with the exception of methyl) have not previously been measured.

Table I: Physical Constants of Ketones

Ketones	Bp, °C	n_D^{20}	$\nu_{C=O}$, cm^{-1} (neat)	Ref
Acetone	55.5	1.3580	1721	a
Methyl ethyl	81	1.3686	1721	b
Methyl isopropyl	94	1.3761	1718	c, d
Methyl <i>t</i> -butyl	105	1.3890	1707	d, e
Methyl phenyl	203.0–203.5	1.5375	1688	f
Ethyl phenyl	98.5 (4 mm)	1.5237	1679	g
Isopropyl phenyl	89 (4 mm)	1.5159	1679	h
<i>t</i> -Butyl phenyl	87–90 (5 mm)	1.5018 ^a	1670	i
Methyl mesityl	179–180 (25 mm)	1.5146	1692	j
Ethyl mesityl	162.0–162.5 (18 mm)	1.5058	1694	k
Isopropyl mesityl	104 (4 mm)	1.5042	1702	l
<i>t</i> -Butyl mesityl	108 (4 mm)	1.5018	1694	m

^a J. Timmermans, "Physico-Chemical Constants of Pure Organic Compounds," Elsevier Publishing Co., New York, N. Y., 1950, p 353.
^b J. Timmermans, ref a, p 360. ^c N. A. Lange, "Handbook of Chemistry," 9th ed, Handbook Publisher Inc., Sandusky, Ohio, 1956, pp 610, 1344. ^d "Handbook of Chemistry and Physics," 45th ed, Chemical Rubber Publishing Co., Cleveland, Ohio, 1964, p C-230.
^e Reference c, p 600. ^f R. R. Dreisbach, "Physical Properties of Chemical Compounds," Vol. I, American Chemical Society, Washington, D. C., 1955, p 353; ref a, p 475; ref d, p C-101. ^g R. R. Dreisbach, ref f, p 365; ref d, p C-506. ^h "International Critical Tables," Vol. III, McGraw-Hill Book Co. Inc., New York, N. Y., 1933, p 46; ref c, pp 648, 1383; ref d, p C-506. ⁱ Reference d, p C-506.
^j V. Meyer and W. Moltz, *Chem. Ber.*, **30**, 1270 (1897); ref 47; ref 32; M. J. Aroney, M. G. Corfield, and R. J. W. Le Fèvre, *J. Chem. Soc.*, 648 (1964). ^k A. Klages, *Chem. Ber.*, **35**, 2245 (1904). ^l R. C. Fuson and C. H. McKeever, *J. Amer. Chem. Soc.*, **62**, 999 (1940).
^m D. V. Nightingale, R. L. Sublett, R. A. Carpenter, and H. D. Radford, *J. Org. Chem.*, **16**, 665 (1951). ⁿ Corrected to 30° from value of 1.5050 obtained at 22° by use of correction factor of $-0.0004/\text{deg}$ for increase in temperature: ref d, p 1307.



and alkyl phenyl ketones⁷ (V) in which the effect of conjugation on dipole moments would be expected. The results would also provide a test of expectations based on the work of Kadesch and Weller.

Experimental Section

Preparation and Purification of Compounds and Solvents. Reagent grade thiophene-free benzene was refluxed overnight or longer with sodium ribbon and fractionated through a 3-ft glass, helix-packed column retaining the constant-boiling fraction, bp 80.0°, n_D^{20} 1.5011. Redistilled material was periodically tested for the presence of water with Karl Fischer reagent.

The alkyl mesityl ketones and *t*-butyl phenyl ketone were synthesized; the other ketones were best commercial grades. All ketones were fractionated, retaining middle cuts. The purity of each ketone was checked by gas chromatography. Physical constants are listed in Table I along with literature references to published physical constants and/or methods of preparation.

Determination of Dielectric Constants. Measurements were made with a heterodyne-beat apparatus modified from types previously described.⁸ The variable oscillator was tuned with a calibrated General Radio Type 722-N precision capacitor and operated at a frequency of 1.8 MHz. The beat-frequency signal from fixed and

and variable oscillators was amplified and applied to vertical plates of an oscilloscope. A standard 1000-Hz signal, generated by a tuning-fork oscillator, was applied to the horizontal plates of the oscilloscope. The resulting 1:1 Lissajous figure was taken as the balance point for all capacitance determinations. The 1000-Hz beat frequency was used in order to lessen the "lock-in" tendency of the two oscillators as their beat frequencies approached zero. The capacitance readings obtained in this manner were reproducible to 0.05 pF.

The experimental cell was of the type designed by Sayce and Briscoe⁹ constructed of two concentric glass tubes. The outer surface of the inner tube and the inner surface of the outer tube were silvered up to approximately two-thirds of the length. Connections were made to the plates by means of platinum wires which passed into the interior of the inner tube and into a side tube sealed to the outer tube.

Prior to each series of determinations, a cell constant was obtained from a capacitance measurement with pure benzene using the known dielectric constant at a given temperature. Designating the capacitance of the cell with air between its plates as C_A and with pure benzene (dielectric constant ϵ_B) in the cell as C_B , capacitance (C_0) of the leads and the surroundings is given by $C_0 = (C_A\epsilon_B - C_B)/(\epsilon_B - 1)$. The dielec-

(8) C. T. Zahn, *Phys. Rev.*, **24**, 400 (1924); A. Weissberger and R. Sängewald, *J. Amer. Chem. Soc.*, **50**, 2332 (1928); A. B. Bryan and I. C. Saunders, *Phys. Rev.*, **32**, 302 (1928); H. Müller and H. Sack, *Phys. Z.*, **31**, 815 (1930); L. E. Sutton, *Proc. Roy. Soc.*, **A133**, 668 (1931).

(9) L. A. Sayce and H. V. A. Briscoe, *J. Chem. Soc.*, 315 (1925).

Table II: Dielectric Constants and Specific Volumes of Ketones in Benzene at 30°

$10^4 w_1$	ϵ_{12}	v_{12}	$10^4 w_2$	ϵ_{12}	v_{12}
	Acetone			<i>t</i> -Butyl Phenyl Ketone	
2.151	2.2941	1.1517	4.111	2.2814	1.1510
5.876	2.3470	1.1521	8.723	2.3009	1.1505
7.468	2.3693	1.1523	11.25	2.3120	1.1502
10.34	2.4104	1.1526	15.92	2.3316	1.1497
	Methyl Ethyl Ketone			Methyl Mesityl Ketone	
2.711	2.2966	1.1518	4.399	2.2854	1.509
5.861	2.3336	1.1521	8.049	2.3049	1.505
8.394	2.3660	1.1524	12.06	2.3268	1.501
11.34	2.3996	1.1527	16.72	2.3495	1.1496
	Methyl Isopropyl Ketone			Ethyl Mesityl Ketone	
3.406	2.2966	1.1519	4.380	2.2837	...
6.380	2.3238	1.1522	9.817	2.3091	...
9.177	2.3502	1.1524	11.88	2.3188	...
12.49	2.3812	1.1528	13.07	2.3236	...
			15.74	2.3371	...
	Methyl <i>t</i> -Butyl Ketone				
4.086	2.2933	1.1519	3.422	...	1.1511
6.302	2.3098	1.1521	6.194	...	1.1509
9.209	2.3307	1.1525	9.817	...	1.1505
11.59	2.3485	1.1527	13.07	...	1.1502
	Methyl Phenyl Ketone			Isopropyl Mesityl Ketone	
			2.994	2.2767	...
4.420	2.3001	1.1508	3.474	2.2771	1.1513
7.998	2.3294	1.1502	5.997	2.2871	1.1509
12.05	2.3634	1.1495	7.312	2.2924	1.1507
15.48	2.3881	1.1489	9.866	2.3019	1.1506
16.73	2.3987	1.1486	10.71	2.3052	...
			13.52	2.3159	1.1502
	Ethyl Phenyl Ketone			<i>t</i> -Butyl Mesityl Ketone	
4.560	2.2941	1.1507	3.737	2.2758	1.1512
8.364	2.3200	1.1502	7.218	2.2873	1.1511
11.75	2.3434	1.1496	10.66	2.2996	1.1506
15.16	2.3672	1.1491	15.27	2.3158	1.1502
	Isopropyl Phenyl Ketone				
4.357	2.2903	1.1512			
8.047	2.3132	1.1505			
12.07	2.3375	1.1500			
15.93	2.3621	1.1495			

tric constant of each solution (ϵ_s) was calculated by the equation, $\epsilon_s = (C_0 - C_s)/(C_0 - C_A)$, where C_s is capacitance of the cell containing the solution.

In order to exclude moisture and oxygen as completely as possible, all solutions were prepared in a drybox under a nitrogen atmosphere. Solutions were transferred in the drybox to flasks equipped with stopcocks terminating with ground-glass joints which fit the inlet port of the dielectric sample cell. This procedure for filling avoided contact of solutions with the atmosphere. For each series of solutions, the most dilute was measured first in order to minimize contamination problems. The precision capacitor was read at 5-min intervals until a constant reading was obtained, indicating that temperature equilibrium had been attained

in sample cell and solution. After a measurement was completed, the cell was emptied by using nitrogen gas pressure, rinsed with benzene, and then dried with dry nitrogen. Air capacitance of the cell was determined before each measurement in order to check that no silver had been removed from the surface of the cell walls.

For temperature control of solutions in the dielectric constant cell, an insulated bath containing 30 gal of mineral oil was used. Previous attempts to use a water bath were unsatisfactory because of marked variation of cell constant with the level of the water. Temperature for measurements was maintained at $30 \pm 0.01^\circ$ by means of a thermistor regulator. The thermostat employed for density determinations was a water bath at 30° . A

Table III: Experimental Data on Ketones

Ketones	MRD , cm^3	β	α_0	${}_{\infty}P_2$, cm^3	μ , ^a D	μ (lit.) (t), ^b D	Ref
Acetone	15.755	+0.10608	14.23	178.72	2.84	2.4 (30) 2.5 (30)	c d
Methyl ethyl	20.297	+0.10429	12.30	184.80	2.86	2.5 (30) 2.76 (25)	e f
Methyl isopropyl	24.84	+0.10345	9.47	187.04	2.83	2.76 (25)	f
Methyl <i>t</i> -butyl	29.381	+0.10303	7.32	176.55	2.70	2.81 (15)	g
Methyl phenyl	34.319	-0.17038	8.25	223.30	3.05	2.6 (30) 2.96 (25)	c h
Ethyl phenyl	40.656	-0.13208	6.645	209.97	2.90	2.88 (25)	h
Isopropyl phenyl	45.425	-0.12686	6.140	217.93	2.93	2.89 (25)	h
<i>t</i> -Butyl phenyl	47.806	-0.11600	4.335	183.43	2.58	2.70 (25)	h
Methyl mesityl	47.945	-0.10552	5.135	158.80	2.81	2.79 (25) 2.81 (25) 2.71 (20)	i j k
Ethyl mesityl	52.487	-0.10256	4.590	208.53	2.76	...	
Isopropyl mesityl	57.029	-0.094377	3.91	201.00	2.64	...	
<i>t</i> -Butyl mesityl	61.571	-0.08673	3.24	190.27	2.50	...	

^a 30°; benzene solvent. ^b Benzene solvent except as noted; temperature (°C) in parentheses. ^c C. R. Murty and D. V. G. L. N. Rao, *J. Sci. Ind. Res. B*, **15**, 346 (1956); C. R. Murty, *Current Sci.*, **25**, 49 (1956); ref 25, p 85. ^d A. Vyas and H. N. Srivastava, *J. Sci. Ind. Res. B*, **17**, 377 (1958); ref 25, p 85. ^e A. Vyas, *ibid.*; ref 25, p 114. ^f G. K. Estok and J. H. Sikes, *J. Amer. Chem. Soc.*, **75**, 2745 (1953); ref 25, p 148. ^g K. L. Wolf and E. Lederle, *Phys. Z.*, **29**, 948 (1928); K. L. Wolf, *Z. Phys. Chem., Abt. B*, **2**, 39 (1929); ref 25, p 216. ^h C. Cherrier, *C. R. Acad. Sci.*, **225**, 1306 (1947); ref 25, pp 328, 363, 391. ⁱ Reference 33; ref 25, p 391. ^j Reference 32; ref 25, p 391; M. J. Aroney, M. G. Corfield, and R. J. W. Le Fèvre, *J. Chem. Soc.*, 648 (1964), in carbon tetrachloride. ^k Reference 2.

two-thermistor bridge circuit between this bath and the oil bath made possible a maximum temperature variation between the two baths of no more than 0.01°.

Densities were measured by means of a 25-ml pycnometer. For calibration purposes the following equation was used.¹⁰ $d_t = 0.87378 + 10668 \times 10^{-7} (25 - t)$, where d is density and t is temperature.

The equation of Halverstadt and Kumler¹¹ was used to calculate solute polarization (${}_{\infty}P_2$) at infinite dilution

$${}_{\infty}P_2 = \frac{3\alpha_0 v_1 M_2}{(\epsilon_1 + 2)^2} + M_2(v_1 + \beta) \frac{\epsilon_1 + 1}{\epsilon_1 + 2}$$

where subscripts 1, 2, and 12 designate solvent, solute, and solution, respectively, $\alpha = \Delta\epsilon/w_2$, $\Delta\epsilon = (\epsilon_{12} - \epsilon_1)$, w_2 is the weight fraction of solute, v is the specific volume ($=1/d$), M is the molecular weight, and ϵ is the dielectric constant. Values of α were determined for each solution and plotted *vs.* w_2 . These linear plots were extrapolated to infinite dilution to obtain values of α_0 using least squares. β was obtained as the slope of a plot of v_{12} *vs.* w_2 . Electronic polarizations (P_E) were taken as equivalent to molar refractions which were calculated from bond refractivities.¹² Atomic polarization (P_A) was taken as 5% of electronic polarization (P_E).¹³⁻¹⁵ Dipole moments (μ) were calculated at 303°K from molar polarizations and molar refractions using the equation of Debye:¹⁶ $\mu = (9KT^{1/2}/4\pi N) \cdot ({}_{\infty}P_2 - P_E - P_A) = 0.22298({}_{\infty}P_2 - 1.05 MRD)^{1/2}$, where T is the absolute temperature, Avogadro's constant¹⁷ is $N = 6.02257 \times 10^{23} \text{ mol}^{-1}$, Boltzmann's

constant¹⁷ is $k = 1.38053 \times 10^{-16} \text{ erg deg}^{-1}$, and MRD is the molar refraction.

Results and Discussion

Weight fractions (w_2), dielectric constants (ϵ_{12}), and specific volumes (v_{12}) for solutions are in Table II; molar refractions (MRD), solute polarizations at infinite dilution (${}_{\infty}P_2$), values of α_0 and β , and dipole moments (μ) are in Table III. Dipole moment values from the literature are also listed in Table III for comparison. The selected literature moments are those reported in benzene solution; however, most of these are at temperatures other than 30° and were calculated by a variety of methods and thus are not completely comparable with each other or the present data.

Methyl Alkyl Ketones. Values for methyl, ethyl, and isopropyl derivatives (Table III) are approximately the same (average 2.84 D). The lower methyl *t*-butyl ketone value (2.70 D) is significantly below values for the other three.

(10) R. J. W. Le Fèvre, "Dipole Moments," 3rd ed, Methuen and Co. Ltd., London, 1953, p 46.

(11) I. F. Halverstadt and W. D. Kumler, *J. Amer. Chem. Soc.*, **64**, 2988 (1942).

(12) R. J. W. Le Fèvre and K. D. Steel, *Chem. Ind. (London)*, **670** (1961).

(13) See ref 10, p 17.

(14) C. P. Smyth, "Dielectric Behavior and Structure," McGraw-Hill Book Co., Inc., New York, N Y., 1955, p 222.

(15) See also J. W. Smith, "Electric Dipole Moments," Butterworth and Co. Ltd., London, 1955, p 24.

(16) P. Debye, *Phys. Z.*, **13**, 97 (1912).

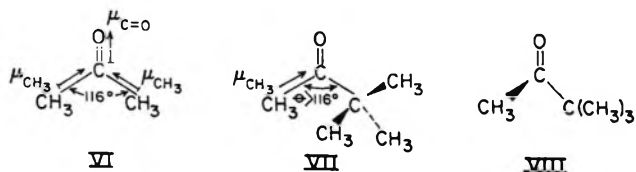
(17) "Handbook of Chemistry and Physics," 45th ed, Chemical Rubber Publishing Co., Cleveland, Ohio, 1964, p F-95.

An explanation for the low moment would appear to be linked to restriction of rotation due to the *t*-butyl group. A scale model shows steric interference between methyl and *t*-butyl groups. If steric interference between methyl and *t*-butyl groups results in a widening of the C-CO-C angle, contribution of the methyl and *t*-butyl group moment vectors to the carbonyl moment would be reduced, thus resulting in a reduced dipole moment for the molecule. Based on certain assumptions, a value for the C-CO-C angle can be calculated. Taking 116° as the C-CO-C angle ($\theta_{\text{C-CO-C}}$) in an unhindered dialkyl ketone¹⁸ (VI), 2.3 D for the bond moment of a carbonyl group,¹⁹ and 2.84 D as the average dipole moment of the three unhindered dialkyl ketones (μ_{R}) in the present work, the group moments of the alkyl groups (μ_{alk}) can be calculated from the equation:²⁰

$$\mu_{\text{R}} - \mu_{\text{C=O}} = 2\mu_{\text{alk}} \sin [(180^\circ - \theta_{\text{C-CO-C}})/2].$$

Using the calculated value of 0.5 D for the alkyl group moments for both the methyl and *t*-butyl moments²¹ in methyl *t*-butyl ketone and the value of the experimentally determined dipole moment of methyl *t*-butyl ketone (2.70 D), the C-CO-C angle in methyl *t*-butyl ketone is calculated to be 134° , a value that appears to be too high. This may be due to the incorrect assumption that the value of the carbonyl group moment is the same²² in the unhindered and hindered ketones. Thus if a value of 2.2 D is taken for $\mu_{\text{C=O}}$ in methyl *t*-butyl ketone (VII), a value of 121° is calculated;²³ the calculated angle is thus seen to be markedly dependent on the value chosen for $\mu_{\text{C=O}}$.

Evidence for a change in the nature of the carbonyl group in methyl *t*-butyl ketone is manifest in the carbonyl stretching frequencies (Table I). Values for methyl, ethyl, and isopropyl derivatives are essentially the same (*ca.* 1720 cm^{-1}) whereas that for the *t*-butyl derivative is significantly lower (1707 cm^{-1}). The reported value²⁴ for di-*t*-butyl ketone (1686 cm^{-1}) is also in accord with this trend and the reported^{25, 26} dipole moment of this ketone also shows a low value of 2.48 D.²⁷ This is in the direction expected for a smaller C-C-O angle (larger C-CO-C angle), thus indicating a decreased double-bond order for C-O stretching. Conversely, for a smaller C-CO-C angle, an increase in carbonyl stretching frequency would be expected.²⁸ The value^{28, 29} for cyclobutanone (1775 cm^{-1}) is in accord with this expectation.³⁰



It is possible that instead of angle widening, an out-of-plane twisting of one of the alkyl groups could explain the results as in VIII (showing methyl out-of-plane). No decision between the two possibilities

(or a combination of the two) can be made at present. An electron diffraction study might furnish information on this point.

Alkyl Phenyl Ketones. Dipole moment values are in Table III. Values for methyl, ethyl, and isopropyl derivatives (3.05, 2.90, and 2.93 D, respectively)³¹ are greater than respective values for the dialkyl ketones as expected on the basis of conjugation of carbonyl with phenyl (greater charge separation). The value for the *t*-butyl derivative (2.58 D), however, is less than the corresponding dialkyl derivative. An explanation for this decrease is evident from examination of scale models in which interference to the coplanar conformation necessary for maximum conjugation occurs between *ortho* hydrogens and the methyls of the

(18) J. D. Swalen and C. C. Costain, *J. Chem. Phys.*, **31**, 1562 (1959), reported $116^\circ 14' \pm 1^\circ$ for the C-CO-C angle in gaseous acetone from electron diffraction measurements; L. E. Sutton, Ed., "Tables of Interatomic Distances and Configurations in Molecules and Ions," Supplement, Special Publication No. 11, The Chemical Society, London, 1958, p 99s.

(19) See ref 14, p 245.

(20) The assumption is also made that the carbonyl moment bisects the C-CO-C angle.

(21) (a) This would seem to be a reasonable assumption on the basis that the dipole moments of alkyl derivatives such as alkyl benzenes,^{21b, c} alkyl halides,^{21d} and alkyl alcohols^{21e} show very little variation. (b) See ref 14, pp 314, 321. (c) A. L. McClellan, "Tables of Experimental Dipole Moments," W. H. Freeman and Co., San Francisco, Calif., 1963, pp 251, 292. (d) See ref 14, p 269. (e) See ref 14, p 301.

(22) See below for evidence from infrared spectra.

(23) (a) Using the empirical equation:^{23b} $\theta = (1974 - \nu)/2.2$ where θ is the C-CO-C bond angle and ν is the position of the infrared carbonyl stretching band in cm^{-1} , a value of 121° is calculated for methyl *t*-butyl ketone using the ir absorption band at 1707 cm^{-1} . (It should be pointed out that the agreement is fortuitous since the value of 2.2 D for $\mu_{\text{C=O}}$ was chosen merely to show that a change of only 0.1 D in this value resulted in a large change in the angle. (b) K. Mislow, "Introduction to Stereochemistry," W. A. Benjamin, Inc., New York, N. Y., 1966, p 48; J. O. Halford, *J. Chem. Phys.*, **25**, 830 (1956). Halford gave the equation $\nu (\text{cm}^{-1}) = 1278 + 68k - 2.2\phi$ and 10.2 ± 0.3 practical units for the stretching force constant. With this average value for k , $\phi = (1972 - \nu)/2.2$ and ϕ for methyl *t*-butyl ketone is calculated to be 120.5° . The value should be noted of this equation in the calculation of C-CO-C angles in unconjugated ketones which can then be used for estimation of carbonyl group moments. The authors thank Professor K. Mislow, Princeton University, for the Halford reference as the source of this equation.

(24) R. M. Stiles, Ph.D. Dissertation, Harvard University as quoted by Halford;^{23b} C. N. R. Rao, G. K. Goldman, and C. Jurie, *J. Phys. Chem.*, **63**, 1311 (1959), reported 1687 cm^{-1} .

(25) A. L. McClellan, "Tables of Experimental Dipole Moments," W. H. Freeman and Co., San Francisco, Calif., 1963, p 339.

(26) C. Cherrier, *Bull. Soc. Chim. Fr.*, 1076 (1948).

(27) (a) However, the solvent and temperature for this determination were not reported.²⁸ On the other hand, a value of 2.79 D was reported^{26, 27b} in benzene at 15° . Unfortunately, because of the various conditions (*e.g.*, temperature) the values are not directly comparable with those in the present paper. (b) K. L. Wolf and E. Lederle, *Phys. Z.*, **29**, 948 (1928); K. L. Wolf, *Z. Phys., Chem., Abt. B*, **92**, 39 (1929).

(28) L. J. Bellamy, "The Infra-red Spectra of Complex Molecules," 2nd ed, John Wiley and Sons, Inc., New York, N. Y., 1958, p 149.

(29) D. H. Whiffen and H. W. Thompson, *J. Chem. Soc.*, 1005 (1946).

(30) (a) The dipole moment reported^{30b, c} is 2.76 D in benzene at 25° . (b) See ref 25, p 107. (c) R. Arndt, H. H. Günthard, and T. Gauthmann, *Helv. Chim. Acta*, **41**, 2213 (1958).

(31) This trend also shows in data reported by C. Cherrier, *C. R. Acad. Sci.*, **225**, 1306 (1947), for methyl, ethyl, isopropyl, and *t*-butyl phenyl ketones in benzene at 25° : 2.96, 2.88, 2.89, and 2.70 D, respectively; however, no explanation was given.

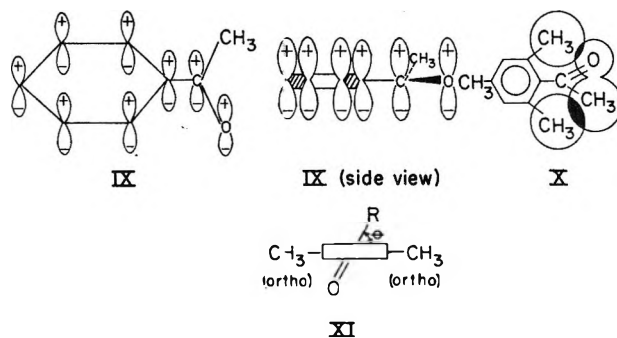
t-butyl group. In the case of methyl phenyl ketone, scale models show little if any interference between *ortho* hydrogens and the methyl group. The methyl groups in ethyl and isopropyl derivatives, however, show interference in certain conformations and not in others. This would account for the largest dipole moment observed for acetophenone and smaller ones for ethyl and isopropyl derivatives.

Alkyl Mesityl Ketones. Dipole moment values are in Table III. The value of 2.81 D (30°) obtained for the methyl derivative checks well with the reported values of 2.81³² and 2.79 D³³ at 25° in benzene. Two important results are notable and require explanation. (1) The values are all *smaller* than respective values for corresponding dialkyl ketones; this result is contrary to that expected on the basis of the postulate of Kadesch and Weller² as discussed earlier in the present paper. (2) The values show a continuous decrease from that of methyl (2.81 D) to *t*-butyl (2.50 D).

In considering possible explanations of the fact that moments of the alkyl mesityl ketones are less than those for the standard dialkyl ketones, the assumption by Kadesch and Weller that the dipole moments of hindered aromatic ketones should approach aliphatic values as resonance was damped out would appear to be invalid. In order to have the same dipole moments, the vector contributions of alkyl groups to the carbonyl dipole vector would have to be equal to those of aryl (mesityl) groups. There is ample evidence that these vectors are not equal. Thus, for example, although the dipole moment values of bromomesitylene (1.53 D)^{34,35} and bromobenzene (1.52–1.57 D)^{36,37} are approximately the same, the values reported for methyl bromide (1.62^{38,39} and 1.84 D^{38,40}) under comparable condition are substantially higher. Furthermore, alkylbenzenes have definite dipole moments ranging from 0.34 to 0.61 D in benzene.^{41,42} Similar trends appear for other halides and substituents that do not exert steric effects on *ortho* methyl groups. Thus, the dipole vector for an aryl group is seen to be less than that of an alkyl (or methyl) group.⁴³ This would tend to reduce the overall dipole moment in accord with experimental observations. This explanation is supported by the observed⁴⁴ dipole moment of 2.53 D for 2,4,6-tribromobenzaldehyde which is lower than that for mesitylaldehyde (2.96 D) and is in the direction expected for inductive electron withdrawal from the ring by the bromines.

Reasonable explanations for the experimentally observed continuous decrease in dipole moments of the mesityl ketones from methyl to *t*-butyl can also be considered. It has been pointed out⁴⁵ that in the case of *ortho*-substituted biphenyls overlap of π orbitals is possible even though the rings may be twisted from coplanarity. The resonance energy resulting from π -orbital overlap of the two phenyl rings varies with \cos^2 of the angle of twist (Figure 1);⁴⁶ thus, even at 45°, 50% resonance is present.^{45–47} A similar situation

can be visualized with mesityl ketones. In acetophenone, maximum π overlap between phenyl ring and carbonyl group can occur when the ring and the plane formed by the carbonyl carbon and oxygen and the methyl group are coplanar (IX). In the case of mesityl ketones because of steric interference between *ortho* methyl groups and the alkyl group (X) (and to a lesser



extent with the oxygen of the carbonyl group), coplanarity is prevented or at least would result in a high-energy eclipsed-type conformation.

Braude and Sondheimer⁴⁸ derived an equation which related the interplanar angle for substituted methyl phenyl ketones and dipole moments: $\cos^2 \theta = (\mu_{\text{obsd}} - \mu_{90}) / (\mu_0 - \mu_{90})$. In the equation θ is the mean interplanar angle (see XI), μ_{obsd} is the observed dipole moment, μ_{90} , the moment for a "completely deconjugated system" (where the plane of the ring and the carbonyl

(32) J. B. Bentley, K. B. Everard, R. J. B. Marsden, and L. E. Sutton, *J. Chem. Soc.*, 2957 (1949).

(33) C. G. Le Fèvre and R. J. W. Le Fèvre, *ibid.*, 1829 (1950).

(34) See ref 25, p 330.

(35) Benzene, 25°; F. Brown, J. M. A. de Bruyne, and P. M. Gross, *J. Amer. Chem. Soc.*, 56, 1291 (1934).

(36) See ref 25, p 173.

(37) Benzene, 25–30°.

(38) See ref 25, p 42.

(39) Benzene, 25°; A. D. Buckingham and R. J. W. Le Fèvre, *J. Chem. Soc.*, 3432 (1953).

(40) Benzene, 25°; A. E. von Arkel and J. L. Snoek, *Rec. Trav. Chim.*, 52, 719 (1933).

(41) See ref 25, pp 251, 292, 332, 336.

(42) Aside from the differences in alkyl group, the range of values is due to determinations under a variety of conditions.

(43) One of the referees stated that when aryl is attached to groups such as -CHO and -CN, the reverse is true.

(44) J. W. Smith, *J. Chem. Soc.*, 4050 (1957).

(45) L. L. Ingraham in "Steric Effects in Organic Chemistry," M. S. Newman, Ed., John Wiley and Sons, Inc., New York, N. Y., 1956, Chapter 11, p 479 ff.

(46) E. G. Spletzer and H. H. Jaffé, Abstracts, 153rd National Meeting of the American Chemical Society, Miami Beach, Fla., April 1967, No. R-33, reported that near-uv spectra of *o*-aminobiphenyls showed significant resonance interaction between perpendicular phenyl rings even in the most sterically hindered biphenyls.

(47) W. M. Shubert and W. A. Sweeney, *J. Amer. Chem. Soc.*, 77, 4172 (1955), noted that although ultraviolet spectra indicated practically complete inhibition of conjugation for methyl mesityl ketone, it still showed a carbonyl vibration shift (decrease) of 18 cm^{-1} from methyl ethyl ketone; however, they did not attempt an explanation of this observation.

(48) E. A. Braude and F. Sondheimer, *J. Chem. Soc.*, 3754 (1955).

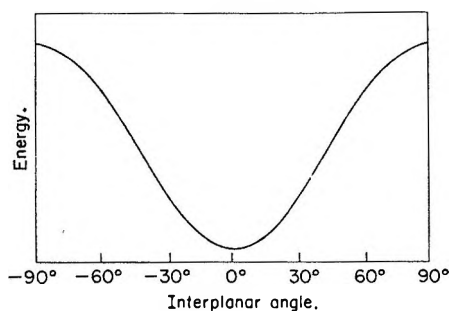


Figure 1. Excess resonance energy of biphenyl over two benzene rings as a function of angle of twist between phenyl groups.

group to alkyl carbon plane are at right angles) was taken as equal to the dipole moment of a saturated ketone (acetone), and μ_0 , the moment for a coplanar configuration, was calculated from appropriately substituted methyl phenyl ketones. The equation was used to calculate angles of twist (θ) from experimental dipole moment data.

It is clear, however, that the Braude-Sondheimer equation is inapplicable to the present dipole moment data on the mesityl ketones since the mesityl ketone dipole moments (μ_{obsd}) are smaller than those of the dialiphatic analogs (μ_{90}). The problem seems to reside in the assumption of the moments of the saturated ketones as standards for the completely deconjugated system. This assumption would appear to be unjustified on the same basis brought out above in the discussion of the dipole moments of the mesityl ketones—that the group moment of an alkyl group is not equivalent to the group moment of an “unconjugated” aryl group. It would seem that a better standard for a deconjugated system would be *t*-butyl mesityl ketone. A scale molecular model (Fisher-Taylor-Hirschfelder) of this compound shows that the *t*-butyl group is in close contact with both *ortho* methyl groups and as a result the carbonyl group to alkyl carbon plane is approximately orthogonal to the plane of the mesityl ring with very little deviation possible. If the value of 2.50 D for *t*-butyl mesityl ketone is taken as the best available standard for the deconjugated system (μ_{90}), the interplanar angles shown in Table IV can be calculated from the Braude-Sondheimer equation using a value of 3.09 D for the conjugated system dipole (μ_0).⁴⁹

Similar calculations can be made for data on the alkyl phenyl ketones using the methyl phenyl ketone moment (3.05 D) for the conjugated system (μ_0) and a corrected value⁵⁰ of 2.46 D for the deconjugated system (μ_{90}). The calculated angles are listed in Table IV. The calculated angles are probably best regarded as average interplanar angles of a minimum energy conformation of the molecule, this lowering of energy of the molecule (with respect to the rotating alkyl-carbonyl group) being related to conjugative interaction as a result of π - π overlap between the mesityl and carbonyl

Table IV: Interplanar Angles (θ) of Alkyl Mesityl and Alkyl Phenyl Ketones Calculated from Braude-Sondheimer Equation⁴⁸

Alkyl group	θ	θ
	Mesityl	Phenyl
Me	44° ^c	0° ^a
Et	48°	30°
<i>i</i> -Pr	61°	27°
<i>t</i> -Bu	90° ^{a,b}	63° ^d

^a Assumed. ^b If the interplanar angle for the standard, *t*-butyl mesityl ketone is slightly less than 90°, then the angles for the other mesityl ketones would be less than those calculated.

^c Braude and Sondheimer⁴⁸ calculated a value of 62° for this compound based on the dipole moment reported by Bentley, *et al.*³² K. Yates and B. F. Scott, *Can. J. Chem.*, **41**, 2320 (1963), calculated a value of 74° based on ultraviolet data in 46–47% sulfuric acid. Yates and Scott point out that strictly speaking, the oscillator strengths and not the extinction coefficients should be used in estimating angles of twist from ultraviolet data with the Braude-Sondheimer equation but that experimental difficulties complicate use of the former. Furthermore, they point out the difficulties in the estimation of a value for the extinction coefficient for the coplanar conformation for *ortho*-dimethyl-substituted compounds and consequently the values for interplanar angles for these types of compounds are “less quantitative” than those for other compounds. These considerations may partially account for the differences between interplanar angle values calculated from ultraviolet data and dipole moment data reported in the present paper. M. J. Aroney, M. G. Corfield, and R. J. W. Le Fèvre, *J. Chem. Soc.*, 648 (1964), however, calculated 90° for the interplanar angle based on comparison between calculated and observed values for molar Kerr constants in carbon tetrachloride. ^d Braude and Sondheimer⁴⁸ reported 34° based on their calculation using ultraviolet data of G. D. Hedden and W. G. Brown, *J. Amer. Chem. Soc.*, **75**, 3744 (1953), taken on *n*-heptane solutions.

groups. Thus, the closer to coplanarity (the smaller the interplanar angle) the more electron delocalization involving carbonyl and mesityl groups and the larger the dipole moment. The least amount of delocalization would occur in the case of *t*-butyl mesityl ketone with the consequence of its having the lowest dipole moment.

Two other possible explanations for the decrease in dipole moments from methyl to *t*-butyl mesityl ketone can be considered. One of these is based on an increase in the angle ($\theta_{\text{C-C-O}}$) between the mesityl and alkyl

(49) This value is obtained by applying a correction of +0.04 D to the experimental moment of 3.05 D obtained for methyl phenyl ketone. The correction is based on reported moments² for mesitylaldehyde (2.96 D) and benzaldehyde (2.92 D) which reflect an increase of 0.04 D for mesitylaldehyde in a comparison of mesityl and phenyl systems where the same carbonyl group is not sterically prevented from conjugation with the ring. Braude and Sondheimer⁴⁸ used a corrected value of 3.03 D.

(50) Obtained by applying a correction of -0.04 D to the experimental moment of 2.50 D for *t*-butyl mesityl ketone (the deconjugated “standard”). The correction is on the same basis as stated in ref 49 which corrects for the decrease in group moment of 0.04 D in going from mesityl to phenyl. The moment of 2.58 D for *t*-butyl phenyl ketone cannot be used as a standard for the deconjugated system since molecular models indicate some “free play” in the *t*-butyl group making the interplanar angle substantially less than 90°.

groups attached to the carbonyl carbon. It would be expected that this angle should increase with the steric requirement of the alkyl group (from methyl to *t*-butyl). On this basis a decrease in the carbonyl stretching frequencies from methyl to *t*-butyl (Table III) would be expected (see discussion above for methyl alkyl ketones). A gradual *increase* is actually observed from methyl to isopropyl and then a decrease to the ethyl ketone value for the *t*-butyl ketone. This lack of correlation would tend to exclude this explanation.

Another possible explanation is based on possible perturbation of the π -electron cloud of the mesityl ring by the alkyl groups. Scale models show that such per-

turbation would increase from methyl to *t*-butyl. Implicit in this suggestion would be a correlation of the degree of perturbation with a reduction of the vector contribution by the mesityl group to the overall dipole moment. This explanation cannot be discounted at present and must be considered as a possibility. Further studies are being carried out in order to attempt to decide more conclusively between possible explanations.

Acknowledgment. The authors express appreciation to the Robert A. Welch Foundation of Houston, Texas, for research grants in partial support of this work.

Ethylene-Maleic Anhydride Copolymers and Derivatives. Potentiometric

Titration and Interactions with Polypeptides¹

by E. Bianchi, A. Ciferri, R. Parodi, R. Rampone, and A. Tealdi

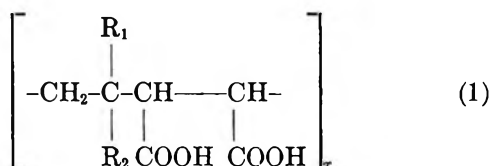
Chemistry Department, University of Genoa, Genoa, Italy (Received June 20, 1969)

The titration behavior of ethylene-maleic anhydride, propylene-maleic anhydride, isobutylene-maleic anhydride, 2-methylpentene-1-maleic anhydride, and styrene-maleic anhydride copolymers was investigated. The carboxyl groups of each copolymer are characterized by two intrinsic pK 's, one of which is increased and the other decreased on increasing the number of carbon atoms on the alkyl side chain of the olefin comonomer. The phenomenon is attributed to an alteration of the effective dielectric constant and its consequent effect on charge-dipole and charge-charge interactions. The titration behavior of the corresponding polycations having dimethylaminopropylmaleimide as comonomer was also investigated. The interaction of the polyanion copolymers with poly-L-lysine and poly-L-ornithine was investigated by determining the conditions for formation of a coprecipitate. The alkyl side chain of the polyanion influences complex formation through the effect it has on the ionization of the carboxyl groups as well as through hydrophobic interactions. The two effects are not, in general, additive.

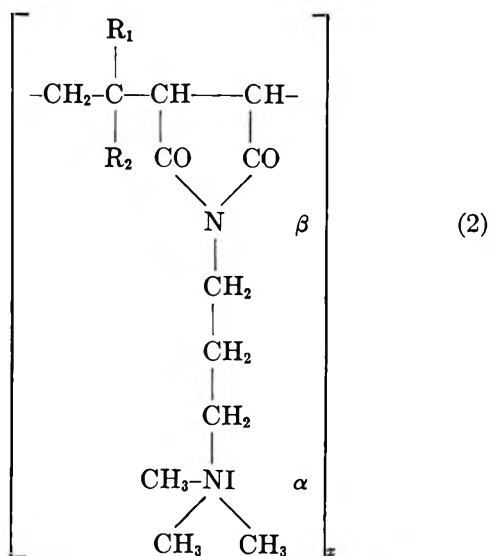
Introduction

Ethylene-maleic anhydride copolymers and their derivatives have recently come to be considered for a number of applications generally involving the formation of insoluble complexes with proteins and viruses.²⁻⁴

Since the physicochemical properties of the corresponding class of polyelectrolytes have not been adequately investigated, we present here a study of the titration behavior of polyanions having the structure



and polycations having the structure



A series of polyelectrolytes corresponding to different R substituents was used. The variation of the alkyl or aromatic substituent affords a method for investigating in a systematic manner the role of steric hindrance on the ionization of titratable groups. The results obtained can possibly be applied to the titration of more complex systems (*i.e.*, the proteins).

Besides the titration behavior of these copolymers, we present here some results pertaining to their interaction with model polypeptides in an attempt to investigate the forces involved in the formation of insoluble complexes between the copolymers and the proteins.

The variation of alkyl and aromatic substituents on the polymer chain backbone also represents a potential variation in the so-called⁵ hydrophobic bonding. This bond is now regarded as a major parameter in the stabilization of the tertiary structure of proteins and possibly contributes to the forces responsible for the formation of a copolymer-protein complex.

Experimental Section

Maleic anhydride copolymers were kindly supplied by Dr. J. E. Fields and Dr. J. H. Johnson of the Monsanto Co. They were described as essentially 1:1 copolymers and were prepared by free radical catalyzed solvent-nonsolvent techniques which traditionally yield relatively narrow molecular weight distributions (*i.e.*,

(1) Thesis submitted by Miss R. Parodi as a partial requirement for the doctoral degree in chemistry.

(2) E. T. Feltz and D. W. Regelson, *Nature*, 196, 642 (1962).

(3) J. H. Johnson, J. E. Fields, and W. A. Darlington, *ibid.*, 213, 665 (1967).

(4) A. H. Sehon, Symposium Series Immunobiological Standard, Vol. IV, Karger, Basel/New York, N. Y., 1967, pp 51-70.

(5) G. Némethy, H. A. Scheraga, and W. Kauzmann, *J. Phys. Chem.*, 72, 1842 (1968).

M_w/M_n to 1.5–2.0). The molecular weight of the ethylene–maleic anhydride copolymer, determined by osmotic pressure in H_2O at 37° , was found to be $M_n = 92,000$. Viscosity measurements in dimethylformamide confirmed the molecular weight (M_v) to be about 100,000.

The essential 1:1 composition of the comonomers was confirmed on the basis of our titration data (yielding the total number of carboxyls in solution) and the known composition (dry weight) of the corresponding solution. Hydrolysis of the anhydrides was performed in the presence of 0.1 *N* NaOH at 90° following the change in the titration behavior with time for over 10 hr. No further change in the titration curve could be detected after 10 hr treatment at 90° . Five different copolymers were used corresponding to the following R substituents

$R_1 = H, R_2 = H$; ethylene–maleic anhydride polyanion copolymer (EMA)

$R_1 = H, R_2 = CH_3$; propylene–maleic anhydride polyanion copolymer (PMA)

$R_1 = CH_3, R_2 = CH_3$; isobutylene–maleic anhydride polyanion copolymer (IBMA)

$R_1 = CH_3, R_2 = C_3H_7$; 2-methylpentene-1–maleic anhydride polyanion copolymer (MMA)

$R_1 = H, R_2 = C_6H_5$; styrene–maleic anhydride polyanion copolymer (SMA)

Hydrolyzed EMA, PMA, and IBMA were soluble in 0.1 *M* KCl, pH 1.5–12, $T = 25^\circ$, at least up to polymer concentrations equal to 0.5% (maximum limit investigated). Under the above conditions MMA was insoluble at pH < 3 and SMA was insoluble at pH < 4.

Dimethylaminopropyl maleimide copolymers, also supplied by Dr. J. E. Fields, were obtained by treating the anhydride precursor with DMAPamine. The degree of polymerization of the maleimide copolymers was, therefore, the same as that of the corresponding maleic anhydride copolymer. Quaternization was performed by suspending the polymers in ethyl acetate, adding a stoichiometric quantity of methyl iodide (calculated mole/mole of dimethylamino groups present), and stirring at 60° for 3 hr. Under the conditions used, no further change in the titration curve was detected by increasing the methyl iodide concentration, the time, or the temperature of reaction. The intrinsic viscosity of the ethylene–dimethylaminopropyl copolymer measured in a 1:1 H_2O –dimethylformamide solution at 25° (pH 1.5) before and after quaternization was found to be 0.74 and 0.64 dl/g, respectively. This result suggests the occurrence of some degradation during the quaternization step.

Three different quaternized copolymers were used corresponding to the following R substituents

$R_1 = H, R_2 = H$; ethylene–dimethylaminopropyl–maleimide polycation copolymer (Ecat)

$R_1 = CH_3, R_2 = C_3H_7$; 2-methylpentene-1–dimethylaminopropylmaleimide polycation copolymer (Mcat)

$R_1 = H, R_2 = C_6H_5$; styrene–dimethylaminopropylmaleimide polycation copolymer (Scat)

The corresponding unquaternized copolymers are indicated as Ecat,unquat; Mcat,unquat; Scat,unquat. Ecat was found to be soluble before and after the quaternization process. Scat and Mcat were also soluble. Scat,unquat and Mcat,unquat precipitated when pH > 7.8.

Model polypeptides poly-L-lysine hydrobromide (PLL) and poly-L-ornithine hydrobromide (PLO) were obtained from Pilot Chemicals. The reported molecular weight was 115,000 for PLL and 90,000 for PLO. Both polymers were completely soluble in the pH range from 1.5 to 11.

Potentiometric titrations were performed as described before⁶ in solutions containing about 50 mg of polymer in 10 ml of 0.1 *M* KCl at 25° . A fresh solution was used in each case taking particular care to start the titration with a clear solution.

Solubility determinations for the polyanion copolymers in the presence of the polypeptides were performed at pH from 2 to 1, $T = 25^\circ$, in the presence of 0.005 *M* KCl by mixing adequate amounts of solutions containing the separate (soluble) polymers at the indicated pH, readjusting the pH, stirring, and visually observing the solutions against a dark background. Observations made after 10 min and after 24 hr from mixing are reported since occurrence of time effects was noticed.

In another set of solubility experiments in the pH range from 2 to 5, adequate amounts of the solutions containing the separate polymers in 0.1 *M* KCl were mixed and stirred under N_2 at $T = 25^\circ$. After equilibration, certainly reached in 48 hr, the amount of precipitate was determined using an EEL nephelometer. At the concentration employed (5.2×10^{-7} equiv/cc for each component polymer) the precipitate was in the form of an opalescent suspension. This allowed the nephelometric determination to yield reproducible data.

Infrared spectra of a film of Ecat was obtained using a Model 225 Perkin-Elmer spectrophotometer. The film was obtained by evaporation (on an Hg surface) of a solution previously maintained for 24 hr at low and high pH.

(6) A. Ciferri, D. Puett, L. Rajzgh, and J. Hermans, Jr., *Biopolymers*, **6**, 1019 (1968).

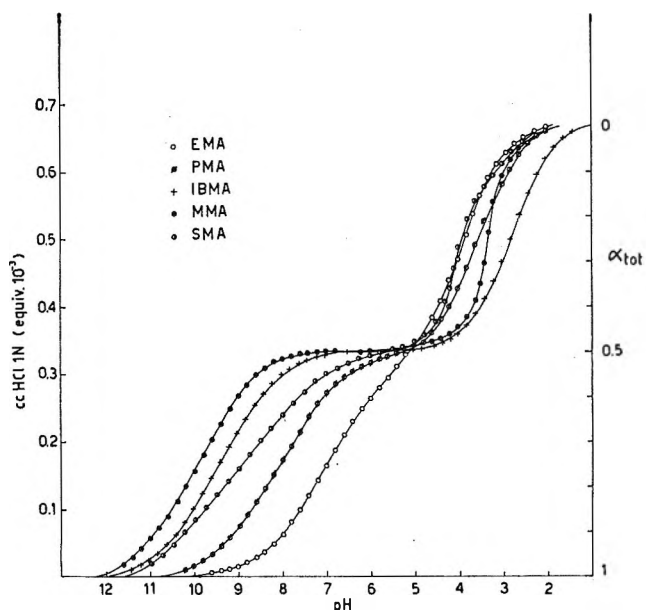


Figure 1. Titration curves for polyanion copolymers at 25° in 0.1 *M* KCl.

Results

Titration curves for EMA, PMA, IBMA, MMA, and SMA are reported in Figure 1, where the volume (in milliliters) of 1 *N* HCl added are reported as a function of the measured pH. The total degree of dissociation, α_{TOT} , is indicated on the right-hand side. We note that the titration of the first carboxyl group is fairly well distinct from that of the second one in the case of PMA, IBMA, MMA, and SMA while the titration of the two carboxyl groups overlap considerably in the case of EMA.

In order to calculate the intrinsic pK , pK_0 , of the carboxyl groups from the apparent pK , pK_{app} , vs. degree of ionization, α , curves,⁶ it is necessary to know the pH vs. α curves for each dissociating group. The difficulty introduced by the overlapping of the titration curves of the two carboxyl groups, particularly in the case of EMA, is overcome on the basis that half of the total equivalents used can be attributed to only one carboxyl group. In this manner pH vs. α curves can be calculated avoiding the use of data near the overlapping region. $pK_{app} = pH - \log [\alpha/(1 - \alpha)]$ vs. α curves thus obtained for the five polyanions are reported in Figure 2. We note that the slopes of the curves are unexpectedly negative in the case of one of the two carboxyl groups of MMA and SMA. The pK_0 values, obtained when the corresponding α is = 0, are collected in Table I and reported in Figure 3, as a function of the number of carbon atoms, n , in the side chains of the olefin comonomer (*i.e.*, 0 for EMA, 1 for PMA, 2 for IBMA, 4 for MMA). In the same figure is also indicated the value of $N = n + 2$, *i.e.*, the total number of carbon atoms in the olefin comonomer. It is seen that an increase of n has a different effect on the ionization of

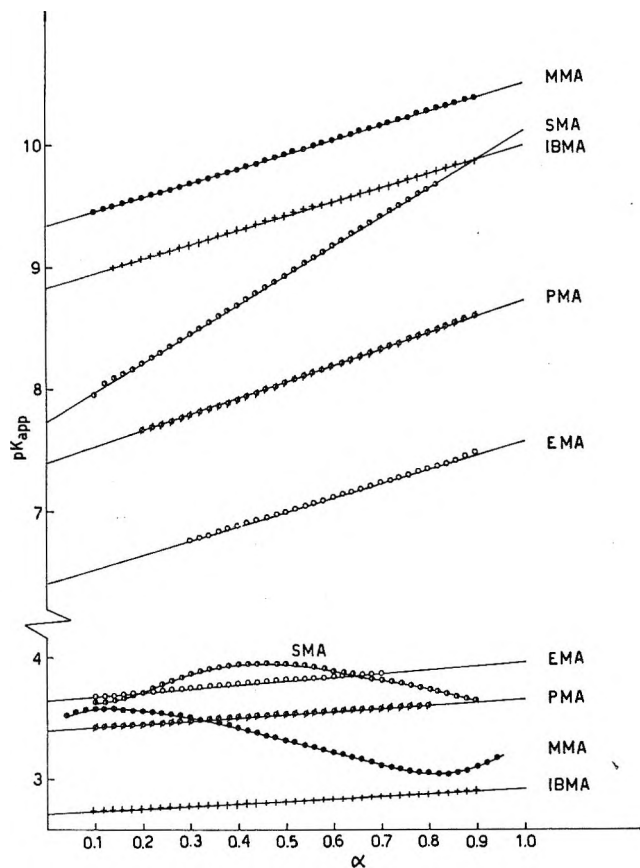


Figure 2. Apparent pK vs. degree of ionization plot corresponding to the data in Figure 1.

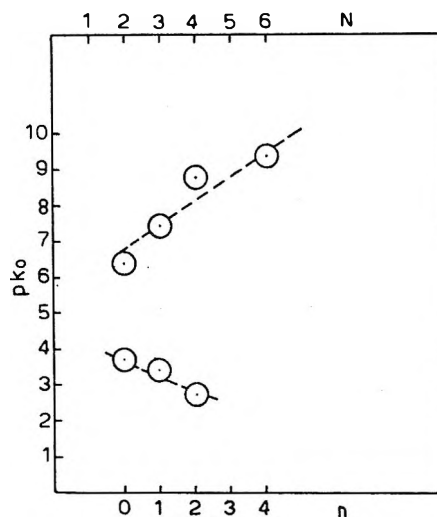


Figure 3. Variation of the intrinsic pK , pK_0 , with the number of carbon atoms, n , in the side chain of the olefin comonomer corresponding to the data in Figure 2. $N (= n + 2)$ is the total number of carbon atoms in the olefin comonomer.

the two carboxyl groups present in each polymer. In particular, the ionization of the more acidic carboxyl group is increased on increasing n while the reverse is true for the weaker carboxyl group.

Table I: Intrinsic pK 's of the Dissociating Groups Present in the Polyanions and Polycations

Polyanion	$pK_{o,A}$	$pK_{o,B}$
EMA	3.65	6.40
PMA	3.40	7.40
IBMA	2.72	8.83
MMA	...	9.35
SMA	...	7.75
Polycation	$pK_{o,\alpha}$	$pK_{o,\beta}$
Ecat,unquat	10.32	4.43
Ecat	...	4.61
Mcat,unquat	(≈ 8)	...
Mcat
Scat,unquat	8.16	...
Scat

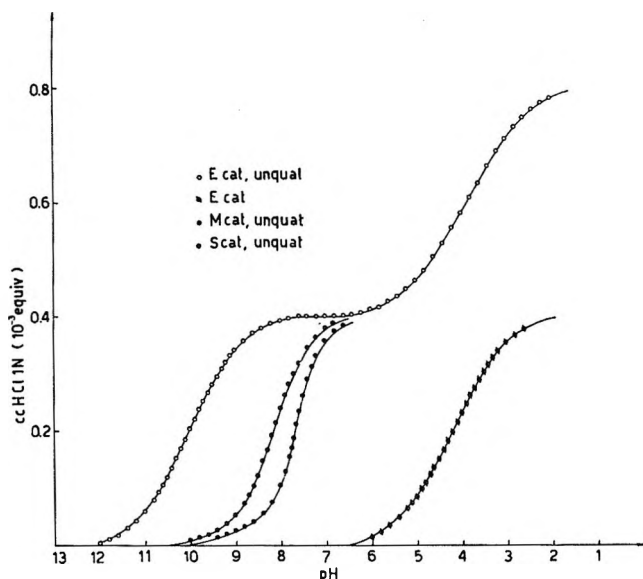
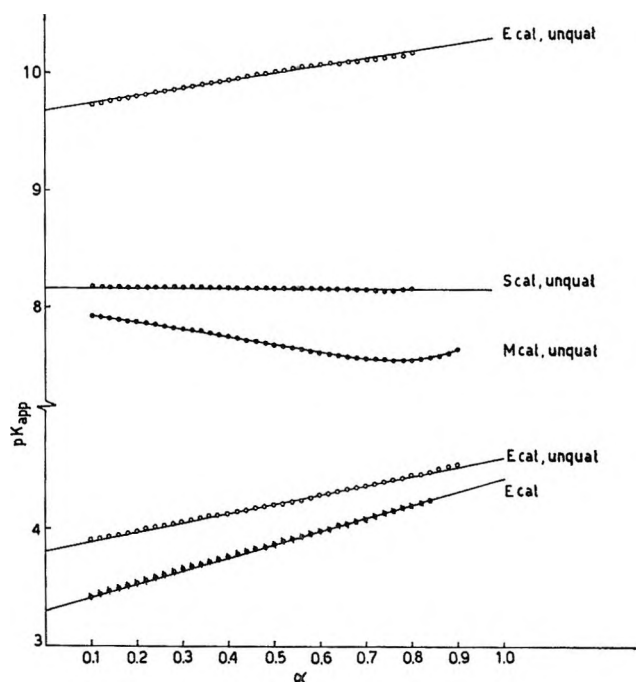
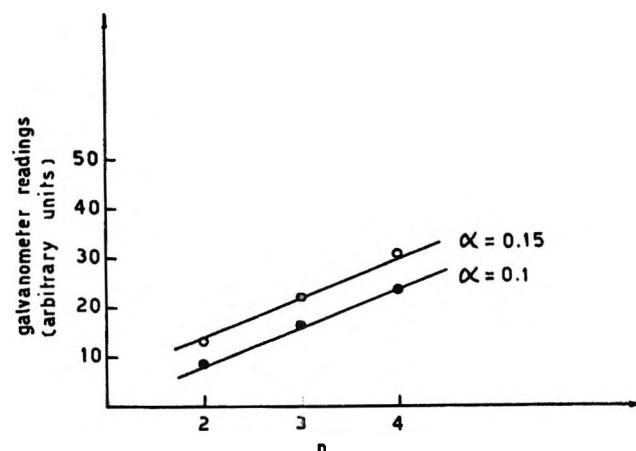


Figure 4. Titration curves for polycation copolymers at 25° in 0.1 M KCl.

Titration curves for the quaternized and unquaternized polycations are reported in Figure 4. We note that there is one titratable group for Ecat and two titratable groups for Ecat,unquat. No titratable groups are evident for Mcat and Scat, whereas one titratable group is evident for both Mcat,unquat and Scat,unquat. The pK_{app} vs. α curves for these polycations are reported in Figure 5 and corresponding pK_o values are collected in Table I. The slope of the pK_{app} vs. α curves for Mcat,unquat is negative while that for Scat is near zero. The infrared spectra of Ecat (previously exposed to high and low pH) revealed the characteristic imide peaks at 5.65 and 5.90 μ .

Titration curves (unreported) for PLL and PLO are similar to those previously reported⁸ and the pK_o values are, respectively, 10.2 and 9.9. From the titration curves it is deduced that when $pH < 7$, $\alpha = 0$ for both


 Figure 5. Apparent pK vs. degree of ionization plot corresponding to the data in Figure 4.

 Figure 6. Turbidity of mixtures of EMA-PLL, PMA-PLL, and IBMA-PLL as a function of the number of carbon atoms, n , in the olefin comonomer of the polyanions. The degree of dissociation for the polyanions is indicated. α for PLL = 0. The temperature is 25° and the concentration of the individual polymers is 5.5×10^{-7} equiv/cc.

polymers (*i.e.*, the polymers are fully charged and in the random coiled conformation).

Figure 6 summarizes the solubility results for mixtures of poly-L-lysine with EMA, PMA, and IBMA at pH 2-5. The direct galvanometric reading of the EEL nephelometer is plotted against the number of carbon atoms n in the olefin comonomer for a constant value of the degree of dissociation on the polyanions (the pH's of the mixtures were chosen, on the basis of the titration curves, so that comparison of the different polyanions could be made at a given α_{TOT}).

Table II: Solubility Characteristics of Mixtures of Polyanion Copolymers with Polypeptides ($T = 25^\circ$, $C_s = 0.005 M$ KCl)

Mixture no.	Polymers	Composition			Appearance			
		Equiv $\times 10^6/10$ cc	Ratio	g/10 cc	10 min after mixing	At pH 2 24 hr after mixing	At pH 1.15, 24 hr after mixing	At pH 1.0, 24 hr after mixing
1	PLL/EMA	339.75/37.75	9:1	0.0071/0.0025	Clear	Clear	...	Clear
2	PLL/EMA	37.75/37.75	1:1	0.0008/0.0025	Precipitate	Precipitate	...	Clear
3	PLL/EMA	3.775/37.75	1:10	0.00008/0.0045	Precipitate	Clear	...	Clear
4	PLO/EMA	339.75/37.75	9:1	0.0066/0.0025	Clear	Clear	...	Clear
5	PLO/EMA	37.75/37.75	1:1	0.00074/0.0025	Clear	Clear	...	Clear
6	PLO/EMA	3.775/37.75	1:10	0.00007/0.0025	Precipitate	Clear	...	Clear
7	PLL/IBMA	319.05/35.45	9:1	0.00667/0.0023	Precipitate	Precipitate	Precipitate	Clear
8	PLL/IBMA	35.45/35.45	1:1	0.00074/0.0028	Precipitate	Precipitate	Precipitate	Clear
9	PLL/IBMA	3.545/35.45	1:10	0.00007/0.0028	Precipitate	Precipitate	Precipitate	Clear
10	PLO/IBMA	319.05/35.45	9:1	0.00622/0.0028	Precipitate	Precipitate	Clear	Clear
11	PLO/IBMA	35.45/35.45	1:1	0.0007/0.0028	Precipitate	Precipitate	Clear	Clear
12	PLO/IBMA	3.545/35.45	1:10	0.00007/0.0028	Precipitate	Precipitate	Clear	Clear

Table II summarizes the solubility results for mixtures containing different proportions of polyanion copolymers with the cationic polypeptides at pH 2-1.

Discussion

Titration Behavior. The effect of the alteration of the alkyl side chains on the ionization of two adjacent carboxyl groups, demonstrated in Figure 3, appears to be one of the most interesting results of this investigation. We suggest the following qualitative interpretation for the different effects of the side chains on the ionization of the two carboxyl groups. The polyanion chain is represented (*cf.* Figure 7) as a sequence of pairs of carboxyl groups alternated with hydrophobic side chains. Two types of carboxyl groups are arbitrarily distinct as type A and type B. For the sake of discussion, the more acidic carboxyls are assigned to group A and the weaker ones to type B. The ionization of the first A-type carboxyl takes place while the neighboring B-type carboxyls are completely un-ionized. It is known that the presence of neighboring dipoles favors the ionization of carboxyl groups. For instance,⁷ the dissociation pK of the carboxyl group in $R-CH_2-COOH$ is 4.87 when $R = CH_3$ and 1.7 when $R = COOH$. If the effect of increasing the number of carbon atoms in the hydrophobic side chain is regarded as a decrease of the effective (local) dielectric constant,⁷ a corresponding increase of the net interaction (favoring ionization) between the charge on the A-type carboxyl and the dipoles on B-type carboxyls should occur, according to general electrostatic considerations, on increasing n .

A different situation arises in the case of the ionization of the first B-type carboxyl which takes place when all A-type carboxyls are essentially ionized. Here the prevailing interaction is of the ion-ion type and must necessarily be a repulsive one, hindering ionization. Therefore, in this case, an increase of n , regarded

as a decrease of the effective dielectric constant,⁷ results in an increase of the net ion-ion interaction and thus in an increase of pK_0 with n .

In the above interpretation the role of the alkyl side chain is an indirect one (*i.e.*, an alteration of the ion-ion or ion-dipole interaction through the local dielectric constant). The possibility of a direct effect of the side chain on the ionization of the A- or B-type carboxyl groups is reduced considering, for instance, the effect of the side chain on the pK_0 's of acetic, propionic, and *n*-butyric acids which are essentially similar. It is gratifying to note that the values of pK_0 which can be extrapolated to $N = 0$ (≈ 4.5 and 5.5) are in good agreement with the values for succinic acid. We also note that the relative strengths of the B-type carboxyls are accurately described⁸ by Newmann's⁹ empirical "rule of six."

The effect of hydrophobic side chains on the ionization of an adjacent group, which has been demonstrated in our synthetic copolymers, may also play a role in the case of more complex copolymers. For instance, some of the anomalous pK_0 's which are often observed in the titration of proteins may be explained in terms of the above considerations.

The behavior of the polycation copolymers is also interpreted in terms of the titration of two functional groups which are indicated as α and β in (2). It is assumed that, upon quaternization, group type α is so strong as to be practically fully ionized at $pH < 12$. The observation of a group with $pK_0 = 10.32$ for Ecat,unquat, $pK_0 \approx 8$ for Mcat,unquat, and $pK_0 = 8.16$ for Scat,unquat is associated with the titration of the unquaternized α group. The difference between these

(7) J. T. Edsall and J. Wyman, "Biophysical Chemistry," Academic Press, Inc., New York, N. Y., 1958.

(8) J. H. Johnson, Monsanto Co., private communication.

(9) M. S. Newmann, "Steric Effects in Organic Chemistry," John Wiley & Sons, Inc., New York, N. Y., 1950.

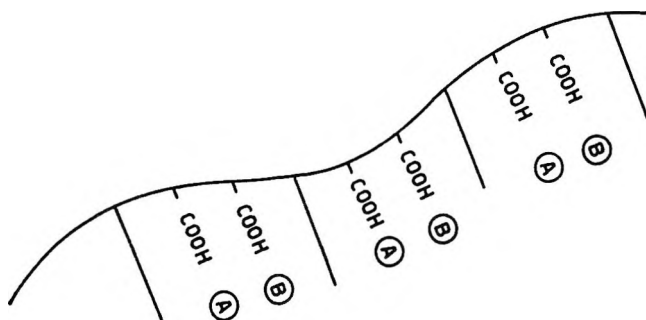


Figure 7. Schematic representation of a polyanion copolymer chain.

pK_o 's can, again, be attributed to the effect of the side chains. Upon quaternization this group is no longer titratable. The occurrence of a second basic group is associated with the titration of group β . This group is titrated in the case of Ecat ($pK_o = 4.43$) and Ecat,unquat ($pK_o = 4.61$) but is not titrated in the case of Mcat, Scat, Mcat,unquat, and Scat,unquat. A pK_o of the order of 4.5 is certainly uncommon for an imide. The possibility that the hydrolysis of the $-\text{CO}-\text{N}-\text{CO}-$ bond has taken place, resulting in amide formation, seems, however, to be ruled out by the spectrophotometric data.

We finally note that the occurrence of zero or negative slopes in the cases of MMA, Mcat,unquat, and Scat,unquat can be associated with some structural transformation occurring during the titration, although the phenomenon is not as sharp as in the case of the crystallization and helix \rightarrow coil transformation of polypeptides⁶ or in the cases of maleic acid + *n*-butyl vinyl ether copolymers¹⁰ and polymethacrylic acid.¹¹ While the phenomenon requires further investigation, we suggest, in view of the limited solubility of these polymers, that it might be associated with an aggregation gradually leading into precipitation.

Interaction with Polypeptides. Insoluble complexes between polypeptides and ethylene-maleic anhydride copolymers can be obtained⁴ as a result of the formation of a covalent bond between an NH_2 group of the peptide chain and a carboxyl group of EMA. Here we consider the occurrence of a coprecipitate between the polyanion copolymers and model polypeptides in the absence of covalent bond formation. The process is of interest in practical applications such as removing viruses from water.³

Preliminary (unreported) results indicated that the formation of a coprecipitate in solutions containing EMA and PLL reached a maximum in the neutral pH range and decreased at the pH extremes when the charge on one of the polymers approached zero. This fact is indicative of the important role of electrostatic interactions in the coprecipitation. If we assume that the polymer to be coprecipitated has a given positive charge, then the order of increasing effectiveness of the

polyanions for precipitation, based solely on electrostatic interactions, could be deduced on the basis of the total degree of dissociation of the polyanions. Using the data in Figure 1, this order should depend on the pH of precipitation. For the alkyl side chain polyanions at pH 4 the order would be



while at pH 8 the order would be



In this classification the role of the alkyl side chain is taken account of only in so far as it affects the dissociation of the carboxyl groups. However, it is conceivable that an increase of the size of the alkyl side chain may favor precipitate formation because of the increased hydrophobic character of the polyanion. The data in Figure 6 and Table II do in fact support the occurrence of this second contribution to the coprecipitation (in addition to electrostatic interaction). The data in Figure 6, pertaining to a situation where the polypeptide is fully ionized (pH < 5), indicate that the amount of precipitate due to an increase of the degree of ionization from $\alpha = 0.1$ to 0.15 for a given polyanion (*i.e.*, $n = \text{constant}$) is about the same as that due to an increase of one carbon atom in the alkyl side chain when $\alpha = \text{constant}$. In fact, on the basis of the data at $\alpha = \text{constant}$ reported in Figure 5, the order for increasing effectiveness for precipitation, based only on hydrophobic interactions, should be



The data in Table II pertain to a situation (pH 1–2) where electrostatic interaction is minimal since the polypeptides (PLL and PLO) are both fully charged while the charge on the polyanions approaches zero. The data indicate the effect of an alteration of the alkyl side chain of the polypeptides, all other conditions being the same. Formation of a precipitate corresponding to the larger side chain of FLL and lack of a precipitate in the case of PLO (compare data at pH 2 for mixtures no. 2 and 5 and at pH 1.5 for mixtures no. 7, 8, 9 and no. 10, 11, 12), confirms that hydrophobic interactions play a part in the formation of insoluble complexes. In addition, the data obtained at pH 1.0 (when the polyanions are certainly uncharged) indicate that any difference in hydrophobicity between EMA and IBMA (and also between PLL and PLO) is not enough, alone, to assure the formation of insoluble complexes. It thus appears that the role of the alkyl side chain of the

(10) P. Dubin and U. P. Strauss, *J. Phys. Chem.*, **71**, 2757 (1967).

(11) A. M. Liquori, G. Barone, V. Crescenzi, F. Quadrioglio, and V. Vitagliano, *J. Macromol. Chem.*, **1**, 291 (1966).

polyanion on complex formation has to be understood in terms of the effect it has on the ionization of the carboxyl groups and of the effect related to hydrophobic interactions. The two effects are not, in general, additive, as is evident on comparing series 3, 4, and 5.

Acknowledgments. The authors are greatly indebted to J. E. Fields, J. H. Johnson, and F. D. Wharton of the Monsanto Company for preparing the copolymers, for many illuminating discussions and very useful advice.

On the Viscosity of Concentrated Aqueous Electrolyte Solutions^{1,2}

by Barry R. Breslau³ and Irving F. Miller

Department of Chemical Engineering, Polytechnic Institute of Brooklyn, Brooklyn, New York 11201
(Received July 7, 1969)

The viscosities of concentrated aqueous electrolytic solutions have been correlated by use of an equation developed by Thomas, for the viscosities of concentrated suspensions of macroscopic spheres. The Thomas equation, $\eta/\eta_0 = 1 + 2.5\phi + 10.05\phi^2$, where η/η_0 is the relative viscosity and ϕ is the particle volume fraction, is a truncated form of a seventh-order regression which has been shown effective for $\phi < 0.25$. For ionic particles, ϕ is related to an "effective" rigid volume by $\bar{V}_e = \phi/c$, where c is the salt concentration; \bar{V}_e is obtained directly from viscosity measurements and is shown to be relatively concentration independent. Analysis of viscosity data for 72 salts in aqueous solution results in an additional correlation of \bar{V}_e with the Jones-Dole B coefficient from which viscosities of concentrated aqueous salt solutions can be estimated. For univalent salts, $B = 2.90\bar{V}_e - 0.018$; for salts involving a multivalent ion, $B = 6.06\bar{V}_e - 0.041$. The difference between these two correlations is attributed to the differences in hydrodynamic effects and ion-solvent interaction.

Introduction

The properties of aqueous electrolytic solutions are highly specific to the individual ions concerned and generalizations are difficult to find. In the case of viscosity, Jones and Dole⁴ developed an empirical equation for the concentration dependence of viscosity of dilute electrolytic solutions, given by

$$\eta/\eta_0 = 1 + A\sqrt{c} + Bc \quad (1)$$

where η and η_0 are the viscosities of the solution and pure solvent, respectively; c is the solute concentration (moles/liter); and A and B are constants specific for the given solute-solvent system.

This well-known equation has undergone extensive investigation, especially with respect to the interpretation of the constants A and B . Falkenhagen, *et al.*,⁵⁻⁷ demonstrated that the square root term was due to long-range interionic forces and that the coefficient A could be theoretically calculated from the Debye-Hückel theory. While no quantitative theory exists for the independent determination of the linear B coefficient, important qualitative determinations have been advanced relating it to ion-solvent interaction.⁸ Since, in general, A/B is $\ll 1$, the second term may be neglected at concentrations above 0.002 M , and eq 1 may be rewritten as

$$\eta/\eta_0 = 1 + Bc; \quad 0.002 M < c < \sim 0.1 M \quad (2)$$

Although the B coefficient is empirically derived, it is a highly specific property of the solute and can be determined by adding individual contributions of the solute constituent ions. Thus

$$B = z_+B_- + z_-B_+ \quad (3)$$

where z_{+-} and B_{+-} refer to the ionic valence and ionic viscosity B coefficient. Cox and Wolfenden⁹ formed tables of ionic B coefficients based on Li^+ and IO_3^- ions; Gurney⁸ and later Kaminsky¹⁰ formed similar tables based on the K^+ and Cl^- ions, assuming that $B_{\text{K}^+} = B_{\text{Cl}^-}$, and corroborated the results of Cox and Wolfenden. Other sources of tables are Stokes and Mills,¹¹

(1) Based on part of a thesis submitted by Barry R. Breslau in partial fulfillment of the requirements for the Ph.D. degree in Chemical Engineering at the Polytechnic Institute of Brooklyn.

(2) The authors gratefully acknowledge financial support for this work from the National Institutes of Health, under Grant No. GM-12013.

(3) Pioneering Research Laboratory, DuPont Co., Wilmington, Del.

(4) G. Jones and M. Dole, *J. Amer. Chem. Soc.*, **51**, 2950 (1929).

(5) H. Falkenhagen and M. Dole, *Phys. Z.*, **30**, 611 (1929).

(6) H. Falkenhagen, and E. L. Vernon, *Phil. Mag.*, **14**, 537 (1932).

(7) H. Falkenhagen, *Phys. Z.*, **32**, 745 (1931).

(8) R. W. Gurney, "Ionic Processes in Solution," McGraw-Hill Book Co., Inc., New York, N. Y., 1953, Chapter 9.

(9) W. M. Cox and J. F. Wolfenden, *Proc. Roy. Soc. (London)*, **A145**, 475 (1934).

(10) M. Kaminsky, *Discussions Faraday Soc.*, **24**, 171 (1957).

Robinson and Stokes,¹² and Asmus.¹³ From these tables, viscosity B coefficients can be constructed for a wide variety of salts with good precision. Equation 2, therefore, could be potentially quite useful for predicting viscosity of electrolytic solutions, were it not restricted to relatively low concentrations ($\sim 0.1 M$).

In the case of suspensions, Einstein¹⁴ developed an equation similar to eq 2, giving the relative viscosity of dilute suspensions of rigid spheres. This equation

$$\eta/\eta_0 = 1 + 2.5\phi \quad (4)$$

where η and η_0 are the viscosity of the suspension and suspending medium, respectively, and ϕ is the particle volume fraction, is based on hydrodynamic considerations alone and is strictly valid only when applied to macroscopic, rigid spheres in the limiting case of infinite dilution. Experimentally, however, it has been found effective to volume fractions as high as $\phi \simeq 0.01$.

A number of workers¹⁵⁻¹⁸ have attempted to relate Einstein's equation (eq 4) to the Jones-Dole equation (eq 2) by performing the transformation

$$\phi = cV \quad (5)$$

where V is an estimate of the molar volume of the solute molecules in solution. The B coefficient can then be related to V by

$$B = 2.5V \quad (6)$$

Estimates of V are often based on the hydrated or crystal radius of the solute ions. In fact, this approach has been used in certain instances to estimate degrees of hydration.¹²

Fuoss and coworkers,^{15,16} working with apparent molar volumes (\bar{V}) obtained from density measurements, were successful in demonstrating a like correspondence between additivity of ion contributions to both B and \bar{V} . They were not able, however, to confirm eq 6, and found it valid only for large ions which can be said to resemble macroscopic particles. For smaller ions, $B/\bar{V} > 2.5$ with the ratio growing as the ions tested became smaller. In particular, Kurucsev, *et al.*,¹⁷ reported that eq 6 is valid only for ions of radius $> 5 \text{ \AA}$.

While very little work has been done in the area of concentrated electrolytic solutions, a considerable effort has been made, both theoretical and empirical, with respect to determining the viscosity of concentrated suspensions.^{19,20} Equations which result can generally be represented by a polynomial of the form

$$\eta/\eta_0 = 1 + 2.5\phi + k_1\phi^2 + k_2\phi^3 + \dots \quad (7)$$

Vand²¹ demonstrated that the addition of the second- and higher order terms to Einstein's equation (eq 4) are due to particle interactions of various types. Thomas²² made a critical analysis of extensive experimental data collected from 16 different sources, and, using statistical techniques, determined the coefficients

of the power series expressed in eq 7 to the seventh degree. These data were obtained with both rotational and capillary viscometers on systems with a range of particle diameters from 0.99 to 435 μ and for such materials as polystyrene, rubber latex, glass, and methyl methacrylate. He further demonstrated that a simple second-degree equation (eq 8) will correlate the experimental data to within 97.5% of the η/η_0 value for $\phi \leq 0.25$.

$$\eta/\eta_0 = 1 + 2.5\phi + 10.05\phi^2 \quad (8)$$

Since, at $\phi = 0.25$, the average particle separation is only 0.35 particle diameter, this equation seems to be valid for quite highly concentrated suspensions.

To date, even though there is considerable work available from suspension theory, no one has been able to relate suspension to solution theory in such a way that viscosities of concentrated electrolytic solutions can be calculated in a general manner.

Proposed Model

In this contribution, eq 8 is taken as the starting point. Performing the transformation presented in eq 5 on eq 8 results in

$$\eta/\eta_0 = 1 + 2.5cV_e + 10.05c^2V_e^2 \quad (9)$$

where we have added the subscript e to V to designate it as an "effective" rigid molar volume. Equation 9 may be rearranged to solve for V_e .

$$V_e = \frac{-2.5c + \sqrt{(2.5c)^2 - 4(10.05c^2)(1 - \eta/\eta_0)}}{2(10.05)c^2} \quad (10)$$

If viscosity-concentration data are available for any given salt, its "effective" rigid molar volume, V_e , may be obtained from eq 10 as a function of concentration. This computation was performed with the aid of an IBM 360/50 computer for 72 different salts; data were obtained from a variety of sources^{11,23,24} covering a

(11) R. H. Stokes and R. Mills, "Viscosity of Electrolytes and Related Properties," Pergamon Press, Oxford, 1965.

(12) R. A. Robinson and R. H. Stokes, "Electrolytic Solutions," 2nd ed, Butterworth, London, 1959.

(13) V. E. Asmus, *Z. Naturforsch.*, **49**, 589 (1949).

(14) A. Einstein, *Ann. Phys.*, **19**, 289 (1906); **34**, 591 (1911).

(15) D. F. T. Tuan and R. M. Fuoss, *J. Phys. Chem.*, **67**, 1343 (1963).

(16) J. F. Skinner and R. M. Fuoss, *ibid.*, **68**, 2998 (1964).

(17) T. Kurucsev, A. M. Sargeson, and B. O. West, *ibid.*, **61**, 1567 (1957).

(18) S. P. Moulik, *ibid.*, **72**, 4682 (1968).

(19) F. R. Eirich, Ed., "Rheology, Theory and Applications," Vol. 1, Academic Press, New York, N. Y., 1956.

(20) T. F. Ford, *J. Phys. Chem.*, **64**, 1168 (1960).

(21) V. Vand, *J. Phys. Colloid Chem.*, **52**, 277 (1948); **52**, 314 (1948).

(22) D. G. Thomas, *J. Colloid Sci.*, **20**, 267 (1965).

(23) N. A. Lange, "Handbook of Chemistry," 10th ed, McGraw-Hill Book Co., Inc., New York, N. Y., 1961.

(24) E. W. Washburn, Ed., "International Critical Tables," Vol. V, McGraw-Hill Book Co., Inc., New York, N. Y., 1929.

Table I: Effective Rigid Molar Volumes of Salts from Viscosity Data

Salt	B , l./mol	No. of data points	Concentration range, mol/l.	Range of V_e calcd, l./mol	\bar{V}_e , l./mol, av value	Std dev, %
CH ₃ COOH	0.117	4	0.125-1.00	0.0391-0.0533	0.0457	12.9
AgNO ₃	0.045	7	1.00-7.00	0.0247-0.0355	0.0304	12.5
Al ₂ (SO ₄) ₃	1.967	4	0.125-1.00	0.1121-0.1180	0.1152	2.08
C ₆ H ₅ NH ₃ Cl	0.319	10	0.098-3.67	0.0892-0.1539	0.1048	18.9
BaCl ₂	0.206	4	0.125-1.00	0.0401-0.0422	0.0414	2.18
Ba(NO ₃) ₂	0.128	4	0.125-1.00	0.0265-0.0331	0.0310	10.0
BeSO ₄	0.601	4	0.125-1.00	0.0472-0.1081	0.0910	32.2
CaCl ₂	0.271	4	0.125-1.00	0.0518-0.0550	0.0538	2.80
Ca(NO ₃) ₂	0.193	4	0.125-1.00	0.0240-0.0409	0.0348	22.4
CdCl ₂	0.306	4	0.125-1.00	0.0454-0.0627	0.0504	16.3
Cd(NO ₃) ₂	0.228	4	0.125-1.00	0.0536-0.0582	0.0553	3.80
CdSO ₄	0.529	4	0.125-1.00	0.0994-0.1122	0.1044	5.25
CoCl ₂	0.371	4	0.125-1.00	0.0648-0.0719	0.0692	4.77
Co(NO ₃) ₂	0.292	4	0.125-1.00	0.0485-0.0560	0.0533	6.2
CoSO ₄	0.593	4	0.125-1.00	0.1008-0.1212	0.1095	8.03
CsCl	-0.052	5	0.598-4.058	-0.0138-(+0.001)	-0.0069	85.5
CsI	-0.113	5	0.284-2.00	-0.0463-(-0.0437)	-0.0454	2.21
CuCl ₂	0.371	4	0.125-1.00	0.0650-0.0823	0.0716	10.5
Cu(NO ₃) ₂	0.293	4	0.125-1.00	0.0557-0.0603	0.0579	3.29
CuSO ₄	0.594	4	0.125-1.00	0.1017-0.1161	0.1096	6.48
FeCl ₃	0.740	4	0.125-1.00	0.0842-0.0924	0.0888	3.95
HBr	0.027	4	0.125-1.00	0.0122-0.0215	0.0154	28.1
HCl	0.062	4	0.125-1.00	0.0244-0.0299	0.0265	9.06
HClO ₃	0.043	4	0.125-1.00	0.0187-0.0227	0.0201	8.95
HClO ₄	-0.011	4	0.125-1.00	-0.0026-(+0.0046)	0.0011	2.91
HNO ₃	0.023	5	0.116-5.806	0.0081-0.0158	0.0117	30.8
H ₃ PO ₄	0.272	4	0.125-1.00	0.0855-0.0957	0.0917	5.24
H ₂ SO ₄	0.184	4	0.125-1.00	0.0259-0.0334	0.0309	11.0
KCl	-0.014	7	1.00-4.00	-0.0012-(+0.0068)	0.0028	104.0
K ₂ CO ₃	0.336	4	0.125-1.00	0.0547-0.0596	0.0574	4.01
KF	0.113	12	0.525-6.445	0.0395-0.0465	0.0416	5.05
K ₃ Fe(CN) ₆	0.117	4	0.125-1.00	0.0163-0.0566	0.0281	68.4
K ₄ Fe(CN) ₆	0.372	4	0.125-1.00	0.0352-0.0389	0.0372	4.57
KI	-0.075	12	0.500-6.00	-0.0289-(+0.0075)	-0.0120	108.0
KNO ₃	-0.058	4	0.125-1.00	-0.0256-(-0.0103)	-0.0180	37.8
KOH	0.102	4	0.125-1.00	0.0408-0.0478	0.0448	6.92
K ₂ SO ₄	0.195	4	0.125-1.00	0.0247-0.0366	0.0324	17.3
LaCl ₃	0.567	3	0.250-1.00	0.1918-0.2145	0.2019	7.92
LiBr	0.105	10	0.597-4.728	0.0314-0.0398	0.0331	7.86
LiCl	0.140	12	0.441-4.964	0.0431-0.0546	0.0471	7.85
LiClO ₃	0.126	15	0.512-8.047	0.0420-0.0524	0.0456	7.03
LiNO ₃	0.101	13	0.0581-8.726	0.0365-0.0484	0.0397	9.06
Li ₂ SO ₄	0.508	4	0.125-1.00	0.0863-0.0976	0.0930	5.26
MgCl ₂	0.371	4	0.125-1.00	0.0639-0.0667	0.0653	2.30
Mg(NO ₃) ₂	0.293	4	0.125-1.00	0.0557-0.0615	0.0590	4.07
MgSO ₄	0.594	4	0.125-1.00	0.0976-0.1127	0.1054	6.07
MnCl ₂	0.420	4	0.125-1.00	0.0660-0.0718	0.0695	37.4
Mn(NO ₃) ₂	0.356	4	0.125-1.00	0.0592-0.0726	0.0644	9.04
MnSO ₄	0.740	4	0.125-1.00	0.1030-0.1109	0.1085	3.50
CH ₃ COONa	0.333	4	0.125-1.00	0.1089-0.1318	0.1210	8.36
NaBr	0.044	14	0.500-7.00	0.0222-0.0413	0.0307	19.9
NaCl	0.079	9	1.00-5.00	0.0338-0.0386	0.0356	4.76
NaClO ₃	0.062	4	0.125-1.00	0.0317-0.0368	0.0336	7.15
NaClO ₄	0.006	4	0.125-1.00	0.0089-0.0173	0.0139	25.9
NaNO ₃	0.040	8	0.972-6.24	0.0191-0.0381	0.0310	21.0
NaOH	0.195	4	0.125-1.00	0.0729-0.0924	0.0809	10.8
Na ₂ SO ₄	0.371	4	0.125-1.00	0.0712-0.0775	0.0738	3.65
NH ₄ Cl	-0.014	4	0.125-1.00	-0.0047-(-0.0003)	-0.0021	90.5
NH ₄ NO ₃	-0.053	4	0.125-1.00	-0.0149-(-0.0113)	-0.0129	13.2
NH ₄ OH	0.102	4	0.125-1.00	0.0083-0.0096	0.0091	6.59
(NH ₄) ₂ SO ₄	0.195	4	0.125-1.00	0.0386-0.0463	0.0430	9.06
NiCl ₂	0.370	4	0.125-1.00	0.0651-0.0681	0.0662	2.11

Table I (Continued)

Salt	B , l./mol	No. of data points	Concentration range, mol/l.	Range of V_e calcd, l./mol	V_e , l./mol, av value	Std dev. %
Ni(NO ₃) ₂	0.292	4	0.125-1.00	0.0583-0.0635	0.0606	3.47
NiSO ₄	0.593	4	0.125-1.00	0.0985-0.1084	0.1039	4.25
Pb(NO ₃) ₂	0.141	4	0.125-1.00	0.0209-0.0354	0.0287	21.6
RbNO ₃	-0.076	7	0.188-2.174	-0.0238-(-0.0101)	-0.0160	38.2
ZnCl ₂	0.356	4	0.125-1.00	0.0608-0.0780	0.0700	10.7
Zn(NO ₃) ₂	0.378	4	0.125-1.00	0.0540-0.0611	0.0580	5.17
ZnSO ₄	0.579	4	0.125-1.00	0.1037-0.1179	0.1107	5.42
C(C ₂ H ₅) ₄ NBr	0.343	1	0.100	0.132	0.132	...
C(C ₂ H ₅) ₄ NCl	0.378	1	0.100	0.132	0.132	...
C(CH ₃) ₄ NCl	0.136	1	0.100	0.057	0.057	...

concentration range from 0.1 (approximately the upper limit of the Jones-Dole equation (eq 2)) to $\sim 8 M$. Since we were primarily interested in high concentration effects, we have only used salts for which data were available to concentrations of at least 1 M . The results of these calculations are presented in Table I.

Analysis of this work brings out a number of interesting points. Although for any given salt there is some variation in V_e with concentration, this variation did not follow any defined trend. Furthermore, when average "effective" rigid molar volumes, \bar{V}_e , were calculated for each salt over the entire concentration range studied, it was observed that the range variation in V_e was most pronounced for those salts having a low value of \bar{V}_e . For example, of the 72 salts investigated, 56 have $\bar{V}_e > 0.03$ l./mol; the relative, average standard deviation of V_e values corresponding to these 56 salts is only 8.7% as compared to 42.5% corresponding to the 16 remaining salts having $\bar{V}_e \leq 0.03$ l./mol. To account for this effect, we need only note that salts with low values of \bar{V}_e have only a minor effect on solution viscosity (see eq 9). Consequently, in these cases the $(1 - \eta/\eta_0)$ term in eq 10 is quite small, and V_e is obtained by taking the difference of two numbers essentially equal in magnitude. This type of calculation tends to magnify any differences which may result from lack of precision in the measured values of η/η_0 and c .

A reasonable conclusion, therefore, that can be drawn from these results is that there exists a unique value of V_e , independent of concentration, and that the observed variation of V_e can be attributed to experimental error. With this as a hypothesis, the calculated average "effective" rigid molar volume, \bar{V}_e , is then the best approximation to the true "effective" molar volume for each salt.

Having thus obtained unique values for \bar{V}_e based on high concentration viscosity data, we seek an additional correlation with the Jones-Dole viscosity B coefficient, which is also unique, but is based on low concentration data. The arguments for such a correlation are purely qualitative and are based on an understanding of the significance of \bar{V}_e .

Embodied in the development of Einstein's equation (eq 4) are the assumptions that (1) the solution is infinitely dilute, (2) the spherical particles move in a continuum, and (3) there is no slip at the surface of the particles. Under the stipulation of infinite dilution, disturbances of the solvent flow pattern, caused by the presence of particles, do not overlap. As the particle concentration increases, a point is reached where perturbations of solvent flow can no longer be treated as being independent. This results in the power series extension of Einstein's equation (eq 7) which forms the basis of the Thomas equation (eq 9) from which \bar{V}_e values are obtained; the restrictions of no slip and a continuous medium (*i.e.*, that the radius of the suspended particle is large in comparison to that of a solvent molecule) are thus still in effect. On a microscopic level ionic particles certainly do not satisfy these restrictions, for not only are they essentially of the same dimensions as the solvent molecules but they move with considerable "slip." The significance of the V_e value thus obtained, therefore, is that of a "fictitious" or "effective" volume; *i.e.*, it is that volume which a mole of solute particles behave like when considered, for purely hydrodynamic reasons, as rigid macroscopic spheres. A particle which has a major effect on neighboring solvent molecules, from physical considerations alone, would be expected to have a higher \bar{V}_e than one which has a lesser effect. Since the B coefficient is an empirical measure of the degree of ion-solvent interaction, a relation should therefore exist, with positive slope, when B is plotted against \bar{V}_e . This plot has been prepared for the 72 salts studied and is presented in Figures 1 and 2. Figure 1 represents a correlation for uni-univalent salts; a least-squares fit of the data presented in Figure 1 results in the following correlation.

$$B = 2.90 \bar{V}_e - 0.018 \quad (11)$$

When values of B are plotted against \bar{V}_e , for salts involving divalent ions, a second linear relationship, different from eq 11, is obtained. Figure 2 presents such a plot for all salts involving a divalent ion. Again,

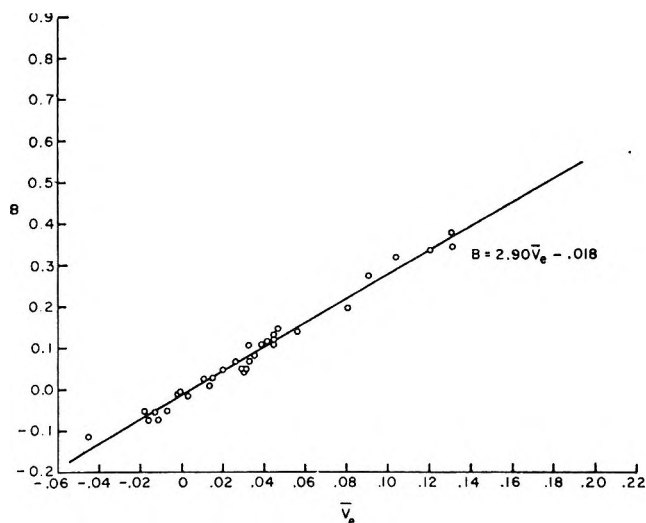


Figure 1. Jones-Dole B coefficient vs. effective rigid molar volume, \bar{V}_e , for 33 uni-univalent salts. Least-squares correlation is given by $B = 2.90 \bar{V}_e - 0.018$; B and \bar{V}_e are given in liters per mole.

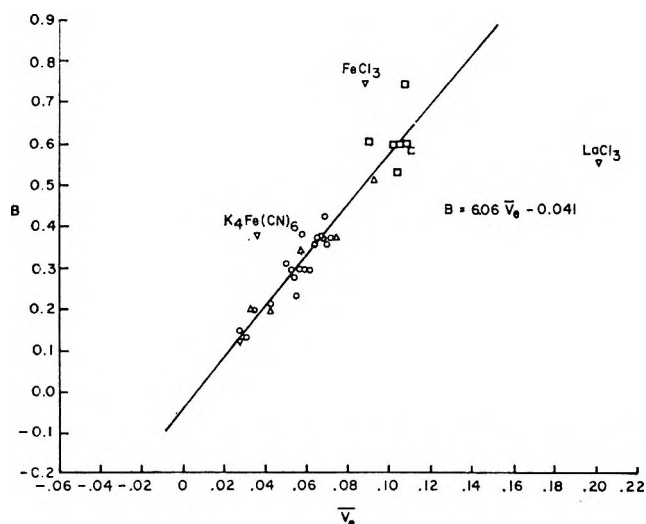


Figure 2. Jones-Dole B coefficient vs. effective rigid molar volume \bar{V}_e for 39 multivalent salts (O, divalent-univalent; Δ , univalent-divalent; \square , divalent-divalent; ∇ , tri- and tetravalent). Least-squares correlation is given by $B = 6.06 \bar{V}_e - 0.041$ (excluding tri- and tetravalent); B and \bar{V}_e are given in liters per mole.

a good straight line is obtained with the least-squares fit resulting in the correlation

$$B = 6.06 \bar{V}_e - 0.041 \quad (12)$$

It should be mentioned here for clarity that it is not reasonable to suppose that a relationship such as

$$B = 2.5 \bar{V}_e \quad (13)$$

should result from these correlations. In the case of comparing Einstein's equation (eq 4) to the modified Jones-Dole equation (eq 2), one compares two linear relationships both valid over the same concentration

range. It is mathematically correct, therefore, to compare coefficients of like terms, resulting in eq 6. In the present case, however, one compares a second-order equation with a first-order equation valid over different concentration ranges

$$\eta/\eta_0 = 1 + Bc \quad (0.002 M < c < 0.1 M) \quad (2)$$

$$\eta/\eta_0 = 1 + (2.5 \bar{V}_e)c + (10.05 \bar{V}_e^2)c^2 \quad (9)$$

$$(\bar{V}_e c < 0.25)$$

Since the coefficient of the square term in eq 9 is always positive

$$B > 2.5 \bar{V}_e \quad (14)$$

a result that is substantiated in eq 11 and 12. Note that one cannot go further than this since it would be incorrect to take the limit of eq 2 and 9 as $c \rightarrow 0$ since, in this case, eq 2 is no longer valid and eq 1 must be used.

Results and Discussion

From the correlation presented above, it is now possible to estimate the viscosity of concentrated solutions of electrolyte with confidence from a knowledge of the B coefficient alone.

From the salt B coefficient, either obtained from the literature or constructed from the B coefficient of the constituent ions, a value of \bar{V}_e is obtained using eq 11 or 12 depending on which is applicable. This value of \bar{V}_e is then used in eq 9 to predict the viscosity of the salt solution at the concentration of interest. Such an estimate should be valid up to concentrations in the 5–6 M region. This approach is demonstrated in Figure 3 in which estimated values for η/η_0 are plotted against measured values (all at 25°) at a series of concentrations up to 5 M for the 72 salts studied in aqueous solution. The applicability of the technique is obvious.

With respect to explaining the difference in slope between the uni-univalent and multivalent correlations, it should be emphasized that in this approach we are comparing two unique properties of a given salt, both pertaining to viscosity, but both the result of different effects. By going to the second-order Thomas equation (eq 9), one tacitly implies that at high concentrations the greatest contribution to the increase in viscosity of an electrolytic solution is due to a strictly hydrodynamic phenomenon, *i.e.*, the interaction of solvent perturbations. This effect should be quite independent of charge type. On the other hand, when working with the modified Jones-Dole equation (eq 2), one implies that the concentration range is one where solvent flow perturbations can be considered independent and, therefore, the increase in viscosity is solely a result of ion-solvent interaction. This interaction is quite substantial for a divalent ion in comparison to a univalent ion of the same size and is reflected in an increased B coefficient.

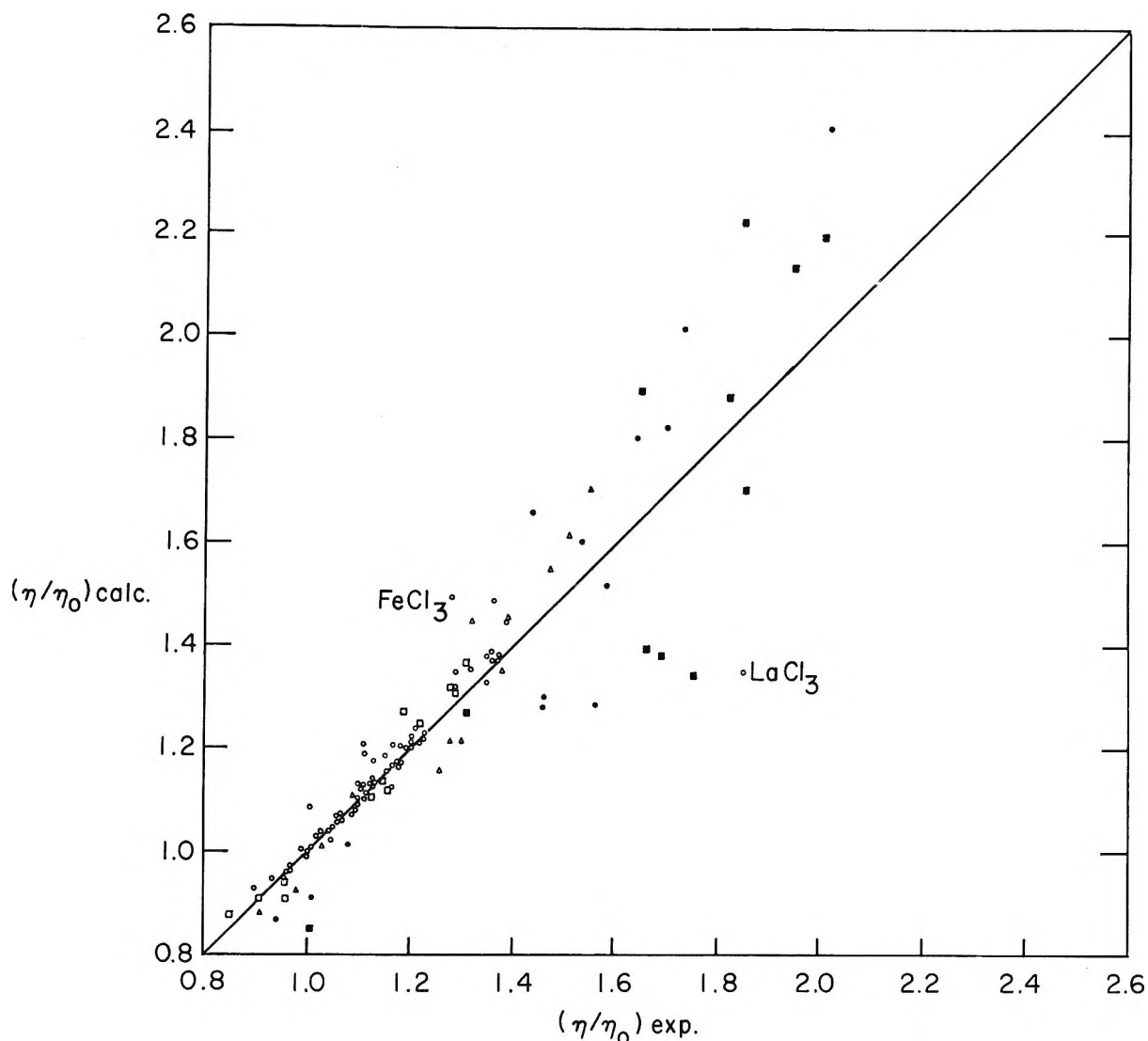


Figure 3. Calculated values of relative viscosity (η/η_0) vs. experimental values (O, 1 M; □, 2 M; △, 3 M; ●, 4 M; ■, 5 M).

cient. This accounts for the fact that for a given \bar{V}_0 value, divalent salts exhibit a marked increase in B values. Note, in particular, that $B = 2.5 \bar{V}_0$ is not to be expected in this case and that all that is required is that the relationship $B = f(\bar{V}_0)$ be one of positive slope.

Merker and Scott²⁵ studied the viscosity of solutions of tetrakis(trimethylsilyl)methane in ten different organic solvents and attempted to correlate their results by use of Einstein's equation (eq 4). The observed viscosities proved to be linear with concentration (at low concentration) but, instead of a slope of 2.5, they found slopes ranging from 0.92 to 3.09.

They explain their results by suggesting that, as a result of solute-solvent interaction, small density changes take place at the interface between solute and solvent molecules. These density changes lead to changes in the microscopic viscosity of the solvent at the interface and, thus, appear as increases or decreases

in the Einstein slope, depending on whether the microscopic viscosity is, respectively, higher or lower than the pure solvent value.

If these arguments are applied to the aqueous systems studied in our work, the implication is that divalent ions, as a result of their higher charge density, tend to induce much more structuring in the solvent water at the interface than do monovalent ions of the same size and, thus, the microscopic viscosity of the solvent water at the interface is higher than it would be for monovalent ions of the same size.

It might be noted that one might expect that the tri- and tetravalent salts would correlate with an equation of still higher slope than eq 12. Unfortunately, there are insufficient data from which to draw a conclusion. The available data are presented in Figure 2.

(25) R. L. Merker and M. J. Scott, *J. Colloid Sci.*, **19**, 245 (1964).

Micellar and Electrolyte Effects upon the H_0'' and H_0''' Acidity Functions¹

by C. A. Bunton and L. Robinson

Department of Chemistry, University of California, Santa Barbara, California 93106 (Received October 1, 1969)

An anionic detergent, sodium lauryl sulfate (NaLS) in dilute acid (0.01–0.1 M HCl) increases $-H_0''$ and $-H_0'''$, based on the ionizations of N-methyl and N,N-dimethyl-*p*-nitroanilines and 1-N-methylamino-4-nitronaphthalene, by up to 0.75 unit for the anilines and 1.25 units for the naphthylamine. Salts decrease the effects of anionic micelles with the sequence for acidity being: no salt > LiCl \sim NaCl \sim NaBr \gg (CH₃)₄NCl. Added cetyltrimethylammonium bromide (CTABr) decreases both $-H_0''$ and $-H_0'''$. Comparison with earlier results on the H_0' and H_R acidity functions shows that micellar effects upon ionization of the H_R indicator tri-*p*-anisylmethanol are considerably larger than on the protonation of primary, secondary, and tertiary aromatic amines. The salt effects upon H_0'' and H_0''' have been measured in the absence of detergent and compared with those on H_0' and H_R . Specific salt effects upon the activity coefficient of the N-methyl-*p*-nitroanilinium ion relative to that of the *p*-nitroanilinium ion are small, but larger effects are observed with the N,N-dimethyl-*p*-nitroanilinium ion which is stabilized, relative to the *p*-nitroanilinium ion by most salts, particularly by those having large, low charge density, anions.

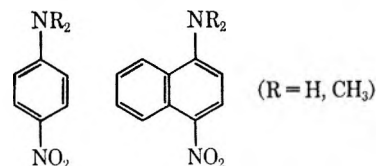
A number of workers have shown that ionic micelles can affect the ionization of indicators,^{2–6} and there are a number of examples of systems in which the pK of an indicator is different in the micellar and aqueous phases, and an anionic micelle should attract protons and other cations.

The incorporation of an ion into an ionic micellar pseudophase depends not only upon the electrostatic interactions between it and the micelle, but also upon the charge density of the ion, and bulky low charge density ions are most strongly incorporated into counterionic micelles,⁷ because of strong hydrophobic interactions between solute and micelle, and low hydration energies of a low charge density ion. These specific effects are important in both kinetic and equilibrium systems.

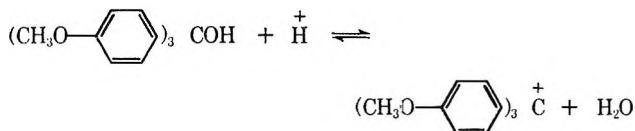
We have shown that anionic micelles of sodium lauryl sulfate, NaLS, increase the acidity of a dilute acid, as measured by the H_0' and H_R scales, and that cationic micelles of cetyltrimethylammonium bromide, CTABr, decrease it.⁶ These results are readily understandable in terms of electrostatic effects. However, the effects on the H_R scale, measured using tri-*p*-anisyl

micelle and the large, low charge density, triaryl carbonium ion.⁶ In neither system could we estimate the effect of micelles upon the hydrogen ion activity, but we could assume that it would not be affected by the indicators, which were present in very low concentrations.

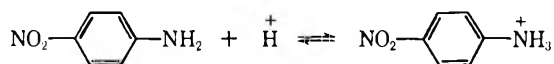
We have now extended these observations to the protonation of secondary and tertiary amines, using either nitroanilines or naphthylamines, because it is known



that there are differences between H_0' , H_0'' and H_0''' acidity scales, determined using primary, secondary and tertiary amines, respectively, especially at high acid concentrations.^{9,10} The differences between these scales and the H_R scale have been shown to depend upon the differing numbers of acidic hydrogen atoms in the conjugate acids which can hydrogen bond to water,^{9,10}



methanol, are much larger than on the H_0' scale mea-



sured using a nitroamine,^{8,9} and we explained these differences in terms of the lower hydration energy of a carbonium as compared with an anilinium ion, and the large hydrophobic interactions between the anionic

(1) Support of this work by the National Science Foundation is gratefully acknowledged.

(2) G. S. Hartley, *Trans. Faraday Soc.*, **30**, 444 (1934).

(3) E. F. J. Duynstee and E. Grunwald, *J. Amer. Chem. Soc.*, **81**, 4540, 4542 (1959).

(4) M. T. A. Behme and E. H. Cordes, *ibid.*, **87**, 260 (1965); M. T. A. Behme, J. G. Fullington, R. Noel and E. H. Cordes, *ibid.*, **87**, 266 (1965).

(5) P. Mukerjee and K. Banerjee, *J. Phys. Chem.*, **68**, 3567 (1964).

(6) C. A. Bunton and L. Robinson, *ibid.*, **73**, 4237 (1969).

(7) C. A. Bunton, L. Robinson, and L. Sepulveda, *J. Amer. Chem. Soc.*, **91**, 4813 (1969), and references cited.

(8) M. A. Paul and F. A. Long, *Chem. Rev.*, **57**, 1 (1957).

(9) E. M. Arnett and G. W. Mach, *J. Amer. Chem. Soc.*, **88**, 1177 (1966).

(10) R. W. Taft, *ibid.*, **82**, 2965 (1960).

and therefore it seemed possible that there would be differences in the micellar effects upon ionization of primary, secondary and tertiary amines. In the present work we used N-methyl-*p*-nitroaniline, N,N-dimethyl-*p*-nitroaniline, and 1-N-methylamino-4-nitronaphthalene. The nitronephthylamine allowed us to examine the effect of bulk in the organic residue.

Added electrolytes have different effects upon the H_0' and H_R acidity scales, and the effects are caused at least in part by specific salt effects upon the relative free energies of the tri-*p*-anisyl carbonium ion and the *p*-nitroanilinium ion.¹¹ We have now examined the specific salt effects upon the H_0'' and H_0''' scales and have taken into account the effects caused by charges in the stabilities of the secondary and tertiary amines in salt solutions.

Experimental Section

Materials. The purification and preparation of solutions of the detergents and electrolytes has been described.^{6,11} N-Methyl-*p*-nitroaniline and N,N-dimethyl-*p*-nitroaniline were commercial samples (Chemical Procurement Co.) which were crystallized from aqueous methanol before use. They had mp 152° for N-methyl-*p*-nitroaniline (lit.¹² 152°) and 164° for N,N-dimethyl-*p*-nitroaniline (lit.¹³ 164°). 1-N-Methylamino-4-nitronaphthalene was prepared by methylation of the amine using dimethyl sulfate¹⁴ and was purified by chromatography over alumina. It had mp 184° (lit.¹⁴ 184–185°).

Measurements of pK_a . The pK_a of N,N-dimethyl-*p*-nitroaniline has been measured,⁹ but the pK_a values for the other indicators were measured spectrophotometrically,⁸ using a Gilford spectrophotometer and 1-cm cells for the aniline and a Cary 15 spectrophotometer and 10-cm cells for the naphthylamine. For N-methyl-*p*-nitroaniline $pK_a = 0.52$ and for 1-N-methylamino-4-nitronaphthalene $pK_a = -0.4$. The naphthylamine derivative is sparingly soluble in water, but with 10-cm cells the absorbances were in the range 0.2–0.8. The detergent solubilizes the amine so that acidity measurements with this amine in detergent solutions were not restricted by its low solubility.

These pK_a are in the ranges expected from the known values of 0.98–1.00 for *p*-nitroaniline,⁸ 0.66 for N,N-dimethyl-*p*-nitroaniline,⁹ and 0.36 for 1-amino-4-nitronaphthalene.⁶

Micellar and Electrolyte Effects on Protonation. The indicator ratios $I = C_B/C_{HB^+}$ were measured spectrophotometrically using a Gilford or Cary spectrophotometer as already described.⁶ The wavelengths were approximately 4080 Å for N-methyl-*p*-nitroaniline, 4230 Å for N,N-dimethyl-*p*-nitroaniline, and 4550 Å for 1-N-methylamino-4-nitronaphthalene. A range of wavelengths was used to allow for spectral shifts caused by the electrolyte or detergent. For any given acid concentration the absorbance was measured in the acid-

electrolyte or acid-detergent mixture and in the same solution but without the acid, and the difference gave the absorbance of the colored species. Because of the basicities of the indicators it was necessary to measure the I values for the nitroanilines in 0.1 *M* HCl in the absence of detergent, and the value of I for 0.01 *M* HCl was then calculated on the assumption that at these acid concentrations it is proportional to C_{H^+} . (This assumption was found to be valid for the primary amines.^{6,8}) For 1-N-methyl amino-4-nitronaphthalene we had to use 1 *M* HCl in the absence of detergent, and therefore the changes in I values and $\Delta H_0''$ for this indicator are less accurate than for the anilines.

Micellization increases the rate of the acid hydrolysis of long-chain alkyl sulfates,¹⁵ but the rate of hydrolysis of lauryl sulfate is very slow under our experimental conditions. However, to minimize any effect due to hydrolysis, freshly made solutions of acid and NaLS were used.

One major problem in the measurements of acidity functions in detergents is that it is virtually impossible to follow a greater than tenfold change in I , and this fact reduces the accuracy of the measurements at high detergent concentrations. To some extent we were able to minimize these problems by using different concentrations of (dilute) hydrochloric acid in the presence and absence of detergent, as was done in our previous work.⁶ The indicator concentrations were N-methyl-*p*-nitroaniline 3×10^{-5} *M*, N,N-dimethyl-*p*-nitroaniline 2×10^{-5} *M*, and 1-N-methylamino-4-nitronaphthalene 3×10^{-6} *M*, and were much lower than the detergent concentrations.

The values of the acidity functions are given by⁸

$$H_0 = pK_a - \log \left(\frac{C_{BH^+}}{C_B} \right) = - \log a_{H^+} \frac{f_B}{f_{HB^+}}$$

(B = ArNR₂)

but because we are concerned with changes in the acidity functions rather than their absolute values uncertainties in pK_a are not a problem, although knowledge of pK_a allows us to calculate the value of the acidity function in the detergent-acid solution.

Solubility Measurements. The solubilities of the nitroanilines were measured in various electrolyte solutions (0.5–2.0 *M*) by saturating the solutions with the amine by leaving the solutions for several days at 25° with occasional shaking. Portions of the solutions

(11) C. A. Bunton, J. H. Crabtree, and L. Robinson, *J. Amer. Chem. Soc.*, **90**, 1253 (1968).

(12) M. Frankel and S. Patai, "Tables for Identification of Organic Compounds," Chemical Rubber Publishing Co., Cleveland, Ohio, 1960, p 175.

(13) "Handbook of Physics and Chemistry," R. C. Weast, Ed., Chemical Rubber Publishing Co., Cleveland, Ohio, 1967, p C119.

(14) V. Vesely and A. Vojtech, *Coll. Czech. Chem. Comm.*, **1**, 104 (1929).

(15) J. L. Kurz, *J. Phys. Chem.*, **66**, 2239 (1962).

were filtered and were then diluted with water, and the absorbance was determined spectrophotometrically.^{8,16,17}

Results

Effects of Micelles. The values of $\Delta H_0''$ and $\Delta H_0'''$ are given in Figures 1 and 2. In most of the experiments the detergent concentrations were considerably larger than those of the indicators and were larger than the critical micelle concentrations, cmc, of the detergents. For NaLS in water¹⁸ cmc = $4 \times 10^{-3} M$, and it is $2.5 \times 10^{-3} M$ in 0.05 M NaOH.¹⁹ For CTABr the corresponding values are $7.8 \times 10^{-4} M$ ²⁰ and $3.2 \times 10^{-4} M$.¹⁹

Added electrolytes and organic solutes generally stabilize micelles and lower the cmc,²¹ and therefore in our systems the cmc should be lower than in water. The simplest theories assume that detergents will have little effect upon rates or equilibria at concentrations below the cmc, but in the present system, as in other cases,⁶ effects are observed below the cmc, either because added solutes promote micellization or because submicellar aggregates are formed.^{7,19,22-24} There is kinetic and structural evidence for these submicellar aggregates.

With increasing concentration of NaLS the values of $-\Delta H_0''$ or $-\Delta H_0'''$ increase to plateaux and in some cases then decrease. The plateaux should be reached when all the indicator is taken up into the micelles, and the fall off at higher concentrations could be caused by the addition of sodium counterions,²⁴ which should hinder incorporation of protons into the Stern layer around the anionic micelle, and by the fact that once sufficient micelles are present to take up all the indicator the addition of other micelles may merely trap protons and keep them away from the indicator.¹⁹ We observed such maxima in measurements of micellar effects upon H_0' ,⁶ and they are frequently observed in kinetic studies of the micellar catalysis of ion-molecule reactions.^{7,19,24,25}

For a given concentration of NaLS added salts decrease the acidity as measured by H_0'' or H_0''' using N-methyl- and N,N-dimethyl-*p*-nitroaniline (Table I).

Table I: Salt Effects upon H_0'' and H_0''' in the Presence of NaLS^a

Salt	$-\Delta H_0''$	$-\Delta H_0'''$
	0.78	0.64
LiCl	0.71	0.52
NaCl	0.69	0.51
(CH ₃) ₄ NCl	0.49	0.41
NaBr	0.70	0.52

^a With 0.01 M HCl and 0.03 M NaLS and 0.03 M salt at 25.0°. The values of $\Delta H_0''$ and $\Delta H_0'''$ are relative to the acidity functions in the absence of detergent.

Table II: Salt Effects upon H_0'' and H_0''' in the Absence of Detergent^a

Salt	C_{salt}	$-\Delta H_0''$	$-\Delta H_0'''$
LiCl	0.50	0.15	0.21
LiCl	1.00	0.33	0.43
NaCl	0.50	0.13	0.19
NaCl	1.00	0.27	0.35
KCl	0.50	0.11	0.17
KCl	1.00	0.22	0.29
(CH ₃) ₄ NCl	0.50	-0.05	0.01
(CH ₃) ₄ NCl	1.00	-0.12	0.00
LiClO ₄	0.50	0.23	0.30
LiClO ₄	1.00	0.40	0.54
NaClO ₄	0.50	0.17	0.27
NaClO ₄	1.00	0.33	0.48
NaBr	0.50	0.16	0.22
NaBr	1.00	0.31	0.40
NaNO ₃	0.50	0.13	0.17
NaNO ₃	1.00	0.26	0.29
NaOTOS	0.50	-0.04	-0.03
NaOTOS	1.00	-0.16	-0.08

^a At 25.0° in 0.1 M HCl, and relative to the values in the absence of added salt.

Table III: Salt Effects upon the Activity Coefficients of N-Methyl and N,N-Dimethyl-*p*-Nitroaniline^a

Salt	f_B''	f_B'''
LiCl	0.14	0.12
NaCl	0.13	0.11
KCl	0.09	0.08
(CH ₃) ₄ NCl	-0.15	-0.13
NaNO ₃	-0.01	-0.05
NaBr	0.06	0.02
LiClO ₄	-0.07	-0.15
NaClO ₄	-0.05	-0.13
NaOTOS	-0.60	-0.86

^a At 25.0° in 1 M salt in the absence of detergent.

Salts Effects on Acidity Functions. The effects of added salts upon H_0'' and H_0''' are shown in Table II. The salt order is very similar to that for H_0' .^{8,11}

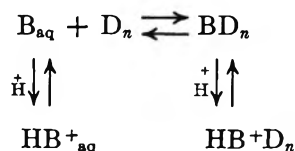
Salt Effects on Solubilities. The activity coefficients of N-methyl- and N,N-dimethyl-*p*-nitroaniline in 1 M

- (16) F. A. Long and W. F. McDevit, *Chem. Rev.*, **51**, 110 (1952).
 (17) M. A. Paul, *J. Amer. Chem. Soc.*, **76**, 3236 (1954).
 (18) M. L. Corwin and W. D. Harkins, *ibid.*, **69**, 679 (1947).
 (19) C. A. Bunton and L. Robinson, *ibid.*, **90**, 5972 (1968).
 (20) E. W. Anacker, R. M. Rush, and J. S. Johnson, *J. Phys. Chem.*, **68**, 81 (1964).
 (21) P. H. Elworthy, A. T. Florence and C. B. Macfarlane, "Solubilization by Surface-Active Agents," Chapman and Hall, London, 1968, Chapter I.
 (22) P. Mukerjee and K. J. Mysels, *J. Amer. Chem. Soc.*, **77**, 2937 (1955).
 (23) T. C. Bruice, J. Katzhendler, and L. R. Fedor, *ibid.*, **90**, 133 (1968).
 (24) R. B. Dunlap and E. H. Cordes, *ibid.*, **90**, 4395 (1968); L. R. Romsted and E. H. Cordes, *ibid.*, **90**, 4404 (1968).
 (25) F. M. Menger and C. E. Portnoy, *ibid.*, **89**, 4698 (1967).

aqueous salt solution determined by solubility measurements are given in Table III. The salt order is that generally found for the activity coefficients of amines and other polar organic solutes.^{11,16,17}

Discussion

Effects of Anionic Micelles. Making the simplest assumptions, the interactions between the micellized detergent D_n and the bases, B, and their conjugate acids can be written as⁶



For the anionic detergent, NaLS, the relation between the acidity functions and detergent concentration in the region in which the indicators and their conjugate acids are present in both the aqueous and micellar phases is complicated,⁶ and it is therefore simplest to consider the values of $-H_0''$ and $-H_0'''$ in the plateau region where B and HB^+ are wholly in the micellar phase.

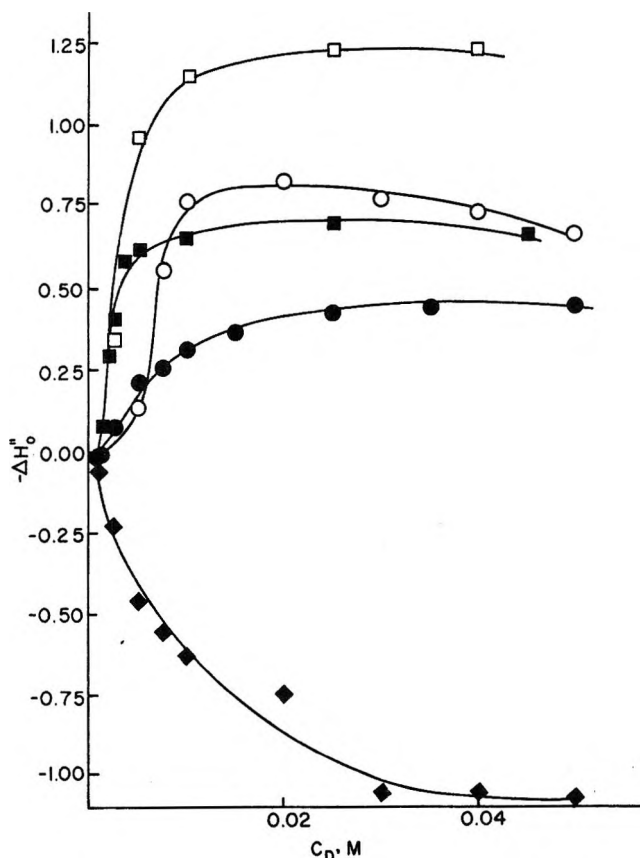


Figure 1. Variation of H_0'' with detergent at 25°. Solid points, 0.1 M HCl; open points, 0.01 M HCl: ● ○, protonation of N-methyl-*p*-nitroaniline in NaLS; ■ □, protonation of 1-N-methylamino-4-nitronaphthalene in NaLS; ◆, protonation of N-methyl-*p*-nitroaniline in CTAB.

In our earlier measurements on H_0' and H_R we found that relatively small amounts of NaLS, 0.005 M, increased $-H_R$ by 2.5 units,⁶ and because of the experimental difficulty in measuring such a large change of acidity with only one indicator this value may underestimate the increase of acidity. The increases in $-H_0'$ were much smaller, being ca. 0.7 unit with *p*-nitroaniline and ca. 1.2 units with 1-amino-4-nitronaphthalene, and these values were only reached with 0.01–0.02 M detergent.⁶

These differences were readily understandable in terms of the greater stability of the carbonium ion in the micellar as compared with the aqueous phase, relative to the behavior of the anilinium ions. The greater bulk of the naphthylamine, and therefore the better binding of it, and its conjugate acid, to the micelle, was responsible for the greater increase of $-H_0'$ using 1-amino-4-nitronaphthalene instead of *p*-nitroaniline.⁶ The present results fit very well into the earlier pattern, and protonation of the primary, secondary, and tertiary amines is less assisted by anionic micelles than is formation of a *p*-trianisyl carbonium ion.

With N-methyl and N,N-dimethyl-*p*-nitroaniline in 0.01 M hydrochloric acid, $-H_0''$ is increased by 0.75 unit at 0.02 M NaLS, and with 1-N-methylamino-4-nitronaphthalene the corresponding increase is 1.25 units (Figures 1 and 2). These increases in acidity function are almost identical with those observed using primary amines⁶ and suggest that the amines and the ammonium ions reside in the outer water rich area of the micelle, and that all the anilinium ions either lose little, or the same amount of, hydration energy in going from the aqueous to the micellar phase. These conclusions accord with nmr and other evidence that polar organic molecules are taken up into the water rich outer layer of ionic micelles and that their polar groups are oriented toward the water molecules which surround the micelles.²⁶ Therefore we ascribe the larger effects of anionic micelles upon H_R as compared with the H_0 acidity functions to the charge delocalization in the bulky carbonium ion which helps it to bind more strongly to the micelle.

In all our studies we find that the increase in acidity function brought about by an anionic micelle is less with 0.1 than with 0.01 M hydrochloric acid (Figures 1 and 2 and ref 6).

Several factors could cause this difference; once there are enough protons to occupy the Stern layer of the micelles addition of further protons will, by virtue of increasing the ionic strength, increase the aggregation number of the micelles and therefore decrease the number of micelles in solution. In addition, acids acting as electrolytes will inhibit incorporation of the

(26) J. C. Eriksson and G. Gilberg, *Acta Chem. Scand.*, 20, 2019 (1966); R. M. Muller and R. H. Birkhahn, *J. Chem. Phys.*, 71, 957 (1967).

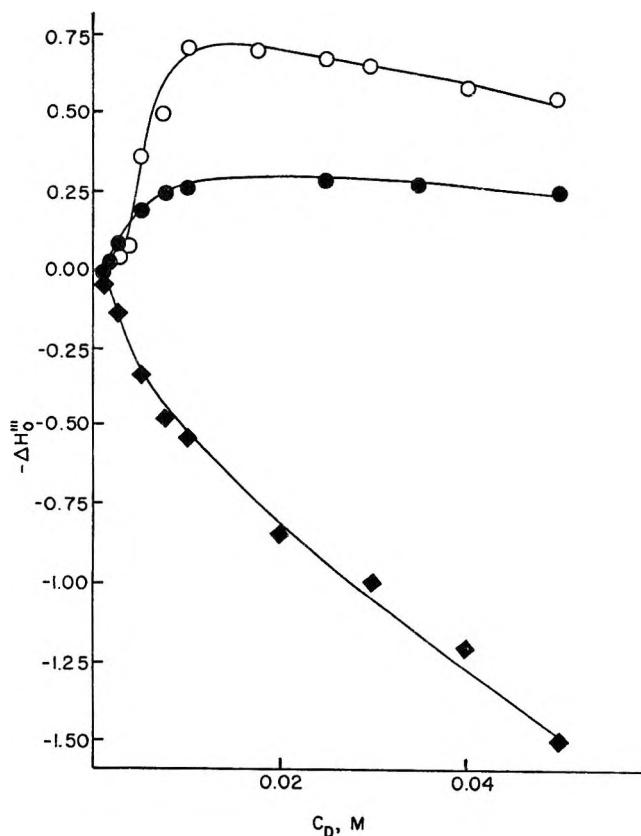


Figure 2. Variation of H_0'' with detergent. Solid points, 0.1 M HCl; open points, 0.01 M HCl; determined using N,N-dimethyl- p -nitroaniline; \bullet , \circ , in NaLS; \blacklozenge , in CTABr.

conjugate acids in the micellar phase. Similar saturation effects have been observed in kinetic systems.¹⁹

Effects of Cationic Micelles. The results are very simple (Figures 1 and 2 and ref 6). The indicators are incorporated into the cationic micelle where they are protected from protonation. (Alternatively, we could say that whereas anionic micelles stabilize the conjugate acids relative to the indicator bases, cationic micelles have the opposite effect.)

In our earlier work we noted that cationic micelles of CTABr were very effective at inhibiting ionization of p -trianisyl carbinol (H_R scale) as compared with protonation of p -nitroaniline (H_0'' scale).⁶ Anionic micelles of NaLS have very similar effects upon H_0' , H_0'' , and H_0''' (Figures 1 and 2 and ref 6), and much larger effects upon H_R . However, cationic micelles of CTABr have different effects on H_0' , H_0'' , and H_0''' ; for example, 0.02 M CTABr decreases $-H_0'$ by 0.6 unit, and $-H_0''$ and $-H_0'''$ by 0.9 unit, suggesting that the cationic micelles stabilize N-methyl and N,N-methyl- p -nitroaniline more than they stabilize p -nitroaniline, and these differences are understandable in terms of the greater detergent solubilization of compounds which contain bulky alkyl groups.

Salt Inhibition of the Detergent Effects. The results in Table I agree with earlier results which showed that

added salts reduced the enhancement of $-H_0'$ or $-H_R$ by anionic micelles of NaLS.⁶ There are many examples of inhibition of micellar catalysis by counterions,^{7,19,24,27} and the ability of a counterion to inhibit micellar catalysis increases with decreasing charge density of the ion. A similar pattern is shown by the present results, and tetramethylammonium ions are much more effective than alkali metal ions. (The low solubility of potassium lauryl sulfate prevented our examining potassium salts.) Added anions appear to have little effect, as shown by the similarity of bromide and chloride ions (Table I).

Salt Effects upon H_0'' and H_0''' . Added salts affect acidity functions by changing the hydrogen ion activity and the activity coefficients of the indicator base and its conjugate acid.^{8,11,17} We can measure the activity coefficients of the indicators in salt solution and can therefore calculate the relative activity coefficients of the proton and the conjugate acid, f_{H^+}/f_{HB^+} , and we can also calculate the activity coefficient of one conjugate acid relative to another. When this treatment was applied to salt effects upon the H_0' and H_R acidity functions it was found that chlorides and nitrates had similar effects upon f_{HB^+}/f_{R^+} but that perchlorates markedly stabilized the tri- p -anisyl carbonium ion (R^+), relative to the p -nitroanilinium ion (HB^+).¹¹

The salt effects upon different acidity scales, e.g., H_0' and H_0'' allow us to relate the activity coefficients, f'_{HB^+} and f''_{HB^+} using eq 1.

$$\Delta \log \left(\frac{f'_{HB^+}}{f''_{HB^+}} \right) = \Delta H_0' - \Delta H_0'' + \Delta \log \left(\frac{f'_B}{f''_B} \right) \quad (1)$$

where Δ indicates the change in the property brought about by the electrolyte in the presence of a low constant acid concentration. A similar equation can be written using the H_0' and H_0''' acidity scales and the activity coefficient ratio, f'_{HB^+}/f''_{HB^+} . Table IV gives the values of the activity coefficients of the tri- p -anisyl carbonium ion and the N,N-dimethyl- and N-methyl- p -nitroanilinium ions, relative to the p -nitroanilinium ion in 1 M salt solutions. These values are calculated using the data given in Tables II and III and ref 8, 11, and 17.

The results in Table IV show that added salts have very similar effects upon the relative stabilities of the p -nitroanilinium and the N-methyl- p -nitroanilinium ions, particularly in view of the uncertainties in the determination of acidity functions.⁸ However, most salts stabilize the N,N-dimethyl- p -nitroanilinium ion relative to the p -nitroanilinium ion, and the effects are largest for those salts which have large, low charge density, anions. To this extent the N,N-dimethyl- p -nitroanilinium ion behaves similarly to the tri- p -anisyl

(27) C. A. Bunton, E. J. Fendler, L. Sepulveda, and K-U. Yang, *J. Amer. Chem. Soc.*, **90**, 5512 (1968).

Table IV: Salt Effects upon Relative Activity Coefficients of the Conjugate Acids^a

Salt	$\Delta \log (f'_{\text{HB}^+}/f''_{\text{HB}^+})$	$\Delta \log (f'_{\text{HB}^+}/f''_{\text{HB}^+})$	$\Delta \log (f'_{\text{HB}^+}/f_{\text{R}^+})^b$
LiCl	0.04	0.16	-0.09
NaCl	0.01	0.11	0.00
KCl	0.01	0.10	
(CH ₃) ₄ NCl	-0.13	-0.03	
NaNO ₃	0.04	0.11	0.04
NaBr	0.09	0.22	0.28
NaCH ₃ SO ₃			0.40
LiClO ₄	0.10	0.32	0.58
NaClO ₄	0.05	0.28	0.59
NaOTOS	-0.03	0.33	

^a For 1 M salt at 25.0°. ^b Reference 11.

carbonium ion with respect to added salts, although the effects of the larger anions, *e.g.*, perchlorate and tosylate are smaller.

These results complement the observations of Arnett and Mach on the specific effects of acids on the H_0' , H_0'' , and H_{R} acidity functions.⁹ Insofar as a primary

anilinium ion should derive more stability from hydrogen bonding than would a corresponding tertiary anilinium ion we would expect all salts to stabilize the tertiary relative to the primary ion, simply because of their lowering of water activity.^{9,10,28} The specific stabilization of a carbonium relative to a primary anilinium ion,¹¹ is evident in this system, but to a lesser extent, and suggests that there are interactions, either direct, or *via* changes in the water structure,²⁹ between the salt anion and the cation of the indicator. We note also the similarities between the interactions between ions of various charge densities and counterions and the interactions between ions and counter ionic micelles. Although the micellar effects are much larger than those of simple electrolytes, they are in the same direction, and examples of this behavior have been provided from studies of both kinetics and equilibria.^{19,30}

(28) R. A. Robinson and R. H. Stokes, "Electrolyte Solutions," Butterworth and Co. Ltd., London, 1965, Appendix 8.

(29) H. S. Frank and M. G. Evans, *J. Chem. Phys.*, **13**, 507 (1945); G. R. Choppin and K. Buijs, *ibid.*, **39**, 2042 (1963).

(30) C. A. Bunton and L. Robinson, *J. Amer. Chem. Soc.*, **90**, 5965 (1968); **91**, 6072 (1969).

The Surface Tension of Polyatomic Liquids and the Principle of Corresponding States

by D. Patterson and A. K. Rastogi

Chemistry Department, McGill University, Montreal, Canada (Received August 12, 1969)

The Prigogine corresponding-states principle for the bulk properties of liquids is extended to their surface tension. Two distinct empirical curves of reduced surface tension against reduced temperature of αT are found, one containing data for simple liquids and the other data for polymers and polyatomic liquids. The Prigogine-Saraga cell model theory of surface tension is then used together with several models of the liquid state, including the recent Flory theory which gives the best results. Good predictions of the empirical curves are found, and the Macleod-Sugden parachor correlation is predicted.

Introduction

Following dimensional considerations of van der Waals, the critical constants have been used to give a principle of corresponding states for the surface tension γ of simple liquids,¹ yielding a common curve of a reduced surface tension

$$\bar{\gamma} = \gamma/k^{1/3}P_c^{2/3}T_c^{1/3} \quad (1)$$

against a reduced temperature, $\bar{T} = T/T_c$. Here k is the Boltzmann constant. This treatment can be

extended to polyatomic molecules by introducing a third characteristic quantity, the acentric factor,² but the reduction procedure must break down for high polymers. Prigogine and collaborators,³ however, have

(1) F. P. Buff and R. A. Lovett in "Simple Dense Liquids," H. L. Frisch and Z. W. Salsburg, Ed., Academic Press, New York, N. Y., 1968, p 17.

(2) J. R. Brock and R. B. Bird, *A.I.Ch.E. J.*, **1**, 174 (1955).

(3) I. Prigogine (with A. Bellemand and V. Mathot), "The Molecular Theory of Solutions," North-Holland Publishing Co., Amsterdam, and Interscience Publishers, Inc., New York, N. Y., 1957, Chapter 17.

proposed a single corresponding-states principle valid for the bulk thermodynamic properties of both simple and polymeric liquids. Roe⁴ has extended it to surface tensions and found two different reduced surface tension curves, $\bar{\gamma}(\bar{T})$, for three high polymers on the one hand and for argon and methane on the other. (The reduced temperature, \bar{T} , is not the ratio T/T_c used by van der Waals and is explained below.) We believe there is an error in Roe's application of the corresponding-states principle to the surface tensions of argon and methane. In this article, we extend the corresponding-states principle for bulk properties to the surface tension in a simpler form than used by Roe. A single $\bar{\gamma}(\bar{T})$ curve is found for some 40 common polyatomic liquids and five high polymers. Liquids such as argon, methane, and nitrogen still give a slightly different curve, however. Cell models of the liquid state give good predictions of the Macleod-Sugden parachor correlation and of the Eötvös constant. The models may be used for the prediction of the surface tension from bulk thermodynamic properties and could be particularly useful in the case of polymeric liquids.

Bulk Reduction Parameters

According to the Prigogine corresponding-states theory,^{3,5} the bulk molar configurational quantities (apart from the combinatorial entropy) of different chain-molecule or spherical-molecule liquids are related to universal dimensionless reduced quantities (with tilde) through reduction parameters (with asterisk)

$$\begin{aligned} V(T,n) &= V^*(n)\bar{V}(\bar{T}); & V^*(n) &= N_0 r(n)(R^*)^3 \\ U(T,n) &= U^*(n)\bar{U}(\bar{T}); & U^*(n) &= N_0 q(n)\epsilon^* \\ S(T,n) &= S^*(n)\bar{S}(\bar{T}); & S^*(n) &= N_0 c(n)k \end{aligned} \quad (2)$$

and

$$\bar{T} = T/T^*; \quad T^* = U^*/S^*; \quad p^* = U^*/V^* \quad (3)$$

Here N_0 is Avogadro's number and n is the number of atoms in the principal chain; ϵ^* and R^* are characteristic depth and distance parameters of the interaction potential between the chain molecules or spherical molecules. The parameters r , q , and c can be considered as numbers of "segments" per chain molecule, but only the value of c can be ascribed an absolute significance. In the theory $3c$ is the number of external (volume-dependent) degrees of freedom of the molecule.

Various models have been used to predict the reduced quantities and obtain the reduction parameters. The original Prigogine cell model for chain-molecule liquids uses a dependence of the configurational energy on volume equivalent to the Lennard-Jones (6,12) energy-distance relation, *i.e.*⁵

$$\bar{U}(\bar{V}) = -2\bar{V}^{-2} + \bar{V}^{-4} \quad (4)$$

More generally for an (m,n) potential

$$\bar{U}(\bar{V}) = \frac{1}{n-m} \left[-n\bar{V}^{-m/3} + m\bar{V}^{-n/3} \right] \quad (5)$$

Flory⁶ and collaborators used the cell partition function and a simple van der Waals energy-volume relation, $\bar{U} = -\bar{V}^{-1}$, equivalent⁵ to putting $m = 3$ and $n \rightarrow \infty$ in eq 5. The reduction parameters for the temperature, T^* , and the pressure, P^* , may be more easily determined than those for the extensive quantities in eq 2. They are related to the isobaric thermal expansion coefficient (α) and the isothermal compressibility (β) through

$$\begin{aligned} T^* &= \bar{\alpha}(\bar{T})/\alpha(n,T) \\ P^* &= \bar{\beta}(\bar{T})/\beta(n,T) \end{aligned} \quad (6)$$

Equations 3 and 6 show that the dimensionless quantity αT is already in reduced form equal to $\bar{\alpha}(\bar{T})\bar{T}$. Using any model, experimental values of αT yield values of \bar{T} and hence T^* . Values of the P^* parameter may be found in turn from experimental values of β through eq 6. In the Flory model, for instance

$$\alpha T = (1 - \bar{V}^{-1/3})/(4/3 \bar{V}^{-1/3} - 1) \quad (7)$$

from which \bar{V} is obtained to give \bar{T} from

$$\bar{T} = \bar{V}^{-1}(1 - \bar{V}^{-1/3}) \quad (8)$$

and P^* is found from eq 6 and

$$\bar{\beta} = \bar{\alpha}\bar{T}\bar{V}^2 \quad (9)$$

The Reduced Surface Tension

The use of bulk properties to reduce the surface tension involves an assumption about the thickness of the surface layer. This was taken by Roe to correspond to the dimension of the chain segment, defined by c ; *i.e.*, it is a sufficient section of the chain to have three external degrees of freedom. Its characteristic intermolecular energy is U^*/N_0c , and the area taken up at the surface is $(V^*/N_0c)^{2/3}$. These two quantities define a reduction parameter for the surface tension

$$\bar{\gamma}(\bar{T}) = \gamma(n,T)/\gamma^*(n) = \gamma(n,T) \left/ \left(\frac{U^*}{N_0c} \right) \left(\frac{V^*}{N_0c} \right)^{-2/3} \right. \quad (10)$$

Apart from a difference of nomenclature, this is the reduced surface tension expression used by Roe.⁴ However, the definitions of the reduction parameters allow the equation to be put in the following form analogous to that used by van der Waals (*i.e.*, eq 1)

$$\bar{\gamma}(\bar{T}) = \gamma(n,T)/\gamma^*(n) = \gamma(n,T)/k^{1/3}P^{*1/3}T^{*1/3} \quad (11)$$

(4) R. J. Roe, *Proc. Nat. Acad. Sci. U. S.*, **56**, 819 (1966).

(5) D. Patterson, S. N. Bhattacharyya, and P. Picker, *Trans. Faraday Soc.*, **64**, 648 (1968).

(6) (a) P. J. Flory, R. A. Orwoll, and A. Vrij, *J. Amer. Chem. Soc.*, **86**, 3507 (1964); (b) A. Abe and P. J. Flory, *ibid.*, **87**, 1838 (1965).

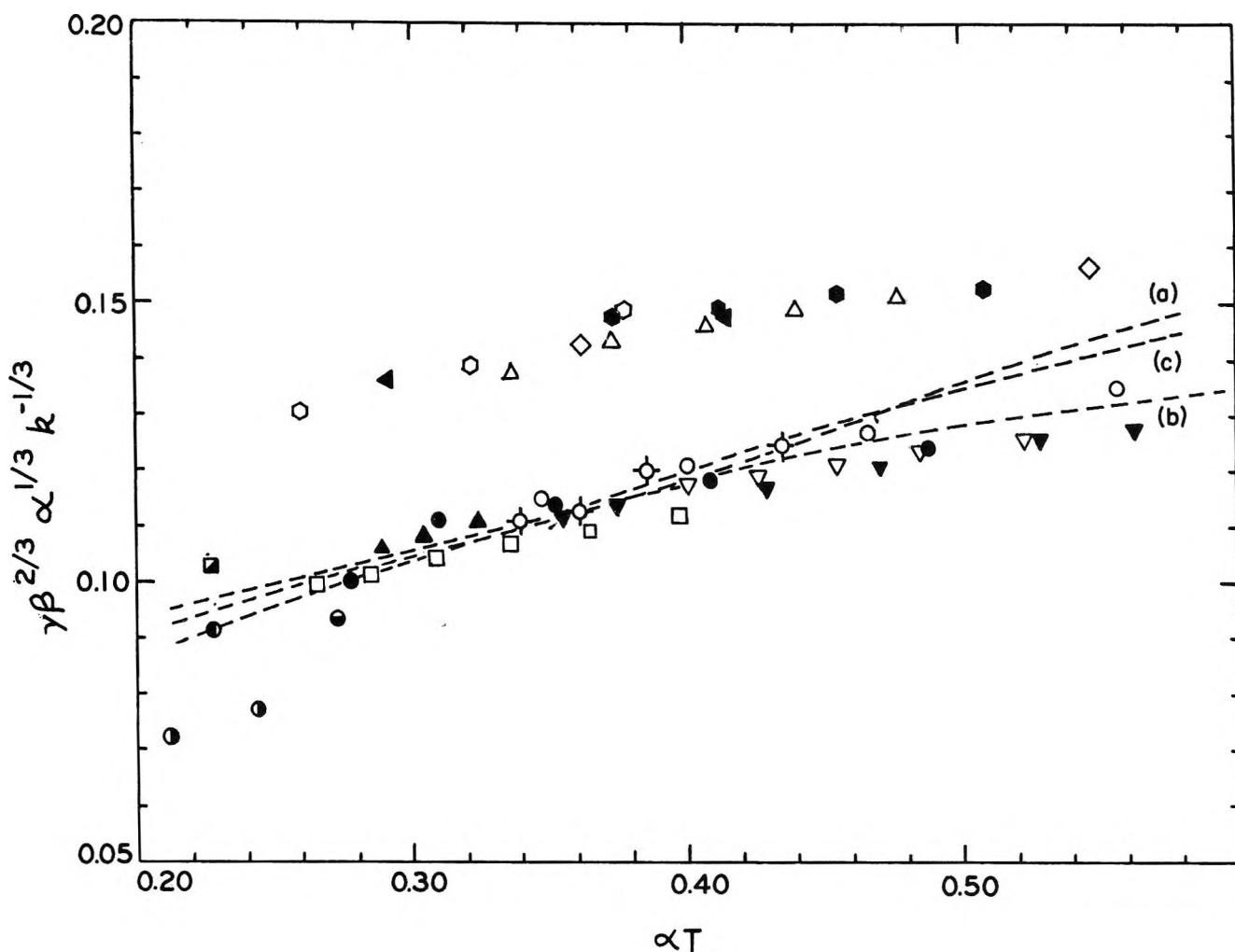


Figure 1. The quantity $\gamma\beta^{2/3}\alpha^{1/3}/k^{-1/3}$ against αT : \bullet , Ar;^{1,7} ∇ , O₂;^{1,7} \diamond , N₂;^{1,7} \circ , C₁;¹ Δ , C₃;⁸ \bullet , C₄;⁸ \circ , C₅;⁸ ∇ , C₆;⁸ ∇ , C₈;⁸ \square , C₁₆;⁸ \blacktriangle , polymethylene;⁹ \odot , polyisobutylene;^{9,10} \ominus , polydimethylsiloxane;⁹ \circ , dimer, trimer, tetramer, and pentamer of dimethylsiloxane;¹¹ \bullet , polyoxypropylene glycol;^{12,13} \blacksquare , polyoxyethylene glycol.^{9,13} For each liquid the first and second references are to the sources of surface tension and equation of state data, respectively. Sources of the equation of state data for the alkanes and dimethylsiloxane oligomers are given in ref 14 and 5, respectively. Dotted lines are theoretical curves using cell model theories with the following (m,n) choices: (a) (6,12); (b) (3, ∞) or Flory model; (c) (6, ∞).

The P^* and T^* parameters are more accessible than those in eq 10. Each of the models used to obtain them is consistent with the Prigogine corresponding-states principle for the bulk properties and hence each gives α and β as functions of values of T obtained from experimental αT . The discovery of a universal $\tilde{\gamma}(\tilde{T})$ function would show that the corresponding-states principle is valid for the surface tension and for bulk properties without, however, implying that the particular model of the liquid is correct.

The bulk properties may be used directly to yield a corresponding-states plot. Equation 6 allows T^* and P^* to be eliminated from eq 11 which then shows that the dimensionless quantity

$$\gamma\beta^{2/3}\alpha^{1/3}/k^{1/3} = \tilde{\gamma}\tilde{\beta}^{2/3}\tilde{\alpha}^{1/3} \quad (12)$$

is a universal function of \tilde{T} or αT for all liquids. We believe this to constitute the most direct test of the corresponding-states principle for surface tension.

The same plot of $\gamma\beta^{2/3}\alpha^{1/3}/k^{1/3}$ against αT is suggested by dimensional considerations and also by eq 1. Using the van der Waals equation of state in reduced form, reduced quantities α and β may be defined by

$$\tilde{\alpha} = T_c\alpha(T,n); \quad \tilde{\beta} = P_c\beta(T,n) \quad (13)$$

Elimination of T_c and P_c from eq 1 then leads to eq 12. However, the corresponding-states principle for bulk properties given by eq 13 is itself unsuccessful when applied to α and β of more complex molecules and requires the introduction of the acentric factor. It therefore seems preferable to regard eq 12 as an extension of the Prigogine corresponding-states principle for bulk properties. Finally, quantities other than α and β , but of dimensions of temperature and pressure, may be used to determine T^* and P^* . In particular, the internal pressure and the cohesive energy might be convenient.

Comparison with Experiment

Figure 1⁷⁻¹⁴ shows $\gamma\beta^{2/3}\alpha^{1/2}/k^{1/3}$ as a function of αT for the normal alkanes from methane to polymethylene over a 100° temperature range, for polyisobutylene over 100°, for four dimethylsiloxane oligomers and the high polymer at 30°, for polyethylene and polypropylene glycol at 20°, and for argon, nitrogen, and oxygen over some 25°. The data separate into two distinct curves. The lower holds for the alkanes from butane to polymethylene and for the other chain-molecule liquids to within $\pm 5\%$ of the mean. Furthermore, the ratio was obtained at 20° for surface tension,¹⁵ and equation of state data¹³ of some 25 other liquids were divided among branched alkanes, esters, ethers, alcohols, and other common solvents. The accuracy of the values of the ratio should be $\sim \pm 3\%$ and they usually fell on the lower curve of Figure 1 to within this value. Benzene and cyclohexane, however, fell 7% higher. The largest deviation was found with 2-propanol, 12% lower than the curve, although methanol, ethanol, 2-butanol, and propanol gave good results. In general it seems that the same corresponding-states principle is obeyed by polyatomic liquids and by chain-molecule liquids from high polymers down to very short chains. The corresponding-states plot for the polyatomic liquids thus permits the surface tension to be calculated from the thermal expansion coefficient and the compressibility. The surface tension data for propane and methane, argon, nitrogen, and oxygen all fall on a single curve some 30% higher. We can offer no explanation for this. It seems surprising that data for butane and higher alkanes lie on the lower curve while propane data are on the upper.

Roe⁴ also found a single $\bar{\gamma}(\bar{T})$ curve using eq 10 for three high polymers, but argon and methane data fell on a curve 50% lower. There was a much greater separation between polymer and simple liquid data than in the present case and the relative position of the curves is opposite. The bulk reduction parameters tabulated by Roe for the simple liquids are clearly in error when compared with those of the polymers which were obtained¹⁶ using the Prigogine model. This is probably due to the assumption that a simple molecule must constitute a segment with three external degrees of freedom, making $c = 1$ in eq 10. This assumption is reasonable but the model gives different results¹⁷ for argon and methane, $c \neq 1$.

We have also obtained (but do not show) experimental curves of $\bar{\gamma}$ against \bar{T} using the $\gamma(T)$ data and the different theoretical models to obtain γ^* and T^* from the α and β data at the appropriate temperatures; *i.e.*, we have used eq 11. This type of plot is another representation or mapping of $\gamma\beta^{2/3}\alpha^{1/2}/k^{1/3}$ against αT . As expected, with each model, a universal curve is found for the polyatomic and chain-molecule liquids which corresponds to the curve in Figure 1.

Cell Model Calculations of the Surface Tension

Prigogine and Saraga¹⁸ have given a simple cell model theory of the surface tension of spherical molecule liquids based on a (6,12) choice of (m,n) in the potential, eq 5. In the following extension to the chain-molecule case, a segment, in moving from the bulk to the surface, experiences an increase of the configurational energy equal to $-M\bar{U}(\bar{V})$ due to the loss of a fraction, M , of its nearest neighbors at the surface. The cell partition function ψ of a segment at the surface is increased due to the loss of constraining nearest neighbors in one direction so that

$$\psi_{\text{surface}}/\psi_{\text{bulk}} = (\bar{V}^{1/3} - 0.5b)/(\bar{V}^{1/3} - b) \quad (14)$$

Here b is a packing factor given by⁵

$$b = \left(\frac{m}{n}\right)^{1/(n-m)}$$

and tends to unity when $n \rightarrow \infty$. The factor $1/2$ introduced in the Prigogine-Saraga theory could presumably be adjusted to another value. The reduced surface tension is then, following eq 3.13 of ref 18

$$\bar{\gamma}\bar{V}^{2/3} = -M\bar{U}(\bar{V}) - \bar{T} \ln \frac{\bar{V}^{1/3} - 0.5b}{\bar{V}^{1/3} - b} \quad (15)$$

with the actual surface tension found through multiplication by γ^* according to eq 11.

The surface energy and entropy are given by

$$\bar{\gamma}_U = -M\bar{U}(\bar{V}); \quad \bar{\gamma}_S = \ln \frac{\bar{V}^{1/3} - 0.5b}{\bar{V}^{1/3} - b} \quad (16)$$

The quantities, \bar{T} , $\bar{\alpha}$, and $\bar{\beta}$ are given as functions of \bar{V} in eq 16-19 of ref 5 for the different models. For example, with the $(3, \infty)$ choice of (m,n) or the Flory model, eq 15 becomes

$$\bar{\gamma}\bar{V}^{2/3} = M - (1 - V^{-1/3}) \ln \frac{\bar{V}^{1/3} - 0.5}{\bar{V}^{1/3} - 1} \quad (17)$$

(7) J. S. Rowlinson, "Liquid and Liquid Mixtures," Butterworth and Co. Ltd., London, 1959, Chapter I.

(8) F. D. Rossini, *et al.*, "Selected Values of Physical and Thermodynamic Properties of Hydrocarbons and Related Compounds," API Research Project 44, Carnegie Press, Pittsburgh, Pa., 1953.

(9) R. J. Roe, *J. Phys. Chem.*, **72**, 2013 (1968).

(10) B. E. Eichinger and P. J. Flory, *Macromolecules*, **1**, 285 (1968).

(11) Dow Corning Technical Bulletin 05-145, Dow Corning Co., Midland, Mich., 1966.

(12) A. K. Rastogi and L. E. St. Pierre, *J. Colloid Interfac. Sci.*, in press.

(13) G. Allen, G. Gee, and G. Wilson, *Polymer*, **1**, 456 (1960); G. Allen, G. Gee, D. Mangaraj, D. Sims, and G. J. Wilson, *ibid.*, **1**, 467 (1960).

(14) D. Patterson and J. M. Bardin, *Trans. Faraday Soc.*, in press.

(15) J. Timmermanns, "Physico-Chemical Constants of Pure Organic Compounds," Elsevier Publishing Co., Inc., New York, N. Y., 1950.

(16) V. S. Nanda and R. Simha, *J. Phys. Chem.*, **68**, 3158 (1964).

(17) T. Someynsky and R. Simha, *Macromolecules*, in press.

(18) I. Prigogine and L. Saraga, *J. Chim. Phys.*, **49**, 399 (1952).

Using the expressions for $\bar{\alpha}$ and $\bar{\beta}$, the quantity $\gamma\beta^{2/3}$. $\alpha^{1/3}/k^{1/3} = \bar{\gamma}\bar{\beta}^{2/3}\bar{\alpha}^{1/3}$ may be calculated as a function of αT . In Figure 1, curves are drawn using three choices of (m,n) : (6,12); (3, ∞) or the Flory theory; and (6, ∞), the original choice of Prigogine and Saraga. The following values of M were found to give the best fit: (6,12), 0.35; (3, ∞), 0.29; (6, ∞), 0.53. Reasonable agreement is found with all of the models. However, the value of M found with the (3, ∞) or Flory theory is the most realistic. On the basis of a close-packed lattice, $M = 0.25$, and if there were any effect of the next-nearest neighbors, the value could be increased somewhat. Values of M with the other models, particularly the (6, ∞), seem too high. We have calculated the surface energy and entropy using the Flory model and eq 16. As in the Prigogine-Saraga work, there is a tendency of the theory to obtain the correct surface tension while giving too low values of the surface energy and entropy.

The Parachor

The Macleod-Sugden correlation states that

$$\gamma = \left(\frac{[P]}{V}\right)^4 = \left(\frac{[P]}{V^* \bar{V}}\right)^4 \quad (18)$$

where $[P]$ is the molar parachor and V the molar volume. For polymers, $[P]$ is expressed per mole of repeat units. In the relation to reduced volume, the reduction parameter V^* is expressed per mole or per mole of polymer repeat units. A least-squares analysis shows that $\bar{\gamma}$ from eq 17 with $M = 0.29$ may be replaced over the temperature range of data by

$$\bar{\gamma} = 0.238/\bar{V}^{3.86} \quad (19)$$

making an error of less than 0.3%. With the exponent changed to 4, the best fit is

$$\bar{\gamma} = 0.247/\bar{V}^4 \quad (20)$$

and a maximum error of 0.9% is made.

A similar treatment was possible with the (6, ∞) model but here the exponent of \bar{V} was 5.6. In the case of the (6,12) model $\bar{\gamma}$ was only imperfectly proportional to \bar{V}^{-n} throughout the whole range of αT , but adequately so in the range of $\alpha T < 0.4$ where the exponent of \bar{V} was found to be 3.3. All of the models therefore are consistent with the parachor correlation. In the case of the (3, ∞) or Flory model, the agreement is remarkably good and the model may be used to predict values of the parachor using bulk thermodynamic properties. Identifying eq 18 and 20, we have

$$[P] = [0.247k^{1/3}P^{*2/3}T^{*1/3}]^{1/4}V^* \quad (21)$$

Values of the parachor calculated from reduction

parameters for the bulk properties agree with those calculated from parachor group contributions to within a few per cent in most cases. Where a greater difference was found, the present values agree better with experiment than those calculated from group contributions.

As an example, Flory, *et al.*,^{6b} listed $P^* = 101$ cal/cm³, $T^* = 4447^\circ\text{K}$, and $V^* = 99.64$ cm³/mol for *n*-hexane obtained from experimental values of β , α , and V at 20° using the Flory model and the procedure outlined above. Equation 21 gives $[P] = 271$ erg^{0.25} cm^{2.5} mol⁻¹, whereas the method of group contributions¹⁹ gives 273, and the value from experimental values of γ is 270 erg^{0.25} cm^{2.5} mol⁻¹. For polydimethylsiloxane, the reduction parameters⁵ are $P^* = 81.5$ cal/cm³, $T^* = 55.3^\circ\text{K}$, and $V^* = 61.76$ cm³/repeat unit of SiO(CH₃)₂. Equation 21 gives $[P] = 165$ erg^{0.25} cm^{2.5} (mol of repeat unit)⁻¹. The corresponding value from group contributions is 154 and from the experimental value of γ , it is 162 in the same units as above. For polyisobutylene, the reduction parameters²⁰ are $P^* = 107$ cal/cm³, $T^* = 7577^\circ\text{K}$, and $V^* = 53.14$ cm³/repeat unit of CH₂(CH₃)₂. Equation 21 gives $[P] = 153$ erg^{0.25} cm^{2.5} (mol of repeat unit)⁻¹. The corresponding value from group contributions is also 153 and from the experimental value of γ , $[P] = 147$ in the appropriate units.

The Eötvös Constant

The polymer analog of the Eötvös constant k_E is

$$k_E = -d(\gamma v^{2/3})/dT \quad (22)$$

where v is the volume per mole of segments of polymer rather than the molar volume as for quasispherical molecules. According to eq 2 and 3, $v = \bar{V}kT^*/P^*$ and the Eötvös constant is $k_E = kd(\bar{\gamma}\bar{V}^{2/3})/dT$, hence a function of \bar{V} . Using the Flory model and eq 17 and performing the differentiation, we have to a good approximation

$$k_E \simeq kN_c^{2/3} \ln \frac{\bar{V}^{1/3} - 0.5}{\bar{V}^{1/3} - 1} \quad (23)$$

This relation shows that k_E increases as the temperature is lowered or as the chain length is increased, as often found experimentally.²¹ For $\alpha T = 0.5$, $k_E = 1.7$ and $\alpha T = 0.25$, $k_E = 2.1$.

Acknowledgment. We gratefully acknowledge the support of the National Research Council of Canada.

(19) O. R. Quayle, *Chem. Rev.* **53**, 439 (1953).

(20) B. E. Eichinger and P. J. Flory, *Macromolecules*, **1**, 285 (1968).

(21) J. R. Partington, "An Advanced Treatise on Physical Chemistry," Vol. 2, Longmans, Green and Co., London, 1951, p 159.

Electrical Conductivity of Suspensions of Conducting Colloidal Particles

by Henry C. Thomas

Department of Chemistry, University of North Carolina, Chapel Hill, North Carolina 27514

and Adrien Cremers

*Institut Wetenschappen v.d. Aardbodem, Catholic University of Louvain, Louvain, Belgium
(Received August 11, 1969)*

The Fricke equation for conductance is applied to suspensions of sodium montmorillonite in sodium chloride solutions. It is shown to be possible to deduce values of micelle concentration, a measure of micelle shape, and a micelle internal conductance which reproduce the data over wide ranges of salt concentration up to about 4 wt % in clay, and at different temperatures. The activation energy for the internal conductance is 4.2 kcal/mol as compared to 3.64 kcal/mol for the limiting aqueous conductance of sodium chloride. It is suggested that this difference may be due to an enhanced water viscosity near the clay surface.

In 1924, Hugo Fricke¹ produced the generalization to ellipsoids of revolution of Maxwell's formula for the overall conductivity of suspensions in conducting media of spheres with an internal conductivity. Although Fricke himself as well as others applied the resulting equation to cases in which the internal conductivity of the particles was either assumed or known to be zero, it has apparently never been adequately tested in cases where a definite internal conductivity must exist. In connection with our work on self-diffusion through colloidal suspensions² we have had occasion to extend earlier work on the conductivity of highly purified clays³ into the region of very dilute solutions and low clay content, where the Fricke equation might be expected to be applicable. It is the purpose of this paper to show that the equation can be quite successful in such cases.

The necessary limitations of the Fricke equation due to the assumptions made in its derivation should first be pointed out. The suspended material is supposed to consist of ellipsoids of revolution in arbitrary orientation with respect to the direction of the applied field. It is further implicitly supposed that the suspended material is isotropic insofar as its conducting properties are concerned. In addition, it is assumed that the suspended particles themselves carry no current because of their own motion in the applied field. Finally, and perhaps of greatest importance, the result is necessarily limited to the case of dilute suspensions. This results from the fact that the electric field in the suspension is considered to be made up of additive contributions from the applied field and from the suspended particles (or micelles), interactions between the latter not being taken into account. Strictly, the result is a typical limiting law and only experiment can decide how far into the region of finite suspension concentrations it can usefully be extended.

Fricke's result can be put into the form

$$k_s - k_g = \frac{(k_s - k_i)\rho R}{1 + \rho R} \quad (1)$$

with

$$\rho = \frac{1}{3} \frac{\rho'}{1 - \rho'} \quad (2)$$

where ρ' is the volume fraction of the suspended micelles and

$$R = \frac{2}{1 + \left(\frac{k_i}{k_s} - 1\right) \frac{M}{2}} + \frac{1}{1 + \left(\frac{k_i}{k_s} - 1\right) (1 - M)} \quad (3)$$

In these expressions k_s is the conductance of suspending solution, k_g is the conductance of the suspension, and k_i is the internal conductance of the colloidal micelles. The quantity M depends only on the average shape of the micelles. It is connected with the axial ratio, a/b , of the corresponding ellipsoid through two expressions, one for oblate spheroids ($a < b$, plates to spheres) and another for prolate spheroids ($a > b$, spheres to needles)

$$M(a < b) = \frac{\phi - \sin \phi \cos \phi}{\sin^3 \phi} \cos \phi \quad (\text{with } \cos \phi = a/b) \quad (4)$$

$$M(a > b) = \frac{1}{\sin^2 \phi} - \left(\frac{1}{2}\right) \frac{\cos^2 \phi}{\sin^3 \phi} \log \frac{1 + \sin \phi}{1 - \sin \phi} \quad (\text{with } \cos \phi = b/a) \quad (5)$$

(1) H. Fricke, *Phys. Rev.*, **24**, 575 (1924).

(2) A. Cremers and H. C. Thomas, *J. Phys. Chem.*, **70**, 3229 (1966).

(3) A. Cremers and H. Laudelout, *J. Chim. Phys.*, **62**, 1155 (1965).

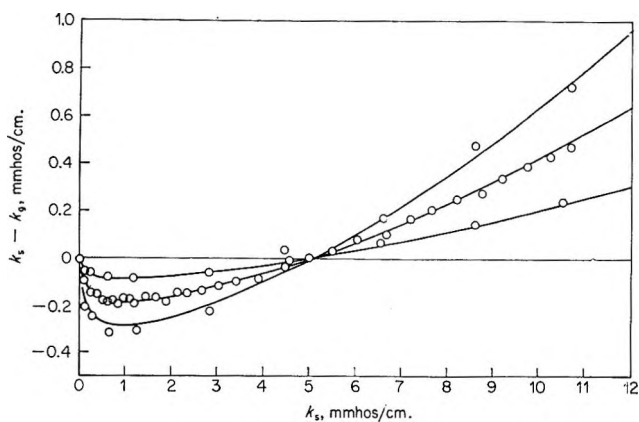


Figure 1. Experimental values of the difference between solution and suspension conductances, $k_s - k_g$, and those calculated from the Fricke equation for $k_i = 5.08$ mmhos/cm, $\rho = 0.011, 0.024, 0.038$, and $M = 0.065$.

For flat plates $M = 0$; for spheres $M = 2/3$; for long needles $M = 1$. All of the above are Fricke's results.

In the following we shall apply eq 1 to the case of suspensions of the sodium form of carefully purified montmorillonite from Camp Berteau, Morocco. The preparation of this material and the conductivity measurements have already been described.² Since it seems to be impossible to learn by direct experiment what size should be assigned to the suspended clay-ion-water micelle, ρ must be taken as an adjustable parameter. The same consideration applies even more certainly to the internal conductivity k_i and to the shape parameter M . We must test the Fricke equation by getting these three quantities from the conductivity data themselves. This would constitute a vitiating circular argument if the values of ρ , k_i , and M so obtained did not bear simple and sensible relations to what is already known about the clay, and if these values did not apply over a wide range of conductivities for various suspensions at various temperatures. We believe we can show that these requirements are fulfilled.

The original conductivity data are to be found in a report to the Petroleum Research Fund of the American Chemical Society.⁴ Generally, conductances have been measured at three temperatures, over a range of NaCl concentration of 0.0001–0.1 N , and for clay content from about 1 wt % to well out of range of validity of the Fricke equation, up to 50 wt % in some cases. The overall reproducibility of the conductance measurements is 0.008 mmho/cm, as seen from eight pairs of replicas. The root-mean-square deviation for the calculated curve in Figure 1 at 25°, for $\rho = 0.024$, is 0.012 mmho/cm, and this is for the difference $k_s - k_g$. Thus in this case the agreement between theory and experiment is essentially perfect. It does not yet appear possible to give meaningful estimates of the accuracy of the parameters ρ , k_i , and M .

The application of the Fricke equation has been

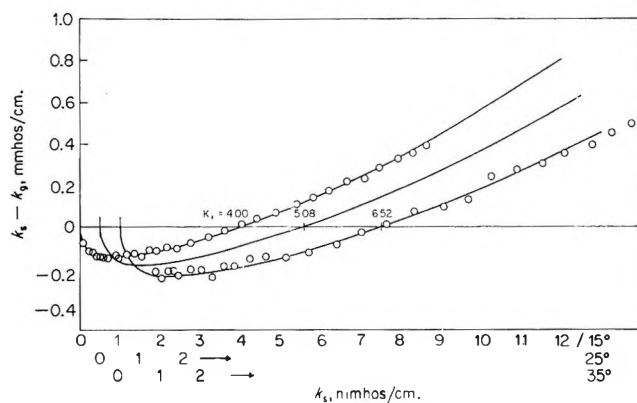


Figure 2. Temperature dependence of the difference between solution and suspension conductances, $k_s - k_g$, and those calculated from the Fricke equation with the indicated values of k_i , $\rho = 0.024$, and $M = 0.065$.

carried out by a least-squares procedure in the following manner. A Fortran program has been constructed which causes the computation of the sum of the squares of the deviations of $k_s - k_g$ as observed and as calculated for a selected set of values of k_i , ρ , and M . If the ranges of the three parameters have been properly selected and, of course, if the data in fact approximately obey the Fricke equation for a fixed set of values of the parameters, a single minimum in the sum of squares can be found by inspecting the output of the computer.

Two clues initially guided this work. Inspection of eq 1 shows at once that if a clay-ion-water micelle does in fact have a definite average internal conductance, the value of $k_s - k_g$ vanishes for $k_i = k_s$, as in any case is physically obvious. In addition, if the value of k_i is independent of ρ , the curves for $k_s - k_g$ vs. k_s , for different values of ρ , should all cross the k_s axis at a single point, at the value of k_i . This is the well-known "isoconductivity point" for clay suspensions as deduced from the Fricke equation. The existence of this nearly constant value of k_i makes the least-squares procedure possible. The second point was the recognition of the fact that the value of ρ could certainly not be expected to be directly calculable from the dry weight of the clay and its density. The size of the micelle is in a sense dictated by our demand that it be describable by the Fricke equation. Whether a fixed and reasonable value of ρ exists, for a given clay content, is to be decided on the basis of the conductivity data. The fact that all these points are correct over a range of values of both ρ and k_s is seen from the actual existence of sharp minima in the various sums of squares produced by the computer for different sets of data.

Figures 1 and 2 give the results of these computations for some of the most complete sets of data. (To avoid crowding, not all experimental points are shown.) As

(4) H. C. Thomas, final report of work under Grant No. PRF 3251-D5.

is seen in Figure 1, single values of k_i , ρ , and M do suffice to reproduce the rather complicated behavior of the data over a range of concentrations which corresponds to a 900-fold change in solution conductance. At the low values of clay content here treated and at a fixed temperature, a single value for the internal conductance suffices for the three different values of ρ .

The Fricke equation is quite insensitive to the value of M , as was long ago pointed out by the original author. It seems probable that differences in the values of M in the range found, 0.05–0.07, are meaningless. The value $M = 0.06$ corresponds to an oblate spheroid of axial ratio $1/25$. Thus the picture of a clay micelle forced on us by this model is that of a pancake 25 broad and 1 thick, entirely consistent with the known mica-like structure of montmorillonite. Of course, the micelles in the suspension must be highly heterogeneous in shape and size, and our model only gives us some average for these.

There is a significant point to be made in connection with the values of ρ' , the volume fraction of micelles as calculated from the values of ρ produced by the least-square process. These are all almost exactly seven times the value of the volume fraction of the dry clay as calculated using 2.7 g/ml as the density of the sodium montmorillonite. This uniform relation adds confidence to the idea that ρ' is a meaningful quantity. If one takes 10 Å as the thickness of a single aluminosilicate sheet and assumes that such a sheet is the basis of a micelle, then the average micelle will be 70 Å thick, corresponding to layers of water molecules 20–30 Å thick to be counted as "belonging to" the clay sheet. It will be of interest to examine potassium and cesium clays for which, because of their greater tendency to flocculate, one would predict a lower volume fraction and a higher value of M , corresponding to more compact micelles.

Table I: Parameters of the Fricke Equation by Least Squares from Conductance Measurements on Sodium Montmorillonite Suspensions

	Condition: wt % clay = 2.34 ± 0.02^a		
	Temp., °C		
	15	25	35
k_i , mmhos/cm	4.00	5.08	6.52
ρ	0.0235	0.0235	0.0230
M	0.065	0.070	0.065

Conditions: 25°, $k_i = 5.0$ mmhos/cm^b

Wt % clay	ρ	M
1.21	0.011	0.050
2.43	0.024	0.059
3.80	0.038	0.042

^a From data obtained at the Catholic University of Louvain, Belgium, 1969. ^b From less abundant data obtained at the University of North Carolina, Chapel Hill, about 1965.

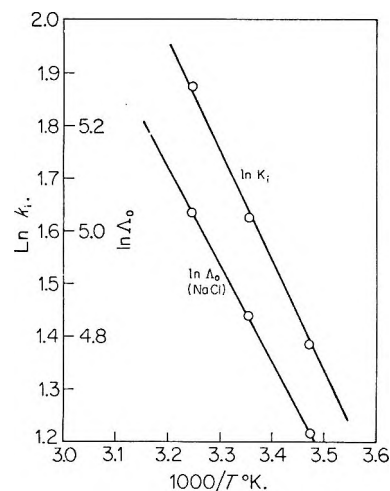


Figure 3. Arrhenius plots for the internal conductance of sodium montmorillonite micelles in sodium chloride solutions, k_i , and of the limiting equivalent conductance of NaCl.

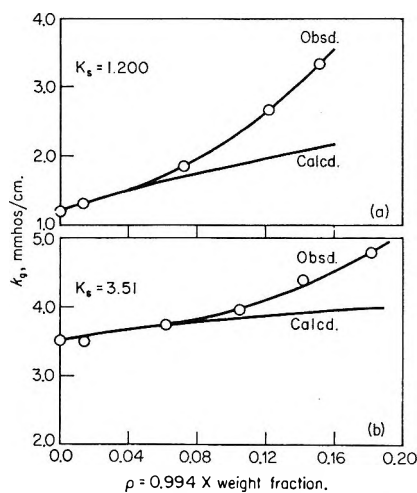


Figure 4. Tests of the range of validity of the Fricke equation into the region of finite clay content, ρ , for different values of the solution conductance: (a) $k_s = 1.200$; (b) $k_s = 3.51$.

If the values of the internal conductance found at different temperatures, Table I, refer to some meaningful average conductivity for ions moving near the clay surface, they should depend on the temperature in much the same way as does a solution conductance. Figure 3 is an Arrhenius plot for $\ln k_i$, together with one for $\ln \Lambda_0$ for NaCl. The "energy of activation" for the surface conduction process is 4.2 kcal/mol and that for the limiting aqueous conductance is 3.64 kcal/mol. It is generally agreed "that the increasing mobility [with temperature] is closely related to the increasing fluidity of water."⁵ The difference between the two energies may indeed be within the experimental error in the $\ln k_i$, but it is in the expected direction if the water adsorbed on the clay surface is in fact more viscous

(5) R. A. Robinson and R. H. Stokes, "Electrolyte Solutions," 2nd ed, Butterworth and Co. Ltd., London, 1959, p 129.

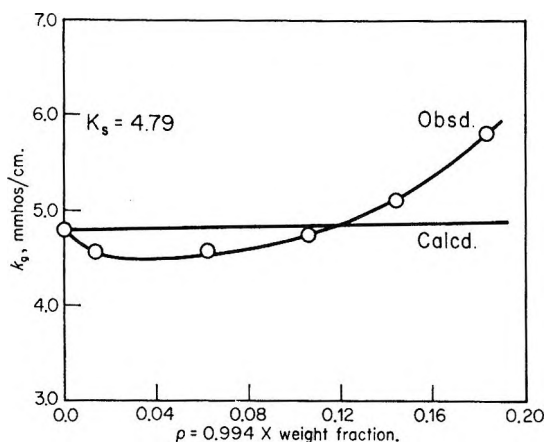


Figure 5. Tests of the range of validity of the Fricke equation into the region of finite clay content, ρ , for $k_s = 4.79$.

than liquid water, as has often been suggested.⁶ A more extensive investigation of this internal conductance would be highly desirable as a means of studying the adsorbed solution in colloidal micelles.

A somewhat unsatisfactory attempt has been made, with the data presently available, to assess the range of validity, as a function of ρ , of the Fricke equation. It is frequently the case with such limiting laws that they provide good approximations well into the region of finite concentrations. The work shown in Figure 1 is sufficient to establish it up to about $\rho = 0.04$ for solution concentrations up to 0.1 *N* in NaCl. Equation 1 solved for k_g gives

$$k_g = \frac{k_s + k_i \rho R}{1 + \rho R} \quad (6)$$

In this form the equation has been applied to data in which conductances were measured for single concentrations of NaCl over a wide range in clay content.³ The internal conductance has been taken to be $k_i = 5.0$ mmhos/cm and the value 0.06 assigned to M . In Figures 4 and 5 are shown the results of these calculations and the data which are supposed to be reproduced. The agreement for the lower solution conductances is quite good up to $\rho = 0.06$ –0.08, but it is far from good for $k_s = 4.79$. If one determines the limiting slope of k_g vs. ρ , at $\rho = 0$, for eq 6, it is found that this slope will be positive, zero, or negative according to whether $k_s < k_i$, $k_s = k_i$, or $k_s > k_i$. For the case of Figure 5 we would have to choose $k_s < 4.7$ mmhos/cm. Now it is indeed probable that k_i is not truly a constant, but one would expect it to increase, not decrease, with solution concentration. In any case there is certainly no good reason to invoke nonconstancy in only one of the three parameters in trying to reproduce the data. We have not attempted more elaborate calculations.

We believe that the above account establishes, or perhaps reestablishes, the Fricke equation as a useful and meaningful tool in the study of colloidal suspensions, and we hope that others will find data for entirely different systems to which the test can be extended.

Acknowledgment. Credit is given to the donors of the Petroleum Research Fund, administered by the American Chemical Society, for support of this research, and by A. C. for support of the Nationaal Fonds von Wetenschappelyk Onderzoek of Belgium.

(6) *E.g.*, P. F. Low, *Isr. J. Chem.*, **6**, 325 (1968).

An Effusion Study of the Reaction of Zirconium

Carbide with Calcium Oxide

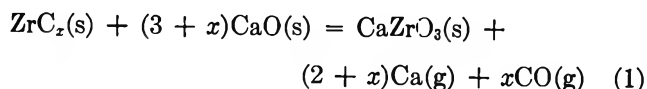
by Juey Hong Rai and N. W. Gregory

Department of Chemistry, University of Washington, Seattle, Washington 98105 (Received October 8, 1969)

Pressure-time studies of the reaction of CaO with ZrC in effusion cells indicate that the rate of reaction is controlled by diffusion of reactant ions through the product layer of CaZrO₃. Extrapolation back to time zero gives total effusion pressures in general agreement with those expected for the reaction $\text{ZrC(s)} + \text{CaO(s)} = \text{CaZrO}_3\text{(s)} + 3\text{Ca(g)} + \text{CO(g)}$ at equilibrium. The behavior of ZrC samples of different carbon content is reported. Experiments on the reaction of ZrO₂ with graphite are also described.

Zirconium carbide is recognized as a nonstoichiometric compound; phases with compositions in the range *ca.* ZrC_{0.55} to ZrC_{0.96} (carbon saturated) have been reported.¹ Available information about thermodynamic properties has been summarized by Storms;¹ properties of the carbon saturated phase have also been tabulated by Schick² and in the JANAF tables.³ Data on the carbon-deficient phases are relatively scarce. Characterization of these materials is confused by their possible inclusion of varying amounts of oxygen. Little definitive work on this aspect of the problem has been published.

We have been interested in the study of oxidation-reduction processes involving zirconium carbide by the effusion method. Observations on the reaction of graphite with ZrO₂ have been reported earlier.⁴ In addition to further work on this system, we now report a torsion-effusion study of the interaction of calcium oxide with zirconium carbide. Calcium zirconate and calcium vapor are shown to be products, along with an additional gas, assumed to be carbon monoxide. The steady-state pressure-time (*P-t*) behavior at various temperatures between 1500 and 1600°K is found to be that expected if the rates of the forward and reverse reactions are diffusion controlled. At various constant temperatures, plots of $1/P$ vs. $t^{1/2}$ are found to be linear; extrapolation to $t = 0$ gives the same "initial pressures" over a range of cell orifice and sample sizes. When these initial pressures are assumed to be equilibrium values, thermodynamic properties calculated are close to those expected for the reaction



Experimental Part

The torsion-effusion apparatus, cells, calibration method and general procedure have been described previously.⁴⁻⁶ The characteristics of the graphite

cells and 2-mil tungsten suspension wires used for the present work are summarized in Table I; torsion cell constants were determined by calibration with the vapor pressure of silver and were verified by measurement of the vapor pressure of copper.⁶ Orifices were cylindrical and a good approximation to knife edge (Clausing factors 0.96-0.97); the outer edges were flared to a hemispherical shape (*ca.* 5-mm diameter) in the $1/8$ -in. cell wall.

Table I: Torsion Cell Constants

Cell	Total orifice area <i>a</i> , cm ² × 10 ⁴	Suspension wire length, cm	Torsion cell constant × 10 ⁴ atm radian ⁻¹
1	3.47	60	7.36
2	5.91	58	4.77
3	6.51	55	5.27
3	6.51	59.2	3.07
4	13.16	40.7	3.40
4	13.16	55	2.42

Two zirconium carbide samples were used: ZrC_T (Titanium Alloy Manufacturing Division of the National Lead Co., Niagara Falls, N. Y.) and ZrC_J (Jet Propulsion Laboratory, Pasadena, California).⁷

(1) E. K. Storms, "The Refractory Carbides," Academic Press, New York, N. Y., 1967.

(2) H. L. Schick, "Thermodynamics of Certain Refractory Compounds," Academic Press, New York, N. Y., 1966.

(3) "JANAF Thermochemical Data," D. R. Stull, Ed., Dow Chemical Co., Midland, Mich.

(4) J. R. Hollahan and N. W. Gregory, *J. Phys. Chem.*, **68**, 2346 (1964).

(5) See the Ph.D. Thesis of J. H. Rai, University of Washington, Seattle, Wash. 98105, 1969.

(6) J. H. Rai and N. W. Gregory, *J. Phys. Chem.*, in press.

(7) These samples were obtained through the Ceramic Engineering Division at the University of Washington. We thank Professors J. I. Mueller and A. D. Miller for providing them and also for helpful discussions relative to this work.

Chemical and X-Ray analysis⁸ of these materials gave the following results.

		Sample T	Sample J
Wt % Zr		86 ± 3	87.5 ± 2
C	Total	13.2 ± 0.2	11.8 ± 0.2
	Free	3.2 ± 0.5	1.1 ± 0.5
O		1.07 ± 0.05	0.75 ± 0.05
Apparent Chemical Formula of Carbide			
(a) if oxygen in carbide phase		ZrC _{0.85} O _{0.07}	ZrC _{0.93} O _{0.05}
(b) if oxygen in separate oxide phase (as ZrO ₂)		ZrC _{0.91}	ZrC _{0.96}
Lattice Parameter Å (from high angle reflections)		4.696	4.698

The uncertainties represent the spread of values for the three or four samples analyzed in each case. When the carbide phase was dissolved in a mixture of 40 ml of 16 M HNO₃, 10 ml of 98% H₂SO₄ and 1-2 ml of 48% HF, the residue appeared to be only free carbon, *i.e.*, no ZrO₂ remained after ignition. Since crystalline ZrO₂ is not appreciably soluble in this acid mixture, these observations indicate that the samples did not contain ZrO₂. However, inasmuch as trace quantities may behave differently when distributed through or on the surface of the carbide, we have represented the apparent formula in two ways: (a) if the oxygen is an integral part of the carbide phase and (b) if the oxygen is present as ZrO₂.

Prior to preparation of the reaction mixture, samples of the carbide were placed in the effusion cell and degassed under vacuum at temperatures up to 1600°K until no angular deflection of the torsion system was apparent. The lattice parameter was unchanged after this treatment. The CaO powder (Allied Chemical, Morristown, New Jersey, Code 1529, 98%) was also heated under vacuum at 300° for 5 to 12 hr. Mixtures, usually in the ratio 1:4 (mol carbide:mol CaO), were then ground together and pressed (1500 psi) into pellets. The pellets were broken into small pieces and about 2.4 g (the maximum that could reasonably be accommodated) placed in the effusion cell. The cell was placed in the vacuum system and brought slowly (over a 2-3 hr period) to within 100° of the desired reaction temperature. The temperature was then raised quickly to the point of interest. Cell displacements were not recorded until about 1 hr after the temperature had been established; initial values were quite high because of further degassing. Steady-state pressures were then observed for periods of 4 to 9 hr.

To aid in identification of products, several experiments were continued for longer periods, *ca.* 22 hr, to

form amounts of solid product detectable by X-ray analysis. Debye-Scherrer X-ray patterns of the remaining solid showed lines of the ZrC phase, CaO, and CaZrO₃; these phases accounted for all lines observed. Following is a comparison of the lines attributed to CaZrO₃ with values listed in the ASTM file (*d* spacings, in Å)

ASTM	4.01	2.87	2.83	2.00	1.651	1.625
Observed	4.01	2.87	2.83	2.01	1.659	1.623

No change in the initial lattice parameters of the carbide phase was detected after this reaction period.

A blank run in which only CaO was placed in the cell showed that contact of this material with the graphite cell wall was insufficient to produce a significant displacement of the cell at the temperatures of interest (by formation of Ca(g) and CO(g)).⁶ Several Knudsen effusion experiments on the reaction of ZrC_T with CaO were carried out at 1518°K. The calcium vapor in the effusate was condensed on a molybdenum liner, which surrounded the cell and extended into the cool region outside the furnace. The quantity collected was determined by chemical analysis and was found to agree with results of the torsion experiments when the reaction was assumed to have the stoichiometry expected for eq 1. Quantitative collection of the effusate was not practical in the torsion apparatus.

No previous report on the reaction of ZrC and CaO has been found in the literature. The phase diagram for the system CaO-ZrO₂ indicates the existence of the compound CaZrO₃.⁹ According to Rabenau, CaZrO₃ has little tendency to dissolve CaO or ZrO₂ at 1400°. ¹⁰

Results and Discussion

Preliminary experiments demonstrated that effusion cell steady-state pressures developed by the reaction of CaO with ZrC were dependent on cell orifice area, sample size, and in a given experiment at constant temperature, decreased with time. Figure 1 shows the behavior of CaO-ZrC_T mixtures and is representative. When, after a period of several hours, the samples were removed, reground, and repressed and the experiment repeated, the *P-t* curve on the second heating was very similar to the first. When the results were plotted in the form $1/P$ vs. $t^{1/2}$, virtually straight lines were obtained. Data at various temperatures for the two different carbide samples are shown in Figures 2, 3, and 4. The following considerations appear to explain the *P-t* relationship.

The rate of reaction (1) may be expected to depend on (i) the rate of reaction at the interface of the solids

(8) The analytical results were obtained by Mr. Satya K. Sarkar, of the Ceramic Engineering Division. We thank him for permission to quote them. S. K. Sarkar, Ph.D. thesis, University of Washington, 1969.

(9) O. Ruff, F. Ebert, and E. Stephan, *Z. Anorg. Allgem. Chem.*, **180**, 219 (1929).

(10) A. Rabenau, *ibid.*, **288**, 221 (1956).

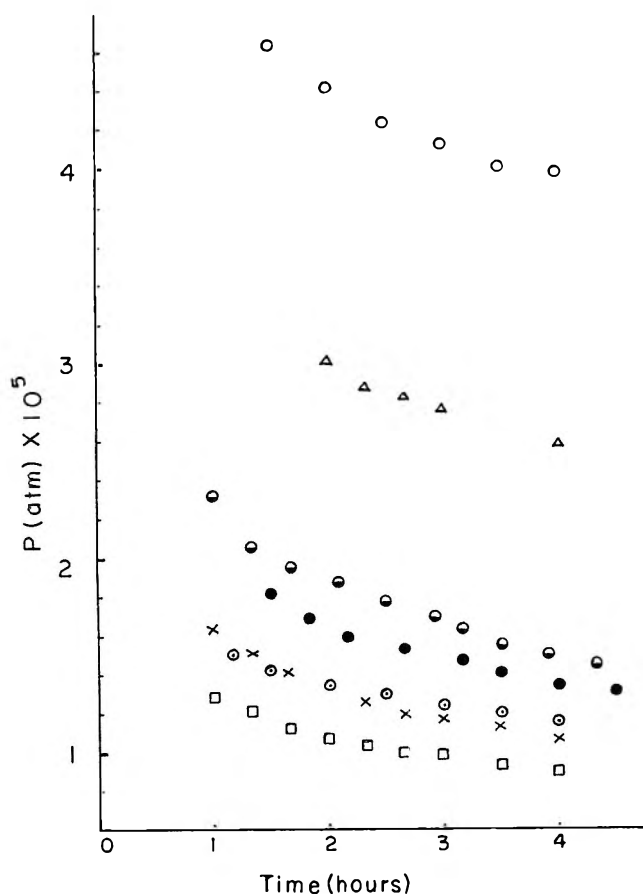


Figure 1. Time dependence of total effusion pressures generated by the CaO-ZrC_2 reaction; symbol, cell no., $T, ^\circ\text{K}$: \circ , 1, 1596; Δ , 3, 1581; \bullet , 3, 1568; \odot , 3, 1543; \ominus , 4, 1578; \times , 4, 1559; \square , 4, 1538.

and, once the reaction is underway, (ii) the rate of diffusion of reactants through the CaZrO_3 product layer. The steady state in the effusion cell is established by the condition: rate of effusion = rate of forward reaction - rate of reverse reaction or

$$k_e a_o P = r_f - r_r \quad (2)$$

where a_o is the total orifice area, P is the total effusion steady-state pressure, and k_e includes the kinetic theory of gas term $(2\pi mkT)^{-1/2}$. If (i) is the rate-determining step, the rate of the forward reaction may be assumed proportional to the interfacial contact area A , i.e., $r_f = k_1 A$. By microscopic reversibility, the rate of the reverse reaction must also be proportional to A and, at the same time, the number of gas molecules striking the interfacial area. It is proposed that the reverse reaction occurs when a particular gas molecule, Ca or CO, strikes a complex at the reaction boundary appropriately formed to lead to conversion of CaZrO_3 to ZrC and CaO ; hence we assume that r_r may be written as $k_2 A P$ (for stoichiometric effusion, P_{Ca} and P_{CO} are each proportional to P , the total pressure).

If instead the rate of reaction is determined by (ii), r_f may be given the form $k_3 A / \eta$, where η is the thickness

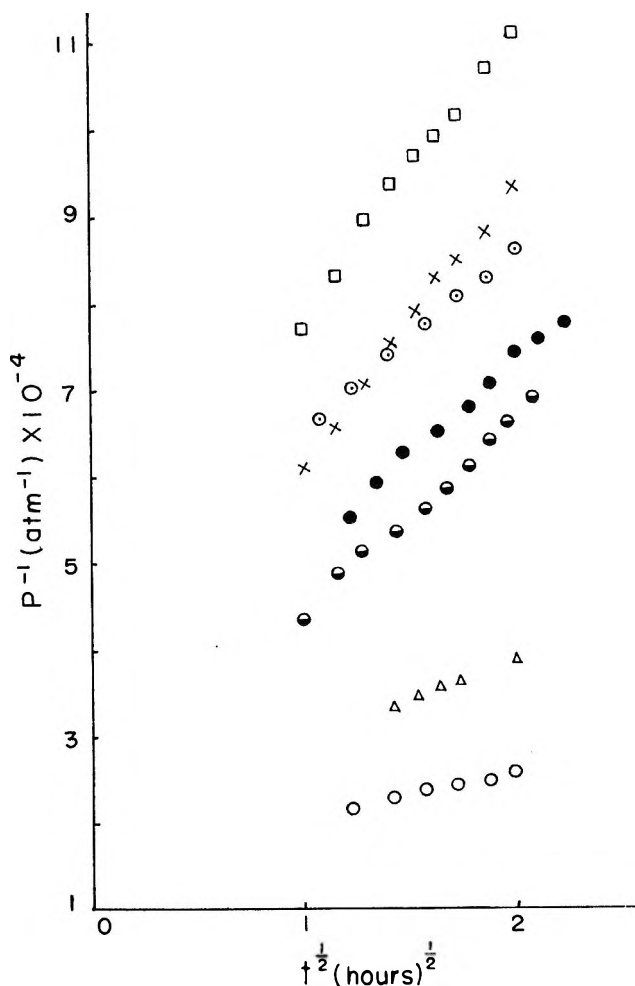


Figure 2. $1/P$ (total effusion pressure) vs. $t^{1/2}$ (time); CaO-ZrC_2 reaction; symbol, cell No. and temperature identification same as designated for Figure 1.

of the product layer; similarly $r_r = k_4 A P / \eta$. If both the phase boundary process and diffusion process are important, we may combine the two effects and (2) becomes

$$k_e a_o P = \frac{1}{\frac{1}{k_1 A} + \frac{\eta}{k_3 A}} - \frac{1}{\frac{1}{k_2 A P} + \frac{\eta}{k_4 A P}} \quad (3)$$

For $a_o = 0$, we may assume that P becomes equal to P_e , the equilibrium pressure; thus $k_1 = k_2 P_e$ and $k_3 = k_4 P_e$. With these substitutions and the assumption that the growth of the product layer follows a parabolic rate law,¹¹ i.e., $\eta = kt^{1/2}$, eq 3 may be reduced to the form

$$\frac{P_e}{P} = 1 + \frac{k_e a_o}{k_2 A} + \frac{k_e a_o k}{k_4 A} t^{1/2} \quad (4)$$

At $t = 0$, (4) reduces to the form discussed for the CaO-graphite reaction (in which no new solid phase is

(11) G. Cohn, *Chem. Rev.*, **42**, 527 (1948); see also N. B. Hannay, "Solid State Chemistry," Prentice-Hall, Inc., Englewood Cliffs, N. J., 1967.

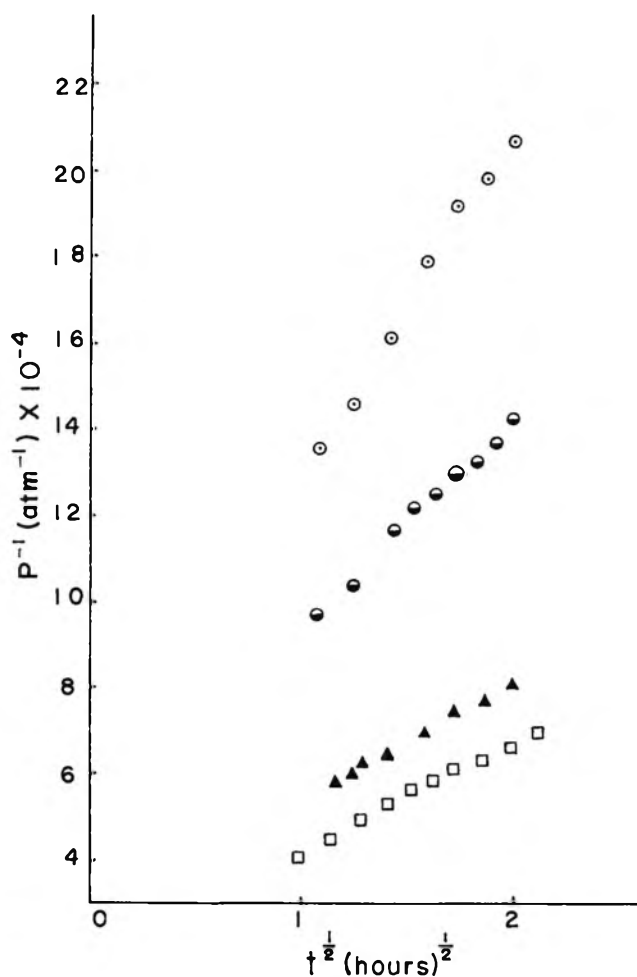


Figure 3. $1/P$ vs. $t^{1/2}$ for the CaO-ZrC_T reaction; cell 4 (symbol, T , °K): □, 1578; ▲, 1546; ●, 1522; ○, 1505.

formed).⁶ If, as time increases, the diffusion process becomes rate controlling, *i.e.*, if $kt^{1/2}/k_4$ becomes significantly larger than $1/k_2$, and if $k_e a_o/k_2 A \ll 1$, eq 4 becomes

$$P_e/P = 1 + k_e a_o k t^{1/2} / k_4 A \quad (5)$$

If A remains virtually constant, (5) corresponds to the experimentally observed relationship between P and t after 1 hr of reaction time.

Equation 5 also accounts for the observed variations in slopes of the $1/P$ vs. $t^{1/2}$ lines in the various experiments. The slopes increase as a_o of the cell is increased, *e.g.*, see Figure 2; the total orifice area of cell 4 is about 4 times larger than that of cell 1. A special experiment in cell 3 with a sample one-half the normal size was found to give a slope roughly twice that of the standard sample as expected if the values A for the two samples are in a 2:1 ratio.

If the $1/P$ vs. $t^{1/2}$ plots are extrapolated to $t = 0$, the "initial pressures," P_i , may be expected to be virtually equal to P_e if the ratio $k_e a_o/k_2 A_i$, where A_i is the initial contact area, is very much smaller than unity. This appears to be the case. The intercepts for the various

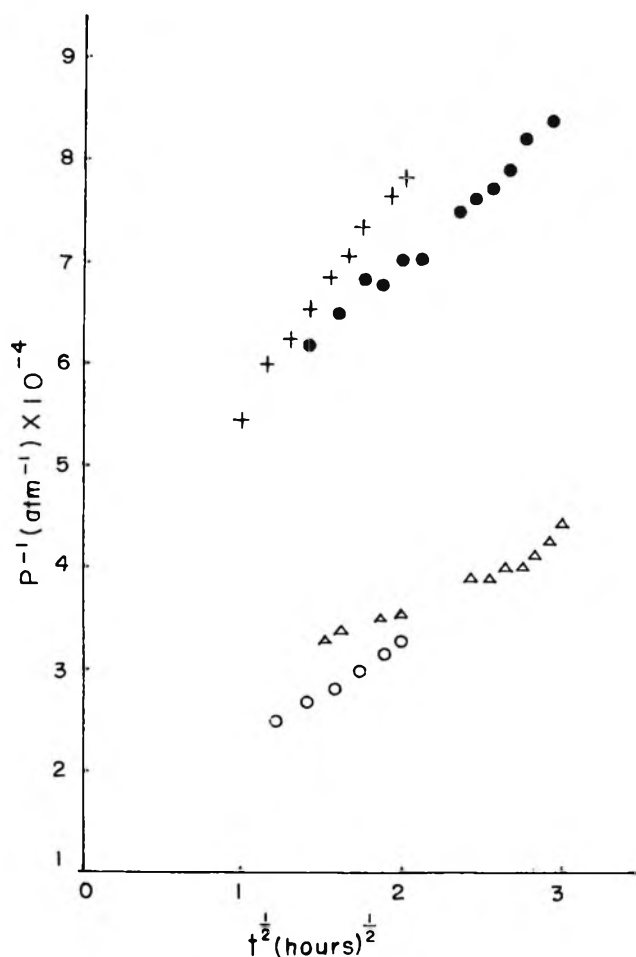


Figure 4. $1/P$ vs. $t^{1/2}$ for the CaO-ZrC_T reaction; symbol, cell no., T , °K; ○, 1, 1594; △, 2, 1563; ●, 2, 1527; +, 4, 1533.

cells show no systematic variation with orifice area. Intercepts were also within experimental error for the experiments in which different size samples were used, although slopes were different. The same result was observed when the mole ratio in the initial mixture was varied from 1:4 to 1:3.

Thermodynamic Aspects. Thermodynamic analysis of the data is complicated by the questionable presence and role of oxygen in the carbide phases. We present first results of calculations based on the assumption that the formulas are ZrC_{0.91}, for ZrC_T, and ZrC_{0.96}, for ZrC_J, respectively. These compositions give rise to the following expressions for $\Delta H^\circ_{298^\circ\text{K}}$ for reaction (1).

For ZrC_{0.96}

$$\Delta H^\circ_{298} = -17.938T \log P_{\text{atm}} + 4.359T - T\Delta(\bar{F}^\circ_{\text{T}} - \bar{H}^\circ_{298})/T \quad (6)$$

For ZrC_{0.91}

$$\Delta H^\circ_{298} = -17.480T \log P_{\text{atm}} + 4.187T - T\Delta(\bar{F}^\circ_{\text{T}} - \bar{H}^\circ_{298})/T \quad (7)$$

where P is the total equilibrium pressure generated by a reaction of form (1). Free energy functions (fef) tabulated by Storms were used for $ZrC_{0.96}$.¹ Values for $ZrC_{0.91}$ were estimated by evaluation of its fef at 3000°K (-23.586) from equilibrium pressures of $Zr(g)$ at this composition, as reported by Storms, carbon activities based on a Gibbs–Duhem treatment of his data,¹² heat capacity data based on measurements by Neel, *et al.*,

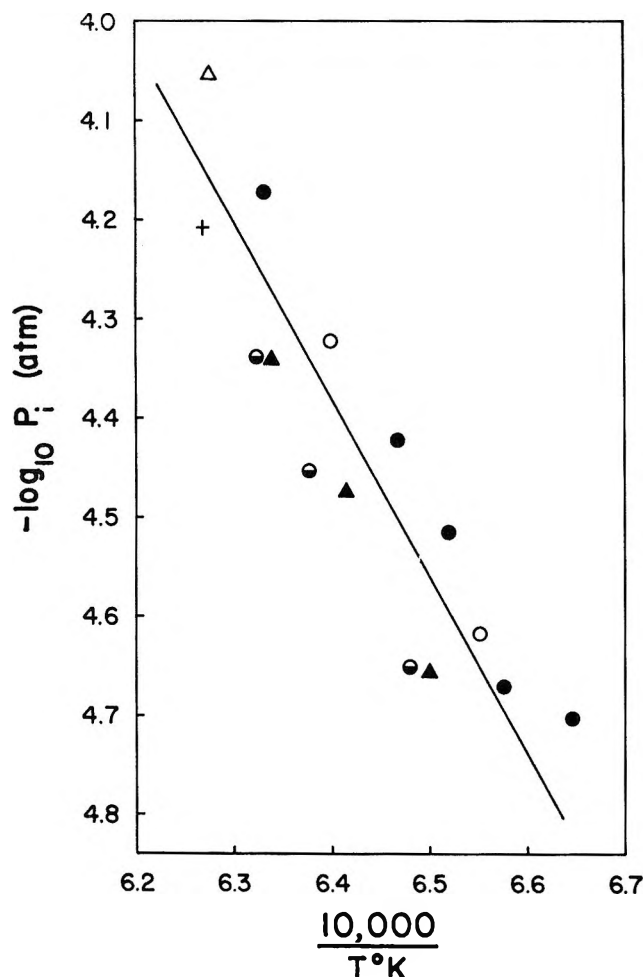


Figure 5. $\log P_i$, atm vs. $1/T$ for the $CaO-ZrC_J$ and $CaO-ZrC_T$ reactions: sample T: Δ , cell 1; \circ , cell 2; \bullet , cell 4; sample J: $+$, cell 1; \ominus , cell 3; \blacktriangle , cell 4. Solid line is the predicted total equilibrium pressure for reaction 1 for $ZrC_{0.96}$, using data of Storms.^{1,14}

on $ZrC_{0.92}$,^{1,13} and the value for the enthalpy of formation based on heat of combustion data.^{1,14} It was then assumed that the ratio of the free energy functions of $ZrC_{0.91}$ and $ZrO_{0.96}$ is the same in our temperature range as found at 3000°K. This approximation appears satisfactory for the niobium carbide system.¹

Free energy functions for $CaZrO_3$ were calculated by extrapolation of calorimetric data of Mezaki, *et al.*,¹⁵ from 1200 to 1600°K and the standard entropy given by King and Kelley.¹⁶ For $Ca(g)$, $CaO(s)$, and $CO(g)$, data given by Kelley¹⁷ and the JANAF tables¹⁸ were

used. Table II lists the results obtained when the P_i values, determined by least-square treatment of the data in the form of eq 5, are assumed to be the total pressures at equilibrium.

Table II: Values for ΔH°_{298} for (1) from Eq 6 and 7

$T, ^\circ K$	$-\log P_i$, (atm)	$-\Delta(\bar{F}^\circ_T - \bar{H}^\circ_{298})/T$, cal deg ⁻¹ mol ⁻¹	ΔH°_{298} , kcal mol ⁻¹
CaO-ZrC _{0.96} mixtures			
1596	4.2042	128.02	331.6
1581	4.3399	128.12	332.5
1578	4.3412	128.12	331.9
1568	4.4555	128.16	331.1
1559	4.4770	128.20	331.9
1543	4.6499	128.24	333.3
1538	4.6579	128.25	332.5
		Average	332.1
CaO-ZrC _{0.91} mixtures			
1594	4.0508	124.88	318.6
1578	4.1699	124.91	318.8
1563	4.3214	124.99	320.1
1546	4.4223	125.01	319.2
1533	4.5168	125.11	319.3
1527	4.6201	125.12	320.8
1522	4.6738	125.12	321.2
1505	4.7031	125.24	318.6
		Average	319.6

The standard deviations are believed to be appreciably less than the absolute uncertainty, estimated at ± 4 kcal. No trend with temperature is observed in either set of data. The enthalpy of formation of the carbide phases may be calculated from these results and standard values for the other components^{17,18} (for $CaZrO_3$, ΔH°_{298} was taken as -418.7 kcal mol⁻¹).¹⁹ For $ZrC_{0.96}$, the value -50.4 ± 4 kcal mol⁻¹ was obtained. This may be compared with -47.0 ± 3 kcal given in the JANAF tables, based on combustion work of Mah,²⁰ and -48.3 kcal mol, based on the formula $-\Delta H^\circ(ZrC_x)_{298} = -7.4 \pm 84.1x - 27.2x^2$ derived by Storms, based on the combustion work of Baker, *et al.*¹⁴

(12) H. W. Schimmelbusch, University of Washington, Seattle, private communication.

(13) D. S. Neel, C. D. Pears, S. Oglesby, Jr., WADD-TR-60-924 (1960).

(14) F. B. Baker, E. K. Storms, and C. E. Holley, Jr., private communication, 1968.

(15) R. Mezaki, E. W. Tilleux, T. F. Jambois, and J. L. Margrave, 3rd Sym. Thermophys. Properties, Lafayette, Ind. (1965).

(16) K. K. Kelley and E. G. King, U. S. Bureau Mines Bulletin No. 592, U. S. Government Printing Office, Washington, D. C., 1961.

(17) K. K. Kelley, U. S. Bureau Mines Bulletin No. 584, U. S. Government Printing Office, Washington, D. C., 1960.

(18) "JANAF Thermochemical Data," D. R. Stull, Ed., Dow Chemical Co., Midland, Mich.

(19) A. S. L'vova and N. N. Feodos'ev, *Zh. Fiz. Khim.*, **38**, 28 (1964).

(20) A. D. Mah, Bureau of Mines, Report of Investigation 6518, U. S. Government Printing Office, Washington, D. C., 1964.

This formula gives $-46.6 \text{ kcal mol}^{-1}$ for $\text{ZrC}_{0.91}$, which was the value used to estimate the free energy function of this phase. The value derived from the result in Table II is $-46.0 \pm 4 \text{ kcal mol}^{-1}$.

For ZrC_J , the van't Hoff slope (Figure 5) gives $\Delta H^\circ_{1550^\circ\text{K}}(1)$ as 352.7 kcal; for ZrC_T , 329.5 kcal. Conversion to 298°K with the heat capacity data cited gives 363 kcal and 339 kcal, respectively, with uncertainties estimated at $\pm 15 \text{ kcal}$. The former is about 9% larger than the *fef* value; the latter about 6% larger. Because of the sensitivity of the van't Hoff slope to temperature errors, we believe the *fef* results are more reliable.

The solid line in Figure 5 represents the predicted total equilibrium pressures of calcium vapor and carbon monoxide for reaction 1 when data tabulated by Storms for $\text{ZrC}_{0.96}$ are used.^{2a} Our results for ZrC_J lie slightly below this line; those for ZrC_T , slightly above. The agreement is well within the combined experimental errors of our study and those of the data used to derive the literature values. The difference between the total pressures observed for our two samples is of the magnitude expected for the difference in composition indicated by the analysis.

Data are not available which would permit us to make a similar comparison based on the assumption that the oxygen content indicated by the analysis is an integral part of the carbide phase. Also we have no assurance that the oxygen content of the phases under the actual effusion conditions remains the same as found in the samples prior to preparation of the reaction mixtures. No change was seen in the carbide lattice parameter following the effusion study; however, this was observed only after cooling the mixture to room temperature. Furthermore, small changes in oxygen content may be difficult to detect in this way. Analysis of the carbide phase following the effusion experiments was not practical because it remained mixed with unreacted CaO and the CaZrO_3 product. Usually less than 10% of the reactants are converted during the effusion period. We can only conclude that the small amount of oxygen which appears to be in these samples does not change the chemical potential of ZrC significantly from that for samples characterized in the literature as $\text{ZrC}_{0.91}$ and $\text{ZrC}_{0.96}$, respectively.

The Reaction of ZrO_2 with Graphite. The earlier effusion study⁴ of the reaction of ZrO_2 with graphite led to the conclusion that either the rate of the reaction was not sufficient to establish near equilibrium pressures or that the reaction was not correctly represented by the equation



The pressures observed were lower than those expected if the carbide phase is $\text{ZrC}_{0.96}$ by a factor of *ca.* 100; the apparent entropy of the reaction was also unreasonable for (8).

We have made some further observations on this system. In particular a quantitative study was made of the pressure-time behavior to see if an extrapolation method similar to that developed for the CaO-ZrC reactions would lead to more satisfactory results. Samples were prepared as described previously.⁴ Experiments in cell 2 confirmed the behavior reported earlier. Very little change of steady-state pressures with time was observed. When cell 4, with its larger orifices, was used, the steady-state pressures fell noticeably with time. Extrapolation of $1/P$ vs. $t^{1/2}$ plots, which were virtually linear, to zero time lead to initial pressures approximately equal to those obtained with cell 2. The addition of up to 5% of CaF_2 , found to decrease the rate of pressure fall-off with time for the CaO-graphite reaction,⁶ had no noticeable effect on steady-state pressures in cell 2.

These observations suggest that the reaction of pressed mixtures of ZrO_2 and graphite under effusion conditions in the temperature range 1422–1520°K establishes an equilibrium-like behavior with a carbide phase distinctly different from $\text{ZrC}_{0.96}$. It is clear, however, that if this phase contains only zirconium and carbon, it cannot be in true equilibrium with graphite. Of the various possibilities, formation of either carbon-deficient ZrC_x or an oxycarbide ZrC_xO_y , with $x + y < 1$, seem most likely. X-Ray diffraction patterns of the effusion cell reaction product after 18 hr of reaction in the cell showed the presence of a ZrC-like phase with a lattice parameter of 4.693 Å (expected for $\sim\text{ZrC}_{0.63}$);^{2a} after 72 hr, the cell parameter had fallen to 4.688 ($\text{ZrC}_{0.59}$?); 4.698 Å is characteristic of the carbon-saturated carbide phase.

Possibly a carbon-deficient phase is formed at the ZrO_2 -graphite interface and "equilibrates" with $\text{CO}(\text{g})$. Estimated free-energy calculations for a phase such as $\text{ZrC}_{0.63}$ in (8), instead of $\text{ZrC}_{0.96}$, gives rise to CO pressures of the magnitude observed. Kinetic studies on the reaction of zirconium with carbon above 2000° by Adelsberg, *et al.*,²¹ show that carbon diffuses through zirconium carbide very slowly, even for carbon-deficient material. From the magnitude of the diffusion coefficients reported, it appears saturation of a $\text{ZrC}_{0.63}$ phase by diffusion of carbon from graphite may not keep pace with the continuous reaction in the effusion cell. Possibly this helps to explain the dilemma that while such a phase accounts for the CO pressures observed, it cannot be truly in equilibrium with carbon. If the composition of such a phase varied with reaction temperature, this would also explain the anomalous values derived for the entropy. The possibility that the phase contains some oxygen cannot be excluded; however, the oxygen activity in the effusion cell, if one assumes

(21) L. M. Adelsberg, L. H. Cadoff, and J. M. Tobin, *Trans. Met. Soc., AIME*, 236, 972 (1966).

it to be fixed by the C-O₂-CO equilibrium, is very low relative to that found over ZrC_zO_y phases with measurable oxygen content.⁸ Chemical analysis of the phase formed in effusion experiments was not practical; it is formed only in small amounts and could not be isolated from the reactant phases.

Acknowledgments. This work was supported in part by National Aeronautics and Space Administration Grant NGL 48-002-004 for "Interdisciplinary Research on the Nature and Properties of Ceramic Materials" and in part by National Science Foundation Grant GP-5608X for the study of "Vaporization Processes."

Mechanism of Polarographic Reduction of Germanium(IV) in Acidic Catechol Medium¹

by R. G. Canham,^{2a} D. A. Aikens, Nicholas Winograd,^{2b} and Glenn Mazepa^{2b}

Department of Chemistry, Rensselaer Polytechnic Institute, Troy, New York 12181 (Received September 3, 1969)

The mechanisms of the preelectrochemical reactions involved in electrodeposition of Ge(IV) from acidic catechol have been studied by means of Koutecky's analysis of the limiting current. Dissociation of the tris-catechol complex and reaction of Ge(OH)₄ with one or two catechol moieties have been identified as the important preelectrochemical steps. The electroactive complexes are the mixed catechol-hydroxy complexes Ge(OH)₂L, Ge(OH)₂L₂, and possibly GeOHL. Adsorption of the electroactive species precedes electroreduction, but electron bridging does not seem to be important. It is postulated that a *trans* effect in the mixed complexes facilitates deposition by increasing the ease of release of the coordination sphere.

The value of the formal heterogeneous rate constant of the Ge(IV)-Ge⁰ couple is extremely low in most electrolytes and the electroreduction of Ge(IV) is usually highly irreversible. Although the reversible reduction potential for Ge(IV) in 1 M acid solution is -0.25 V *vs. sce*,³ no reduction is observed at the dropping-mercury electrode prior to the onset of hydrogen evolution at approximately -1 V *vs. sce*.⁴ This behavior appears to be representative and the polarographic half-wave potential of Ge(IV) in most electrolytes is displaced approximately 1 V from the reversible value, with values ranging from -1.3 V *vs. sce* in 0.1 M Na₂EDTA⁵ to -1.6 V *vs. sce* in 0.1 M KCl.⁶ Catechol effectively catalyzes the reduction of Ge(IV), however, and in acidic catechol medium the half-wave potential is shifted as far positive as -0.4 V *vs. sce*. The ability of catechol and related compounds to catalyze the reduction of Ge(IV) was first reported by Konopik,⁷ who proposed that the electroactive species was the diprotonated form of the tris-catechol complex of Ge(IV), H₂GeL₃. Recently, however, Konopik and Kalvoda⁸ reexamined the mechanism and, in a novel application of Job's method to polarographic kinetic currents, demonstrated the existence of two electroactive complexes. The first species, a 1:1

complex, predominates at pH 1 and the second species, a 1:2 complex, predominates at pH 3.5. Although this study clearly established the existence of the two electroactive species, it was not possible, however, to define the precise nature of either the electroactive species or the preelectrochemical reactions.

This paper reports a detailed study of the polarographic reduction of Ge(IV) in acidic catechol solution based on the Koutecky treatment of preelectrochemical reactions. The preelectrochemical reactions leading to the electroactive species are identified and the significance of the nature of the coordination of the several electroactive species is discussed.

(1) Supported in part by Grants GP 5668X and GP 9577 from the National Science Foundation. Abstracted in part from the B.S. thesis of N. W., Rensselaer Polytechnic Institute, 1967.

(2) (a) Participant, NSF Summer Institute in Instrumental Analysis, Rensselaer Polytechnic Institute, 1968. (b) NSF undergraduate research participant.

(3) B. Lovrecek and J. O'M. Brockris, *J. Phys. Chem.*, **63**, 1368 (1959).

(4) B. Lovrecek and L. Duic, *J. Electroanal. Chem.*, **10**, 151 (1965).

(5) P. Valenta and P. Zuman, *Anal. Chim. Acta*, **10**, 591 (1954).

(6) Gh. Sauvenier and G. Duckyaerts, *ibid.*, **13**, 396 (1955).

(7) N. Konopik, *Monatsh. Chem.*, **91**, 717 (1960).

(8) R. Kalvoda and N. Konopik, *Z. Anal. Chem.*, **244**, 30 (1969).

Experimental Section

Reagents. Distilled water and reagent grade materials were used throughout except as noted. Stock solutions 0.01 M in Ge(IV) were prepared by dissolution of 550 mg of GeO₂ (Fairmount Chemical Co., Newark, N. J.) in 100 ml of 0.1 M NaOH. The solution was filtered through a glass frit, and the filtrate was acidified with HCl to pH 5 and diluted to 500 ml. Aliquots were analyzed for Ge(IV) content by titration with standard base in the presence of excess catechol as described by Bevilard.⁹ Catechol stock solutions were prepared by solution of weighed quantities of Eastman grade catechol in deoxygenated water. The polarographic supporting electrolyte was 1.00 M NaCl-HCl. The pH values of solutions were determined using an expanded-scale pH meter standardized with four 1.00 M NaCl-HCl solutions 1.00 × 10⁻³, 1.00 × 10⁻², 1.00 × 10⁻¹, and 1.00 M in HCl, respectively. Solutions were deoxygenated prior to addition of catechol, and addition of concentrated base to solutions containing free catechol was avoided.

Equipment. A standard H cell with an sce as reference electrode and a potassium chloride-agar salt bridge was used. The dropping-mercury electrode had a drop time of 5.0 sec at a column height of 105 cm. The cell resistance was 140 ohms and no corrections for ir drop were made. The cell was thermostated at 25.0° ± 0.1°. A Sargent Model XXI recording polarograph was used without damping.

Results

Limiting Currents. Plots of the logarithm of the limiting current for reduction of 10⁻⁴ M Ge(IV) at 25° in 1 M NaCl-HCl from pH 0 to pH 4 are given in Figures 1 and 2. The catechol concentration corresponding to each curve is indicated numerically by the value of pL adjacent to the curve. Currents calculated from the proposed rate laws are denoted by solid lines.

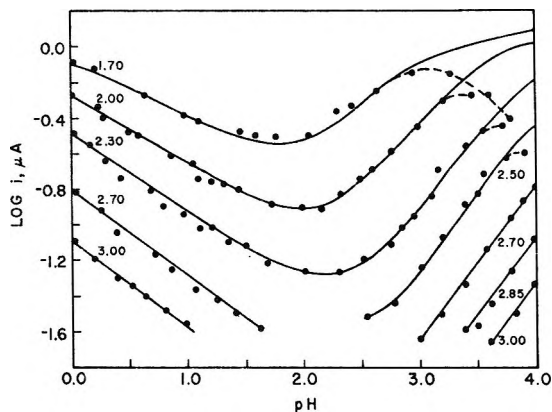


Figure 1. Limiting current for reduction of Ge(IV) from acidic catechol solution at low catechol concentrations. Solid lines represent currents calculated on the basis of the proposed complex formation mechanism. Numerals indicate pL values.

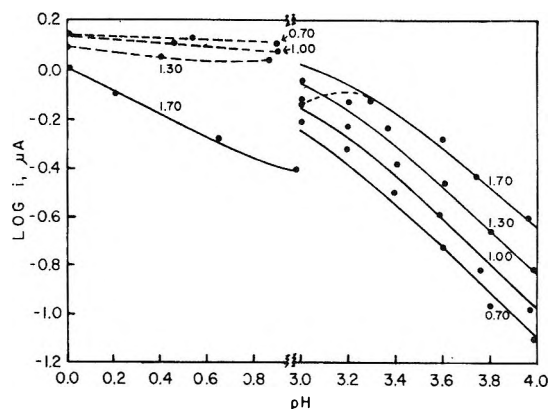


Figure 2. Limiting current for electrodeposition of Ge(IV) from acidic catechol solution at high catechol concentrations. Solid lines represent currents calculated on the basis of the proposed complex formation and dissociation mechanisms. Numerals indicate pL values.

Dashed lines are used in Figure 2 to connect experimental current values at low pH and high catechol concentrations which are nearly diffusion controlled and in both Figure 1 and Figure 2 to connect several experimental points that deviate substantially from the calculated values. The diffusion current, estimated from the dependence on the catechol concentration of the limiting current at pH 0, is 1.42 μA. The uncertainty in measuring limiting currents increases substantially for currents less than 0.025 μA, and currents less than this value have not been reported.

No correction has been made for the influence of solution viscosity which even at the highest catechol concentrations is relatively minor. The viscosity of the pH 1 electrolyte is increased only 6% from 10⁻³ M catechol to 0.2 M catechol, the highest concentration studied. This increase in viscosity corresponds to a decrease in diffusion current of only 3% or 0.02 log unit whereas this increase in catechol concentration causes a net increase in current of 50-fold or 1.7 log units.

The limiting current shows the expected transition from strict kinetic control at the lower values to pure diffusion control at the higher values, as judged by the dependence of the current on the mercury column height. Currents less than 0.2 μA are essentially purely kinetic in nature and are independent of the mercury column height while currents greater than 1 μA are essentially diffusion controlled and vary with the square root of the mercury column height.

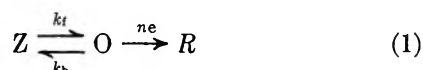
Kinetic currents are strictly first order in germanium over the usual polarographic concentration range provided catechol is present in large excess. As an example, for a solution 10⁻² M in catechol and pH 1, the ratio of the limiting current in microamperes to the Ge(IV) concentration in millimoles per liter is 1.93 ±

(9) P. Bevilard, *Bull. Soc. Chim. Fr.*, 21, 296 (1954).

0.05 for Ge(IV) concentrations between 10^{-4} and 2×10^{-3} M. For Ge(IV) concentrations above 2×10^{-3} M, the current does not increase in proportion to the germanium concentration, probably because the concentration of catechol begins to limit the current.

Discussion

Interpretation of Limiting Currents. For polarographic limiting currents controlled by the rate of a preelectrochemical step, Koutecky's analysis^{10,11} of the limiting current provides a powerful approach to study of the mechanism of the preelectrochemical step. This analysis is applicable to electrode reactions of the type exemplified by the cathodic reaction in eq 1 where Z represents an electroinactive species, O represents the electroactive species, R represents the electrode reaction product, and k_f and k_b denote, respectively, the rate constants of the forward and reverse steps of the preelectrochemical reaction. The limiting current, i , is



related to the diffusion current, i_d , and the values of k_f and k_b by the Koutecky variable, χ , and the Koutecky function, $F(\chi)$, as shown in eq 2.

$$\chi = k_f \sqrt{i} / \sqrt{k_b} \\ i/i_d = F(\chi) \quad (2)$$

Quantitative application of Koutecky's analysis requires that the preelectrochemical reaction be first order or pseudo first order in both Z and O. This requirement was easily satisfied with respect to catechol by restricting the catechol concentrations to values of 10^{-3} M or higher, thereby ensuring that the catechol concentration was at least tenfold greater than the Ge(IV) concentration. This approach could not be used to ensure that the hydrogen ion concentration was held essentially fixed, however, because it was desired to study the reaction at pH values up to 4 and it was necessary to maintain the Ge(IV) concentration at 10^{-4} M in order to obtain sufficiently large polarographic currents. Further, the use of pH buffers was deliberately avoided because it was feared that the components of suitable buffers would interfere by complexing Ge(IV). Hence, at pH 4 hydrogen ion is not present in excess over Ge(IV), and the possibility that diffusion of hydrogen ion controls the Ge(IV) reduction current must be considered. Comparison of the limiting current for reduction of Ge(IV) at pH 4 with the current which would be supported by diffusion of 10^{-4} M hydrogen ion indicates clearly, however, that the Ge(IV) reduction current at pH 4 is not limited significantly by diffusion of hydrogen ion. Reduction of Ge(IV) at pH 3-4 requires two hydrogen ions and the diffusion current for reduction of 10^{-4} M Ge(IV) is 1.4 μ A. On the conservative assumption that the diffusion

coefficient of the hydrogen ion equals that of Ge(IV), the limiting current for reduction of 10^{-4} M Ge(IV) at pH 4 would be 0.7 μ A if diffusion of hydrogen ion were the current-limiting step. The limiting current at pH 4 does not exceed 0.23 μ A, however, or one-third the value which could be supported by diffusion of hydrogen ion. Hence diffusion of hydrogen ions does not significantly influence the Ge(IV) reduction current at pH 4. By the same reasoning it also follows that diffusion of hydrogen ion is not the current-limiting step at lower pH values. This reasoning is confirmed by the observation that limiting currents less than 20% of the diffusion-limited value are purely kinetic in nature. As an example, at pH 3.66 and with a catechol concentration of 0.1 M, lowering the mercury column reservoir from 90 to 40 cm caused the limiting current to decrease only 7%, as compared to a decrease of 33% for a diffusion-limited current.

Application of Koutecky's analysis to the limiting-current data in Figures 1 and 2 together with knowledge of Ge(IV) complex formation indicates that electroreduction of Ge(IV) in acidic catechol solution involves both complex formation and complex dissociation reactions. In the dilute hydrochloric acid solutions employed in this study Ge(IV) exists as germanic acid, Ge(OH)₄.¹² The hydroxide ions in the coordination sphere of Ge(IV) can undergo not only simple displacement by the entering ligand, but also direct acid-base reaction with protons. Hence, in order to define the reaction precisely, it is necessary to determine the reaction order of Ge(OH)₄ with respect to both hydrogen ion and catechol.

The preelectrochemical pathway involves complex formation reactions between Ge(OH)₄ and catechol if either the catechol concentration or the pH is low. The preelectrochemical step involves partial dissociation of the tris-catechol complex of Ge(IV) if both the pH and the catechol concentration are high. The formulation of χ and establishment of proposed mechanisms for the complex formation reaction and the dissociation reaction are discussed separately below.

Current Control by Complex Formation. For pH values between 0 and 4 and catechol concentrations between 1×10^{-3} M and 2×10^{-2} M, the limiting current at fixed pH increases with increasing catechol concentration. Hence the preelectrochemical reaction leading to the electroactive species must involve reaction of Ge(OH)₄ with catechol.

Data for this range of variables are given in Figure 1 where the points represent experimental limiting currents and the solid lines represent the current calculated from the value of χ defined by eq 3. The

$$\chi = 66C_H^{1/2}C_{H,L} + 3.5C_H^{-1}C_{H,L}^2 \quad (3)$$

(10) J. Koutecky, *Collect. Czech. Chem. Commun.*, **18**, 597 (1953).

(11) J. Weber and J. Koutecky, *ibid.*, **20**, 980 (1955).

(12) R. L. Benoit and P. Clerc, *J. Phys. Chem.*, **65**, 676 (1961).

limiting current at pH 0 is determined by the first term, and the limiting current at pH 4 is determined by the second term, while the limiting current near pH 2 is controlled by both terms. Observed and calculated currents agree within 15% or less with one notable exception, the consistent deviation observed for $2 \times 10^{-2} M$ catechol (pL 1.70) above pH 2.5. Here the observed current falls below the calculated current, and the deviation increases with increasing pH until at pH 4 the calculated current exceeds the observed current by a factor of 4. The onset of this deviation coincides with conversion of a significant fraction of $\text{Ge}(\text{OH})_4$ to GeL_3^{2-} which lowers the concentration of $\text{Ge}(\text{OH})_4$. The formation of GeL_3^{2-} from $\text{Ge}(\text{OH})_4$ via eq 4 was studied by Antikainen,¹³ who reported that the equilib-



rium constant at 25° in 0.1 *M* KCl is 0.17. This value predicts approximately 50% conversion of $\text{Ge}(\text{OH})_4$ to GeL_3^{2-} at pH 3. This result has only qualitative significance in 1 *M* NaCl-HCl, of course, but appears to be entirely consistent with the pH dependences of the observed and calculated limiting currents. The discrepancy between the observed and calculated currents at pH 3 is, of course, much less than the factor of 2 suggested by the equilibrium concentrations of $\text{Ge}(\text{OH})_4$ and GeL_3^{2-} , because the equilibrium between the two species is relatively mobile.

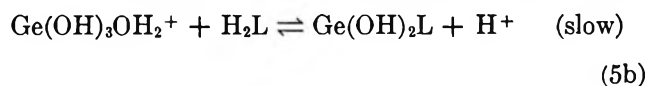
As the catechol concentration is increased above $2 \times 10^{-2} M$, the onset of the formation of GeL_3^{2-} and the resultant deviation of the experimental limiting current from the values calculated from eq 3 move to lower pH values. Establishment of the preelectrochemical reaction at intermediate pH values is complicated by the presence of significant amounts of both $\text{Ge}(\text{OH})_4$ and GeL_3^{2-} , but only $\text{Ge}(\text{OH})_4$ is present at substantial concentration at catechol concentrations up to $2 \times 10^{-1} M$ for pH values below 1 and the analysis is straightforward. Limiting currents for this range of pH and for catechol concentrations between 2×10^{-2} and $2 \times 10^{-1} M$ are given in the left side of Figure 2. The current increases steadily with increasing catechol concentration, and for the highest catechol concentrations, the current is essentially diffusion controlled. The direct dependence of the current on the catechol concentration shows clearly that complex formation is the predominant preelectrochemical mechanism. Observed currents for the intermediate catechol concentrations, however, consistently fall 10–15% above the values calculated from eq 3. The reason for this discrepancy is not clear, but it may be related to adsorption of catechol, which has been shown by Kalvoda and Konopik⁸ to be extensive.

Formulation of Rate Laws. Because the form of χ is determined by the forms of both the forward and reverse rate laws of the preelectrochemical reaction, establishment of the form of χ usually does not permit

unambiguous assignment of the forward and reverse rate laws. A number of pairs of forward and reverse rate laws are generally consistent with a given form of χ and are thus equally acceptable in a mathematical sense. Fortunately, all but one of the mathematically acceptable pairs of forward and reverse rate laws can usually be eliminated on the basis of kinetic considerations. As an example, the first term in eq 3 is consistent both with the reaction pair in which a forward reaction second order in hydrogen ion is coupled with a reverse reaction third order in hydrogen ion and with the reaction pair in which a forward reaction first order in hydrogen ion is coupled with a reverse reaction first order in hydrogen ion. In the absence of known acid-base reactions that could account for the second and third orders of the first reaction pair with respect to hydrogen ion, this pair appears implausible and has been rejected in favor of the second pair which is first order in hydrogen ion in each direction. In a similar manner, evaluation of each χ term generally leads to the result that one pair of forward and reverse rate laws is more attractive kinetically than other alternatives.

Complex Formation Mechanisms. The presence of two additive terms in eq 3 for χ indicates the existence of two independent paths leading to formation of electroactive species from $\text{Ge}(\text{OH})_4$ and catechol. The nature of the mechanism and the identity of the electroactive species are discussed below in detail for each path.

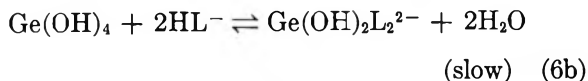
The first term of eq 3 leads to a forward rate law first order in catechol and first order in hydrogen ion coupled with a reverse rate law zero order in catechol and first order in hydrogen ion. Thus, both formation and dissociation of the electroactive species are catalyzed by hydrogen ion. Several plausible mechanisms are consistent with the orders of the forward and reverse steps with respect to catechol and hydrogen ion, and all lead to formation of the mixed complex, $\text{Ge}(\text{OH})_2\text{L}$, as the electroactive species. The sequence in eq 5 has been selected as both consistent with the properties of the reactants and capable of providing an energetically



favorable path. Protonation of $\text{Ge}(\text{OH})_4$ in the initial equilibrium step 5a provides a favorable site for ligand displacement through conversion of a coordinated hydroxide ion to the more loosely bonded water molecule. This step is followed by replacement of the water molecule by catechol in rate step 5b. This step is probably facilitated by simultaneous proton transfer from catechol to coordinated hydroxide in a concerted mechanism.

(13) P. J. Antikainen, *Acta Chem. Scand.*, 22, 2867 (1968).

Analysis of the second term in eq 3 indicates that the preelectrochemical reaction is second order in catechol in the forward direction and second order in hydrogen ion in the reverse direction. The mechanism proposed for this reaction is given in eq 6 and the electroactive



species is the bis-hydroxyl-bis-catechol complex, $\text{Ge}(\text{OH})_2\text{L}_2$. Deprotonation of catechol in equilibrium step 6a is followed by attack of the monoprotonated catechol on $\text{Ge}(\text{OH})_4$. The attack by the two monoprotonated catechol moieties described by eq 6b probably occurs in two consecutive steps rather than one concerted step. Koutecky¹⁴ has shown that the form of χ for a two-step reaction of this type is dimensionally identical with the form of χ for a single-step reaction, and the first order of the successive steps is more plausible than the second order of a single complex-formation step. As with the mechanism outlined in eq 5, simultaneous proton transfer from the entering catechol to coordinated hydroxide probably facilitates the ligand exchange by providing a concerted pathway.

Current Control by Dissociation of GeL_3^{2-} . For catechol concentrations of $2 \times 10^{-2} M$ and above and pH values between 3 and 4, the limiting current at constant pH decreases with increasing catechol concentration, and the limiting current at fixed catechol concentration increases with decreasing pH. These facts indicate that the preelectrochemical reaction is dissociation of a germanium(IV)-catechol complex involving protons. The relative stabilities of germanium(IV)-catechol complexes indicate that the complex undergoing dissociation is GeL_3^{2-} . For catechol concentrations of $2 \times 10^{-2} M$ and above, conversion of $\text{Ge}(\text{OH})_4$ to GeL_3^{2-} via eq 4 is driven essentially to completion above pH 3, and Bevilard⁹ has shown that intermediate complexes are not present in appreciable amounts. Limiting currents for this range of variables are given in the right-hand side of Figure 2, where the solid lines represent the currents calculated from χ as defined by eq 7. Observed and calculated currents

$$\chi = 3.0C_{\text{H}}C_{\text{H}_2\text{L}}^{-1/2} \quad (7)$$

generally agree within 15% or better except near pH 3 for a catechol concentration of $2 \times 10^{-2} M$, where the experimental current drops sharply below the calculated value. This deviation is attributed to the incomplete formation of GeL_3^{2-} under these conditions and is consistent with the value of the formation constant of GeL_3^{2-} . For the higher catechol concentrations, the experimental current near pH 3 is somewhat above the value calculated from eq 7. This deviation may represent the onset of an additional dissociation mecha-

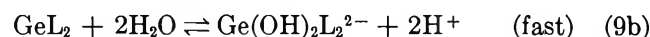
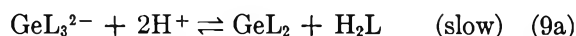
nism, but the data are insufficient for quantitative evaluation of this possibility.

Complex Dissociation Mechanism. Of the mechanisms consistent with χ as defined by eq 7, two appear to be relatively plausible in terms of kinetics. Both involve loss of a single catechol molecule from GeL_3^{2-} , and the resulting bis-catechol complexes differ only in respect to the number of coordinated hydroxide ions.

The first mechanism, in which the forward reaction is first order in hydrogen ion, is described by eq 8. Pro-



tonation of the complex and partial removal of one catechol group in the first step are followed by coordination of an hydroxide to Ge(IV) and protonation of the catechol anion to yield GeL_2OH^- . The second mechanism is second order in hydrogen ion in both forward and reverse directions and is described by eq 9.



Protonation and removal of catechol in the first step is followed by hydrolysis of GeL_2 to yield the bis-hydroxy complex $\text{Ge}(\text{OH})_2\text{L}_2^{2-}$. As with eq 6, the steps in eq 9 probably proceed in a stepwise manner. Hence, both eq 8 and eq 9 represent kinetically plausible mechanisms and the electroactive species may be either the mono-hydroxy complex GeOHL_2^- or the bis-hydroxy complex $\text{Ge}(\text{OH})_2\text{L}_2^{2-}$. Fortunately, the differences between the two electroactive species are minor and the major structural aspects of the electroactive species are clearly defined.

Adsorption Effects. Although neither the Koutecky analysis of the limiting current nor the dependence of the limiting current on the mercury column height gives any direct evidence of adsorptive processes, other studies indicate clearly that adsorption plays an important part in electrodeposition of Ge(IV) from acidic catechol solution. Through drop-time studies, Konopik¹⁵ has shown that germanium(IV)-catechol complexes are adsorbed at potentials less negative than $-1.4 V$ vs. sce. The desorption of complexed Ge(IV) at $-1.4 V$ vs. sce is reflected in the polarogram as a broad current minimum, an indication that adsorption of the electroactive species precedes electrodeposition. Adsorption of the electroactive species was confirmed by Kalvoda and Konopik⁸ by means of ac polarography and rapid-sweep voltammetry. Bard¹⁶ found that the polarogram of tin(IV) in acidic pyrogallol exhibits a broad minimum that is associated with desorption of

(14) J. Koutecky, *Collect. Czech. Chem. Commun.*, **19**, 1093 (1954).

(15) N. Konopik, *Monatsh. Chem.*, **92**, 8 (1961).

(16) A. J. Bard, *Anal. Chem.*, **34**, 266 (1962).

the electroactive pyrogallol complex. Adsorption of the electroactive complex is fast and equilibrium surface coverage is attained throughout the drop life. The strong similarity of the polarography of tin(IV) in pyrogallol to the polarography of Ge(IV) in catechol suggests that adsorption of germanium(IV)-catechol complexes is also very fast and this would explain the failure to detect adsorption control by varying the mercury column height. Because the rate of adsorption of the electroactive species is much faster than the rate of its formation, the rate of formation remains the current-controlling step. The failure to detect a significant influence of adsorption with changes in catechol concentration is puzzling, however, because Konopik¹⁵ has shown that catechol is strongly adsorbed at the mercury electrode. Adsorption of catechol would in general be expected to influence the rate of the preelectrochemical steps and the value of χ through the change in double-layer structure,¹⁷ but the influence of the catechol concentration on the rate of the preelectrochemical reaction agrees well with the Koutecky analysis which neglects adsorptive effects. Evidently, the net effect of adsorption on the rate of the overall electrode reaction must be relatively small.

The mechanistic significance of adsorption in the electrodeposition of germanium(IV)-catechol complexes is conjectural, but it appears that ligand bridging is probably not involved. Ligand bridging by hydroxide appears unlikely because the reduction of

Ge(OH)₄ is far less reversible than the reduction of the electroactive germanium(IV)-hydroxide-catechol complexes. The half-wave potential of the electroactive complexes varies from -0.4 to -0.7 V *vs. sce*, whereas the half-wave potential of Ge(OH)₄ is -1.6 V *vs. sce*. Participation by hydroxide as an effective bridge for reduction of germanium(IV)-catechol-hydroxide complexes is difficult to reconcile with the highly irreversible reduction of Ge(OH)₄. It is tempting to attribute ligand-bridging properties to catechol, but it is difficult to envision an efficient mechanism for charge transfer involving the delocalized π electrons.

The fact that only mixed catechol-hydroxide complexes are electroactive suggests that the coordination sphere as a whole may control electroactivity in a less direct manner than ligand bridging. Removal of the coordination sphere must make a major contribution to the activation energy for electrodeposition, and an inhomogeneous coordination sphere would be expected to facilitate concerted displacement. The labilization of one ligand by a second coordinated *trans* to the first, the so-called *trans* effect, is well established in homogeneous ligand-exchange reactions,¹⁸ and it is probable that such effects are important in electrode reactions of metal complexes also.

(17) P. Delahay, "Double Layer and Electrode Kinetics," Interscience Publishers, New York, N. Y., 1965, pp 207-208, 293-298.

(18) J. Lewis and R. G. Wilkins, "Modern Coordination Chemistry," Interscience Publishers, New York, N. Y., 1960, pp 133-140.

Adsorption of Blood Proteins on Metals Using Capacitance Techniques

by G. Stoner

Department of Materials Science, School of Engineering and Applied Science, University of Virginia, Charlottesville, Virginia 22901

and S. Srinivasan

Electrochemical and Biophysical Laboratories of the Vascular Surgical Services, Department of Surgery and Surgical Research, State University of New York, Downstate Medical Center, Brooklyn, New York 11203 (Received September 17, 1969)

A differential capacity method was applied to the measurement of adsorption of proteins on solid metal electrodes. The differential capacity is measured by observing the square-wave current output response of two working electrodes in series to a small triangular voltage input. The double-layer capacity is then recorded as a function of electrode potential by a slow potential scan input into the potentiostated circuit. Capacity curves are first compared on mercury, gold, and platinum in pure solutions with reported literature values obtained by electrocapillary and ac bridge techniques. The coverages (θ) of the amino acids glycine and tryptophan and the blood proteins fibrinogen, thrombin, and Hageman factor on mercury and platinum are then computed for various concentrations using the Frumkin equation, which relates θ to the measured capacity. Glycine and Hageman factor were found not to adsorb appreciably on mercury or platinum whereas tryptophan, fibrinogen, and thrombin all adsorbed appreciably on both mercury and platinum. The adsorption results on mercury are in agreement with previous work using electrocapillary methods.

Introduction

Over the last twenty years, considerable evidence has been accumulated to show that the interfacial reaction of thrombosis on the blood vessel wall and on prosthetic materials depends on the electrochemical characteristics of the solid-solution interface.¹⁻⁴ Thrombosis on conducting materials is found to be accelerated at potentials above 100 mV nhe and inhibited at negative potentials. This reaction is thus probably triggered by the interaction of one or more of the blood coagulation factors on the blood vessel wall or on the prosthetic materials at the more positive potentials. One of the characteristics of the adsorption of species on conducting surfaces from electrolytic solutions containing the adsorbates is its potential dependence. Thus, in the present work, the adsorption of some amino acids (the basic units of proteins) and some blood coagulation factors was determined on metal electrodes as a function of potential.

One of the methods of obtaining information on adsorption of species on electrodes is by a determination of the capacity at the metal-solution interface as a function of potential. Bridge methods have been mainly used for capacity measurements.⁵⁻⁷ While these methods have proved useful for a determination of the capacity on mercury, several problems have been encountered in the extension of these methods to solid electrodes, these include time and frequency variation of capacitance due to unevenness of surface, adsorption pseudo-capacity, dielectric relaxation, and impurities in solution and on the electrode.⁸ A sine-wave voltage, superimposed on a triangular potential sweep, coupled with an ac impedance bridge has been used by Breiter⁹ to

measure capacitance. Recently, Gileadi and Tshernikovski¹⁰ have developed an instrument for the measurement of capacities across solid electrode-solution interfaces. In this method, a *triangular wave* in which the frequency and amplitude could be varied is superimposed between two small electrodes which are maintained at the same dc potential, and the amplitude of the resulting square wave is a measure of the capacity across the solid-solution interface. Thus, by making the measurements with varying dc potentials of the test electrodes it is possible to obtain the capacity of the electrode as a function of potential.

The present work reports the following series of experiments, a few of which were carried out as a check of the method of Gileadi and Tshernikovski and the remainder of which were done with the purpose of obtaining adsorption characteristics of some amino acids and blood coagulation factors.

1. Determination of the capacity-potential relation

- (1) P. N. Sawyer, "Biophysical Mechanisms in Vascular Homeostasis and Intravascular Thrombosis," Appleton-Century-Crofts, New York, N. Y., 1965.
- (2) P. N. Sawyer and S. Srinivasan, *Amer. J. Surg.*, **114**, 42 (1967).
- (3) S. Srinivasan and P. N. Sawyer, *J. Advan. Med. Instrum.*, **3**, 116 (1969).
- (4) G. Stoner and L. Walker, *J. Biomed. Mat. Res.*, **3**, 645 (1969).
- (5) D. C. Grahame, *Chem. Rev.*, **41**, 441 (1947).
- (6) D. C. Grahame, *J. Amer. Chem. Soc.*, **63**, 1207 (1941); **68**, 301 (1946); **71**, 2975 (1949).
- (7) K. Muller, Ph.D. Thesis, University of Pennsylvania, 1965.
- (8) S. D. Argade and E. Gileadi, in "Electrosorption," E. Gileadi, Ed., Plenum Press, New York, N. Y., 1967, p 87.
- (9) M. W. Breiter, *Electrochim. Acta*, **7**, 533 (1962).
- (10) E. Gileadi, N. Tshernikovski, and V. Amdursky, Proceedings of 19th Meeting of C.I.T.C.E., Detroit, Mich., 1968.

on mercury electrodes in 0.1 *m* NaCl in 1 *N* NaOH for comparison of the results on the liquid metal with those of the classical work of Grahame,^{5,6} who used bridge techniques. Experiments were also carried out in 0.1 *N* HCl for which there are the recent data of Bockris, Gileadi, and Muller.⁷

2. Determination of the capacitance-potential relations on the solid metals: Au and Pt in 10^{-3} *M* HClO₄. These metals were selected because of the fact that it is possible to work on them over a wide range of potential in which there are no competing reactions such as hydrogen or oxygen adsorption, metal dissolution, etc. The HClO₄ electrolyte was chosen because there is the recent work of Argade⁸ which may be used for confirmatory purposes.

3. Determination of the capacitance-potential relations on Hg and on Pt in 0.1 *M* NaCl containing varying concentrations of tryptophan and glycine. The reason for selecting these amino acids is that they are basic amino acids in blood protein, and tryptophan is strongly adsorbing on mercury while glycine is not.¹¹ Hg is the simplest metal to work with and its surface is reproducible. Platinum was selected for the reason given above. In addition, the capacity measurements were made on mercury in 0.1 *M* NaCl solution containing fibrinogen, thrombin, and Hageman factor. These compounds are actively involved in the intrinsic blood coagulation sequence.¹² From the capacity-potential relations, the coverage-potential relations of the adsorbates tryptophan, fibrinogen, and thrombin were obtained, according to the theory of Frumkin.¹³

Experimental Section

1. *Electrical Components.* The capacity meter, designed and developed by Gileadi and Tshernikovski, has been adequately described in the literature.¹⁰ The measured capacity in the form of a square wave was monitored on a Tektronix 546 storage oscilloscope. The magnitude of the capacity was recorded as a function of potential on a Hewlett-Packard Model 2D X-Y recorder. The potential of the working electrodes was varied using an Elron CP-1 potentiostat and Elron CHP-1 function generator.

2. *Cells, Electrodes, and Solutions.* The present method is most accurate when the series (solution) resistance between the two working electrodes is very small. Thus the distance between the electrodes was kept at a minimum by using a Teflon disk containing two concentric mercury electrodes (Figure 1) or two sputtered film electrodes (Figure 2) in the case of solid metals.

In alkaline and neutral solution, calomel reference electrodes were used and in acid solutions with the solid metals, reversible hydrogen electrodes were used. The solutions were prepared with conductivity water ($\rho > 2 \times 10^6$) and reagent grade chemicals. The mercury was triple distilled (Bethlehem Instruments) and the sput-

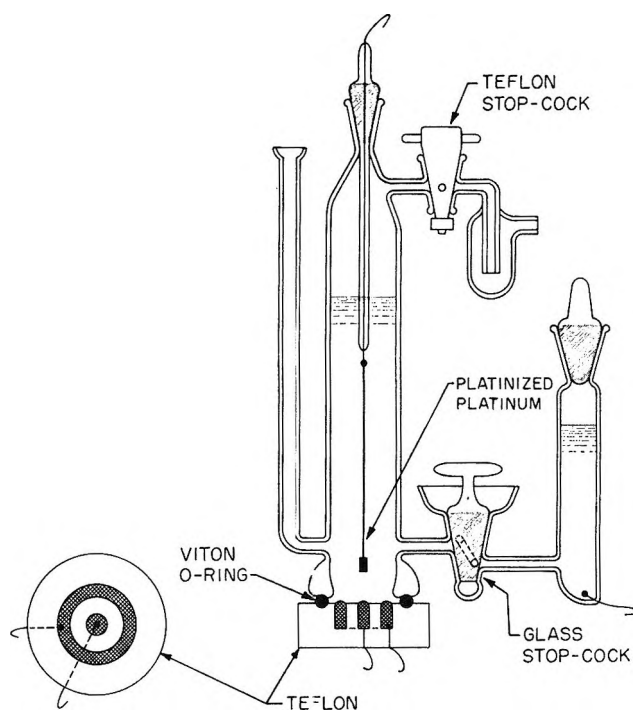


Figure 1. Cell for measurement of differential capacity on mercury.

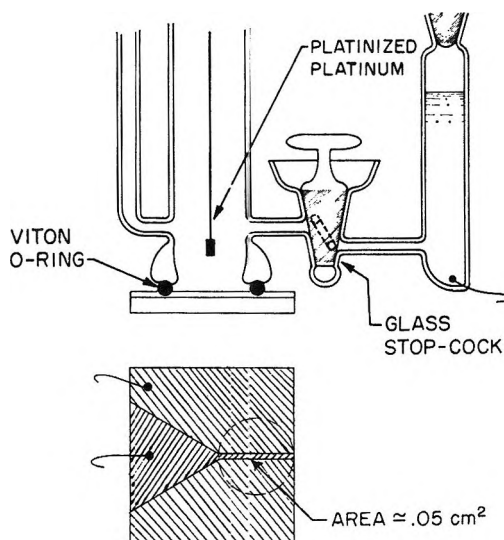


Figure 2. Cell for measurement of differential capacity on solid metals.

tered electrodes were prepared in a manner described elsewhere.¹⁴ Solutions of the protein fibrinogen and Hageman factor were prepared as described elsewhere.^{4,14} Pure bovine thrombin was obtained through the courtesy of W. Seegers.

(11) G. Stoner, *J. Biomed. Mat. Res.*, **3**, (1969).

(12) W. Seegers, "Blood Clotting Enzymology," Academic Press, New York, N. Y., 1967.

(13) A. N. Frumkin and B. B. Damaskin, "Modern Aspects of Electrochemistry," No. 3, J. O'M. Bockris and B. E. Conway, Ed., Butterworth and Co. Ltd., London, 1964.

(14) J. O'M. Bockris, B. D. Calan, and G. E. Stoner, *Chem. Inst.*, **1**, 273 (1969).

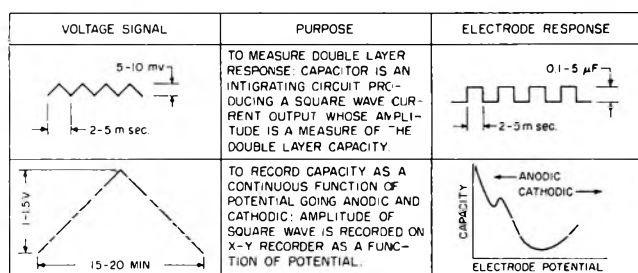


Figure 3. Schematic of potential sequence in capacity measurements.

3. *Procedure.* The capacity was recorded in the anodic and cathodic branches of a slow triangular potential scan and the criteria for an acceptable measurement were (i) suitable square wave form was obtained by varying the frequency of the triangular wave input; (ii) the lack of any hysteresis in the recorded capacity in the anodic and cathodic branches of the curve was achieved by reducing the overall scan rate to about 10^{-3} V/sec. (Since the low range of the Elron instrument is 10^{-2} V/sec, a 1/10 potential divider was used across the input of the potentiostat.) These procedures are illustrated in Figure 3.

Results

1. *Comparison with Other Methods.* (i) *Measurements on Mercury.* Capacity-potential curves in 0.1 M NaCl and 1 M NaOH are compared with the work of Grahame^{5,6} in Figure 4 and for 0.1 M HCl with Muller⁷ in Figure 5. The above authors used ac bridge and electrocapillary methods.

(ii) *Measurements on Solid Metals.* Figures 6 and 7 compare the respective capacity values on platinum and gold (in the neighborhood of the potential of zero charge) with the ac bridge work of Argade⁸ in dilute HClO₄ solutions. The values of the capacity are higher

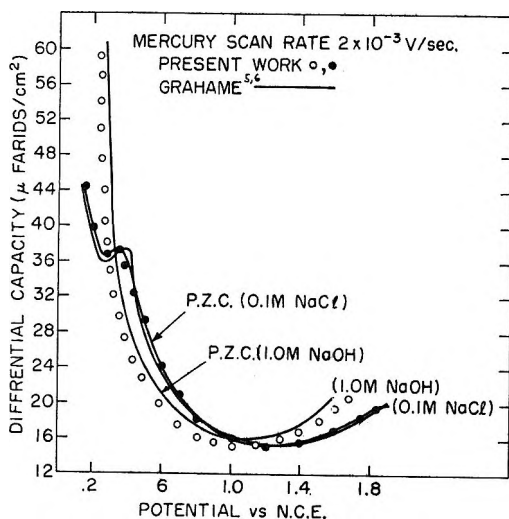


Figure 4. Capacity as a function of electrode potential in 1 M NaOH and 0.1 M NaCl on mercury.

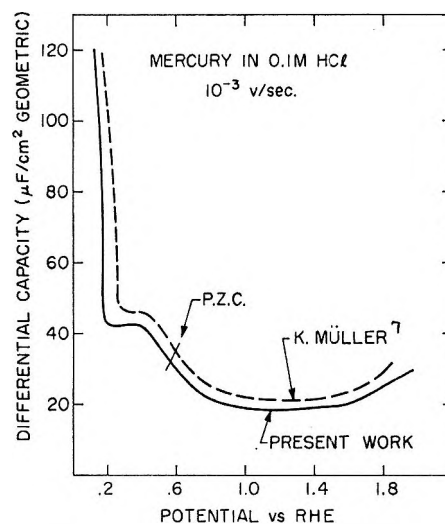


Figure 5. Capacity as a function of electrode potential in 0.1 M HCl on mercury.

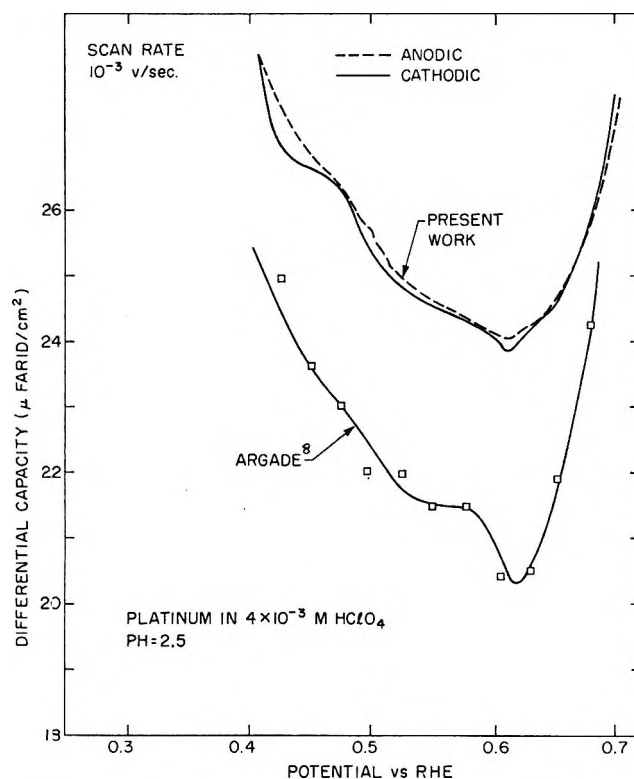


Figure 6. Capacity as a function of electrode potential in dilute HClO₄ solutions on platinum.

in the present work (probably due to differences in absolute electrode area or roughness factor); however, the shape of the curves and the characteristic minima are comparable.

2. *Effect of Various Blood Proteins and Relevant Amino Acids on Capacity-Potential Curves.* (i) *Measurements on Mercury.* Capacity-potential curves are shown in Figure 8 for the amino acids glycine and tryptophan. Figure 9 shows the effect of the protein thrombin.

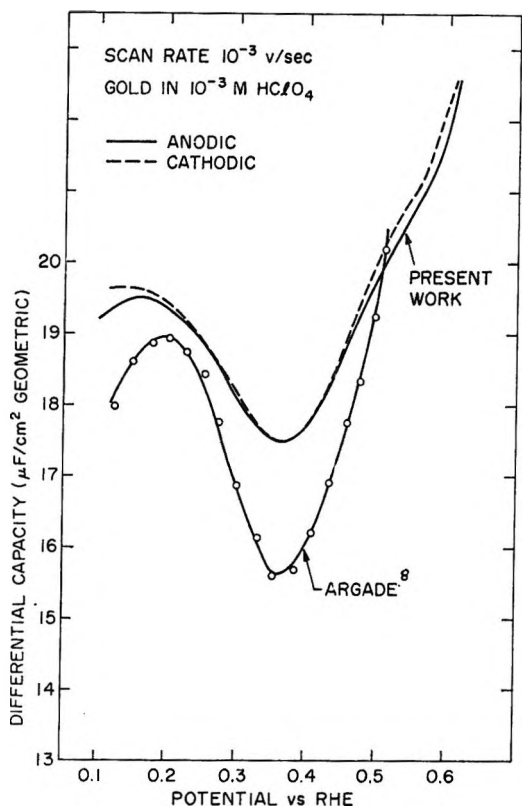


Figure 7. Capacity as a function of electrode potential in dilute HClO₄ solutions on gold.

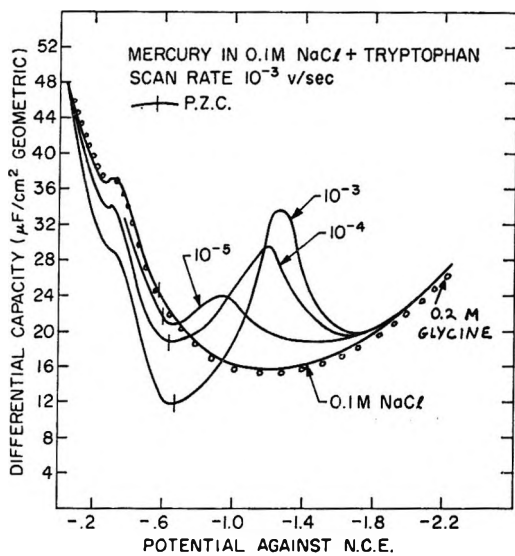


Figure 8. Capacity as a function of potential in glycine and various concentrations of tryptophan on mercury.

(ii) *Measurements on Platinum.* Capacity-potential curves for glycine and various concentrations of tryptophan are given in Figure 10. The effects of two proteins which are active in the blood clotting sequence, fibrinogen and thrombin, on the differential capacity are shown in Figures 11 and 12. Four concentrations (0.1, 1, 10, and 100 times physiological concentration) of

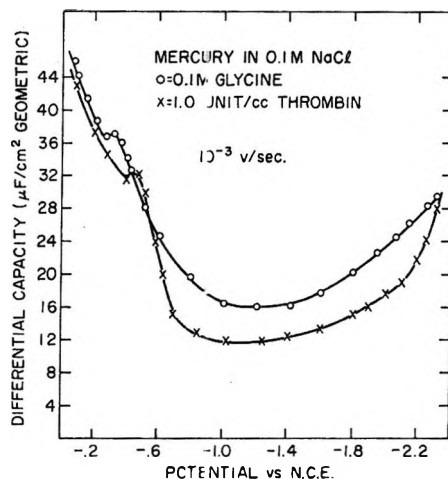


Figure 9. Capacity as a function of potential in solutions of thrombin on mercury.

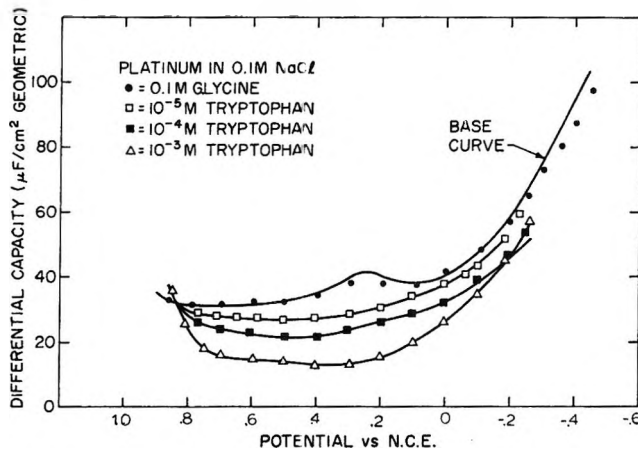


Figure 10. Capacity as a function of potential in various concentrations of tryptophan on platinum.

a third blood protein, Hageman factor (Factor XII), did not lower the base (0.1 M NaCl) curve.

Discussion

1. *Evidence for Using Technique of Gileadi and Tshernikovski for Measurements of Double-Layer Capacities on Metals in Solution.* (i) *Experiments on Mercury.* Extensive work has been done on this metal using bridge techniques.^{5,6} The present measurements of the capacity as a function of potential in 1 M NaOH, 0.1 M NaCl, and 0.1 M HCl (Figures 4 and 5) are in good agreement with the corresponding C-V relations obtained by other investigators using bridge techniques. This agreement lends considerable support to the method of Gileadi and Tshernikovski, whose technique has several advantages over the bridge technique in that (a) the method is simple and more rapid; (b) the capacity is readily recorded while the potential is varied linearly with time at any desired rate; in this way by choosing the appropriate sweep rate, the effect of impurities in solution could be minimized; (c) the method can be used both on liquid

and solid metals; and (d) bridge methods are for bridge techniques; it is necessary to use very small electrodes. Though in the present method there are advantages of small electrodes, measurements are still possible on electrodes of large areas.

(ii) *Experiments on Gold and Platinum.* The present results on platinum and on gold in HClO_4 are comparable with those of earlier work using bridge techniques. However, one observes a shift in the C - V curves of the present work. Higher capacities, recorded at any potential in this work, may be due to the differences in the roughness factors of the electrodes—the capacities are represented per unit geometric area of the test electrode.

2. *Method for the Calculation of the Coverage of Proteins as a Function of Potential from the Capacity-Potential Plots.* There are two possible approaches to obtaining information on coverage as a function of potential from the capacity-potential plots. In one, which is a tedious procedure but perhaps more accurate, the C - V curve is integrated twice with respect to the potential (which gives a plot of the surface tension *vs.* potential) followed by a differentiation of the surface tension with respect to the activity of the component whose adsorption behavior is to be ascertained. For this method, it is necessary to know the potential of zero charge (which is necessary to obtain the constant of integration of C *vs.* V) and also the surface tension at any one potential which is necessary to evaluate the second integration constant. These constants are not readily available. Thus, the alternative method was chosen to obtain the coverages of the proteins as a function of potential of the test electrode. Here, the empirical equation proposed by Frumkin¹³

$$C_\theta = C_0(1 - \theta) + \theta C_{\theta=1}$$

which relates the measured capacity C_θ to the degree of coverage (θ) is used. C_0 and $C_{\theta=1}$ represent the capacities when $\theta = 0$ and $\theta = 1$, respectively. Though this equation is approximate, it has proved to be valid in the determination of adsorption of methanol on platinum from capacity measurements; there was good agreement in the coverage-potentials relations using this method and a transient technique.¹⁵ In order that this equation may be applied it is necessary to know C_0 and $C_{\theta=1}$. The first, C_0 , is obtained from the capacity-potential relations in control solutions with no adsorbate. To obtain $C_{\theta=1}$ it is necessary to carry out the C - V measurements varying the concentration of adsorbate in solution and make the assumption the $C_{\theta=1}$ is the value of the minimum capacity for the highest concentration of adsorbate in solution. Generally one may observe a plateau in the region corresponding to the capacitance minimum (Figures 9-12). In the case of highly adsorbable materials, the minimum of the C - V plots may occur at fairly low concentrations. A problem with this method will be encountered if the capacity

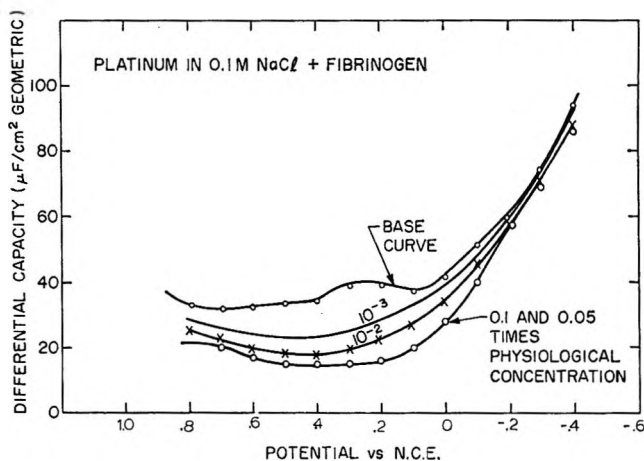


Figure 11. Capacity as a function of potential for various concentrations of fibrinogen on platinum.

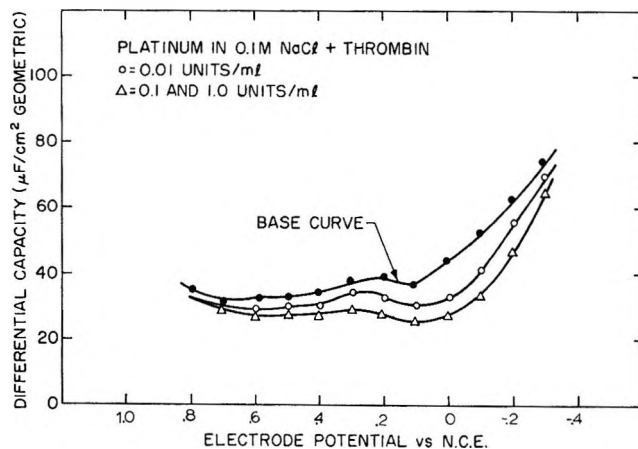


Figure 12. Capacity as a function of potential in solutions of thrombin on platinum.

in the presence of the adsorbate exceeds that on the absence of the adsorbate over certain potential regions. In the present work, this was found only on mercury in solution containing tryptophan at fairly anodic and cathodic potentials. Even in these cases, it is possible to obtain coverage information in the region where this anomaly does not exist.

3. *Adsorption Characteristics of Tryptophan on Mercury and on Platinum.* Due to the fact that the capacity-potential curves on mercury in 0.1 M NaCl containing tryptophan (in varying concentration) intersects the control C - V curve (with no tryptophan), it is possible to determine the θ - V relation only over a short potential region (Figure 13). The adsorption at any potential is markedly dependent on concentration. There is a steep fall in the coverage at highly anodic potentials. The adsorption maximum for 10^{-3} M concentration of tryptophan in solution occurs at a potential of ~ 0 V *vs.* sce.

(15) M. W. Breiter, *Electrochem. Acta*, **7**, 533 (1962).

The adsorption of tryptophan on platinum from 0.1 M NaCl solution containing varying concentrations of tryptophan shows the typical type of parabolic θ -V behavior¹⁶ for organic compounds on solid electrode

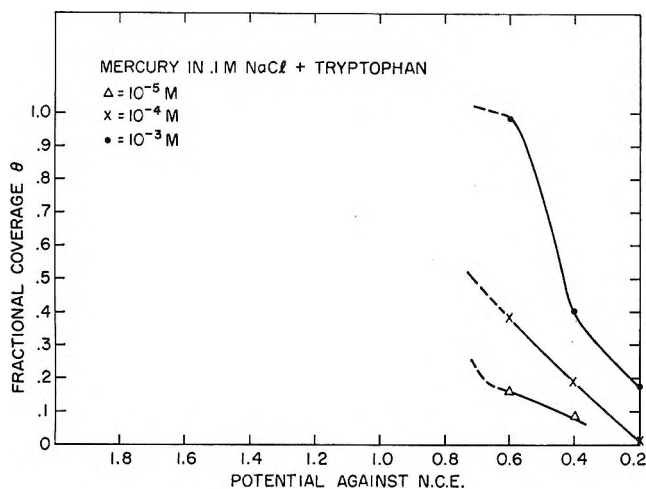


Figure 13. Fractional coverage of tryptophan as a function of potential on mercury.

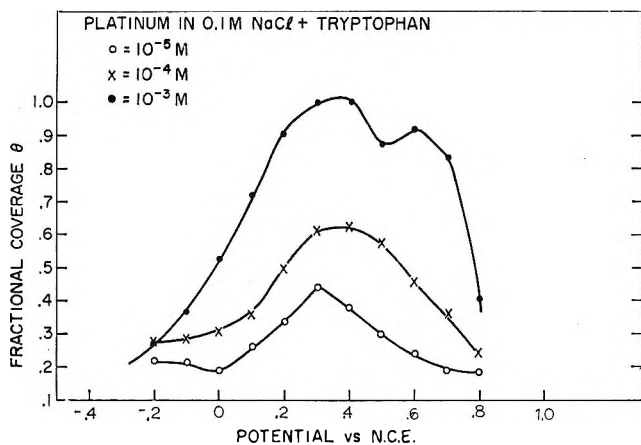


Figure 14. Fractional coverage of tryptophan as a function of potential on platinum.

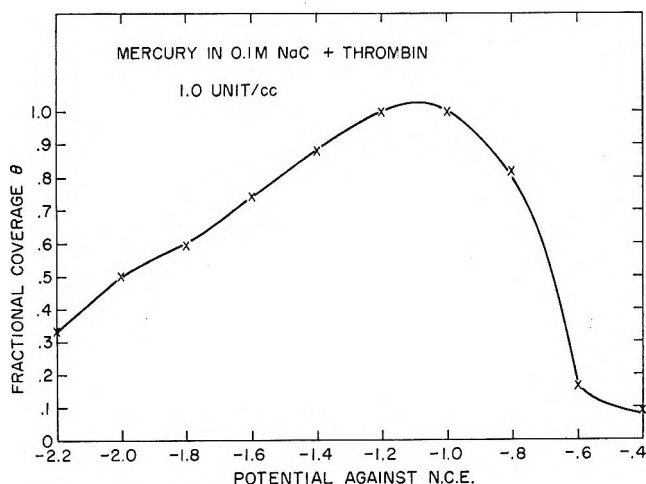


Figure 15. Fractional coverage of thrombin as a function of potential on mercury.

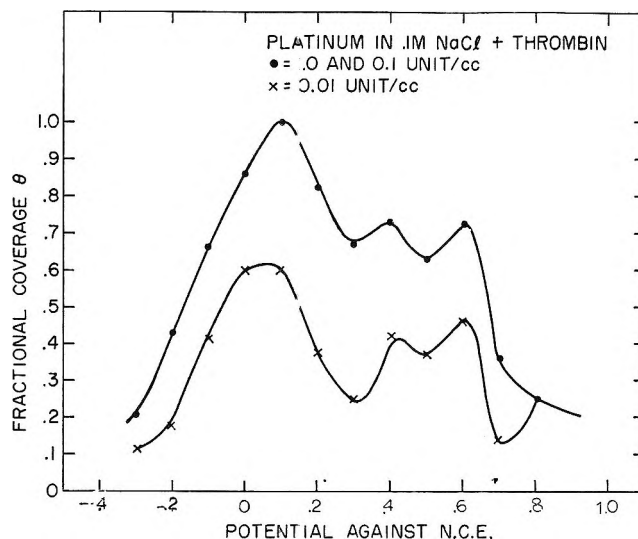


Figure 16. Fractional coverage of thrombin as a function of potential on platinum.

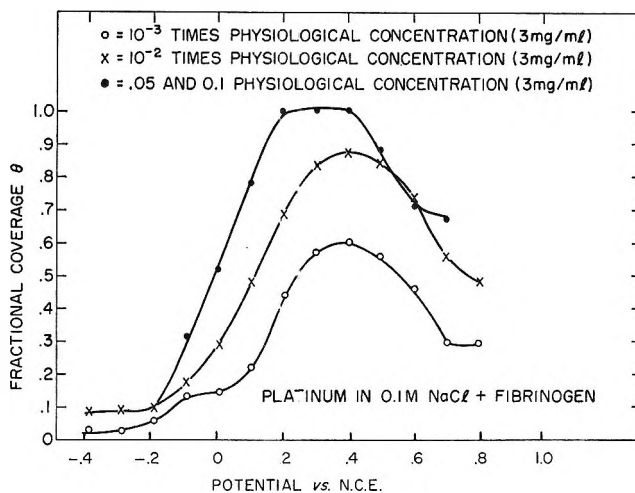


Figure 17. Fractional coverage of fibrinogen as a function of potential on platinum.

(Figure 14). There is again a marked concentration dependence of adsorption. There appears to be no shift in the potential of maximum adsorption (~ 0 V vs. sce) with concentration of tryptophan. As on mercury, there is strong adsorption of tryptophan on platinum.

4. Adsorption of Thrombin on Mercury and on Platinum. Only one concentration of thrombin was used in the studies on mercury. The assumption was made that the coverage is unity in the minimum of the C-V relation on mercury in 0.1 M NaCl at this concentration of thrombin. The results show that there is a significant adsorption of thrombin over a considerable range of potential (Figure 15). The adsorption maximum is quite cathodic (-1.1 V vs. sce). The results of this work are in fair agreement with coverage data obtained from electrocapillary data.¹¹

(16) E. Gileadi, B. T. Rubin, and J. O'M. Bockris, *J. Phys. Chem.*, **69**, 3335 (1965).

The shapes of the coverage-potential relations for thrombin in Pt show an unusual type of behavior—more than one maximum (Figure 16). Evidence was obtained for full coverage here at the highest peak because the same minimum capacity was obtained for the two higher concentrations of thrombin in solution. There is no shift in the position of the maximum with change of concentrations of thrombin in solution. The potential at the highest peak is about 0.1 V *vs.* sce. The region of adsorption is quite extensive (~ 1 V).

5. *Adsorption of Fibrinogen on Platinum.* Fibrinogen plays an important role in the clotting mechanism.¹⁷ Its adsorption is quite strong even at concentrations which are less than physiological (maximum adsorption is observed at 0.05–0.1 of physiological concentrations). Parabolic θ - V relations are obtained (Figure 17). The potential of maximum adsorption appears to be independent of concentration and has a value of about 0.4 V. Adsorption is significant even at low concentrations of fibrinogen over a potential range of nearly 1 V. The fall in adsorption at potentials cathodic to the potential of maximum adsorption (V_m) is steeper than that at potentials anodic to V_m .

6. *Nonadsorbability of Hageman Factor.* It is interesting to note that the capacity-potential relation on platinum is identical in the presence and in the absence of Hageman factor, which is the blood component initiating the blood coagulation mechanism. This important result indicates that Hageman factor does not trigger the reaction by an adsorption mechanism. This was confirmed by electrocapillary measurements on mercury in 0.1 M NaCl with and without Hageman factor in solution.

Conclusions

The following conclusions may be reached from the present work. (i) The capacitance meter developed by Gileadi and Tshernikovski is a satisfactory instrument for capacity measurements on mercury and on solid metals. (ii) Tryptophan adsorbs strongly on mercury as well as on platinum. The coverage potential relations are quasi-parabolic. (iii) The coverage-potential relations of thrombin on platinum show more than one maximum. Thrombin is also a strongly adsorbing compound, though at more negative potentials. (iv) Fibrinogen shows the adsorption characteristics of simple organic compounds (*e.g.*, hydrocarbons, alcohols). Maximum adsorption occurs at a potential of 0.4 V *vs.* sce. (v) Hageman factor does not adsorb on mercury or platinum. It is possibly activated by a collision with surfaces of certain (positive)¹⁸ charge characteristics.

Acknowledgments. The authors wish to thank Professors A. Catlin, E. Gileadi, and P. N. Sawyer for valuable discussions, suggestions, and encouragement of this work. Financial support from the National Institute of Dental Research, Grant DE-2111-05 (for G. S.) and from the Artificial Heart Program, National Heart Institute, National Institutes of Health, Contract No. PH43-68-75 (for S. S.) is gratefully acknowledged. S. S. is the recipient of a Career Scientist Award from the Health Research Council, City of New York, Contract No. I 542.

(17) K. Laki, "Fibrinogen," Marcel Dekker, Inc., New York, N. Y., 1968.

(18) L. Vroman, *Thromb. Diath. Haemorrhag.*, **10**, 445 (1963).

Electrical Conductivity of the Nickel Oxide- α -Ferric Oxide System

by Jae Shi Choi and Ki Hyun Yoon

Department of Chemistry, Yonsei University, Seoul, Korea (Received August 4, 1969)

The electrical conductivity of polycrystalline samples of the NiO- α -Fe₂O₃ system containing 2.1, 4.2, 8.2, 10, 19.2, 34.8, and 41.6 mol % of NiO has been measured in the temperature range of 400 to 1100° under oxygen pressures from 1.12×10^{-6} to 152 mm, using a new contact method which has been devised in this laboratory. It was found that, for a given temperature, the slope of log conductivity vs. mole per cent of NiO is negative up to a certain mole per cent of added NiO, becoming positive for further increase in NiO concentration. This inversion point was found to move toward higher values of NiO concentration at higher temperatures. This is explained according to the controlled valency principle. The variation of conductivity with temperature is described. Fermi degeneracy is found to occur above about 34.8 mol % of the added NiO.

Introduction

A quantitative investigation of the electrical conductivity of NiO- α -Fe₂O₃ system has not been published since 1960, when Lord and Parker¹ reported on the electrical resistivity of nickel ferrite. Their experimental results were limited to the investigation of the influence of oxygen pressures on the electrical properties of this material.

This investigation has been undertaken to determine the inversion point (decrease to increase) of the electrical conductivity of NiO- α -Fe₂O₃ as a function of the amount of added NiO by analyzing the results of conductivity measurements made over a range of oxygen partial pressures on samples of varying relative composition. It is generally believed that the conductivity of a semiconducting oxide can be shifted in the direction of increased P conductivity or decreased N conductivity by doping small proportions of lower valency cations and that the reverse is true for higher valency cation doping. Because the only necessary conditions for the doping effect are solubility in the solid state and a similarity of cation radii, the electrical properties of the NiO- α -Fe₂O₃ system seem to be similar to that of ZnO² doped Li₂O. The electrical conductivity of the NiO- α -Fe₂O₃ system depends on temperature and the ambient oxygen pressure in the sintering process. In these measurements, thermal hysteresis was negligible. Since electrical conductivity has been correlated with defect structure, the influence of oxygen pressure of the sintering process in the preparation of the spinel NiO- α -Fe₂O₃ system is important. With high oxygen pressure during sintering, the NiO- α -Fe₂O₃ system turns to a P type semiconductor and under low oxygen pressure it converts to an N type.¹ The explanation of the conduction mechanism is given by applying the principle of controlled valency.³⁻⁶

Sample Preparation

Specpure NiO powder from Johnson Matthey Co. and α -Fe₂O₃, which was prepared from chemically pure

FeCl₂ and KOH by the wet method according to the procedure of Balz,⁷ were used for the preparation of NiO- α -Fe₂O₃. The sample was identified as α -Fe₂O₃ by X-ray diffraction.

NiO and α -Fe₂O₃ were weighed precisely, mixed in varying proportions, ball-milled for 15 hr in a C₂H₅OH solution, and then dried at 150°. Three grams of the powder mixture was made into a pellet containing four Pt leads (length 10 mm, radius 0.04 mm) with 0.6 g of powder between leads under a pressure of 2 tons/cm². This pellet was presintered for 3 hr at 800° and then sintered for 3 hr at 1200° under oxygen pressure and then cooled rapidly.

A difficult problem in the measurement of electrical conductivity is the contact method. In this laboratory, the 4 Pt leads were inserted into the NiO- α -Fe₂O₃ powder at equal intervals and the combination compressed under high pressure and sintered to allow interdiffusion of both cations. By this method, contact resistance is kept constant with temperature change and good contact between the four Pt leads and sample is maintained.

Experimental Section

The experimental apparatus used is shown in Figure 1. The vacuum system was connected to a Cenco Hyvac force pump through an EC GF-20A oil diffusion pump. The pressure was measurable down to 10^{-6} - 10^{-6} mm. Among the four Pt leads which were in contact with the sample, the two inside leads were connected to a battery through an ammeter. Before the sample was inserted, it was first polished with abrasive

- (1) H. Lord and R. Parker, *Nature*, **188**, 929 (1960).
- (2) K. Hauße and A. L. Vierk, *Z. Phys. Chem.*, **196**, 160 (1950).
- (3) W. Schottky, *ibid.*, **B29**, 33f (1935).
- (4) C. Wagner, and W. Schottky, *ibid.*, **B11**, 163 (1930).
- (5) E. J. W. Verwey, P. W. Haaijman, F. C. Romeijn, and C. W. Van Oosterhout, *Philips Research Repts.*, **5**, 173 (1950).
- (6) G. Brouwer, *ibid.*, **9**, 366 (1954).
- (7) W. Balz, *Badische Anilin and Soda Fabric., Fr.* **1**, 357, 866 (1964).

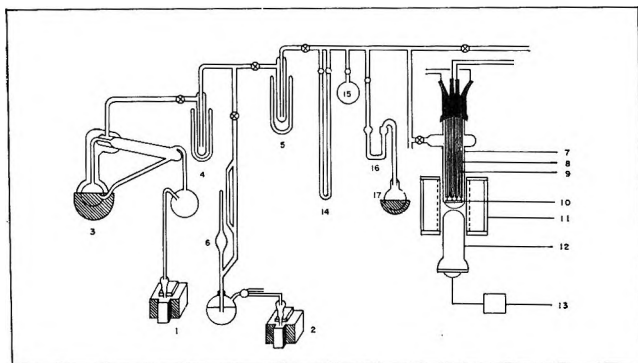


Figure 1. Schematic drawing of the furnace assembly and vacuum system: 1, 2, rotary pumps; 3, diffusion pump; 4, 5, Dry Ice traps; 6, McLeod gauge; 7, quartz tube; 8, Vycor tube; 9, Pt lead; 10, NiO- α -Fe₂O₃ sample; 11, furnace; 12, Pt-Rh thermocouple; 13, ammeter; 14, manometer; 15, O₂ storage tank; 16, CaCl₂ tube; 17, KClO₃ flask.

paper of silicon carbide, etched in dilute HNO₃, washed with distilled water, dried, and connected to the Pt leads of the sample container. When the temperature and the oxygen pressure were adjusted to the desired values, the stopcock which connected the vacuum system and sample container was closed. After 1 hr of annealing,⁸ the temperature was raised by increments of 20°. The dc current in the sample was measured with a Hewlett-Packard dc microvolt ammeter and the dc voltage was measured with a Leeds & Northrup K-2 potentiometer. The galvanometer used was a Leeds & Northrup Type E galvanometer whose sensitivity is 0.005 μ A/mm. The current in the sample was kept below 1.5 mA.⁹ Typical analyses of these samples show that they contain 40 ppm, mainly Cu, Si, Al, and Pb.

Experimental Results

The results of the electrical conductivity measurements are shown in Figure 2. Log conductivity for seven different samples is plotted *vs.* the reciprocal of absolute temperature. We may note that for every curve a straight line is obtained. The slope is negative and its value depends on the concentration of NiO. From samples 1 to 4 the slope becomes more negative, while at higher concentrations of NiO the curves become almost flat, showing that the temperature dependence becomes less for higher concentrations of NiO.

The electrical conductivity isotherms of various compositions in NiO- α -Fe₂O₃ systems are presented in Figure 3. The clusters of points show conductivity values at the same temperature under the different oxygen pressures for the same sample.

Figure 4 shows the results of isobarics in which log σ is plotted against $1/T$. At high temperatures there is little variation in the value of log σ over the whole pressure range. As seen already in Figure 4, noting points falling on the same position indicate that the

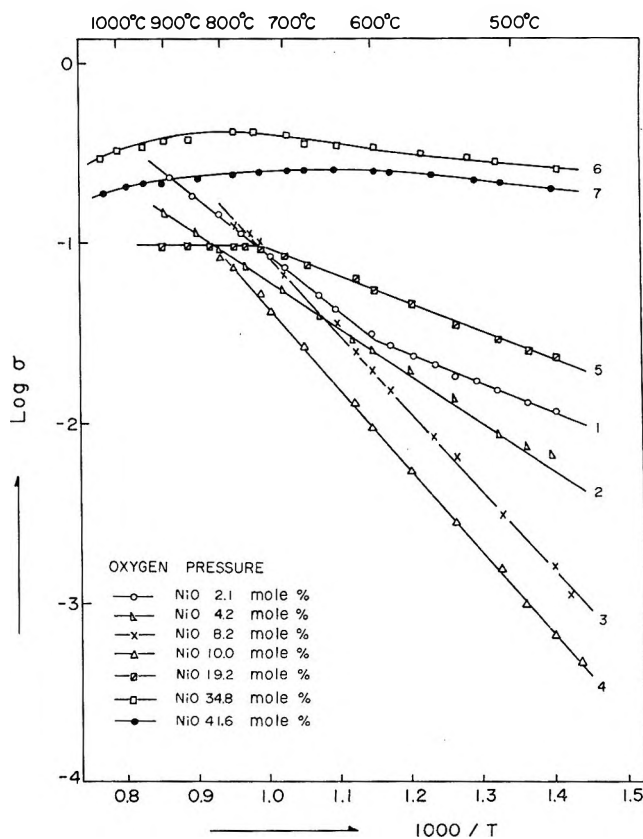
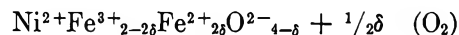


Figure 2. Representative temperature dependence of conductivity of composition in the system NiO- α -Fe₂O₃.

conductivity is nearly independent of the ambient oxygen pressure.

Discussion

Since the sintering was done under low oxygen pressure (152 mm) the excess Ni³⁺ ions, which were dissolved in the NiO- α -Fe₂O₃ lattice, were reduced completely to Ni²⁺ ions and the electrons which were released from the oxygen reduced the Fe³⁺ ions to Fe²⁺ ions; Fe³⁺ + e \rightarrow Fe²⁺. This may be represented by¹



Thus the electrons function as the carriers. Also thermoelectric power showed that all samples had negative Seebeck coefficients. Therefore, as shown in Figure 4, the electrical conductivity is not affected by the partial oxygen pressure regardless of the doped NiO mole percentage. As shown in Figure 3 the increase in the amount of the doped NiO, according to the principle of controlled valency, prevents the process Fe³⁺ + e \rightarrow Fe²⁺ conduction mechanism of the NiO- α -Fe₂O₃ system. Because the number of conduc-

(8) R. S. Toth, R. Kilson, and D. Trivich, *J. Appl. Phys.*, **31**, 1117 (1960).

(9) W. J. Moore, "Physical Chemistry," Prentice-Hall, Inc., Englewood Cliffs, N. J., 1962.

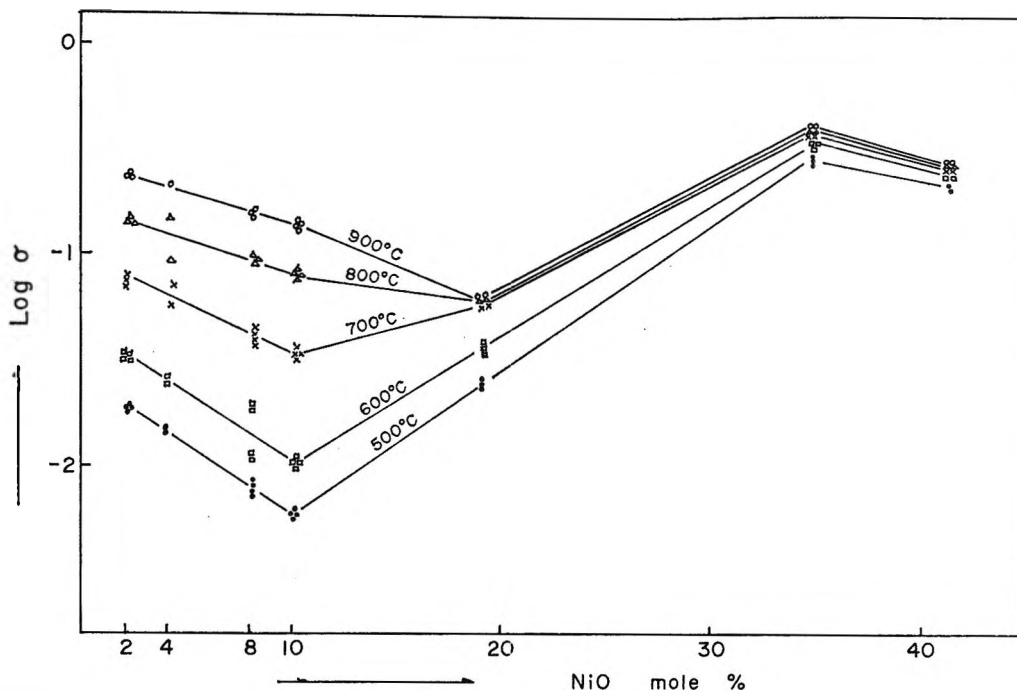


Figure 3. Values of conductivity of NiO- α -Fe₂O₃ as the function of the amount of NiO added. Clusters of points show conductivity values measured at different oxygen pressure for the same sample.

tion electrons is decreased, the electrical conductivity is decreased. In the NiO- α -Fe₂O₃ system, when the amount of doped NiO is increased to more than about 10 mol %, the conductivity increases due to the in-

creasing positive holes arising from Ni³⁺ ions dissolved in the NiO- α -Fe₂O₃ lattice through an excess amount of nickel oxide. In other words, the concentration carrier in the NiO concentration region then mostly converts to positive holes due to the excess NiO. As a result, the electrical conductivity increases due to the increasing doped nickel oxide in the NiO- α -Fe₂O₃ system.

With increasing temperature, independent of oxygen pressure, the inversion point (decrease to increase) of the electrical conductivity shows a tendency to move in the direction of increasing mole percentage of nickel oxide. The reason, in general, is that when α -Fe₂O₃ is in its pure state, it begins to reduce. Fe³⁺ + e → Fe²⁺, at 1388°;¹⁰ but in the case of the ferrite, it reduces at a rather lower temperature and the amount of Fe²⁺ increases in proportion to the increases of temperature. Therefore the initial slope of conductivity vs. NiO concentration is shallower at high temperatures (cf. Figure 3). Furthermore, according to the controlled valency principle, more electrons occur by the process Fe³⁺ + e → Fe²⁺ as the temperature increases, requiring additional Ni²⁺ ions, so the inversion point moves to the right.

The decrease of conductivity above around 34.8 mol % of added NiO is not clear.

In Figure 2, sample 1 shows that the inversion point appears around 600°. Above this temperature range the intrinsic conductivity of α -Fe₂O₃ appears rather than the impurity (NiO) effect. Below this temperature

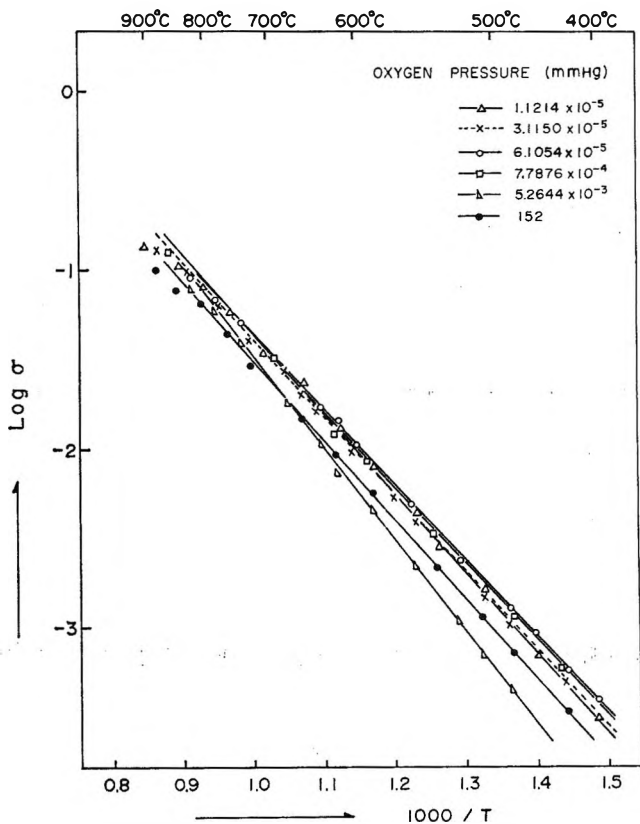


Figure 4. Conductivity isobars of NiO- α -Fe₂O₃ as a function of 10³/T. Sample: 10 mol % of NiO doped α -Fe₂O₃.

(10) R. G. Richard and J. White, *Trans. Brit. Ceram. Soc.*, 53, 233 (1954).

range it becomes an extrinsic semiconductor because of the doped NiO. Therefore it does not satisfy the general semiconductor equation, $\sigma = Ae^{-E/RT}$,¹¹ but shows a higher electrical conductivity. Sample 6 and 7, which show little change in conductivity over the temperature range 400–900°, show Fermi degeneracy because of a very high concentration of nickel oxide and conduction electrons in the system of NiO- α -Fe₂O₃. Above 900° the carrier concentration is constant because of the complete ionization of the donors; on the other hand the mobility of the carriers decreases with rising temperature due to the "impurity scattering"¹² because of the excess nickel oxide. Therefore the electrical conductivity is reduced.

The values of the electrical conductivity measured both as the temperature was raised and lowered are similar. Therefore the sample was in a state of thermal equilibrium at the moment of measurement. It appears that the new contact method devised in this laboratory is satisfactory.

Acknowledgment. The authors are grateful to the Graduate School of Yonsei University and Ministry of Science and Technology of Korea for support of the experimental work.

(11) L. G. Uitert, *J. Chem. Phys.*, **23**, 1883 (1955).

(12) N. B. Hannay, "Semiconductors," Reinhold Publishing Corp. New York, N. Y., 1959.

Electron Paramagnetic Resonance Studies of Silver Atom Formation and Enhancement by Fluoride Ions in γ -Irradiated Frozen Silver Nitrate Solutions

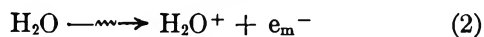
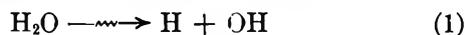
by Barney L. Bales¹ and Larry Kevan²

Department of Physics and Department of Chemistry, University of Kansas, Lawrence, Kansas 66044
(Received July 14, 1969)

The γ radiolysis of AgNO₃ ices at 77°K produces trapped Ag⁰, OH, and NO₂. Addition of fluoride ion increases Ag⁰, prevents NO₂ formation, increases the total number of observable spins, and increases the linear range of the dose-yield curve for Ag⁰. The initial Ag⁰ yields are $G(\text{Ag}^0) = 1.2$ in 1 M AgNO₃ and $G(\text{Ag}^0) = 3.2$ in 1 M AgNO₃-0.5 M KF. These effects indicate that fluoride ion acts as an efficient hole trap for H₂O⁺ and prevents electron-hole recombination. Low fluoride concentrations are effective; thus some H₂O⁺ is mobile.

Introduction

The radiolysis of ice has been the subject of much research³ and is understood in terms of the initial reaction scheme given in (1) and (2). The details of the



fate of the electron and the hole depend on the nature of the solutes present in the ice and, to some extent, on the phase of the ice.⁴ Shields⁵ and Zhitnikov and Orbeli⁶ have shown that γ -irradiated silver salt solutions at 77°K yield silver atoms which were attributed^{5,7} to the electron-capture reaction



The epr spectra of Ag⁰ were analyzed, but no quantita-

tive data on yields or on the reactions occurring in the frozen system were reported. One interesting observation was that fluoride ion enhanced the yield of Ag⁰ in the irradiated silver salt ices. Shields⁵ inferred that fluoride ion "promotes" the reactivity of electrons with

(1) Department of Physics.

(2) Department of Chemistry. Address inquiries to this author at Department of Chemistry, Wayne State University, Detroit, Mich. 48202.

(3) L. Kevan in "Radiation Chemistry of Aqueous Systems," G. Stein, Ed., Interscience Division, John Wiley & Sons, Inc., New York, N. Y., 1968, pp 21-72.

(4) H. Hase and L. Kevan, *J. Phys. Chem.*, **73**, 3290 (1969).

(5) L. Shields, *J. Chem. Phys.*, **44**, 1685 (1966); *Trans. Faraday Soc.*, **62**, 1042 (1966); L. Shields and M. C. R. Symons, *Mol. Phys.*, **11**, 57 (1966).

(6) R. A. Zhitnikov and A. L. Orbeli, *Fiz. Tverd. Tela.*, **7**, 1929 (1965); *Sov. Phys. Solid State*, **7**, 1559 (1966).

(7) B. L. Bales and L. Kevan, *Chem. Phys. Lett.*, **3**, 484 (1969).

Ag^+ but did not suggest a mechanism. In this work we investigate the radiation chemistry of AgNO_3 frozen solutions and the mechanisms which lead to Ag^0 and its enhancement by fluoride ion. The relative radical yields and the magnitude of the fluoride effect change drastically with dose. The fluoride effect can be explained by hole trapping by fluoride to prevent electron-hole recombination.

Experimental Section

Reagent grade chemicals and triple-distilled water were used to prepare the solutions. Concentrations were determined by the solute weight. Nondegassed solutions were used since degassing of solutions had no effect on the radical yields measured in the solid state. Drops containing $5 \mu\text{l}$ of solution were dropped directly into liquid nitrogen in which they rapidly froze to form opaque, spherical samples. Because of their opacity the samples were considered to be largely polycrystalline. This type of sample preparation avoids the use of any irradiation cells which could contribute impurities and background epr signals. In order to have maximum sensitivity, 8–12 spherical samples were irradiated and measured as a single sample. The samples were immersed in liquid nitrogen and were irradiated in the dark in a cobalt-60 γ irradiator at a dose rate of 0.4 Mrad/hr. The dose rate was measured by ferrous sulfate dosimetry using $G(\text{Fe}^{+3}) = 15.5$.

After irradiation, the samples were poured into a quartz epr insertion-type dewar together with liquid nitrogen thus keeping the sample temperature at 77°K . Helium gas was bubbled through the liquid nitrogen in the dewar above the microwave cavity to eliminate bubbling within the cavity which is a source of noise. A Varian X-band reflection-type epr spectrometer using 100-kHz field modulation was used to make the measurements. Field modulation and microwave power amplitudes were kept low enough to avoid modulation broadening or power saturation. Radical yields per 100 eV of energy deposited by the γ irradiation (G value) were found by comparing the doubly integrated first derivative spectra in the irradiated silver nitrate samples with the uncorrected trapped-electron spectrum in irradiated $10 M$ NaOH. The G value for the uncorrected trapped-electron spectrum was taken to be 2.1.³

Results

Figure 1 shows epr spectra of γ -irradiated $1 M$ AgNO_3 (Figure 1a) and $1 M$ AgNO_3 - $0.5 M$ KF (Figure 1b). The dose was 3.0 Mrads and the measurements were taken a few minutes after irradiation. The spectra are similar to those reported in the literature.^{5,6} Figure 1a consists of features due to Ag^0 , the groups of lines split by approximately 500 G; OH, the central doublet; and NO_2 , the central triplet which is partially obscured by the hydroxyl radical. The stick diagrams in the

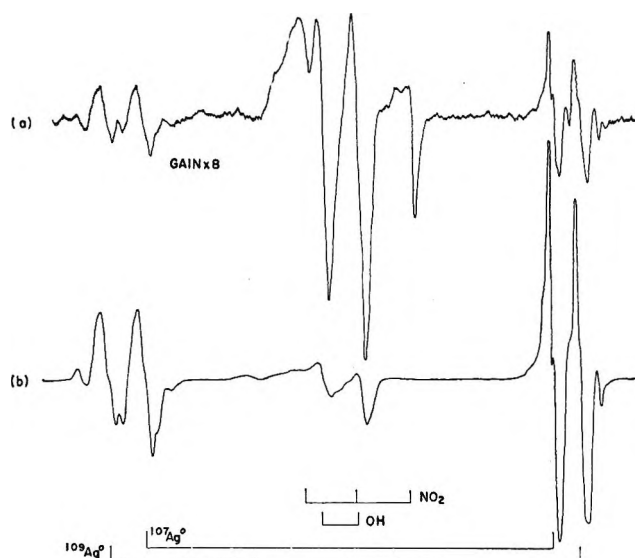


Figure 1. First-derivative epr spectra of γ -irradiated frozen solutions at 77°K : (a) $1 M$ AgNO_3 ; (b) $1 M$ AgNO_3 - $0.5 M$ KF. Note that the spectrometer gain in (a) is a factor of 8 larger than in (b). Dose is 3.0 Mrads.

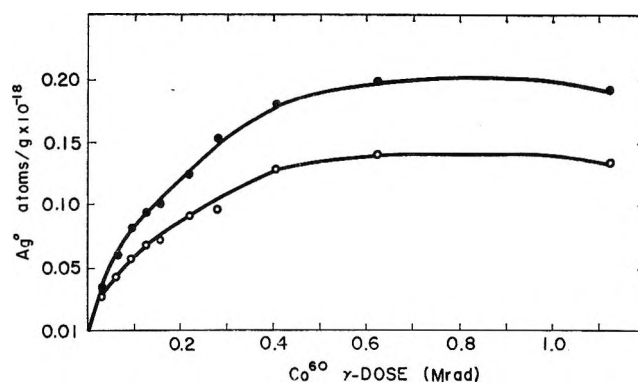


Figure 2. Number of Ag^0 atoms per gram as a function of γ -irradiation dose at 77°K : ●, $1 M$ AgNO_3 ; ○, $0.1 M$ AgNO_3 .

figure show the positions of the main features. Figure 1b is similar to Figure 1a except that no NO_2 is detected (even at high gain) and the yield of Ag^0 is much larger. Note that the spectrometer gain in Figure 1a is higher by a factor of 8 than in Figure 1b and that the hydroxyl radical yield in the two systems is comparable.

The doubling of the features due to Ag^0 results because naturally occurring silver has two spin $1/2$ isotopes which are almost equally abundant. The complexity of the epr of Ag^0 is due to g anisotropy and to the fact that the silver atoms are trapped in several sites of different symmetry, a fact which has been interpreted⁷ as being due to different water dipole orientations in the solvation shell of Ag^0 . Full details on the epr parameters of Ag^0 in various sites are reported in ref 7. The relative concentration of Ag^0 in various sites is time dependent at 77°K , but the total Ag^0 concentration depends only on irradiation dose.⁷ Measurements of

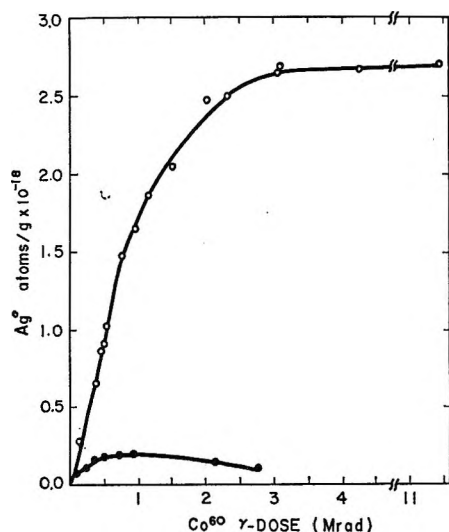


Figure 3. Number of Ag^0 atoms per gram as a function of γ -irradiation dose at 77°K : O, 1 M AgNO_3 - 1 M KF ; ●, 1 M AgNO_3 .

Ag^0 concentration require double integrations of rather complex spectra rather than peak-to-peak line intensity measurements and this is the main source of error in determining silver atom yields. It is estimated that relative silver yields are accurate to $\pm 15\%$ and absolute silver yields (as determined by comparison with the trapped-electron yield in irradiated 10 M NaOH) are accurate to $\pm 30\%$.

The Ag^0 yield as a function of dose is given in Figure 2 for 1 M AgNO_3 and 0.1 M AgNO_3 . These results are not completely reproducible when solutions of AgNO_3

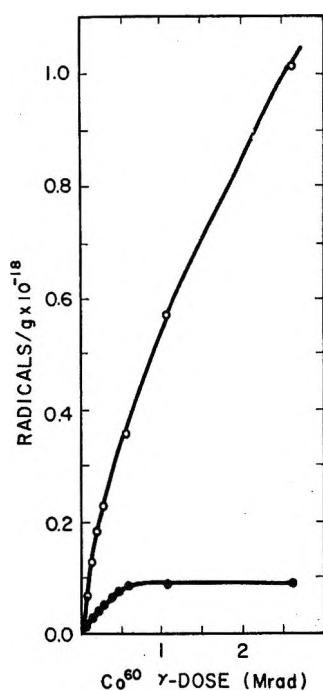


Figure 4. Number of radicals per gram in 1 M AgNO_3 as a function of γ -irradiation dose at 77°K : O, OH; ●, NO_2 .

which have been allowed to "age" are used. The reproducibility of several samples from the same solution is $\pm 10\%$ while samples prepared from freshly made solutions give less intense signals. The reported results are all for freshly made solutions. The yield-dose curve in Figure 2 is linear only to doses less than 0.05 Mrad .

Figure 3 shows the yield-dose curve over a wider dose range in 1 M AgNO_3 and in 1 M AgNO_3 - 1 M KF . In the presence of fluoride, the linearity of the yield-dose curve for Ag^0 is increased to about 1.0 Mrad . Also in the fluoride-containing system the silver atom concentration reaches a plateau at high dose, whereas in the AgNO_3 system without fluoride, the Ag^0 concentration goes through a maximum and decreases at very high doses. At these high doses the nonfluoride-containing samples change from bright yellow to brown.

Table I: Initial G Values of Paramagnetic Species^a at 77°K

	Ag^0	OH	NO_2	Reference
Ice	...	0.8	...	3
1 M KNO_3 ^b	0.36 ± 0.10	This work
1 M KNO_3 - 0.5 M KF ^b	0.09 ± 0.03	This work
1 M AgNO_3 - 0.5 M KF	3.2 ± 0.5	1.5 ± 0.4	0.0	This work
1 M AgNO_3	1.2 ± 0.2	1.5 ± 0.4	0.20 ± 0.06	This work

^a The errors quoted are relative to $G(\text{e}_t^-) = 2.1$ in 10 M NaOH .

^b Irradiated and measured in the dark.

Figure 4 gives the yield-dose curve of NO_2 and OH in 1 M AgNO_3 . As is illustrated in Figure 1, the OH yield is not a function of fluoride concentration while NO_2 is not produced in fluoride-containing silver nitrate ice. The yield of OH at low dose was estimated by comparing the peak-to-peak height of the low-field line of the apparent doublet in ice and silver nitrate ice. The NO_2 yield was determined by measuring the peak-to-peak height of the high-field line. A factor was determined relating the peak-to-peak height to the integrated area by doubly integrating the NO_2 spectrum in γ -irradiated HNO_3 ice and correcting for a small line-width difference. The results were compared with the trapped electron in irradiated 10 M NaOH to calculate the yield. The yield-dose curves of OH in 1 M AgNO_3 and ice are similar except that the absolute yield is larger in the former. The yield-dose curves of NO_2 in 1 M AgNO_3 and 1 M KNO_3 are somewhat different: the initial yield is less in the former (Table I), but the linearity extends over a longer dose range. The curve is linear in potassium nitrate to $\sim 0.05\text{ Mrad}$ while in silver nitrate the curve is linear to $\sim 0.25\text{ Mrad}$.

Table I gives the initial G values of the paramagnetic species in ice, and in ice containing AgNO_3 , $\text{AgNO}_3\text{-KF}$, KNO_3 , and $\text{KNO}_3\text{-KF}$. At low doses, Ag^+ increases the production of OH and decreases the yield of NO_2 . In 1 M AgNO_3 , fluoride does not affect the OH yield, eliminates NO_2 , and enhances Ag^0 . The epr spectrum of irradiated 1 M AgNO_3 at low dose is composed of approximately 41% Ag^0 , 52% OH , and 7% NO_2 . In the presence of 0.5 M fluoride a corresponding spectrum consists of 68% Ag^0 and 32% OH . At higher doses, due to the differences in the dose-yield curves of the various paramagnetic species, the difference in total spin concentration and per cent Ag^0 concentration can vary vastly as is evident in Figure 1 where the total spin concentration is larger in Figure 1b by 200% while the silver yield ratio in Figure 1b is 20 times that in Figure 1a.

The effect of fluoride ion concentration on the Ag^0 yield in irradiation of 1 M AgNO_3 ice is shown in Figure 5 for a low dose (0.03 Mrad) and a high dose (4.5 Mrads). The fluoride ion is quite effective in enhancing Ag^0 even at low concentrations. A yield of NO_2 is observed at low dose up to a concentration of $\sim 10^{-3}\text{ M}$ KF . Above 10^{-3} M KF only CH and no NO_2 is observed. However, at concentrations above about

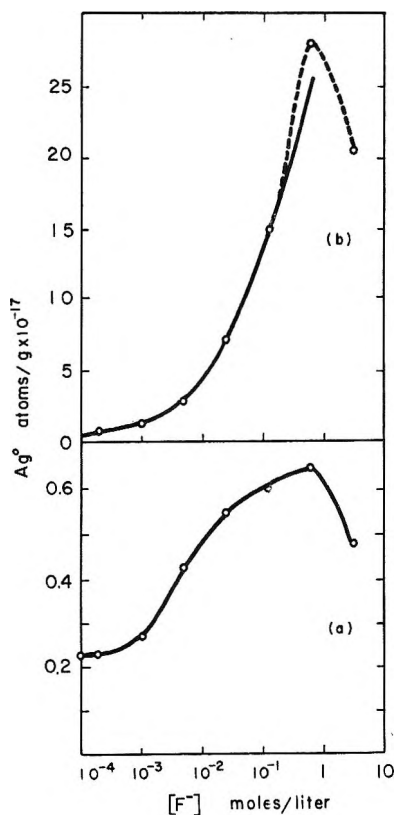


Figure 5. Number of Ag^0 atoms per gram in γ -irradiated 1 M AgNO_3 at 77°K as a function of fluoride concentration: (a) γ dose 0.03 Mrad; (b) γ dose 4.5 Mrads. The solid line in (a) is a smooth curve through the experimental points. The solid line in (b) is a plot of $[\text{F}^-]^{1/2}$.

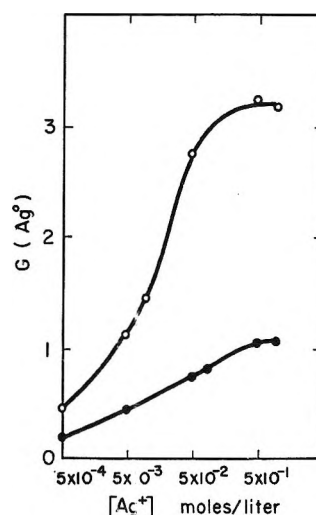


Figure 6. Initial $G(\text{Ag}^0)$ as a function of silver nitrate concentration: \circ contains 1 M KF ; \bullet contains no KF . Dose is 0.04 Mrad.

0.5 M KF , a new three-line spectrum whose perpendicular features are $g_{\perp} = 2.005$ and $A_{\perp} = 63 \pm 2\text{ G}$ appears. The parallel features are obscured somewhat by the overlapping lines of the various radicals around $g = 2$. This spectrum is similar to those attributed in the literature^{8,9} to NO_3^{2-} and is identified here as such. Further confirmation is provided by the fact that irradiation by ultraviolet light converts our spectrum assigned to NO_3^{2-} into NO_2 . This conversion by ultraviolet is characteristic of NO_3^{2-} . Note that the Ag^0 concentration reaches a maximum at about 0.5 M KF and decreases at higher fluoride concentration.

A search was made for the spectrum of F_2^- in $1\text{ M AgNO}_3\text{-}3\text{ M KF}$ by looking for perpendicular epr features at $g_{\perp} = 2.023$ and $A_{\perp} = 296\text{ G}$,¹⁰ but no evidence for this species was found.

The yield of silver atoms as a function of silver nitrate concentration is given in Figure 6, in the presence and in the absence of fluoride ion. The silver atom yield has a very nonlinear dependence on the silver nitrate concentration and also shows a very strong enhancement due to fluoride ion even at very low concentrations of Ag^+ . The yields of OH and NO_2 show similar nonlinear behavior with silver nitrate concentrations.

The effect of added fluoride ion on the radicals produced in the radiolysis of 0.5 M KNO_3 was also briefly investigated (Table I). The addition of 0.5 M KF to 0.5 M KNO_3 causes the NO_2 radical to be reduced by a factor of about 4 and causes the NO_3^{2-} radical to be increased by a factor of 2-3.

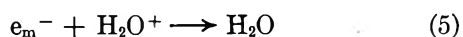
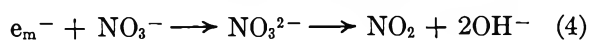
(8) P. B. Ayscough and R. G. Collins, *J. Phys. Chem.*, **70**, 3128 (1966).

(9) B. G. Ershov, A. K. Pikaev, B. Ya. Glazunov, and V. I. Spitsyn, *Dokl. Akad. Nauk SSSR*, **149**, 663 (1963).

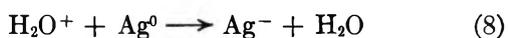
(10) P. W. Atkins and M. C. F. Symons, "The Structure of Inorganic Radicals," Elsevier Publishing Co., Amsterdam, 1967, p 115.

Discussion

A. Primary Reactions in AgNO₃ Ices. The primary species produced in the radiolysis of ice are given in reactions 1 and 2. At 77°K the directly produced OH radicals are trapped, but the H atoms are mobile. The H atoms back-react to some extent with OH radicals and also react with each other to form H₂. In this work, we are primarily concerned with the reactions of the electrons and holes produced in reaction 2, both of which are considered to be mobile. In NaNO₃ ice, the mobile electrons react with the anion as shown in reaction 4.^{8,9} From the suggested correlation of mobile electron reaction rates with solutes in ice,¹¹ electrons are expected to react several times faster with Ag⁺ than with NO₃⁻ in AgNO₃ ices. The reduced NO₂ yield and the absence of NO₃²⁻ in AgNO₃ ice compared to NaNO₃ ice bear this out. Some electrons must recombine with holes as portrayed in reaction 5. In addition to reaction 5, holes react by reactions 6 and 7 in NaNO₃ ice.¹²

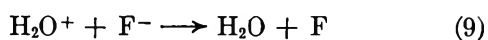


As shown in Figure 2 the yield-dose curve is linear to less than 0.05 Mrad. This suggests that there is another reaction which destroys Ag⁰ at relatively low concentration. We suggest that the reaction is (8). The postulate that mobile holes reduce the Ag⁰ yield at low concentrations is supported by the fluoride effects discussed below. If reaction 8 is primarily



responsible for the shape of the yield-dose curve, then it implies that some H₂O⁺ can travel considerable distances in ice without participating in reaction 6.

B. Hole Trapping by Fluoride Ion. The addition of fluoride ion to silver nitrate ices has several dramatic effects. It (a) increases the Ag⁰ yield, (b) prevents the formation of NO₂ at low γ doses, (c) increases the total number of observable trapped paramagnetic species, and (d) increases the linear range of the yield-dose curve for Ag⁰. All of these effects can be explained by the assumption that fluoride ion acts as an efficient hole trap for H₂O⁺ as indicated by reaction 9. The com-



petition of (9) and (8) increases the Ag⁰ yield and increases the linear range of the yield-dose curve of Ag⁰. The competition of (9) with (7) prevents the formation of NO₂. This, in fact, supports the mechanism of NO₂ formation by hole reactions.¹² Finally, competition of (9) with (5) increases the total number of observable trapped paramagnetic species by allowing more electrons to react with Ag⁺.

Reaction 9 is postulated to form trapped fluorine atoms. If the fluorine atoms are trapped as such, they would not be expected to show an epr spectrum in the solid phase because of a strong spin-orbit interaction which probably broadens the lines beyond detection.

A search was made for the known epr spectrum¹⁰ of F₂⁻, but no evidence for it was found. The fact that fluoride ion exhibits its effects at very low concentrations also argues against the involvement of F₂⁻. In work on frozen chloride solutions, Cl₂⁻ is formed only at concentrations above 0.5 M.¹³ The possibility that a silver fluoride complex is responsible for the effects observed can also be ruled out because the fluoride effects occur at such low fluoride concentrations.

If fluoride ion indeed acts as a hole trap, it should also do so in other systems. To test this, the effect of fluoride on the radical yields in irradiated KNO₃ ice was examined (Table I). It was predicted that the NO₂ yield, which is mainly formed by reaction 7, would be decreased while the NO₃²⁻ yield would be increased. This is precisely what was observed as shown in Table I. The decrease in the NO₂ yield was expected because of competition of reaction 9 with 7. Also, competition of (9) with (5) allows more electrons to participate in reaction 4 in the absence of silver ions. The NO₂ yield is slightly smaller in AgNO₃ ice compared with KNO₃ ice. This is expected because in AgNO₃ ice most of the electrons react with Ag⁺, whereas in the KNO₃ ice most of the electrons react with NO₃⁻ and form a small amount of NO₂.

C. Radical Yields. The radiolysis of pure ice at 77°K produces $G(OH) = 0.8$.³ Addition of AgNO₃ causes reaction 3 to compete with (5). This causes the OH yield to increase by reaction 6 relative to pure ice because fewer holes undergo reaction 5. The NO₂ arises largely from (7). In 1 M AgNO₃, Table I shows that the total yield of trapped-electron species (Ag⁰) is a little smaller than the total yield of trapped-hole species (OH + NO₂). Some H₂ may be formed as is postulated in pure ice.³ However, within the experimental error the yields of electron and hole species are approximately equivalent.

Figure 6 shows that the increase in Ag⁰ with AgNO₃ concentration is quite sublinear and that the Ag⁰ yield plateaus at 0.5 M AgNO₃. The Ag⁰ yield is approximately linear with either the square root or cube root of the silver ion concentration from 5×10^{-4} to 5×10^{-2} M Ag⁺ but deviates considerably at higher concentrations. This concentration dependence is consistent with scavenging electrons by Ag⁺ from recombination reaction 5 if H₂O⁺ and e_m⁻ are considered to be diffusing from an initial inhomogeneous distribution in

(11) L. Kevan, *J. Amer. Chem. Soc.*, **89**, 4238 (1967).

(12) L. Kevan, *J. Phys. Chem.*, **68**, 2590 (1964).

(13) D. M. Brown and F. S. Dainton, *Nature*, **209**, 195 (1966).

spurs.^{12,14} The cube root dependence has usually been applied to scavenging in irradiated aqueous solutions¹⁵ while the square root dependence has more recently been applied to ion scavenging in irradiated organic liquids.¹⁴ Both correlations fail at high solute concentrations as is also found here.

The effect of added KF as a hole trap has been discussed. It is striking that the optimum concentration of KF (0.5 M) increases the maximum, initial $G(\text{Ag}^0)$ from 1.2 to 3.2. This high value is reasonable for the maximum ionization yield of electrons in the system. This means that reaction 5 is nearly eliminated in 1 M AgNO_3 -0.5 M KF. Note that both electron and hole traps are necessary to achieve this condition.

The concentration dependence of the enhancement of Ag^0 by F^- is quite sublinear (Figure 5) and approximately fits square root or cube root dependencies on the F^- concentration. The fit is better at high doses than at low doses. As discussed above for the Ag^+ concentration dependence, this is expected for ion scavenging in irradiated systems.

D. Mobile and Nonmobile Holes. In the presence of F^- , NO_2 is eliminated. Thus F^- is a better hole trap than NO_3^- in ice at 77°K; *i.e.*, F^- effectively competes with NO_3^- in reaction 7. Fluoride ion increases the initial Ag^0 yield by scavenging holes from reaction 5. On the other hand, the OH yield is unaffected by F^- so F^- does not scavenge the holes in reaction 6. We suggest that there may be two populations of holes which are differentiated by their reactivity. One H_2O^+ population readily undergoes reaction 6 with an H_2O

molecule in its own solvation shell, is not appreciably mobile, and is not scavengeable. The yield of these nonmobile holes is the maximum OH yield in AgNO_3 ice ($G = 1.5$). The other H_2O^+ population reacts only slowly, if at all, by reaction 6, is mobile, and can be scavenged. This mobile hole yield is given by the increase in Ag^0 due to F^- ($G = 2$).

If we postulate the existence of two types of holes in ice, how can they be described physically? We suggest that the mobile hole is unrelaxed; that is, it has the same geometry as a neutral water molecule so charge conduction is facile. Reaction 6 is inefficient because charge conduction is rapid. The nonmobile hole is relaxed and has attained a new equilibrium geometry consistent with the loss of one electron from the neutral molecule. The relaxed hole readily undergoes proton-transfer reaction 6 but charge conduction is slow because of the change in geometry required. This physical description of two types of holes in ice is rather analogous to a recent proposal by Hamill for two types of holes (dry and hydrated) in liquid water radiolysis.¹⁶

Acknowledgment. This research was supported by NASA, the AEC, and the Air Force Rocket Propulsion Laboratory. This is AEC, Document No. COO-1528-35. We wish to thank Dr. P. Hamill for helpful discussions.

(14) J. M. Warman, K. D. Asmus, and R. H. Schuler, *Advances in Chemistry Series*, No. 82, American Chemical Society, Washington, D. C., 1968, p 25.

(15) H. A. Schwartz, *J. Amer. Chem. Soc.*, **77**, 4960 (1955).

(16) W. M. Hamill, *J. Chem. Phys.*, **49**, 2446 (1968).

A Molecular Structure Study of Cyclopentene¹

by Michael I. Davis² and T. W. Muecke

Department of Chemistry, The University of Texas at Austin, Austin, Texas 78712 (Received November 25, 1968)

The molecular structure of cyclopentene has been determined by the gas-phase electron diffraction technique. The C=C double-bond length was found to be 1.343 ± 0.010 Å. The value obtained for the average length of the C—C single bonds was 1.533 ± 0.007 Å. Only a rough estimate of the difference between the lengths of the two distinct types of C—C single bonds could be made. The five-membered ring was found to be puckered by $29.0 \pm 2.5^\circ$. A value of $111.0 \pm 1.2^\circ$ was obtained for the CCC bond angles adjacent to the double bond.

Introduction

To the best of our knowledge, there has been only one previous attempt to determine the molecular structure of cyclopentene.³ From the microwave spectrum, values were obtained for the rotational constants of the ground and lowest excited vibrational states. Since 18 parameters are required to describe the equilibrium geometry, numerous assumptions were required to enhance the three pieces of experimental information. It was found, from that study, that the ring is puckered by more than 20° .

Several studies have been made of norbornadiene,^{4,5} the general features of which are in good agreement. A comparison of the structural parameters of cyclopentene and norbornadiene might provide some insight into the manner in which the molecular strain is distributed through their respective carbon skeletons.

Experimental Section

Intensity data were collected photographically at distances of 100, 50, and 25 cm from the scattering center. The de Broglie wavelengths of 0.05663 Å was determined from gold foil diffraction patterns. The sample reservoir was maintained at a temperature of -16° , while the nozzle was presumably close to room temperature. Exposure times ranged from 10 to 120 sec. Transmission values were obtained from traces of microdensitometer records at an interval of $\Delta s = 0.25$ Å⁻¹ for the two shortest camera distances and 0.125 Å⁻¹ for the longest. The preliminary data-handling and background-insertion procedures were carried out along lines described in a previous paper.⁶ Reference 6 also contains the theoretical expressions employed in the analysis and appropriate source references.

Structure Determination

When an undamped version of the molecular scattering curve was Fourier inverted, the resulting radial distribution curve was found to possess several distinctive features (see Figure 1). The peak at 1.1 Å is a composite of five nonsymmetry-related C—H bond contributions. The C=C bond peak is sufficiently well

isolated from that of the C—C single bonds to provide a tolerable estimate of its length. It is evident that there is no appreciable difference between the lengths of the two types of C—C single bond. The contribution at 2.2 Å is attributable to nonbonded C—H atom pairs. The larger peak at 2.4 Å contains contributions from all three distinct types of nonbonded C—C pairs. Its sharpness indicates that the three internuclear distances are very nearly identical. The peaks at 3.0 and 3.4 Å contain the contributions of the longer C—H atom pairs.

Assuming that the molecule possesses a plane of symmetry (see Figure 2), five parameters are required to describe the equilibrium geometry of the ring. The knowledge that the two C—C single bond lengths and the three C—C nonbonded distances are within a few hundredths of an ångstrom of their respective mean values made it possible to obtain a fairly good estimate of the ring structure at an early stage of the investigation.

Thirteen extra parameters would have been needed to determine all of the hydrogen positions unambiguously. This amount of information is not available from our data. Thus it was assumed that the five types of C—H bond are of identical length. The hydrogen atoms bonded to C(3) and C(4) were assumed to be coplanar with carbons 2, 3, 4, and 5. The bisectors of the HCH bond angles at C(1) and C(2) were assumed to coincide with the bisectors of the corresponding CCC angles. Further, the HCH planes at C(1) and C(2) were assumed to intersect the CCC planes perpendicularly.

(1) Material supplementary to this article has been deposited as Document No. NAPS-00707 with the ASIS National Auxiliary Publications Service, c/o CCM Information Corp., 909 3rd Ave., New York, N. Y. 10022. A copy may be secured by citing the document number and by remitting \$1.00 for microfiche or \$3.00 for photocopies. Advance payment is required. Make checks or money orders payable to: ASIS-NAPS.

(2) Department of Chemistry, The University of Texas at El Paso, El Paso, Texas 79999.

(3) G. W. Rathjens, Jr., *J. Chem. Phys.*, **36**, 2401 (1962).

(4) (a) T. W. Muecke and M. I. Davis, *Trans. Amer. Crystallogr. Ass.*, **2**, 173 (1966); (b) Y. Morino, K. Kuchitsu, and A. Yokozeki, *Bull. Chem. Soc. Japan*, **40**, 1552 (1967); (c) G. Dallinga and L. H. Toneman, to be submitted for publication.

(5) W. C. Hamilton, Ph.D. Dissertation, California Institute of Technology, 1955.

(6) M. I. Davis and H. P. Hanson, *J. Phys. Chem.*, **69**, 4091 (1965).

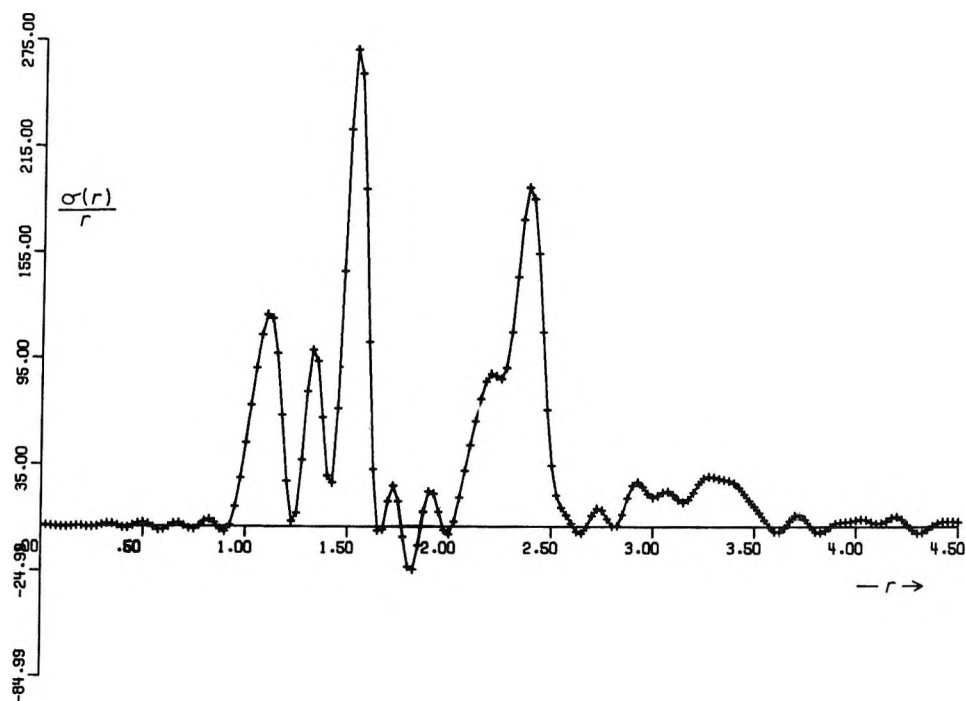


Figure 1. Radial distribution curve for cyclopentene (no damping).

Much of the structural analysis was carried out using a cyclic process of univariant parameter adjustments. Considerable use was also made of the least-squares procedure.⁷ The assumption was adopted throughout that those atom pairs whose radial distribution curve

contributions lie under the same peak should be assigned identical vibrational amplitudes.

There are two somewhat ambiguous features of this investigation. It was possible to determine the HCH bond angles to within a few degrees. There are, however, two distinctly different values of the C(3)C(4)H(4) bond angle that appear to conform with our data. The value of 121° is about what one might have predicted. The other value of 143° is not. It was the larger of the two values that gave the slightly better correlation between theoretical and experimental molecular scattering curves.

One would anticipate that the C-C single bonds that are adjacent to the double bond would be a few hundredths of 1 \AA shorter than those that are not. Our data were not adequate to provide verification of this feature. Two separate analyses were performed. In one, the C-C single bonds were assumed to be all of identical length; in the other the difference between the two types of bond length was included as a refinement parameter.

Some relatively naive calculations were carried out to investigate the sensitivity of the rotational constants to the difference between the two C-C bond lengths and to variation of the C(3)C(4)H(4) bond angle.

Results

The results of this investigation are set out in Table I. In view of the two ambiguous features, several sets of parameters are given. It is apparent that most of the structural features are relatively insensitive to

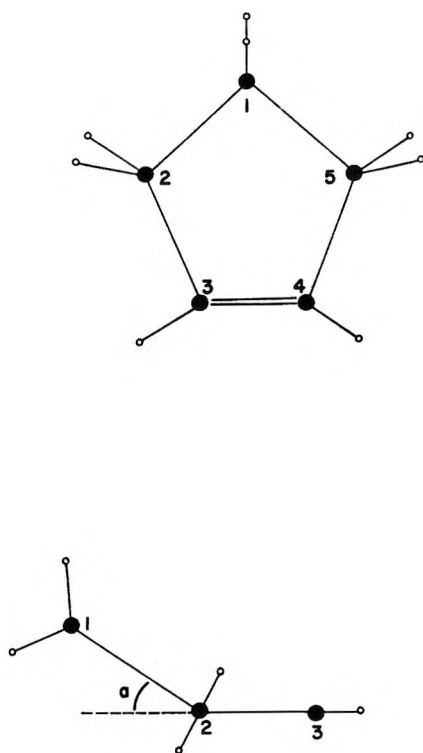


Figure 2. Cyclopentene molecule: top, projection perpendicular to the plane containing carbons 2, 3, 4, and 5; bottom, projection along an axis parallel to C_2-C_3 .

(7) K. Hedberg and M. Iwasaki, *Acta Crystallogr.*, 17, 529 (1964).

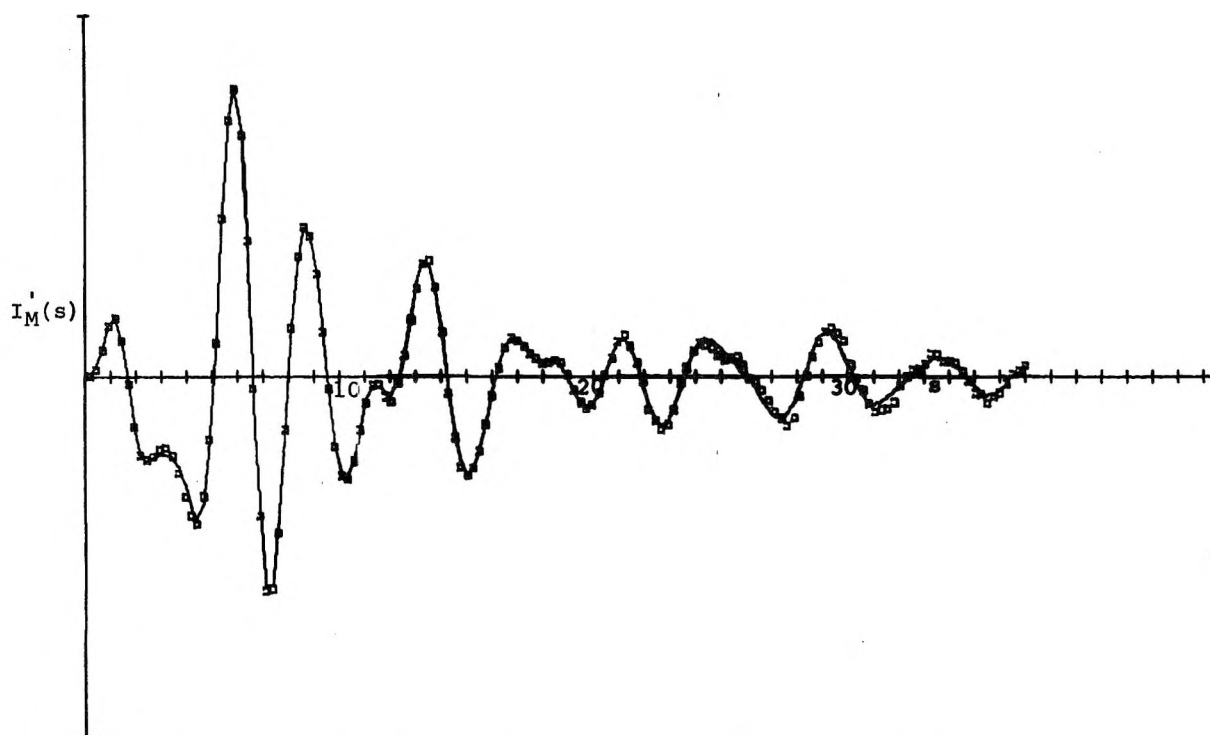


Figure 3. Molecular scattering curves for cyclopentene: \square , experimental, $s = 3.0\text{--}37 \text{ \AA}^{-1}$; —, theoretical.

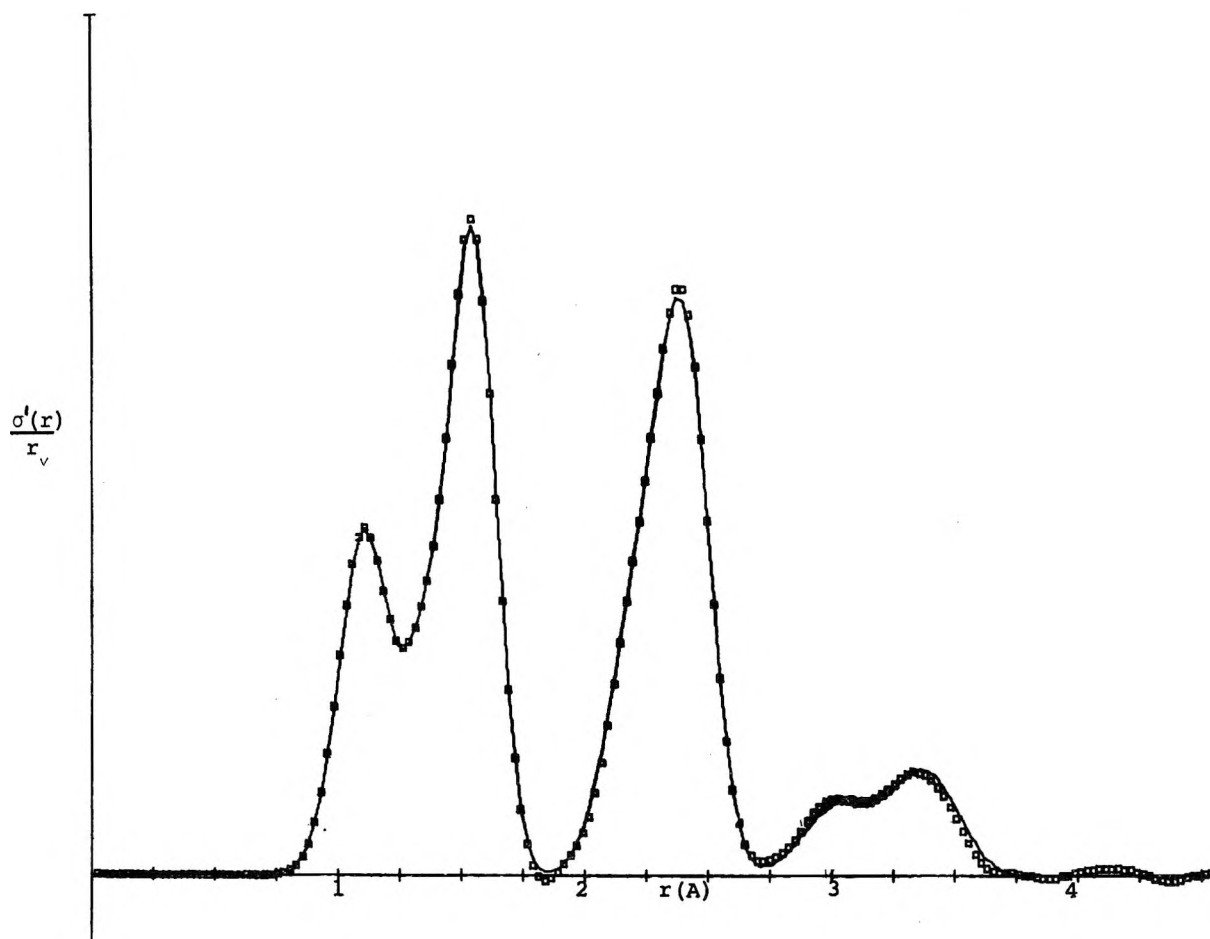


Figure 4. Cyclopentene. Radial distribution curves for cyclopentene: \square , experimental; —, theoretical ($k = 0.003$). Theoretical version obtained by Fourier inversion of the corresponding molecular scattering curve.

Table I: Cyclopentene Molecular Structure Parameters

	a	b	c	d
$r(C_1-C_2)$, Å	1.546	...	1.544	0.035
$r(C_2-C_3)$, Å	1.519	...	1.519	0.030
$r(C-C)_{av}$, Å	(1.533)	1.533	(1.533)	0.007
$r(C=C)$, Å	1.342	1.343	1.341	0.010
$r(C-H)_{av}$, Å	1.098	1.098	1.096	0.006
$C_2C_3C_4$, deg	111.0	110.9	111.2	1.2
Pucker, deg	28.8	29.2	28.8	2.5
$H_1C_1H_1$, deg	104.8	101.0	104.8	e
$H_2C_2H_2$, deg	101.8	102.6	101.8	e
$C_3C_4H_4$, deg	143.5	143.6	121.8	e
$l(C=C)$, Å	0.035	0.034	0.032	0.015
$l(C-C)_{av}$, Å	0.046	0.047	0.046	0.020 ^f
$l(C-C)_{nb}$, Å	0.054	0.055	0.055	0.020
$l(C-H)$, Å	0.059	0.059	0.059	0.005
$l(C_1-H_2)$, Å	0.075	0.076	0.074	e
$l(C_2-H_3)$, Å	0.092	0.104	0.107	e
$l(C_1-H_3)$, Å	0.076	0.075	0.079	e

^a C_1-C_2 and C_2-C_3 treated as distinguishable entities; CCH = 143.5°. ^b C_1-C_2 and C_2-C_3 treated as being identical; CCH = 143.6°. ^c CCH = 121.8°. ^d Confidence limits. ^e Parameters evaluated by unitary parameter adjustment method but not treated as parameters in least-squares procedure. ^f Confidence range diminishes to ± 0.005 Å when $r(C_1-C_2)$ is assumed equal to $r(C_2-C_3)$.

either the difference between the two types of C-C single bond length or the variation of the CCH angle. In the latter case one finds that changing the CCH angle from 121 to 143° switches the lengths of two pairs of nonbonded C-H atom pairs.

The standard errors of the least-squares calculation were doubled to account for data correlation and further multiplied by 2.5 to give the limits of confidence values cited.

Theoretical and experimental versions of the radial distribution and molecular scattering curves are shown in Figures 3 and 4, respectively. Such changes as occur in these curves as one switches from one set of parameters to another are too small to be discernible on this scale.

Discussion

The C-H, C=C, and average C-C single bond length values all appear to be normal. The $C(1)C(2)C(3)$ and $C(2)C(1)C(5)$ bond angles are both about 6° less than the tetrahedral value. The $C(2)C(3)C(4)$ angle is some 9° less than the trigonal value. None of these features is significantly affected by the two ambiguous aspects of the investigation.

The individual HCH bond angle values are somewhat sensitive to both the C-C single bond length difference and the value of the $C(3)C(4)H(4)$ bond angle. The average of the two HCH angles, however, remains more or less constant. The average value may then be taken to be fairly reliable while the individual differences are clearly not well established.

Table II: Cyclopentene Rotational Constants (Mc)

Microwave ^a	—CCH = 143°—		—CCH = 121°—	
	(C_1-C_2) = (C_2-C_3)	(C_1-C_2) - (C_2-C_3) = 0.027 Å	(C_1-C_2) = (C_2-C_3)	(C_1-C_2) - (C_2-C_3) = 0.027 Å
7294	7391	7391	7255	7244
7227	7105	7093	7195	7194
3950	3959	3953	3948	3942

It is perhaps surprising that the HCH values should be less than tetrahedral. While we are satisfied that our value is the best that could be obtained from the analysis, its reliability is marginal in view of the approximations made concerning the hydrogen positions.

When some appropriate quantitative estimate of the degree of correlation between the theoretical and experimental molecular scattering curves is plotted as a function of the $C(3)C(4)H(4)$ bond angle, the resulting curve possesses two well-defined minima that are separated by a fairly sizable peak. The relative depths of the two minima are moderately sensitive to the values chosen for the other parameters but the general features of the curve are not. There are no indications from our experiment as to which of the two values should be preferred although the smaller value of 121° is evidently the more acceptable in terms of precedent.

While changing the CCH angle from 121 to 143° appears to have very little effect upon the appearance of the molecular scattering and radial distribution curves, it does make a fair difference to the rotational constants. When the rotational constants calculated for models with the two different CCH angles are compared with those obtained from the microwave spectrum³ (see Table II), it is seen that the value of 121° gives the better set of the two.

The value of 29° for the puckering angle represents a considerable departure from planarity. While the resulting decrease in the CCC bond angles must inevitably introduce extra strain, it is accompanied by a withdrawal of the CH_2 groups from the unfavorable eclipsed orientation.

Table III: Cyclopentene and Norbornadiene Corresponding Bond Lengths and Angles^a

	C_5H_8	C_7H_{12}		
	this work	Ref 4a	Ref 4b	Ref 5
$r(C_1-C_2)$, Å	1.543	1.567	1.573	1.558
$r(C_2-C_3)$, Å	1.513	1.549	1.522	1.522
$r(C_3=C_4)$, Å	1.342	1.357	1.339	1.333
$C_2C_1C_5$, deg	102.)	96.5	92.0	96.7
$C_1C_2C_3$, deg	103.)	96.0	99.0	96.4
$C_2C_3C_4$, deg	111.)	108.5	107.7	109.1
Pucker, deg	28.8	57.3	57.5	55.1

^a Carbon atoms numbered in accordance with cyclopentene structure.

The results of our investigation are presented together with those of three studies of norbornadiene (see Table III). It is of interest to note that while none of the investigations can rightly be claimed to have determined unambiguously the difference between the two types of single C-C bond length, each of them reports that the single bonds adjacent to the double bond is the shorter.

The dihedral puckering angle in cyclopentene is approximately half the corresponding norbornadiene angle. That the latter compound should be the more strained is of course to be expected. If the deviations of the bond angles from tetrahedral or trigonal values may be used as a measure of the manner in which the strain is distributed through the carbon skeletons, it is evident that the distribution is fairly uniform.

A Refinement Procedure for Determining the Crystallite Orientation

Distribution Function¹

by W. R. Krigbaum

Department of Chemistry, Duke University, Durham, North Carolina (Received August 18, 1969)

One obtains the most complete information concerning the crystallite orientation in a polycrystalline sample through use of the crystallite orientation distribution function. Nevertheless, in some instances one may desire better resolution in the representation of the distribution than is offered by the current procedure. A successive refinement procedure is proposed which is based upon the close analogy between the determination of a crystal structure and determination of the crystallite orientation distribution function. Its application is illustrated using four pole figures for a fiber texture sample of isotactic polystyrene. The refinement effects a marked improvement, as judged by comparison of the observed and recalculated plane-normal profiles and by the behavior during refinement of the standard deviations of the plane-normal distributions and of the crystallite orientation distribution.

I. Introduction

A wide variety of polycrystalline materials occurs among the polymers, metals, and minerals. Preferred orientation of the crystalline regions in such samples may be investigated by X-ray diffraction. In this way one obtains information concerning the preferred orientation of each Bragg plane examined, and these data may be summarized concisely by the pole figure diagrams. The preferred orientation of different samples may be compared qualitatively through use of averages such as $\langle \cos^2 \chi_i \rangle$, where χ_i is the angle between the i th plane normal and the drawing direction. However, a collection of pole figure diagrams for a single sample implicitly contains information which is both more general and more useful, namely, the distribution of orientations of the crystallographic unit cells. Mathematical procedures have been developed for deducing this information in the form of the crystallite orientation distribution^{2,3} or its equivalent in the case of a sample having fiber symmetry, the inverse pole figure.⁴⁻⁶ Once the crystallite orientation distribution function has been determined, it may be used to compute pole figures for unmeasured planes. The

procedure, as generalized by Roe,³ may be applied to samples of arbitrary texture, and its application has been illustrated for both fiber symmetry⁷⁻⁹ and the more general case of biaxial texture.¹⁰ The crystallite orientation distribution function offers the most complete representation which can be gained from a given set of pole figure data. Nevertheless, in some instances one might desire higher resolution than the current procedure offers.

(1) Supported by the National Aeronautics and Space Administration under the Sustaining University Program. Project Grant NGL 34-001-005.

(2) R.-J. Roe and W. R. Krigbaum, *J. Chem. Phys.*, **40**, 2608 (1964).

(3) R.-J. Roe, *J. Appl. Phys.*, **36**, 2024 (1965).

(4) H. J. Bunge, *Monatsber. Deut. Akad. Wiss. Berlin*, **1**, 400 (1959); **2**, 479 (1960); **3**, 97, 285 (1961); **5**, 293 (1963).

(5) H. J. Bunge, *Acta Cryst.*, **15**, 612 (1962).

(6) H. J. Bunge and H. Sanderman, *Monatsber. Deut. Akad. Wiss. Berlin*, **5**, 343, (1963).

(7) W. R. Krigbaum and R.-J. Roe, *J. Chem. Phys.*, **41**, 737 (1964).

(8) W. R. Krigbaum and Y. I. Balta, *J. Phys. Chem.*, **71**, 1770 (1967).

(9) D. W. Baker, H. R. Wenk, and J. M. Christie, *J. Geol.*, **77**, 144 (1969).

(10) W. R. Krigbaum, T. Adachi, and J. V. Dawkins, *J. Chem. Phys.*, **49**, 1532 (1968).

Concerning the matter of resolution, we recall that the crystallite orientation distribution function is represented as a series of polynomials.² The coefficients in this series are determined by solving a set of simultaneous linear equations, and the number of terms which may be retained is governed by the number of pole figures measured experimentally and by the symmetry elements present in the sample. As an illustration of the latter dependence we observe that, in order to evaluate the coefficient(s) A_{lm} (and B_{lm}) having $l = 22$ for a fiber texture sample, the number of pole figures required is: cubic (2), hexagonal (4), trigonal (8), orthorhombic (12), and triclinic (45). The fidelity of the calculated crystallite orientation distribution depends, of course, on the order of the harmonic terms retained. The resolution requirement in any particular case depends upon the character of the preferred orientation. If the pole figures are sharply peaked, a large number of terms will be needed for an adequate representation. Thus, if one encounters a highly oriented sample belonging to a crystal class of low symmetry—for example, triclinic or monoclinic—it may not be possible to obtain experimental data for a sufficient number of Bragg planes to achieve an adequate representation. Even for a crystal class of higher symmetry, it may happen that the crystalline regions are quite small or highly imperfect, so that only a limited number of Bragg planes diffract adequately for convenient study. Finally, experience indicates that the set of simultaneous equations often becomes ill conditioned in the higher coefficients due to errors in the experimental pole figures, in which case the polynomial series must be terminated short of the anticipated limit. If the resolution is low for any of the above reasons, the reconstructed pole figures will have their maxima lowered and broadened, and spurious oscillations will be introduced due to series termination errors.

II. Proposed Refinement Procedure

We propose a possible method for improving the resolution which involves a successive refinement procedure. This is suggested by the close parallel between the method used to deduce the crystallite orientation distribution function from pole figures and that used to determine a crystal structure from single-crystal diffraction data. In the latter case the structure amplitudes measured in reciprocal space and the electron density sought in real space are connected *via* a Fourier transform. The analogs in the present problem are the pole figures in reciprocal space and the crystallite orientation distribution in real space. In the crystal structure problem the number of observed structure amplitudes greatly exceeds the number of parameters sought; however, the phase angles, which are required to calculate the electron density, are not directly observable. One fruitful approach involves deduction

of a trial structure—for example, by use of the Patterson function—which may be used to calculate both the structure amplitudes and their phases. A combination of the observed structure amplitudes with the calculated phases leads, through an inverse transform, to an electron density distribution. Hopefully, this structure will be more nearly correct than the trial structure, in which case it replaces the trial structure and one is ready to perform a second cycle of refinement. We propose to obtain a better approximation for the crystallite orientation distribution in a similar fashion. In this case the problem of unknown phases is absent, but the solution is limited by the number of measured pole figures. As we shall see, this limitation also applies to the quality of the representation of each pole figure which is used as input information in determining the crystallite orientation distribution. Our procedure seeks to relax both of these limitations.

Let us assume that N pole figures have been determined, and let l_{\max} be the maximum term whose coefficient can be evaluated for the particular sample in question. We first solve the crystallite orientation distribution function using, for the maximum term, some value $\lambda < l_{\max}$. This function is then used to reconstruct the N measured pole figures and to compute an additional ΔN unmeasured pole figures. Comparison of the N reconstructed pole figures with those determined experimentally will reveal certain discrepancies arising from series termination errors. As mentioned above, the principal maxima will be more diffuse, and oscillations will appear in the reconstructed pole figures. Using this comparison as a guide, one smooths the oscillations and sharpens the principal maxima in the ΔN unobserved pole figures. These ΔN smoothed pole figures are then combined with the N measured pole figures to begin a second cycle, this time retaining more terms in the series. One might perform this cycle several times, increasing ΔN and the number of polynomial coefficients determined, in order to improve successively the agreement between the recalculated and measured pole figures. The key to this procedure is that as additional terms are added, it becomes possible to utilize a more faithful representation of the measured pole figures for solution of the crystallite orientation distribution, and hence each cycle draws from a larger store of input information.

III. An Illustrative Example

As an illustration of the application of this refinement procedure we consider data for a uniaxially oriented isotactic polystyrene sample, V-3, which has been described elsewhere.¹¹ This particular sample was melted and quenched, drawn to an elongation ratio of 5 at 110°, and crystallized approximately 5% by heating for 11 min at 137°.

(11) W. R. Krigbaum and S. Maruno, *J. Polym. Sci., A*, **2**, 1733 (1968).

Table I: Crystallographic Data for All Plane Normals Utilized in the Analysis

No.	hkl	2θ	θ_i	Φ_i	ρ_i^a
1	30 $\bar{3}$ 0	14.07	90.00	0.00	1.00
2	2240	16.19	90.00	30.00	1.00
3	21 $\bar{3}$ 1	18.30	42.83	19.11	1.00
4	11 $\bar{2}$ 3	41.65	11.44	30.00	0.00
5	41 $\bar{5}$ 0	21.47	90.00	10.89	0.60
6	10 $\bar{1}$ 2	27.24	9.94	0.00	0.00
7	42 $\bar{6}$ 1	28.31	61.68	19.11	0.60
8	2022	28.54	29.32	0.00	0.40
9	52 $\bar{7}$ 0	29.41	90.00	16.11	0.80
10	51 $\bar{6}$ 1	29.46	62.88	8.95	0.80
11	21 $\bar{3}$ 2	29.62	24.88	19.11	0.40
12	5491	39.51	69.94	26.33	0.60
13	4372	39.63	46.84	25.29	0.50
14	7291	41.26	70.79	12.22	0.00

^a Weights used in the final (third) cycle.

The crystal structure of isotactic polystyrene has been examined by Natta, Corradini, and Bassi.¹² They assigned polystyrene to one of the two rhombohedral space groups $R\bar{3}c$ or $R3c$. The dimensions of the unit cell, as indexed using a hexagonal lattice, are $a = b = 21.9 \text{ \AA}$ and $c = 6.65 \text{ \AA}$. For the purpose of the present illustration we will treat polystyrene as pseudohexagonal and will employ diffraction data for four plane normals. During the course of the analysis, unmeasured pole figures were reconstructed for an

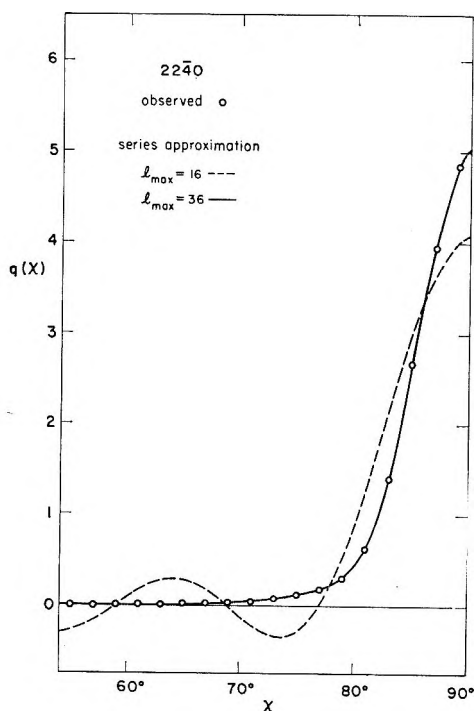


Figure 1. Comparison of the polynomial representation obtained for the 2240 profile using $l_{\max} = 16$ (dashed curve) and $l_{\max} = 32$ (full curve). Circles represent the experimental data.

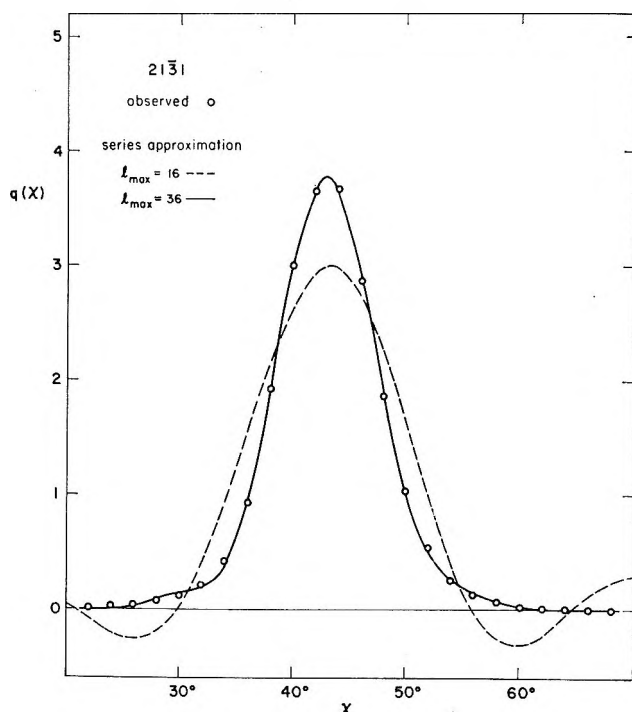


Figure 2. Same as Figure 1 for the 21 $\bar{3}$ 1 profile.

additional 10 planes. The pertinent crystallographic data for these 14 planes are given in Table I. The observed planes are numbered 1-4.

As mentioned above, the individual pole figures are fitted by a series of Legendre polynomials, and it is the coefficients of this series which are utilized in solving the simultaneous equations for the coefficients in the harmonic representation of the crystallite orientation distribution. The maximum coefficient in the latter series which can be evaluated in the present case of pseudohexagonal crystal symmetry and four pole figures is $l_{\max} = 22$. In the first cycle the crystallite orientation distribution function was calculated retaining $l = 16$ as the maximum coefficient. Figures 1 and 2 offer a comparison of the observed profiles (circles) for two of the pole figures and the representation obtained using $l_{\max} = 16$ (dashed curve) and $l_{\max} = 36$ (full curve). The dashed curves therefore represent the actual input information to the problem at this initial stage. The four observed pole figures were recalculated, and the ten unobserved pole figures were constructed, through use of the crystallite orientation distribution function with $l_{\max} = 16$.

The foregoing is just the procedure used heretofore, and we are now ready to test the proposed refinement procedure. Using a comparison of the measured and recalculated pole figures as a guide, we smooth the oscillations and sharpen the principal maximum somewhat for each of the ten unobserved pole figures. These ten smoothed profiles and the four observed

(12) G. Natta, P. Corradini, and I. W. Bassi, *Nuovo Cimento, Suppl.* **1**, 15, 68 (1960).

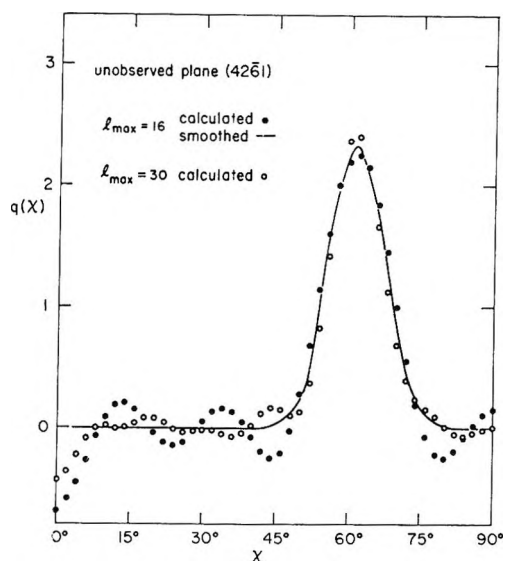


Figure 3. An illustration of the smoothing procedure for the unmeasured profile $42\bar{6}1$. See text for discussion.

pole figures were next fitted to Legendre polynomials retaining $l_{\max} = 30$, and this information was utilized to solve a second approximation to the crystallite orientation distribution function truncated after $l = 30$.

The smoothing procedure for the unmeasured pole figures is illustrated for the $42\bar{6}1$ plane in Figure 3. The filled circles represent the pole figure constructed from the crystallite orientation distribution keeping, as the maximum polynomial, $l_{\max} = 16$. This exhibits rather pronounced oscillations. The smoothed representation is shown by the full curve. The principal maximum has been somewhat sharpened, and its abscissa value increased. The open circles in Figure 3 show the reconstructed pole figure given by the second approximation to the crystallite orientation distribution function ($l_{\max} = 30$). Comparison with the result of the first cycle (filled circles) reveals that the oscillations are now more nearly damped, and the principal maximum is higher and sharper. The smoothing of this second reconstructed pole figure is easier. Once again, we are entitled to sharpen and raise the principal maximum somewhat.

For the third and final cycle coefficients up to and including $l = 36$ were employed to represent the observed and unmeasured pole figures for eleven of the best-behaved planes. This number of plane normals would permit solution of the coefficient having $l_{\max} = 64$, so that we may use the least-squares procedure already described² for solution of the system of simultaneous equations. The weights assigned to the individual plane normals for this final cycle appear in column six of Table I.

IV. Evaluation

One test of the correctness of the crystallite orientation distribution function is furnished by comparison of

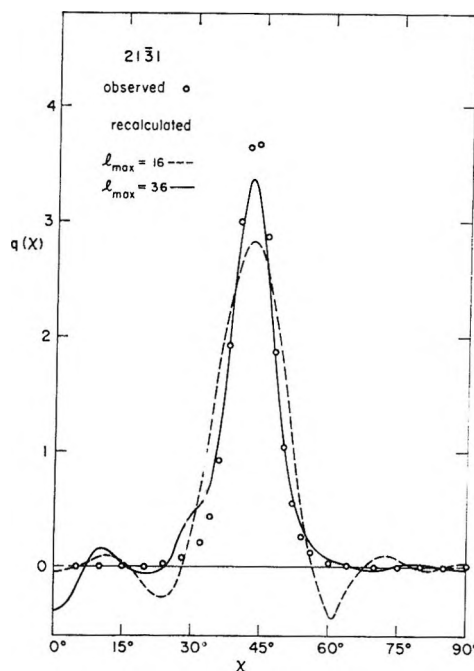


Figure 4. Comparison of the measured profile (circles) for the $(21\bar{3}1)$ reflection with those reconstructed from the crystallite orientation distribution function with $l_{\max} = 16$ (dashed curve) and $l_{\max} = 36$ (full curve).

the recalculated pole figures with those determined experimentally. Figures 4 and 5 illustrate such a comparison for two plane normals. The dashed and full curves represent the recalculated profiles using $l_{\max} = 16$ (first cycle) and $l_{\max} = 36$ (third cycle),

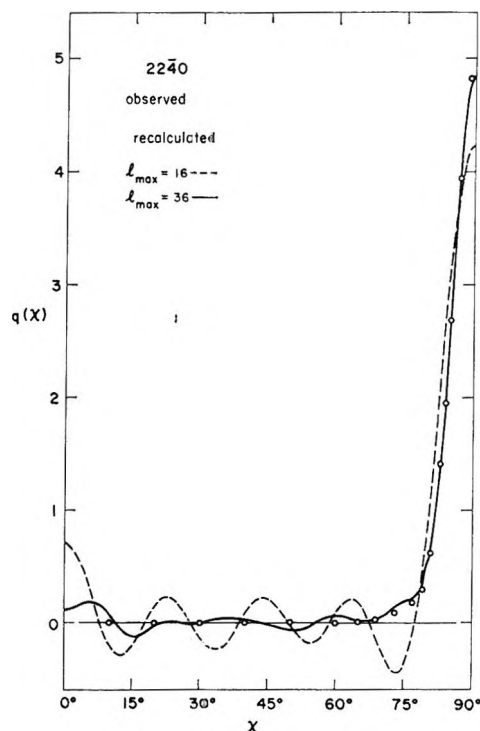


Figure 5. Same as Figure 4 for the $(22\bar{4}0)$ plane.

respectively, while the experimental observations are shown by circles. The full curves are clearly better representations of the observed profiles.

A more quantitative assessment of the series termination error can be gained from the standard deviation, σ_q . If the plane-normal distribution, $q(\cos \chi)$, is approximated by a series of Legendre polynomials terminated at $l_{\max} = \lambda$

$$q_l(\cos \chi_l) \cong \sum_{l=0}^{\lambda} Q_l^t P_l(\cos \chi_l) \quad (1)$$

then²

$$\sigma_q^2 = \int_{-1}^1 [q_l(\cos \chi_l)]^2 d(\cos \chi_l) - \sum_{l=0}^{\lambda} (Q_l^t)^2 \quad (2)$$

The σ_q values obtained for $l_{\max} = 16, 22, \text{ or } 36$ are shown in part A of Table II. The series termination error varies from one plane normal to another, but the decrease in σ_q with increasing l_{\max} is quite marked for all planes.

Table II: Evaluation of the Refinement Procedure

hkl	A. Values of σ_q			B. Values for σ_w	
	16	22	36	max	σ_w
30 $\bar{3}$ 0	0.379	0.218	0.047	16	0.849
22 $\bar{4}$ 0	0.444	0.193	0.017	22	0.330
21 $\bar{3}$ 1	0.420	0.176	0.025	36	0.013
11 $\bar{2}$ 3	0.673	0.372	0.058		
Av	0.479	0.240	0.037		

The crystallite orientation distribution for the case of hexagonal crystal symmetry may be expressed in spherical harmonics as

$$w(\xi, \phi) = \sum_{\substack{l=0 \\ \text{even}}}^{\infty} A_{l0} P_l^0(\xi) + 2 \sum_{\substack{l=2 \\ \text{even}}}^{\infty} \sum_{m=6}^l A_{lm} P_m^m(\xi) \cos m\phi \quad (3)$$

where m takes the values 6, 12, 18, If the series is truncated at $l_{\max} = \lambda$, the standard deviation, σ_w , of the finite series from the true $w(\xi, \phi)$ is given by

$$\sigma_w^2 = 2\pi \sum_{l>\lambda}^{\infty} \sum_{m=-l}^l A_{lm}^2 \quad (4)$$

An exact evaluation of σ_w is not possible since the A_{lm} values are not known for $l > \lambda$. However, Roe and Krigbaum² have suggested the approximate relation

$$\sigma_w^2 = \frac{1}{\pi} \sum_{l>\lambda}^{\infty} (l + 1/2) \langle Q_l^2 \rangle \quad (5)$$

where the angular brackets $\langle \rangle$ designate an average over all observed reciprocal lattice vectors. Equation 5 is based upon the approximate relation

$$\langle Q_l^2 \rangle = 2\pi^2 (l + 1/2)^{-1} [A_{l0}^2 + 2 \sum_{m=6}^l A_{lm}^2] \quad (6)$$

We must first check to see that this relation is obeyed in the present case. Figure 6 offers such a test. Here the triangles represent values of Q_l^t , averaged over the 11 reflections employed in the investigation, while the circles represent values for the right-hand member of eq 6. An approximately linear relation is obtained if the logarithms of these quantities are plotted as a function of l^2 . A similar functional dependence was observed earlier for fiber texture samples of polyethylene terephthalate.⁸ In Figure 6 the triangles and circles are represented reasonably well by a single line. If this linear relationship is assumed to extend beyond the range of l values shown, then eq 5 may be rewritten as

$$\sigma_w^2 = \frac{1}{\pi} \int_{\lambda+2}^{\infty} (l + 1/2) a e^{-bl^2} dl \quad (7)$$

From Figure 6, $a = 0.387$ and $b = 7.51 \times 10^{-3}$. The σ_w values estimated in this way are shown in part B of Table II. This criterion also indicates that a remarkable improvement in the crystallite orientation distribution function has resulted from application of the refinement procedure.

We conclude from this illustrative example that the successive refinement procedure can effect a substantial improvement in resolution of the crystallite orientation distribution function which can be deduced from a given set of pole figure data. This conclusion is based upon a comparison of the observed and recalculated plane-normal profiles, and upon the behavior of σ_q and σ_w during the refinement. The example presented involved a very small number of pole figures for a material having high crystal symmetry. In this case

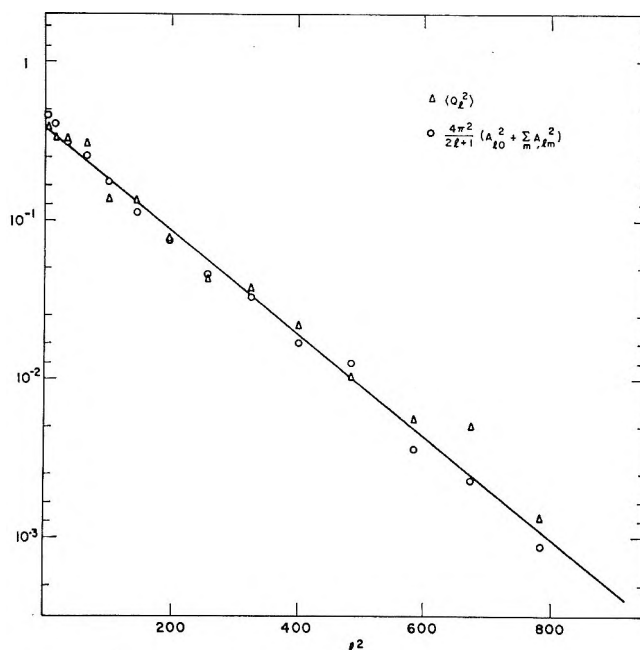


Figure 6. A test of eq 6 (see text).

the stated limitation upon the maximum l , based upon the number of pole figures and the sample symmetry, could be overcome. We recognize that a material of low crystal symmetry may present a more severe test of the refinement procedure, and an example of this type is

currently under investigation. We have not depicted the crystallite orientation distribution function for polystyrene V-3 since we intend to present a more complete investigation of several isotactic polystyrene samples at a later time.

First Quantum Corrections to the Second Virial Coefficient of a Stockmayer Gas

by M. McCarty, Jr.

Research Institute for Advanced Studies, Martin Marietta Corporation, Baltimore, Maryland 21227

and S. V. K. Babu

Department of Physics, State University of New York at Stony Brook, Stony Brook, New York 11790
(Received August 25, 1969)

The first-order translational and rotational quantum corrections to the second virial coefficient of a Stockmayer gas are calculated. These terms can be significantly larger than similar terms calculated with zero dipole moment. The quantum corrections are generally small in the region where $B(T)$ data exist; however, for H_2O and NH_3 they make contributions of as much as 10% near room temperature.

The Stockmayer potential (hereafter SP) consisting of a Lennard-Jones 6-12 potential plus a term to account (in the far field approximation) for dipole-dipole interactions is the potential most frequently employed to correlate observed second virial coefficients, $B(T)$, of polar molecules.¹ It is not uncommon that the best fit of the experimental data is obtained with values of the potential parameter, ϵ , sufficiently large that the reduced temperature, $T^* = kT/\epsilon$, can be less than 1.0 in the range of temperatures where $B(T)$ can be measured. For the Lennard-Jones potential, quantum mechanical corrections to $B(T)$ can become significant at values of $T^* < 1$.² Since the SP for the same value of ϵ corresponds, on the average, to a stronger attractive interaction than the Lennard-Jones potential it was felt that the quantum corrections for the SP could be of significance even for the relatively massive molecules usually encountered.

The theory germane to calculating the quantum corrections to $B(T)$ for angular dependent potentials was developed by Chang and Uhlenbeck.³ Their development is strictly applicable only to diatomic molecules. Although the extension to a generalized asymmetric rotor appears formally straightforward, this was not attempted since our present results indicate that the extensive additional computation would be of little practical value. It is felt, however, that the here

computed correction term for rotation (*vide infra*) should serve as a satisfactory first approximation to the actual term if the moment of inertia used in B^* is chosen (when possible) parallel to the dipole moment. Applied to the SP, the Chang-Uhlenbeck formulas yield

$$B^*(T^*) = B(T)/b_0 = B_{cl}(T^*) + \Lambda^{*2}B_{tr}^*(T^*) + B^*B_{rot}^*(T^*) + O(\Lambda^{*4}) + O(B^{*2})$$

where

$$b_0 = 2\pi\tilde{N}\sigma^3/3; \quad \Lambda^{*2} = h^2/(\sigma^2M\epsilon)$$

$B_{cl}(T^*)$ is the classical reduced second virial coefficient for the SP

$$\varphi^* = SP/4\epsilon = X^{-12} - X^{-6} - gX^{-3}t^*/\sqrt{2}$$

$$X = r/\sigma \quad t^* = \mu^2/(\epsilon_0^3\sqrt{8})$$

$$g = 2 \cos \theta_1 \cos \theta_2 - \sin \theta_1 \sin \theta_2 \cos(\varphi_1 - \varphi_2)$$

$$B_{tr}^*(T^*) = (2\pi T^*)^{-3} \iint \left(x \frac{d\varphi^*}{dx} \right)^2 \exp(-4\varphi^*/T^*) dx d\Omega$$

(1) J. O. Hirschfelder, C. F. Curtiss, and R. B. Bird, "Molecular Theory of Gases and Liquids," John Wiley & Sons, Inc., New York, N. Y., 1954, p 211.

(2) See, for example, ref 1, p 422.

(3) C. S. Wang Chang, Doctoral Dissertation, University of Michigan, 1944, as reported in ref 1, p 434.

$$B_{\text{rot}}^*(T^*) = t^{*2}/(4\pi T^{*2}) \iint X^{-4} L \exp(-4\varphi^*/T) dx d\Omega$$

$$L = \left(\frac{\partial g}{\partial \theta_1}\right)^2 + \left(\frac{\partial g}{\partial \theta_2}\right)^2 + \left(\frac{\partial g}{\partial \varphi_1} \csc \theta_1\right)^2 + \left(\frac{\partial g}{\partial \varphi_2} \csc \theta_2\right)^2$$

$$B^* = \hbar^2/(2IkT)$$

$$d\Omega = \sin \theta_1 \sin \theta_2 d\theta_1 d\theta_2 d(\varphi_1 - \varphi_2)$$

and the angles θ_1 , θ_2 , and $(\varphi_1 - \varphi_2)$ are defined in Figure 1. The integrals can be evaluated by first expanding the term, $\exp(gX^{-3}t^*\sqrt{8}/T^*)$, in a Maclaurin series. The resulting integrals over $d\Omega$ are readily evaluated by an easily derived recursion formula (*vide infra*). The

remaining integrals are most conveniently evaluated using the relations

$$B_m^{n*} = -3 \int_0^\infty X^{2+n} g_m dx$$

$$g_m = \begin{cases} \exp(-4(X^{-12} - X^{-6})/T^*) & m = 0 \\ r^{-6m} \exp(-4(X^{-12} - X^{-6})/T^*) & m \geq 1 \end{cases}$$

$$B_{m+2}^{n*} = 1/2 B_{m+1}^{n*} + \frac{6m - n - 3}{48} T^* B_m^{n*}$$

Both B_0^{n*} and B_1^{n*} can be evaluated by the rapidly

Table I^a

T^*	$t^* = 0^{b,c}$	$t^* = 0.25^b$	$t^* = 0.50^b$	$t^* = 0.75^b$	$t^* = 1.0^b$	$t^* = 1.25^b$	$t^* = 1.50^b$	$t^* = 1.75^b$	$t^* = 2.0^b$
0.5	3.05161	4.66362	14.2885	70.5727	493.87	4503.69	50403.6	664694	1.00558E + 7
	0	2.01409	15.2472	101.634	807.16	7862.69	91502.4	1.23697E + 6	1.90224E + 7
0.6	1.67256	2.27886	5.28397	18.0769	82.9272	479.497	3334.76	26927.3	246156
	0	1.03458	6.41955	30.9657	163.321	1010.88	7310.44	60493.2	561916
0.7	1.05461	1.33591	2.57607	6.86665	23.5207	98.6684	488.8	2777.17	17690.9
	0	0.622872	3.43036	13.5095	54.2462	244.633	1259.81	7328.87	47404.9
0.8	0.729172	0.879234	1.49067	3.32383	9.21201	30.5258	117.489	512.849	2489.63
	0	0.414713	2.11581	7.29343	24.2877	87.234	349.273	1559.25	7677.27
0.9	0.537685	0.626051	0.966566	1.88734	4.46028	12.3556	39.1761	139.431	547.839
	0	0.295759	1.43284	4.50872	13.1594	40.0046	132.348	481.393	1915.7
1	0.415582	0.471573	0.678651	1.19708	2.50052	6.02259	16.3941	49.6217	164.681
	0	0.221639	1.0352	3.05324	8.10121	21.7519	62.141	192.327	645.652
1.2	0.27409	0.300393	0.392417	0.599716	1.04952	2.06435	4.49671	10.7184	27.6715
	0	0.138041	0.615146	1.6694	3.91274	8.89842	20.7378	50.8816	132.868
1.4	0.197775	0.212075	0.260379	0.362082	0.562583	0.963978	1.8014	3.63747	7.87446
	0	9.44522E - 2	0.409289	1.05725	2.30147	4.73188	9.70309	20.448	45.0041
1.6	0.151545	0.160139	0.188489	0.245492	0.350672	0.544362	0.910637	1.62974	3.10089
	0	6.88535E - 2	0.293027	0.733343	1.52266	2.9338	5.53221	10.5235	20.5649
1.8	0.121171	0.126727	0.144747	0.179802	0.241471	0.348325	0.536302	0.876288	1.5118
	0	5.25272E - 2	0.220802	0.540812	1.08751	2.00519	3.5709	6.32709	11.3645
2	0.09999	0.103785	0.115942	0.139018	0.17819	0.243023	0.350989	0.534391	0.854179
	0	4.14651E - 2	0.172766	0.416709	0.819134	1.46409	2.50372	4.21688	7.12541
2.5	6.80158E - 2	6.97521E - 2	0.075203	8.51473E - 2	0.101072	0.125515	0.162676	0.219503	0.307593
	0	2.55025E - 2	0.104813	0.246913	0.468846	0.799433	1.28594	2.0057	3.08652
3	5.05769E - 2	5.15138E - 2	5.44211E - 2	5.96036E - 2	6.76237E - 2	7.93959E - 2	9.63456E - 2	0.120671	0.155767
	0	1.73563E - 2	0.070795	0.164631	0.306779	0.51	0.794001	1.18885	1.74048
5	0.023591	2.37718E - 2	2.43222E - 2	2.52672E - 2	2.66498E - 2	2.85351E - 2	3.10142E - 2	3.42111E - 2	3.82926E - 2
	0	6.16565E - 3	2.48612E - 2	5.66953E - 2	0.102725	0.164527	0.244298	0.34501	0.470619
10	9.31649E - 3	9.33878E - 3	9.40598E - 3	9.51908E - 3	9.67977E - 3	9.89048E - 3	1.01544E - 2	1.04757E - 2	1.08592E - 2
	0	1.6185E - 3	6.4903E - 3	1.46647E - 2	2.62249E - 2	4.12898E - 2	6.00167E - 2	8.26043E - 2	0.109297

^a Notation: $aEb = a \times 10^b$. ^b Top entry is $B_{\text{tr}}(T^*)$, lower entry is $B_{\text{rot}}(T^*)$. ^c Note that when $t^* = 0$, B_{tr}^* is the reduced first correction term for the Lennard-Jones 6-12 potential. The short table of $B(T^*, 0)$ given in ref 1, p 422, contains several errors.

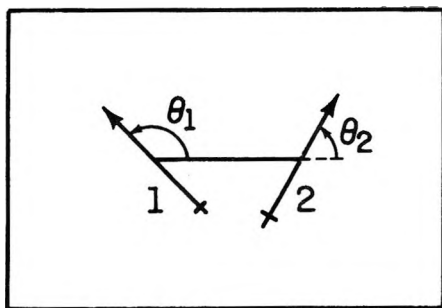


Figure 1. Sketch defining θ_1 and θ_2 in the Stockmayer potential. The angle $\varphi_1 - \varphi_2$ is the angle by which the second dipole protrudes from the plane defined by the first dipole and the line connecting the centers of the dipoles.

convergent series given by Nosanow and Mayer.⁴ The results for B_{Tr} and B_{rot} are

$$B_{tr}^* = - (2\pi^2 T^{*3})^{-1} \sum_{k=0}^{\infty} \frac{8^k}{(2k)!} \left(\frac{t^*}{T^*} \right)^{2k} \times$$

$$\left[G_k B_{k+2}^{-2} T^* (12k + 22) - B_{k+1}^{-2} \times \right.$$

$$\left. \left(T^* G_k (6k + 5) + t^{*2} G_{k+1} \frac{6k + 7}{2k + 1} \right) \right]$$

$$B_{rot}^* = - \frac{2}{3} \sum_{k=0}^{\infty} \frac{8^k}{(2k)!} \left(\frac{t^*}{T^*} \right)^{2k+2} I_k B_{k+1}^{0^*}$$

where

$$G_k = \frac{1}{8\pi} \int g^{2k} d\Omega$$

$$G_0 = 1 \quad G_{k+1} = (k + 1.5)^{-2} [4^k + G_k (k + 1)(k + 0.5)]$$

$$I_k = \frac{1}{8\pi} \int L g^{2k} d\Omega = 2(G_k - G_{k+1} + 3H_k)$$

$$H_k = \frac{1}{8\pi} \int \cos^2 \theta_1 g^{2k} d\Omega$$

$$H_0 = 1/3; \quad H_{k+1} = (k + 2.5)^{-1} (k + 1.5)^{-1} (H_k (k + 1)(k + 0.5) + 4^k)$$

After computing $B_0^{-2^*}$ and $B_1^{-2^*}$ ($B_0^{0^*}$ and $B_1^{0^*}$ are simply related to the tabulated second virial coefficient and its temperature derivative for the Lennard-Jones 6-12 potential) both B_{tr}^* and B_{rot}^* were computed to six significant figures. These are tabulated in Table I. Since for the species usually considered Λ^{*2} is in the range of 10^{-2} to 10^{-3} , it is seen that the translational corrections will generally be unimportant for values of $T^* > 1$. Likewise, for $T^* > 1.0$ it will occur that $B^* B_{rot}^* \ll B_{cl}^*$. However, for those species whose calculated SP parameters indicate that values of $T^* < 1$

are in the experimentally accessible region, the quantum corrections should be taken into account.

Of the molecules for which the Stockmayer parameters have been determined, the quantum corrections were generally found to be less than 2% at the lowest temperature for which $B(T)$ data exists.⁵ Two exceptions to this are H_2O and NH_3 for which calculations indicated that the quantum correction terms were on the order of 10%, at the lowest temperature for which $B(T)$ data are available. For both of these species the data reported in ref 6 were employed to determine the parameters, ϵ/k and b_0 , both with and without the correction terms. The results for H_2O are summarized in Table II, where it is seen that including the quantum corrections leads to only a very slight improvement in the calculated second virial coefficients. Similar results were found for NH_3 except that a much smaller difference between the values of ϵ/k determined with and without the correction terms was found (without the quantum corrections $\epsilon/k = 335.02^\circ K$, $b_0 = 23.416$ cc/mol; with corrections $\epsilon/k = 334.69^\circ K$, $b_0 = 22.68$ cc/mol).

Table II

$T, ^\circ C$	$-B(T),^a$ cc/mol	$B(\text{calcd}) -$ $B(\text{obsd}),^b$ cc/mol	$B(\text{calcd} -$ $B(\text{obsd}),^c$ cc/mol	Quantum corrections to $B(\text{calcd}),^d$ cc/mol
40	976	-0.98	-0.25	139.70
70	638	1.65	0.45	69.49
100	450	0.78	-0.02	38.78
150	284	0.39	0.59	17.64
200	197	-0.64	0.12	9.45
300	112	-1.86	-0.77	3.69
400	72	-2.51	-1.48	1.85

^a Data reported in ref 6. ^b $B(\text{calcd})$ determined using $\epsilon/k = 375.92^\circ K$, $b_0 = 23.3539$, and neglecting quantum corrections. ^c $B(\text{calcd})$ determined using $\epsilon/k = 360.049$, $b_0 = 22.319$ and including the quantum corrections.

In summary, it appears that quantum corrections to the second virial coefficient of a Stockmayer gas can be significant even well above room temperature. However, for the purposes of correlating data, potential parameters can be determined which yield satisfactory agreement between the calculated and experimental second virial coefficients while ignoring the quantum corrections.

(4) L. H. Nosanow and J. E. Mayer, *J. Chem. Phys.*, **28**, 874 (1958).

(5) See ref 1, pp 214, 217 for references to original data.

(6) L. Monchick and E. A. Mason, *J. Chem. Phys.*, **35**, 1676 (1961).

Phosphorus 2p Electron Binding Energies. Correlation with Extended Hückel Charges

by M. Pelavin,¹ D. N. Hendrickson,² J. M. Hollander,¹ and W. L. Jolly²

Department of Chemistry of the University of California and the Inorganic Materials Research and Nuclear Chemistry Divisions of the Lawrence Radiation Laboratory, Berkeley, California 94720
(Received July 9, 1969)

Phosphorus 2p electron binding energies were measured for 53 phosphorus compounds. Phosphorus atom charges, calculated for some of the compounds by means of a noniterative as well as an iterative extended Hückel molecular orbital method, are correlated with the measured phosphorus 2p binding energies. The electronic structure of the cyclic phosphonitrilic chloride trimer, (NPCl₂)₃, is briefly discussed.

I. Introduction

Core-electron binding energies, as determined by X-ray photoelectron spectroscopy, have been found to be chemically shifted and to be correlated to effective atomic charge.³ Thus core-electron binding energies have been shown to be correlated to formal oxidation states in sulfur^{3,4} and chlorine^{3,5} compounds and to fractional atomic charges in sulfur,³ nitrogen,^{6,7} and carbon⁸ compounds. The methods for calculating the fractional atomic charges used in these correlations include a modification of Pauling's method,⁹ the CNDO molecular orbital method,¹⁰ and the extended Hückel molecular orbital (EHMO) method.¹¹

In this paper, an attempt is made to correlate phosphorus 2p electron binding energies with phosphorus atom charges calculated by the EHMO method. The simple EHMO method as well as an iterative variation¹² of the EHMO method are used to calculate the phosphorus atom charges, and the phosphorus atom input parameters are varied to find the set which gives the best correlation of binding energy with calculated charge.

II. Experimental Section

Photoionization of the phosphorus 2p electrons was accomplished by using Mg K α X-radiation (1253.6 eV). A description of the iron-free, double-focusing magnetic spectrometer used to determine the kinetic energies of the photoelectrons has appeared previously.^{3,13} In this study, as in previous studies, the carbon 1s signal from the pump oil which formed as a film on the samples served as a convenient reference. For all compounds three measurements of the phosphorus peak were carried out, each followed by calibration with the pump oil carbon peak.

All the phosphorus compounds studied were solids; powdered samples were brushed onto double-faced conducting tape mounted on an aluminum plate, which served as a heat and electron sink. Some instances of decomposition (X-ray induced, thermal, or chemical)

were noticed and will be mentioned in the Results section.

Some of the phosphorus compounds were purchased; many were kindly provided by Dr. J. Van Wazer. *trans*-Mn(CO)₄P(C₆H₅)₃Cl, (*cis*-PP)Mn(CO)₃I,¹⁴ and Mn(CO)₅(AP)I¹⁴ were supplied by Dr. G. Nelson, and compounds 46-50 were obtained from L. Kramer. Samples of (NPCl₂)₃,¹⁵ (NaPO₂NH)₃,¹⁵ P₄OH,¹⁶ and

- (1) Nuclear Chemistry Division of the L. R. L.
- (2) Department of Chemistry of the University of California and Inorganic Materials Research Division of the L. R. L.
- (3) K. Siegbahn, C. Nordling, A. Fahlman, R. Nordberg, K. Hamrin, J. Hedman, G. Johansson, T. Bergmark, S.-E. Karlsson, I. Lindgren, and B. Lindberg, "ESCA Atomic Molecular and Solid State Structure Studied by Means of Electron Spectroscopy," Almquist and Wiksells AB, Stockholm, 1967.
- (4) A. Fahlman, K. Hamrin, J. Hedman, R. Nordberg, C. Nordling, and K. Siegbahn, *Nature*, **210**, 4 (1966).
- (5) A. Fahlman, R. Carlsson, and K. Siegbahn, *Ark. Kemi*, **25**, 301 (1966).
- (6) R. Nordberg, R. G. Albridge, T. Bergmark, U. Ericson, A. Fahlman, K. Hamrin, J. Hedman, G. Johansson, C. Nordling, K. Siegbahn, and B. Lindberg, *Nature*, **214**, 481 (1967); R. Nordberg, R. G. Albridge, T. Bergmark, U. Ericson, J. Hedman, C. Nordling, K. Siegbahn, and B. J. Lindberg, *Ark. Kemi*, **28**, 257 (1968).
- (7) J. M. Hollander, D. N. Hendrickson, and W. L. Jolly, *J. Chem. Phys.*, **49**, 3315 (1968); D. N. Hendrickson, J. M. Hollander, and W. L. Jolly, *Inorg. Chem.*, **8**, 2642 (1969).
- (8) R. Nordberg, U. Gelius, P. F. Hedén, J. Hedman, C. Nordling, K. Siegbahn, and B. J. Lindberg, submitted to *Ark. Kemi*.
- (9) L. Pauling, "The Nature of the Chemical Bond," 3rd ed, Cornell University Press, Ithaca, N. Y., 1960, p 97.
- (10) J. A. Pople, D. P. Santry, and G. A. Segal, *J. Chem. Phys.*, **43**, S130 (1965).
- (11) R. Hoffmann, *ibid.*, **39**, 1397 (1963).
- (12) P. C. Van der Voorn and R. S. Drago, *J. Amer. Chem. Soc.*, **88**, 3255 (1966).
- (13) J. M. Hollander, M. D. Holtz, T. Novakov, and R. L. Graham, *Ark. Fysik*, **28**, 375 (1965); T. Yamazaki and J. M. Hollander, *Nucl. Phys.*, **84**, 505 (1966).
- (14) *cis*-PP and AP are the bidentate olefin phosphine ligands 2-*cis*-propenylphenyldiphenylphosphine and 2-allylphenyldiphenylphosphine, respectively; see G. Nelson and L. Interrante, *Inorg. Chem.*, **7**, 2059 (1968).
- (15) "Inorganic Syntheses," Vol. 6 and 11, McGraw-Hill Book Co., New York, N. Y., 1960 and 1968.
- (16) J. H. Krueger, Ph.D. Thesis, University of California, Berkeley, Calif., 1961.

trans-Rh(CO)Cl(P(C₆H₅)₃)₂¹⁵ were prepared by standard synthetic procedures.

III. Theory

The theoretical aspects of the determination of core-electron binding energies have been considered previously.^{3,7,17} The core-electron binding energy E_b is referred to the Fermi level of the sample. Knowledge of the energy of the X-radiation, $E_{x\text{-ray}}$, the kinetic energy of the photoelectron, E_{kin} , and the work function of the spectrometer material (aluminum), ϕ_{spec} , allows the calculation of the core-electron binding energy

$$E_b = E_{x\text{-ray}} - E_{\text{kin}} - \phi_{\text{spec}}$$

The binding energies of core electrons are influenced by potentials arising from the net charge on atoms in the particular molecule as well as by the lattice potential of neighboring molecules.^{3,7,17} It has been found that the binding energy increases with increasing oxidation state (*i.e.*, actually the effective charge) of the particular atom.

IV. Calculations

Two basic modifications of the extended Hückel molecular orbital method were used. In both cases computations were performed with a CDC 6600 computer using a Fortran IV program. The first modification was that formulated by Hoffmann.¹¹ In the extended Hückel method no assumptions have to be made concerning hybridization. The Coulomb integrals were approximated by valence-state ionization potentials (vsip) as determined by Hinze and Jaffé.¹⁸ The ionization potential for a phosphorus 3d electron was taken as 3.00 eV.¹⁹ Orbital exponents were obtained by using Slater's rules²⁰ except where noted. Calculations were completed with use of three variations for the off-diagonal Hamiltonian elements: the arithmetic mean (eq 1), the geometric mean (eq 2), and Cusachs' approximation²¹ (eq 3)

$$H_{ij} = 1.75S_{ij}(H_{ii} + H_{jj})/2 \quad (1)$$

$$H_{ij} = 2S_{ij}(H_{ii}H_{jj})^{1/2} \quad (2)$$

$$H_{ij} = S_{ij}(H_{ii} + H_{jj})(2 - |S_{ij}|)/2 \quad (3)$$

Here H_{ii} is the negative of the vsip, and S_{ij} is the usual overlap integral.

The second modification of the extended Hückel method used in this work was an iterative type.¹² The Coulomb integrals were set equal to the negative of the appropriate neutral atom vsip's, corrected for net atomic charge q_i , where K was taken as 2.00 eV per unit charge.

$$H_{ii} = H_{ii}^\circ - Kq_i \quad (4)$$

The Slater exponents μ_i were also taken as charge dependent, assigned by an extension of Slater's rules

$$\mu_i = \mu_i^\circ + 0.35q_i/n^*$$

Here n^* is the effective principal quantum number, and μ_i° is the exponent for the i th orbital on a neutral atom. The net atomic charges q_i were obtained in each cycle by an application of Mulliken's population analysis.²² In our self-consistent extended Hückel calculations we elected to use the Cusachs' approximation (eq 3) for the off-diagonal Hamiltonian elements. The calculational procedure consisted of iterating until the atomic charges were self-consistent to at least 0.01.

Cartesian coordinates were obtained from Program PROXYZ,²³ the molecular parameters were obtained from crystal structure determinations²⁴⁻²⁶ or from estimates.

Phosphorus atomic charges were also calculated by the simple Pauling method.⁹ The ionic character (I_{AB}) of a bond between atoms A and B is taken as a function of the atom electronegativities χ_A and χ_B

$$I_{AB} = 1.0 - e^{-0.25(\chi_A - \chi_B)^2} \quad (5)$$

The atom electronegativities can be taken as charge-dependent functions, the prescription for correction of neutral atom electronegativities being simply that the electronegativity is increased two-thirds of the way to the electronegativity of the element next in the periodic table for each unit positive charge. Hydrogen cannot be treated by this simple correction formula, but it was found that the phosphorus charges in the molecules studied in this work were affected only slightly by correcting χ_H for charge by some reasonable amount.

Within the valence-bond formalism the net charge q_A on an atom A is given by

$$q_A = Q_A + \sum_{B \neq A} I_{AB} \quad (6)$$

where Q_A is the formal charge on atom A and the summation is over all the bonds to atom A. The calculational process is iterative because of the charge-dependent atom electronegativities; "self-consistent" atomic charges result. In no case did we use a valence-bond representation indicative of 3d phosphorus orbital participation as has been done in the case of sulfur compounds.³

(17) C. S. Fadley, S. B. M. Hagström, J. M. Hollander, M. P. Klein, and D. A. Shirley, *Science*, **157**, 1571 (1967); C. S. Fadley, S. B. M. Hagström, M. P. Klein, and D. A. Shirley, *J. Chem. Phys.*, **48**, 3779 (1968).

(18) J. Hinze and H. H. Jaffé, *J. Amer. Chem. Soc.*, **84**, 540 (1962).

(19) D. P. Santry and G. A. Segal, *J. Chem. Phys.*, **47**, 158 (1967).

(20) J. C. Slater, *Phys. Rev.*, **36**, 57 (1930).

(21) L. C. Cusachs and J. W. Reynolds, *J. Chem. Phys.*, **43**, S160 (1965); L. C. Cusachs, J. W. Reynolds, and D. Barnard, *ibid.*, **44**, 835 (1966).

(22) R. S. Mulliken, *ibid.*, **23**, 1333, 1841, 2338, 2343 (1955).

(23) P. M. Kuznesof, Quantum Chemistry Program Exchange (Indiana University) QCPE 94 (1966).

(24) "Table of Interatomic Distances," L. E. Sutton, Ed., Special Publication No. 11, The Chemical Society, Burlington House, London, 1958, and No. 18, Supplement, 1965.

(25) For (C₆H₅)₃P, see J. Daly, *J. Chem. Soc.*, 3799 (1964).

(26) For P₄S₁₀ and P₄S₇, see A. Vos and E. Wiebenga, *Acta Cryst.*, **8**, 217 (1955).

V. Results and Discussion

The work function of the spectrometer material was arbitrarily assigned a value of 4.0 eV, for normalization purposes.⁷

Correlation with Charges Obtained from Extended Hückel Molecular Orbitals. Phosphorus 2p electron binding energies determined for over 50 compounds are listed in Tables I and II. The range of binding energy shifts was found to be about 8 eV. In the case of 25 of these compounds, noniterative extended Hückel molecular orbital calculations were made by using eq 1, both without and with 3d orbitals on the phosphorus atom. The resultant phosphorus atom charges are given in Table I. It can be seen that the calculated phosphorus atom charge is, except in a few cases, unaffected by inclusion of 3d orbitals.

In Figure 1 the measured phosphorus 2p binding energies are plotted against the noniterative extended Hückel-calculated phosphorus charges. The correlation of these two quantities can be seen to be poor.

Table I: Phosphorus 2p Binding Energies and Extended Hückel Calculated Charges

Compound no.	Compound	Binding energy, eV	Calculated phosphorus atom charge		
			without 3d	with 3d	Iterative ^b with 3d
1	NH ₄ PF ₆	137.3	3.723	3.806	2.505
2	(NPF ₂) ₃	134.5	2.321	2.277	0.961
3	(CH ₃ PS ₂) ₂	133.4	1.502	1.591	0.764
4	P ₄ S ₁₀	134.0	1.515	1.390	
5	(C ₆ H ₅) ₂ PS	132.3		2.194	
6	<i>n</i> -(C ₆ H ₅) ₄ P ⁺ Cl ⁻	132.3	1.173	2.525	
7	(C ₆ H ₅) ₃ P	130.6		0.999	
8	P ₄ S ₃	130.5 ^c	0.324 ^d	0.338 ^d	0.303 ^d
			0.048	0.148	0.122
9	P _{red}	130.1 ^c	0	0	0
10	KPF ₂ O ₂	134.8	3.578	3.547	1.956
11	(NH ₄) ₂ PFO ₃	134.1	3.490	3.443	1.815
12	Na ₂ H ₂ P ₂ O ₇	133.9	3.387	3.387	1.767
13	KH ₂ PO ₄	133.9		3.669	1.785
14	(NH ₄) ₂ CH ₃ PO ₃	133.8	2.905	3.041	1.435
15	C ₆ H ₅ CH ₂ PO ₃ H ₂	133.8	2.846	3.284	
16	HOPO(NH ₂) ₂	133.6	2.832	3.083	1.465
17	Na ₄ P ₂ O ₇	133.3	3.374	3.354	
18	Na ₃ PSO ₃	133.0	2.936	2.622	1.361
19	Na ₃ (PO ₂ NH) ₃	133.0	2.892 ^e	3.062 ^e	
20	BaHPO ₃	132.9	2.844	2.790	1.420
21	(C ₆ H ₅) ₃ PO	132.7		2.744	
22	K ₂ HPO ₄	132.7		3.621	2.001
23	KH ₂ PO ₂ ·H ₂ O	132.4	2.236	2.201	1.189
24	Na ₃ PO ₄	132.1	3.413	3.621	1.544
25	P ₄ S ₇	134.3		1.370	
		132.7		0.266	

^a Completed using arithmetic off-diagonal approximation (eq 1). ^b Charges are self-consistent to at least 0.01. ^c A second peak at 134.5 eV was attributed to a decomposition product. ^d There are two different types of phosphorus in P₄S₃; the more positive number in each case refers to the unique phosphorus atom. For purposes of plotting, an average charge value was used. ^e Calculation with assumed $r_{P-N} = 1.70 \text{ \AA}$.

This is in contrast to our nitrogen work⁷ where a reasonably good correlation was found with the same variation of the noniterative extended Hückel method (*i.e.*, the arithmetic mean off-diagonal approximation).

Table II: Some Phosphorus 2p Binding Energies

Compound no.	Compound	Phosphorus 2p electron binding energy, eV
26	Mn(CO) ₄ P(C ₆ H ₅) ₃ Cl	131.2
27	(<i>cis</i> -PP)Mn(CO) ₃ I ^d	133.2
28	Mn(CO) ₃ (AP)I ^b	133.0
29	<i>trans</i> -Rh(CO)Cl(P(C ₆ H ₅) ₂) ₂	131.6
30	Tris- α -naphthylphosphine	130.9
31	<i>o</i> -[(C ₆ H ₅) ₂ C ₆ H ₅] ₂ P	134.3
32	P ₃ N ₅	133.2
33	(NaPO ₃) ₃	134.0
34	(NaPO ₃) ₄ ·4H ₂ O	134.1
35	P ₄ OH	129.9 ^c
		133.1
36	Phosphotungstic acid	133.0 ^d
37	(C ₆ H ₅ O) ₃ PO	134.2
38	(C ₆ H ₅ S) ₃ P	134.4
39	Na ₅ P ₃ O ₁₀ form I	133.6
40	NaPO ₃ glass	134.5
41	P ₄ S ₅	132.0
		134.9 (sh)
42	BP	129.5
43	<i>cis</i> -PP ^a	131.3
		132.6 (sh)
44	PBr ₅	138.4 ^e
45	POBr ₃	134.4
46	Riboflavin 5'-phosphate	133.5
47	O-Phosphoserine (<i>dl</i>)	133.5
48	Barium phosphoglyceric acid	133.5
49	O-Phosphothreonine (<i>dl</i>)	133.7
50	O-Phosphoethanolamine	134.1
51	CrP	128.8 ^f
52	MnP	129.3 ^g
53	(C ₆ H ₅ CH ₂)(C ₆ H ₅) ₂ P ⁺ Cl ⁻	132.5

^a The ligand *cis*-PP is the bidentate 2-*cis*-propenylphenyldiphenylphosphine. ^b The ligand AP is the bidentate 2-allylphenyldiphenylphosphine. ^c Two peaks observed for P₄OH in the ratio of about 2:1, the lower binding energy peak the larger. See the Discussion for further particulars. ^d A second peak at 134.2 eV was observed, attributed to something other than starting material, for peak increased between successive scans while the 133.0-eV peak decreased. ^e A second larger peak was found at 134.4 eV, probably assignable to the oxidation product POBr₃. ^f A second peak was observed at 133.8 eV, due probably to an oxidation product. ^g A second peak was observed at 133.2 eV, due probably to an oxidation product.

Extensive modifications of the input data were tried (see Table III). The phosphorus 3d orbital was contracted by arbitrarily assigning the Slater exponent a value of 1.6 (this value is in the range suggested by Fogleman, *et al.*²⁷). The effect of this can be seen to be negligible for the series of molecules in Table III.

(27) W. W. Fogleman, D. J. Miller, H. B. Jonassen, and L. C. Cusachs, *Inorg. Chem.*, **8**, 1209 (1969).

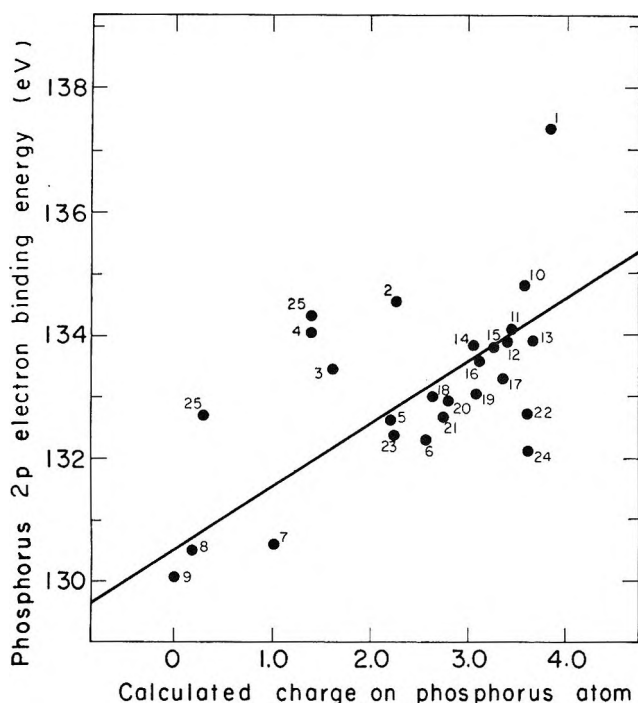


Figure 1. Plot of phosphorus 2p binding energies vs. noniterative extended Hückel calculated charges on phosphorus atoms.

In the second modification the phosphorus 3d orbital was contracted, and its vsip was changed from 3.0 to 7.0 eV (see column 3, Table III). The resultant phosphorus charges were appreciably changed, but the correlation was *not* markedly improved for the seven compounds considered. The last two columns in Table III list the phosphorus charges resulting from changing the input vsip's for the phosphorus 3s and 3p orbitals. Again, a plot of the data shows little improvement in the correlation. Finally, the character of the off-diagonal approximation used in our noniterative

Table III: Noniterative Extended Hückel Calculated^a Net Phosphorus Atom Charges Resultant from Various Input Parameter Modifications

Molecule	Phosphorus atom charge and input parameter modification			
	$\mu(\text{P}_{3d}) = 1.6$	$\mu(\text{P}_{3d}) = 1.6$ vsip(P _{3d}) = 7.0 eV	vsip(P _{3s}) = 17.0	vsip(P _{3p}) = 11.5
PFO ₃ ²⁻	3.442	2.880	3.579	3.761
PSO ₃ ³⁻	2.746	1.943	2.881	3.096
PF ₂ O ₂ ⁻	3.554	3.057	3.683	3.858
(CH ₃ PS ₂) ₂	1.215	0.494	1.709	2.022
P ₄ S ₃	0.260 ^b	-0.181 ^b	0.437 ^b	0.690 ^b
PF ₆ ⁻	0.019	-0.202	0.196	0.305
HPO ₄ ²⁻	3.792	3.259	3.933	4.086
PO ₄ ³⁻	3.524	3.054	3.810	4.017

^a Equation 1 used for off-diagonal terms. ^b See footnote d in Table I.

Table IV: Noniterative Extended Hückel Calculated Net Phosphorus Atom Charges Resultant from Two Off-Diagonal Approximations

Molecule	Phosphorus atom charge	
	Geometric H_{ij} ^a	Cusachs' H_{ij} ^b
PF ₂ O ₂ ⁻	4.191	3.739
PFO ₃ ²⁻	4.131	3.676
PSO ₃ ³⁻	3.610	3.205
(CH ₃ PS ₂) ₂	2.963	2.182
P ₄ S ₃	0.993 ^c	0.870
PF ₆ ⁻	0.464	0.276
HPO ₄ ²⁻	4.574	4.198
PO ₄ ³⁻	4.402	4.068
	3.727	3.305

^a Equation 2. ^b Equation 3. ^c See footnote d in Table I.

extended Hückel calculations was changed to both the geometric mean (eq 2) and the Cusachs variation (eq 3). The calculated phosphorus atom charges in a series of nine compounds for both of these approaches is given in Table IV. The data obtained using the Cusachs and geometric mean approximations showed essentially the same correlation as found in Figure 1.

It seemed at this point that the inability to obtain even a moderate correlation of measured phosphorus 2p binding energy with noniterative extended Hückel-calculated phosphorus charge was a manifestation of some inherent problem(s) in the calculational method. This belief was nurtured, as stated above, by our success with nitrogen 1s data⁷ as well as with recent boron 1s data.²⁸ Concerning the reality of phosphorus atom charges obtained from this simple extended Hückel method, Sichel and Whitehead²⁹ have found a good linear correlation of the phosphorus nuclear magnetic resonance chemical shifts of the methylphosphines with calculated charges on phosphorus. Unfortunately, this is not a diversified series of phosphorus compounds. An attempt to correlate the phosphorus charges given in Table I with reported phosphorus chemical shifts³⁰ was a marked failure. This failure could be attributed either to some inadequacy in the noniterative extended Hückel method (applied to phosphorus compounds) or more probably to differing average electronic excitation energies³¹ throughout the series of molecules.

Considering the distribution of points in Figure 1, it is interesting to note that compounds 10–24 are molecules containing P–O bonds. Perhaps the simple extended Hückel method has tended to overemphasize the polarity of these P–O bonds and as such has assigned

(28) D. N. Hendrickson, J. M. Hollander, and W. L. Jolly, unpublished work.

(29) J. M. Sichel and M. A. Whitehead, *Theor. Chim. Acta*, **5**, 35 (1966).

(30) J. W. Emsley, J. Feeney, and L. H. Sutcliffe, "High Resolution Nuclear Magnetic Resonance Spectroscopy," Vol. 2, Pergamon Press, New York, N. Y., 1966, p 1139.

(31) J. A. Pople, *J. Chem. Phys.*, **37**, 53 (1962).

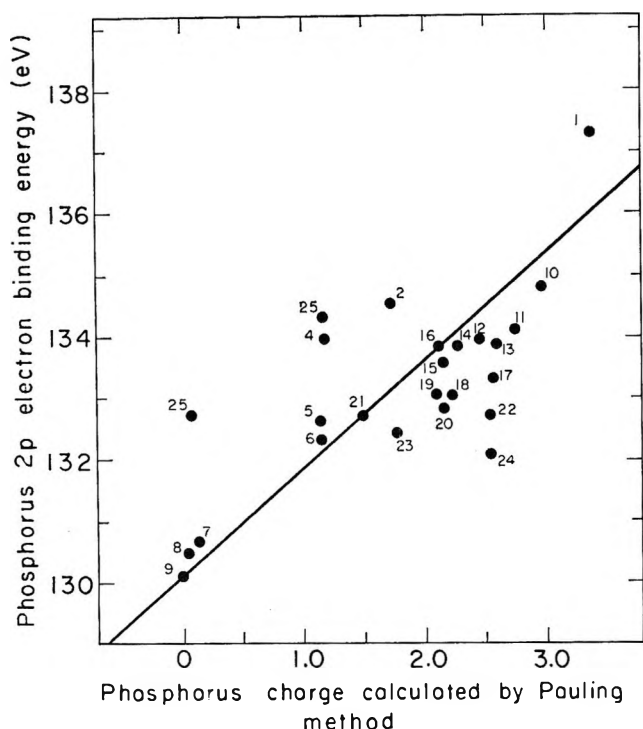


Figure 2. Plot of phosphorus 2p binding energies vs. phosphorus atom charges calculated by Pauling method using neutral atom electronegativities.

excessive positive charge to the phosphorus atoms. It does seem unrealistic that the phosphates 13, 22, and 24 should have essentially the same net phosphorus

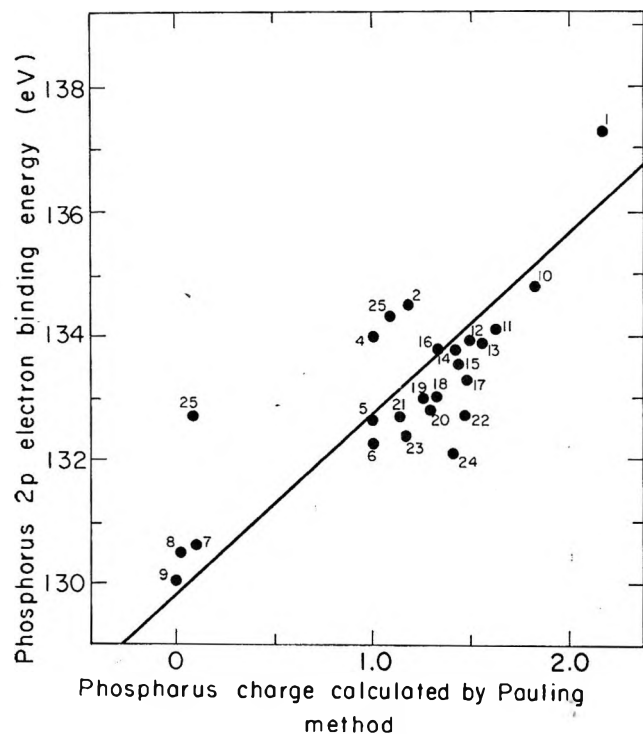


Figure 3. Plot of phosphorus 2p binding energies vs. phosphorus atom charges calculated by Pauling method using charge-dependent atom electronegativities.

charges as that obtained for the hexafluorophosphate ion (1). Some support for this proposal of overemphasis of P-O bond polarity can be gained by reverting to two variations of the Pauling method⁹ of calculation of net atomic charges.

In analogy with our noniterative extended Hückel calculations, phosphorus charges for the compounds in Figure 1 were obtained by a straightforward application of eq 4 and 5, using neutral-atom electronegativities. The resultant charges are plotted in Figure 2 vs. the phosphorus 2p binding energies. The similarity of distribution of points in Figures 1 and 2 is striking. If the other modification of the Pauling method is invoked, we would expect this iterative "self-consistent" method to accomplish two goals: (1) over-all decrease in all net charges, and (2) reduction in tendency to overemphasize particular bond polarities. In Figure 3 we can clearly see that the first expectation is met; the phosphorus charge range is essentially halved from that in Figure 2. The improved correlation depicted in Figure 3 tends to support the second expectation.

Having accepted this interpretation of the lack of correlative ability, it seemed reasonable that a more modern version of the extended Hückel method would be warranted, a version where the Hamiltonian is charge dependent.¹² Using charge-dependent valence state ionization potentials (eq 4) coupled with the Cusachs approximation (eq 3) for the off-diagonal Hamiltonian terms, we obtained the phosphorus charges given in Table I. All phosphorus charges are appreciably reduced when using this iterative extended Hückel method. In fact the same order of reduction occurred in this case as with the simple Pauling method. Unfortunately, these self-consistent extended Hückel-calculated phosphorus charges gave little improvement in the correlation with phosphorus 2p binding energies (see Figure 4).

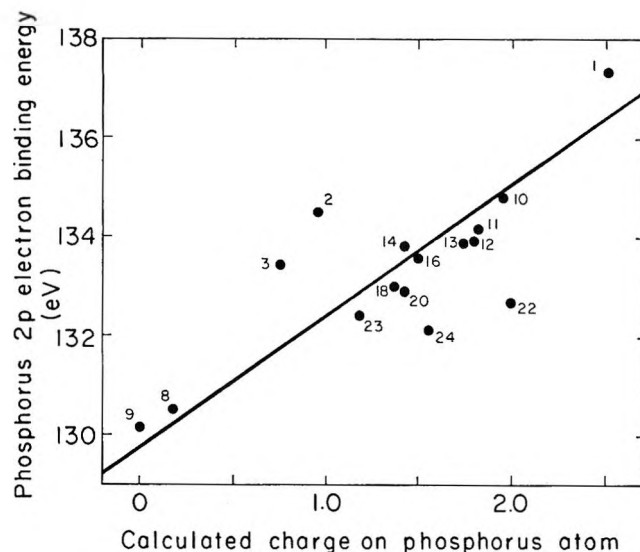


Figure 4. Plot of phosphorus 2p binding energies vs. iterative extended Hückel calculated charges on phosphorus atoms.

Although at this point one might tend to lose hope of obtaining a good correlation, it must be remembered that the iterative extended Hückel method used here still contains a gross approximation. The charge correction of all vsip's by the same factor seems unrealistic. A better approach would be to use valence orbital ionization potentials, which have been tabulated for the atoms as a function of charge and configuration.³²

Electronic Structure of Phosphonitrilic Chloride Trimer. As a by-product of this study we obtained an extended Hückel description of the cyclic phosphonitrilic chloride trimer ((NPCl₂)₃). Calculations were completed with use of a planar structure for (NPCl₂)₃ coupled with known molecular dimensions.²⁴ Two different descriptions have been given for the electronic π system above and below the plane of the ring. Dewar, *et al.*,³³ concluded that there are "islands" of π character, each involving three-centered π bonds centered at a nitrogen atom. Craig and Paddock³⁴ suggested unequal participation of the 3d_{zz} and 3d_{yz} (the molecular plane is the x - y plane) orbitals would result in a continuous π -molecular orbital around the ring.

The π -type (e'' and a_2'' in D_{3h}) molecular orbitals resulting from both the noniterative and iterative extended Hückel treatments showed unequal 3d_{zz} and 3d_{yz} participation, in agreement with the suggestion of Craig and Paddock. The 3d participation was somewhat greater in the iterative case. In both cases the molecular orbital ordering was found to be $\dots e''(2) - e''(2)a_2''(2)a_2''*a_1'' \dots$. The ionization potential of (NPCl₂)₃ has been determined to be 10.26 eV,³⁵ which compares with the eigenvalue of the highest filled orbital, $a_2''(-12.00$ eV in the iterative calculation). The electronic spectrum of (NPCl₂)₃ has a broad peak at 199 m μ (6.23 eV).³⁶ The iterative calculations predict an ${}^1E'$ ($a_2''* \leftarrow e''$) transition at 8.77 eV consisting essentially of the transition of a nitrogen 2p_z electron into the phosphorus 3d orbitals.

Decompositions. In the case of some of the compounds studied, two peaks were observed in the P_{2p} spectrum where only a single peak was expected. It was usually easy to assign the peak arising from the compound under study, either by peak position or by observing a change in the relative areas of the two peaks. Both elemental red phosphorus and tetraphosphorus trisulfide (see Table I) gave a second peak at 134.5 eV in addition to their assigned peaks. In each case the assignment was made on the basis of peak position, since little time dependence was noted in the spectrum. For red phosphorus the decomposition peak was the larger, whereas the opposite was found for P₄S₃. This probably parallels their reactivities with water vapor; red phosphorus reacts slowly with water vapor and oxygen at normal temperatures, while under "ordinary conditions" P₄S₃ is unaffected by exposure to the atmosphere.³⁷ In fact, the red phosphorus

oxidation is accelerated markedly by small concentrations of silver (we used silver-based conducting tape!).³⁸ The decomposition product in each of these cases is then a mixture of the oxy acids of phosphorus, which probably had formed on the surface before we loaded the samples into the spectrometer.

The appearance of two peaks (see Table II) in the spectra of the metal phosphides CrP and MnP is not easily explained. Hydrolysis of a phosphide should give only gaseous phosphine, but apparently there was some surface oxidation.

Two phosphorus peaks would be expected for the compound P₄OH probably in the ratio of 3:1.³⁹ As noted in Table II a sample of P₄OH (1 day old) gave two peaks in the ratio of 2:1 with binding energy values of 129.9 and 133.1 eV, respectively. A portion of the same sample was stored for a week in a capped bottle, and the phosphorus spectrum was rerun. Two peaks were again found, still in the ratio of 2:1. The smaller peak, however, had moved to a binding energy of 134.0 eV while the larger peak remained fixed. The sample was then kept in air overnight, and the phosphorus spectrum was rerun. This spectrum showed peaks at 13.00 and 134.0 eV binding energy in the ratio of 1:1. Apparently we were observing initially the P₄OH 3:1 pattern with some surface (or bulk?) impurity.

Applications. The effect of metal coordination on the charge of a ligand atom can be studied by this method. From the measurements on triphenylphosphine, the triphenylphosphine coordinated complexes (Table II, compounds 26 and 29), and the phosphonium salt, compound 53, it can be seen that coordination of the triphenylphosphine ligand decreases the charge on the phosphorus atom. This is analogous to results obtained for the NH₃ ligand.⁷

Unfortunately, it does not seem that at present phosphorus photoelectron spectroscopy on biological compounds will be definitive, at least insofar as the type of phosphorus atom is concerned. This can be seen by the small changes in binding energy for the compounds 46-50 in Table II.

Acknowledgment. This work was supported by the U. S. Atomic Energy Commission.

(32) H. Basch, A. Viste, and E. B. Gray, *Theor. Chim. Acta*, **3**, 458 (1965).

(33) M. J. S. Dewar, E. A. C. Lucken, and M. A. Whitehead, *J. Chem. Soc.*, 2423 (1960).

(34) D. P. Craig and N. L. Paddock, *Nature*, **181**, 1052 (1958).

(35) C. E. Brion, D. J. Oldfield, and N. L. Paddock, *Chem. Commun.*, 226 (1966).

(36) N. L. Paddock, *Quart. Rev.*, **18**, 168 (1964).

(37) J. Van Wazer, "Phosphorus and Its Compounds," Vol. 1, Interscience Publishers, Inc., New York, 1958, N. Y., pp 118, 297.

(38) M. Silverstein, G. Nordblom, C. Dittrich, and J. Jakabein, *Ind. Eng. Chem.*, **40**, 301 (1948).

(39) H. Harnisch, *Z. Anorg. Allg. Chem.*, **300**, 261 (1959).

Chemical Reaction during Electromigration of Ions

by J. Deman and W. Rigole

Laboratorium voor Fysische Scheikunde, University of Ghent, Belgium, (Received June 23, 1969)

It is shown what happens when reactive ions of opposite charge, present in different regions of a conducting medium, meet each other in the course of electromigration. If the computations are confined to precipitation reactions, theory predicts that a reaction region will narrow till a sharp reaction front is formed. The direction of movement of this front and its velocity are calculated, and the correctness of the formulas is briefly checked by some experiments.

It is possible to prepare an electric conductor which consists of a sequence of electrolytic solutions of different composition. Electrophoresis theory¹⁻³ describes the change in concentration distributions accompanying application of direct current. However, so far no attempt has been made to investigate what happens when ions which react with each other, and which initially were present in separate regions, are brought together by electromigration.

In our treatment, we have chosen conditions as simple as possible. First it is supposed that the reactive ions are of opposite sign, and that the regions containing them are arranged so that mere application of current will bring them together.

Further, the calculations are carried out on the assumption that a variation of the concentration of the reaction products does not influence the concentration of the reactants to a noticeable degree. Consequently, all kinds of reactions are included of which the equilibrium constants are small enough.

The reaction products may be either charged or not. However, for the sake of brevity, we confine our present computations to the uncharged case. In the theory, therefore, only precipitation reactions are explicitly treated. This reaction type fulfills the requirements mentioned above. Moreover, experience has shown that with precipitates the effects that are to be described are easily observed visually. Diffusion is left out of consideration together with the influence of products originating in electrode reactions.

The field strength is supposed to be constant with time and to be uniform over the whole conductor. As will be pointed out further on, this condition is fulfilled when the conducting medium contains a nonreactive electrolyte in a uniform concentration largely exceeding the concentrations of the reactive ions. It should be realized that owing to this assumption the connection between the present theory and general electrophoresis theory is seriously loosened.

It is clear that in experimental work, a means has to be devised to impede relative displacements which are not caused by the applied direct current. Agar gel proved to be most suitable for this purpose.

In this medium, convection may be neglected and the precipitate remains at the place where it was actually formed.

Hermans⁴ has taken diffusion as the driving force for the ionic displacement and arrived at conclusions which are in good analogy to ours.

While moving through a region in which reaction products are present, ions in solution will exchange with those bound in the products. In another paper it will be shown that owing to these exchange reactions a separation between different ionic species can be obtained.

Preliminary Remarks

Suppose the conducting medium is an aqueous gel column. At the anodic side, a part of the column is made to contain the positive ionic species A^{a+} . In another region nearer to the cathodic compartment the anionic species L^{l-} is placed. When direct current is sent through, these ionic regions will move closer to each other and will produce the precipitate A_lL_a at the section of meeting.

We introduce the notation m_A, m_L : effective electrophoretic mobilities of A^{a+} respective to L^{l-} (the term "effective" is used to emphasize that sorption of the ions to the gel molecules results in a decrease of apparent mobility); c_A, c_L : concentrations expressed in g equiv/cm³; E : the electric field strength supposed to be uniform over the whole gel column. (Not only the column has a constant cross-sectional area but there is also a large excess of nonreactive electrolyte. As a consequence, it can be assumed that E is not affected by precipitation and also that the constraint that otherwise would be imposed on the concentrations and mobilities of the reactive ions in their respective regions, falls away); $v = mE$: the ionic velocity; P : in the gel medium the precipitate is very finely dispersed, therefore the term "concentration"

(1) F. Kohlrausch, *Ann. Phys. Chem.*, **62**, 209 (1897).

(2) D. C. Henry and J. Brittain, *Trans. Faraday Soc.*, **29**, 798 (1933).

(3) V. P. Dole, *J. Amer. Chem. Soc.*, **67**, 1119 (1945).

(4) J. J. Hermans, *J. Colloid Sci.*, **2**, 387 (1947).

tration of precipitate" appears allowable. This concentration is denoted by the symbol P and is expressed in g equiv of either the cationic or anionic species present in the precipitate per cm^3 .

Ideal behavior with respect to constant activity coefficients and constant mobilities is assumed. Variation of effective mobility with sorption is neglected.

The positive x axis points in the direction in which the positive ions move. That part of the gel column in which precipitation is actually taking place is called the "reaction." A reaction region narrows itself to a "reaction front." That part of the column in which precipitate is present is called the "product region." Of the general precipitation reaction



the solubility product is

$$K_s = [A^{a+}]^1 [L^{1-}]^a$$

With square brackets, the concentrations are expressed in mol/l. When expressed in g equiv/ cm^3 (symbols c_A and c_L), the solubility product becomes

$$K_{AL} = c_A^1 c_L^a = a!^a (10^{-3})^{1+a} K_s \quad (1)$$

K_{AL} is, as is K_s , constant at a given temperature.

Formation of a Reaction Region

Suppose an experiment in which the regions A^{a+} and L^{1-} are initially separated. Because of diffusion, concentration gradients arise at the edges of these regions (Figure 1). Because of their greater concentration, A^{a+} ions which are present at point p are able to precipitate the L^{1-} ions which a time before were in equilibrium with the A^{a+} ions of point q . At the same moment, the A^{a+} ions of q react with the L^{1-} ions which a time before were in equilibrium with the A^{a+} ions of point r . Consequently, A^{a+} ions are precipitated at points p and q simultaneously. It follows that a reaction region is established.

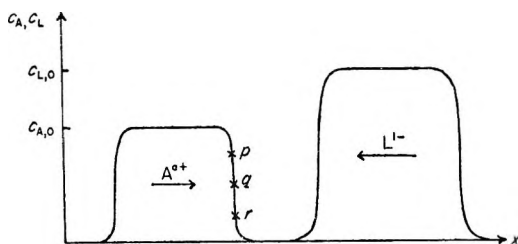


Figure 1. Ionic regions with their initial concentration distributions.

The Differential Equation

In the reaction region, ions are disappearing during their movement, by precipitation. Exact mathematical description requires the formulation of the material balance.

Let us take an infinitesimal section $dydz$ of the conductor. Ions A^{a+} originally present at this section will have covered a distance $m_A E dt$ after a time dt . In this way a volume $m_A E c_A dy dz dt$ is filled by A^{a+} which has passed the section. Hence the amount of A^{a+} which passed the section is

$$m_A c_A E dy dz dt \quad (a)$$

The amount of A which leaves the volume at the opposite section is

$$m_A c_A E dy dz dt + m_A E \frac{\partial c_A}{\partial x} dx dy dz dt \quad (b)$$

The increase in A is (a) - (b), or

$$-m_A E \frac{\partial c_A}{\partial x} dx dy dz dt$$

When we divide by the volume $dx dy dz$ and time dt , we obtain the increase of total amount per unit of volume and of time

$$-m_A E \frac{\partial c_A}{\partial x}$$

This increase is also equal to the sum of the changes in concentrations c_A and P per unit time

$$\frac{\partial c_A}{\partial t} + \frac{\partial P}{\partial t} = -m_A E \frac{\partial c_A}{\partial x}$$

For L we obtain

$$\frac{\partial c_L}{\partial t} + \frac{\partial P}{\partial t} = m_L E \frac{\partial c_L}{\partial x}$$

P is eliminated by subtraction

$$\frac{\partial c_A}{\partial t} - \frac{\partial c_L}{\partial t} = -E \left(m_A \frac{\partial c_A}{\partial x} + m_L \frac{\partial c_L}{\partial x} \right)$$

c_L can be expressed in function of K_{AL} and c_A by means of (1).

$$\left(a c_A^{\frac{1+a}{a}} + 1 K_{AL}^{\frac{1}{a}} \right) \frac{\partial c_A}{\partial t} = -E \left(a m_A c_A^{\frac{1+a}{a}} - 1 m_L K_{AL}^{\frac{1}{a}} \right) \frac{\partial c_A}{\partial x} \quad (2)$$

After integration we arrive at

$$\left(a c_A^{\frac{1+a}{a}} + 1 K_{AL}^{\frac{1}{a}} \right) x - E \left(a m_A c_A^{\frac{1+a}{a}} - 1 m_L K_{AL}^{\frac{1}{a}} \right) t = \varphi(c_A) \quad (3)$$

$\varphi(c_A)$ is a function which can be determined with the aid of the concentration distribution at $t = 0$.

Evolution of the Concentration Gradients in the Reaction Region

From eq 2 and 1 we can derive v_{c_A} i.e., the velocity with which a given c_A is displaced in the reaction region

$$v_{c_A} = - \frac{\left(\frac{\partial c_A}{\partial t}\right)}{\left(\frac{\partial c_A}{\partial x}\right)} = \frac{am_{AC_A} - lm_{LC_L}}{ac_A + lc_L} E \quad (4)$$

Since the denominator is positive, a given c_A will move in the direction of the positive x axis if $am_{AC_A} > lm_{LC_L}$. When $am_{AC_A} < lm_{LC_L}$, the direction of movement is reversed. Because of the c_A gradient in the reaction region, a c_A exists which does not move. The condition is $am_{AC_A} = lm_{LC_L}$ or

$$c_{A,st} = \left[\left(\frac{lm_L}{am_A} \right)^a K_{AL} \right]^{\frac{1}{1+a}}$$

It can be demonstrated that the reaction region will narrow itself around the fixed section x_{st} until the reaction front is formed. Indeed, when eq 4 is differentiated with respect to c_A , (with c_L treated as a function of c_A according to the constraint of eq 1), then the result is

$$\frac{dv_{c_A}}{dc_A} = \frac{al(m_A + m_L) \left(c_L - c_A \frac{dc_L}{dc_A} \right)}{(ac_A + lc_L)^2} E$$

Both numerator and denominator are positive. It follows that with greater concentration c_A , the velocity v_{c_A} increases. When v_{c_A} is positive (movement to the cathode), then greater c_A values will move faster than smaller ones. If v_{c_A} is negative, the velocity in the

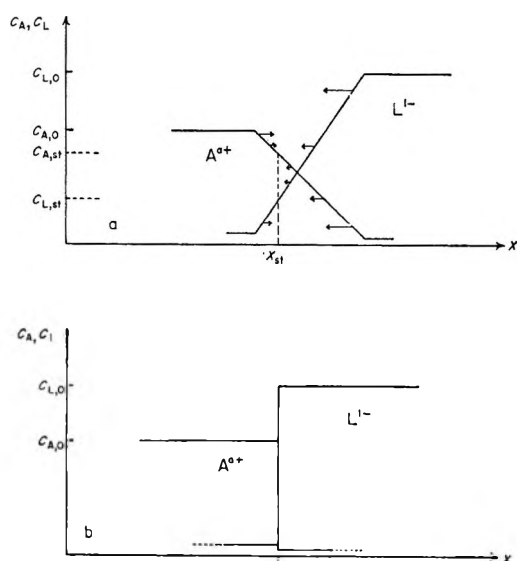


Figure 2. a, Formation of a reaction front; directions and lengths of arrows indicate directions and magnitudes of velocities (schematic). b, Concentration distribution after formation of the front.

direction of the anode decreases with greater c_A value (Figure 2a).

The c_L -values follow the c_A -values to which they are linked by eq 1. The argument makes itself clear, when we substitute c_A in eq 2 by c_L by means of eq 1. We obtain

$$\left(aK_{AL}^{\frac{1}{1+a}} + lc_L^{\frac{a+1}{1+a}} \right) \frac{\partial c_L}{\partial t} = - E \left(am_A K_{AL}^{\frac{1}{1+a}} - lm_{LC_L}^{\frac{a+1}{1+a}} \right) \frac{\partial c_L}{\partial x}$$

Since

$$K_{AL}^{\frac{1}{1+a}} = c_A c_L^{\frac{a}{1+a}}$$

It follows

$$(ac_A + lc_L) \frac{\partial c_L}{\partial t} = -E(am_{AC_A} - lm_{LC_L}) \frac{\partial c_L}{\partial x}$$

$$v_{c_L} = \frac{am_{AC_A} - lm_{LC_L}}{ac_A + lc_L} E$$

the same equation as eq 4.

Summarizing, we state that the reaction region is narrowing and the concentration gradients are growing more steep at the fixed section x_{st} .

We have seen earlier that when the ionic regions first make contact with each other, a reaction region will develop because concentration gradients exist at the edges of the regions (Figure 1). However, the bulk of the ions A^{2+} and L^{-} is present in uniform concentration $c_{A,0}$ and $c_{L,0}$ in their respective regions. Since uniform concentrations give no rise to a reaction region (this will become evident in the following paragraph), it is obvious that the narrowing tendency of the reaction region will result in a discontinuity in the concentrations (reaction front), when contact is made between $c_{A,0}$ and $c_{L,0}$ (Figure 2b).

At the section of discontinuity

$$c_{A,0} \text{ falls to concentration } \frac{K_{AL}^{\frac{1}{1+a}}}{c_{L,0}^{\frac{a}{1+a}}}$$

$$c_{L,0} \text{ falls to concentration } \frac{K_{AL}^{\frac{1}{1+a}}}{c_{A,0}^{\frac{a}{1+a}}}$$

Another Approach

Equation 3 can be written as

$$x = \frac{\varphi(c_A)}{\left(ac_A^{\frac{1+a}{a}} + lK_{AL}^{\frac{1}{a}} \right)} + \frac{E \left(am_{AC_A}^{\frac{1+a}{a}} - lm_{LC_L} K_{AL}^{\frac{1}{a}} \right) t}{\left(ac_A^{\frac{1+a}{a}} + lK_{AL}^{\frac{1}{a}} \right)} \quad (3')$$

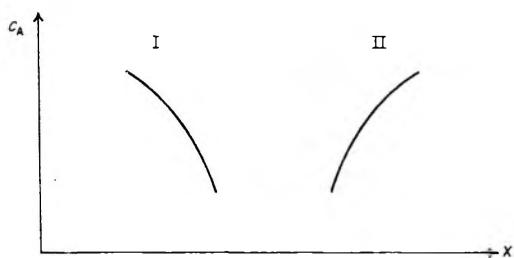


Figure 3. Concentration distributions at $t = 0$.

at $t = 0$

$$x = \frac{\varphi(c_A)}{\left(\frac{1+a}{ac_A^a} + 1K_{AL}^{\frac{1}{a}}\right)} = S_0(c_A)$$

The inverse function of $S_0(c_A)$ is denoted by $c_A = s_0(x)$. It describes the concentration c_A in function of x at $t=0$. There are two possibilities since c_A may either increase or decrease with increasing abscissa (Figure 3).

Equation 3' is composed by the initial function $S_0(c_A)$ to which is added a term which describes the change with time. Partial differentiation with respect to c_A leads to

$$\left(\frac{\partial x}{\partial c_A}\right)_t = S_0'(c_A) + \frac{El(1+a)c_A^{\frac{1}{a}}(m_A + m_L)K_{AL}^{\frac{1}{a}}}{\left(\frac{1+a}{ac_A^a} + 1K_{AL}^{\frac{1}{a}}\right)^2}$$

A discontinuity in c_A will develop if $\partial c_A / \partial x \rightarrow \infty$ i.e., $\partial x / \partial c_A \rightarrow 0$. The second term at the right-hand side is always positive. As a consequence, $(\partial x / \partial c_A)_t$ can never be zero when $S_0'(c_A)$ is positive (curve II). A curve of type I has a negative $S_0'(c_A)$ value and $(\partial x / \partial c_A)_t$ approaches zero with time.

Figure 4 shows what happens. We have taken separately the concentration gradients of region A^{a+}

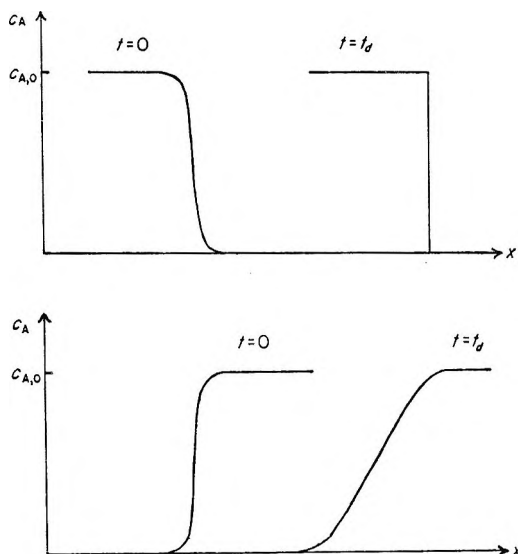


Figure 4. Evolution of the concentration gradients in a reaction region.

in Figure 1. It is evident that the uniform concentration $c_{A,0}$ does not exert any influence on the discontinuity after its formation.

Because the front moves and regions A^{a+} and L^{1-} will be gnawed off (see following paragraph), we can discern four stages: 1, formation of a reaction region; 2, formation of a discontinuity in the ionic concentrations (reaction front); 3, movement of the front till the concentration gradient at the rear end of the ion region is reached; and 4, breakdown of the front and reinstallation of a reaction region.

Displacement of the Reaction Front

It is assumed that at both sides of the front a uniform concentration exists (Figure 2b). The velocity of the front is denoted as v_f . The amount of an ionic species precipitated at the front per unit time is equal to the difference between the velocity of the ion and that of the front, multiplied by the fall in ionic concentration. Thus

$$(m_A E - v_f) \left[c_{A,0} - \left(\frac{K_{AL}}{c_{L,0}^a}\right)^{\frac{1}{a}} \right] = (m_L E + v_f) \left[c_{L,0} - \left(\frac{K_{AL}}{c_{A,0}^1}\right)^{\frac{1}{a}} \right] = |v_f| P$$

whence

$$v_f = \frac{m_A \left[c_{A,0} - \left(\frac{K_{AL}}{c_{L,0}^a}\right)^{\frac{1}{a}} \right] - m_L \left[c_{L,0} - \left(\frac{K_{AL}}{c_{A,0}^1}\right)^{\frac{1}{a}} \right]}{\left[c_{A,0} - \left(\frac{K_{AL}}{c_{L,0}^a}\right)^{\frac{1}{a}} \right] + \left[c_{L,0} - \left(\frac{K_{AL}}{c_{A,0}^1}\right)^{\frac{1}{a}} \right]} E \tag{5}$$

The concentration of the precipitate is

$$P = \frac{\left| (m_A + m_L) \left[c_{A,0} - \left(\frac{K_{AL}}{c_{L,0}^a}\right)^{\frac{1}{a}} \right] \left[c_{L,0} - \left(\frac{K_{AL}}{c_{A,0}^1}\right)^{\frac{1}{a}} \right] \right|}{\left| m_A \left[c_{A,0} - \left(\frac{K_{AL}}{c_{L,0}^a}\right)^{\frac{1}{a}} \right] - m_L \left[c_{L,0} - \left(\frac{K_{AL}}{c_{A,0}^1}\right)^{\frac{1}{a}} \right] \right|} \tag{6}$$

When $d_{A,0}$ is the initial length of the A^{a+} region and d_p the length of the product region after all the A^{a+} ions have made contact with L^{1-} , then

$$\frac{d_p}{d_{A,0}} = \frac{c_{A,0} - \left(\frac{K_{AL}}{c_{L,0}^a}\right)^{\frac{1}{a}}}{P}$$

Substitution of P yields

$$\frac{d_p}{d_{A,0}} = \frac{m_A \left[c_{A,0} - \left(\frac{K_{AL}}{c_{L,0}^a}\right)^{\frac{1}{a}} \right] - m_L \left[c_{L,0} - \left(\frac{K_{AL}}{c_{A,0}^1}\right)^{\frac{1}{a}} \right]}{(m_A + m_L) \left[c_{L,0} - \left(\frac{K_{AL}}{c_{A,0}^1}\right)^{\frac{1}{a}} \right]} \tag{7}$$

In most cases $(K_{AL}/c_{L,0}^a)^{\frac{1}{2}}$ and $(K_{AL}/C_{L,0}^1)^{\frac{1}{2}}$ are negligible with respect to $c_{A,0}$ and $c_{L,0}$, respectively. With good approximation, we may then write

$$v_f = \frac{m_A c_{A,0} - m_L c_{L,0} E}{c_{A,0} + c_{L,0}} \quad (5')$$

$$P = \left| \frac{(m_A + m_L) c_{A,0} c_{L,0}}{m_A c_{A,0} - m_L c_{L,0}} \right| \quad (6')$$

$$\frac{d_p}{d_{A,0}} = \frac{m_A c_{A,0} - m_L c_{L,0}}{(m_A + m_L) c_{L,0}} \quad (7')$$

Some cases of practical importance can be discerned. We confine ourselves to the simple formulas 5' and 6'.

1'. When $m_A c_{A,0} = m_L c_{L,0}$, the front does not move ($v_f = 0$). All the precipitate accumulates at one definite section of the gel column ($P \rightarrow \infty$). In practice the width of the product region is not infinitesimally small because diffusion of the reactant ions has been neglected.

2'. When $m_A c_{A,0} \neq m_L c_{L,0}$, the part of the column containing precipitate increases steadily. The product region is bordered sharply at both sides. One border remains stationary; this is the section where the reactant ions met each other initially. The other border is the reaction front. When $m_A c_{A,0} > m_L c_{L,0}$, then the front moves in the direction of the cathode. The velocity increases when $c_{A,0}/c_{L,0}$ is taken greater. When $m_A c_{A,0} < m_L c_{L,0}$, then v_f is negative and the front moves in the opposite direction.

3'. When simultaneously $m_A \gg m_L$ and $c_{A,0} \gg c_{L,0}$ then v_f and P are approaching to their respective limiting values v_{c_A} and $c_{L,0}$. On the other hand, v_f approaches to v_{c_L} and P to $c_{A,0}$ when at the same time $m_L \gg m_A$ and $c_{L,0} \gg c_{A,0}$.

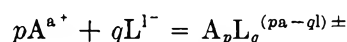
The theory of diffusion of ions into gels containing precipitating ions has been given by Hermans. He comes to the conclusion that also in that case a reaction front will be formed. This front will be displaced due to a difference between $\partial^2 m_A / \partial x^2$ and $\partial^2 m_L / \partial x^2$. It is obvious that displacement of the front by diffusion can be taken into account only if we refrain from our assumption of constant mobilities.

Discussion

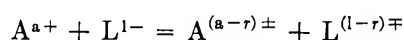
We have verified the conclusions of the theory by experiments. A column of agar gel at 1% (wt/vol) containing the indifferent electrolyte KCl (0.2 N) was used. The precipitation reaction studied was $\text{Co}^{2+} + 2\text{OH}^- \rightarrow \text{Co}(\text{OH})_2$, $pK_s = 15.6$ at 25°. At first

the concentrations were chosen so that the blue-green precipitation band extended in the direction of the cathode. We found that the moving side of the band was very sharply bordered (reaction front). When the hydroxyl concentration is enhanced, keeping the cobalt concentration constant, the precipitate becomes more dense and the velocity of the front decreases. Finally, with hydroxyl concentrations which are high enough, the direction of movement of the front is reversed. The ratio $[\text{Co}^{2+}]/[\text{OH}^-]$ at which the front does not move is found to be 2.11 ($\text{Co}^{2+} = 10^{-2} N$, $\text{OH}^- = 4.73 \times 10^{-3} N$). When computed theoretically with the aid of equation 5' using the effective mobilities $m_{\text{Co}^{2+}} = 45$ and $m_{\text{OH}^-} = 125.9$ determined in separate experiments, we found a ratio of 2.79. The agreement is to be called satisfactory bearing in mind that in the computation, no account has been taken of the nonuniformity of the electric field strength. Moreover, the exact temperature at the reaction front was not known. As already pointed out, the theory is applicable as such to other ionic reactions with uncharged reaction products provided the equilibrium constant is small enough. If the latter is not the case, then the concentrations of the reactants are to be regarded as dependent on the concentration of the product. Consequently, an attempt to an exact treatment will have to surmount some serious mathematical difficulties. It is our opinion that also in this case formation of an abrupt reaction front may be expected. Indeed a reaction region will continue to narrow as long as concentration gradients exist, the greater concentrations moving faster than the smaller ones.

When the reaction products are charged as, e.g., in a complex-forming reaction



or in a redox reaction



then many possibilities are open depending on the direction of movement and the velocity which the products assume. Due to this movement, the length of the product region can be either shortened or extended. It is conceivable that a product, say $\text{Fe}(\text{CNS})_6^{3-}$, moves more quickly in the direction of the anode than the reaction front between CNS^- and Fe^{3+} . The front, as we have defined it, will then be situated behind the place where the victims of the battle are found.

Predicted Properties of the Super Heavy Elements. I. Elements

113 and 114, Eka-Thallium and Eka-Lead¹

by O. L. Keller, Jr., J. L. Burnett, T. A. Carlson, and C. W. Nestor, Jr.

Oak Ridge National Laboratory, Oak Ridge, Tennessee 37830 (Received June 11, 1969)

The probable existence of an island of nuclear stability centered on element 114 makes the prediction of chemical and physical properties of elements in this region important for their identification. These elements may be produced using proposed heavy ion accelerators, or they may even be found in nature. The values derived from extrapolations in Mendeleev's periodic system and theoretical calculations are presented in the following table.

	Element 113, Eka-Thallium	Element 114, Eka-Lead
Chemical group	IIIA	IVA
Atomic weight	297	298
Most stable oxidation state	+1	+2
First ionization potential, eV	7.4	8.5
Second ionization potential, eV		16.8
Oxidation potential, V	$M \rightarrow M^+ + e^-$ -0.6	$M \rightarrow M^{2+} + 2e^-$ -0.9
Metallic radius, Å	1.75	1.85
Ionic radius, Å	1.48	1.31
Atomic volume, cm ³ (g-atom) ⁻¹	18	21
Density, g/cm ³	16	14
Mp, °K	700	340
Bp, °K	1400	420
Heat of vaporization, kcal (g-atom) ⁻¹	31	9
Heat of sublimation, kcal (g-atom) ⁻¹	34	10
Debye temp, °K	70	46
Entropy, cal deg ⁻¹ (g-atom) ⁻¹ (25°)	17	20

A number of theoretical papers² have appeared recently indicating that islands of nuclear stability exist around elements 114 to 126. Several laboratories in the U. S., Western Europe, and Russia are proposing to build heavy ion accelerators to explore this region of the periodic table. Work is also progressing here and abroad in the search for super heavy elements in nature. As an aid in designing experiments for the necessary chemical identification of the accelerator products and to assist in the search for possible naturally occurring isotopes of the super heavy elements, we present in this and succeeding papers values for certain physical and chemical properties predicted on the basis of Mendeleev's periodic system and theoretical calculations. In this first paper, we present our results for elements 113 and 114.

Ionization Potentials

Element 114 occurs in group IVA of the periodic system. The eigenvalues of Ge, Sn, Pb, and 114 free atoms and their free +1 ions have been calculated using a relativistic Hartree-Fock-Slater (HFS(Rel)) program developed at Oak Ridge.³ The Slater-Latter approximation with an exchange factor of 1.5 is used

for the exchange potential. A $7s^27p^2$ configuration for 114 was assumed in accordance with the relativistic Dirac-Slater calculations of Waber, Cromer, and Liberman.⁴ The eigenvalue of the $P_{1/2}$ electron is taken as an approximation to the ionization potential. The theoretical and experimental ionization potentials together with their differences are presented in Table I.

The Δ 's for 114 were obtained by extrapolating the Δ 's of Ge, Sn, and Pb with the best straight line to 114. These Δ 's were then used to obtain the "experimental" ionization potentials of 114.

Our procedure for obtaining a semiempirical value of the first ionization potential for element 114 was also checked using eigenvalues from the relativistic Hartree-Fock solution (kindly supplied by Joseph B. Mann from

(1) Research sponsored by the U. S. Atomic Energy Commission under contract with the Union Carbide Corp.

(2) (a) For an excellent review see G. T. Seaborg, *Ann. Rev. Nuclear Sci.*, **18**, 53 (1968); (b) S. G. Nilsson, S. G. Thompson, and C. F. Tsang, *Phys. Lett.*, **28B**, 458 (1969).

(3) C. W. Nestor, T. C. Tucker, T. A. Carlson, L. D. Roberts, F. B. Malik, and C. Froese, "Relativistic and Non-Relativistic SCF Wave Functions for Atoms and Ions from $Z = 2$ to 80," ORNL-4027; for a related paper using a Wigner-Seitz boundary condition see *Phys. Rev.*, **174**, 118 (1968).

(4) J. T. Waber, D. T. Cromer, and D. Liberman, ref 2a, p 105.

Table I: Ionization Potentials^a (Group IVA)

	I			II		
	HFS(Rel)	Exptl	ΔI	HFS(Rel)	Exptl	ΔII
Ge	6.44	7.88	1.44	14.63	15.93	1.30
Sn	6.14	7.34	1.20	13.54	14.63	1.09
Pb	6.46	7.42	0.96	14.07	15.03	0.96
114	7.77	8.49	0.72	15.97	16.75	0.78

^a Values in electron volts.**Table II:** HFS(Rel) Eigenvalues (eV) of Outermost $S_{1/2}$ and $D_{5/2}$ Electrons (Group IVA)

	Ge	Sn	Pb	114
$S_{1/2}$	14.69	13.19	14.32	16.63
$D_{5/2}$		31.99	24.90	17.66

unpublished data). The extrapolated value obtained was within 0.3 eV of that given in Table I.

The eigenvalues of the outermost $S_{1/2}$ and $D_{5/2}$ electrons for the free atoms are listed in Table II. It is seen that the eigenvalues for the s and p electrons are not approaching each other in energy as one goes to higher atomic numbers although the s and d electrons are. This is important in the considerations of the valence of 114 where tetravalency requires promotion of an s electron for sp^3 hybridization.

Since element 113, with a $7s^27p$ configuration,⁴ occurs in group IIIA, the eigenvalues of the $P_{1/2}$ orbitals of Al, Ga, In, Tl, and 113 were calculated using the HFS(Rel) program.³ The differences between the calculated and experimental values were extrapolated to obtain the first ionization potential of 113 (Table III).

To inspect the possibility of the formation of hybrid orbitals, the outermost $S_{1/2}$ and $D_{5/2}$ eigenvalues are

Table III: First Ionization Potential (eV) (Group IIIA)

	HFS(Rel)	Experimental	Δ
Al	4.89	5.98	1.09
Ga	4.99	6.00	1.01
In	4.87	5.78	0.91
Tl	5.24	6.11	0.87
113	6.53	7.36	0.83

Table IV: HFS(Rel) Eigenvalues (eV) of Outermost $S_{1/2}$ and $D_{5/2}$ Electrons (Group IIIA)

	$S_{1/2}$	$D_{5/2}$
Al	10.2	
Ga	11.66	26.78
In	10.7	24.4
Tl	11.99	19.42
113	14.5	14.4

given in Table IV. Although the d and s orbitals approach each other in energy with increasing Z , their difference from the p electron remains large as in the 114 case.

Validity of Extrapolations to Elements 113 and 114

We estimate the properties of elements 113 and 114 mainly by extrapolating the properties of the lighter members of the respective groups to which 113 and 114 have been assigned. The basic validity of such extrapolations rests on this assignment. The most important evidence available on this question is contained in Tables I–IV. The results of our “state of the art” HFS(Rel) calculations show that the 7p electrons have a markedly different energy than the 7s and 6d. The p electrons are therefore the valence electrons which we expect to be the necessary condition to allow extrapolations in the periodic table.

Oxidation States

The outstanding periodic characteristic of the group IVA elements is their increasing stability in the II oxidation state relative to the IV as one goes to higher atomic numbers. C and Si are almost always tetravalent, and Ge shows only very weak divalency. Sn chemistry is about evenly divided between divalency and tetravalency, and Pb is most stable in the II state with only weak tetravalent qualities. Drago⁵ shows from thermodynamic considerations that this trend arises from a decrease in the strength of the covalent bonds formed by the metal atom as the atomic number increases in this group. From the point of view of valence bond theory, the tetravalent state is made possible by sp^3 tetrahedral hybridization. In order for all four valence electrons to be used in bonding, strong enough covalent bonds must be formed to supply both the promotion energy for one s electron and the Gibbs free energy required for compound stability. When only weak covalent bonds can be formed, as in most lead compounds, only the p electrons participate in bonding.

Drago explains the weakening of the covalent bonding with increasing Z with the following two considerations. (1) In the higher Z elements the valence electrons are spread over a larger volume so that less overlap with the orbitals of the anion results. (2) The heavier elements have more inner electrons to repel the inner electrons of the bonded anion.

Since 114 has the largest atomic volume and the most inner electrons of any group IV element, sp^3 hybridization will probably be very unimportant and thus element 114 will be weakly, if at all tetravalent. The expected most stable valence of 114 is +2. However, since the outermost s and d electrons in 114 have approximately equal energies, it may be possible to form a volatile hexafluoride.

(5) R. S. Drago, *J. Phys. Chem.*, **62**, 353 (1958).

The stable oxidation state of the group IIIA elements tends toward +1 from +3 with increasing atomic number. The +3 state is attained through sp^2 trigonal hybridization. Drago⁵ shows that the trend toward +1 stability in the IIIA elements arises from the same considerations that explain the tendency toward +2 stability in the IVA elements. The most stable oxidation state for element 113 is therefore expected to be +1. As in the case of 114, however, we also suggest the possible existence of a volatile hexafluoride.

Metallic and Ionic Radii

Metallic radii for 12-coordination are given by Wells⁶ and Pauling⁷ (Table V). Since 114 is expected to have, like Pb, a cubic close-packed structure (face-centered cubic) the 12-coordinate radii are the proper ones for extrapolation.

We assume that the change in radius between Pb and 114 will be the same as between Sn and Pb since similar electronic configurations are passed over in each case. We take the metallic radius (1.85 Å) as the average of the Pauling and Wells values.

The ionic radii⁷ can be extrapolated in a similar manner to obtain 1.28 Å as the crystal radius of 114^{2+} . There is a relation between ionic radii and 12-coordinate metallic radii of Ge, Sn, and Pb, however, in that their difference is 0.50 (Table VI). This indicates that the ionic radius of 114 should be 1.35 Å. We take the average of the extrapolated and calculated values, 1.31 Å, as the ionic radius of 114^{2+} .

We assume that 113 has a hexagonal closest packed structure like thallium. The 12-coordinate metallic radii given by Wells⁶ for In and Tl extrapolate to a metallic radius of 1.75 Å for 113 (Table VII). The ionic radii⁷ extrapolate to 1.48 Å. Extrapolating

Table V: Metallic Radii for 12-Coordination (Å)

	Pauling	Δr	Wells	Δr	
Ge	1.44		1.39	0.19	
Sn	1.62	0.18	1.58	0.17	
Pb	1.70	0.08	1.75	0.17	
114	1.78	0.08	1.92		Av 1.85

Table VI: Ionic Radii

	Ionic radius, Å (Pauling)	Pauling metallic radius minus ionic radius	Wells metallic radius minus ionic radius
Ge	0.93	0.51	0.46
Sn	1.12	0.50	0.46
Pb	1.20	0.50	0.55
		Av 0.50	Av 0.49

Table VII: Radii

	Metallic (Wells), Å	Ionic (Pauling), Å	$R(\text{metallic}) - R(\text{ionic})$
Ga	1.53	1.13	0.40
In	1.67	1.32	0.35
Tl	1.71	1.40	0.31
113	1.75	1.48	0.27

$R(\text{metallic}) - R(\text{ionic})$ to 113 yields 0.27. The 12-coordinate metallic radius minus 0.27 yields 1.48 Å the same as the extrapolated value.

Density and Atomic Volume

We assume 114 has the same structure as Pb, *i.e.*, fcc with four atoms per unit cell. Using the metallic radius of 1.85 Å, the density of 114 is calculated to be 14 g cm^{-3} and the g-atomic volume 21 cm^3 (g-atom)⁻¹ (Table VIII).

Oxidation Potential

The oxidation potentials of Sn, Pb, and 114 are obtained from the free energy of the reaction⁸



using the relation

$$\Delta G = -2E^\circ = \Delta H - T\Delta S \quad (2)$$

where ΔG = Gibbs free energy (eV) and E° = oxidation potential (V).

The enthalpy change for the change in state (1) is, using the Born-Haber cycle

$$\begin{aligned} \Delta H = & [\Delta H_s^{298} + (I + II) + \\ & \Delta H_{\text{hyd}}(M^{2+}(\text{g})) - 2\Delta H_{\text{hyd}}(H^+(\text{g})) - \\ & -2(IP)(H(\text{g})) - \Delta H_{\text{diss}}(H_2(\text{g}))] \quad (3) \end{aligned}$$

where ΔH_s^{298} = heat of sublimation of the metal at 298°K, $I + II$ = sum of first two ionization potentials, $\Delta H_{\text{hyd}}(M^{2+}(\text{g}))$ = hydration energy of the gaseous metal ion, $\Delta H_{\text{hyd}}(H^+(\text{g}))$ = hydration energy of the gaseous hydrogen ion (-11.14 eV), $IP(H(\text{g}))$ = ionization potential of the hydrogen atom (13.595 eV), $\Delta H_{\text{Diss}}(H_2(\text{g}))$ = heat of dissociation of the hydrogen molecule (4.52 eV).

The heat of sublimation of metallic 114 is obtained from the plot of the heats of sublimation of Si, Ge, Sn, and Pb *vs.* row of the periodic table (Figure 1 and Table IX). The curve is fitted by the equation

$$\Delta H_s^{298} = 105 - 14.9\chi + 0.6\chi^2 - 0.7\chi^3$$

(6) A. F. Wells, "Structural Inorganic Chemistry," 3rd ed, Oxford University Press, Oxford, 1962.

(7) L. Pauling, "The Nature of the Chemical Bond," 3rd ed, Cornell University Press, Ithaca, N. Y., 1960.

(8) C. S. G. Phillips and R. J. P. Williams, "Inorganic Chemistry," Oxford University Press, Oxford, 1965.

Table VIII: Thermodynamic Quantities^a of Groups IVA and IIIA Elements¹⁰⁻¹²

Element	Bp, °K	Mp, °K	ΔH_v , kcal mol ⁻¹	Trouton's constant	θ , °K	V , cm ³ (g-atom) ⁻¹	ρ , g cm ⁻³
Si	2950(?)	1683			670	12.04	2.330
Ge	3100	1210	79.9	25.8	370	13.64	5.3234
Sn	2960	505	69.4	23.4	190 (white)	16.29	5.75 (gray) 7.29 (white)
Pb	2024	600.6	42.88	21.2	95	18.27	11.34
114	420	340	9.3	22	46	21	14
Al	2720	932	70.2	25.8	420	10.0	2.71
Ga	2510	303	61.2	24.4	333	11.80	5.91
In	2320	429.32	54.1	23.3	110	15.76	7.3
Tl	1740	577	38.74	22.2	89	17.22	11.85
113	1400	700	31	22	70	18	16

^a Bp, boiling point; mp, melting point; ΔH_s^{298} , heat of sublimation; ΔH_v , heat of vaporization at the bp; θ , Debye temperature; V , atomic volume; ρ , density.

Table IX: Oxidation Potential of Element 114^{a,b}

Element	ΔH_s^{298}	Ionization energy	$\Delta H_{\text{hyd}}(M^{2+}(\text{g}))$	$\bar{S}^\circ_{M^{2+}(\text{aq})}$	$\bar{S}^\circ_{M(\text{s})}$	$-T\Delta S$ (eq 1)	Calculated oxidation potential (eq 1)	Experimental oxidation potential (eq 1)
Sn	3.12	21.97	-15.8	$-(1.7 \times 10^{-4})$	5.3×10^{-4}	-0.2	+0.15	+0.14
Pb	2.03	22.45	-15.1	0	6.7×10^{-4}	-0.2	+0.11	+0.13
114	0.44	25.24	-14.3	2.2×10^{-4}	8.7×10^{-4}	-0.2	-0.9	

^a All quantities in appropriate units with energies in electron volts. ^b $S^\circ_{\text{H}_2(\text{g})} = 13.5 \times 10^{-4}$ eV deg⁻¹. ΔH for reaction $2\text{H}^+(\text{aq}) + 2\text{e}^- = \text{H}_2(\text{g})$ is -9.4 eV.

Table X: Oxidation Potential of Element 113^{a,b}

Element	ΔH_s^{298}	Ionization energy	$\Delta H_{\text{hyd}}(M^+(\text{g}))$	$\bar{S}^\circ_{M^+(\text{aq})}$	$\bar{S}^\circ_{M(\text{s})}$	$-T\Delta S$	Calculated oxidation potential	Experimental oxidation potential
Tl	1.86	6.11	-3.22	12.8×10^{-4}	6.6×10^{-4}	-0.4	+0.35	+0.34
113	1.47	7.36	-3.11	13.7×10^{-4}	7.4×10^{-4}	-0.4	-0.6	

^a All quantities in appropriate units with energies in electron volts. ^b $0.5S^\circ_{\text{H}_2(\text{g})} = 6.8 \times 10^{-4}$ eV deg⁻¹. ΔH for reaction $\text{H}^+(\text{aq}) + \text{e}^- = 0.5\text{H}_2(\text{g})$ is -4.7 eV.

where $(\chi + 3)$ equals the appropriate row of the periodic table. Letting $\chi = 4$ (for the seventh row) we calculate $\Delta H_s^{298}(114) = 10$ kcal (g-atom)⁻¹.

The hydration energy is calculated from the Born equation modified to give the correct oxidation potentials for Sn and Pb⁸

$$\Delta H_{\text{hyd}} = -\frac{7.32z^2}{r + 0.74} \text{ eV} \quad (4)$$

where z = charge on the ion and r = ionic radius (Pauling) (Å). Calculated values are given in Table IX.

The entropy change for the change in state is

$$\Delta S = S^\circ_{\text{H}_2(\text{g})} + \bar{S}^\circ_{M^{2+}(\text{aq})} - 2\bar{S}^\circ_{\text{H}^+(\text{aq})} - S^\circ_{M(\text{s})} \quad (5)$$

where $S^\circ_{\text{H}_2(\text{g})}$, the entropy of ideal diatomic hydrogen gas at 298°K = 31.21 cal deg⁻¹ mol⁻¹ (13.53×10^{-4} eV deg⁻¹); $S^\circ_{M(\text{s})}$ = entropy of the metal; and $\bar{S}^\circ_{\text{H}^+(\text{aq})} = 0$ by convention. $\bar{S}^\circ_{M^{2+}(\text{aq})}$, the entropy of the aqueous metal ion, was calculated using the equation of Powell and Latimer.⁹ The standard entropy of 114 metal (20 eu (g-atom)⁻¹) was obtained by extrapolation of the entropies of Si, Ge, Sn, and Pb *vs.* row of the periodic table (Figure 2 and Table IX)

$$\bar{S}^\circ_{M^{2+}(\text{aq})} = \frac{3}{2}R \ln A + 37 -$$

$$270 \frac{z}{(r + 2)^2} \text{ cal deg}^{-1} \quad (6)$$

(9) R. E. Powell and W. M. Latimer, *J. Chem. Phys.*, **19**, 1139 (1951).

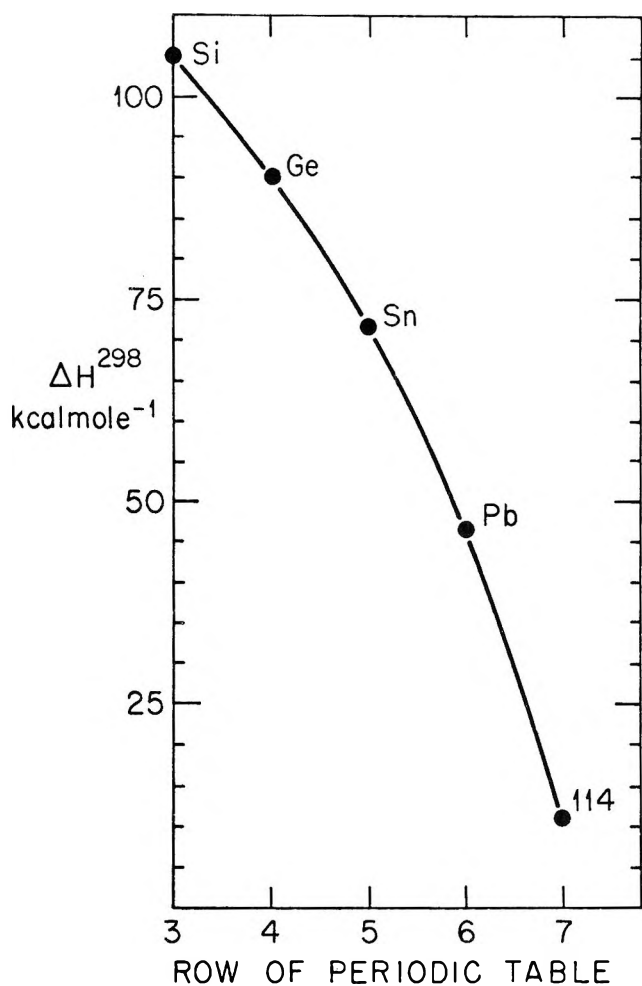


Figure 1. Heat of sublimation of element 114.

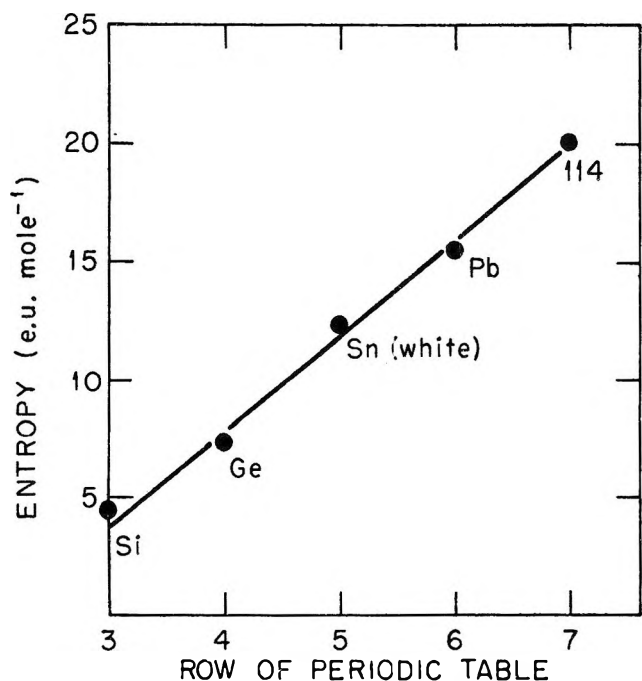


Figure 2. Entropy of elemental 114 (298°K).

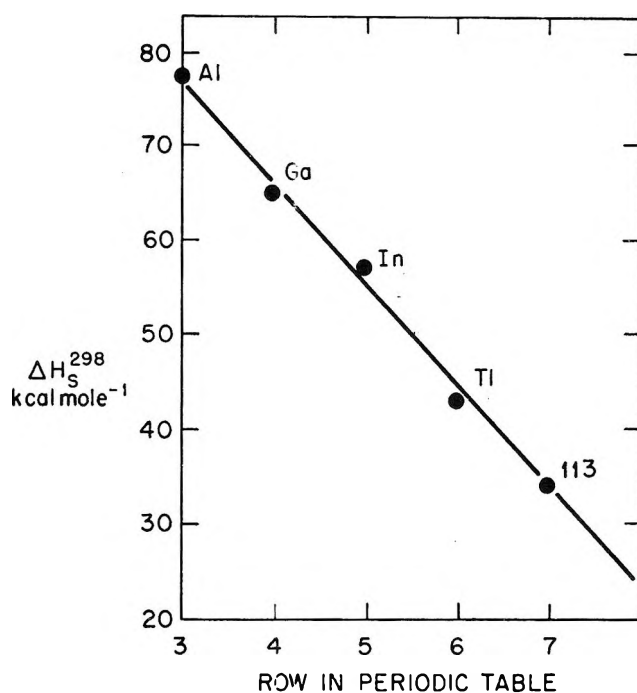


Figure 3. Heat of sublimation of element 113.

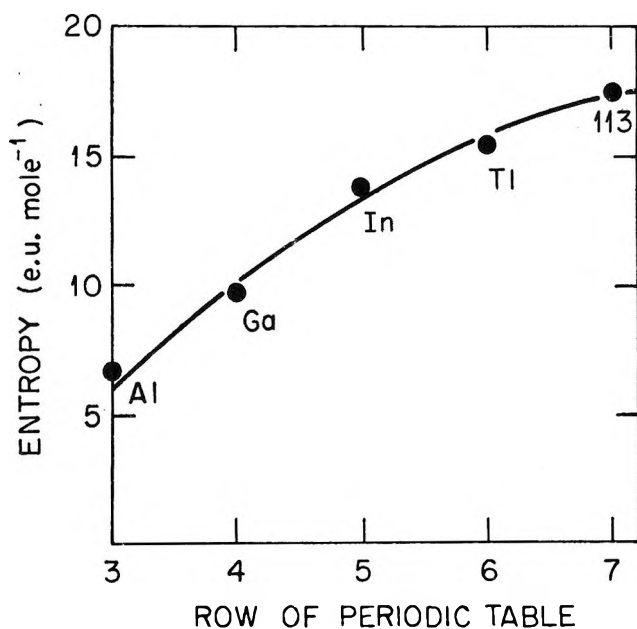


Figure 4. Entropy of elemental 113 (298°K).

where z = charge, A = atomic weight, and r = ionic radius (Pauling), in ångströms. The oxidation potential of 114 is calculated to be -0.9 V (American convention) (Table IX).

The oxidation potential of 113 is obtained in a manner analogous to that used for 114.

The hydration energies of Tl and 113 were calculated using eq 4 with an additive constant of 0.87 \AA to the ionic radius.⁸ The heat of sublimation, ΔH_s^{298} , and the elemental entropy were obtained by extrapolation (Figures 3 and 4 and Table X). The oxidation po-

tential of 113 is calculated to be -0.6 V (American convention). Element 113 is therefore estimated to be somewhat more noble than thallium, being similar to copper in this respect ($\text{Cu} = \text{Cu}^+ + e^-; E^\circ = -0.521$ V).

Boiling Points and Melting Points

The boiling points of Si, Ge, Sn, and Pb do not lend themselves to extrapolation to 114. As seen in the discussion of the oxidation potential, the heats of sublimation can be extrapolated. The heat of vaporization, ΔH_v , is assumed to be 8.3% less than the heat of sublimation, the same as lead. Using Trouton's rule and an entropy of vaporization of 22 eu, we calculate a boiling point for 114 of 420°K (Table VIII).¹⁰⁻¹²

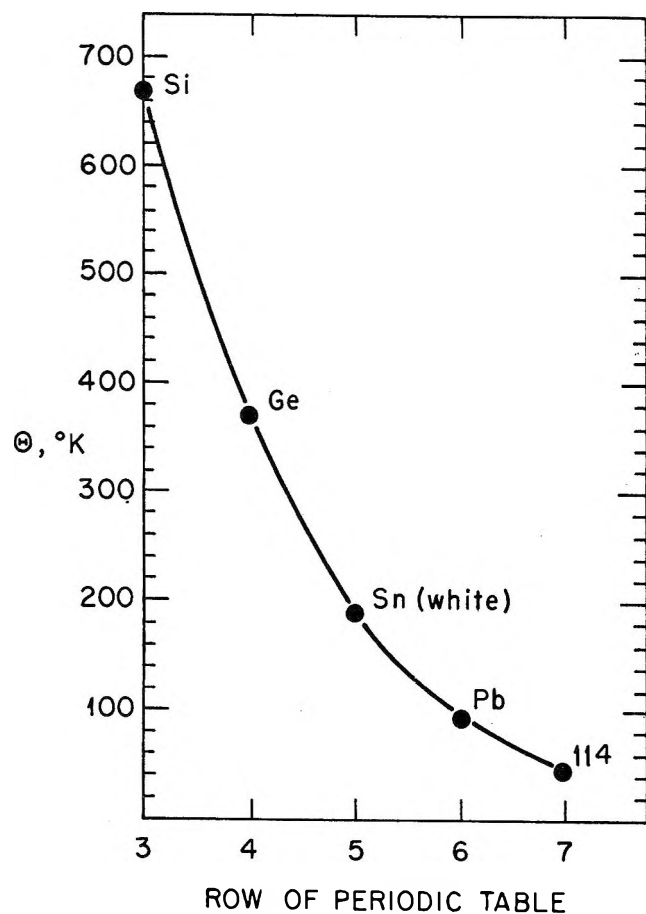


Figure 5. Debye temperature of element 114.

The melting point of a substance is a structure-dependent property and frequently is difficult to obtain by a simple extrapolation over a series where different structures are involved. Silicon, Ge, and gray Sn have the diamond structure; white Sn, which has typical metallic properties, is tetragonal, and Pb has the face-centered cubic (cubic closest packed) structure. We assume the latter for 114.

We obtain the melting point through the Lindemann melting point formula for close-packed metals¹³

$$T_m = \frac{\theta^2 A V^{2/3}}{D^2} \quad (7)$$

where θ = the Debye temperature, A = atomic weight, V = molar volume, and D is found empirically to be about $120 \text{ cm g}^{1/2} \text{ }^\circ\text{K}^{1/2}$. The Debye temperature for Si, Ge, white Sn, and Pb is plotted in Figure 5 using values from Mendelssohn.¹¹ We used the Debye

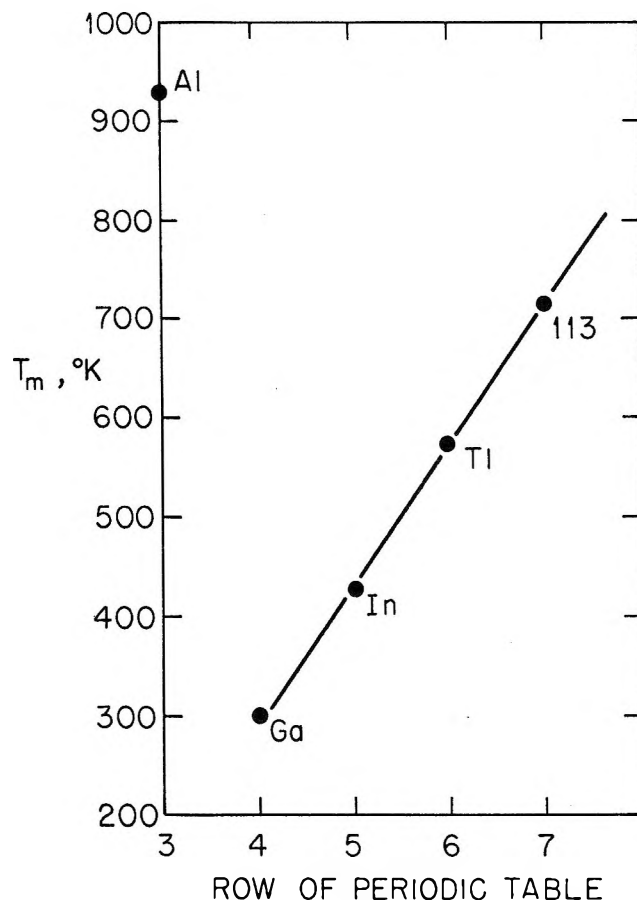


Figure 6. Melting point of element 113.

temperature of white tin for our extrapolation. If gray tin ($\theta = 212^\circ\text{K}$) is used a negative θ for 114 is obtained. Since white tin (tetragonal) has typical metallic properties whereas gray tin (diamond) does not, the use of the former may be sufficient to provide a transition between the diamond structures of Si and Ge to the fcc structure of Pb allowing a reasonably ac-

(10) D. R. Stull and G. C. Sinke, "Thermodynamic Properties of the Elements," American Chemical Society, Washington, D. C., 1956.

(11) K. Mendelssohn, "Cryophysics," Interscience Publishers, Inc., New York, N. Y., 1960.

(12) G. V. Samsonov, "Handbook of the Physicochemical Properties of the Elements," IFI/Plenum, New York, N. Y., 1968.

(13) N. H. March, "Liquid Metals," Pergamon Press, Oxford University Press, Oxford, 1968.

curate extrapolation to 114. The data are fitted by the equation

$$\theta = 670 - 372\chi - 73\chi^2 - 6\chi^3$$

where $(\chi + 3) =$ row of the periodic table. Letting $\chi = 4$ gives $\theta = 46^\circ\text{K}$ for 114 and a melting point of 340°K (Table VIII).

Although Ga is orthorhombic, In is tetragonal, and Tl is hexagonal, their melting points extrapolate in a straight line to a melting point of 710°K for 113 (Figure 6). In this case, the Debye temperature of Al, Ga, In, and Tl could not be extrapolated. Extrapolating only In and Tl yields $\theta = 70^\circ\text{K}$ for 113. Using this value in Lindemann's formula gives a melting point of 690°K . We take the average of 700°K as the melting point of element 113.

The heat of sublimation, (ΔH_s^{298}) , of 113 is obtained by extrapolation to be 34 kcal mol^{-1} (Figure 3). The heat of vaporization is assumed to be 10% less ($\Delta H_v = 31 \text{ kcal mol}^{-1}$). Using a Trouton's constant of 22, the boiling point is calculated to be 1400°K (Table X).

Discussion

In general, the chemistry of 114 is expected to be similar to that of divalent lead. The calculated oxidation potential of -0.9 V indicates, however, that 114 is considerably more noble. The large negative oxidation potential coupled with a large polarizability should enable 114^{2+} to form strong complexes with anions in spite of its large ionic radius. In excess halogen acid, for example, complexes of the type $114X_n^{(n-2)-}$ should be quite stable. A complex analogous to the plumbite ion is also expected. The sulfate and sulfide should be extremely insoluble. The acetate and nitrate would be soluble. The covalent nature of the acetate should prevent hydrolysis, as in the case of lead, but the nitrate may show extensive hydrolysis.

The chemistry of 113 is expected to be similar to that of the thallos ion although 113^+ should form complexes more easily. Our predicted radius of 113^+ is 1.48 \AA , the same as Rb^+ , and is not much larger than Tl^+ itself (1.40 \AA). The large polarizability and moderately large negative oxidation potential of -0.6 V will increase the binding of anions to 113^+ , but the large radius will counteract these effects to quite an extent. For example, the solubility of TlCl in water is not increased by adding hydrochloric acid or ammonia in contrast to the behavior of AgCl . The 113^+ ion should tend toward the behavior of Ag^+ in these properties. The chloride, bromide, iodide, sulfide, and chromate of 113^+ should have low solubilities while the nitrate and fluoride should be quite soluble. Thallos hydroxide is soluble and a strong base. The 113^+ ion may, however, form only a slightly soluble oxide whose solution is alkaline readily absorbing carbon dioxide from the air. Like argentous and aurous oxides, the oxide of 113^+ may be soluble in ammonia.

Uncertainties in Predicted Properties

Although the fundamental validity of extrapolation in the periodic table to the properties of 113 and 114 appears well founded, it is nonetheless difficult within the scope of this paper to discuss all of the assumptions and uncertainties in each of our estimates. There are two estimates, however, which appear to us to be questionable, and we will discuss those in some detail. The worst case is probably the melting point of 114 because we had to use (with little justification) the Debye temperature of white tin rather than gray tin in the extrapolation. The Lindemann melting point formula is a further approximation. Although there are difficulties with the method, the melting point itself appears acceptable from an intuitive point of

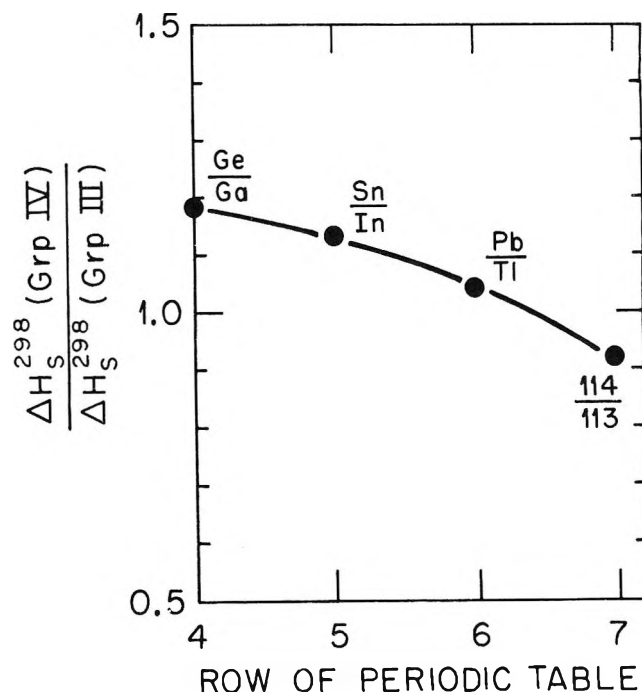


Figure 7. Row correlation of heats of sublimation of 113 and 114.

view. In the other questionable case, the heat of sublimation (and boiling point) of 114, the opposite is true. Although the extrapolation appears to be reasonable, the results appear from an intuitive point of view to be far too low. The extrapolation was carried out (Figure 1) by fitting a polynomial, the only other method being "eye-balling." The latter method allows the investigators judgment to be exercised to the maximum, and a value perhaps as high as about 20 kcal mol^{-1} could be obtained. Thus the "eye-balling" method could increase ΔH_s^{298} by as much as about 100%. Since the polynomial fits the data in a perfectly smooth and satisfactory way, however, it is difficult to see why we should not let the periodic

table govern the extrapolation rather than our "intuition."

There is, however, another way to extrapolate to ΔH_s^{298} of element 114. This involves essentially correlating by row as well as by column. If the ratio of the heats of sublimation for corresponding elements in groups IIIA and IVA are extrapolated to the seventh row (Figure 7), we obtain (by fitting a polynomial) a ratio of 0.87 for 114/113 (Figure 7). (Inclusion of the Si/Al ratio raises this ratio to 0.97.) The value of ΔH_s^{298} of element 114 obtained is 29.6 kcal mol⁻¹, a value which cannot even remotely fit into the group IVA sequence (Figure 1). We must, therefore, choose between the two methods. The group IVA extrapolation (Figure 1) can be viewed as less reliable than the group IIIA extrapolation (Figure 3) since all group IIIA elements are metallic whereas group IVA elements are graded from nonmetallic to metallic. Unfortunately, in the row type of extrapolation (Figure 7), we are probably only emphasizing this discrepancy by taking ratios involving elements with quite different properties.

Since the properties of Si, Ge, Sn, and Pb are more strongly correlated in a group way than in a row way, we accept the group extrapolation (Figure 1) as the more reliable method for predicting ΔH_s^{298} for element 114. Within this framework, we could, however, extrapolate only through Ge, Sn, and Pb leaving off Si. This would raise ΔH_s^{298} to 15 kcal mol⁻¹ ($\Delta H_s^{298} = 90 - 14.5\chi - 3.5\chi^2$) from our accepted value 10 kcal mol⁻¹.

Our other estimates do not involve such apparent problems.

Although extrapolating across 32 elements involves a certain amount of bravado, and numerous assumptions are involved, we feel that our estimates are sufficiently accurate to prove useful in the search for superheavy elements.

Acknowledgment. It is a pleasure to express our thanks to Dr. Glenn T. Seaborg for suggesting this study. His insight and interest were important in the development of the ideas presented here.

Radiation-Induced *cis-trans* Isomerization of Solutions of 2-Pentene in Cyclohexane

by J. W. F. van Ingen and W. A. Cramer

Interuniversitair Reactor Instituut, Delft, The Netherlands (Received September 8, 1969)

The *cis-trans* isomerization of solutions of 2-pentene in cyclohexane has been studied at room temperature as a function of pentene concentration. Effects of various additives, notably CH₃OH, NH₃, piperidine, O₂, I₂, CCl₄, C₂H₅Br, N₂O, C₇F₁₄, and SF₆ were investigated. In the presence of I₂, C₂H₅Br, and SF₆ a chain reaction occurs, as is evident from the very high isomerization yields. A chain reaction is also observed in the 2537-Å photolysis of solutions containing C₂H₅Br and 2-pentene. It is suggested that Br and I atoms and SF₅ radicals act as chain carriers. In the absence of a chain reaction, isomerization proceeds *via* excited 2-pentene molecules, formed by charge transfer from C₆H₁₂⁺ to the olefin and subsequent neutralization with electrons or negative ions.

Introduction

Formation of hydrogen, cyclohexene, and dicyclohexyl from irradiated cyclohexane is reduced in the presence of olefins. In previous work we have investigated the γ radiolysis of solutions of a number of olefins, including 2-pentene, with special emphasis on the effects of these additives on the hydrogen yield and the yield of saturated hydrocarbons corresponding with the olefins.¹ Evidence has been presented that charge

transfer from cyclohexane positive ions to olefins occurs if energetically possible. This can result in reduced decomposition of solvent molecules and in sensitized reactions of the solute, such as the radiation-induced *cis-trans* isomerization of 2-butene in dodecane.² We

(1) J. W. F. van Ingen and W. A. Cramer, to be published in *Trans. Faraday Soc.*

(2) R. B. Cundall and P. A. Griffiths, *Discussions Faraday Soc.*, **36**, 111 (1963).

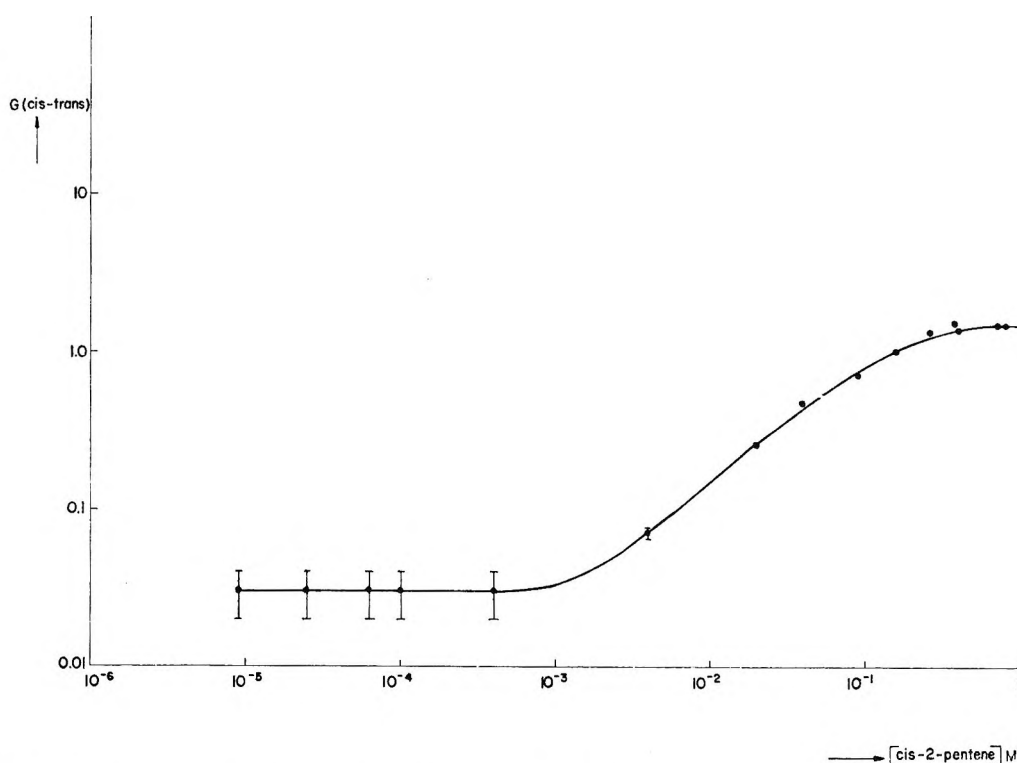


Figure 1. The *cis* → *trans* isomerization of 2-pentene in cyclohexane as a function of solute concentration.

have studied the γ -radiation-induced *cis*–*trans* isomerization of 2-pentene in cyclohexane as a function of 2-pentene concentration and in the presence of various additives. The results described in this paper give information about the mechanism of energy transfer from solvent to solute and also about the processes by which isomerization can take place.

Experimental Section

Cyclohexane (Merck Uvasol) was distilled from sodium in an 80-plate column; no impurities could be detected afterward by gas chromatographic analysis. The purification of *cis*-2-pentene has been described.¹ *trans*-2-Pentene (Fluka purum, $\geq 99\%$) was used as such. Methanol (Baker Analyzed, $\geq 99.5\%$) was dried on Mg and carbon tetrachloride (U.C.B. p.a., $\geq 99.9\%$) on MgSO_4 . Ammonia (Fluka, puriss, $\geq 99.8\%$), SF_6 (Baker, $\geq 98\%$), and N_2O (Loos and Co., $\geq 99.7\%$) were passed through a trap at -196° to remove traces of water. Perfluoromethylcyclohexane (Imperial Smelting, $>98\%$), O_2 (Air Products, $>99.5\%$), NO (Baker, $>99\%$), $\text{C}_2\text{H}_5\text{Br}$ (U.C.B., $>99\%$), and piperidine (Fluka puriss. p.a., $>99\%$) were used without further purification.

Degassing and irradiation procedures have been described.³ Dose rate and total dose were, respectively, 0.7×10^{17} eV/(g min) and 4×10^{19} eV/g, unless stated otherwise. Photolysis experiments were carried out in Vycor cells at 2537 \AA , using a Hanovia low-pressure mercury lamp. Rates of product formation were similar to those in the radiolysis experiments.

The *cis*- and *trans*-2-pentene were separated from cyclohexane at 60° on a 0.2-m column containing 40% squalane on Embacel 60–80 mesh. This column was coupled with a 4-m column containing 25% ethylene glycol on Embacel 60–8) mesh, which served to separate, at 8° , *cis*- and *trans*-2-pentene. Due to incomplete separation the accuracy of $G(\text{trans} \rightarrow \text{cis})$ measurement was only $\pm 10\%$.

Results

G values for *cis* → *trans* isomerization of 2-pentene are shown in Figure 1 as a function of solute concentration. At higher concentrations the curve levels off at a G value of ca. 1.5. The G value for *trans* → *cis* isomerization has been measured at *trans*-2-pentene concentrations varying from 2.7 – $4.5 \times 10^{-1} M$. At these concentrations, the observed G value of 1.0 ± 0.1 was constant within experimental error.

Information about the mechanism of *cis*–*trans* isomerization was obtained by investigating the effects of additives on $G(\text{isom})$. Among the additives studied were positive ion scavengers (CH_3OH , NH_3 , and piperidine), electron scavengers (CCl_4 , N_2O , C_7F_{14} , I_2 , $\text{C}_2\text{H}_5\text{Br}$, SF_6), free radical scavengers (CCl_4 , O_2 , I_2 , $\text{C}_2\text{H}_5\text{Br}$), and a quencher of excited molecules (O_2). Results are shown in Table I. The effects of $\text{C}_2\text{H}_5\text{Br}$ and SF_6 are remarkable in that they cause very high isomerization yields, indicating that chain reactions are operative. Even at lower doses, the thermodynamically

(3) W. A. Cramer and G. J. Piet, *Trans. Faraday Soc.*, **63**, 1402 (1967).

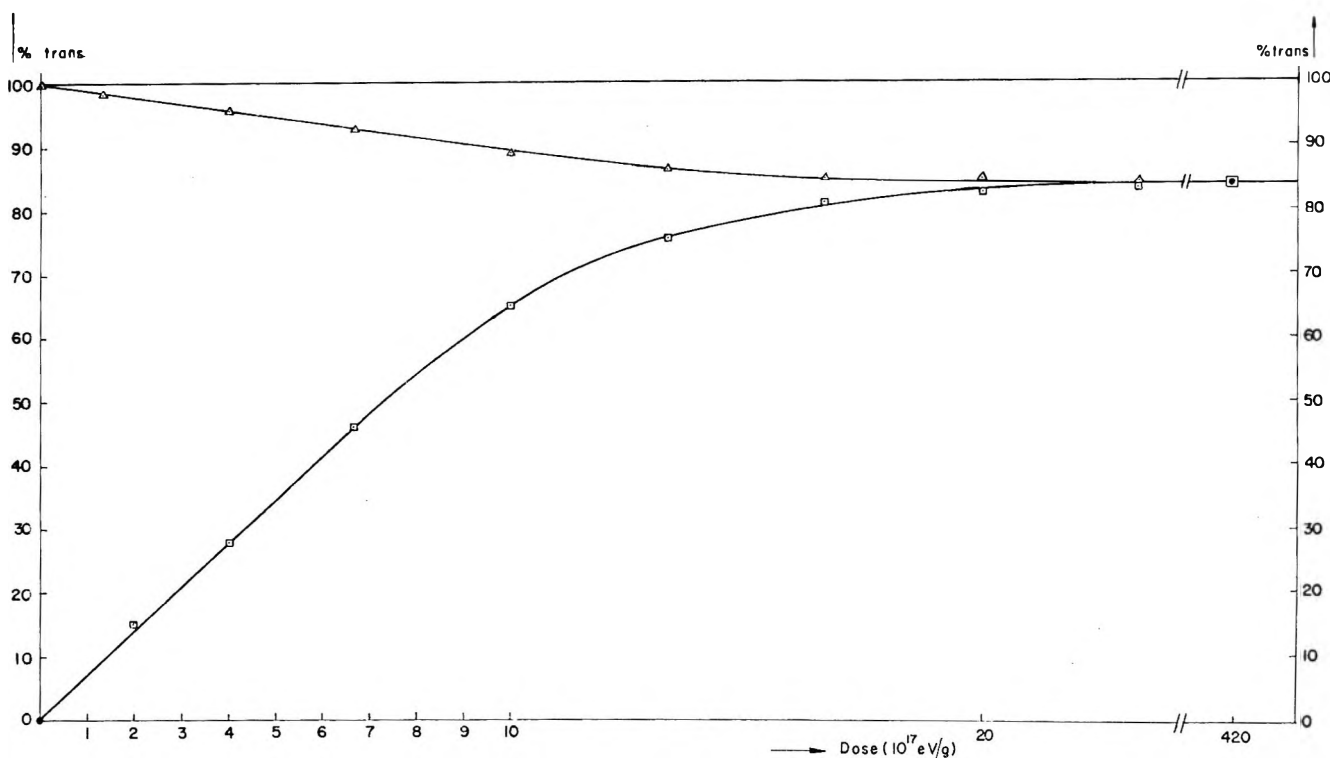


Figure 2. Effect of dose on isomer composition in solutions containing 0.1 *M* 2-pentene and 0.1 *M* SF₆.

Table I: Effects of Additives on the Radiation-Induced *cis* → *trans* Isomerization of 2-Pentene in Cyclohexane.

Additive	Concn, <i>M</i>	[<i>cis</i> -2-Pentene], <i>M</i>	<i>G</i> (isomer)	Δ <i>G</i> (isomer)
CH ₃ OH	5×10^{-1}	2×10^{-1}	0.35	-0.8
NH ₃	3×10^{-1}	4×10^{-1}	0.50	-1.0
	5×10^{-1}	4×10^{-1}	0.60	-0.9
O ₂	1×10^{-1}	3×10^{-1}	0.70	-0.6
C ₂ F ₄	0.5×10^{-1}	2×10^{-1}	0.70	-0.5
CCl ₄	1×10^{-1}	1.5×10^{-1}	1.6	0.6
N ₂ O	1×10^{-1}	1.5×10^{-1}	1.7	0.7
I ₂	1×10^{-1}	3.1×10^{-1}	8.8	7.4
C ₂ H ₅ Br	1×10^{-1}	1.0×10^{-1}	}complete isomerization	>300
SF ₆	1×10^{-1}	1.0×10^{-1}		

determined equilibrium of 84% *trans*- and 16% *cis*-2-pentene was obtained. In solutions containing 0.1 *M* *cis*-2-pentene, the dose required to obtain this equilibrium was *ca.* 2×10^{19} eV/g in the presence of 0.1 *M* C₂H₅Br and *ca.* 2×10^{18} eV/g when 0.1 *M* SF₆ was present. Figure 2 shows the isomer composition as a function of dose in solutions originally 0.1 *M* in *cis*-2-pentene or *trans*-2-pentene and 0.1 *M* in SF₆. A *G* value of about 5000 for the *cis* → *trans* isomerization can be calculated from the initial slope of the curve. Similar experiments at 0.01 *M* *cis*-2-pentene and 0.1 *M* SF₆ indicated a *G* value of *ca.* 1600.

It has been reported that *cis*-*trans* isomerizations of olefins can be catalyzed by I[•] and Br[•]⁵⁻⁸ atoms and also

by some radicals.⁸ To clarify the mechanism by which the radiation-sensitized chain isomerization proceeds, we have compared the γ and uv (2537 Å) induced reactions in solutions containing 0.1 *M* *cis*-2-pentene and 0.1 *M* C₂H₅Br. The effects of a number of additives were also studied in these systems. The same additives were used in irradiated solutions containing SF₆

(4) R. M. Noyes, G. Dickinson, and V. Schomaker, *J. Amer. Chem. Soc.*, **67**, 1319 (1945).

(5) H. Steinmetz and R. M. Noyes, *ibid.*, **74**, 4141 (1952).

(6) M. A. Golub, *J. Polym. Sci.*, **25**, 373 (1957).

(7) M. A. Golub, *J. Amer. Chem. Soc.*, **80**, 1794 (1958).

(8) M. A. Golub, *ibid.*, **81**, 54 (1959).

and *cis*-2-pentene. Results of these investigations are shown in Tables II and III. The radiation dose, used in these experiments, was about twice as high as required for complete isomerization with only *cis*-2-pentene and C₂H₅Br or SF₆ present as solutes.

Table II: Effects of Additives on γ and UV-Sensitized *cis* \rightarrow *trans* Isomerization of Solutions of 0.1 M 2-Pentene and 0.1 M C₂H₅Br in C₆H₁₂

Additive	M	% <i>cis</i>	% <i>trans</i>	Type of radiation
—		16	84	uv
CH ₃ OH	0.5	16	84	uv
NH ₃	0.1	~100	...	uv
	0.5	~100	...	uv
O ₂	0.1	~100	...	uv
—		16	84	γ
CH ₃ OH	0.5	16	84	γ
NH ₃	0.3	~100	...	γ
	0.5	~100	...	γ
O ₂	0.1	~100	...	γ

Table III: Effects of Additives on Radiation-Induced *cis* \rightarrow *trans* Isomerization of Solutions of 0.1 M 2-Pentene and 0.1 M SF₆ in C₆H₁₂

Additive	M	% <i>cis</i>	% <i>trans</i>
—		16	84
CH ₃ OH	0.5	16	84
NH ₃	0.3	~100	...
	0.5	~100	...
O ₂	0.5	~100	...

Discussion

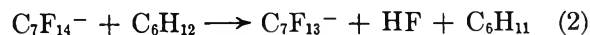
Occurrence and Mechanism of Energy Transfer and Isomerization. Energy absorption in various components of a mixture of hydrocarbons is approximately proportional to the respective electron densities of these components. It is therefore evident from the observed *G* values for isomerization that a sensitized reaction of the solute occurs. Reactions of alkyl radicals and H atoms with the solute cannot account for the observed results.² Chain reactions involving free radicals, charged species, or excited molecules can also be excluded, as scavengers of these intermediates have only limited effects on the *G*(isom) (the large increase in the presence of SF₆, C₂H₅Br, and I₂ will be discussed later). Hence, the results suggest that energy (either charge or excitation) is transferred from solvent to solute. The actual mechanism by which this energy transfer proceeds can be deduced from results obtained in the presence of additives reacting with electrons, positive ions, and excited molecules (Table I).

In the presence of positive ion scavengers (CH₃OH, NH₃, piperidine), a reduction is observed in *G*(isom). This may be considered as evidence for a mechanism in which cyclohexane positive ions react with the olefin. Charge transfer from C₆H₁₂⁺ to olefins has been shown to occur if the olefins have a lower ionization potential than cyclohexane, as is the case with 2-pentene.¹ The dependence of *G*(isom) on 2-pentene concentration confirms a charge-transfer mechanism, as is evident from the following observations. It is known that, at very low concentrations, positive ion scavengers cannot compete with geminate ion recombination but can only react with free ions. The contribution of this reaction remains approximately independent of scavenger concentration until, at higher concentrations, the scavenger starts to compete with inhomogeneous recombination reactions.^{9,10} The results in Figure 1 show exactly this dependence of *G*(isom) on scavenger concentration.

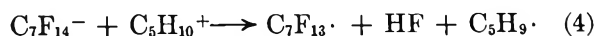
The contribution of charge transfer can be enhanced by increasing the lifetime and hence the reaction probability of solvent positive ions. This can be achieved by adding electron scavengers. An increase in *G*(isom) was indeed observed upon addition of N₂O or CCl₄ (Table I; the very high yields in the presence of I₂, C₂H₅Br, and SF₆ will be discussed later). However, *G*(isom) was reduced when perfluoromethylcyclohexane (C₇F₁₄) was added as electron scavenger. This additive reacts with electrons according to reaction 1.¹¹⁻¹³



The observed reduction in *G*(isom) is not inconsistent with the proposed charge-transfer mechanism if it is assumed that the pentene positive ion does not isomerize, but that isomerization proceeds only *via* an excited state, formed by recombination of C₅H₁₀⁺ with a negative ion or an electron, and furthermore, that the reaction between C₅H₁₀⁺ and C₇F₁₄⁻ (or C₇G₁₃⁻ according to Rajbenbach¹⁴) does not produce an excited pentene molecule. In agreement with this suggestion is the proposed sequence of reactions 2 and 3.¹⁴



Alternatively, reaction 4 may also contribute, followed by (5)



(9) F. Williams, *J. Amer. Chem. Soc.*, **86**, 3954 (1964).

(10) S. J. Rzed and J. M. Warman, *J. Chem. Phys.*, **49**, 2861 (1968).

(11) L. A. Rajbenbach, *J. Amer. Chem. Soc.*, **88**, 4275 (1966).

(12) L. A. Rajbenbach, *J. Chem. Phys.*, **47**, 242 (1967).

(13) N. H. Sagert, *Can. J. Chem.*, **46**, 95 (1968).

(14) L. A. Rajbenbach, *J. Phys. Chem.*, **73**, 356 (1969).

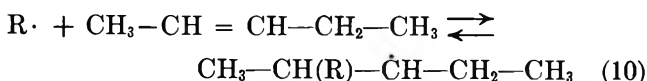
The observed reduction in $G(\text{isom})$ when O_2 is present is consistent with a mechanism involving excited pentene molecules. (Cundall and Griffiths suggested isomerization of 2-butene in dodecane to occur *via* proton transfer from the solvent positive ion to the olefin, followed by rearrangement and proton loss to a negative ion.² However, with such a mechanism one would expect the effects of C_7F_{14} , N_2O , and other e^- scavengers to be qualitatively similar. Moreover, the reduced yields with O_2 present would be difficult to explain.) Hence the following reactions are proposed.



Assuming that k_6 is equal for *cis*- and *trans*-2-pentene, one can calculate from the "plateau" G values for *cis* \rightarrow *trans* and *trans* \rightarrow *cis* isomerization, for k_8/k_9 a value equal to 1.5. (A value of 1.0 for this ratio was observed in benzene solutions.¹⁵) If, for each $\text{C}_5\text{H}_{10}^+$ ion, one precursor for the isomerization reaction ($\text{C}_5\text{H}_{10}^*$) is formed, then the calculated G value for scavenged ions at the highest pentene concentrations used (Figure 1) is equal to $(k_8 + k_9)/k_9 \times G(\textit{cis} \rightarrow \textit{trans})_{\text{max}} = 2.5$. This yield will be larger if the formation of $\text{C}_5\text{H}_{10}^*$ is less efficient. A G value ≥ 2.5 agrees fairly well with estimates of the total ion yield in C_6H_{12} of 3-4.¹⁶ From the limiting yield of $G(\text{isom})$ at low pentene concentration the $G(\text{free ion})$ can be estimated. $G(\text{f.i.}) \geq (k_8 + k_9)/k_8 \times G(\textit{cis} \rightarrow \textit{trans})_{\text{C}_6\text{H}_{12} \rightarrow 0} = 0.05$. Again, this yield does not differ much from the generally accepted value of *ca.* 0.1. A value smaller than 0.1 might actually be expected as, at the olefin concentrations and the radiation doses used, a considerable fraction of the pentene will be isomerized. Moreover, cyclohexene is formed and this product competes with pentene for cyclohexane positive ions.¹⁷

Isomerization of 2-Pentene by a Chain Mechanism. It has been discussed that the increase in $G(\text{isom})$ in the presence of electron scavengers such as N_2O and CCl_4 is due to an increased lifetime of cyclohexane positive ions. However, the large yields when I_2 , $\text{C}_2\text{H}_5\text{Br}$, or SF_6 are added (Table I) clearly require another explanation. The very high values for $G(\text{isom})$ especially when SF_6 and $\text{C}_2\text{H}_5\text{Br}$ are present indicate that a chain reaction occurs.

It is known that Br atoms as well as some S-containing radicals can catalyze *cis-trans* isomerizations of olefins according to reaction 10.⁵⁻⁸



Iodine atoms can initiate the same reaction, but they are much less reactive at room temperature. Hence,

the observed increase in $G(\text{isom})$ with I_2 present is probably the result of a catalytic effect of I atoms. (It is of interest to note that in presence of I_2 no increase in $G(\text{isom})$ of 2-butene in dodecane was observed² whereas preliminary experiments indicate very high yields for the isomerization of 0.1 *M cis*-stilbene in cyclohexane. Evidently, the effect of I atoms depends strongly on the olefins involved.) Formation of these atoms in solutions containing I_2 may occur by dissociative electron capture and also by reactions of alkyl radicals and H atoms with I_2 . A similar mechanism may be involved in the presence of $\text{C}_2\text{H}_5\text{Br}$ and SF_6 . Bromine atoms may be formed in reactions 11 and 12.



To confirm the role of Br atoms, solutions of 2-pentene and $\text{C}_2\text{H}_5\text{Br}$ in cyclohexane were irradiated with light of 2537 Å. This causes dissociation of $\text{C}_2\text{H}_5\text{Br}$ into Br atoms and C_2H_5 radicals. It was indeed observed that complete isomerization also occurred in these experiments but only when $\text{C}_2\text{H}_5\text{Br}$ was present. Further evidence for the proposed mechanism was obtained by comparing effects of additives on the chain reaction in the γ and uv experiments. The results (Table II) show similar effects of the additives in the two sets of experiments. As expected, CH_3OH has no effect in the presence of $\text{C}_2\text{H}_5\text{Br}$. Ammonia and piperidine, on the other hand, known to react with halogen atoms,¹⁸ completely suppress the chain reaction. This is also observed in the presence of O_2 . The effect of O_2 seems to be related to the structure of the reacting olefins as was the case with the catalytic effects of I atoms. For example, no effect of O_2 has been observed in the I-catalyzed thermal isomerization of esters of cinnamic acid¹⁹ whereas we have found in preliminary experiments that a similar isomerization reaction of stilbene was strongly reduced by O_2 . Possibly, oxygen can react irreversibly with addition complexes of I atoms and some olefins.

The chain reaction observed upon addition of SF_6 requires some additional comment. It has recently been reported that the radiation-induced *cis-trans* isomerization of 2-butene in cyclohexane in the vapor phase proceeds by a chain reaction in the presence of SF_6 .²⁰ SF_6^- was suggested to be the chain carrier. However, the observed suppression of the reaction in the presence

(15) M. A. Golub, L. L. Stephens, and J. L. Brash, *J. Chem. Phys.*, **45**, 1503 (1966).

(16) A. Hummel, *ibid.*, **49**, 4840 (1968).

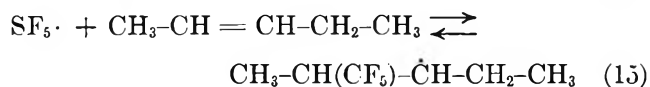
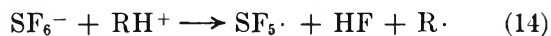
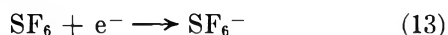
(17) W. A. Cramer and G. J. Piet, to be published in *Trans. Faraday Soc.*

(18) A. M. Halpern and K. Weiss, *J. Phys. Chem.*, **72**, 3863 (1968).

(19) W. J. Muizebelt, private communication.

(20) R. W. Hummel, *Nature*, **218**, 1050 (1968).

of O₂ could not be explained. Our results in solutions containing SF₆ and in particular the effects of additives, which are similar to those in solutions containing C₂H₅Br, suggest a mechanism involving free radicals. The following reactions are proposed



Results obtained by Golub indicate that some S-containing radicals are more efficient as catalysts for *cis-trans* isomerizations than Br atoms.⁶ This is consistent with our observation that complete isomerization of 0.1 M *cis*-2-pentene requires ca. 2×10^{19} eV/g with

0.1 M C₂H₅Br present and ca. 2×10^{18} eV/g in the presence of 0.1 M SF₆.

Sagert, *et al.*, have concluded from reduced yields of C₁₂H₂₂ in solutions containing SF₆ that reaction 14 does not occur in cyclohexane.²¹ However, this conclusion was based on the assumption that SF₅ radicals will react with C₆H₁₂ to form C₆H₁₁ radicals. Our results indicate that reaction 14 probably does occur but that SF₅ radicals do not effectively abstract H atoms from cyclohexane. This can account for the decrease in *G*(C₁₂H₂₂) as measured by Sagert, *et al.*

Acknowledgment. The authors wish to express their gratitude to Mrs. C. E. C. Van Tieghem and N. de Boer for their assistance in the experiments.

(21) N. H. Sagert and A. S. Blair, *Can. J. Chem.*, **45**, 1351 (1967).

NOTES

Fitting Data with the β Distribution

by Gordon H. Fricke, Donald Rosenthal,

Department of Chemistry and Institute of Colloid and Surface Science, Clarkson College of Technology, Potsdam, New York 13676

and George Welford

Health and Safety Laboratory, U. S. Atomic Energy Commission, New York, New York 10014 (Received July 16, 1969)

The β function, which is a two-parameter distribution function, has wide applicability¹⁻³ but has not received much attention from chemists. However, we have recently used the cumulative β distribution to fit density distribution data of glass beads from which a frequency distribution was calculated.⁴ The β probability density function has been used successfully to fit particle size distributions obtained from light scattering and from light and electron microscopy. Complete and incomplete β functions have been used to calculate the quality factor (QF) for degraded heavy-particle spectra observed in solar flare activity.⁵

The function is presented here in a number of figures which show the broad range of cumulative and non-cumulative characteristic shapes. Least-squares fits of the β distribution to a number of common distribution functions, which are of interest to chemists, give reasonable fits.

The β distribution function is the ratio of the incomplete β function to the complete β function

$$I_x(p, q) = \frac{\beta_x(p, q)}{\beta(p, q)} \quad (1)$$

where

$$\beta_x(p, q) = \int_0^x x^{p-1}(1-x)^{q-1} dx \quad (2)$$

and

$$\beta(p, q) = \int_0^1 x^{p-1}(1-x)^{q-1} dx \quad (3)$$

The β function is defined for $0 \leq x \leq 1$, $0 \leq p$, and $0 \leq q$. One of the properties of the β function is

$$I_x(p, q) = 1 - I_{1-x}(q, p) \quad (4)$$

This means that each noncumulative distribution has a

(1) M. Abramowitz and I. A. Stegun, Ed., "Handbook of Mathematical Functions with Formulas, Graphs and Mathematical Tables," National Bureau of Standards, Applied Mathematics Series, No. 55, U. S. Government Printing Office, Washington, D. C., 1964.

(2) G. J. Hahn and S. S. Shapiro, "Statistical Models in Engineering," John Wiley & Sons, Inc., New York, N. Y., 1967.

(3) D. Osborn and R. Madey, "Mathematics of Computation," Vol. 22, Lane Press Inc., Burlington, Vermont, 1968, p 159.

(4) G. H. Fricke, D. Rosenthal, and G. Welford, *Anal. Chem.*, **41**, 1866 (1969).

(5) R. Madey and T. E. Stephenson, "Proceedings of the Second Symposium on Protection against Radiation in Space," NASA SP-71, U. S. Government Printing Office, Washington, D. C., 1965, p 229.

Table I: The β Distribution

	Symmetric	Skewed	J and reverse J	U and skewed U	Linear
Noncumulative					
Cumulative					
General conditions	$p > 1, q > 1$ $p = q$	$p > 1, q > 1$	Both not equal one	$p < 1, q < 1$...
Specific conditions	...	(a) Pos skewed $p < q$ (b) Neg skewed $q < p$	(a) J shape $p \geq 1, q \leq 1$ (b) Reverse J $p \leq 1, q \geq 1$	(a) Symmetric $p = q$ (b) Pos skewed $q < p$ (c) Neg skewed $p < q$	(a) Horizontal $p = 1, q = 1$ (b) Neg 45° slope $p = 1, q = 2$ (c) Pos 45° slope $p = 2, q = 1$
Values used for figures	(a) $p = 2.0,$ $q = 2.0$ (b) $p = 10.0,$ $q = 10.0$	(a) $p = 1.5,$ $q = 3.0$ (b) $p = 5.0,$ $q = 1.5$	(a) $p = 8.0,$ $q = 1.0$ (a') $p = 1.5,$ $q = 0.8$ (b) $p = 1.0,$ $q = 5.0$	(a) $p = 0.5,$ $q = 0.5$ (b) $p = 0.9,$ $q = 0.5$ (c) $p = 0.5,$ $q = 0.8$	(a) $p = 1.0,$ $q = 1.0$ (b) $p = 1.0,$ $q = 2.0$ (c) $p = 2.0,$ $q = 1.0$

mirror image obtained by reversing the numerical values of p and q .

The β probability density function is given as

$$f_x(p,q) = \frac{x^{p-1}(1-x)^{q-1}}{\beta(p,q)} \quad (5)$$

The parameters p and q both influence the shape of the distribution.

The complete β function can be evaluated as a ratio of Γ functions¹

$$\beta(p,q) = \frac{\Gamma(p)\Gamma(q)}{\Gamma(p+q)} \quad (6)$$

From eq 6 it is obvious that

$$\beta(p,q) = \beta(q,p) \quad (7)$$

The incomplete β function may be evaluated by the method of Osborn and Madey³ or by a standard IBM computer program.⁶ Values of the β distribution calculated for eq 1 have been tabulated for values of p and q from 0.5 to 50.⁷

Statistical estimates of the values of p and q can be made from the average value and the variance.² These initial estimates can be used as starting values for a

fitting procedure which finds the "best" values of p and q by minimizing the sum of the squares of the differences between the experimental points and the points calculated from the β distribution. Minimization or maximization of some other function of the differences between the experimental and calculated points might be used.⁸

After the "best" values of p and q have been located, the mean (expected value), the mode (peak or minimum of a monomodal distribution), and the variance may be calculated^{1,2}

$$\text{mean} = \frac{p}{p+q} \quad (8)$$

$$\text{mode} = \frac{p-1}{p+q-2} \quad (9)$$

$$\text{variance} = \frac{pq}{(p+q)^2(p+q+1)} \quad (10)$$

(6) "System/360 Scientific Subroutine Package," 360 A-CM-03X, Version III, 4th ed, International Business Machines Corp., White Plains, N. Y., 1968, p 78 ff.

(7) K. Pearson, "Tables of Incomplete Beta-Function," Cambridge University Press, New York, N. Y., 1934.

(8) R. Deutsch, "Estimation Theory," Prentice-Hall, Inc., Englewood Cliffs, N. J., 1965.

Table II: Distributions Fitted to β Distribution

Name of distribution	Probability density function	Values of parameters	"Best" values of distribution parameters		$E, \%$ (eq 11)
			p	q	
Normal	$\frac{1}{\sigma\sqrt{2\pi}} \exp[-(x - \mu)^2/2\sigma^2]$	$\mu = 0.00$ $\sigma = 1.00$	10.65	10.65	0.77
Log normal	$\frac{1}{\sigma x\sqrt{2\pi}} \exp[-(\ln x - \ln \mu)^2/2\sigma^2]$	$\mu = 1.00$ $\sigma = 1.00$	1.48	12.77	4.60
Lorentz	$\alpha / \left[\left(\frac{1}{\lambda} - \frac{1}{\lambda_0} \right)^2 + \beta^2 \right]$	$\lambda_0 = 260$ $\alpha = 2.37 \times 10^{-4}$ $\beta = 1.54 \times 10^{-4}$	46.99	109.91	5.84
Γ	$\frac{\lambda^\eta}{\Gamma(\eta)} x^{\eta-1} e^{-\lambda x}$	$\lambda = 2.00$ $\eta = 4.00$	3.20	8.65	2.68
χ^2 (special case of Γ distribution)	$[2^{\nu/2} \Gamma(\nu/2)]^{-1} x^{(\nu/2)-1} e^{-x/2}$	$\nu = 5.00$ (deg of freedom) $\nu = 25.00$ (deg of freedom)	2.20 7.71	8.22 10.44	2.32 3.06
Zeroth-order logarithmic ⁹	$\frac{\exp[-(\ln x - \ln x_M)^2/2\sigma^2]}{\sigma x_M \sqrt{2\pi} \exp(\sigma^2/2)}$	$x_M = 0.399$ $\sigma = 0.074$	4.93	5.83	2.19

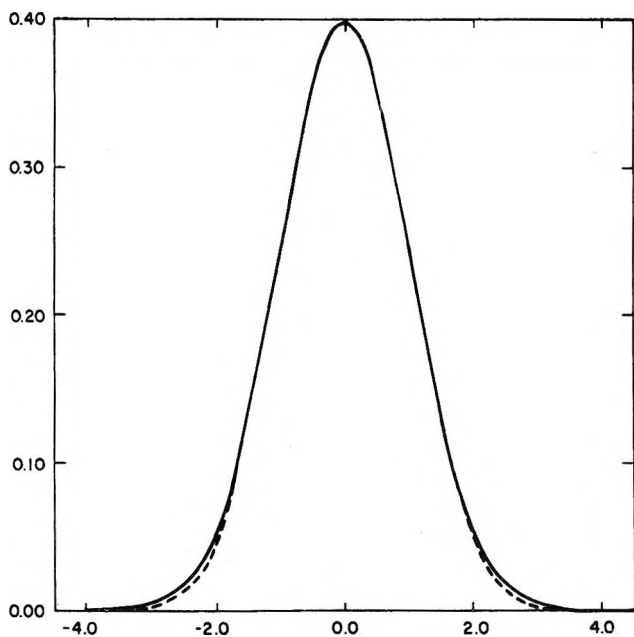


Figure 1. Normal distribution fitted with β distribution (Table II); —, normal distribution; - - - -, β distribution.

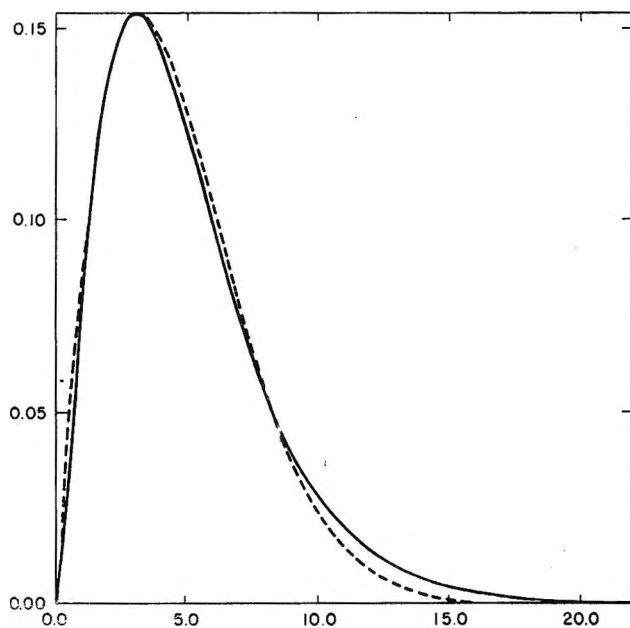


Figure 2. χ -Square distribution (five degrees of freedom) fitted with β distribution (Table II; —, χ -square distribution; - - - -, β distribution).

The shape estimators, $\sqrt{\beta_1}$ (measure of skewness) and β_2 (measure of kurtosis) may also be calculated from the shape parameters p and q .^{1,2}

The wide range of shapes of the β distribution is illustrated by the figures in Table I. All figures, except the noncumulative J and U shape curves, have been normalized to give a maximum ordinate value of 1. These figures are merely representative of the shapes which the β distribution has.

The β distribution has been least-squares-fitted to a number of common distribution functions. The results are presented in Table II.⁹ The relative error,

E , in per cent, is obtained by dividing the standard deviation from regression, SD_{reg} with $N - 2$ degrees of freedom, by the value of the noncumulative function at its peak

$$E = \frac{SD_{reg}}{\text{maximum}} \times 100 \quad (11)$$

where

$$SD_{reg} = \sqrt{\frac{\sum (f_{exptl.} - f_{calcd.})^2}{N - 2}} \quad (12)$$

(9) W. F. Espenscheid, M. Kärker, and E. Matijević, *J. Phys. Chem.*, 68, 3093 (1964).

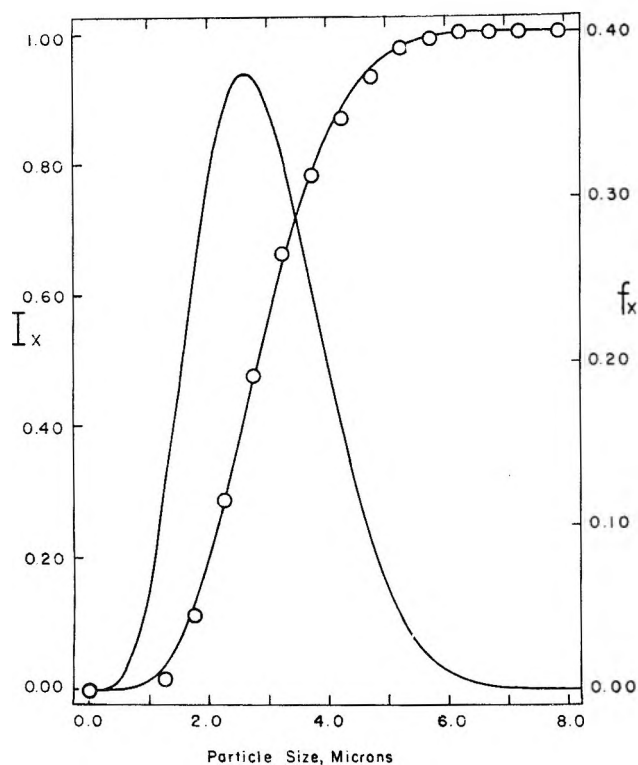


Figure 3. Size distribution of emulsion data fitted with β distribution. Experimental cumulative number fraction, I_x . f_x is the frequency distribution in microns⁻¹.

Figures 1 and 2 represent the β distribution fitted to the normal distribution and the χ^2 distribution (five degrees of freedom), respectively. Although the fits are not perfect, the shape of the curves has been followed quite well.

Figure 3 shows a cumulative size distribution of particles from a homogenized emulsion of a 1% w/v α -monostearin in a water-water-oil system with an equal volume of 0.5% w/v sodium stearate in water. The data points, which have been least-squares-fitted with the β distribution from 0 to 11 μ , represent the cumulative fraction of the number of particles. The values of p and q for the β distribution obtained are 5.39 and 14.90, respectively. The data have been plotted from 0 to 8 μ . The frequency distribution was calculated from the derivative of the β distribution using the least-squares values of p and q .

It should be noted that a contour map of p vs. q with SD_{reg} as the third dimension may have a number of minima. The procedure used to locate the values of p and q was a method of steepest descent. Initially, contour maps, using reasonable intervals of p and q , were constructed by the computer. A search was made near areas of the contour map which appeared to have minima. The values of p and q corresponding to the lowest value of E found are given in Table II. The goodness of fit obtained by the β distribution may be improved by a judicious choice of data points at the extremes of the curve. Extending or eliminating

data points, where I_x is approximately 0 or 1 or where f_x is 0, may be advantageous.

A number of useful statistical functions and distributions may be obtained directly from integer and half-integer values of the β distribution function, $I_x(p, q)$.¹ These include the hypergeometric function, the binomial distribution, the negative binomial distribution, Student's t distribution, the F distribution (variance ratio), and the distribution for two independent random variables X_1^2 and X_2^2 , which follow the χ^2 distribution with ν_1 and ν_2 degrees of freedom, respectively.

In conclusion it can be said that the β distribution function has been shown to have a wide range of shapes and should be considered when shapes of distributions for experimental data are investigated. It has the advantage of being able to cover the range of distribution shapes commonly in use.

Acknowledgment. The authors wish to thank Dr. Richard Madey and Mr. David Osborn for making available their computer program for evaluation of the β function, Dr. Chao Huang for the light scattering and electron micrograph data, and Dr. H. H. G. Jellinek for the emulsion size distribution data. The AEC Health and Safety Laboratory provided partial support for this research and furnished G. H. F. with a research fellowship.

The Product Energy Distribution on Photolysis of 3-Methyl-1-Pyrazoline

by F. H. Dorer

Department of Chemistry, California State College, Fullerton, Fullerton, California 92631 (Received September 8, 1969)

The partitioning of the excess energy between the cyclic hydrocarbon and nitrogen products of the photolysis of 1-pyrazolines has been found to be non-random; the internal degrees of freedom of the hydrocarbon fragment receive only about 62% of the available energy.^{1,2} The energy distribution between products of the decomposition of these symmetric 1-pyrazolines (symmetric in the sense that both rupturing C-N bonds are equivalent) can be at least qualitatively rationalized by a model in which the hydrocarbon portion of the molecule would have to undergo little structural change on formation of the product,

(1) F. H. Dorer, *J. Phys. Chem.*, **73**, 3109 (1969).

(2) T. F. Thomas, C. I. Sutin, and C. Steel, *J. Amer. Chem. Soc.*, **89**, 5107 (1967). For purposes of consistent comparison, the results quoted are those obtained when RRKM unimolecular rate theory (R. A. Marcus, *J. Chem. Phys.*, **20**, 359 (1952)) is used for the rate calculations.

but the N-N bond distance must considerably shorten on forming nitrogen. In a recent communication³ Baur noted that for 1-pyrazoline decomposition it is possible that there is simultaneous rupture of the two C-N bonds resulting in essentially complete separation of the two fragments before geometric relaxation can occur,^{4,5} and consequently, if the transition state lifetime were short enough, a large fraction of the excess energy could be stored as vibrational excitation of the nitrogen.

This concept suggests that it might be possible, by using a 1-pyrazoline for which the rupturing C-N bonds are not equivalent, to alter the potential energy surface sufficiently for the decomposition reaction such that the product energy distribution would reflect the change in the nature of the transition state. As an extreme, differences in the bond strengths of the rupturing C-N bonds might be great enough to cause the elimination reaction to become a stepwise process which could allow a greater degree of geometric relaxation of the N-N bond and concomitant energy randomization before separation of the fragments. This is perhaps the explanation of why vibrationally excited vinylcyclopropane has been observed in the pyrolysis of 3-vinyl-1-pyrazoline,⁵ but even though the reaction is 41 kcal mol⁻¹ exothermic, we have not found "hot" methylcyclopropane in the pyrolysis of 4-methyl-1-pyrazoline at pressures as low as 2×10^{-3} Torr.⁶

We, therefore, have carried out this short study of the partitioning of energy between the methylcyclopropane and nitrogen produced on photolysis of 3-methyl-1-pyrazoline in order to see what effect a relatively small difference in the strengths of the two rupturing C-N bonds of this molecule might have on the product energy distribution.

Experimental Section

Beginning with the reaction of hydrazine with crotonaldehyde, the 3-methyl-1-pyrazoline was synthesized by the same procedure as used for the synthesis of 4-methyl-1-pyrazoline.^{1,7} The final product was purified by gas chromatography using a carbowax column.

The photolysis run procedure has been previously outlined.¹ However, the following two modifications to this procedure are contained in the present work. A Bausch and Lomb high intensity monochromator (Model No. 5, 7.4 m μ /mm dispersion, 22.2-m μ bandpass) with an Osram HBO 200 mercury lamp was used as the source of 3130-Å radiation. The photolysis runs were carried out at room temperature in quartz cells 50 mm in diameter with total volume of 172 cm³ and 491 cm³ instead of the spherical Vycor reactors used for the 4-methyl-1-pyrazoline work. Photolysis times were of the order of 1 hr.

The products were analyzed by gas chromatography using the flame ionization detector in the same manner as previously described.¹

Results and Discussion

The pressure dependence of the relative amounts of C₄ hydrocarbons produced by the 3130-Å photolysis of a dilute mixture of 3-methyl-1-pyrazoline in propane is given in Table I. In addition to these products propylene and ethylene result from a cleavage reaction characteristic of 1-pyrazoline photolysis,⁸ but their contribution to the hydrocarbon products is no greater than 14% and need not concern us here.

There is a small amount of C₄ olefins formed at even the highest pressures. These could be products of vibrationally excited methylcyclopropane (MCP*) isomerization, or they may come from an olefin producing reaction in the primary photodecomposition step. The experimental unimolecular rate constant for the isomerization of MCP* formed in the primary process calculated from

$$k_a = \omega \frac{(\text{butene-1} + \text{butene-2} + \text{isobutene})}{\text{MCP}} \quad (1)$$

where ω is the specific collision frequency of MCP* with the bath molecules, will therefore represent an upper limit for k_a . If olefin formation in the primary process is independent of pressure, or if, as found for 4-methyl-1-pyrazoline photolysis, its importance decreases at lower pressures,¹ the experiments in the lowest pressure region will, of course, most accurately reflect the magnitude of k_a . The values of k_a calculated from the data of Table I are illustrated in Figure 1. Collision diameters of 5.6 Å for MCP and 4.8 Å for propane were used to calculate ω .

The relationship of the experimental unimolecular rate constant to the microscopic unimolecular rate constant for isomerization of MCP* with energy E , k_E , and the energy distribution function, $f(E)$, is

$$k_a = \omega \frac{\sum_E^{E_T} k_E f(E)}{\sum_E^{E_T} \frac{\omega f(E)}{k_E + \omega}} \quad (2)$$

The manner in which the RRKM calculations of k_E were carried out and how eq 2 is evaluated are contained in ref 1.

From the available thermochemical data one calculates that the decomposition of 4-methyl-1-pyrazoline to MCP and nitrogen is 41 kcal mol⁻¹ exothermic.¹ The differences in the heats of hydrogenation of 3- and

(3) S. H. Baur, *J. Amer. Chem. Soc.*, **91**, 3688 (1969).

(4) R. J. Crawford and A. Mishra, *ibid.*, **88**, 3963 (1966).

(5) R. J. Crawford and D. M. Cameron, *Can. J. Chem.*, **45**, 691 (1967).

(6) F. H. Dorer, unpublished results.

(7) R. J. Crawford, A. Mishra, and R. J. Dummel, *J. Amer. Chem. Soc.*, **88**, 3959 (1966).

(8) R. Moore, A. Mishra, and R. J. Crawford, *Can. J. Chem.*, **46**, 3305 (1968).

Table I: Relative Amounts of C₄ Hydrocarbon Products as a Function of Total Pressure^a

Pressure, Torr	$C_{4i}/\sum_{i=1}^5 C_{4i}$				
	MCP	<i>i</i> -C ₄ H ₈	<i>trans</i> -C ₄ H ₈ -2	<i>cis</i> -C ₄ H ₈ -2	C ₄ H ₈ -1
683 ^b	0.929	0.036	0.035
270 ^b	0.888	0.055	0.057
1.64	0.720	0.022	0.053	0.091	0.121
1.60	0.734	0.018	0.053	0.080	0.115
1.14	0.727	0.018	0.054	0.081	0.121
0.91	0.701	0.020	0.060	0.090	0.128
0.76 ^c	0.697	0.021	0.059	0.092	0.131
0.59	0.618	0.031	0.079	0.112	0.160
0.24	0.562	0.043	0.098	0.112	0.185
0.21	0.582	0.035	0.094	0.120	0.169
0.051	0.501	0.041	0.114	0.116	0.227
0.050	0.520	0.042	0.113	0.113	0.211
0.047 ^c	0.461	0.033	0.117	0.139	0.250
0.018	0.425	0.051	0.135	0.127	0.262
0.017	0.414	0.052	0.137	0.124	0.273

^a The 3130-Å photolysis of a 31:1 mole ratio mixture of propane and 3-methyl-1-pyrazoline. ^b Because of the very high (>100:1) propane:pyrazoline ratios of these mixtures the amount of *trans*-C₄H₈-2 could not be quantitatively measured. ^c A Hanovia 550-W lamp with the appropriate solution filter used as the radiation source (see ref 1).

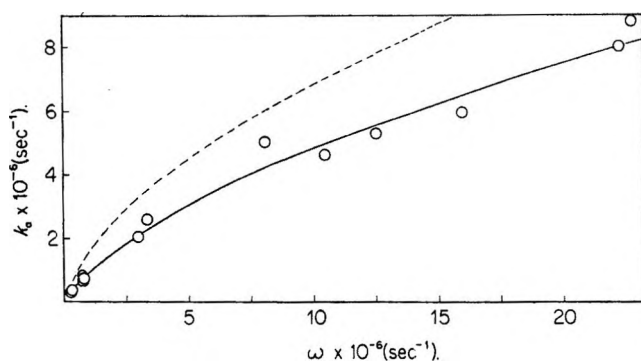


Figure 1. The experimental and calculated values of k_a as a function of ω . The solid line is a calculated curve with $E_{mp} = 80$ kcal mol⁻¹ and $\sigma = 18$ kcal mol⁻¹. For comparison, the broken line is a calculated curve with $E_{mp} = 85$ kcal mol⁻¹ and $\sigma = 14$ kcal mol⁻¹.

4-methylcyclopentene⁹ would indicate that the decomposition of 3-methyl-1-pyrazoline would be 1.5 kcal mol⁻¹ less exothermic, and consequently, the total available energy is 1–2 kcal mol⁻¹ less than the 132 kcal mol⁻¹ available on 3130-Å photolysis of 4-methyl-1-pyrazoline. Again, $f(E)$ was assumed to be Gaussian.

The theoretical curve that best fits the experimental data is illustrated in Figure 1; it is one for which the most probable energy, E_{mp} , is 80 kcal mol⁻¹ and the dispersion, σ , is 18 kcal mol⁻¹. This represents an upper limit to the most probable energy of the formed MCP*, a value that is 2 kcal mol⁻¹ less than E_{mp} observed for the 4-methyl-1-pyrazoline system.¹

Comparison of σ values is less meaningful because of the uncertainty as to the extent of olefin formation from the primary photodecomposition process in the present work.

Pyrolysis studies of some alkyl-1-pyrazolines,⁴ azoethane,¹⁰ and isopropylazomethane¹¹ indicate that a methyl group on the 3 position instead of the 4 position of the 1-pyrazoline ring lowers its activation energy for decomposition to alkylcyclopropanes and nitrogen by ~ 1 kcal mol⁻¹. Evidently this small change in the potential energy surface has not decreased the most probable energy of the nitrogen fragment by even one vibrational quanta, since such a change would mean there would be 5 to 6 kcal mol⁻¹ more energy available to be distributed to the remaining degrees of freedom, and therefore, a relatively more energetic MCP* (>82 kcal mol⁻¹) would be formed in this system as compared to 4-methyl-1-pyrazoline photolysis. Changes in the experimental technique may account for a part of the 2 kcal mol⁻¹ difference in E_{mp} , but certainly the present value is no greater than the 82 kcal mol⁻¹.

Although it alters the relative amount of olefin formation in the primary photodecomposition process,^{1,8} substitution of methyl group in the 3 position instead of the 4 position little affects the partitioning of energy between the MCP and nitrogen fragments. If this structural change causes a great enough perturbation of the potential energy surface to at least partially affect a stepwise breaking of the CN bonds, rather than a ring-like transition state with equivalent CN bonds, for the cyclopropane forming reaction, these results imply that the transition state lifetime is too short (<10⁻¹¹ sec)¹² to allow any greater intramolecular re-

(9) A. Labbauf and F. D. Rossini, *J. Phys. Chem.*, **65**, 479 (1961).

(10) Private communication by D. F. Swinehart to J. B. Levy and B. K. W. Copeland, *J. Amer. Chem. Soc.*, **82**, 5314 (1960).

(11) H. C. Ramsperger, *ibid.*, **51**, 2134 (1929).

laxation of the vibrational energy stored in the N-N bond to the vibrational modes of the hydrocarbon fragment that would be expected of such a mechanism.³ Not surprisingly perhaps, greater structural changes are evidently necessary in order to sufficiently alter the potential energy surface to affect the reaction product energy distribution.

Acknowledgment. This work has been supported by grants from the National Science Foundation and the Research Corporation.

(12) D. W. Placzek, B. S. Rabinovitch, and F. H. Dorer, *J. Chem. Phys.*, **44**, 279 (1966); D. L. Bunker, *ibid.*, **40**, 1946 (1964).

Glass Structure and Electrochemical Selectivity

by Michael L. Hair

Research and Development Laboratories, Corning Glass Works, Corning, New York 14830 (Received September 9, 1969)

The use of aluminosilicate glasses as specific ion electrodes is well known and the effect of glass composition on the monovalent ion selectivity has been the subject of many studies by Eisenman and his coworkers.¹ These workers have noted a correlation between the M^+/Al^{3+} ratio in the glass and the K^+-Na^+ ion selectivity of the resultant electrode. This is shown in Figure 1 where the data for sodium aluminosilicate glasses were reproduced from Eisenman.^{2,3} The empirical curve is based on experimental data and illustrates three points of significance.

1. Over a range of compositions there is an approximately linear relationship between Na^+/Al^{3+} and the logarithm of the K^+-Na^+ selectivity constant. This has been expressed by Eisenman in the form

$$\log K_{NaK}^{Pot} = 7.42 \log \frac{Na^+}{Al^{3+}} - 3.2$$

2. When M^+/Al^{3+} is less than unity, the selectivity constant K_{NaK}^{Pot} is a maximum (*i.e.*, the glass is Na^+ selective) and it does not depend on the M^+/Al^{3+} ratio.

3. When M^+/Al^{3+} is large, there is a deviation which results in an apparent minimum in the K_{NaK}^{Pot} selectivity constant (*i.e.*, maximum K^+ selectivity). This deviation is attributed by Eisenman to "water swelling" of the sites and glasses in this region are used to prepare K^+ -selective electrodes.

All glasses contain dissolved "water" in the form of hydroxyl groups and this effect has been quantitatively investigated by Scholze⁴ using infrared spectroscopy. Two major bands can be observed in the infrared spectrum of most silicate glasses, and these appear at about

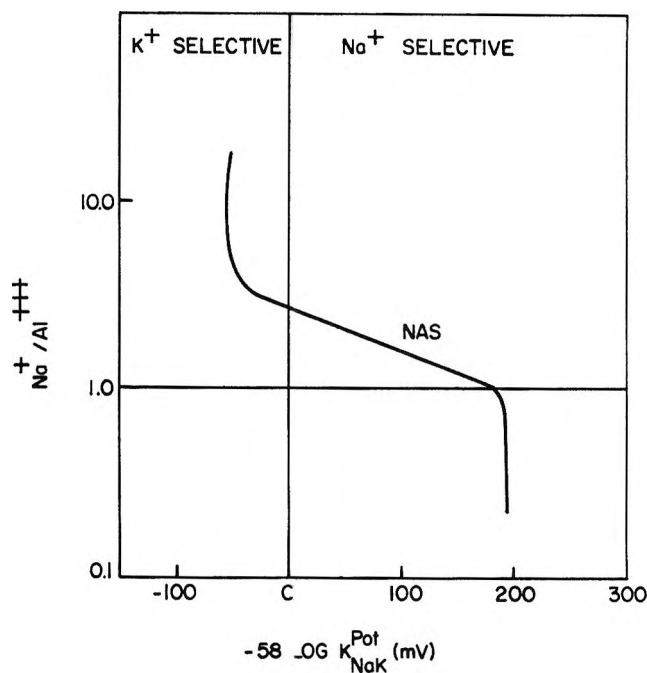


Figure 1. Dependence of Na^+-K^+ selectivity on the alkali cation to aluminum ratio in glass. The curve plots the empirical relationship between K_{NaK}^{Pot} and Na^+/Al^{3+} (at constant 50 atom %). The vertical line separates K^+ -selective from Na^+ -selective compositions.

2.85 and 3.6 μ . Only the 2.85- μ band is observed in fused silica and it is therefore attributed to an Si-OH group which is slightly perturbed by the silica environment. The 3.6- μ band occurs in the spectrum of simple alkali silicate glasses and is attributed to an Si-OH group which is more perturbed by a different environment. Scholze has provided data on the relative concentrations of these two bands in a series of sodium aluminosilicate glasses, and his results on the percentage of water which is present as the 2.85- μ band have been plotted as a function of $\log Na^+/Al^{3+}$ in Figure 2. Visual comparison of these results with the Eisenman selectivity plot suggests that there is a correlation between the percentage of water present as the 2.85- μ band and the electrochemical selectivity of the glasses.

Thus, when the Na^+/Al^{3+} ratio is less than 1, the infrared spectra show that all the water is present as the 2.85- μ group. These glasses are selective to Na^+ in the presence of K^+ , and the degree of selectivity is independent of the actual Na^+/Al^{3+} ratio.

When Na^+/Al^{3+} is between 1 and 2.5, there is an approximately linear relationship between $\log Na^+/Al^{3+}$ and the per cent OH in the 2.85- μ band. A similar linear relationship exists in this range between $\log Na^+/Al^{3+}$

(1) G. Eisenman, "Glass Electrodes for Hydrogen and Other Cations," Marcel Dekker, New York, N. Y., 1967.

(2) G. Eisenman in "Advances in Analytical Chemistry and Instrumentation," Vol. 4, C. N. Reilly, Ed., 1965, p 345.

(3) G. Eisenman, *Biophys. J.*, **2**, 270 (1962).

(4) H. Scholze, *Glastech. Ber.*, **32**, 142 (1959).

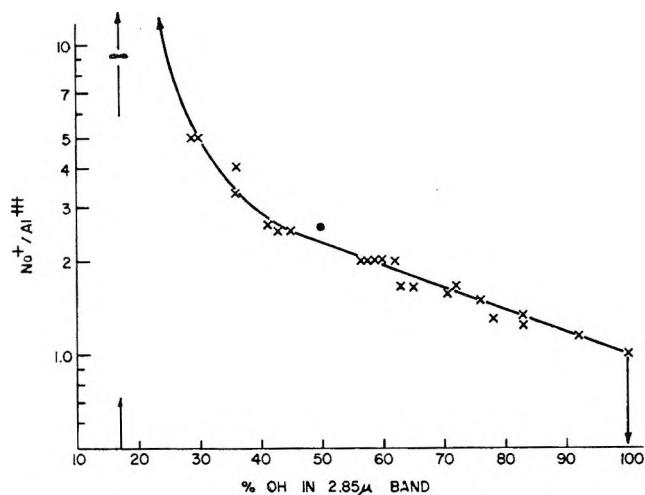


Figure 2. Dependence of the relative concentrations of OH in the 2.85- μ band on the $\text{Na}^+/\text{Al}^{3+}$ ratio for a series of sodium aluminosilicate glasses of silica content between 45 and 70%. Solid circle represents $N_{\text{E}^+}/\text{Al}^{3+}$ ratio at zero selectivity placed at 50% OH content (data from Scholze⁴).

and $\log K_{\text{NaK}}^{\text{pot}}$. When $\text{Na}^+/\text{Al}^{3+}$ is greater than 2.5, there are deviations from the straight line. The minimum Na^+-K^+ selectivity parallels a minimum percentage of the 2.85- μ band. In view of these correlations the selectivity data obtained from Figure 1 have been plotted against the relative hydroxyl concentrations (Figure 3). A surprisingly good linear relationship is obtained between the relative hydroxyl concentrations and $\log K_{\text{NaK}}^{\text{pot}}$ throughout the complete range of glass compositions for which adequate data are available. The gross upward deviations from linearity which appear in Eisenman's $\log \text{Na}^+/\text{Al}^{3+}$ vs. $\log K_{\text{NaK}}^{\text{pot}}$ plot and which are explained away by "water swelling" are normalized by the hydroxyl concentration plot.

Eisenman's theory of the electrochemical selectivity of alkali aluminosilicate glasses is based on the presence of two types of ion-exchange sites in the glass. These are considered to be the weakly acidic, high field strength, SiO^- sites which have a selectivity order $\text{H}^+ > \text{Li}^+ > \text{Na}^+ > \text{K}^+ > \text{Rb}^+ > \text{Cs}^+$ and the strongly acidic, low field strength, $(\text{Al}-\text{O}-\text{Si})^-$ sites which exhibit a selectivity order exactly opposite to that of the SiO^- site. The addition of Na^+ to an aluminosilicate glass "screens" the $(\text{Al}-\text{O}-\text{Si})^-$ site and lowers the effective field strength. Thus, when $\text{Na}^+/\text{Al}^{3+}$ is less than 1, the properties of the individual $(\text{Al}-\text{O}-\text{Si})^-$ sites were considered to be independent of the alkali content (Figure 1). When $\text{Na}^+/\text{Al}^{3+}$ is greater than 1, it was considered that increasing the Na^+ concentration weakens the site and makes Na^+ less preferred relative to K^+ . This model explains the low sodium and the linear portion of the curve, but does not explain the deviations at high Na^+ concentrations. In view of the success of the hydroxyl ratio correlation at

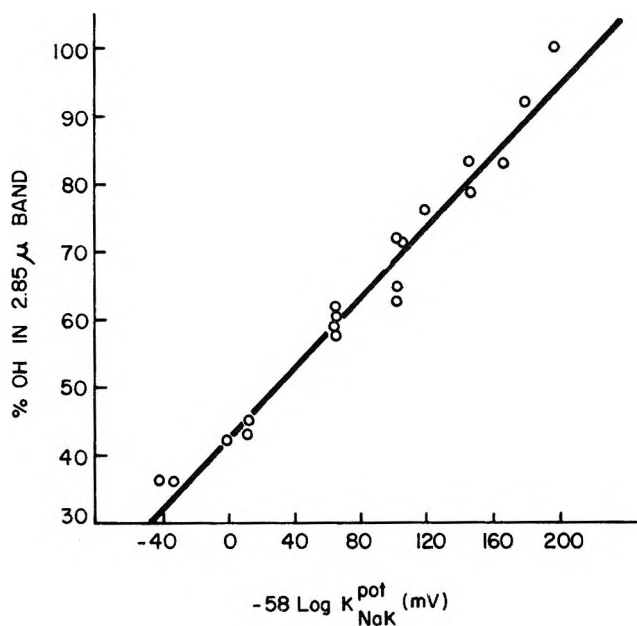
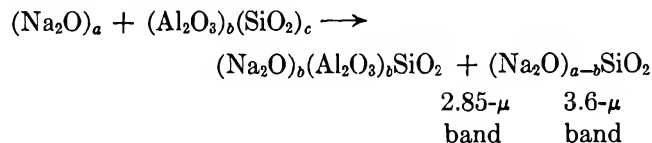


Figure 3. Plot showing the relation between the amount of water present in the glass as the 2.85- μ band and $\log K_{\text{NaK}}^{\text{pot}}$.

all compositions, some extension of Eisenman's model seems in order.

It is now widely believed that simple sodium silicate glasses are not homogeneous but exist as two phases which, under certain circumstances, can be clearly observed with the electron microscope.⁵

A previous study of the ratio of the concentrations of "water" bands in simple alkali silicate glasses suggested that the 2.85- and 3.6- μ bands can be ascribed to two different internal structures in the glass.⁶ These are a "pure" silica environment and a sodium silicate environment of variable composition. With aluminosilicate glasses, two analogous environments are again envisaged. These are an aluminosilicate phase and a sodium silicate phase. The water distributes itself between these two phases, giving rise to OH bands at 2.85 and 3.5 μ , respectively. If it is assumed that the concentration of OH groups is directly proportional to the number of sites, then the hydroxyl data are understandable in terms of the electrochemical selectivity. As Na_2O is added to an aluminosilicate glass, it is considered that the following rearrangement occurs



If $b > a$, the 3.6- μ band cannot be produced. If $a > b$, then the 3.6- μ band is produced. This substitution is

(5) E. A. Porai-Koshits and V. I. Averjanov, *J. Non-Cryst. Sol.*, **1**, 29 (1968).

(6) M. L. Hair, submitted for publication.

approximately linear up to $\text{Na}^+/\text{Al}^{3+} = 2.5$, at which point the hydroxyls are almost evenly distributed between the 2.85- μ and the 3.6- μ bands. Within the limits of experimental error, this also corresponds to the ratio at which Eisenman notes a change from K^+ to Na^+ selectivity.

It is tempting therefore, to ascribe the ion selectivity of glass electrodes to the superimposition of two types of sites in the glass. The one which is Na^+ selective (2.85 μ) can constitute 100% of the sites, whereas the other (3.6 μ) which is K^+ selective, can apparently constitute no more than about 70% of the sites. This accounts for the highly selective Na^+ electrodes that can be obtained and the poor selectivity of the available K^+ glass electrodes.

Nicol'skii⁷ has reported that in electrodes containing only small quantities of alumina (less than 7%), a distinct step occurs when the electrode potentials of a series of sodium aluminosilicate glasses are plotted against pH. These results were taken as indicating contributions to the electrode potentials by $(\text{SiO})^-$ and $(\text{Al-O-Si})^-$ sites.

The role of the hydrated layer which must be formed before glasses become K^+ selective is still vague. The present correlation suggests that if the layer is directly important in ordering the selectivity, then the underlying glass structure directly controls the leaching and structure of the gelatinous layer which in turn controls the ion selectivity.

The present model differs from the Eisenman model in that the K^+ selectivity is associated with the phase that gives rise to the 3.6- μ band—*i.e.*, the sodium silicate phase or the Si-O^- - Na^+ structure. Sodium silicate glasses are known to be leachable to give molecular sieve type materials which have pore sizes between 2 and 7 Å in diameter.⁸ This is the same order of magnitude as the "pores" observed in sintered porous glasses which gave rise to similar K^+ - Na^+ selectivity⁹ and suggests that a pore size effect could be important in determining ion selectivity. The role of the alumina in the glass is seen to be of less importance. An alkali silicate glass, rich in soda, would be predicted to give high K^+ - Na^+ selectivity on the basis of relative hydroxyl concentrations. Such glasses are notoriously soluble in water (as distinct from leachable) and the role of the alumina may be primarily to provide stability to the glass network in high-alkali glasses. (Alumina is renowned in the glass industry as the great homogenizer.)

Similarly, a pure silica would be predicted to give high Na^+ - K^+ selectivity. Such a membrane, however, would have very high resistance and, in this case, the role of the alumina could be the purely practical one of allowing the addition of Na_2O to reduce the resistance, without causing formation of the 3.6- μ phase.

Addendum

A reviewer has commented on the emphasis placed on the correlation between the composition at which the selectivity changes from potassium to sodium and the distribution of the hydroxyls. Quite rightly, he points out that this composition would be completely different had I chosen K^+ - Li^+ or K^+ - Rb^+ and suggests that some insight into the question might be obtained by looking at lithium aluminosilicate or potassium aluminosilicate glass compositions rather than the sodium aluminosilicates. Unfortunately, the small amount of data in the literature does not permit the corresponding plots for lithium and potassium aluminosilicate glasses to be drawn. However, the data do show that lithium glasses lie well above and potassium glasses lie well below the curve drawn for sodium glasses in Figure 2—just as they do in Eisenman's selectivity plot.² The general trend is thus established but more data are needed to confirm an exact relationship.

(7) B. P. Nicol'skii, M. M. Shul'ts, E. A. Materova, and A. A. Belijusten, *Dokl. Akad. Nauk SSSR*, **140**, 641 (1961).

(8) L. S. Yastrebova, A. A. Bessonov, S. S. Khvashev, *Tseolity, Ikh Sin., Svoistva Primen., Mater. Vses. Soveshch. Tseolitam*, **2nd**, 1964, 229 (1965). See *Chem. Abstr.* **64**, 19149c (1966).

(9) I. Altug and M. L. Hair, *J. Phys. Chem.*, **72**, 2976 (1968).

The Anomalous Frequency Effect in Conductometric Measurements at High Dilution

by Estella K. Mysels,¹

Chemistry Department, University of Southern California, Los Angeles, California 90007

Piet C. Scholten,

Philips Research Laboratories, Eindhoven, The Netherlands

and Karol J. Mysels

R. J. Reynolds Tobacco Company, Winston-Salem, North Carolina 27102 (Received September, 22, 1969)

The precise and accurate measurement of conductivity of dilute solutions is an important tool in the study of both aqueous and nonaqueous electrolytes. The necessity of a solvent correction makes it generally desirable to use dilution cells capable of determining the resistance of both the solvent and the solution and therefore requires the measurement of a wide range of resistances extending to high values. Alternating current is usually used in these measurements and this can lead, and has led, to significant errors. Jones and

(1) To whom correspondence should be sent at Salem College, Winston-Salem, N. C. 27108.

his students² have analyzed most of these, particularly the "capacitive shunt" effect, and have shown that they can always be detected by a *decreasing* measured resistance at increasing frequencies. Hence, a resistance independent of frequency has been accepted as a criterion of accurate measurement.

The literature reports, however, instances of measured resistances *increasing* with frequency. This anomalous effect has been variously explained without detailed analysis. Thus, Nichol and Fuoss³ ascribed it to higher order terms in the capacitive shunt effect, Hawes and Kay⁴ to the polarizability of glass, and Mukerjee, Mysels, and Dulin⁵ to the presence of induction in windings of an electric motor. In the two cases where equivalent conductivity values were involved,^{4,5} extrapolations to zero frequency were used although the exact method is not reported.

We have again encountered this anomalous frequency effect, and as the previous explanations did not seem pertinent or sufficient, a more detailed study was undertaken. Our results indicate that the effect is due to a capacitive leakage to the ground and that extrapolation to zero frequency is indeed correct and should be done on the basis of frequency squared from quite low frequencies.

Experimental Section

Resistances were measured on a Jones-Dyke bridge⁶ with a General Radio Type 1232-A null detector. Auxiliary high-quality resistors (General Radio Co. Type 500) served either to shunt the measured cell or to extend the measuring arm of the bridge. Both procedures gave equivalent results. The Wagner ground of the bridge was balanced for each measurement. The cell was of the type described by Daggett, Bair, and Kraus⁷ with the configuration of the lead arms somewhat modified to reduce the Jones shunt effect. This basically is a 1000-ml erlenmeyer flask with a small bulb containing the electrodes connected to the side of this flask by two channels, one very near the bottom and the other vertically above it. The lead arms extend sideways from the bulb. The cell constant was 0.2254. The cell was immersed in a thermostated oil bath. Within the bath were a number of metallic accessories, such as a cooling coil, a heater, a temperature sensor, and, particularly, a riser enclosing the motor of the magnetic stirrer.⁵ These, as well as the steel thermostat vessel, were grounded. The data reported are for distilled water containing three different levels of dissolved CO₂.

Results and Interpretation

A typical variation of measured resistance as a function of frequency is given in Figure 1. The line drawn from the intercept through the first two points is a parabola corresponding to a linear extrapolation on an ω^2 plot. It may be seen that the effect is significant

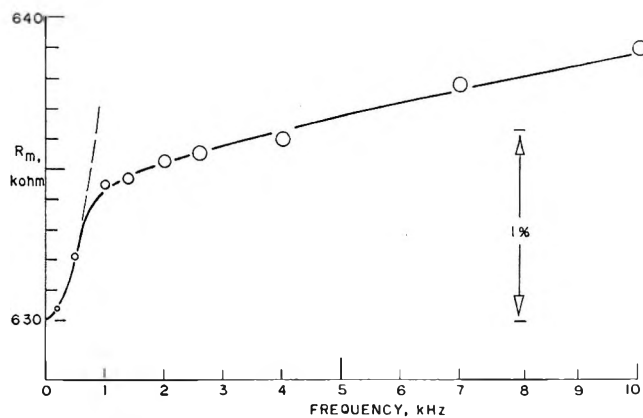


Figure 1. Typical variation of the measured resistance with frequency when cell resistance is about 0.5 megohm.

and that linear extrapolation along either the high-frequency or the low-frequency part can lead to quite different results than the one shown.

We attribute this effect to a leakage to the ground along a resistance in series with a capacitance. The principal capacitance is believed to be between the bottom of the erlenmeyer part of the cell and the magnetic stirrer mechanism. The resistance is that of the electrolyte within the cell, particularly in the channels between the measuring bulb and the erlenmeyer flask.

Figure 2 shows the essential elements of the system including the equal fixed arms of the bridge, the true cell resistance R_t , the measuring resistance R_m , and the resistance to the ground R_g , along with its series capacitance C_g . For simplicity, the latter is assumed to be connected to the middle of R_t , which corresponds to the position of the narrow channels between the bulb and the erlenmeyer. C_t is the true parallel capacitance of the cell and C_m is the measuring capacitance. Other capacitances are omitted since they do not enter the calculation. C_t includes two items: the true parallel capacitance of the cell due mainly to its parallel disk electrodes acting as condenser plates and the effective series capacitance due to electrode polarization. The impedance of the latter is negligible when the electrodes are even lightly platinized and especially when the measured resistance is large. C_t is then essentially a function of the cell constant K and for aqueous solutions given by $1.1 \times 10^{-12} \times 80 / (K \times 4\pi)$ F so that in our measurements C_t is about 31 pF. When the bridge and the Wagner ground are both balanced, the two

(2) (a) G. Jones and G. M. Bollinger, *J. Amer. Chem. Soc.*, **53**, 411 (1931); (b) G. Jones and S. M. Christian, *ibid.*, **57**, 272 (1935).

(3) J. C. Nichol and R. M. Fuoss, *J. Phys. Chem.*, **58**, 696 (1954).

(4) J. L. Hawes and R. L. Kay, *ibid.*, **69**, 2420 (1965); see p 2423 top.

(5) P. Mukerjee, K. J. Mysels, and C. I. Dulin, *ibid.*, **62**, 1390 (1958).

(6) P. H. Dyke, *Rev. Sci. Instr.*, **2**, 379 (1931).

(7) H. M. Daggett, E. J. Bair, and C. A. Kraus, *J. Amer. Chem. Soc.*, **73**, 799 (1951).

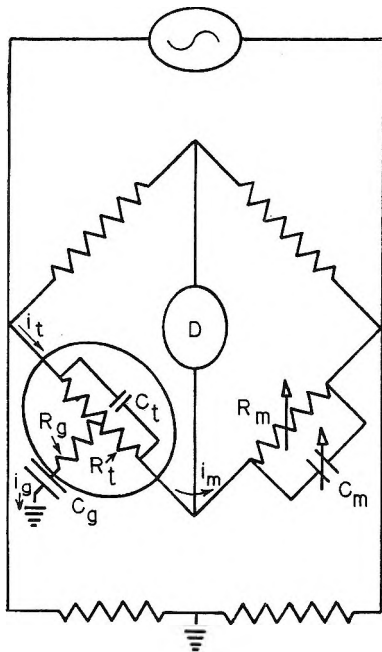


Figure 2. Schematic diagram of the Wheatstone bridge with Wagner ground at the bottom and with the error-causing $R_g - C_g$ bypass to the ground from the middle of the measured resistance R_t .

terminals of the detector are at ground potential. Hence, the system must satisfy the conditions

$$i_t = i_m + i_g \quad (1)$$

$$i_t(Z_t/2) + i_m(Z_t/2) = i_m Z_m \quad (2)$$

$$i_m(Z_t/2) = i_g Z_g \quad (3)$$

where Z denotes the complex impedance of the element indicated by the subscript and i the corresponding current with the exception that i_t is the current in only the left part of R_t .

Solution of these equations is simplified if one takes into account the postulated nature of the stray resistance and capacitance. C_g is constant if the position of the cell remains constant in the apparatus and C_t is also constant as explained above. Hence, we can write

$$C_g = \gamma C_t \quad (4)$$

where γ is a constant. R_g and R_t are both due to the same electrolyte filling the cell, the former to the portion in the channels and the latter to that between the electrodes. Hence, they must be proportional to each other and we can write

$$R_g = \rho R_t \quad (5)$$

where ρ is a constant > 1 .

The exact solution of eq 1-3 gives for the error Δ in the measured resistance

$$\Delta \equiv R_m - R_t =$$

$$\frac{\omega^2 R_t^3 C_t^2 \gamma^2 (4\rho + 1 + 4\omega^2 R_t^2 \rho C_t^2)}{16 + 4\omega^2 R_t^2 C_t^2 [4 + 2\gamma + \rho \gamma^2 (4\rho + 1)] + 4\omega^4 R_t^4 \rho C_t^4 \gamma^2 (4\rho - 1)} \quad (6)$$

This difference is indeed positive and for low frequencies approaches zero proportionately to the square of the frequency. This explains then qualitatively our observations and permits the determination of the true resistance by such an extrapolation.

Further support for this explanation can be obtained by evaluating the characteristics of the postulated leakage to the ground; *i.e.*, ρ and C_g should both be constant. To simplify, we neglect 1 in comparison with 4ρ and γ and 1 in comparison with $\rho^2 \gamma^2$. Equation 6 can then be rewritten as

$$\frac{R_t \omega^2}{\Delta} = \frac{4}{R_t^2 \rho C_t \gamma^2 (1 + \omega^2 R_t^2 C_t^2)} + 4\rho \omega^2 \quad (7)$$

As the product $R_t^2 C_t^2$ is of the order of 10^{-9} , the first term on the right is essentially constant and a plot of eq 7 on a ω^2 scale should reduce all data to a set of parallel lines having different intercepts. These intercepts can thus be obtained but are very small and of the order of the scatter of the data. Figure 3 therefore shows our data according to eq 7 after subtracting these intercepts. It may be seen that, up to a frequency of about 7 kHz, the points lie close to a single straight line passing through the origin. At the highest frequency (10 kHz) there are marked methodical deviations increasing with the resistance of the cell. These are of little importance in normal measurements, and we attribute them to the emergence of residual shunt effects. The slope of this line is equal to ρ and gives the value of 25 for the ratio of R_g to R_t which is reasonable.

The low-frequency limit of eq 7 can be written as:

$$\frac{4\Delta}{R_t^3 \rho} = \omega^2 C_g^2 \quad (8)$$

Since R_t , Δ , and ρ have been evaluated, the value of C_g may be obtained from the slope of a plot of this relation. The points scatter considerably since they depend on the small values of Δ at low frequencies but give a value of about 10 pF for C_g which is reasonable.

The simplification introduced in obtaining eq 7 and 8 is therefore consistent with the values obtained, *i.e.*, $\rho = 25$ and $\gamma = 0.3$, which gives $\rho^2 \gamma^2 = 56$. The same approximations seem to remain valid over the probable range of conditions of interest.

Equation 8 can be rewritten as

$$\Delta = \frac{\omega^2 R_t^3 \rho C_g^2}{4} \approx \frac{\omega^2 R_m^3 \rho C_g^2}{4} \quad (9)$$

which shows that for any experimental arrangement,

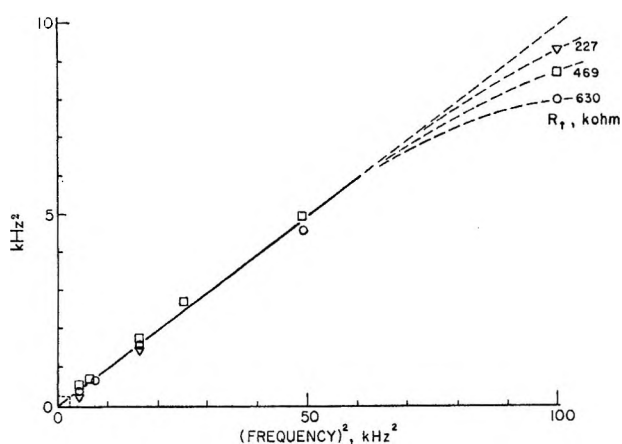


Figure 3. Agreement of data with eq 8. Additional 10 points not shown are located in the small dashed rectangle near the origin. The ordinate shows $R_t f^2 / \Delta$ minus the small intercepts (see text).

once the two constants have been evaluated, the correction can be readily applied to any measurement at a low enough frequency (500 Hz or below).

It may be noted that the calculated measuring capacitance is

$$\frac{C_t [R_t - (R_t \gamma / 4) + \Delta(2 - \rho \gamma) - \omega^2 R_t^2 \rho C_t^2 \gamma (R_t + \Delta)]}{(R_t + \Delta)(1 - \omega^2 R_t^3 \rho C_t^3 \gamma)} \approx C_t - C_g / 4 \quad (10)$$

The approximation involves the neglect of the very

small terms in Δ and in $R_t C_t$. Hence, the error in the measured capacitance is negative and very small.

Conclusion

Because of the very different grounding system used by Hawes and Kay⁴ it is possible that our analysis does not apply to their system. It certainly can account, however, for the anomalies observed in the more conventional systems of Nichol and Fuoss³ and of Mukerjee, *et al.*⁵ The effect can, of course, be minimized by careful design of the constant-temperature bath and especially of the stirring arrangement to avoid any leakage of the current from the bridge circuit against which Jones has warned already.⁸ Any residual effects can be precisely corrected for by proper extrapolation or by eq 9. Thus, the range of accurate cell resistance measurements can be extended to at least 500 kilohms from the 10 kilohms recommended by Jones¹ and the 50 kilohms shown to be possible with dip cells by Nichol and Fuoss.³ Hence, the range of concentrations over which a solvent correction measured in the same cell can be applied to give an accurate conductance value can be correspondingly increased.

Acknowledgment. This work was supported in part by PHS Research Grant GM 10961-03 from the Division of General Medical Services, Public Health Service.

(8) G. Jones and R. C. Josephs, *J. Amer. Chem. Soc.*, **50**, 1049 (1928).

COMMUNICATIONS TO THE EDITOR

Density of Liquid Uranium

Sir: The density of liquid U was examined as part of a continuing study of the physical properties of liquid actinide elements. A knowledge of the volume change associated with the solid to liquid transformation is of fundamental importance in the study of liquid metals. The majority of metallic elements exhibit approximately 3% volume expansion during the melting process,¹ except for two classes of elements which contract during melting. One class consists of the semimetallic elements with open or layer-like solid structures, such as Bi, Sb, and Ga, which apparently transform to a more densely packed liquid phase. The other class consists of only the rare earth element Ce and the actinide element Pu which exhibit volume contractions for the melting of rather dense bcc solid phases. These changes are 0.8 and 2.4% volume contraction for Ce² and Pu,³ respectively. A change in the electronic configuration of the atoms in metallic Ce has been proposed by Jayaraman⁴ to explain its volume contraction.

The volume change associated with the melting of the bcc solid phase of γ -U has not been measured directly, although the density of liquid U has been reported previously by Grosse, Cahill, and Kirshenbaum.⁵ When their results for the density of the liquid are compared with the calculated density of the solid at the melting point, a volume contraction during the melting of U is implied. Because of the significance of this implication on the electronic structure of metallic U, the density of liquid U was redetermined and is reported here.

A pycnometric technique, previously described,³ was utilized for this investigation. In this technique small tantalum pycnometers were filled at test temperatures. An especially reduced zirconia crucible was used as the liquid metal container in order to minimize the oxidation of the U. The substoichiometric zirconia crucible was formed when a commercially available, impervious ZrO₂ crucible was heated in a high vacuum furnace in the presence of zirconium metal for 4 days at 1450° and approximately 10⁻⁶ Torr residual pressure. The U was of high purity, 99.96 wt % U, with the major impurities (in ppm) being: Al, 12; Fe, 64; Ni, 14; Si, 43; C, 146; other metallics, 152. The isotopic composition was 0.24 wt % ²³⁵U and 99.76 wt % ²³⁸U. The density values were not adjusted to any other isotopic composition.

The measured density values, listed in Table I, were fitted to a straight-line function of temperature by the least-squares method. The equation of the line was

$$\rho \text{ (g/cm}^3\text{)} = (19.520 - 16.01)10^{-4}T(\text{°K})$$

with a standard deviation of ± 0.016 g/cm³. The present values are approximately 3.5% lower near the melting point and the temperature coefficient is slightly larger than the values given by the previous investigators.⁵ The deviation between the two sets of data is greater than the standard deviation given for either measurement. No explanation of this deviation is obvious, especially since experimental data were not given in the original publication; however, surface tension forces on the suspension wire of the sinker often cause an apparent density increase in the Archimedean method used by Grosse, *et al.*

Table I: Density of Liquid Uranium

Temp, °C	Density, g/cm ³
1137	17.252
1162	17.215
1180	17.225
1206	17.149
1245	17.082

The significant result of the present measurement is that the density of liquid U is less than the density of the solid, as shown by the following calculations. Although the density of α -U has not been measured at the melting point, an estimate based upon thermal expansion and X-ray data⁶ indicates it would have a density of 17.65 g/cm³ and a molar volume of 13.48 cm³/g-atom. The present data indicate a liquid density at the melting point of 17.27 g/cm³ and a molar volume of 13.77 cm³/g-atom. A volume expansion during melting of approximately 2.2% is indicated, therefore, very similar to the average of 3% found for most metals and unlike the volume contraction shown by Ce and Pu.

These calculations were supported by examination of the pycnometers after filling which indicated a volume

(1) A. R. Ubbelohde, "Melting and Crystal Structure," Clarendon Press, Oxford, 1965, pp 170-171.

(2) L. J. Wittenberg, D. Ofte, and W. G. Rohr in "Rare Earth Research II," Karl S. Vorres, Ed., Gordon and Breach Science Publishers Inc., New York, N. Y., 1964, pp 257-275.

(3) C. Z. Serpan, Jr., and L. J. Wittenberg, *Trans. AIME*, **221**, 1017 (1961).

(4) A. Jayaraman, *Phys. Rev.*, **137A**, 179 (1965).

(5) A. V. Grosse, J. A. Cahill, and A. D. Kirshenbaum, *J. Amer. Chem. Soc.*, **83**, 4665 (1961).

(6) C. R. Tipton, Jr., Ed., "Reactor Handbook," Vol. 1, 2nd ed. Interscience Publishers, New York, N. Y., 1960, pp 111 and 119.

contraction during the freezing process. This conclusion was based upon the observation that for metals like Ce and Pu, with known volume expansions during solidification, a drop of liquid was forced to the tip openings of the pycnometers. No such liquid droplets were noted for the pycnometers used for U.

The conclusion of volume expansion during melting of U is in keeping with two direct observations made of this phase transformation. During interfacial tension measurements Rosen, Chellew, and Feder⁷ estimated a 3% volume expansion. Recently, the phase diagram⁸ of U has been published and an initial positive slope of 4.1°/kbar noted for the change in the melting point as a function of pressure. By use of the Clapeyron equation and the heat of fusion,⁹ 2900 cal/g-atom, the solid → liquid volume change calculated from the phase diagram is +0.35 cm³/g-atom, in good agreement with the value of +0.29 cm³/g-atom, calculated from this work.

(7) C. L. Rosen, N. R. Chellew, and H. M. Feder, *Nucl. Sci. Eng.*, **6**, 504 (1959).

(8) N. Asami, M. Yamada, and S. Takahashi, *Nippon Kinzoku Gakkaishi*, **31**, 389 (1967).

(9) H. Savage and R. D. Seibel, USAEC Report ANL-6702, Argonne National Laboratory, Argonne, Ill., Sept 1963.

(10) Mound Laboratory is operated by Monsanto Research Corp. for the U. S. Atomic Energy Commission under Contract No. AT-33-1-GEN-53.

MONSANTO RESEARCH CORPORATION WILLIAM G. ROHR
MOUND LABORATORY¹⁰ LAYTON J. WITTENBERG
MIAMISBURG, OHIO 45342

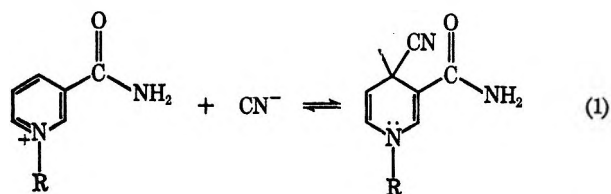
RECEIVED AUGUST 15, 1969

Secondary Valence Force Catalysis. XI.

Enhanced Reactivity and Affinity of Cyanide

Ion toward N-Substituted 3-Carbamoylpyridinium Ions Elicited by Ionic Surfactants

Sir: It has been established that rate and equilibrium constants for a number of organic reactions are altered in the presence of dilute solutions of ionic surfactants.^{1,2} We now wish to report an additional example, the addition of cyanide ion to N-substituted 3-carbamoylpyridinium ions, which is unusual in several respects. The principal features of this reaction are the following.



First, the rate and equilibrium constants for the reaction shown in eq 1 are markedly increased by low concentrations of cationic surfactants. In Table I, rate and

equilibrium constants in the presence of 0.02 M solutions of a series of *n*-alkyltrimethylammonium ions are collected. The largest association constant found, 4800 M⁻¹, for the reaction of the N-hexadecyl substrate in the presence of the *n*-hexadecyl surfactant, is more than 25,000 times larger than that for the model reaction, addition of cyanide to N-propyl-3-carbamoylpyridinium ion in surfactant-free aqueous solutions under comparable conditions.³ The largest second-order rate constant observed, 13.3 M⁻¹ sec⁻¹, for the reaction of the N-hexadecyl substrate in the presence of the *n*-hexadecyl surfactant, is 950 times greater than that for the same model reaction.³ These increases are substantially greater than those usually elicited by dilute surfactant solutions.^{1,2} It seems likely that a principal driving force for the surfactant-dependent reactions is destabilization of the cationic substrates by the cationic surface of the micelles relative to the zwitterionic transition states and uncharged products.

Table I: Rate and Association Constants for the Addition of Cyanide to a Series of N-Substituted 3-Carbamoylpyridinium Ions in the Presence of a Series of *n*-Alkyltrimethylammonium Bromides in Aqueous Solution at 25°^a

Substrate	Surfactant			
	Decyl	Dodecyl	Tetradecyl	Hexadecyl
Octyl				0.21; 135
Decyl			1.10; 530	1.35; 710
Dodecyl		2.5; 1100		5.8; 4000
Tetradecyl	0.28; 330		6.6; 3600	10.4; 4500
Hexadecyl		6.4; 4500		13.3; 4800

^a Surfactant concentration is 0.02 M throughout. In each case, the entries in the table are second-order rate constants in units of M⁻¹ sec⁻¹ followed by association constants in units of M⁻¹.

Second, at a constant concentration of a given surfactant, rate and equilibrium constants for the reactions increase with increasing hydrophobicity of the substrate. This behavior is best illustrated by the rate and equilibrium constants measured in the presence of *n*-hexadecyltrimethylammonium ion (Table I). This behavior is, in the case of the rate constants at least, not the consequence of incorporation of an increasing fraction of the substrates into the micelles with increasing substrate hydrophobicity. Measurement of rate con-

(1) (a) J. L. Kurz, *J. Phys. Chem.*, **66**, 2239 (1962); (b) C. A. Burnton, E. J. Fendler, L. Sepulveda, and K.-U. Yang, *J. Amer. Chem. Soc.*, **90**, 5512 (1968); (c) R. B. Dunlap and E. H. Cordes, *ibid.*, **90**, 4395 (1968); (d) R. B. Dunlap and E. H. Cordes, *J. Phys. Chem.*, **73**, 361 (1969); (e) M. T. A. Behme, J. G. Fullington, R. Noel, and E. H. Cordes, *J. Amer. Chem. Soc.*, **87**, 266 (1965); (f) L. R. Romsted and E. H. Cordes, *ibid.*, **90**, 4104 (1968); (g) C. Gitler and A. Ochoa-Solano, *ibid.*, **90**, 5004 (1968); (h) T. C. Bruice, J. Katzhendler, and L. R. Feder, *ibid.*, **90**, 1333 (1968).

(2) For a review, see E. H. Cordes and R. B. Dunlap, *Accounts Chem. Res.*, **2**, 239 (1969).

(3) R. B. Lindquist and E. H. Cordes, *J. Amer. Chem. Soc.*, **90**, 1269 (1968).

stants for these reactions as a function of surfactant concentration reveals that catalysis is maximal at 0.01 *M*, or less, surfactant and that rate constants either remain constant or decrease slightly at higher surfactant concentrations. At all surfactant concentrations investigated, 0.005–0.03 *M*, that order of reactivity as a function of substrate structure noted in Table I is observed. Since the concentration of surfactant is generally about 200 times greater than that of substrate, it is likely that the substrates themselves do not alter the micellar structure significantly. Thus, the data provide evidence for the suggestion of Gitler and Ochoa-Solano¹⁸ that hydrophobic interactions may contribute to activation energies for reactions in micellar systems. Such contributions might result from movement of the ionic head group of the substrates into the environment occupied by the nonionic dihydropyridine moiety of the products as the hydrophobic interactions between substrate and micelle are accentuated. This suggestion is consistent with the observation that the absorption maxima of the substrates in the presence of 0.02 *M* hexadecyltrimethylammonium bromide change uniformly from 271.3 to 272.3 *mμ* as the N substituent is changed from decyl to hexadecyl.⁴

Third, the surfactant-dependent reactions are made less favorable by salts. For example, association constants are 2300, 860, and 300 *M*⁻¹ for 0.0, 0.1, and 0.5 *M* added sodium chloride for the reaction of the N-tetradecyl substrate in the presence of 0.02 *M* tetradecyltrimethylammonium bromide at 30°. Second-order rate constants for this reaction decrease from 7.1 to 3.1 to 0.8 *M*⁻¹ sec⁻¹ for the same concentrations of sodium chloride. The effectiveness of anions as inhibitors increases in the order F⁻ < NO₃⁻ < Cl⁻ < Br⁻, which is related to but not identical with the relative inhibitory capacity of these anions for the surfactant-dependent basic hydrolysis of esters.^{1f}

Fourth, the affinity and reactivity of cyanide toward pyridinium ions are increased by zwitterionic surfactants. For example, rate and association constants for the addition of cyanide to N-dodecyl-3-carbamoylpyridinium bromide in the presence of 0.02 *M* dodecyl-dimethylammoniopropanesulfonate at 25° are, respectively, 1.0 *M*⁻¹ sec⁻¹ and 1100 *M*⁻¹. These figures indicate increases of 71- and 5700-fold in reactivity and affinity of cyanide for this pyridinium ion elicited by the zwitterionic surfactant. This is the only case known to us in which an organic reaction is subject to marked promotion by a zwitterionic surfactant. The source of the rate and affinity increases is not evident.

Finally, these reactions are subject to promotion by sonicated aqueous dispersions of ovoid lecithin. Rate and association constants for the addition of cyanide to N-dodecyl-3-carbamoylpyridinium bromide are increased 13- and 350-fold over control values in the presence of 4 × 10⁻⁴ *M* lecithin. As above, this reaction appears to be the only case identified in which a non-

enzymatic reaction is promoted by biological surfactants (with the exception, of course, of those reactions in which substrate solubilization is the important factor). Promotion by sonicated dispersions of lysolecithin and sphingomyelin has also been observed.

All of the above reactions have been followed spectrophotometrically at 340 *mμ* in aqueous solution. The temperature was maintained at 25° unless noted otherwise. Values of pH were maintained in the vicinity of pH 10 through use of dilute triethylamine buffers.

Acknowledgment. E. H. C. expresses his appreciation to the Escuela de Química, Universidad Central, for hospitality during a visit during which a portion of this research was conducted. We are indebted to Procter and Gamble, Inc., for a gift of the dodecyl-dimethylammoniopropanesulfonate.

(4) Related experiments have been described by P. Mukerjee and A. Ray, *J. Phys. Chem.*, **70**, 2144 (1966).

(5) Career Development Awardee of the National Institutes of Health. Research Fellow of the Alfred P. Sloan Foundation. This work was supported by Grant AM 08232 from the National Institutes of Health and by Grant GB 8132 from the National Science Foundation.

ESCUELA DE QUIMICA, FACULTAD DE CIENCIAS J. BAUMRUCKER
UNIVERSIDAD CENTRAL M. CALZADILLA
CARACAS, VENEZUELA M. CENTENO
G. LEHRMANN

DEPARTMENT OF CHEMISTRY P. LINDQUIST
INDIANA UNIVERSITY D. DUNHAM
BLOOMINGTON, INDIANA 47401 M. PRICE
B. SEARS
E. H. CORDES⁶

RECEIVED DECEMBER 2, 1969

Solvent Polarity in Electrochemical and Other Salt Solution Studies

Sir: Electrochemical techniques are very useful for the generation of reactive species in organic solvents. The subsequent behavior of these species may be followed by a number of techniques, including that of cyclic voltammetry.¹ Other methods, *e.g.*, potential step methods, can be and have been used to study the subsequent chemical reaction.² The rate constant *k* for the process $O + ne \rightleftharpoons R$; $R \xrightarrow{k} D$ can thus be determined.

R can be a neutral or charged species and may react through a transition state with a charge separation quite different from that of the initial state. In such cases, *k* will be very sensitive to the polarity of solvent.

(1) P. Delahay, "New Instrumental Methods in Electrochemistry," John Wiley and Sons, New York, N. Y., 1954. Also see R. S. Nicholson and I. Shain, *Anal. Chem.*, **35**, 706 (1964).

(2) W. M. Schwarz and I. Shain, *J. Phys. Chem.*, **69**, 30 (1965); **70**, 854 (1966); J. T. Lindquist and R. S. Nicholson, *J. Electroanal. Chem.*, **16**, 445 (1968).

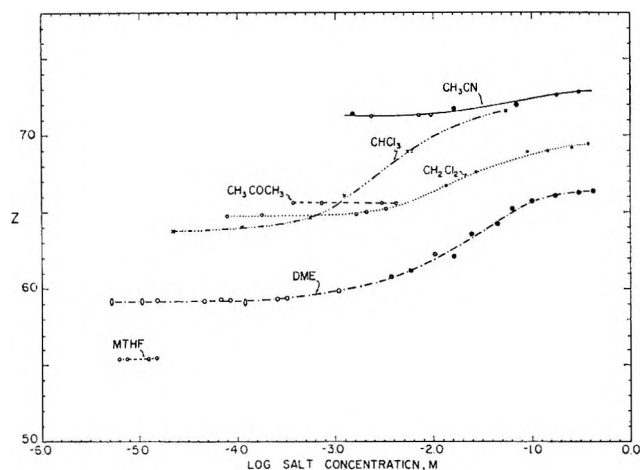


Figure 1. A plot of Z value vs. the negative of the logarithm of salt concentration for a number of nonpolar solvents. Open circles (\circ) represent measurements made with pure 1-ethyl-4-carbomethoxy-pyridinium iodide; closed circles (\bullet) are based on solutions of tetra-*n*-butylammonium perchlorate containing sufficient (7% or less) 1-ethyl-4-carbomethoxy-pyridinium iodide to permit facile observation of the charge-transfer maximum. Circles with diagonal lines (g) are derived from measurements on solutions of tetra-*n*-butylammonium perchlorate containing 15% 1-ethyl-4-carbomethoxy-pyridinium iodide (DME solutions). Data for acetonitrile and chloroform solutions (containing 0.13 M ethanol) are taken from ref 6 and are shown as \otimes (CH_3CN) or \times (CHCl_3). All other solvents were highly purified and degassed.

We wish to point out that the electrolyte required in the solutions for adequate conductivity (*e.g.*, 0.1 M tetra-*n*-butylammonium perchlorate (TBAP)) markedly raises the polarity of the solvent over that of the pure material. We have utilized Z values as a measure of the polarity of such solutions. Z values are empirical measures of solvent polarity based on the position of the charge-transfer band of 1-ethyl-4-carbomethoxy-pyridinium iodide.³ Our results show that, the lower the polarity of the pure solvent, the greater the increase in polarity brought about by a particular concentration of salt. Some solvents will exhibit a somewhat greater (or lesser) change than this rough generalization implies (*e.g.*, chloroform).

Data on the Z values of 1,2-dimethoxyethane (DME), acetonitrile, and other solvents relevant to electrochemistry are presented in Figure 1 as a log (salt concentration) vs. Z -value plot. The Z values of the pure solvents are derived by extrapolating Z -value measurements to infinitely dilute solutions.

The Z -value increment for the change from zero

salt to 0.1 M TBAP is quite large for DME (~ 6.8 kcal/mol) and significant for acetonitrile (1.5 kcal/mol). It is remarkable that the limiting Z value for very high concentrations of TBAP in DME is close (*ca.* 66.4 kcal/mol) to the Z value found for molten tri-*n*-hexylammonium perchlorate (66.9 kcal/mol).⁴

A Z -value increment of 2.8 kcal/mol can increase the rate of an electron-transfer reaction by a factor of 10, as shown for the case of 1-ethyl-4-carbomethoxy-pyridinium radical and 4-nitrobenzyl chloride.⁵ Electron-transfer reactions are clearly among the elementary processes to be considered for the reactions of species generated electrochemically, and a proper consideration of solvent polarity is necessary for comparison with kinetic results obtained by other means.

Salt effects in low polarity media can be studied by means of Z -value measurements. The charge-transfer bands observed for 1-ethyl-4-carbomethoxy-pyridinium iodide (*i.e.*, the Z values) exhibit much greater sensitivity to increases in salt concentration above $3 \times 10^{-4} M$ in DME and methylene chloride than below that concentration (Figure 1). A similar effect is observed in chloroform solutions.⁶ Electrostatic interactions may be responsible for these salt effects since dielectric relaxation measurements on tetraalkylammonium picrate salts in benzene do not support the notion that ionic aggregates more complex than ion pairs are present in solutions below 0.01 M .⁷⁻⁹

We suggest that Z -value measurements will provide intrinsically useful information on organic salt solutions and that they will be useful for the interpretation of kinetic data derived through electrochemical experiments.

(3) Cf. E. M. Kosower, "An Introduction to Physical Organic Chemistry," John Wiley and Sons, New York, N. Y., 1968, Section 2.6.

(4) J. E. Gordon, *J. Amer. Chem. Soc.*, **87**, 4347 (1965).

(5) E. M. Kosower and M. Mohammad, *ibid.*, **90**, 3271 (1968).

(6) E. M. Kosower, *ibid.*, **80**, 3253 (1958).

(7) Cf. Table 2.13 in ref 3.

(8) G. Williams, *J. Phys. Chem.*, **63**, 534 (1960).

(9) M. Davies and G. Williams, *Trans. Faraday Soc.*, **56**, 1619 (1960).

(10) To whom correspondence should be addressed.

(11) Support from the Army Research Office (Durham) and the National Institutes of Health is gratefully acknowledged.

DEPARTMENT OF CHEMISTRY
STATE UNIVERSITY OF NEW YORK
STONY BROOK, NEW YORK 11790

M. MOHAMMAD
E. M. KOSOWER^{10,11}

RECEIVED DECEMBER 19, 1969